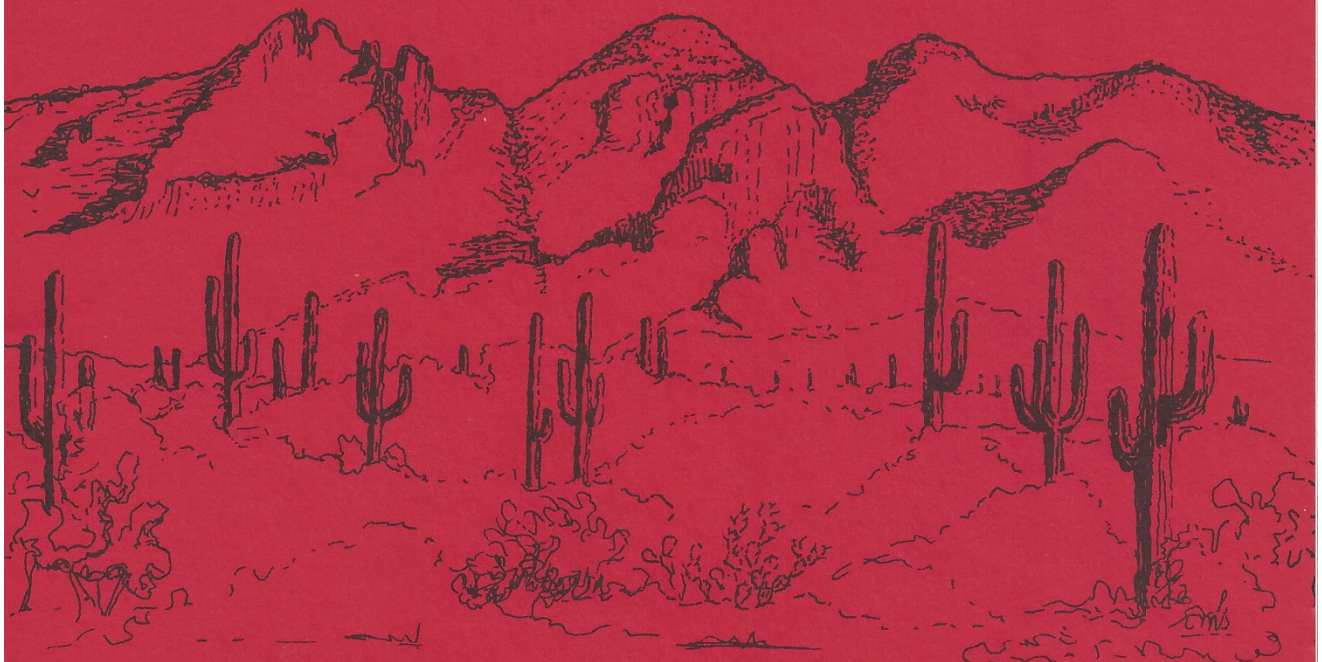




**Geophysical Surveys Near  
Tucson International Airport**

**Geophysics Field Camp 2013  
LASI-13-1  
May 15, 2013**



# **Geophysical Surveys Near Tucson International Airport**

**Geophysics Field Camp 2013  
LASI-13-1  
May 15, 2013**

Alaa E. Alam  
Mohammed Alabkari  
Ahmed Mohammed A. Albahrani  
Abdulrahman M. Aljarbou  
Ada R. Dominguez  
Mohammed Ghallab  
Khaliza Binti Khalid  
Amber L. Keske  
Sophie Morrell  
Ben K. Sternberg  
Wanjie Feng  
Xavier Zapata-Ríos

## **Abstract**

The Tucson International Airport Area (TIAA) Superfund site is an approximately ten square mile area in southeast Tucson, Pima County, Arizona in which several known contaminated water plumes have been identified, which are the result of improper disposal of industrial waste from multiple sources during the past sixty years. The most prominent of these contaminants are 1, 4-dioxane, hexavalent Chromium, and trichloroethylene (TCE), which exist in varying concentrations throughout the site. Groundwater contamination in Tucson was first identified in the 1950's; however TIAA was not recognized as a Federal Superfund site until 1982. Since then, much work has been carried out in an attempt to fully understand and remediate the contamination in the area. This study focusses on four areas within the TIAA: Samsonite North, Aero Park Blvd South (EW line), Aero Park Blvd South (NS line), and EPA-03. Several geophysical techniques have been used to understand the subsurface structure in the area and to better understand the contamination plume and its movement. Using the Transient Electromagnetic (TEM) technique at three sites: Samsonite North, Aero Park Blvd South (NS line and EW line), and EPA-03, it was found that there was a low-resistivity region going through the EPA-03 site, two low-resistivity regions through Aero Park Blvd South (NS line), and three low-resistivity zones through Aero Park Blvd South (EW line). These channels were consistent with the overall orientation of water flow in the region which is toward the Northwest. These zones may indicate higher moisture content, and this may be caused by porous, water-filled channels passing through the sites. These zones could also indicate non-porous clay-rich regions, which would also be low resistivity. The effect of a pipeline on the measurements in the Samsonite North area made it difficult to reach any useful conclusions at this site.

## **Acknowledgements**

The University of Arizona Geophysics Field Camp class, GEN/GEOS 416/516, would like to thank the U.S. Geological Survey, Arizona Water Science Center for providing the funding for this project. Without this funding and support, we would not have been able to offer the class this year.

Fred Tillman, USGS Hydrologist, Tucson, organized the permits and coordinated the logistics for this project. He provided an introduction to the site and the project objectives in one of our first classes. His assistance in the field and his understanding of the regional geology were of great help to the students.

Jamie P. Macy, USGS Hydrologist, Arizona Water Science Center, Flagstaff Programs, assisted with all of the surveys in the field. His willingness to share his expertise in the collection, processing and interpretation of TEM data was an invaluable resource to the students in the class.

We are grateful to Don Pool for allowing us to use the seismometers, and training us on the use of the Geopsy software and the H/V analysis interpretations. We also thank Roy Johnson for providing us with the necessary P-wave information and for helping us with the interpretation of the detected boundary.

Thanks to James Callegary for his assistance with the EM 31 data.

Zonge Engineering provided data processing software programs to the class. Zonge Engineering has played a vital role in our Geophysics Field Camp for the past 26 years. We sincerely appreciate that they have continued to provide our students with the opportunity to use state-of-the-art electrical geophysics methods.

# Table of Contents

Abstract

Acknowledgement

## 1. Introduction

- 1.1 History of Site
- 1.2 Current Issues with the TIAA Superfund Site
- 1.3 Project Outline

## 2. Location Maps

- 2.1 Geographic location
- 2.2 Transient electromagnetic soundings (TEM) locations
- 2.3 Electromagnetic Induction (EM31) transect locations
- 2.4 Passive seismic locations
- 2.5 Cultural interference

## 3. EM31 Surveys

- 3.1 Introduction
- 3.2 Overview and Technique
- 3.3 Data Processing
- 3.4 TEM Interference
- 3.5 Interpretation
- 3.6 Summary

## 4. Transient Electromagnetic (TEM) Survey and STEMINV Inversion

- 4.1 Introduction
- 4.2 Location
- 4.3 Instrumentation and Field Procedures
- 4.4 Data Processing

## 4.5 Layered-Earth Modeling

## 5. EMIGMA Inversion of Transient Electromagnetics

### 5.1 Introduction

### 5.2 Procedures

### 5.3 Processing results

### 5.4 Interpretation

## 6. Passive Seismic Surveys

### 6.1. Introduction

### 6.2. Methods

#### 6.2a. Instrumentation and Field Procedures

#### 6.2b. Data Processing

#### 6.2c. Subsurface Interpretation of H/V Results

### 6.3. Data and Results

#### 6.3a. Seismometer T6B75 H/V and H/V Rotate Analysis

#### 6.3b. Seismometer T6B77 H/V and H/V Rotate Analysis

#### 6.3c. Seismometer A834 H/V and H/V Rotate Analysis

### 6.4. Data Interpretation

### 6.5. Discussion and Conclusions

## 7. TEM Summary and Conclusions

## 8. References

Appendix A. GPS coordinates of transient electromagnetic soundings (TEM), EM31 and passive seismic surveys

Appendix B. Zonge, smooth-model TEM (STEMINV) inversions for all loops.

Appendix C. EMIGMA inversions for all loops.

# **1. Introduction**

## **1.1 History of Site**

The Tucson International Airport Area (TIAA) Superfund site covers approximately ten square miles in the northern part of the Tucson Basin in Pima County, Arizona (Figure 1.1) including the Tucson International Airport, northeastern portions of the Tohono O'Odham Indian Reservation, residential areas of the Cities of Tucson and South Tucson, and the Air Force Plant #44 Raytheon Missile Systems Company (AFP44). Groundwater from wells within this region provided drinking water to over 47,000 people prior to 1981 (EPA). Since 1942 more than twenty facilities have operated at the TIAA, such as aircraft and electronics facilities, fire drill training areas, and unlined landfills. Many of these operations led to the large-scale disposal of waste (such as metals, chlorinated solvents, and other contaminants) directly into the soil or unlined pits. While smaller sources of soil and groundwater contamination were found at the Burr-Brown Corporation, Arizona Air National Guard Base and the former West-Cap of Arizona facilities, the most important sources of contamination, were identified at the airport area and AFP44; the latter being the largest contributor (EPA).

Due to early concerns in the 1950s, when unusually high chromium levels were detected in City of Tucson municipal wells just west of AFP44 and complaints of a foul chemical odor from private wells west of the airport, improper waste disposal at TIAA facilities was halted by the early 1970s (EPA). The results of a 1981 investigation involving groundwater sampling from city municipal water wells within the TIAA, conducted by EPA and the City of Tucson, found unsafe levels of trichloroethylene (TCE) in several wells (EPA). TIAA was officially identified as a superfund site in 1982, and soon thereafter a large plume of groundwater contamination one-half mile wide and five miles in length was identified (EPA). In 1987, AFP44 began a groundwater treatment system, and in 1994 the Tucson Airport Remediation Project began to treat Volatile Organic Compounds from groundwater. The discovery of 1,4-dioxane in TARP wells, AFP44, and several other localized areas in 2001 led the Air Force to install an advanced oxidation treatment facility to remove groundwater 1,4-dioxane (EPA).

## 1.2 Current Issues with the TIAA Superfund Site

Several contaminants have been detected in the TIAA Superfund Site: 1,4-dioxane, hexavalent Chromium, and trichloroethylene (TCE). The contaminant 1,4-dioxane was first discovered in 2001, and is present in the groundwater through the TIAA (EPA). It has been determined to be carcinogenic, and although no federal standard has been determined, the EPA proposed its minimum cancer “risk level” to be 0.35 ppb. It is currently being treated with Advanced Oxidation (AO), which uses hydrogen peroxide and oxygen, because it cannot be removed by releasing it into the atmosphere since it is easily dissolved with water (EPA). Hexavalent Chromium, also present, exceeds the established minimum standard of 0.02 ppb. In 2011, the EPA health advisory for 1,4-Dioxane changed from 3.0 ppb to 0.35 ppb (EPA). In order to accommodate this, Tucson Water began planning and designing a new treatment facility to remove this contaminant from the water. It will work in conjunction with the TARP facility and aims to produce up to 8 million gallons of purified water each day (EPA).

The contamination plume is moving in a northwestern direction at a rate of 100 ft/year. However, due to recent water management changes, the water influx has increased, accelerating the movement of the plume. Another complication is that the contamination plume would have originally stayed in the unsaturated zone, but, due to the fact that there are over 400 wells in the area, this has led to the contamination plume moving deeper, further exacerbating the problem (EPA) (Figure 1.2).

## 1.3 Project Outline

Several studies have been conducted around TIAA to understand the subsurface structure, determine aquifer properties, groundwater flow, and plumes of contamination. The present study is focusing on four areas in the western part of the Tucson International Airport: Samsonite North, Aero Park Blvd south-north and east-west transects, and EPA-03. The objective of this study is to contribute to the understanding of subsurface structure around the Tucson International Airport.

We have applied several geophysical techniques to understand the subsurface features and their influence on the movement of the contamination plume. A transient electromagnetic survey was

conducted over 3 areas: Samsonite North, Aero Park Blvd and EPA-03. Passive seismic records were also collected at the Aero Park Blvd and EPA-03. Metal detectors and EM31 measurements were used to try to identify any underground sources of interference, such as pipes or power lines that could interfere with the TEM. The following chapters discuss our findings.

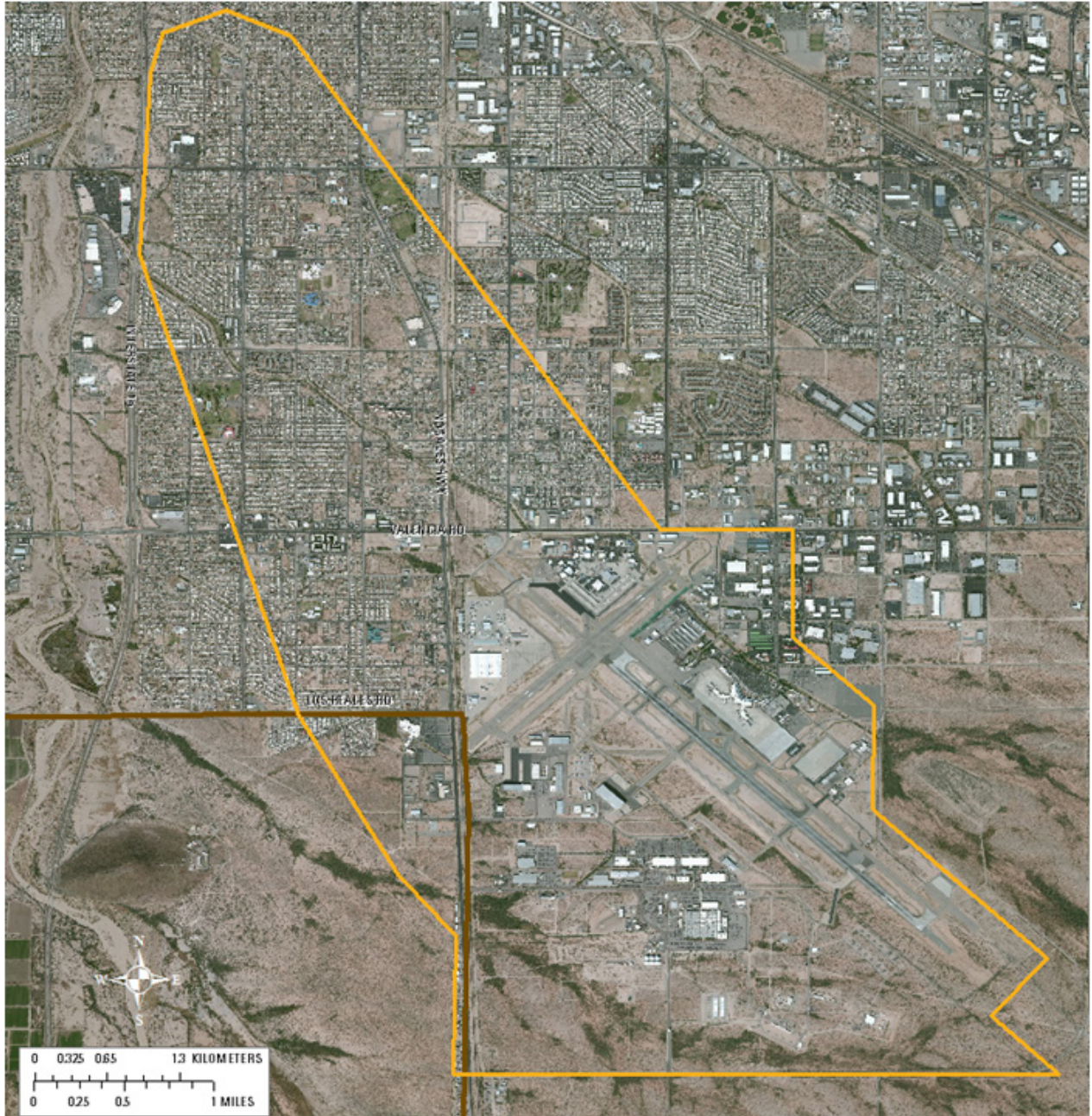


**Figure 1.1:** Aerial map showing the Superfund site (contained in the polygon). Courtesy of Fred Tillman, USGS (2013).

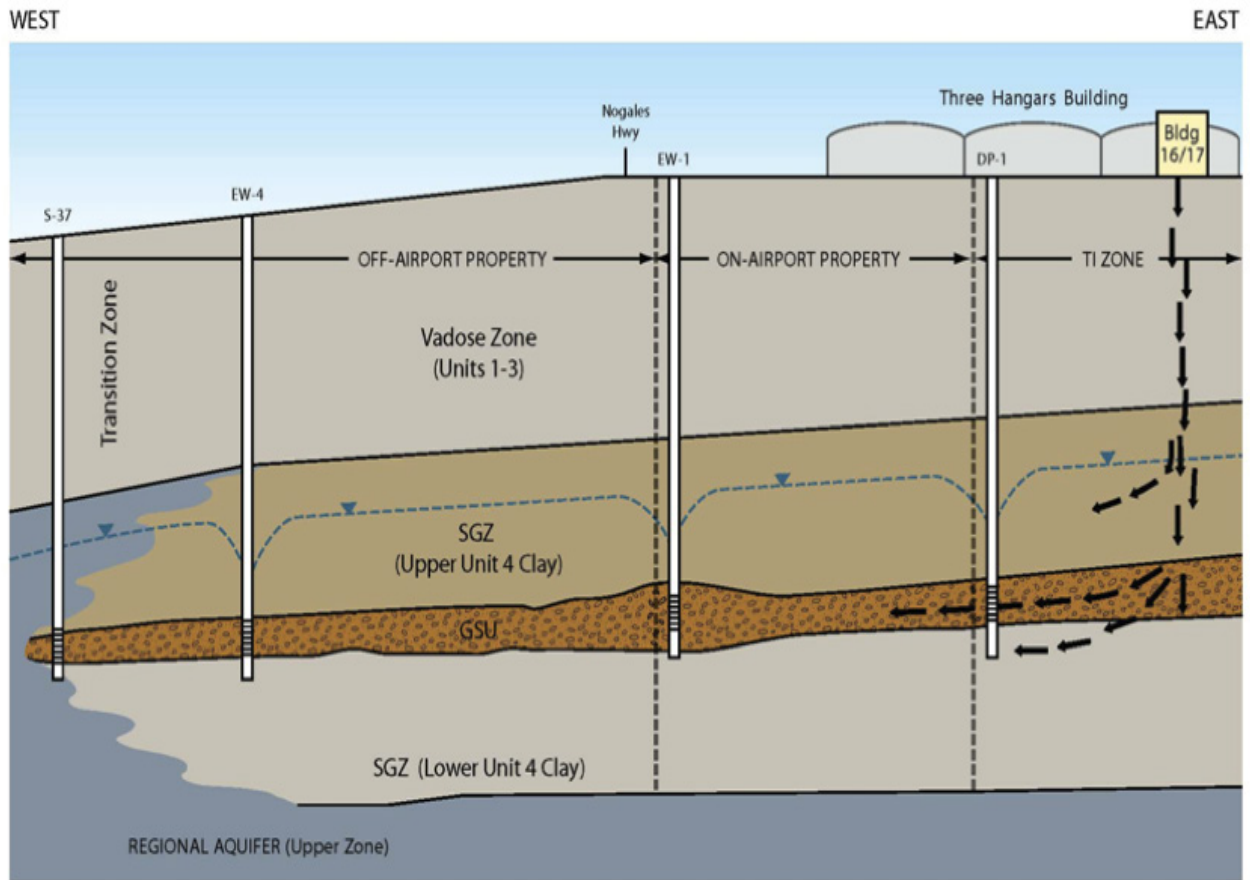


**Figure 1.2:** Cross-sectional schematic showing the hydrogeological sections and general flow of contamination plume (depicted by arrows) (Conestoga-Rovers and Associates, 2012).

## 2. Locations

### 2.1 Geographic location

The study area is located in the southern part of the city of Tucson, enclosed between the UTM coordinates 503,000 to 505,000 East and 3,554,300 to 3,554,900 North. Four different properties were studied: 1. Samsonite North, 2. Aero Park Blvd South south-north line, 3. Aero Park Blvd South east-west line and 4. EPA-03. The four properties are located in the west and south western part of the Tucson International Airport (Figure 2.1).

### 2.2 Transient electromagnetic soundings (TEM) locations

Transient electromagnetic soundings (TEM) in the study area were recorded with 20m x 20 m, 50m x 50m and 100 m x 100 m loops.

#### 2.2.1 TEM 20 x 20 m loops

The coordinates of the 20m x 20 m loops' centers can be found in Tables A.1 and A.2. At the property Samsonite North (1) we used 8 loops. Along the Aero Park Blvd south-north line we used 9 loops and at the east-west line 23 loops. The EPA-03 site was surveyed with 5 loops (Figure 2.2 - Figure 2.5).

#### 2.2.2 TEM 50 x 50 m loops

Five 50 x 50 m loops were used at approximately the center of the Aero Park Blvd east-west line instead of 100 x 100 m loops because of limitation of space to complete 100 m loops (Figure 2.6). The coordinates of the 50m x 50 m loops' centers can be found in Table A.3.

#### 2.2.2 TEM 100 x 100 m loops

100 m loops were used in three out of the four surveyed properties. Three 100 x 100 m loops were used along the Aero Park Blvd south-north line. Six loops along the east-west line and one loop at the EPA-03 property. The coordinates of the 100m x 100 m loop centers and corners can be found in Tables A.4 and A.5. (Figures 2.7 - 2.9)

### 2.3 Electromagnetic Induction (EM31) transect locations

Electromagnetic induction (EM31) transects were surveyed at the Aero Park Blvd south-north line and east-west line. Two additional transects were surveyed at the EPA-03 property (Figures 2.10-2.12). EM31 readings were recorded every meter along transects. Some reference point locations are given in Table A.6.

### 2.4 Passive seismic locations

Passive seismic stations were located along the Aero Park Blvd south-north line, east-west line and EPA-03. Data from 16 Seismic stations were collected (Figure 2.13-Figure 2.16) (Table A.7)

### 2.5 Cultural interference

At the Samsonite north site, approximately 10 m towards the west from the TEM 20 x 20 m loops, we located an anomaly detected by a Fisher TW-6 metal and pipe detector. This anomaly had a south-north orientation and it was not found in the general water supply and sewage system maps (Figure 2.2). At the Aero Park Blvd south-north line there are water pipes running along a south-north direction at a distance larger than 30 m from the 100m loops border. At the Aero Park Blvd east-west line water pipes run beneath the loops 24100 and 25100 and approximately 10 m south from loops 26000, 27000, 28000 and 29000 (Figure 2.4). At the property (4) EPA-03 no cultural interference was mapped within the area surveyed.

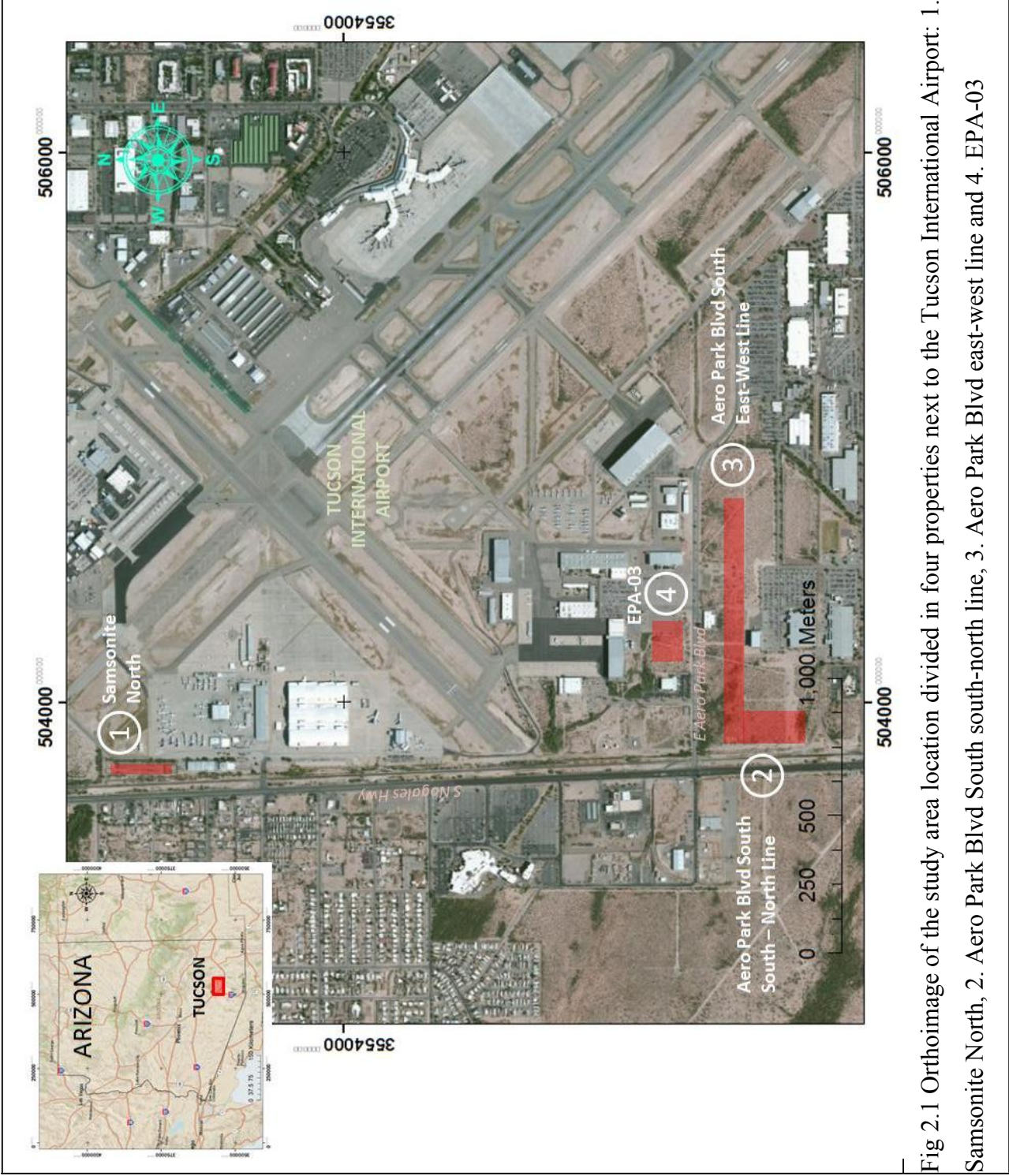


Fig 2.1 Orthoimage of the study area location divided in four properties next to the Tucson International Airport: 1. Samsonte North, 2. Aero Park Blvd South south-north line, 3. Aero Park Blvd South east-west line and 4. EPA-03

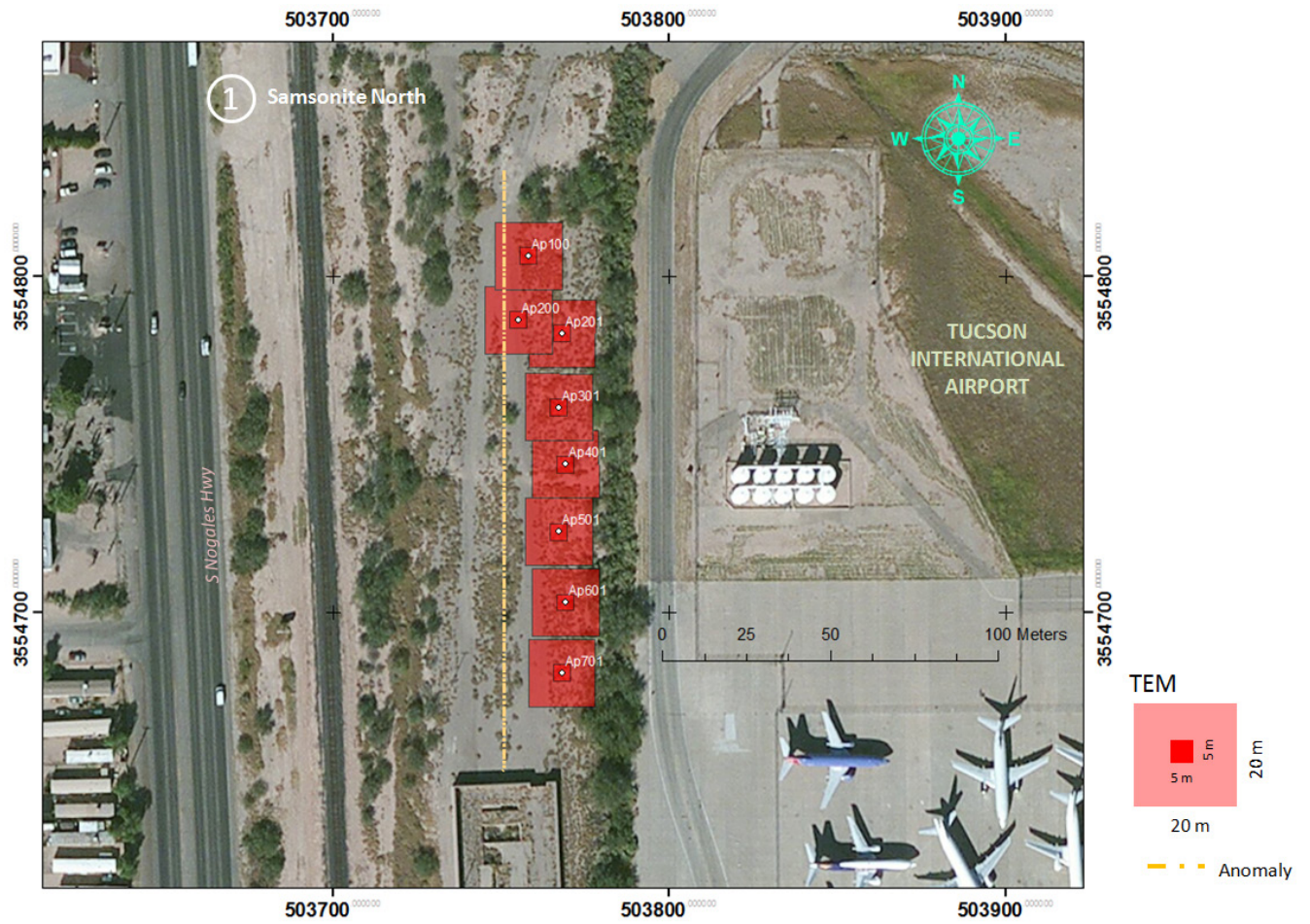


Fig 2.2 Eight 20 m x 20 m TEM loops at the Samsonite North site and anomaly detected in the field with a Fisher TW-6 metal and pipe detector (yellow line).



Fig 2.3 Nine 20 m x 20 m TEM loops at the Aero Park Blvd South: South-North line.

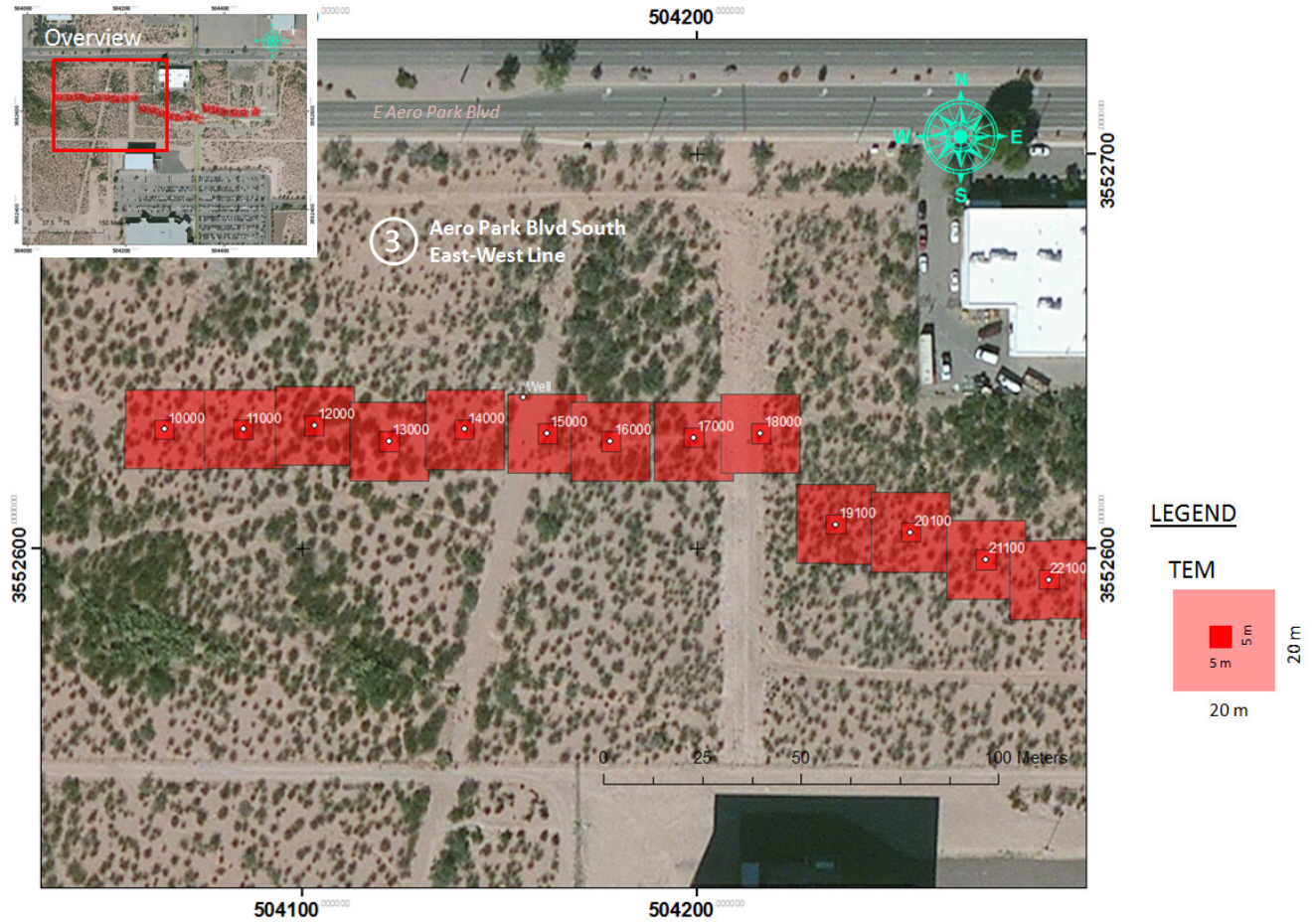


Fig 2.4a Twenty three 20 m x 20 m TEM loops at the Aero Park Blvd South: East-West line.

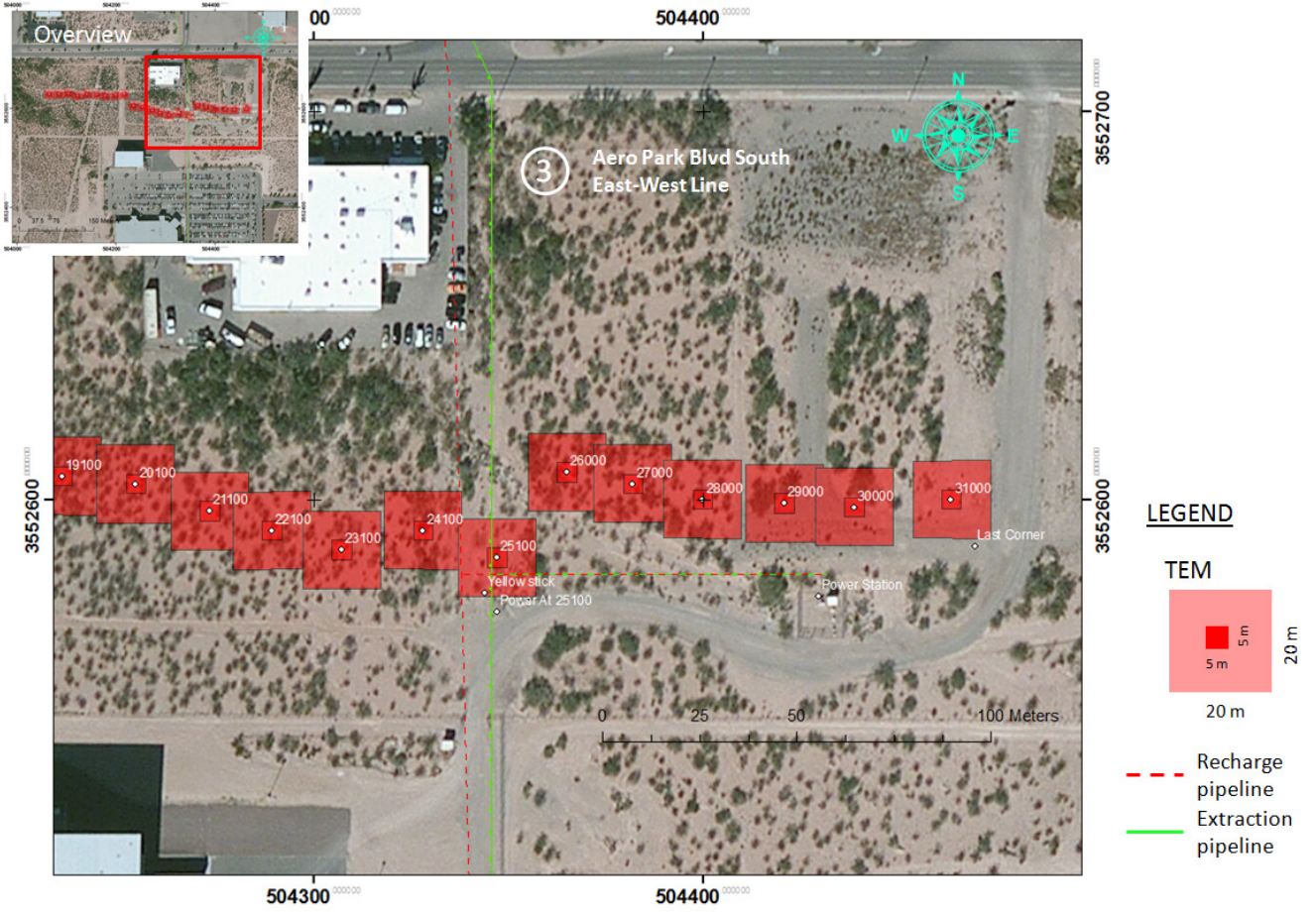


Fig 2.4b Twenty three 20 m x 20 m TEM loops at the Aero Park Blvd South: East-West line.

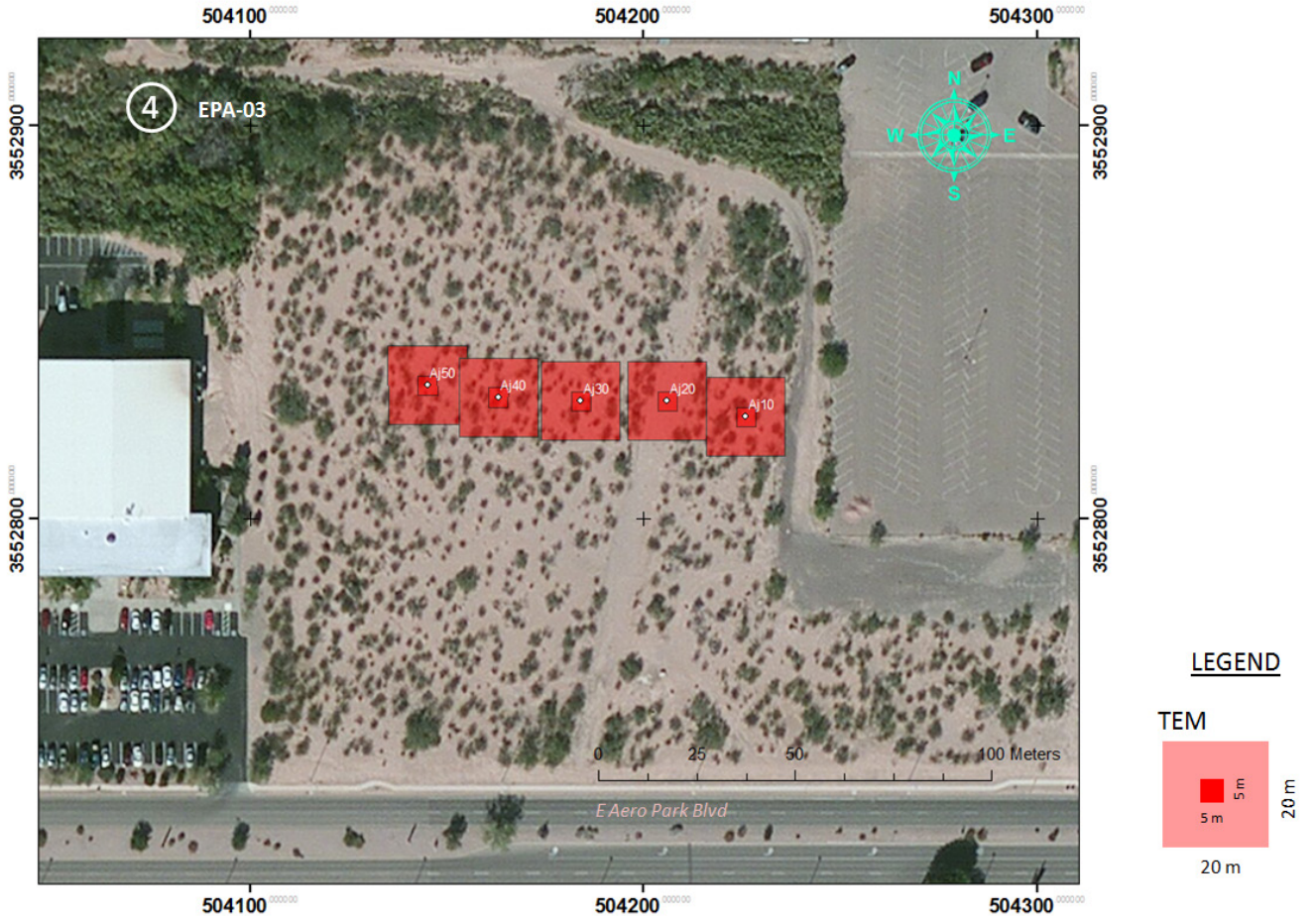


Fig 2.5 Five 20 m x 20 m TEM loops at the EPA-03 site.



Fig 2.6 Five 50 m x 50 m TEM loops at approximately the center of the Aero Park Blvd east-west line.

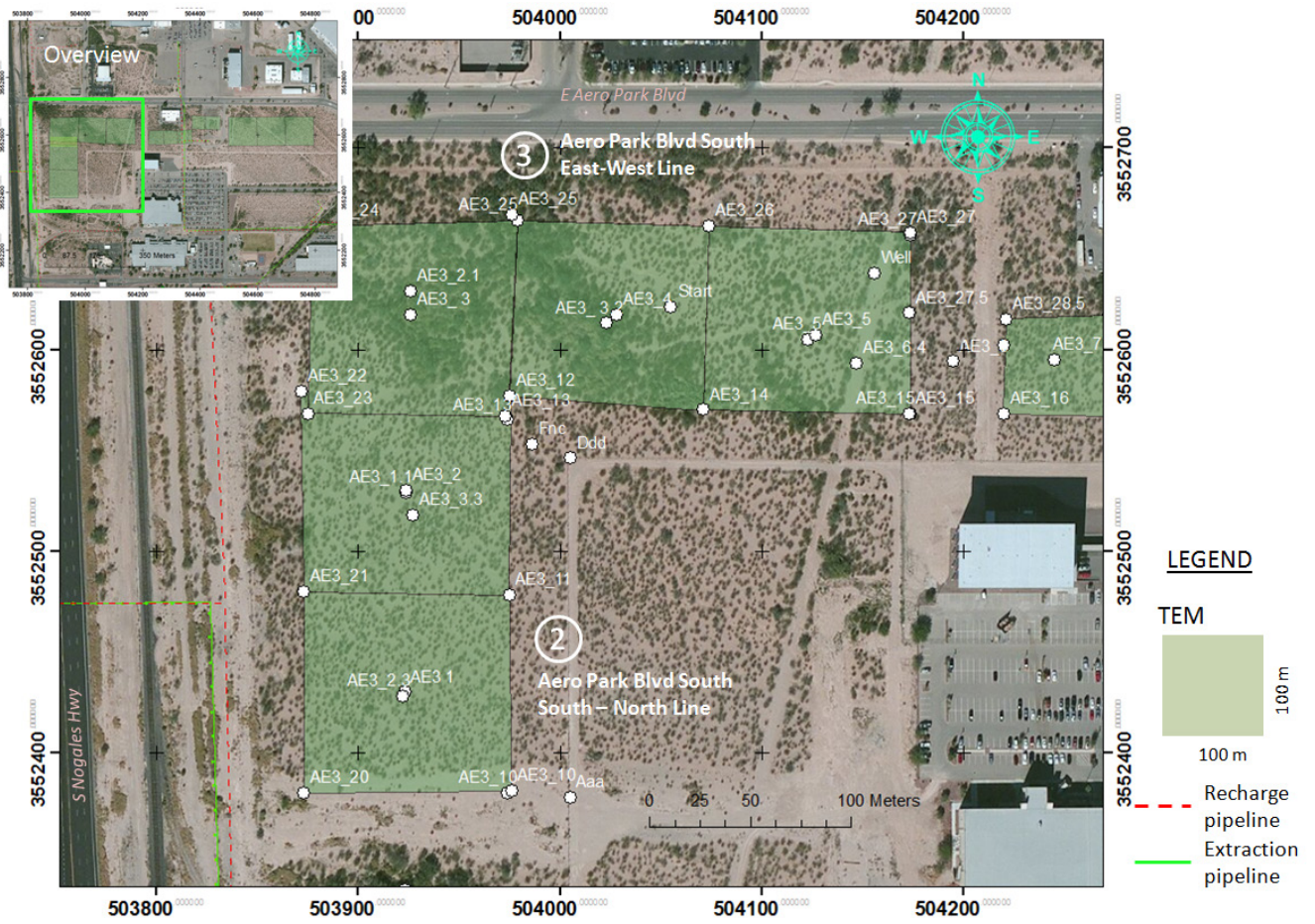


Figure 2.7 100 m x 100 m TEM loops at the Aero Park Blvd south-north line and Aero Park Blvd east-west line.



Figure 2.8 100 m x 100 m TEM loops at the Aero Park Blvd east-west line.



Figure 2.9 100 m x 100 m TEM loop at the EPA-03.

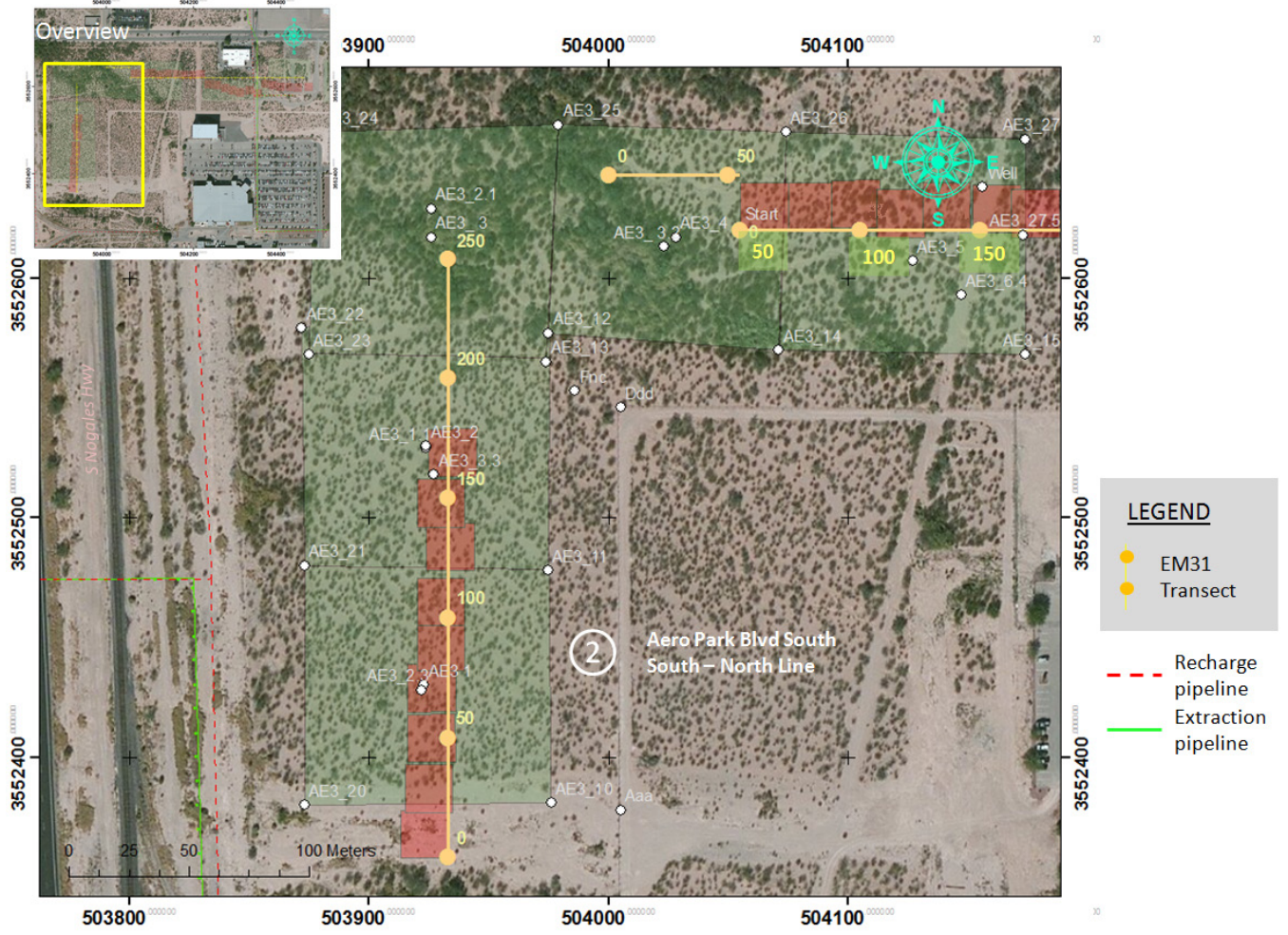


Figure 2.10 EM31 transect along the Aero Park Blvd south-north line and western part of the Aero Park Blvd east-west line.

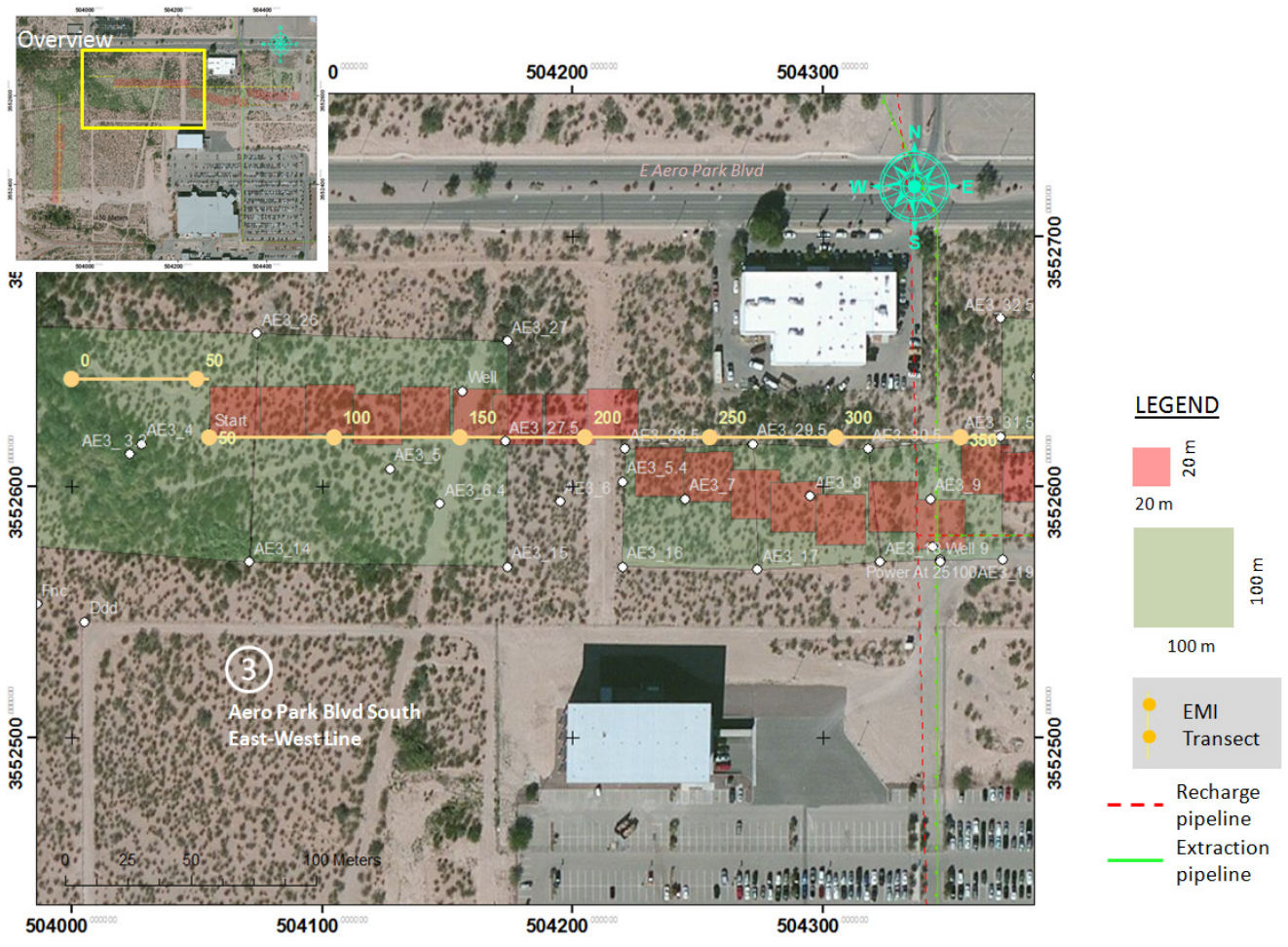


Figure 2.11a EM31 transect along Aero Park Blvd east-west line.

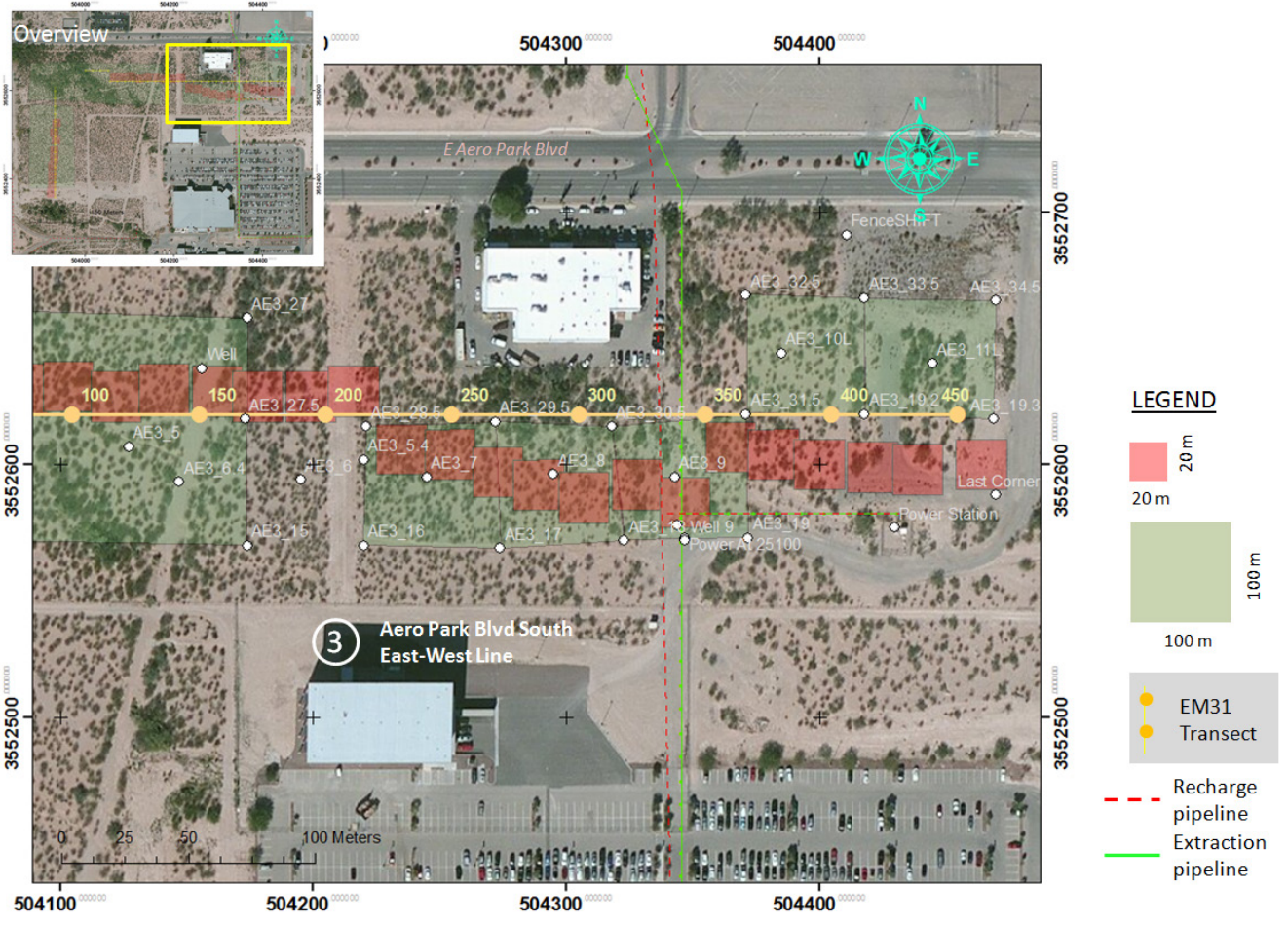


Figure 2.11b EM31 transect along Aero Park Blvd east-west line.

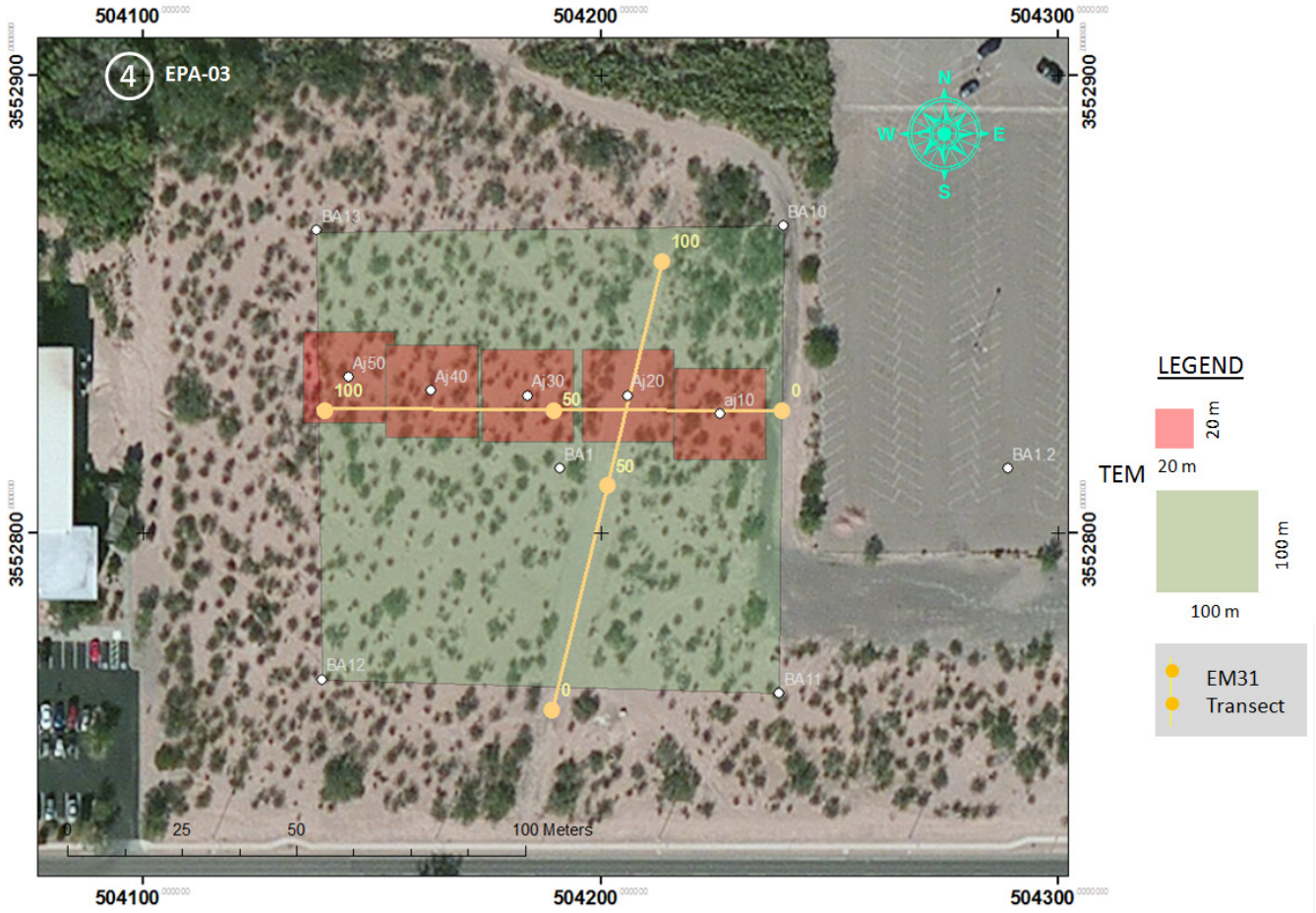


Figure 2.12 EM31 transects in the EPA-03 property.

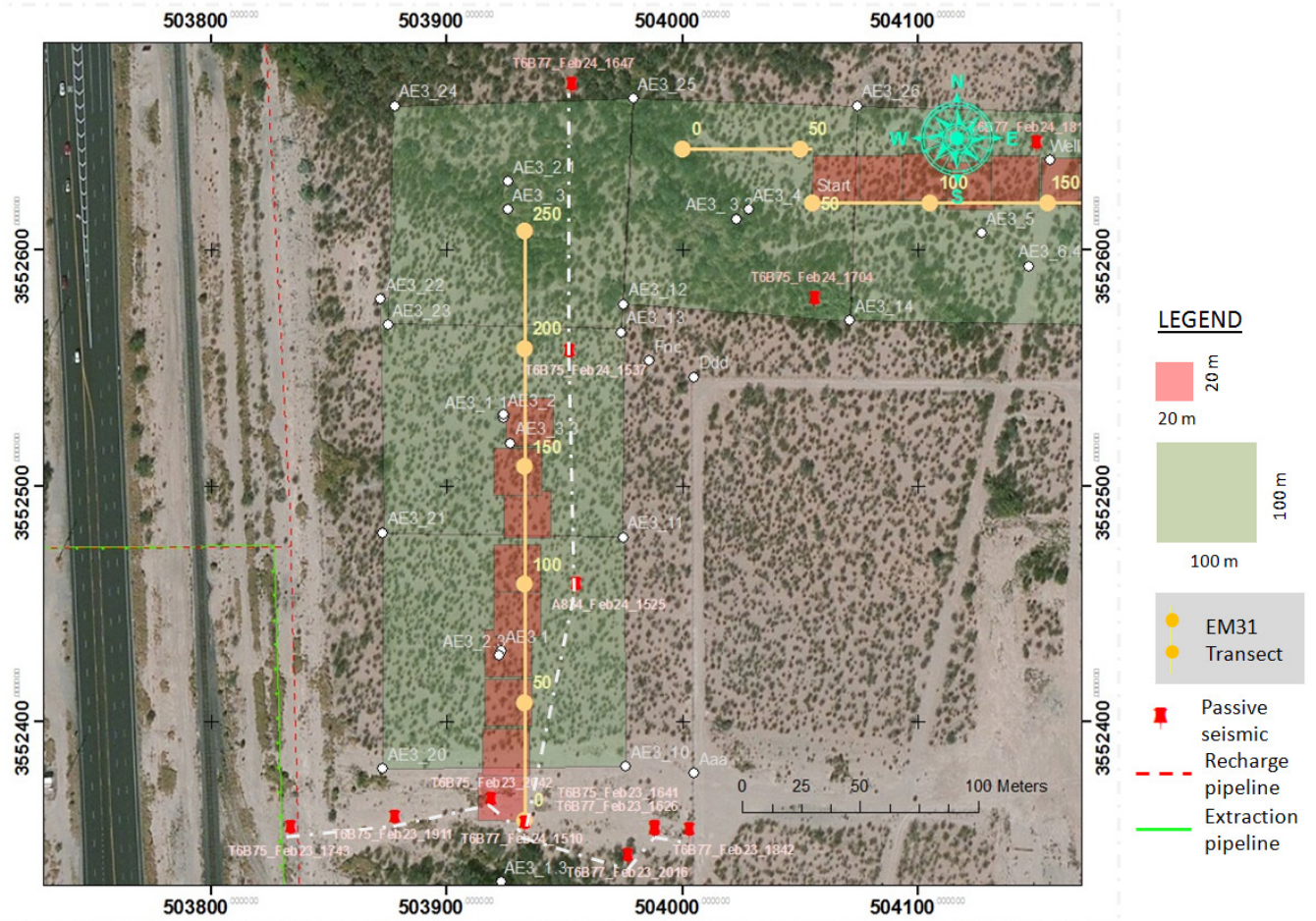


Figure 2.13 Passive seismic survey points in the Aero Park Blvd south-north line.

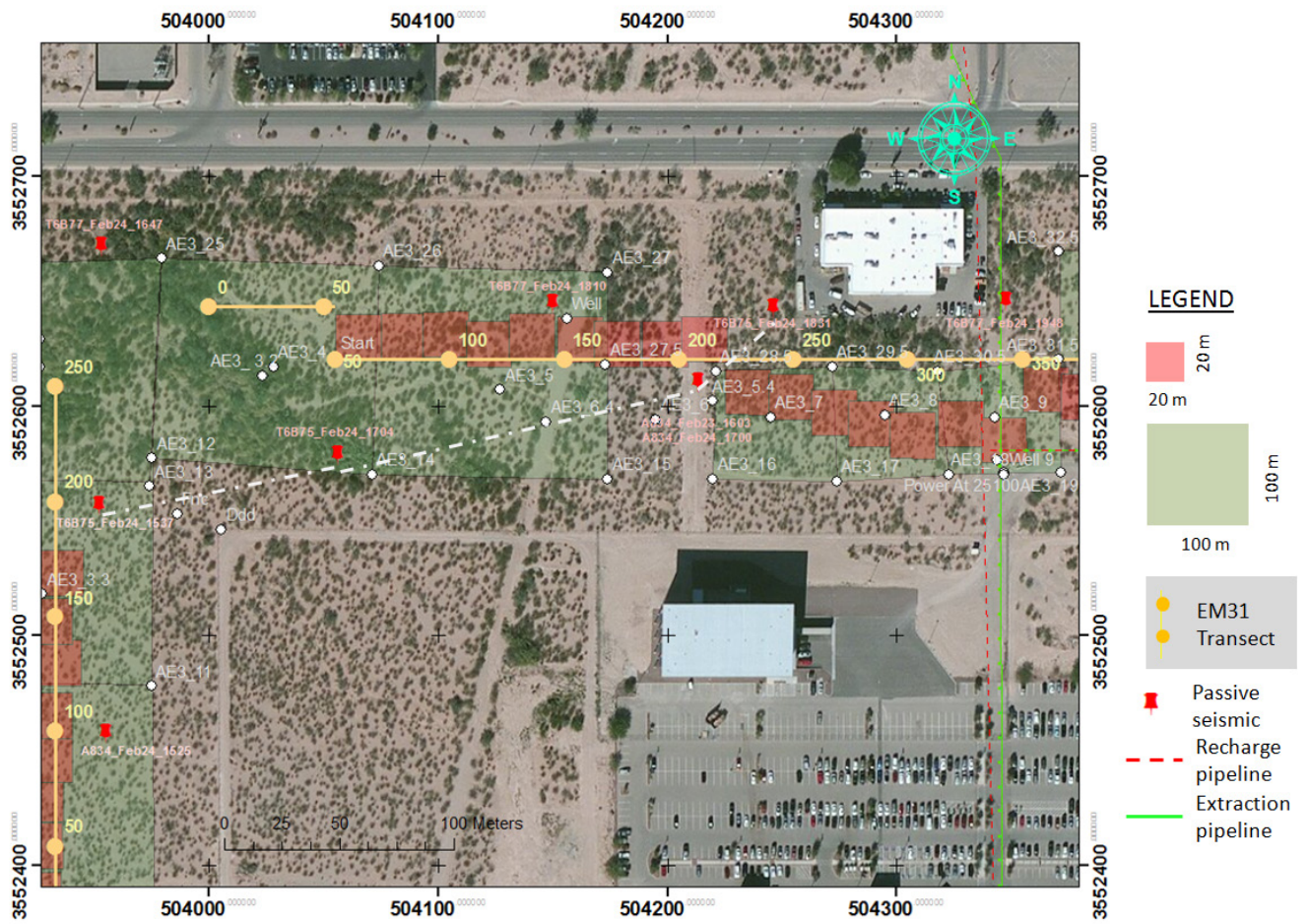


Figure 2.14 Passive seismic survey points in the Aero Park Blvd east-west line.

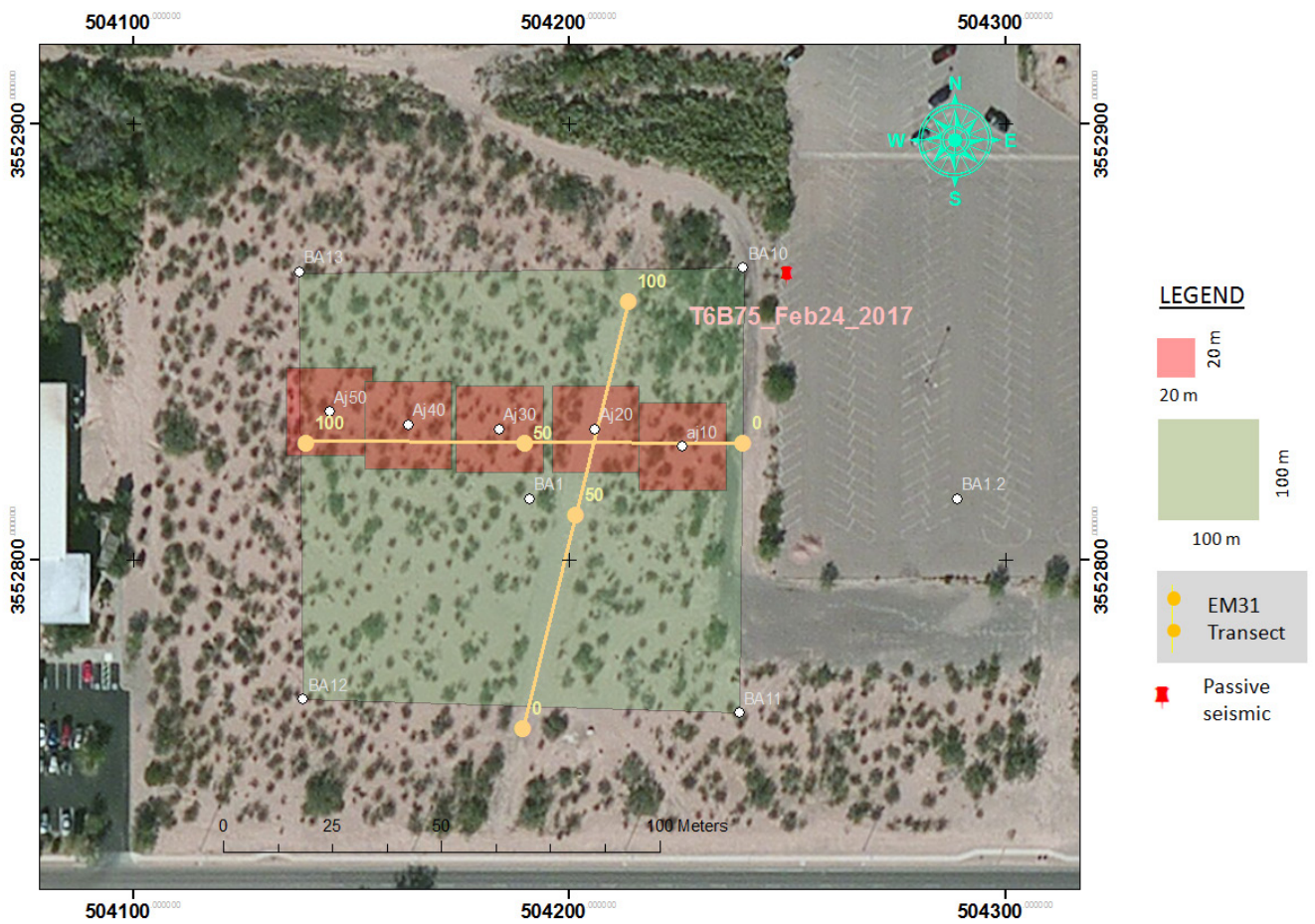


Figure 2.15 Passive seismic survey points in the EPA-03 property.

## **3. EM31 Surveys**

### **3.1 Introduction**

The purpose of the EM31 data was to locate and interpret any possible sources of interference that may affect the TEM data, including underground pipes and power lines. Data were collected at all 3 sites: Samsonite North, Aero Park Blvd and EPA-03. The Aero Park Blvd Site was separated into 2 lines. The first line (Aero Park Blvd N-S line) ran from south to north for 250 meters, where the vegetation became too dense to continue (Figure 2.10). The second line (Aero Park Blvd W-E line) ran from west to east for 450m. This line had a 20-meter N-S offset at the 50-meter mark, because of the dense vegetation (Figure 2.10). Two lines were collected at the EPA-03 site, one south to north and the other west to east (Figure 2.12). Notes were taken on any possible visible sources of interference that may affect the acquisition of the data and the data itself. Each of the 3 localities contained varying amounts of vegetation, ranging from moderate to dense, which made acquisition of data difficult in certain areas.

### **3.2 Overview and Technique**

For each line surveyed, measurements were taken with the EM31 parallel to the line as well as perpendicular, all with the instrument held at the horizontal coplanar orientation. Both conductivity and in-phase measurements were taken, plotted and analyzed for all lines. Most of the segments on which data were gathered at Aero Park Boulevard were 100 meters long, with measurements taken at one-meter intervals, totaling 250 meters from south to north and 450 meters from west to east. The segments measured at the EPA-03 site were 100 meters long, with measurements taken at two-meter intervals, totaling 100 meters from south to north and 100 meters from west to east. Due to the heavily vegetated nature of the terrain, perpendicular measurements were much more difficult to make consistently than their parallel counterparts, resulting in consistently more scattered perpendicular data than parallel data. The brush also caused difficulties in laying out the measuring tape, which was used to define and track our intervals of measurement. Areas that produced questionable data were repeated for verification purposes, and relevant environmental observations were noted.

Such environmental observations included a utility access hole near the beginning (around 20-30 meters) of the North-South Aero Park line, which was located about 40 meters away and corresponds to a positive anomaly in that conductivity data set. Another utility access hole was observed on the West-East Aero Park line at 360 meters, which read “POWER LINES.” This observation corresponds to a very large anomaly in the conductivity data.

### **3.3 Data Processing**

Once the data were collected, it was imported into Excel and plotted in separate scatter plots displaying the conductivity (mS/m) and in phase components (ppt). The original and repeated data were plotted on the same graphs for easy comparison. This made anomalous data between the two weekends obvious and allowed correlation on any suspected pipelines or any other sources of interference.

### **3.4 TEM Interference**

Inconsistent, anomalous data were not attributed to proximity of the transient electromagnetics (TEM) equipment until near the completion of the first data set at Aero Park Blvd. Experimental observations involving EM31 data collection at various distances from the TEM equipment (both transmitting and not transmitting) led to the following conclusions: (1) The proximity of the TEM significantly affects the EM31 conductivity and in-phase data; (2) this effect was notably worse during TEM transmission; and (3) The effect decreases rapidly with distance from the edge of the TEM loop. The next day it was observed as well that there is a positive relationship between TEM loop size and distance from the edge of the loop necessary for unaffected data collection. Figures 3.1 and 3.2 show the aforementioned experimental data collected, which show the drop-off of conductivity values associated with movement away from the TEM equipment. On the edge of a loop (Figure 3.2) the conductivity increased 17mS/m at one point. While the TEM was transmitting, the values for conductivity and in phase fluctuated wildly on the data logger, explaining how such irregular anomalies were created in our data. The wire itself had a minor effect on the conductivity value (between 2-4 mS/m), but not as significant as when the TEM was transmitting.

This effect rendered data collected from the Samsonite site unreliable, as EM31 data were collected alongside active TEM data collection (due to the small size of the site), producing scattered, uninterpretable plots. Scattered data points corresponding to hypothesized TEM interference from the first Aero Park data set are prominent, but separable from the reliable data, since the area was larger and therefore had less overall TEM interference. Due to uncertainties about the first Aero Park data set, all of the lines at Aero Park were repeated with clear communication via walkie-talkies with the TEM crew regarding proximity and periods of transmission to avoid any further TEM interference in the EM31 data. It was also observed that walkie-talkie outgoing transmission affected the data, though not as severely, and it was easily avoided. A comparison of the two Aero Park data sets demonstrates that there was very little TEM interference in the second set compared to the first (Figures 3.3-3.6).

### **3.5 Interpretation**

One major anomaly was identified on the Aero Park Blvd N-S line between 0-30 meters (Figures 3.3 and 3.4). This anomaly was suspected to be due to TEM interference on the first weekend, but a repeat of this area produced the same results with the TEM 100 meters away. Around 40 meters to the east (level with 25 meters on our line) there was an unlabeled utility access hole cover, that was not present on any pipeline maps. This implies a pipeline runs west to east and bisects our N-S line. After this anomaly the conductivity values slowly decline between 30-75 meters from 15-10 mS/m. The in-phase component shows a very small increase where the suspected pipeline lies, however this is not present in the repeated data, so could be a result of TEM interference.

On the second line; Aero Park Blvd W-E line, one major anomaly was located at approximately 360 meters along the line. This anomaly correlated well with a known set of pipes that is documented in the maps (Figure 3.12) and shown on the graphs (Figures 3.5-3.6). However, a utility access hole cover was found approximately 20 meters south of our line, which read "POWER LINES", though nothing related to power lines is shown in any of the maps near that location. It is possible that the power lines are not shown on the maps we have. The anomaly can be identified as a trough and peak in both the conductivity and in phase plots (Figures 3.5-3.6), followed thereafter by an increase in conductivity towards the end of the data sets from 20-

25 mS/m. The location of the extraction pipe labeled in the maps corresponds with the inflection point seen in the anomaly, making it the probable cause of the anomaly. An abrupt increase in the in phase component is visible at 50 meters along this line. At this point there is a 20-meter offset in the data due to the dense vegetation. The data were also collected on different days, indicating that the offset in the data was likely due to the calibration of the equipment.

For both of the Aero Park Blvd lines the dense vegetation made data acquisition difficult, particularly when perpendicular measurements were being taken. This resulted in the perpendicular plots looking scattered when compared to the parallel data (Figures 3.4 and 3.6), however the anomalies are still easy to identify over this background noise.

At the EPA-03 site the data collected were smooth compared to the Aero Park Blvd data. No obvious anomalies were present, although a general northeast increase in conductivity can be observed (Figures 3.7-3.10). There were less terrain issues at this site, however a few outliers are present, likely due to isolated areas of vegetation.

### **3.6 Summary**

The purpose of collecting EM31 data was to find potential sources of interference for the TEM. In summary, two main areas of potential interference were discovered, between 0-30 meters in Aero Park Blvd N-S line and around 360 meters in Aero Park Blvd W-E line. The anomaly in the W-E line correlates with a known set of pipes that is shown on the maps (Figure 3.12). The anomaly in the W-E line does not correlate to any plotted pipes or power lines, however a utility access hole cover to the south indicates that a pipeline may be present. Identification of TEM interference of EM31 data collection was key to explaining random outliers in the data. Other outliers are explained by errors from changes in terrain (gradual or choppy, such as with heavy vegetation) and possible changes in instrument calibration. In general, the data not affected by manholes or the TEM are smooth, indicating that there are no significant unexplained sources of interference for the TEM data. The perpendicular lines are somewhat more irregular than parallel lines as they proved troublesome to collect.

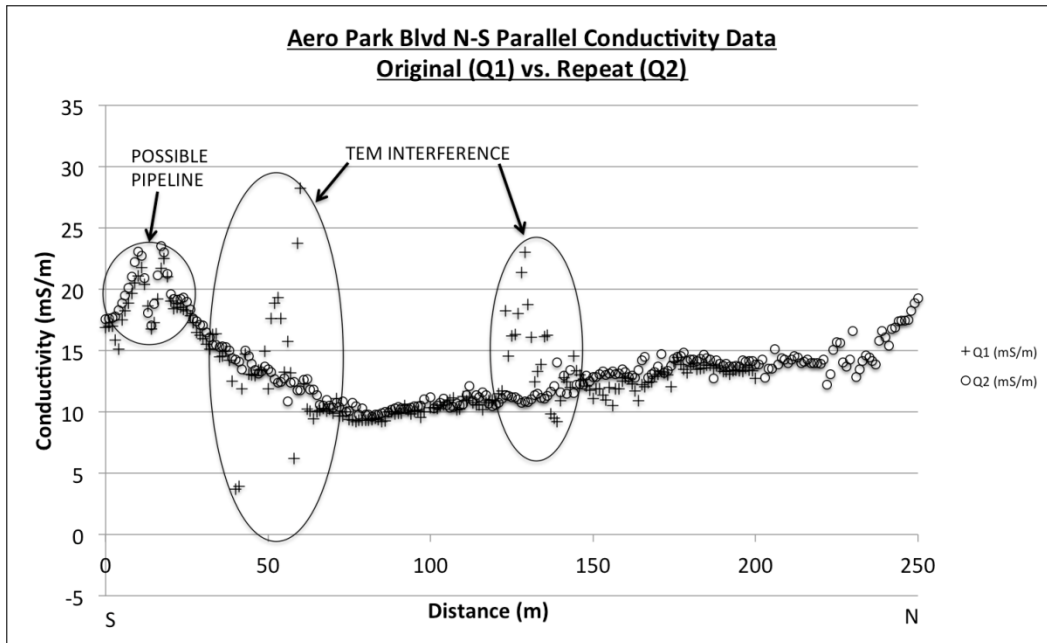
<b><u>Parallel</u></b>	<b><u>Conductivity, Q (mS/m)</u></b>	<b><u>In Phase, IP (ppt)</u></b>
TEM transmitting	25.6	-3.3
TEM transmitting	26.9	-5.2
TEM not transmitting	20.3	1.64
TEM not transmitting	20.3	1.02
TEM 40m east	18.3	-0.22
TEM 40m east	18.2	-0.24
<b><u>Perpendicular</u></b>		
TEM transmitting	25.3	-18.7
TEM transmitting	24.8	-17.9
TEM not transmitting	16.2	0.12
TEM not transmitting	15.8	0.23
TEM 40m east	19.2	1.25
TEM 40m east	19.2	1.15

Figure 3.1: Table of values recorded to test effect of TEM interference. A large increase in conductivity and a decrease of the In-Phase component is observed. This data were recorded 3m to the west of the TEM equipment, over the wire.

<b><u>Parallel</u></b>	<b><u>Conductivity, Q (mS/m)</u></b>	<b><u>In Phase, IP (ppt)</u></b>
TEM transmitting	30.4	18.45
TEM transmitting	28.4	18.62
TEM transmitting	29.9	18.72
TEM not transmitting	19.5	0.11
TEM not transmitting	18.9	0.07
<b><u>Perpendicular</u></b>		
TEM transmitting	37.46	-1.19
TEM transmitting	36.6	-1.11
TEM transmitting	36.4	-1.25
TEM not transmitting	20.46	-1.32
TEM not transmitting	20.32	-1.39

Figure 3.2: Table of values recorded to test effect of TEM interference. A large increase in conductivity is noticeable when the TEM is transmitting compared to when it is not. These values were recorded over the corner of a TEM loop.

3.3a



3.3b

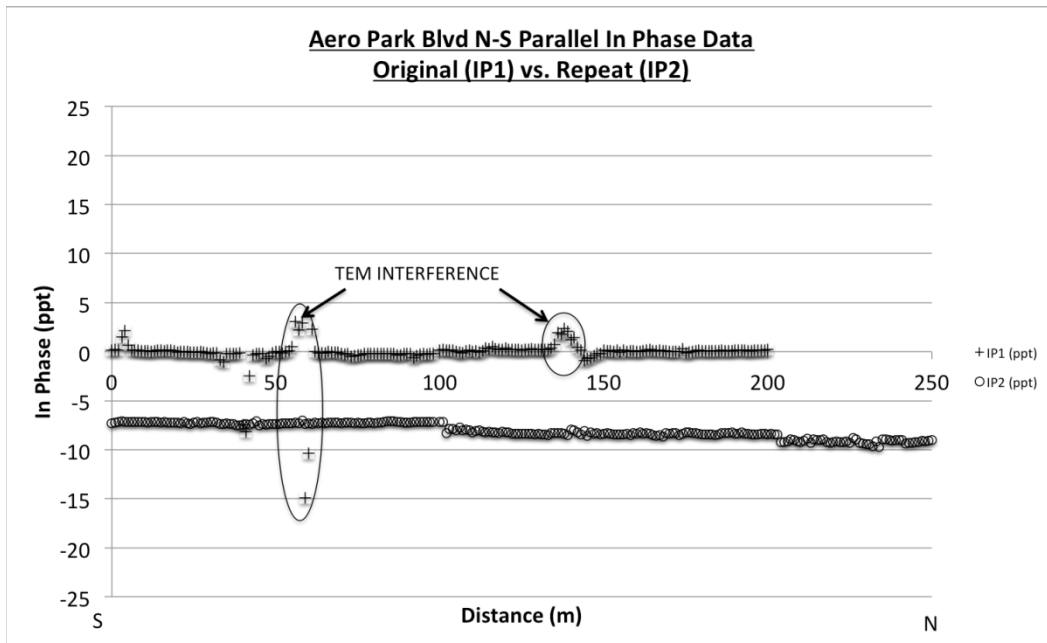
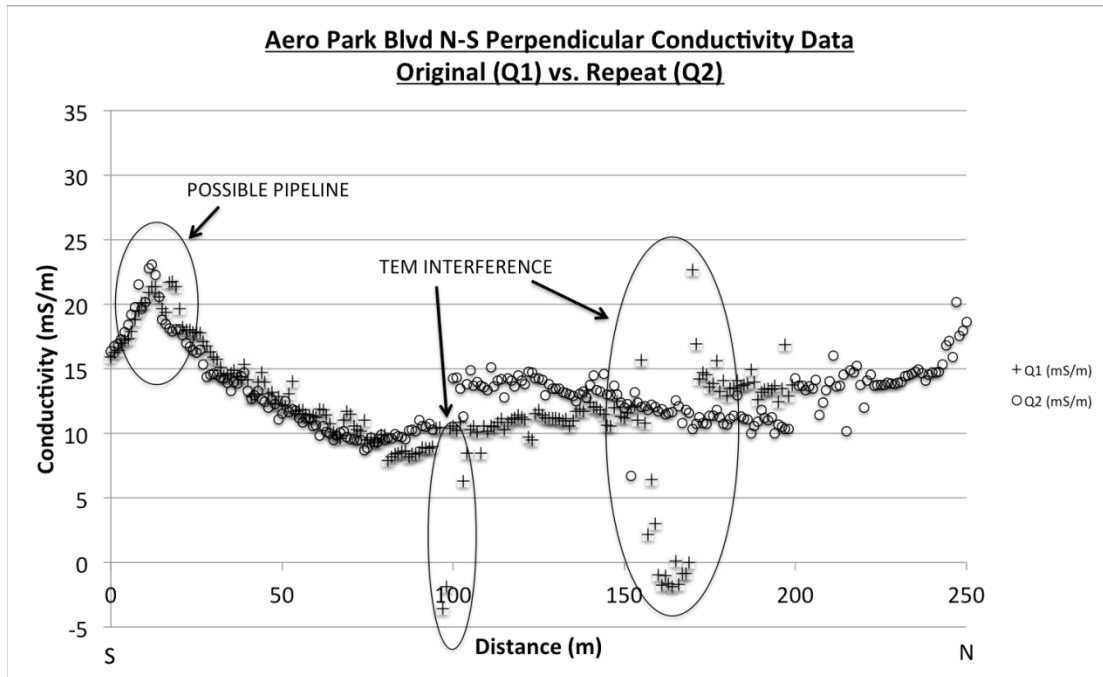


Figure 3.3a: Parallel conductivity data for the Aero Park Blvd N-S line. Two areas of major TEM interference are present in the original data that are not present in the repeated data. Possible pipe is expressed by anomaly between 0-30 meters. This anomaly was consistent between the original and repeat data, so is unlikely a result of TEM interference. 3.3b: In-phase data for the N-S line. Though less apparent, anomalies are present in the same locations as the conductivity data.

3.4a



3.4b

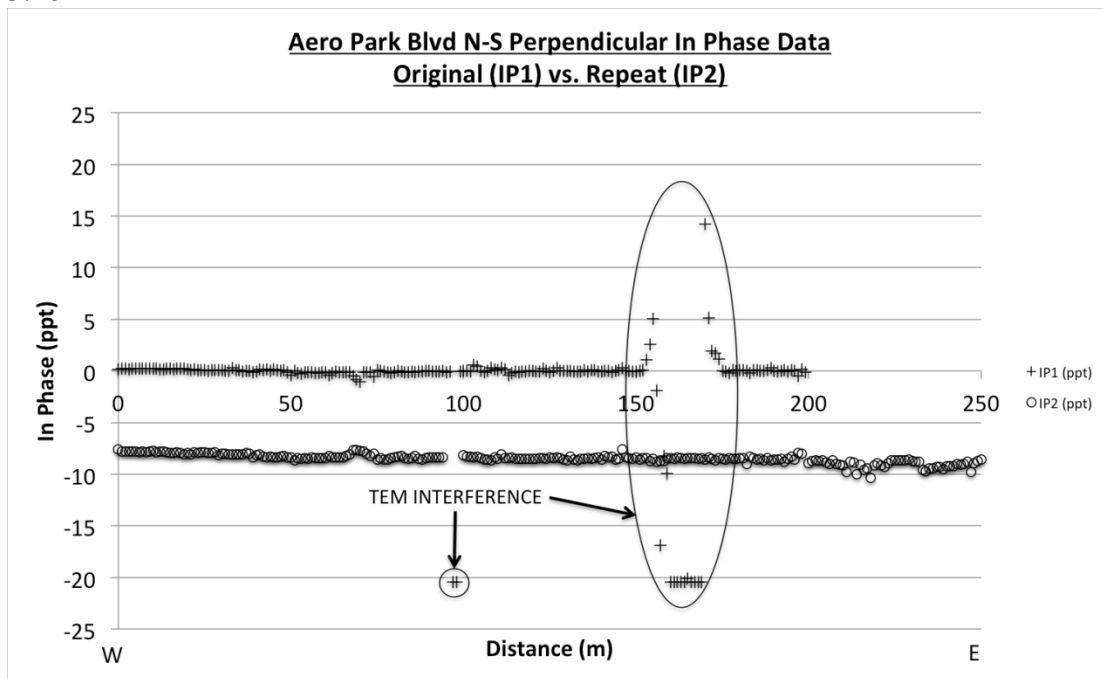
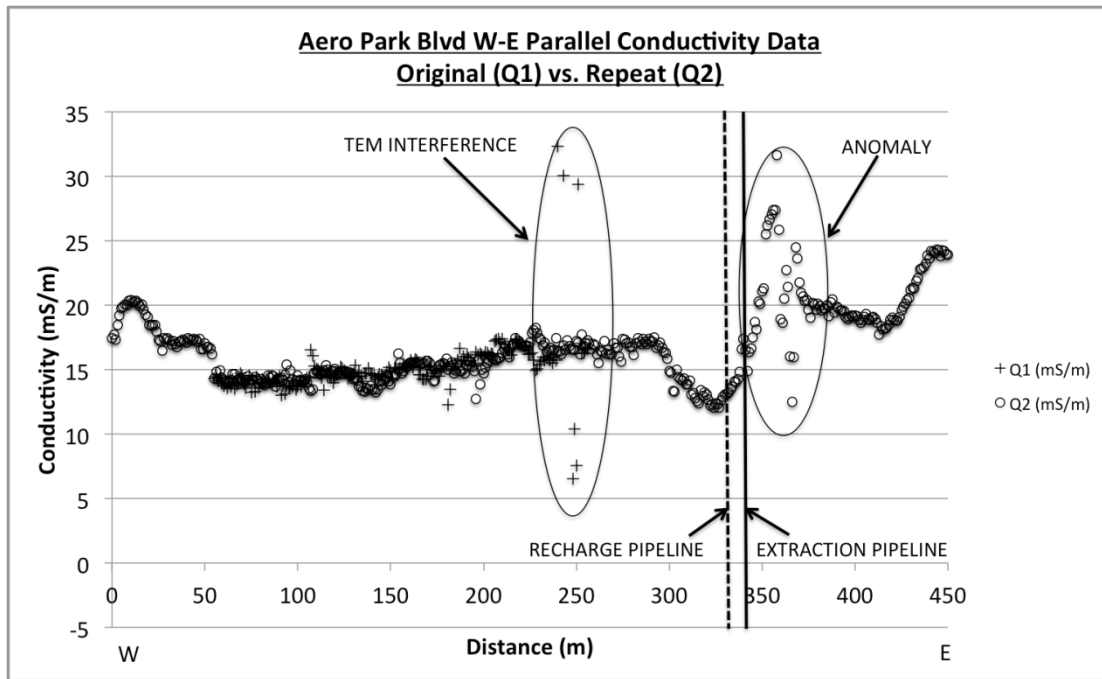


Figure 3.4a: Perpendicular conductivity data for the Aero Park Blvd N-S line. Two areas of TEM interference are present in the original data. The anomaly is still present between 0-30 meters with a similar expression as in the parallel data. 3.4b: The interference is also present in the in phase data. There is no expression of the suspected pipeline between 0-30 meters.

3.5a



3.5b

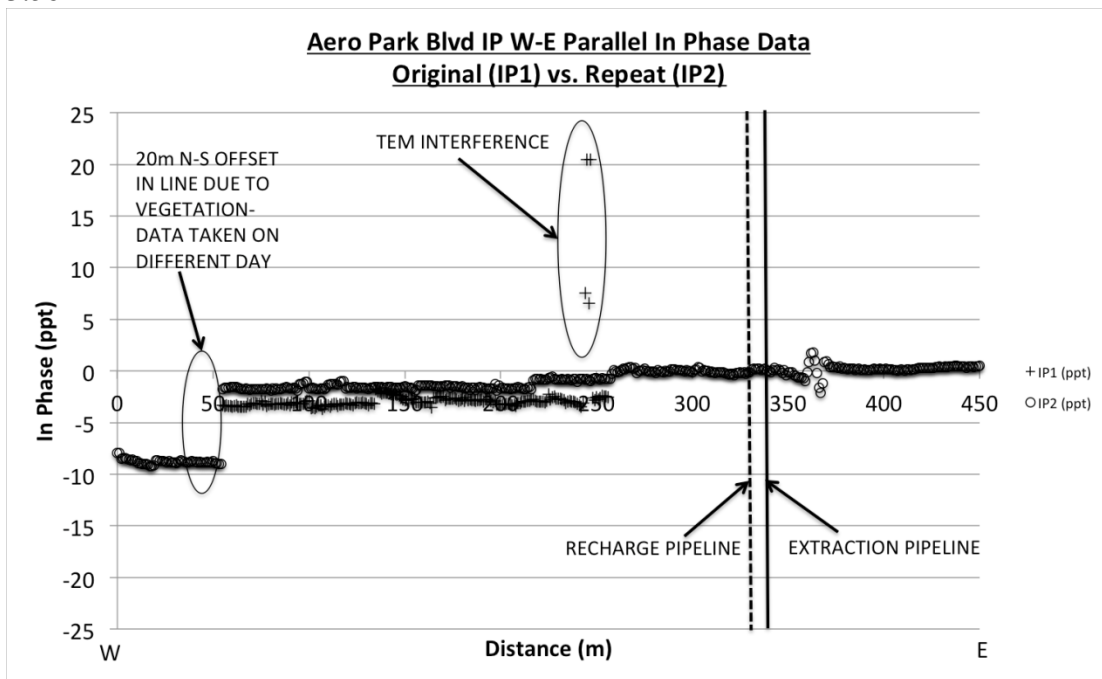
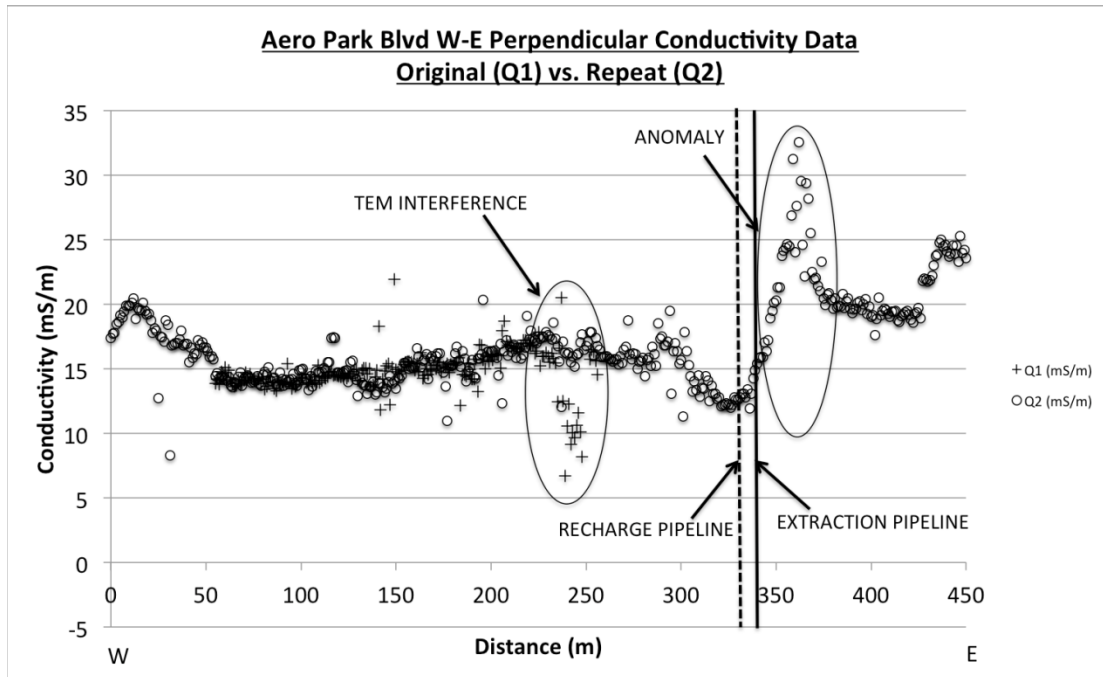


Figure 3.5a: Conductivity data for the Aero Park Blvd W-E line. There is only one area of TEM interference present around 250m along the line. Slight anomaly near the start of line is likely due to heavy vegetation making data acquisition difficult. Around 360m along the line an anomaly is present that correlates well with a known extraction pipeline. 3.5b: The interference is also present in the in phase data with a small expression of the pipeline present. An offset in the in phase data is probably due to calibration differences in the equipment, as the data were recorded on a different day.

3.6a



3.6b

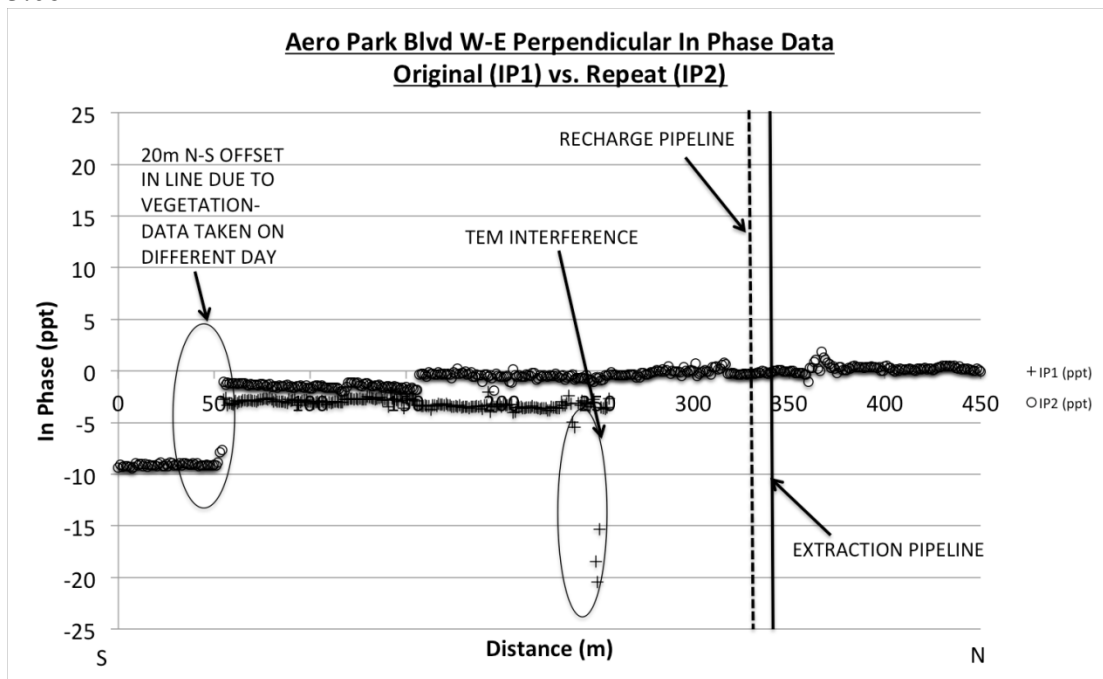
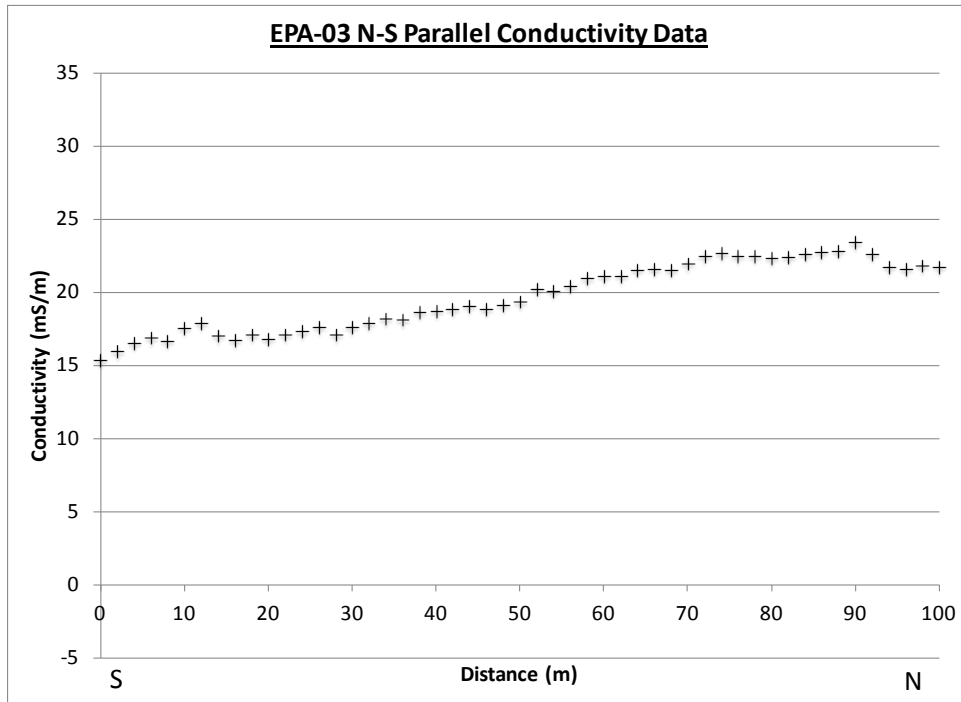


Figure 3.6a: Conductivity data for the Aero Park Blvd W-E line. This data are less consistent than the parallel data, due to the trouble in acquisition. In one area around 250 meters, the data are even messier, most likely due to TEM interference. The pipeline is still visible around 360 meters and is followed by a gradual increase in conductivity. 3.6b: Same offset in data as Figure 3.5b. In-phase data are more consistent than the conductivity. The TEM interference is clearer in this data set. There is only a small anomaly present expressing the presence of the power line.

3.7a



3.7b

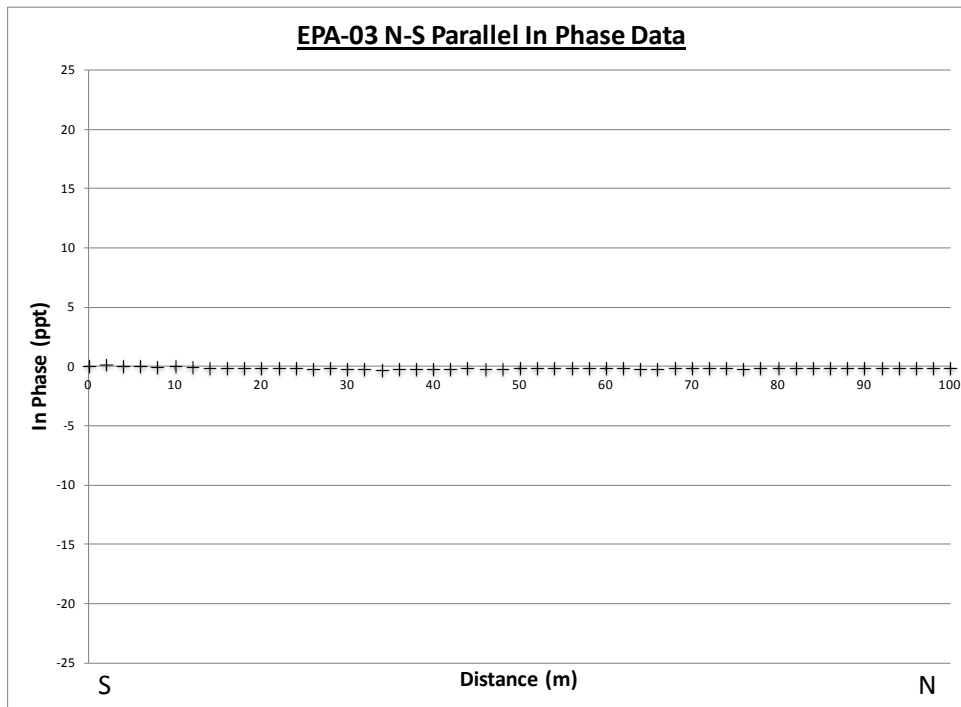
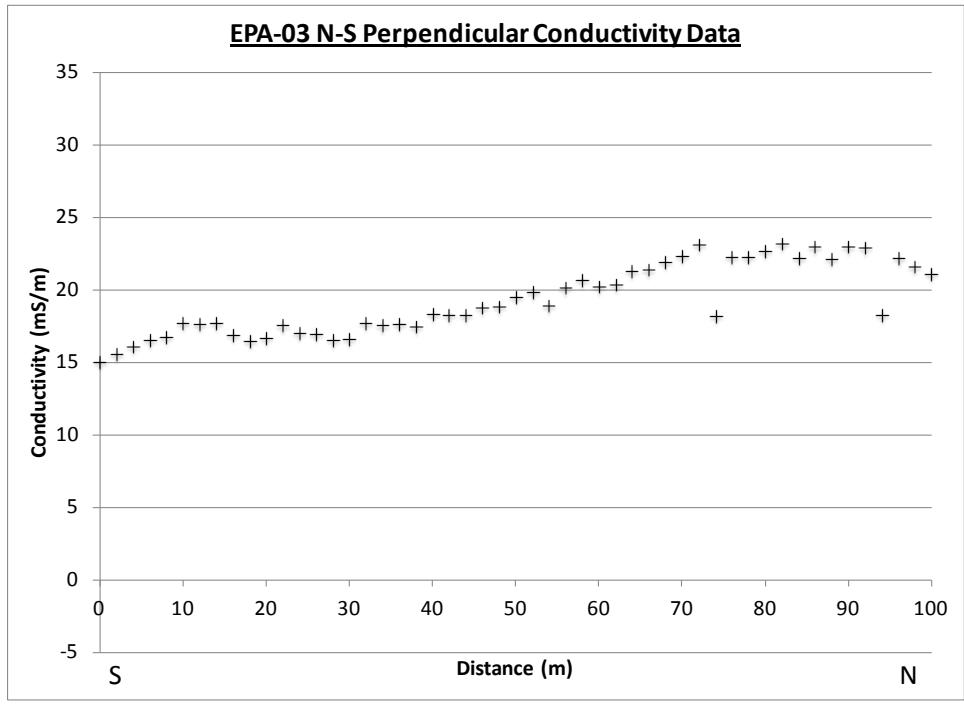


Figure 3.7a: The parallel N-S conductivity data are increasing slightly to the north, but are otherwise smooth. No significant anomalies in the data, and there were no visual observations of potential sources of anomaly. Figure 3.7b: The in-phase data are very flat around 0.

3.8a



3.8b

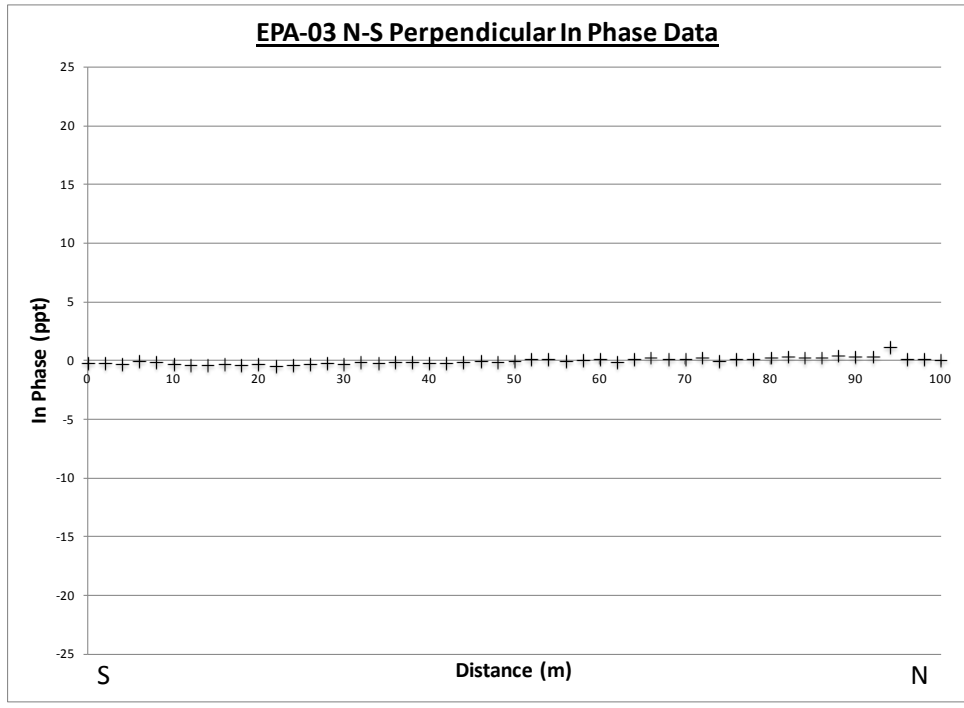
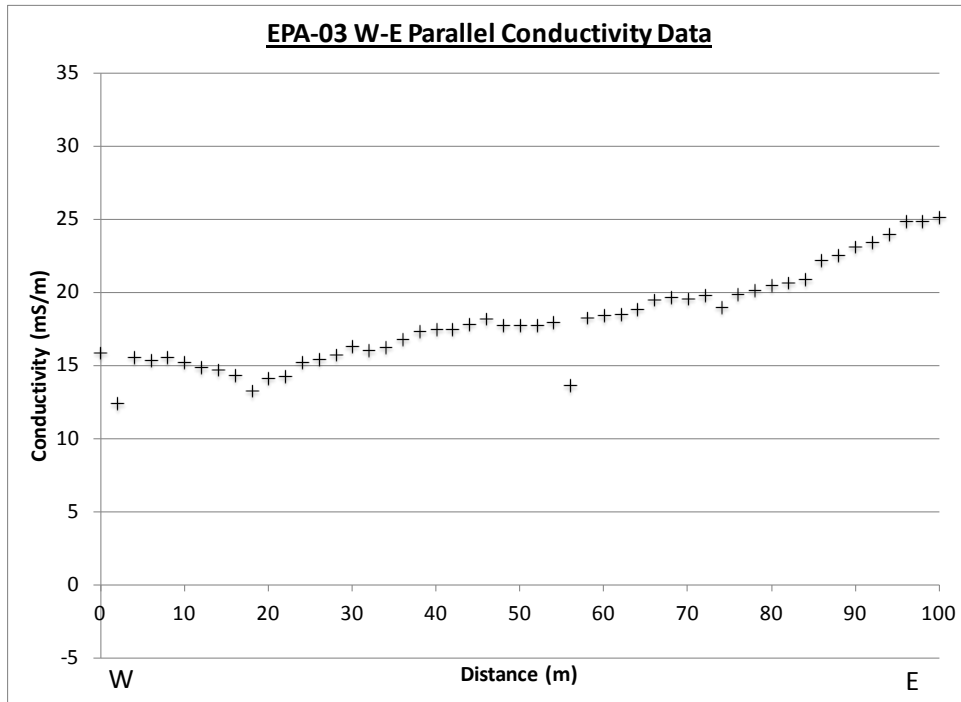


Figure 3.8a: Similar to Figure 3.7, the conductivity increases slightly and smoothly to the north. Figure 3.7b, the in-phase data are flat around 0. Data are somewhat messier due to difficulties in perpendicular data collection.

3.9a



3.9b

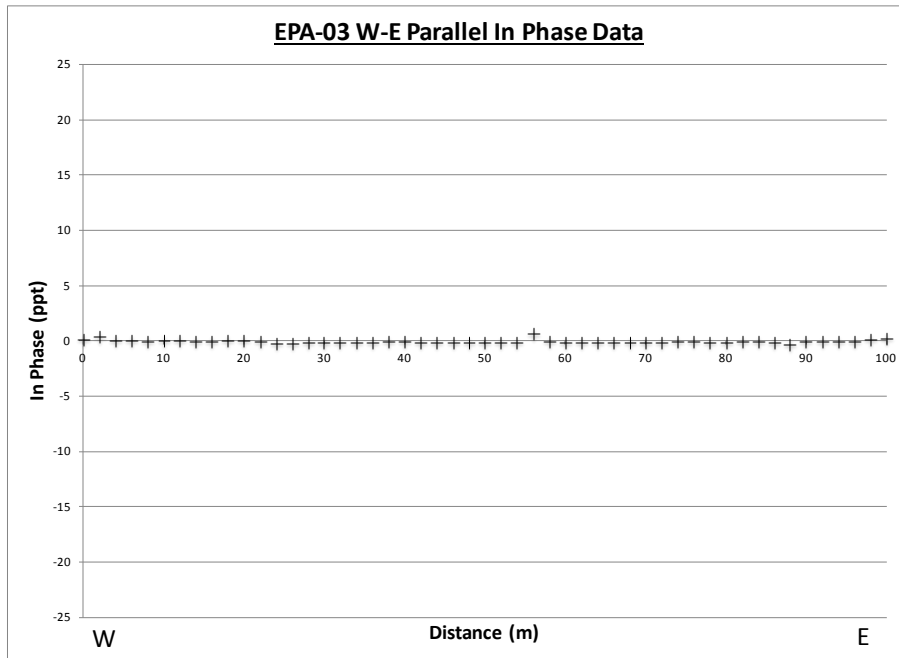
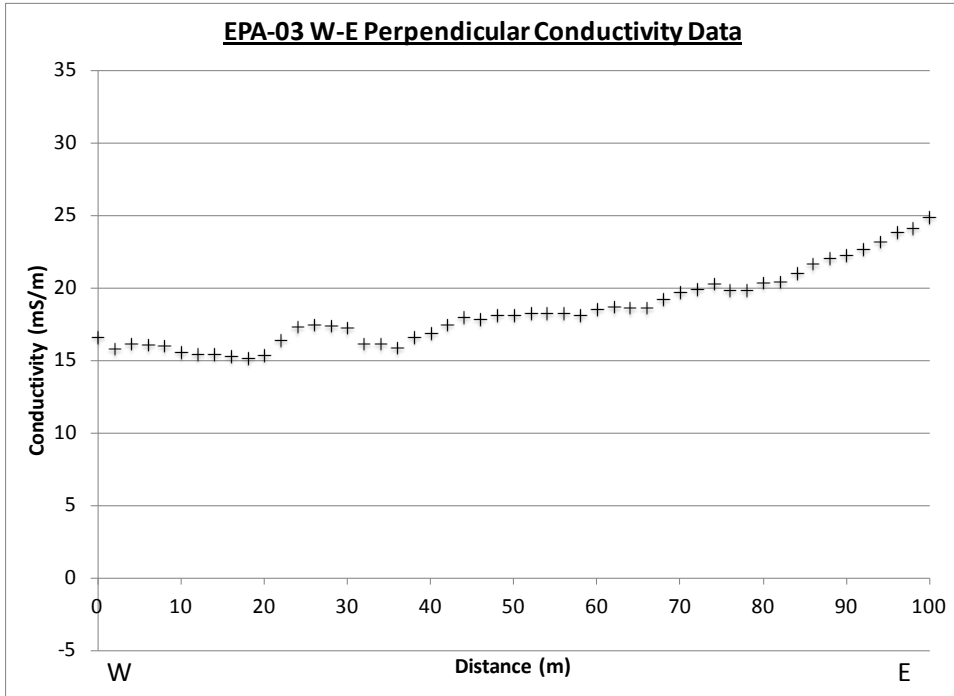


Figure 3.9a: The conductivity in the W-E parallel data increases slightly to the east. There were again no significant anomalies in the data, and there were no visual observations of potential sources of anomaly. Figure 3.9b: The in-phase data are again mostly flat around 0.

3.10a



3.10b

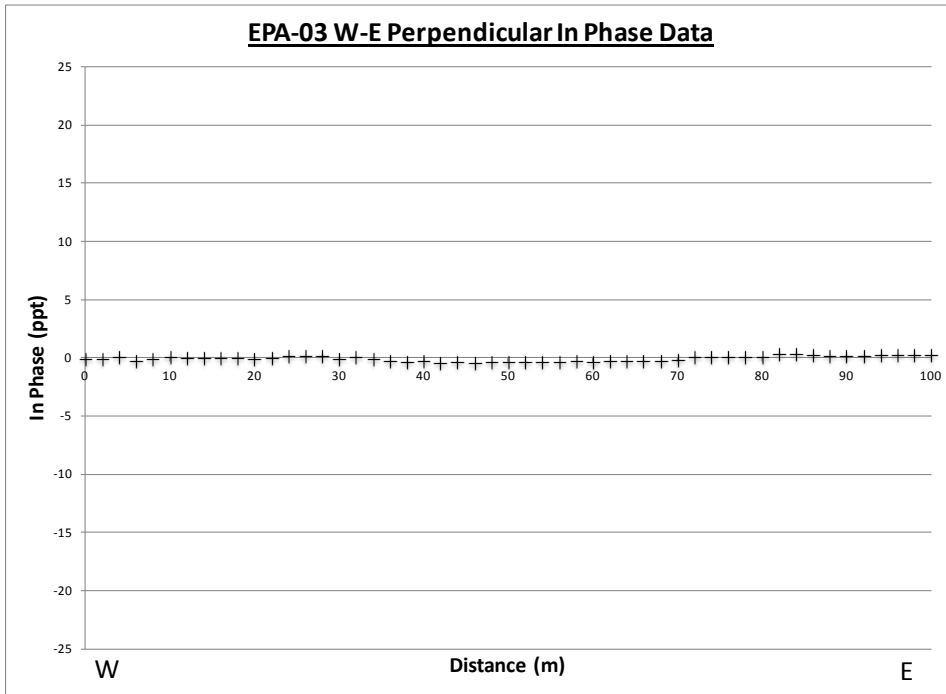


Figure 3.10a: Similar to 3.9, W-E conductivity increases slightly to the east. Figure 3.10b, the in-phase data are flat around 0.

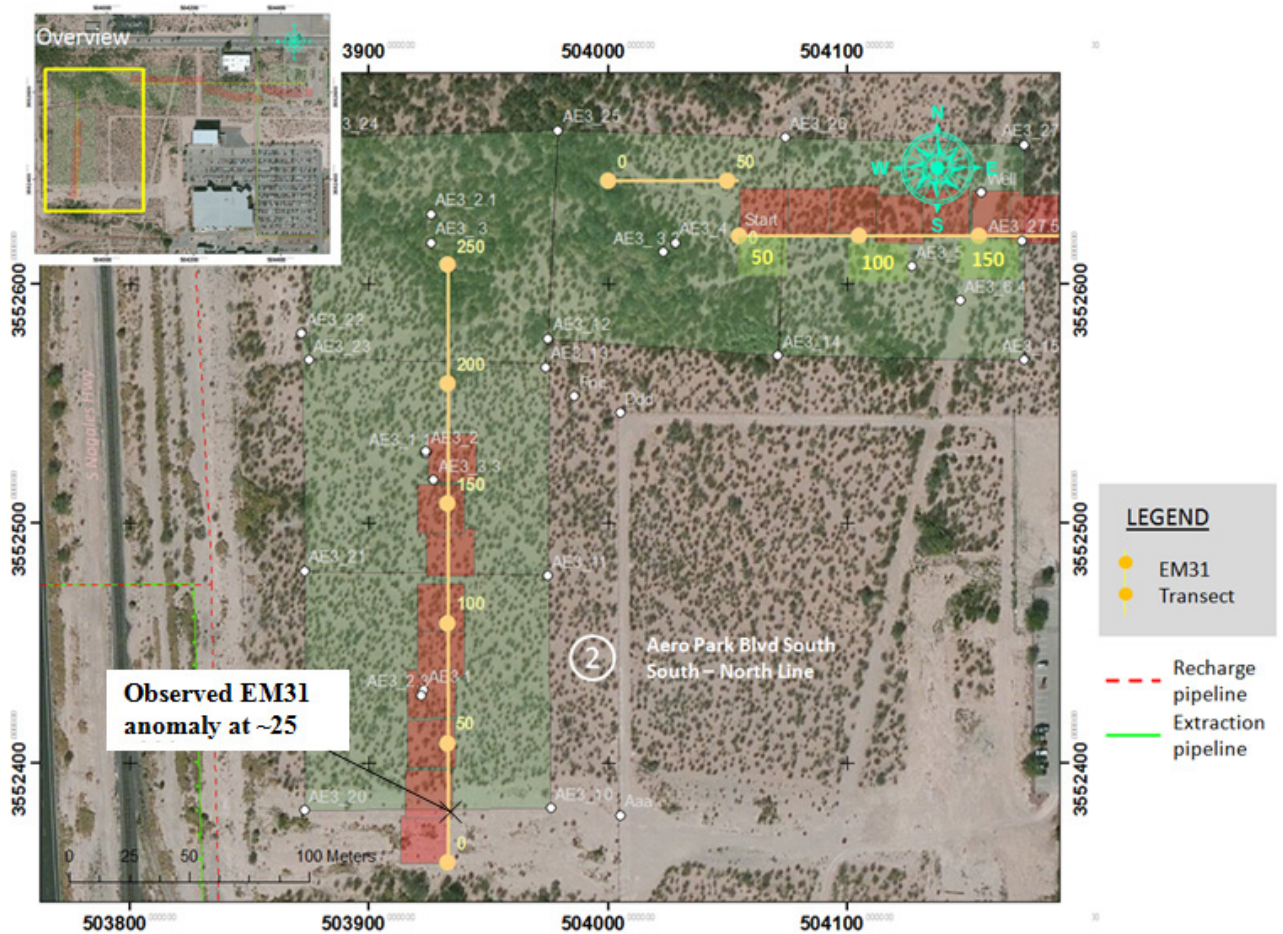


Figure 3.11: Map displaying observed anomaly at approximately 25m on the Aero Park Blvd N-S Line. This anomaly does not correlate with any visible pipe or power lines.

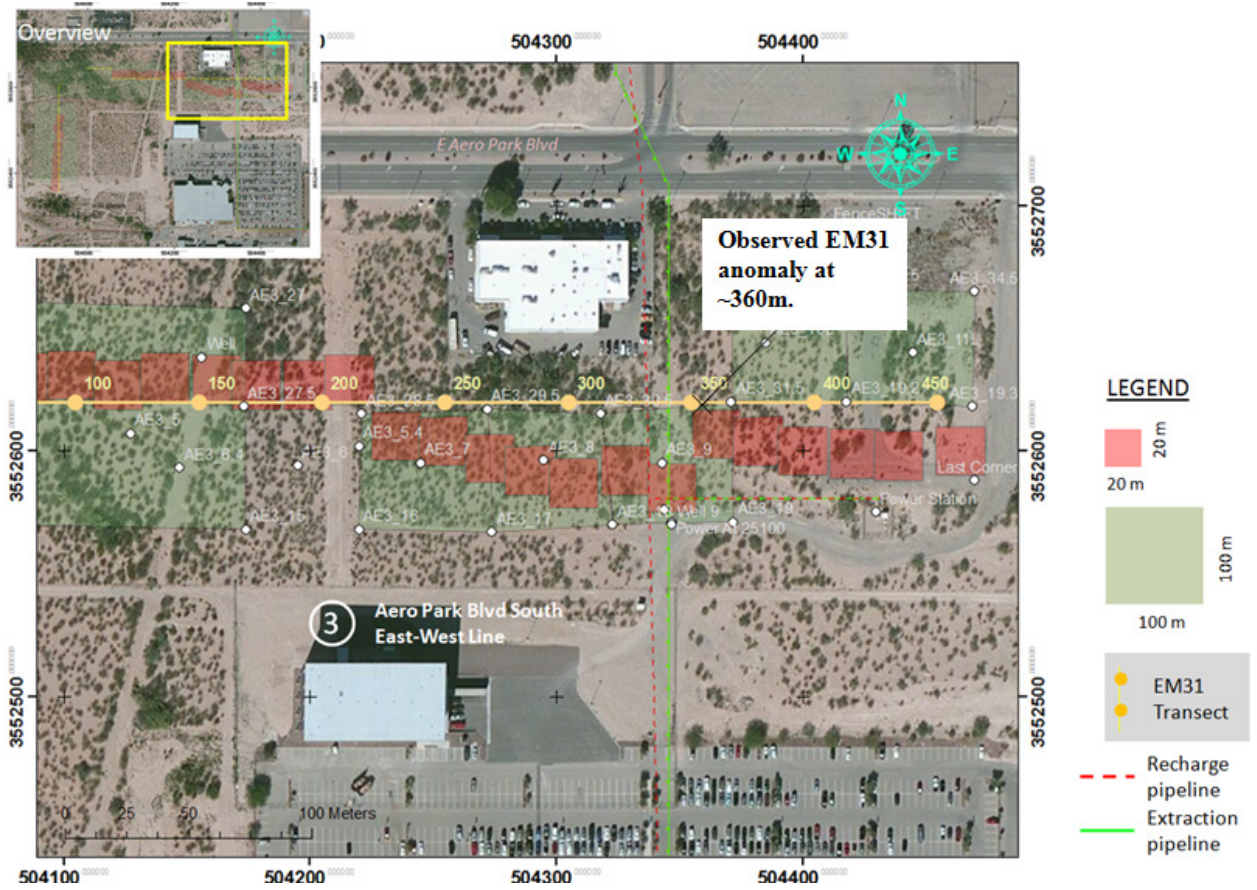


Figure 3.12: Map displaying observed anomaly at approximately 360m along Aero Park Blvd W-E Line. This anomaly correlates well with a set of pipes plotted on the maps.

## **4. Transient Electromagnetic (TEM) Surveys**

### **4.1 Introduction**

The main target for our Transient Electromagnetic (TEM) survey is mapping the potential buried porous channels which could control the subsurface flow of contaminants. In general, the TEM method can find the conductivity of the subsurface to a maximum of 3 to 5 times the loop size. However, in our survey we assumed a more conservative depth of about 2-3 times the loop size. For more information about the TEM method, see the paper “Introduction to TEM” (Zonge 2009). The work was done over two weekends in three different areas: Samsonite N, Aero Park Blvd South (two lines S-N and W-E), and EPA-03 shown in Figure 2.1. The Samsonite N area was only studied in the first weekend using 20x20 transmitter loops. In the first weekend, transmitter loops of size 20x20 meters were used; however, in the second weekend transmitter loops of sizes 100x100 meters were used and some 50x50 meters loops were used as well in restricted space areas.

### **4.2 Location**

In the first weekend, all TEM transmitter loops were 20x20 meter loops. The first site in which TEM was used was the Samsonite site. At this site, 8 loops were laid out going north to south. After running the first two loops, AP100 and AP200, the line of loops was shifted east 20 meter due to a pipeline running beneath the original loop line as shown in Figure 2.2.

The second site was the Aero Park Blvd. South site. The first loop line was running south to north, consisting of 9 loops as shown in Figure 4.2. Then, shifting a 100 m north to avoid being close to a fence, a total of 22 loops were run going west to east as shown in Figure 2.4.

The final site, EPA-03, had 5 loops going east to west as shown in Figure 2.5.

### **4.3 Instrumentation and Field Procedures**

Two different TEM setups were used for this study, a NanoTEM and ZeroTEM system. The equipment used for the NanoTEM system is a 20x20 meters transmitter loop, a GDP32-II

multi-channel receiver, a NT-20 transmitter, and an inner receiver loop of size 5x5 meters (Zonge 2012, Zonge 2013a). The NT-20 transmitter is used with the 20x20 meter loop to produce a magnetic field, which is received by the GDP32-II that is connected to the inner loop to measure the decaying secondary magnetic field. This decay curve can be used to find the resistivity of the earth. In the ZeroTEM system, a transmitter loop of 100x100 meters or a loop of 50x50 meters was used based on the availability of sufficient area. An XMT-32 transmitter controller and a ZT-30 transmitter were used for the ZeroTEM system instead of the NT-20 transmitter, and instead of the inner receiver loop we used a receiver coil that is connected to the GDP32-II (Zonge 2013b, Zonge 2013c). The GDP32-II and the XMT-32 are synchronized together by an internal resonating crystal and TEM surveys were made at 32 and 16 Hz repetition frequencies for both the 100x100 meters and 50x50 meters loops. However, the frequencies used for the 20x20 transmitter loops were 64 and 32 Hz. The current used for the 20x20 loops was 3.0 Amps, 6.0 Amps for the 50x50 loops, and 3.5 Amps for the 100x100 loops. The power source was a single 12 V battery for the 20x20 loop and two 12 V batteries for the 50x50 and 100x100 loops. These instruments were manufactured by Zonge International (formerly - Zonge Engineering).

We tried to keep the transmitter loops away from fence lines, pipelines, power lines and other cultural features that could affect the measurements. In the Samsonite N area, a metal detector indicated the presence of a conductive line, possibly a buried metal pipe. Therefore, after the first two loops, the loops were shifted 20 meters toward the East to avoid the buried conductor.

#### **4.4 Data Processing**

The TEM data obtained from the surveys were stored in the GDP32-II receiver and then downloaded and saved, in its raw form, to a laptop computer in the Laboratory for Advanced Subsurface Imaging (LASI) at the University of Arizona. The raw data were sorted and organized and then processed using Zonge International's proprietary suite of software called DATPRO. Then, the data were trimmed or edited for values that had a large error or were inconsistent with the decay trend. The file was then run through STEMINV, in order to invert the measured data into a smooth model of the resistivity variation with depth. The one-dimensional

inversion figures for each TEM site are shown in Appendix B. A comparison of the measured decay curve data and the best-fit calculated decay curve is shown on the left side of each figure in Appendix B, and in red are the values considered too noisy that were deleted prior to the smooth inversion. In the Aero Park Blvd. east-west line, loop 18000 was skipped due to its closeness to the building shown in Figure 2.4. Also, loop AP601 was skipped due to a power line inside the loop. On the right side of the Figures found in Appendix B, a plot of the best-fit smooth model of resistivity versus depth is shown.

#### **4.5 Layered-Earth Modeling**

A display of the TEM data was produced using Golden Software's Surfer 9. The input data were the inverted data from STEMINV and grid processed by the Kriging method. The input file consisted of three columns, which are the horizontal distance between a loop corner and its side's midpoint, elevation of the loop, and resistivity. Then, the models were plotted using contour maps. The contour steps and scale bar were created such that they are logarithmic. The produced contour maps show the distance along the sides of the loops, real elevation, and resistivity of the layer such as shown in Figure 4.1. The lower x-axis (distance) is the distance starting from the center of the loop, and the upper x-axis is the station number.

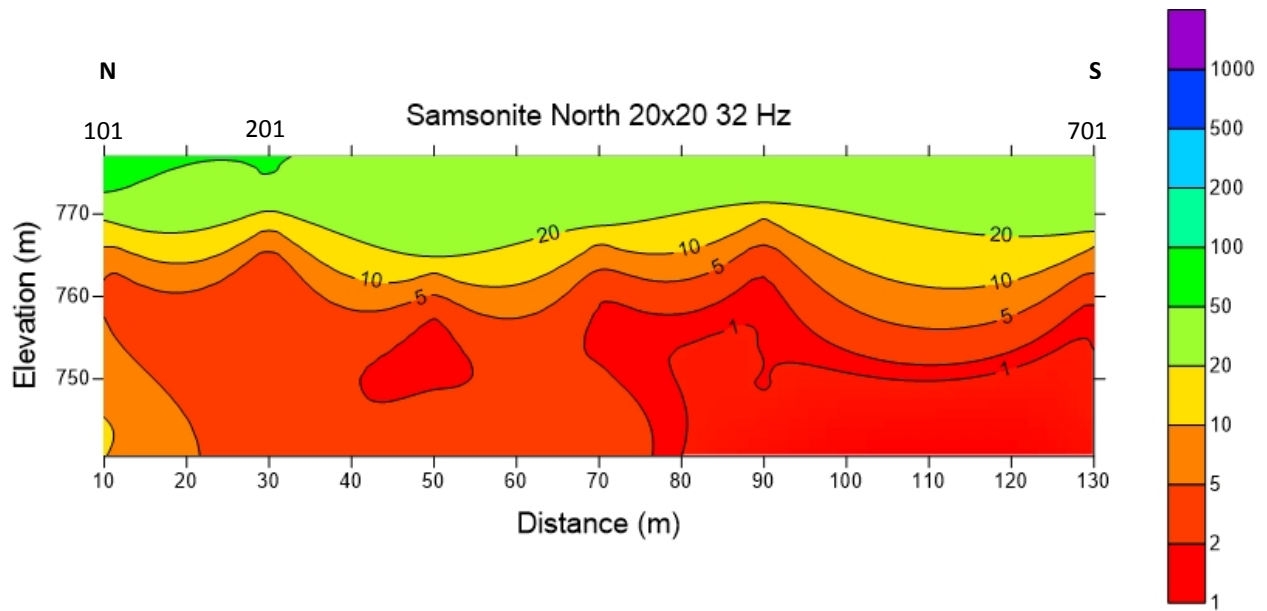


Figure 4.1 Samsonite North site with 20x20 loops running 32 Hz.

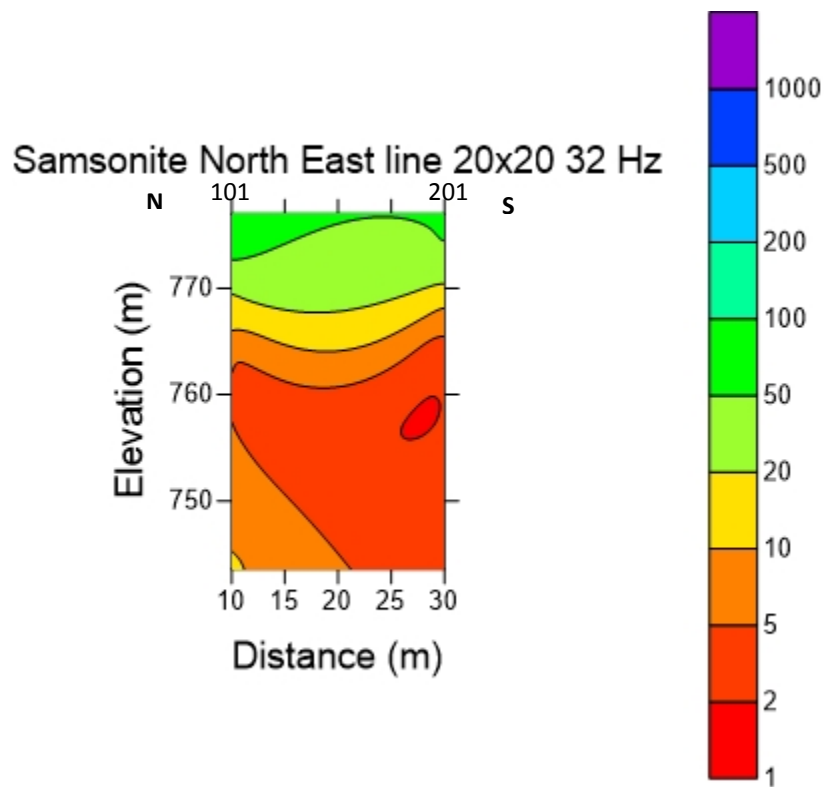


Figure 4.2 Samsonite North site East line with 20x20 loops running 32 Hz.

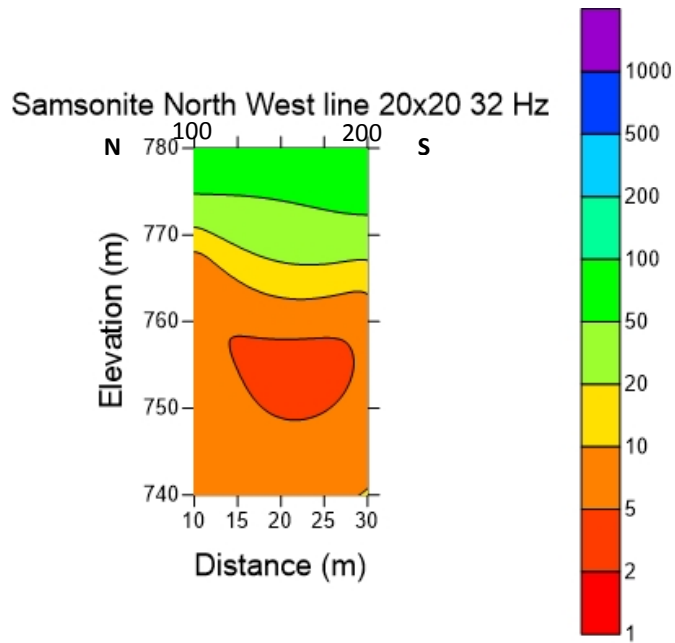


Figure 4.3 Samsonite North site West line with 20x20 loops running 32 Hz.

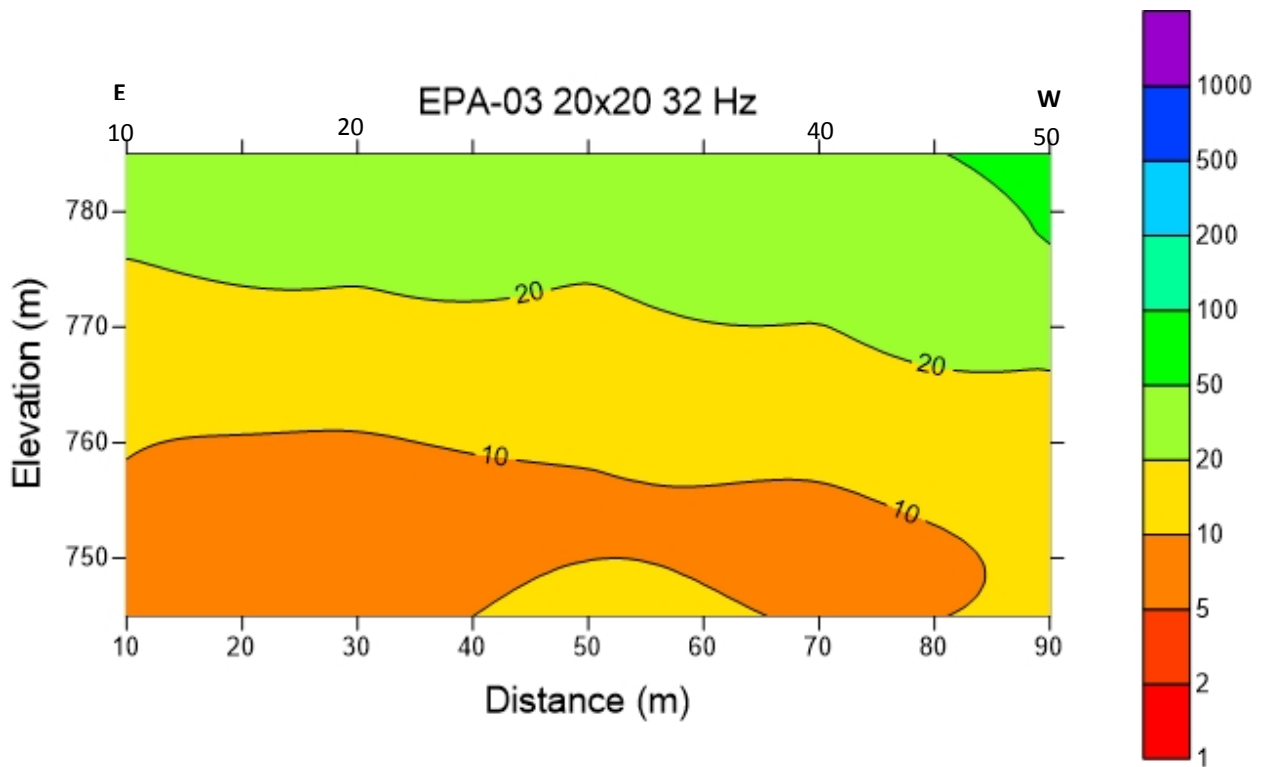


Figure 4.4 EPA-03 site with 20x20 loops running 32 Hz.

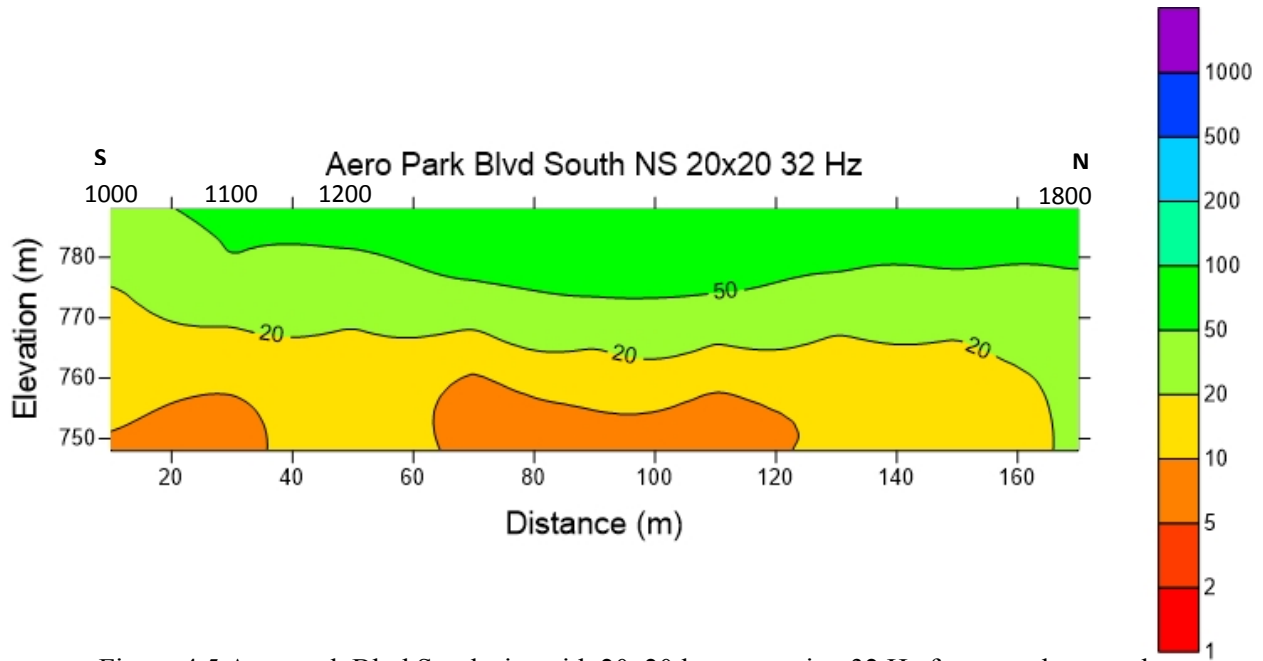


Figure 4.5 Aero park Blvd South site with 20x20 loops running 32 Hz from south to north.

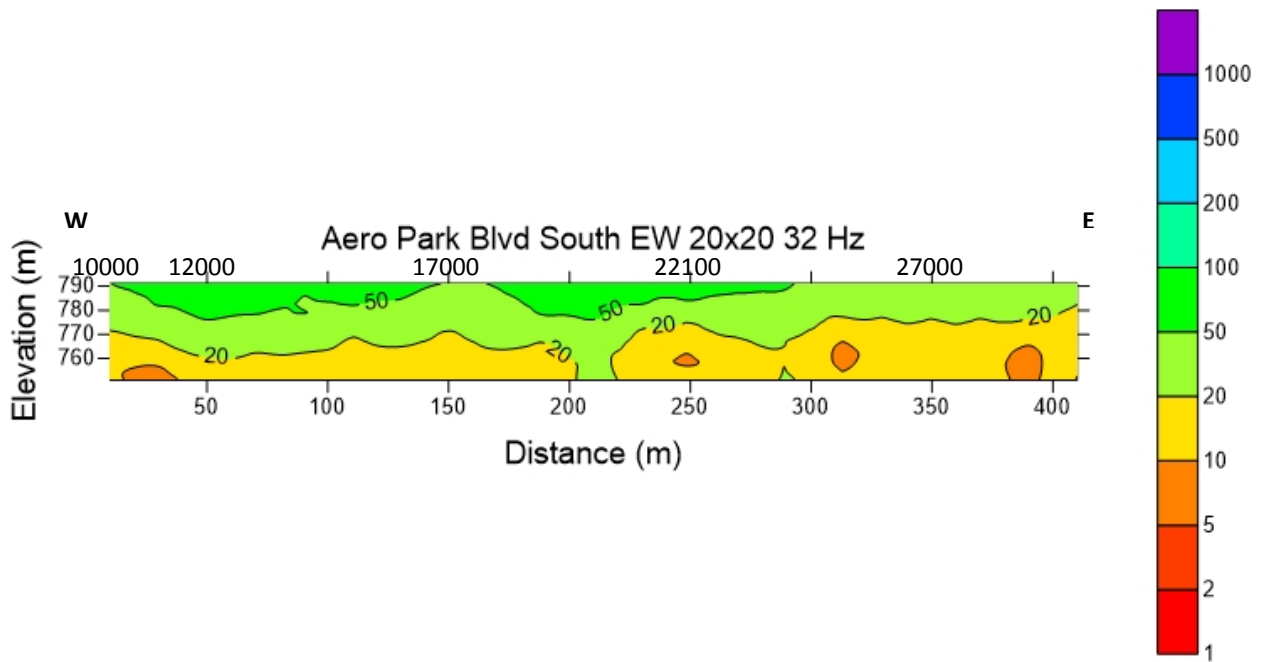


Figure 4.6 Aero Park Blvd South site with 20x20 loops running 32 Hz from west to east.

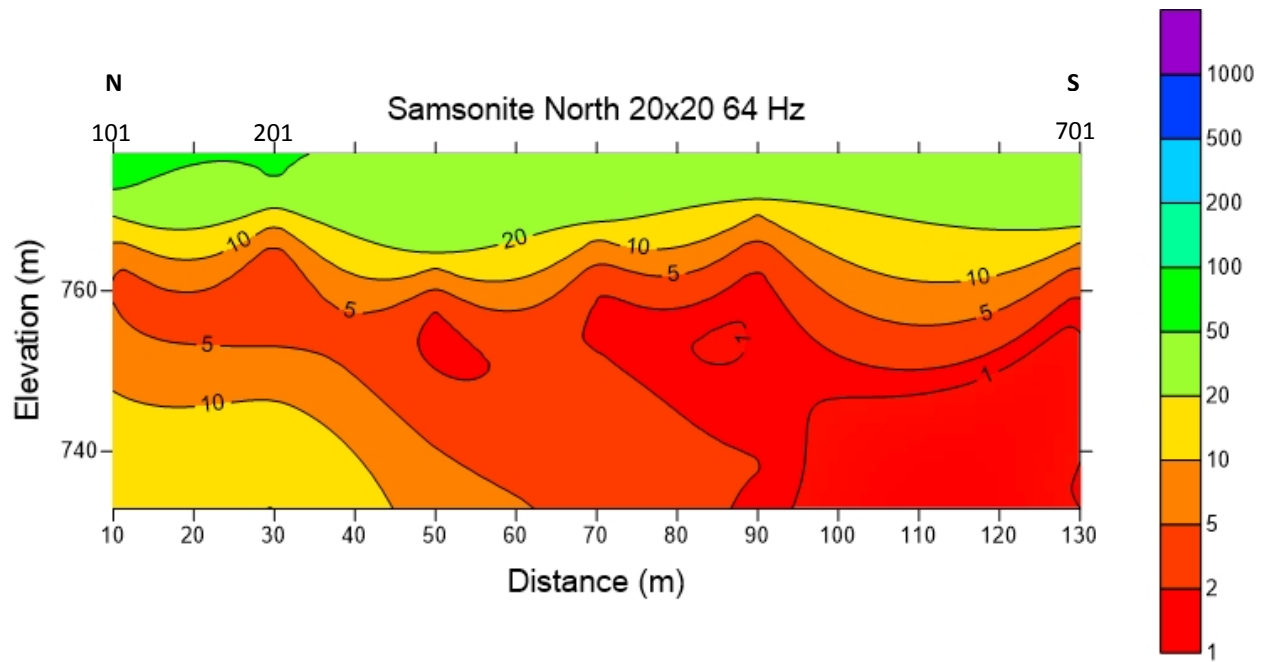


Figure 4.7 Samsonite North site with 20x20 loops running 64 Hz.

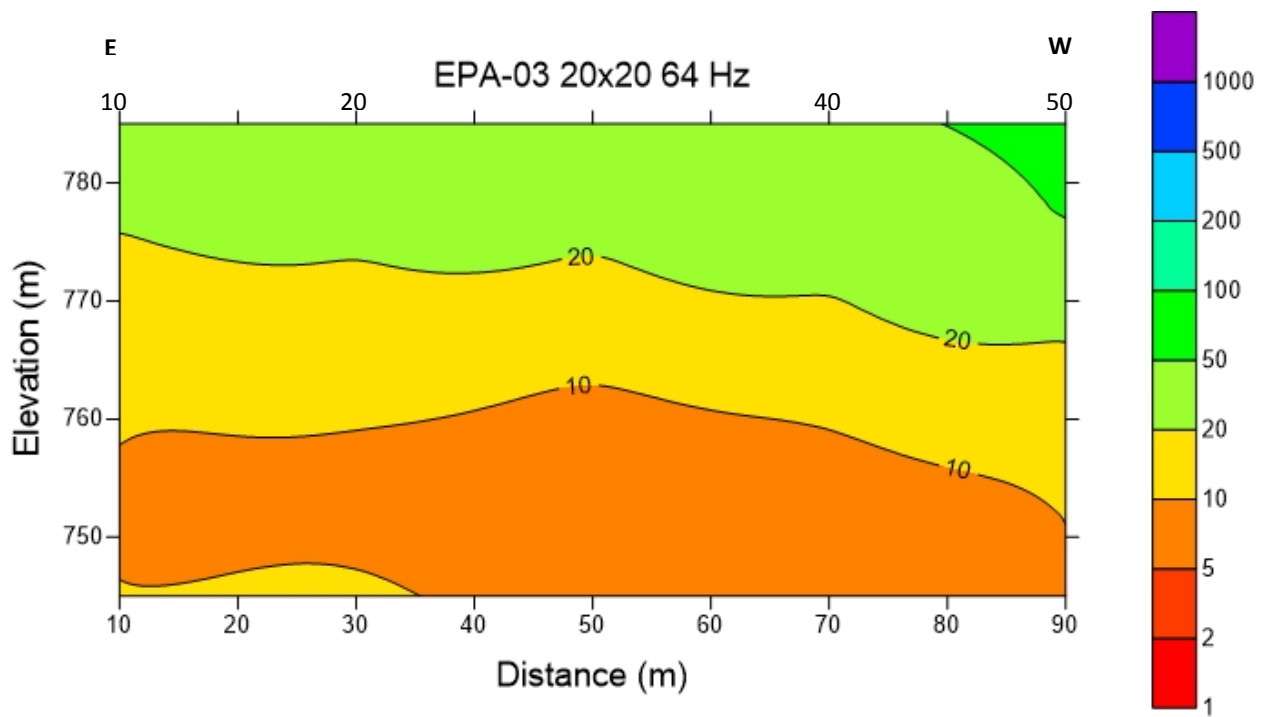


Figure 4.8 EPA-03 site with 20x20 loops running 64 Hz.

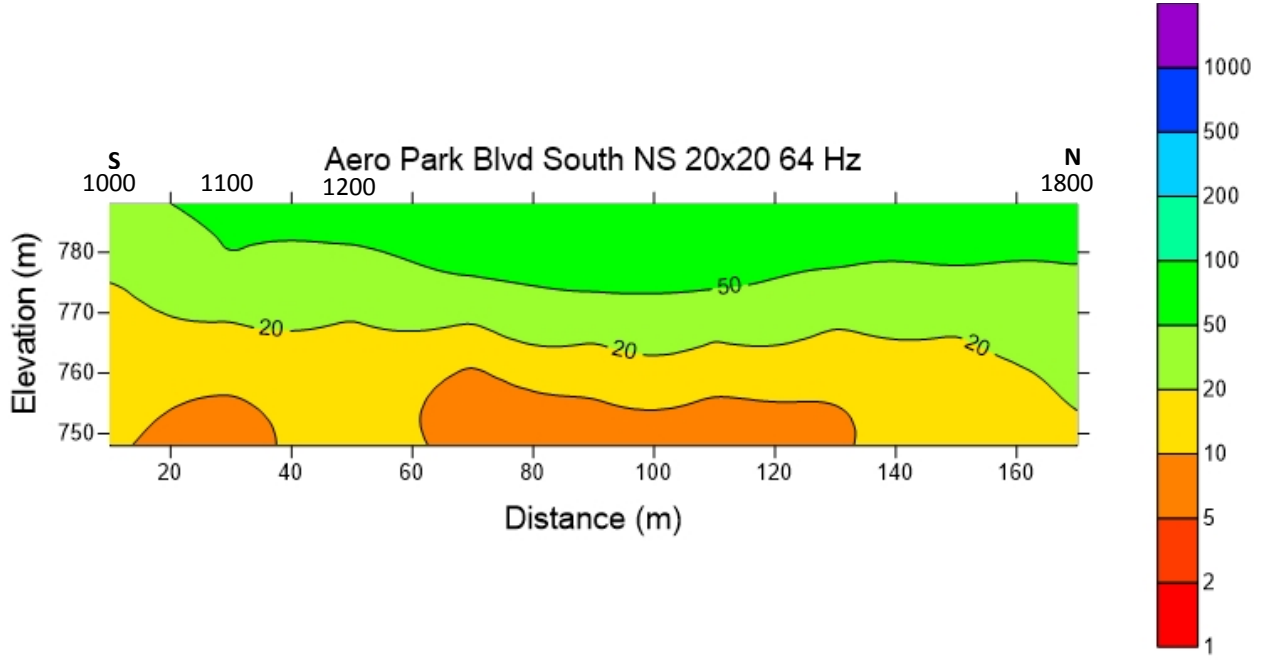


Figure 4.9 Aero Park Blvd South site with 20x20 loops running 64 Hz from south to north.

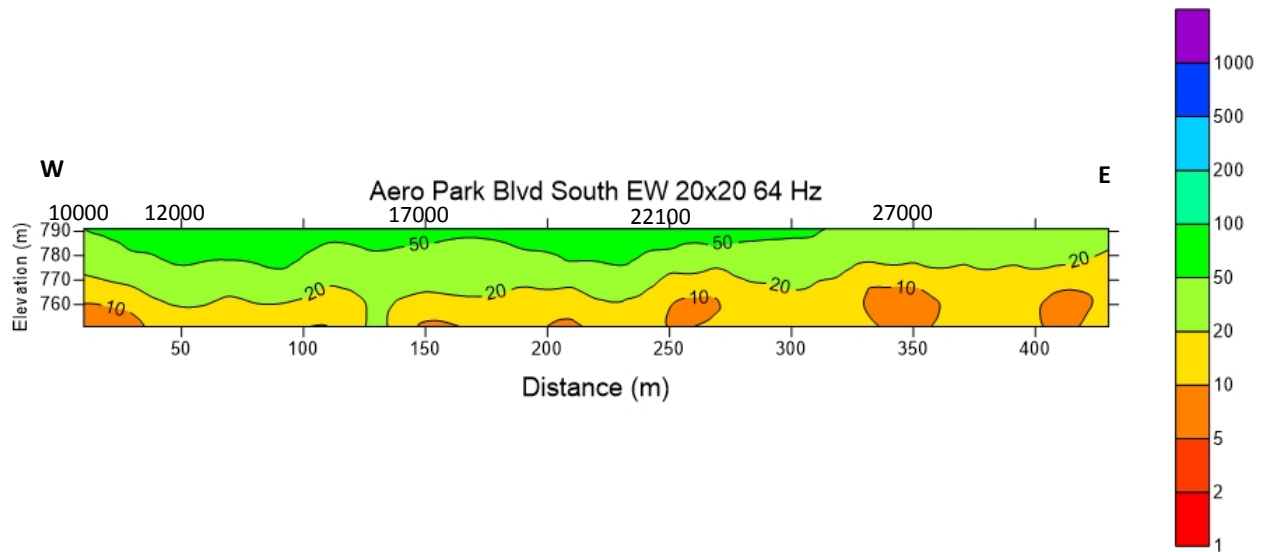


Figure 4.10 Aero Park Blvd South site with 20x20 loops running 64 Hz from west to east.

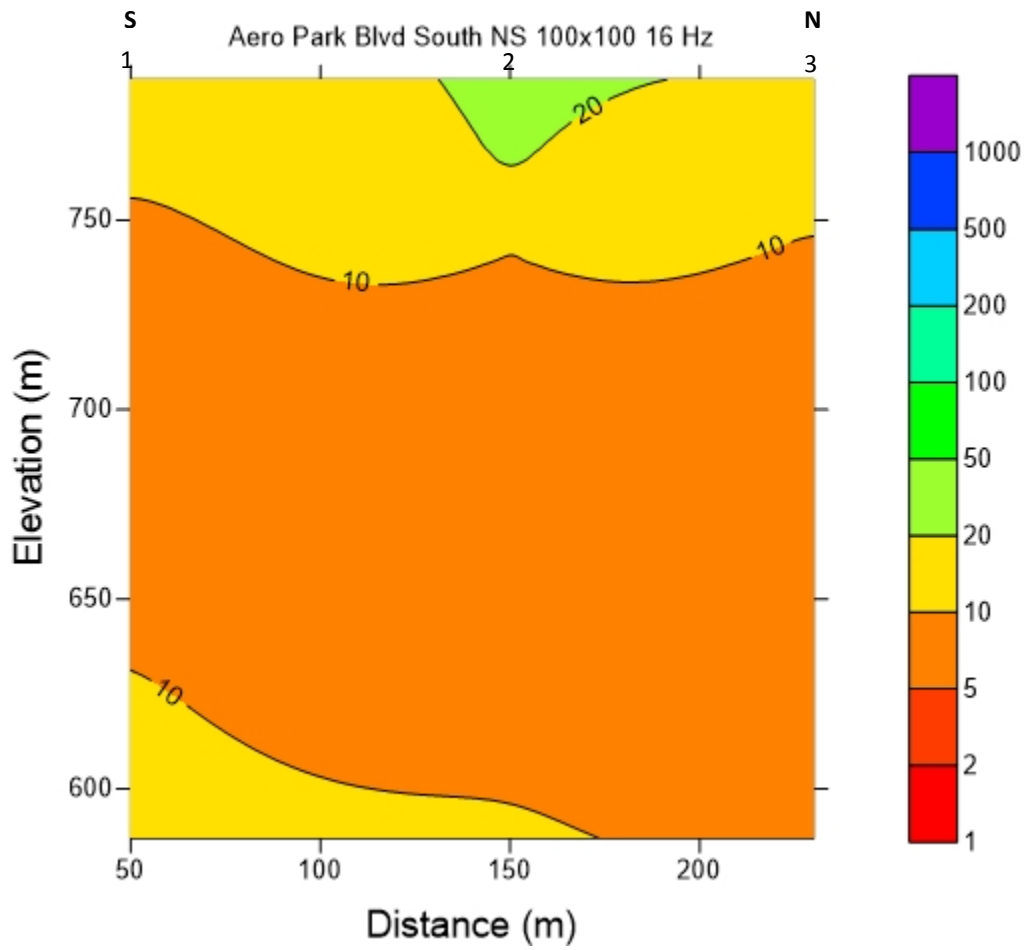


Figure 4.11 Aero Park Blvd South site with 100x100 loops running 16 Hz from south to north.

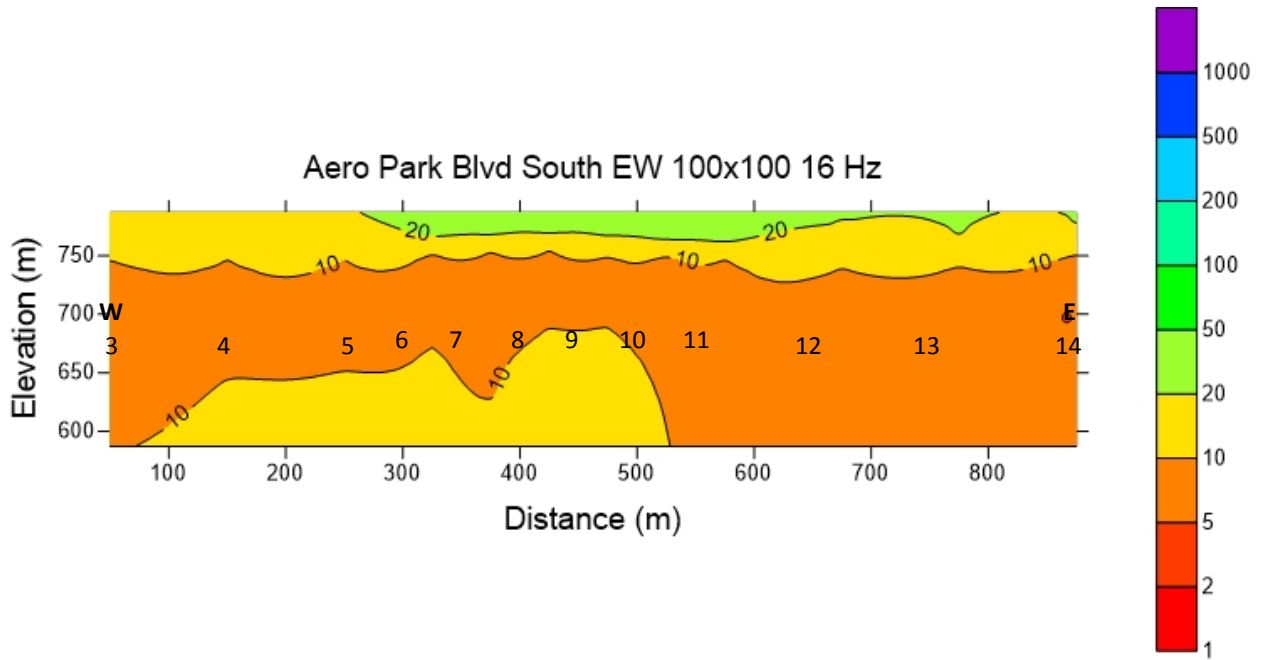


Figure 4.12 Aero Park Blvd South site with 100x100 loops running 16 Hz from west to east.

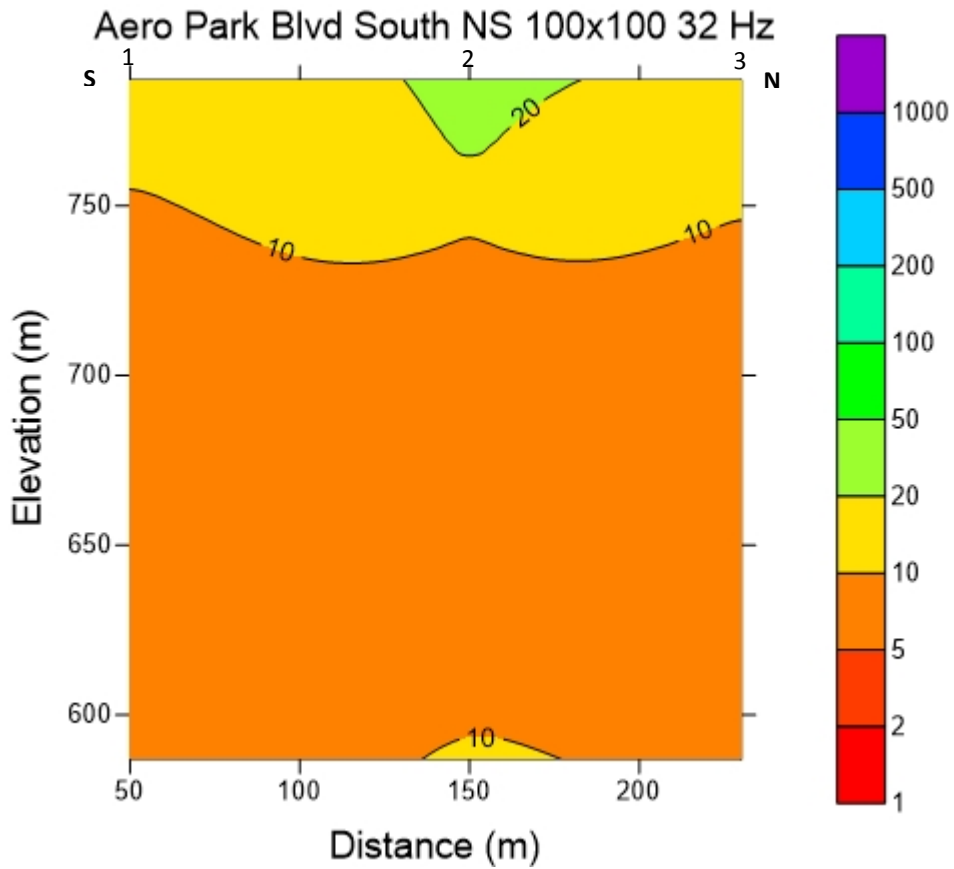


Figure 4.13 Aero Park Blvd South site with 100x100 loops running 32 Hz from south to north.

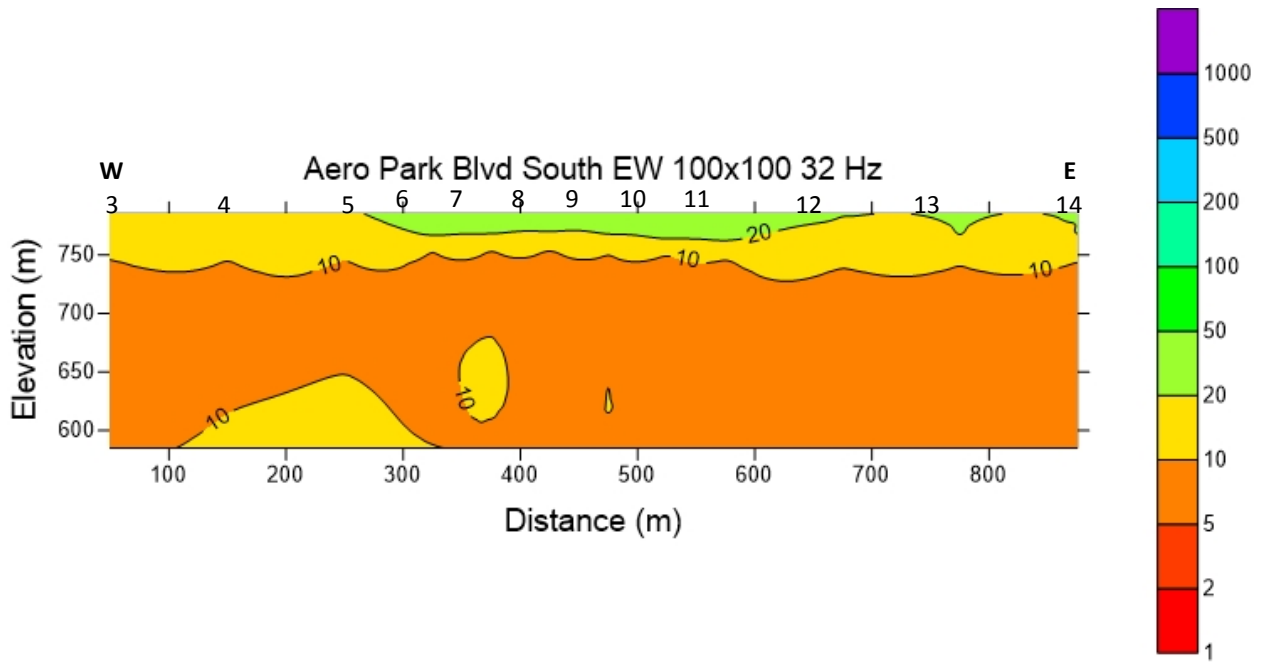


Figure 4.14 Aero Park Blvd South site with 100x100 loops running 32 Hz from west to east.

## **5. EMIGMA Inversion of Transient Electromagnetics**

### **5.1 Introduction**

EMIGMA 8.6 from PetrosEikon, Inc. is a commercial program for modeling, inversion and interpretation of geophysical electromagnetic methods. In this project, EMIGMA was used to process our TEM field data. By using the processing functions and inversion functions of EMIGMA, we can compare the inversion results from EMIGMA and STEMINV in order to obtain a better understanding of the subsurface targets.

### **5.2 Procedures**

To process TEM field data using EMIGMA, the first step is processing the TEM field data using the TEMAVG program, i.e. the Zonge International averaging program, to produce an average (.avg) file, which is a readable file for EMIGMA. Before inverting the data, we need to delete noisy data. The deleted points should be the same as used in the STEMINV smooth inversion method in order to compare the inversion results. And finally, we invert the TEM field data by 1D inversion. In this project, we used the 1D Occam inversion method. After obtaining the inversion models for TEM field data, we produced a cross section using Golden Software's SURFER 11. We then compared the inversion results of the two methods.

### **5.3 Processing results**

#### **5.3.1 32HZ, 20×20m Loop**

##### **① Samsonite N. NS**

In this profile, the initial models we used for the 1D Occam inversion are 40 layers with 2 m for each layer for points Y=0 and Y=60m, and 30 layers with 3m each layer for points Y=20, 40, 80 and 120m (The decay curves are shown in Appendix C). The misfit for this profile is less than 5%.

The inversion results are shown in Figure 5.1. Compared with the STEMINV inversion results in Figure 4.1, we can see that the resistivity trend is similar. Both resistivity sections are decreasing from high resistivity in the shallow layers to low resistivity in the deep layers.

### ② Samsonite N. East

In this profile, the initial models we used for the 1D Occam inversion are 30 layers with 2 m each layer (see the decay curves in Appendix C). The misfit for this profile is less than 5%.

The inversion results are shown in Figure 5.2. Compared with Figure 4.2, the STEMINV inversion results, the resistivity trends are similar, but the resistivity values are different. The shallow-layer resistivity of Figure 4.2 is higher and the deeper resistivity is lower.

### ③ Samsonite N. West

In this profile, the initial models we used for the 1D Occam inversion are 30 layers with 2 m each layer (see the decay curves in Appendix C). The misfit for this profile is less than 5%.

The inversion results are shown in Figure 5.3. Compared with Figure 4.3, the STEMINV inversion results, the resistivity trends are similar, but the resistivity values are different. The shallow resistivity of Figure 4.3 is higher and the middle layer resistivity is lower.

### ④ EPA-03. EW

In this profile, the initial models we used for the 1D Occam inversion are 35 layers with 2 m each layer (see the decay curves in Appendix C). The misfit for this profile is less than 5%.

The inversion results are shown in Figure 5.4. Compared with Figure 4.4, they have very similar inversion results. The EMIGMA model shows more detail in the shallow area.

### ⑤ Aero Park Blvd.S.NS

In this profile, the initial models we used for the 1D Occam inversion are 40 layers with 2 m each layer for first 3 points  $Y=0$  ,  $Y=20m$  and  $Y=40m$ , and 30 layers with 3m each layer for

other 6 points Y=60, 80, 100, 120, 140 and 160m (see the decay curves in Appendix C). The misfit for this profile is less than 5%.

The inversion results are shown in Figure 5.5. Compared with Figure 4.5, the STEMINV inversion results, the resistivity trends are the same, but the resistivity values are different. The shallow layer resistivity of Figure 5.5 is higher and it has a lower resistivity in the deep zone.

### **⑥Aero Park Blvd.S.EW**

In this profile, the initial models we used for the 1D Occam inversion are 30 layers with 3 m each layer (see the decay curves in Appendix C). The misfit for this profile is less than 5%.

The inversion results are shown in Figure 5.6. Compared with Figure 4.6, the resistivity trends are the same, but the resistivity values are different. The shallow layer resistivity of Figure 5.6 is higher and it has a lower resistivity in the deep zone.

### **5.3.2 64HZ, 20×20m Loop**

#### **①Samsonite N. NS**

In this profile, the initial models we used for the 1D Occam inversion are 30 layers with 3 m each layer (see the decay curves in Appendix C). The misfit for this profile is less than 5%.

The inversion results are shown in Figure 5.7. Compared with Figure 4.7, the resistivity trends are similar, but in the depth zone from 750m to 738m deep and stations from 0 to 60m, and in the shallow zone between 20m and 60m, the resistivity values are different from STEMINV inversion results.

#### **②EPA-03. EW**

In this profile, the initial models we used for the 1D Occam inversion are 30 layers with 3 m each layer (see the decay curves in Appendix C). The misfit for this profile is less than 5%.

The inversion results are shown in Figure 5.8. Compared with Figure 4.8, the inversion results are similar, just with a little difference in the last two points.

### **③Aero Park Blvd.S.NS**

In this profile, the initial models we used for the 1D Occam inversion are 30 layers with 3 m each layer (see the decay curves in Appendix C). The misfit for this profile is less than 5%.

The inversion results are shown in Figure 5.9. Compared with Figure 4.9, the inversion results are similar, just with a little difference in the shallow zone between 60m and 120m. In the deeper zone, the resistivity in Figure 5.9 is much higher.

### **④Aero Park Blvd.S.EW**

In this profile, the initial models we used for the 1D Occam inversion are 30 layers with 3 m each layer (see the decay curves in Appendix C). The misfit for this profile is less than 5%.

The inversion results are shown in Figure 5.10. Compared with Figure 4.10, the inversion results are similar, just with a little difference in the shallow area between 40m and 200m. In this zone, the resistivity in Figure 5.10 is much higher. Figure 5.10 has more detail in the shallow zone.

## **5.3.3 16HZ, 100×100m Loop and 50×50m Loop**

### **①Aero Park Blvd.S.NS**

In this profile, the initial models we used for the 1D Occam inversion are 30 layers with 10 m each layer (see the decay curves in Appendix C). The misfit for this profile is less than 1%.

The inversion results are shown in Figure 5.11. Compared with Figure 4.11, the inversion results are similar, but the resistivity values are different and the inversion result in Figure 5.11 has more detail than that in Figure 4.11.

### **②Aero Park Blvd.S.EW**

In this profile, the initial models we used for the 1D Occam inversion are 30 layers with 10 m each layer (see the decay curves in Appendix C). The misfit for this profile is less than 1%. And for the 50X50m loop, we deleted the first time channel due to its divergence in the inversion, but it was not deleted in the STEMINV inversion.

The inversion results are shown in Figure 5.12. Compared with Figure 4.12, the inversion results are quite different, but from the shallow to the deeper layers, the resistivity trend is similar. The resistivity values are much lower in the deep zone in Figure 5.12. Due to the deletion of the first time channel for 50m loop, from 250m to 550m, the shallow responses are different.

#### **5.3.4 32HZ, 100×100m Loop and 50×50m Loop**

##### **①Aero Park Blvd.S.NS**

In this profile, the initial models we used for the 1D Occam inversion are 30 layers with 10 m each layer (see the decay curves in Appendix C). The misfit for this profile is less than 1%.

The inversion results are shown in Figure 5.13. Compared with Figure 4.13, the inversion results are similar, but the resistivity values are different and the inversion results in Figure 5.13 have more detail than that in Figure 4.13.

##### **④Aero Park Blvd.S.EW**

In this profile, the initial models we used for the 1D Occam inversion are 30 layers with 10 m each layer (see the decay curves in Appendix C). The misfit for this profile is less than 1%. And, again, for the 50X50m loop, we deleted the first time channel due to its divergence in inversion, but it was not deleted in the STEMINV inversion.

The inversion results are shown in Figure 5.14. Compared with Figure 4.14, the inversion results are quite different, but from the shallow to the deep, the resistivity trend is similar. The resistivity values are much lower in the deep zone in Figure 5.14. Due to the deletion of the first time channel for 50m loop, from 250m to 550m, the shallow layer responses are different.

#### **5.4 Interpretation**

1. For Samsonite N. site, the four EMIGMA inversion results (Figures 5.1, 5.2, 5.3 and 5.7) and the four STEMINV inversion results(Figures 4.1, 4.2, 4.3 and 4.7) all show that in this area the resistivity values are decreasing with depth, and in the deep zone, the sections contain low resistivity values. Though the cross sections of the other areas have a similar resistivity trend,

the anomalies are mainly limited to a small area, not to the whole section. The most likely cause for this is that there is a parallel metal pipeline near the profile.

2. For EPA-03, the two EMIGMA inversion results (Figure 5.4 and Figure 5.8) and the two STEMINV inversion results (Figure 4.4 and Figure 4.8) all indicate the same resistivity change from the shallow to the deep. There are differences between the 32Hz and 64Hz inversion results. This could be caused by the pre-processing of the raw data, including deletion of some noisy time channels. The anomalies are mainly concentrated in the east area of this profile from 0 to 60m.

3. In the area of the Aero Park Blvd. S. NS line, for the 20m loop, there are two anomalies in the deep part, from points 10m to 20m and from 50m to 100m, both in the EMIGMA (Fig 5.5 and Figure 5.9) and STEMINV results (Fig 4.5 and Figure 4.9). These are possibly caused by increased water in this zone. For the 100m loop (Fig 5.11 and Figure 5.14), there is a low resistivity feature at the first point from 760m to 740m elevation, i.e. from 30m to 50m deep. The EM31 also shows this feature.

4. In the area of Aero Park Blvd. S. EW line, the two EMIGMA inversions results (Figure 5.6 and Figure 5.10) for the 20m loop and the two STEMINV inversion results (Figure 4.6 and Figure 4.10) for the 20m loop all give a low-resistivity response in the deep part of the section, around point 360m, which also shows up in EM31 data. Between 0-20m, 200-240m and 380-400m, there are low-resistivity responses. There is a resistivity valley around the point 100m for 64Hz both in EMIGMA (Fig 5.10) and STEMINV (Fig 4.10), but which doesn't show up in 32Hz. This could be caused by the different deletion of time channels for the two methods. The 20 Ohm-m boundary in the 32Hz and 64Hz EMIGMA inversion results may be showing a basin in this area. For the 100m loop, there is a structure from points 250m to 450m with elevation of 720-750m, depth of about 30-60m. This may show an increased water concentration in this zone. Around point 400m, from 120m deep to 200m deep, there is a low-resistivity response, which is possibly a response to a pipeline. It also shows up in the EM31 profile.

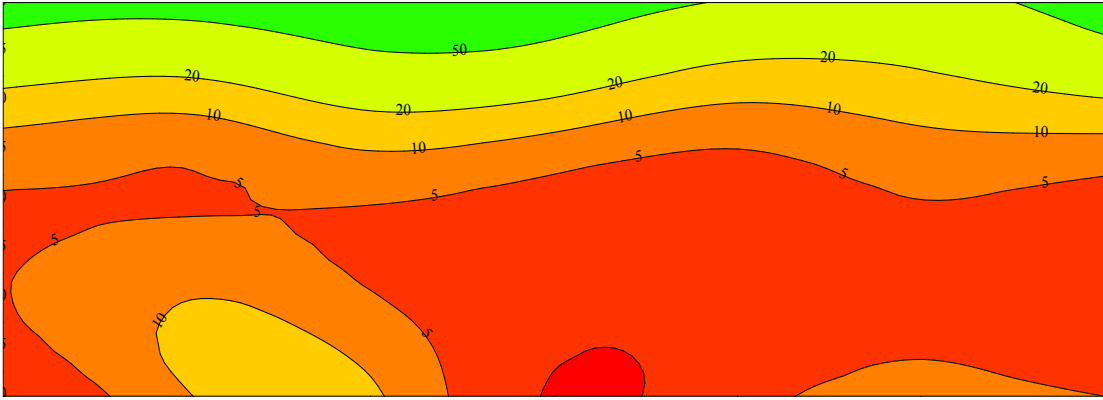


Fig 5.1 Inversion results of Samsonite North, NS line field data

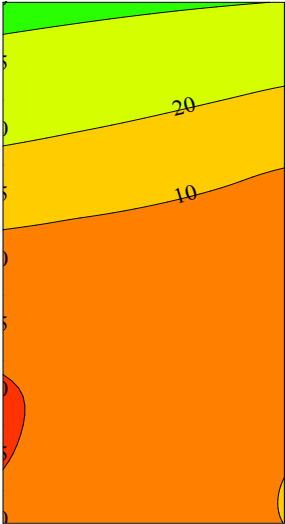


Fig 5.2 Inversion results of Samsonite North, East line field data

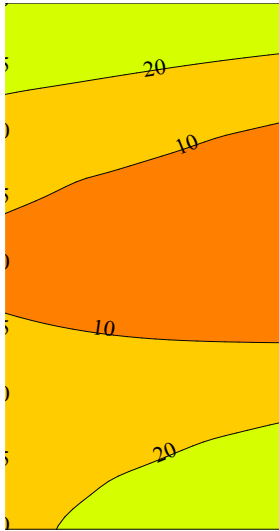


Fig 5.3 Inversion results of Samsonite North, West line field data

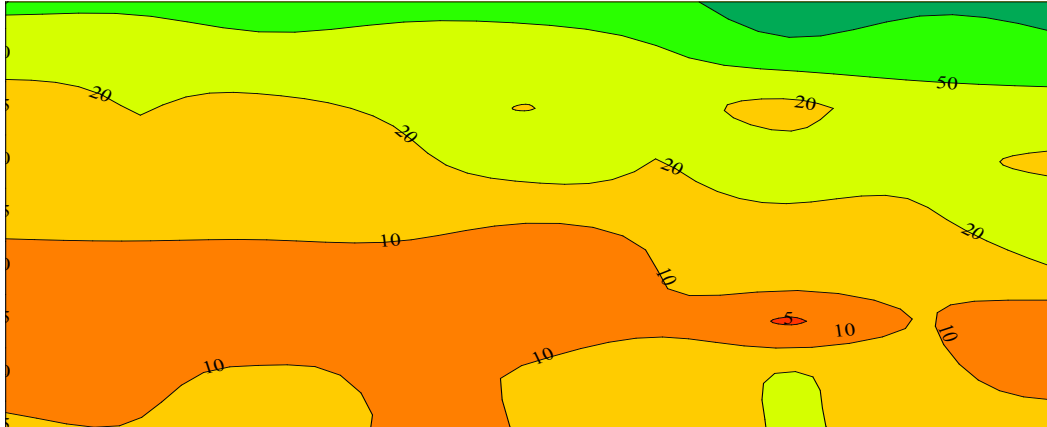


Fig 5.4 Inversion results of EPA-03, EW line field data

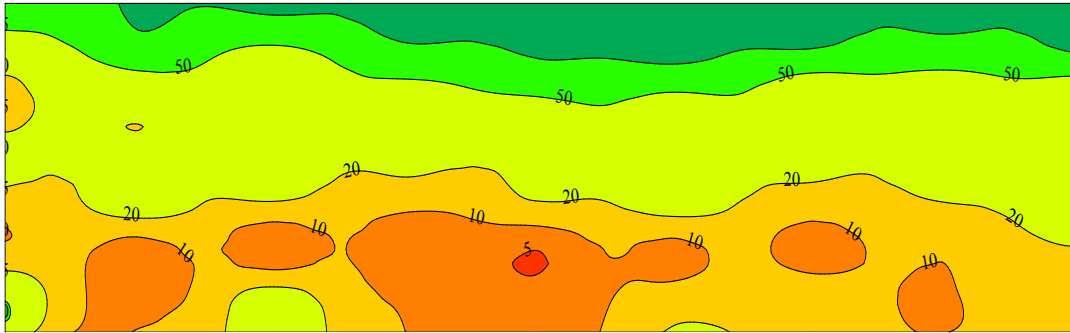


Fig 5.5 Inversion results of Aero Park Blvd. S. NS line field data

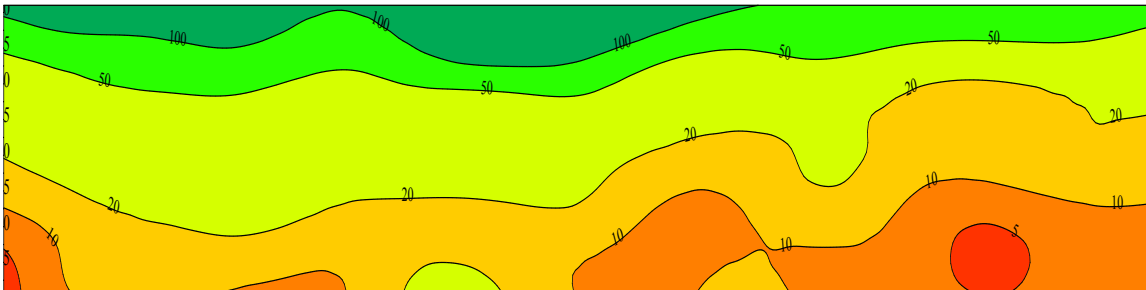


Fig 5.6 Inversion results of Aero Park Blvd. S. EW line field data

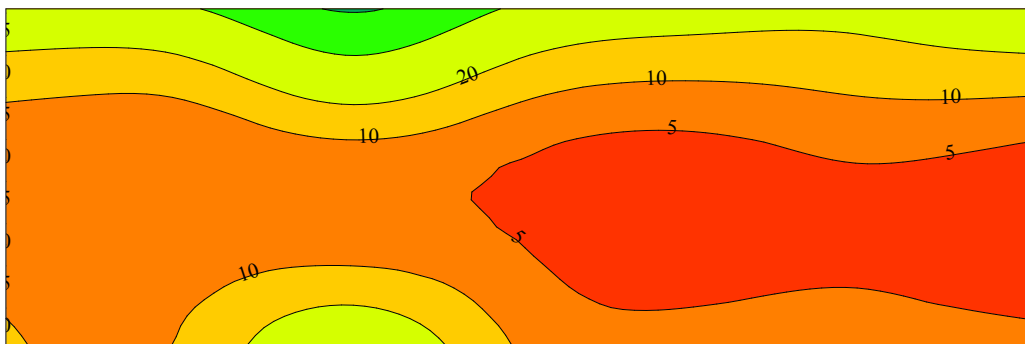


Fig 5.7 Inversion results of Samsonite North, NS line field data

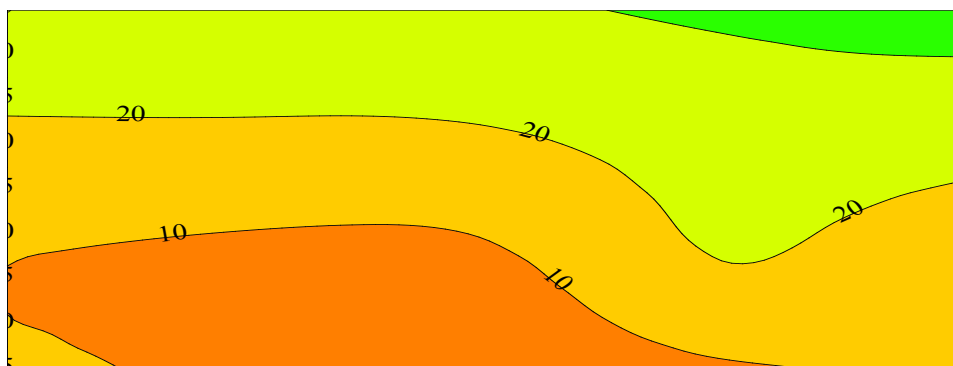


Fig 5.8 Inversion results of EPA-03, EW line field data

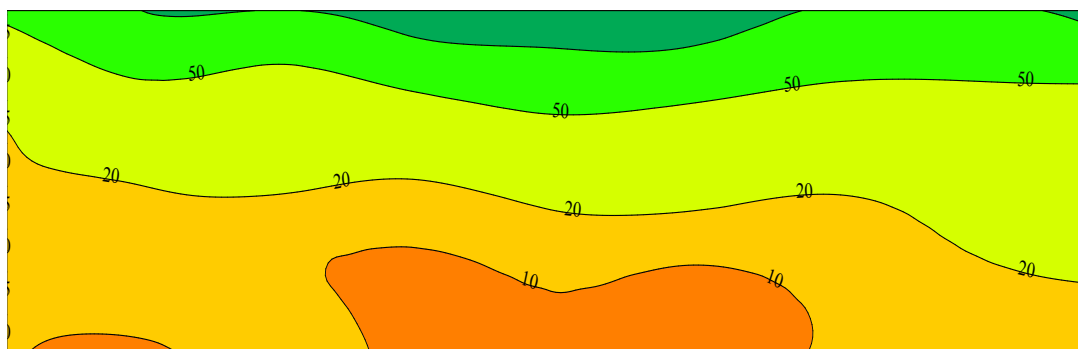


Fig 5.9 Inversion results of Aero Park Blvd. S. NS line field data

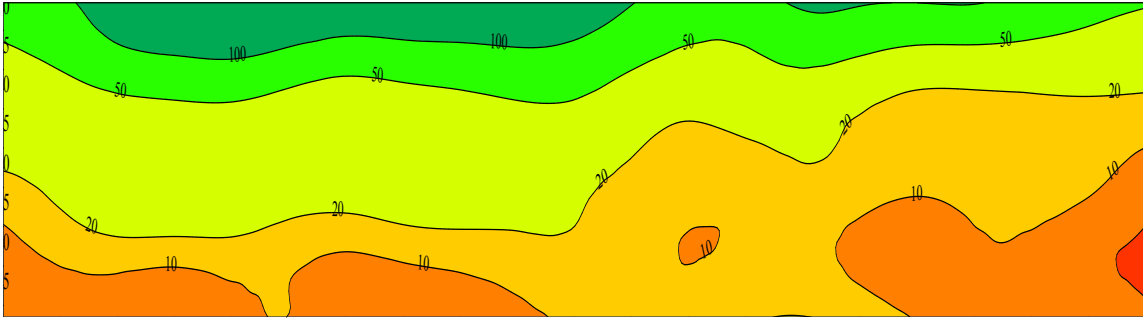


Fig 5.10 Inversion results of Aero Park Blvd. S. EW line field data

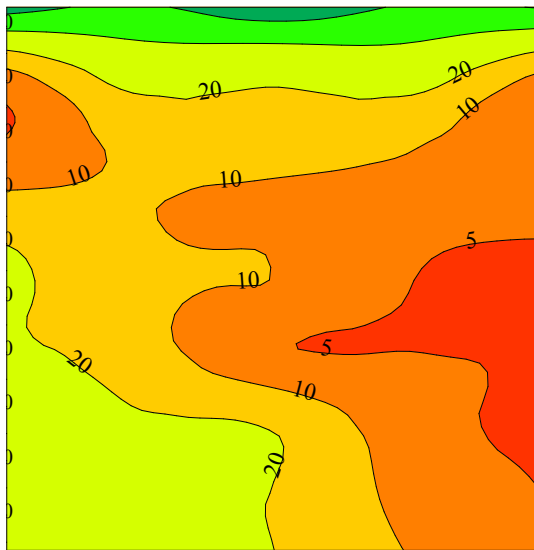


Fig 5.11 Inversion results of Aero Park Blvd. S. NS line field data

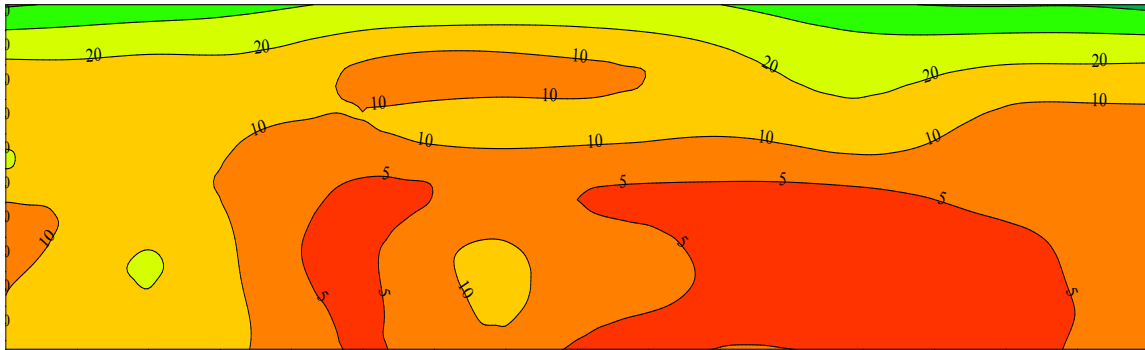


Fig 5.12 Inversion results of Aero Park Blvd. S. EW line field data

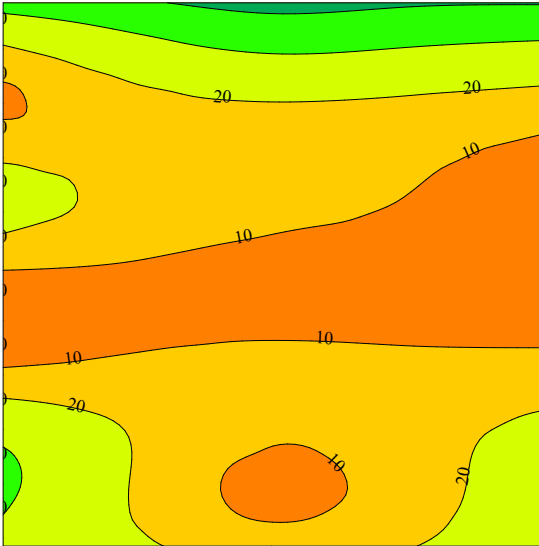


Fig 5.13 Inversion results of Aero Park Blvd. S. NS line field data

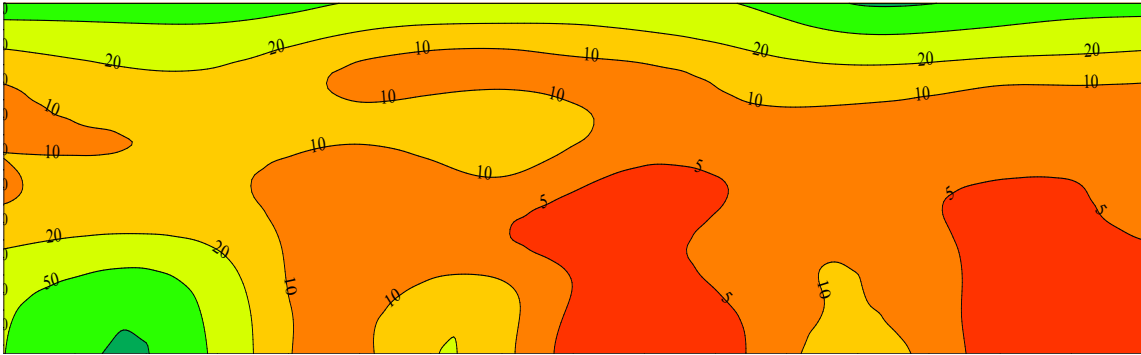


Fig 5.14 Inversion results of Aero Park Blvd. S. EW line field data

## **6. Passive Seismic Analysis**

### **6.1. Introduction**

This section focuses on the use of the passive seismic technique in order to understand the subsurface structure for our study area. H/V spectral ratio and H/V rotate analyses were performed on ambient vibrations. These techniques are implemented in low seismicity regions where the use of local seismic noise sources is a cost-effective way to gather seismic data. This method is not intended to be used as a standalone technique and should be supplemented by other methods, especially considering that it is still in its experimental stage (SESAME,2004)

H/V spectral ratio and H/V rotate analyses on ambient vibrations are useful methods for studying the characteristics of soil deposits. It provides information about the interior of the earth without the use of destructive methods. The noise source is passive and close to the seismometers which eliminates the use of an active source as in other seismic techniques. The waves produced by the noise will pass through the rocks and will be reflected and recorded by the seismometer. When the wave passes through different media, its velocity will change and thus, it can provide information about the seismic properties of the rocks in the area. A significant change in the seismic properties of the subsurface is shown as a peak on the H/V spectral ratio. However, it can only detect a high impedance contrast between layers. The near-surface shear wave velocity helps in estimating the depth and boundary of layers with different seismic properties. It is used along with the natural frequency of the soil obtained from the H/V spectral ratio.

### **6.2. Methods**

The following section describes the methods necessary to achieve the purposes of this study, including the field, processing, and analysis methods.

## 6.2a. Instrumentation and Field Procedures

The data were collected at the Aero Park Boulevard South and EPA-03 sites (Figures 6.1, 6.2, and 6.3). The measurements are based on single stations with three recorded components: north, east, and vertical. Three seismometers were used in the study, Guralp T6B75, T6B77, and A834, the latter of which was used as the base seismometer. A gravimeter plate was used throughout the survey to act as leveling plate. The duration of data recordings is shown in Table 6.1.

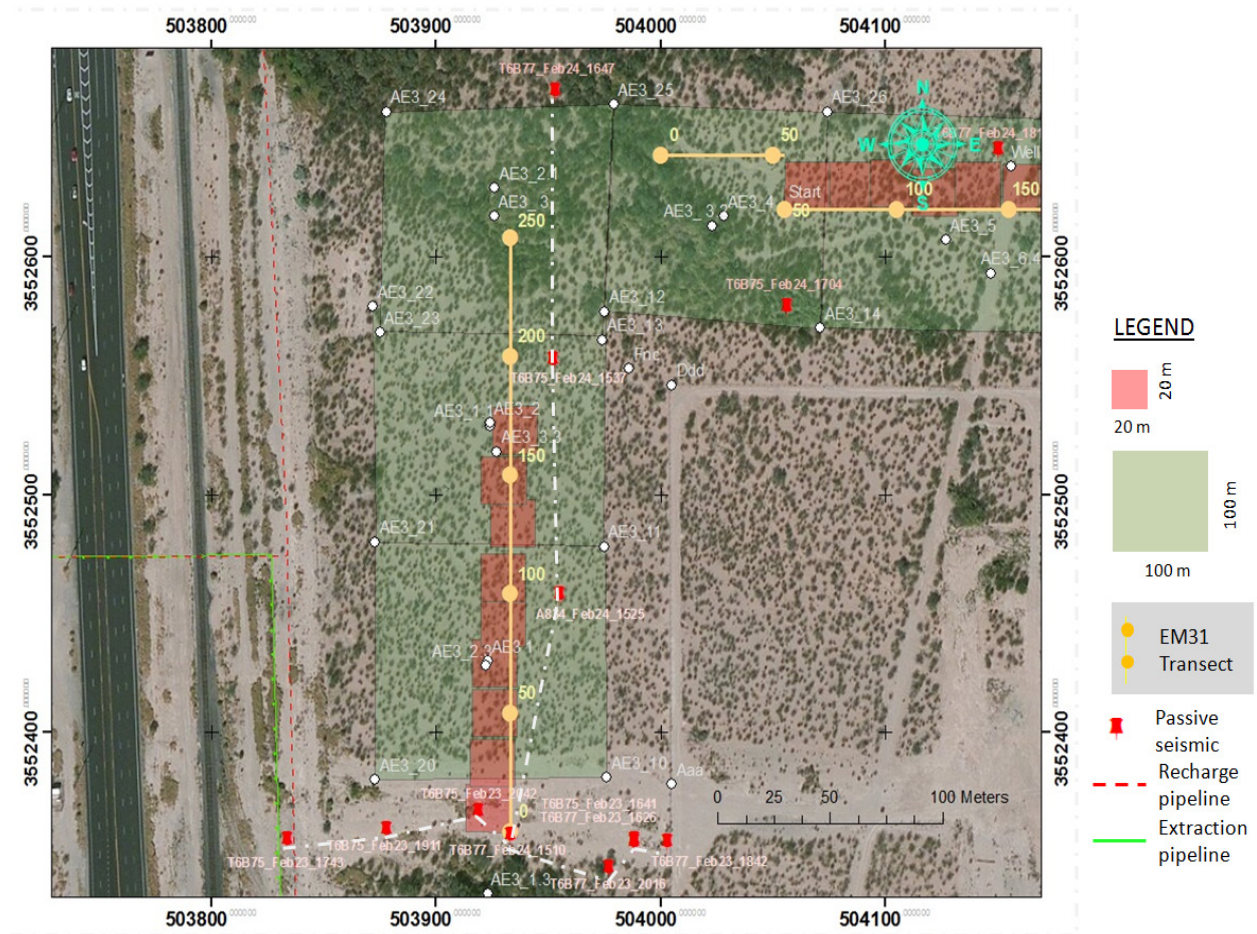


**Figure 6.1:** Map showing locations of seismometers and seismic lines 1 & 2 oriented E-W and N-S respectively in the western part of Aero Park Boulevard South. Seismometers are marked with red pins. Seismic lines are marked with a white dashed line.

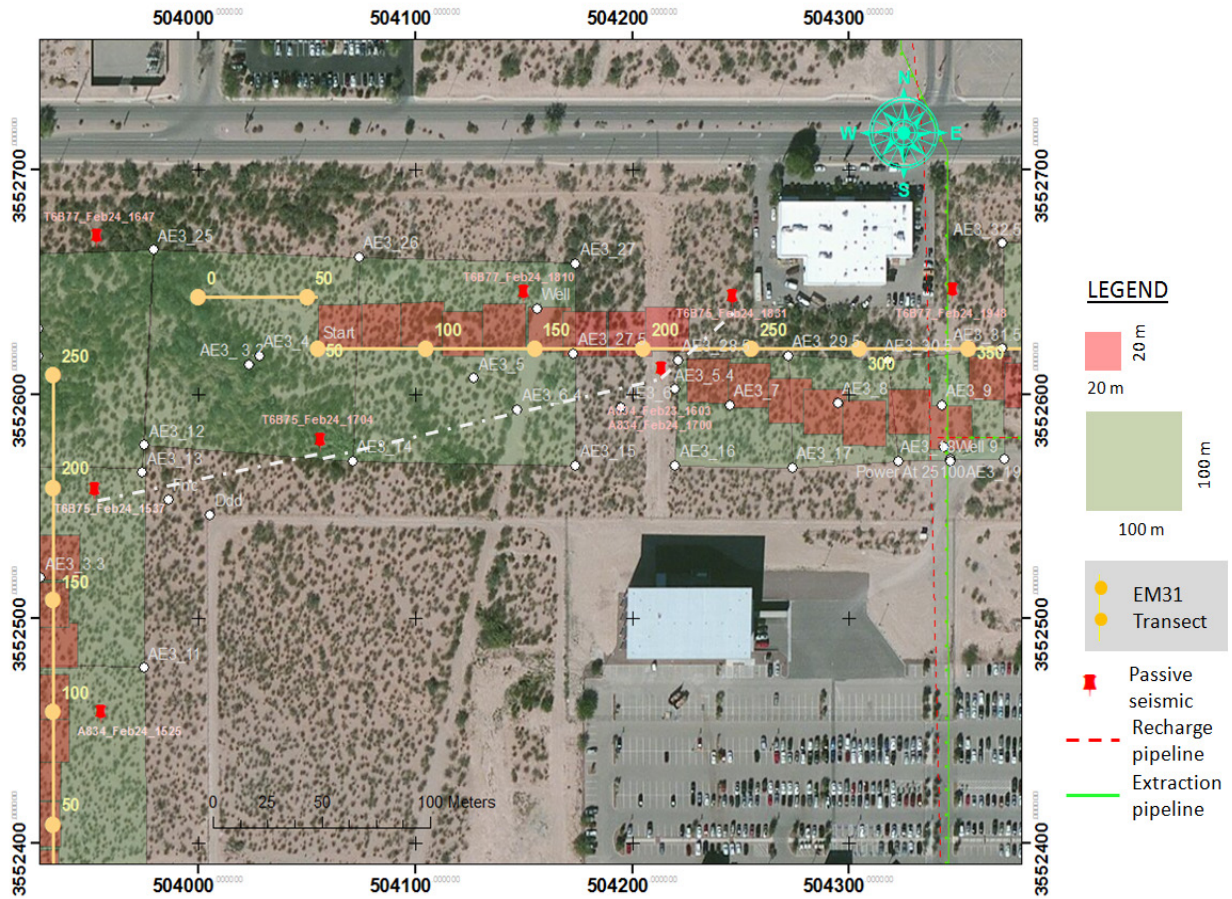


**Figure 6.2:** Map showing locations of seismometers and seismic line 3 oriented E-W in the northern part of Aero Park Boulevard South. Seismometers are marked with red pins. Seismic line is marked with a white dashed line.

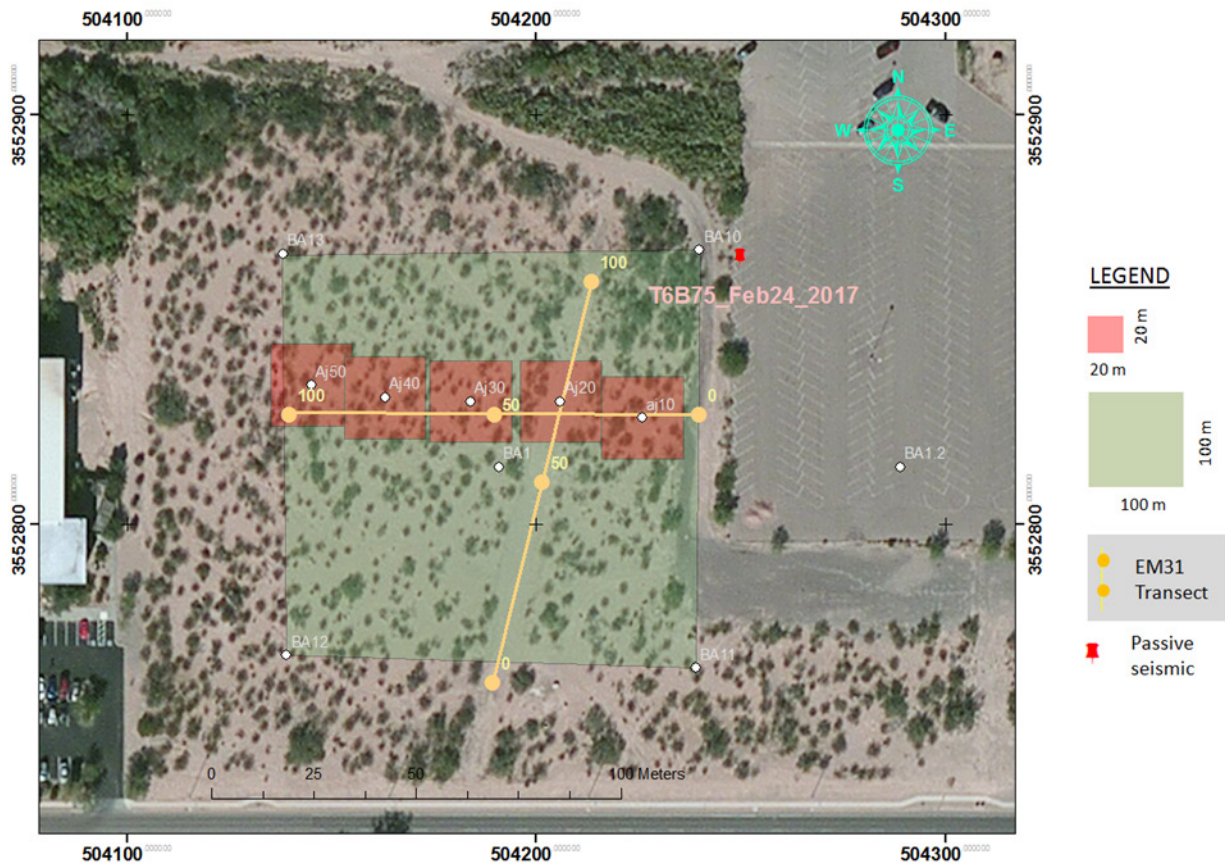


**Figure 6.3:** Map showing location of seismometer in EPA-03 site. Seismometer is marked with red pin.

**Table 6.1:** Duration of seismic recordings at each station, with their UTC coordinates. (Note: the seismometer bolded and marked with an asterisk was excluded in this study because of saturated data probably due to constant wind).

<b>Station</b> <b>(Seismometer_Date_Start</b> <b>Time (UTC))</b>	<b>Location</b>		<b>Duration</b> <b>(hours:minutes)</b>
	<b>Northing</b>	<b>Easting</b>	
T6B75_Feb23_1641	3552354	503988	0:53
T6B75_Feb23_1743	3552354	503834	1:09
T6B75_Feb23_1911	3552358	503878	1:16
T6B75_Feb23_2042	3552366	503919	2:18
T6B75_Feb24_1537	3552556	503952	1:18
T6B75_Feb24_1704	3552578	504056	1:12
T6B75_Feb24_1831	3552642	504246	1:03
T6B75_Feb24_2017	3552865	504250	1:04
A834_Feb23_1603	3552610	504214	7:03
A834_Feb24_1525	3552457	503955	1:13
A834_Feb24_1700	3552610	504214	3:58
T6B77_Feb23_1626	3552353	503988	1:33
T6B77_Feb23_1842	3552353	504003	1:27
T6B77_Feb23_2016	3552342	503977	1:01
<b><i>T6B77_Feb23_2125*</i></b>	<b><i>3552375</i></b>	<b><i>503980</i></b>	<b><i>1:42</i></b>
T6B77_Feb24_1510	3552356	503933	1:01
T6B77_Feb24_1647	3552669	503953	1:09
T6B77_Feb24_1810	3552644	504150	1:12
T6B77_Feb24_1948	3552645	504348	0:17

## **6.2b. Data Processing**

The data collected in the field were then processed by merging them and using the previously mentioned H/V and H/V Rotate analyses with the use of the Geopsy program (Wathelet et al., 2008; Di Giulio et al., 2006). A high pass filter set at 0.04 Hz was applied to the entire signal processing to remove the lower frequency ranges in order to maintain the higher frequencies, thus improving the signal-to-noise ratio. Anti-triggering on raw and filtered data was applied on some of the signals in order to remove transient noise. The anti-triggering was not applied on the signals that resulted in few or zero selected windows. Default parameters were used for window width set at 25 seconds, the Konno & Ohmachi smoothing type was set at 40, the cosine taper was set to 5% width, and the horizontal components were based on the squared average.

## **6.2c. Subsurface Interpretation of H/V Results**

The H/V spectral ratio is the ratio between the Fourier amplitude spectra of the horizontal (H) to vertical (V) components of ambient noise vibrations. H/V rotate analysis shows the H/V in the horizontal plane as a function of azimuth (SESAME, 2004). The H/V Rotate analysis is done in order to determine the source direction. If the source ranges from the azimuth values of 0 to 180 degrees, this indicates that it is being recorded by the seismometer as coming from all directions. If, on the other hand, it does not cover the entire azimuth range (i.e. it is ellipsoidal), this indicates that the source is coming from a concentrated direction. The possible sources of noise used for this passive seismic study are wind, vehicles from nearby roads, aircraft in the vicinity due to the proximity of our field site to the Tucson International Airport, vegetation and root movement near seismometers, locomotives, and pedestrian traffic.

By using the Geopsy software for signal processing (Wathelet et al., 2008; Di Giulio et al., 2006), plots of azimuth versus frequency, and H/V vs. frequency, were generated for H/V rotate and H/V ratio, respectively. A local P-wave velocity ( $V_p$ ) of 5700 ft/s for the depths of 0 to 290 meters was used from Loy (1990) (Pers. comm. Roy Johnson). The local surface S-wave velocity ( $V_s$ ) was then calculated from the determined P-wave velocity by using the equation below:

$$\sigma = \frac{V_P^2 - 2*(V_S^2)}{2*(V_P^2 - V_S^2)} \quad \text{(Equation 6.1)}$$

where  $\sigma$  is a Poisson's ratio of 0.15 for shallow unconsolidated sand (Bachrach, 2002). This yielded a  $V_s$  value of 3657.6 ft/s or 1114.8 m/s. Afterwards, the depths of the layers corresponding to H/V peaks were calculated by using the equation below (SESAME, 2004):

$$h = \frac{V_s}{4*f} \quad \text{(Equation 6.2)}$$

Here,  $V_s$  is the surface shear wave velocity,  $h$  is the depth of the layer and  $f$  is the corresponding frequency peak determined from the H/V analysis (see table 6.2). Lastly, once the layer depth has been calculated for each station, three generalized seismic cross-sections were created by matching the layer depths with the corresponding seismic measurement.

### 6.3. Data and Results

Once the data were collected and processed, the boundary depths were calculated using their corresponding H/V ratio peaks. Table 6.2 shows the calculated depths with their corresponding H/V peaks. Note that, with the exception of two measurements, only one boundary was detected. This might be due to only one boundary having a large enough impedance contrast to be detected by the passive seismic method. Additionally, the majority of the H/V ratio peaks had a frequency of 1 Hz, giving a depth range of 223 - 395 meters. In the case where a shallow boundary around 20 meters in depth was detected, it might be an artificial reading since it could only be replicated with two measurements.

Furthermore the H/V rotate, H/V peaks and photographs of some of the seismometer measurements are shown in Figures 6.4 to 6.19.

**Table 6.2:** Table showing the H/V to depth conversions. (Note: the bolded measurement with an asterisk could not be analyzed due to saturated signals from strong winds).

<b>Seismometer Measurement</b>	<b>H/V Peak 1 (Hz)</b>	<b>Depth 1 (m)</b>	<b>H/V Peak 2 (Hz)</b>	<b>Depth 2 (m)</b>
T6B75_Feb23_1641	1.119	249.1	-	-
T6B75_Feb23_1743	0.839	332.2	-	-
T6B75_Feb23_1911	0.726	383.9	-	-
T6B75_Feb23_2042	0.867	321.6	-	-
T6B75_Feb24_1537	1.013	275.1	-	-
T6B75_Feb24_1704	1.099	253.6	-	-
T6B75_Feb24_1831	1.089	255.9	-	-
T6B75_Feb24_2017	0.706	394.8	-	-
A834_Feb23_1603	0.864	322.5	-	-
A834_Feb24_1525	0.729	382.4	-	-
A834_Feb24_1700	0.950	293.3	-	-
T6B77_Feb23_1626	1.250	223.0	13.65	20.4
T6B77_Feb23_1842	1.084	257.1	14.15	19.7
T6B77_Feb23_2016	1.021	273.0	-	-
<b>T6B77_Feb23_2125*</b>	-	-	-	-
T6B77_Feb24_1510	1.024	272.1	-	-
T6B77_Feb24_1647	1.186	235.1	-	-

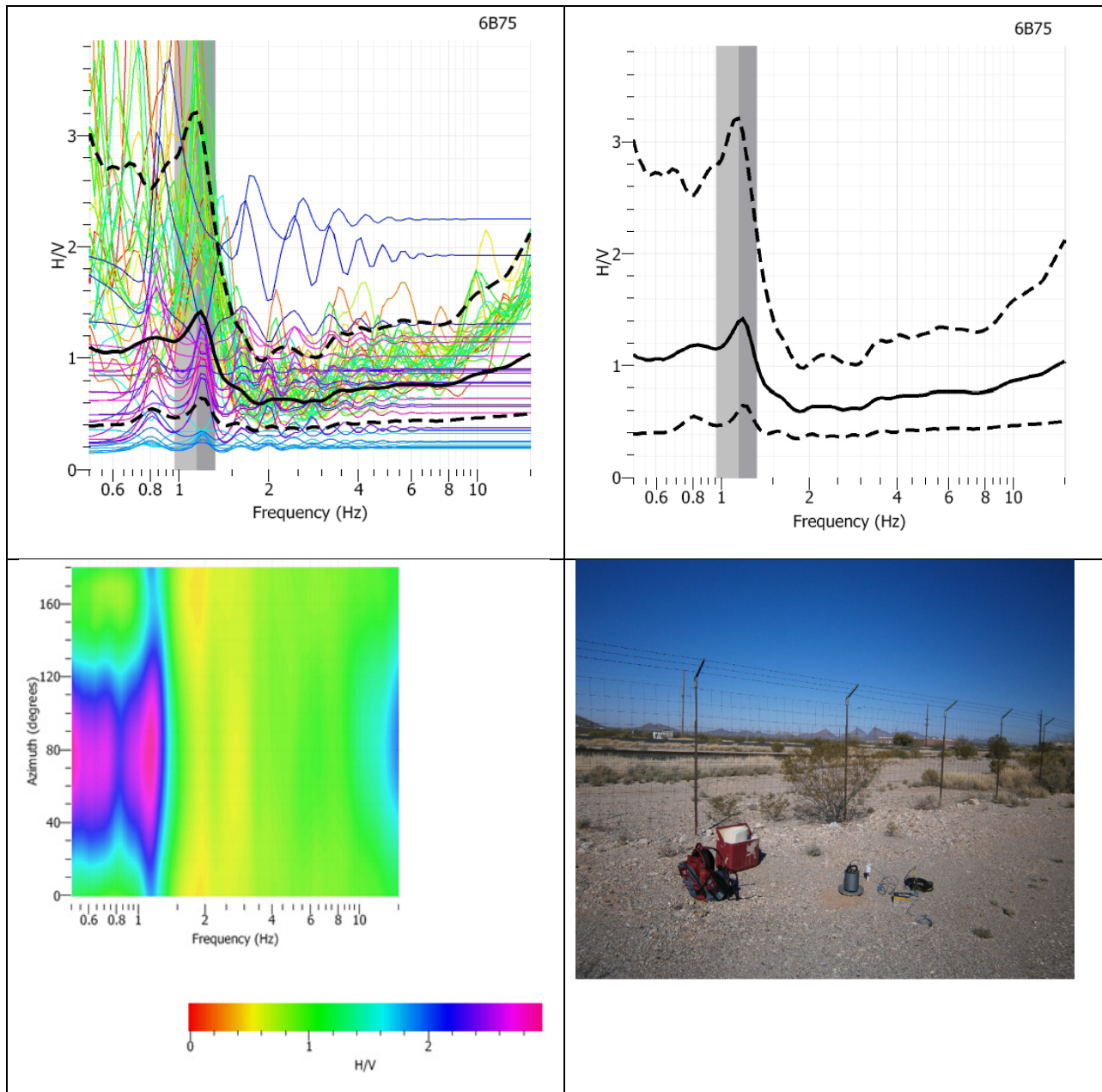
T6B77_Feb24_1810	1.093	255.1	-	-
T6B77_Feb24_1948	1.192	233.8	-	-

### 6.3a. Seismometer T6B75 H/V and H/V Rotate Analysis

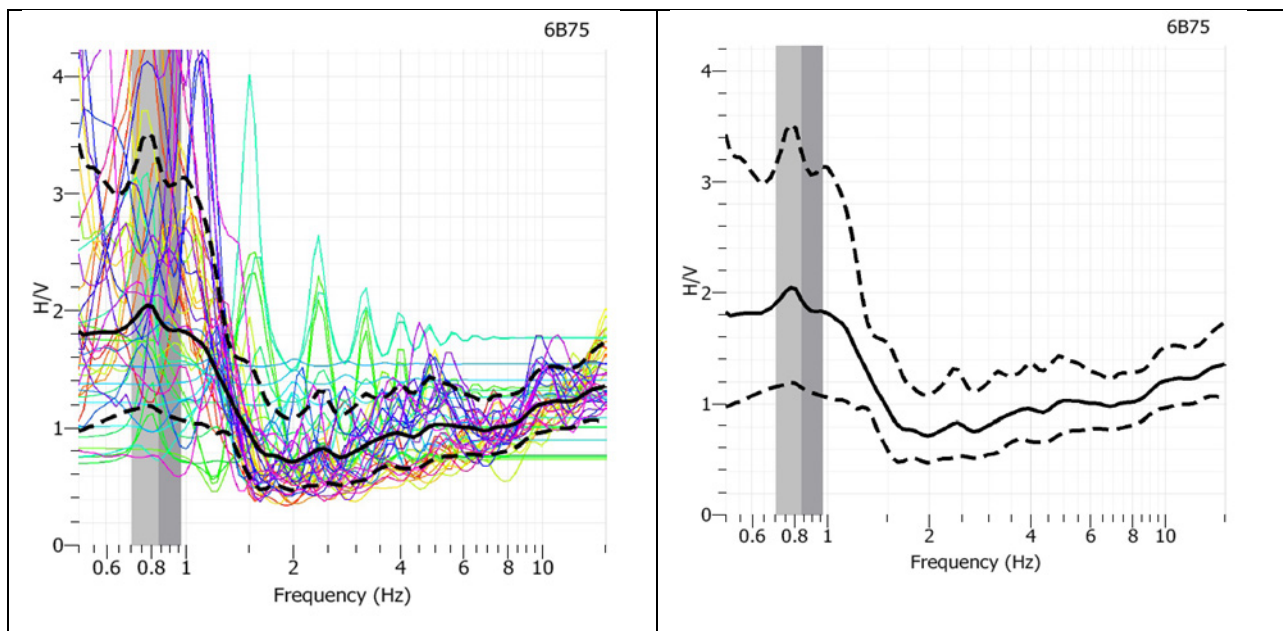
Measurements with seismometer T6B75 can be seen in Figures 6.4 through 6.11, with their corresponding H/V spectral ratios (both the average peaks and the composite of individual window peaks) from which the boundary depths were calculated, and the H/V rotate results are plotted, indicating the direction of the source of noise. In the case of the H/V spectral ratio analysis, the colored curves show the H/V spectral ratio for each of the individual windows. The solid black curve shows the average of H/V ratios and the black dotted lines are the standard deviation values.

Measurement T6B75\_Feb23\_1641 (Figure 6.4) was placed near a busy road. As is visible from the H/V analysis, there was some significant noise recorded. One peak was recorded at 1.119 Hz, with a corresponding depth of 249 meters. The source of the signal might come from several directions, but there might be a localization of the source in the road. Measurement T6B75\_Feb23\_1743 (Figure 6.5) was located close to some sparse high and low vegetation, and an observation well, also experienced some significant noise due to the proximity of vegetation. One H/V peak was detected at 0.839 Hz, which corresponds to a depth of 332 meters. The source comes from one direction. Measurement T6B75\_Feb23\_1911 (Figure 6.6) was surrounded by low vegetation, has a high signal-to-noise ratio, suggesting that low vegetation does not seem to have much effect on the seismometer readings. The source was also recorded from all directions. An H/V peak was detected at 0.726, with a corresponding depth at 384 meters. Measurement T6B75\_Feb23\_2042 (Figure 6.7) was located in a vegetation-free area halfway between nearby buildings and a busy road. There was low seismic noise and the source is concentrated in one direction. The H/V peak is 0.867 Hz, with a corresponding depth of 322 meters. Measurement T6B75\_Feb24\_1537 (Figure 6.8) had a source coming from all direction, and has an H/V peak of 1.013 Hz, which has a corresponding depth of 275 meters. Measurement T6B75\_Feb24\_1704 (Figure 6.9) had a source coming from all directions, and had some slight seismic noise. An H/V peak was detected at 1.099, with a corresponding depth of 254 meters. Measurement

T6B75\_Feb24\_1831 (Figure 6.10) had a source concentrated in one direction, and there was some slight noise. One H/V peak was detected at 1.089 Hz, giving a corresponding depth of 256 meters. Lastly, measurement T6B75\_Feb24\_2017 (Figure 6.11) had a source that was concentrated in one direction and experienced some slight noise. An H/V peak was present at 0.706 Hz with a corresponding depth at 395 meters. The majority of the H/V spectral peaks were detected around 1 Hz, indicating that only one boundary had a large enough acoustic impedance to be detected.



**Figure 6.4:** Measurement T6B75\_Feb23\_1641 (and T6B75\_Feb23\_1743) with (a) individual H/V window peaks, (b) mean H/V peak of 1.119 Hz (corresponding depth: 249.06 m), and (c) H/V rotate analysis, indicating a seismic source that seems to arrive in the directions between 40 and 120 degrees, and (d) a photograph showing the seismometer measurement taken approximately 70 meters from a busy road.



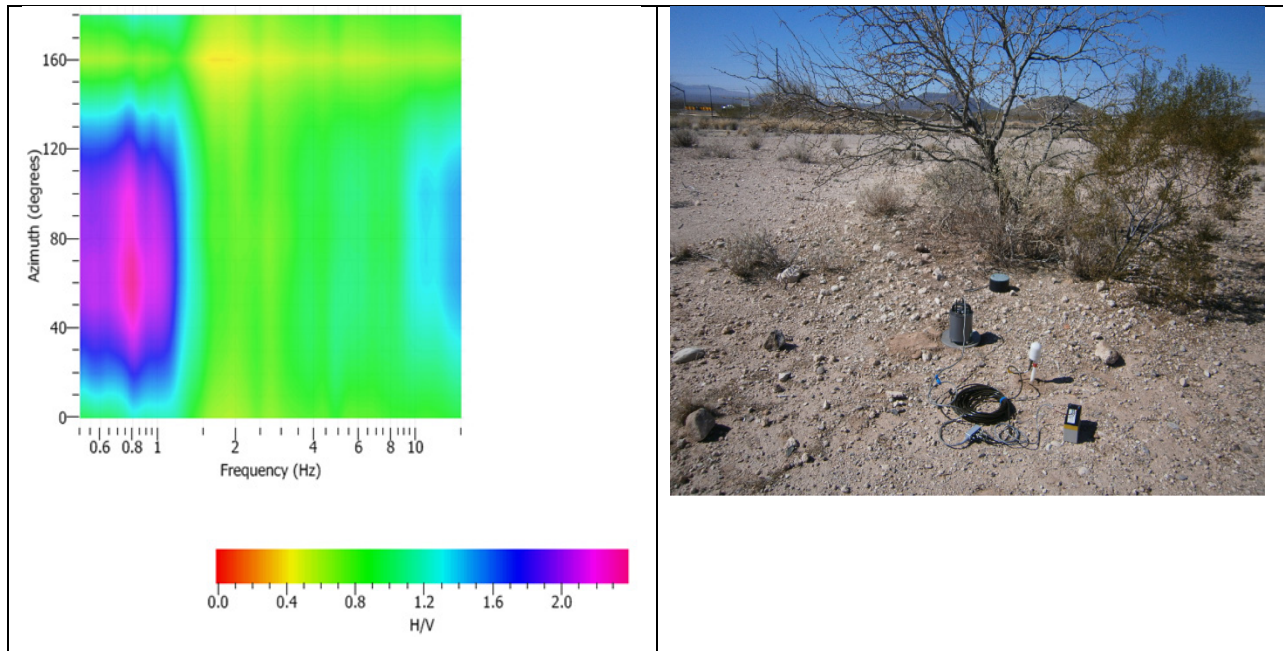


**Figure 6.5:** Seismometer measurement T6B75\_Feb23\_1743 with (a) individual H/V window peaks, (b) mean H/V peak of 0.839 Hz (corresponding depth: 332.18 m), and (c) H/V rotate analysis, indicating a seismic source that seems to arrive in the directions between 10 and 130 degrees, and (d) a photograph showing the seismometer measurement taken approximately close to taller, sparse vegetation and an observation well.

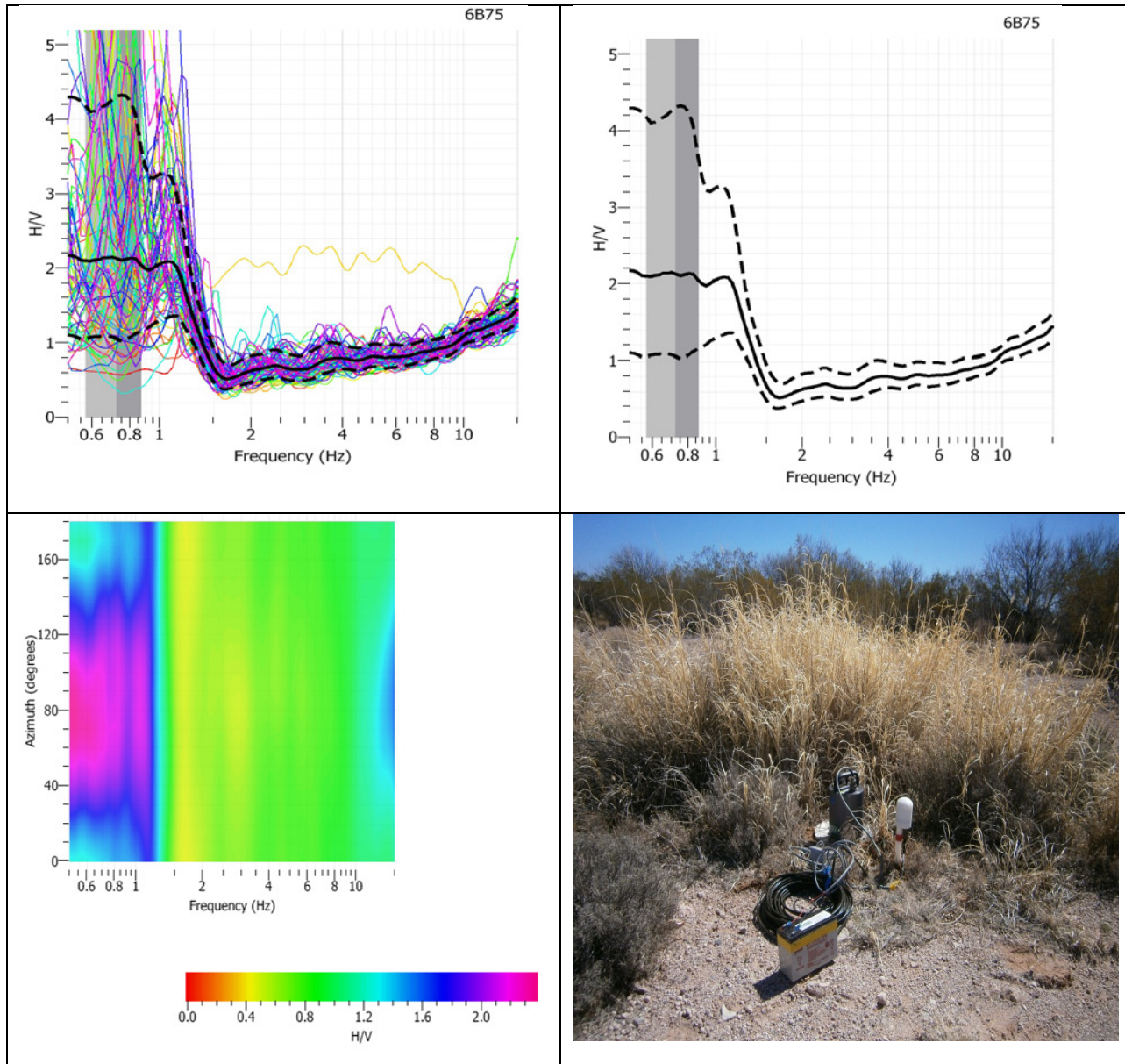


**Figure 6.6:** Seismometer measurement T6B75\_Feb23\_1911 with (a) individual H/V window peaks, (b) mean H/V peak of 0.726 Hz (corresponding depth: 383.88 m), and (c) H/V rotate analysis, indicating a seismic source that seems to arrive in the directions between 40 and 120 degrees, and (d) a photograph showing the seismometer measurement taken close to low vegetation.

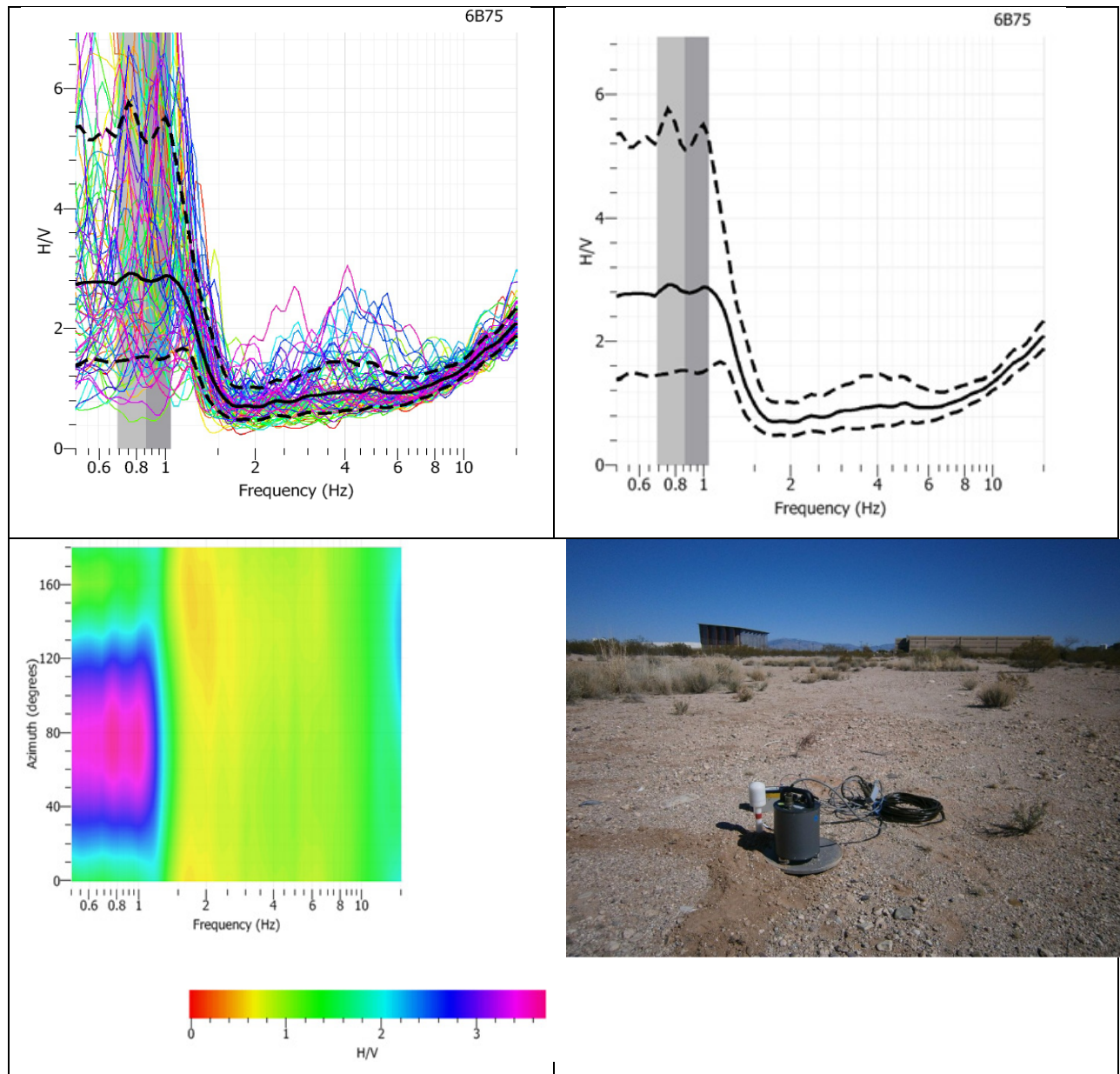


**Figure 6.7:** Seismometer measurement T6B75\_Feb23\_2042 with (a) individual H/V window peaks, (b) mean H/V peak of 0.867 Hz (corresponding depth: 321.45 m), and (c) H/V rotate analysis, indicating a seismic source that seems to arrive in the directions between 40 and 120 degrees, and (d) a photograph showing the seismometer measurement taken halfway between nearby buildings and busy road.

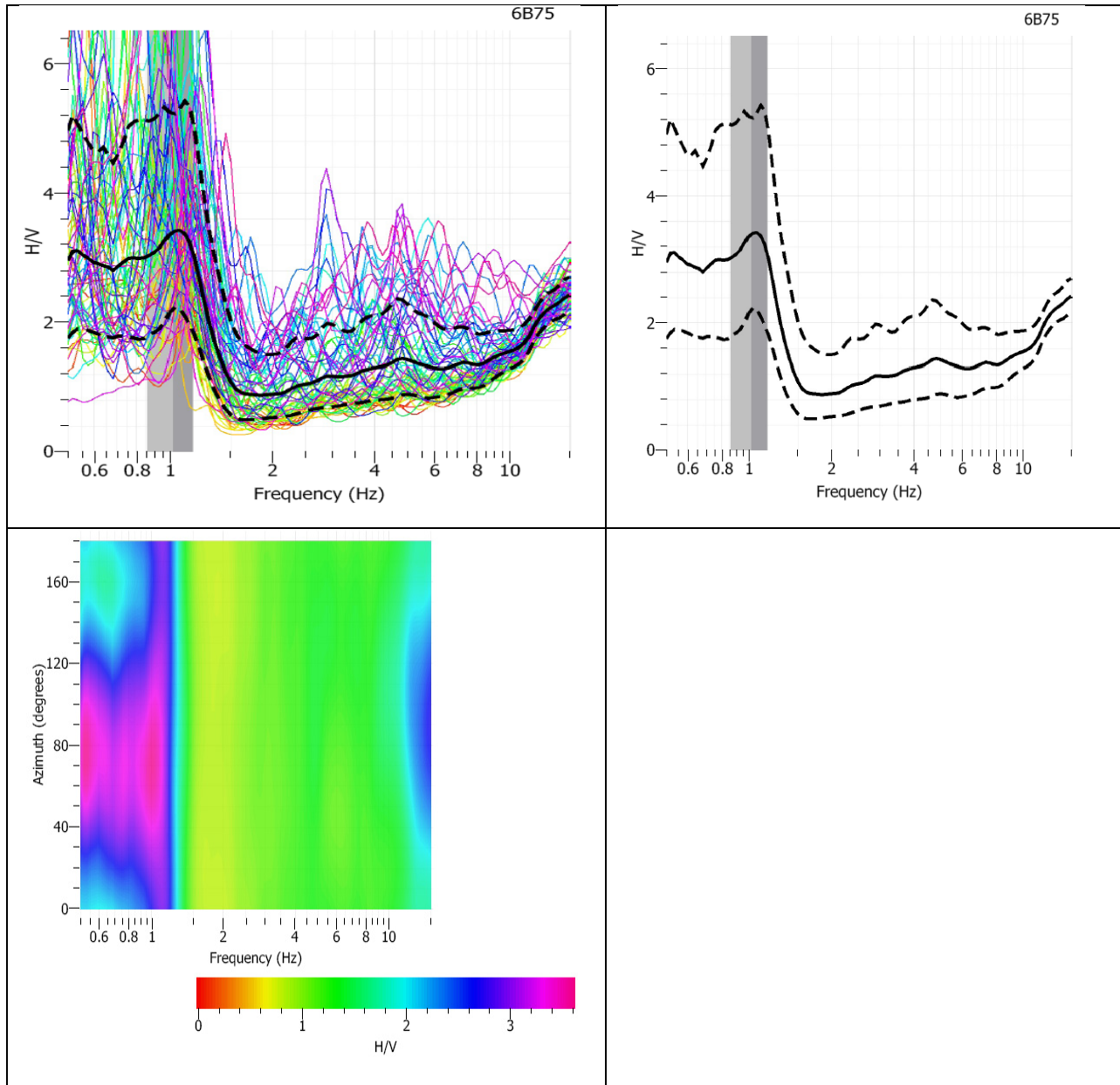


**Figure 6.8:** Seismometer measurement T6B75\_Feb24\_1537 with (a) individual H/V window peaks, (b) mean H/V peak of 1.013 Hz (corresponding depth: 275.1 m), and (c) H/V rotate analysis, indicating a seismic source that seems to arrive from all directions.

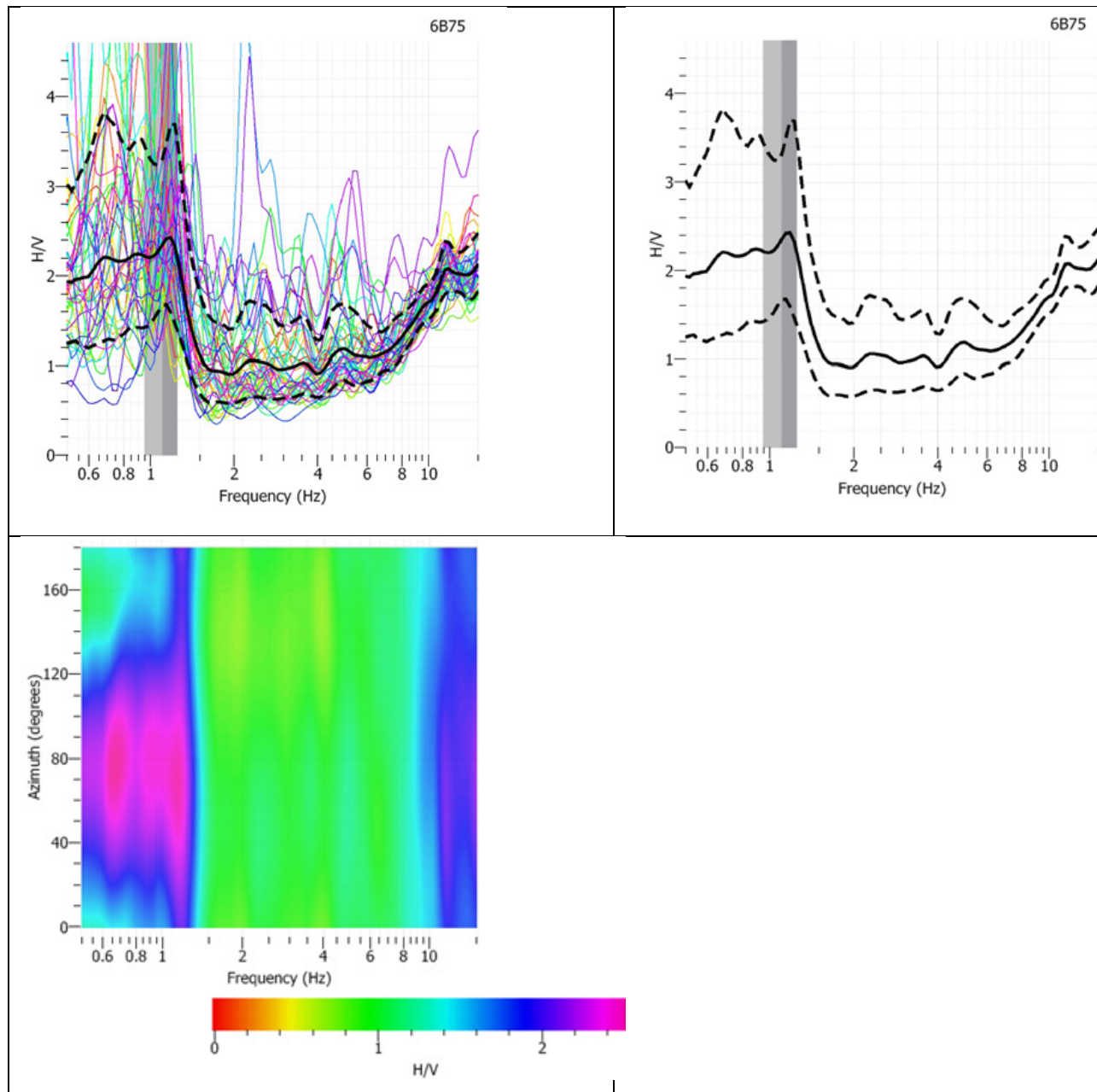


**Figure 6.9:** Seismometer measurement T6B75\_Feb24\_1704 with (a) individual H/V window peaks, (b) mean H/V peak of 1.099 Hz (corresponding depth: 253.59 m), and (c) H/V rotate analysis, indicating a seismic source that seems to arrive from 40 – 120 degrees.

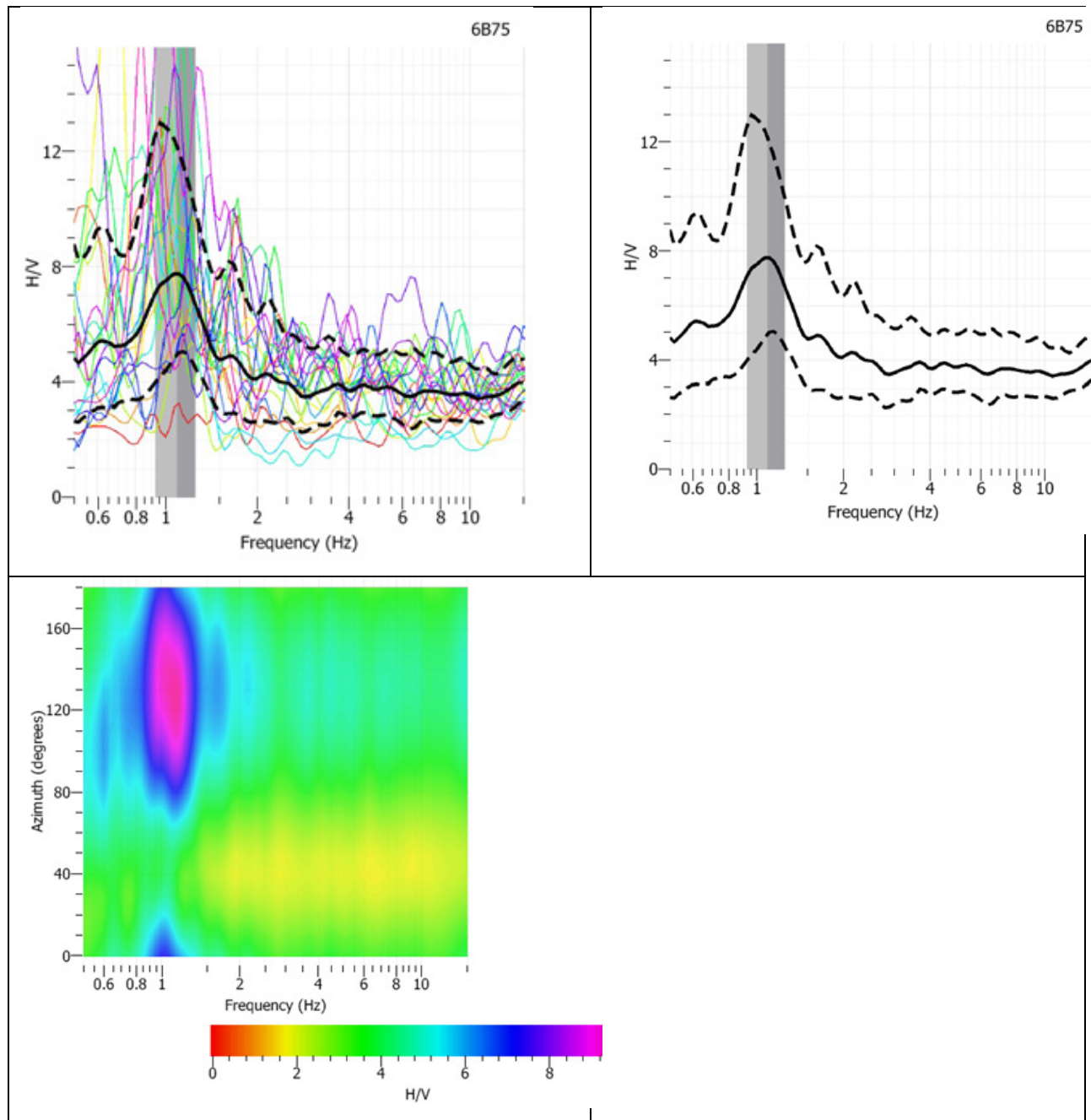


**Figure 6.10:** Seismometer measurement T6B75\_Feb24\_1831 with (a) individual H/V window peaks, (b) mean H/V peak of 1.089 Hz (corresponding depth: 255.92 m), and (c) H/V rotate analysis, indicating a seismic source that seems to be concentrated in one direction along azimuths between 80 and 180 degrees.

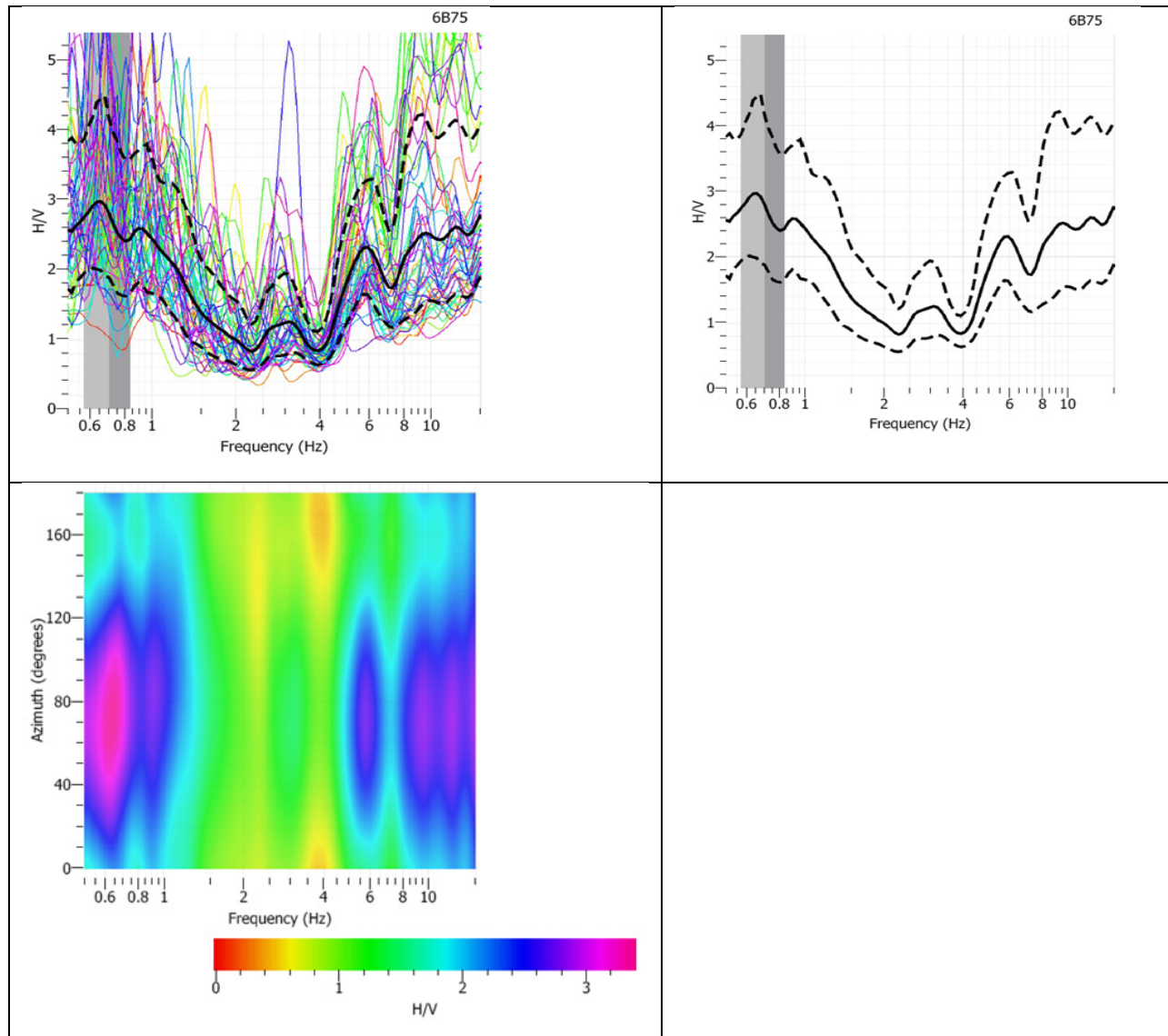


**Figure 6.11:** Seismometer measurement T6B75\_Feb24\_2017 with (a) individual H/V window peaks, (b) mean H/V peak of 0.706 Hz (corresponding depth: 394.76 m), and (c) H/V rotate analysis, indicating a seismic source that seems to be concentrated in one direction, at EPA-03.

### **6.3b. Seismometer T6B77 H/V and H/V Rotate Analysis**

This section focuses on the H/V and H/V rotate analyses for seismometer measurements for the Guralp T6B77 presented in Figures 6.12 through 6.18. Seismometer measurement T6B77\_Feb23\_1626, which was taken in an open area with no nearby vegetation (Figure 6.12) has a mean H/V peak 1 of 1.25 Hz, with a corresponding depth of 223 m, and a mean peak 2 of 13.65 Hz, which corresponds to a depth of 20.4 m. Its H/V rotate analysis, indicating a seismic source that seems to arrive in all directions. Seismometer measurement T6B77\_Feb23\_1842 was taken near an electrified fence (Figure 6.13). It has a mean H/V peak 1 of 1.084 Hz, with a corresponding depth of 257 m, and a mean peak 2 of 14.15 Hz, which corresponds to a depth of 19.7m. Its H/V rotate analysis indicates a seismic source that seems to arrive from all directions. Seismometer measurement T6B77\_Feb23\_2016, taken near a tall tree with roots beneath the seismometer (Figure 6.14) has a mean H/V peak of 1.021 Hz that corresponds to a depth of 273 m. Its H/V rotate analysis suggests a seismic source that seems to arrive from all directions. Seismometer measurement T6BD77\_Feb24\_1510 (Figure 6.15) has a mean H/V peak 1.024 Hz, and corresponding depth of 272 m. Its H/V rotate analysis implies a seismic source that seems to arrive from all directions. Seismometer measurement T6B77\_Feb24\_1647 (Figure 6.16) has a mean H/V peak of 1.186 Hz and has a corresponding depth of 235 m. Its H/V rotate analysis indicates seismic sources that concentrate from north and south. Seismometer measurement T6B77\_Feb24\_1810 (Figure 6.17) has a mean peak at 1.092 Hz and has a corresponding depth of 255m. Its H/V rotate analysis indicates seismic sources from all direction. Seismometer measurement T6B77\_Feb24\_1948 (Figure 6.18) with (a) has a mean H/V peak at 1.192 Hz, with corresponding depth of 234 m. Its H/V rotate analysis suggests seismic sources that arrive from all directions.

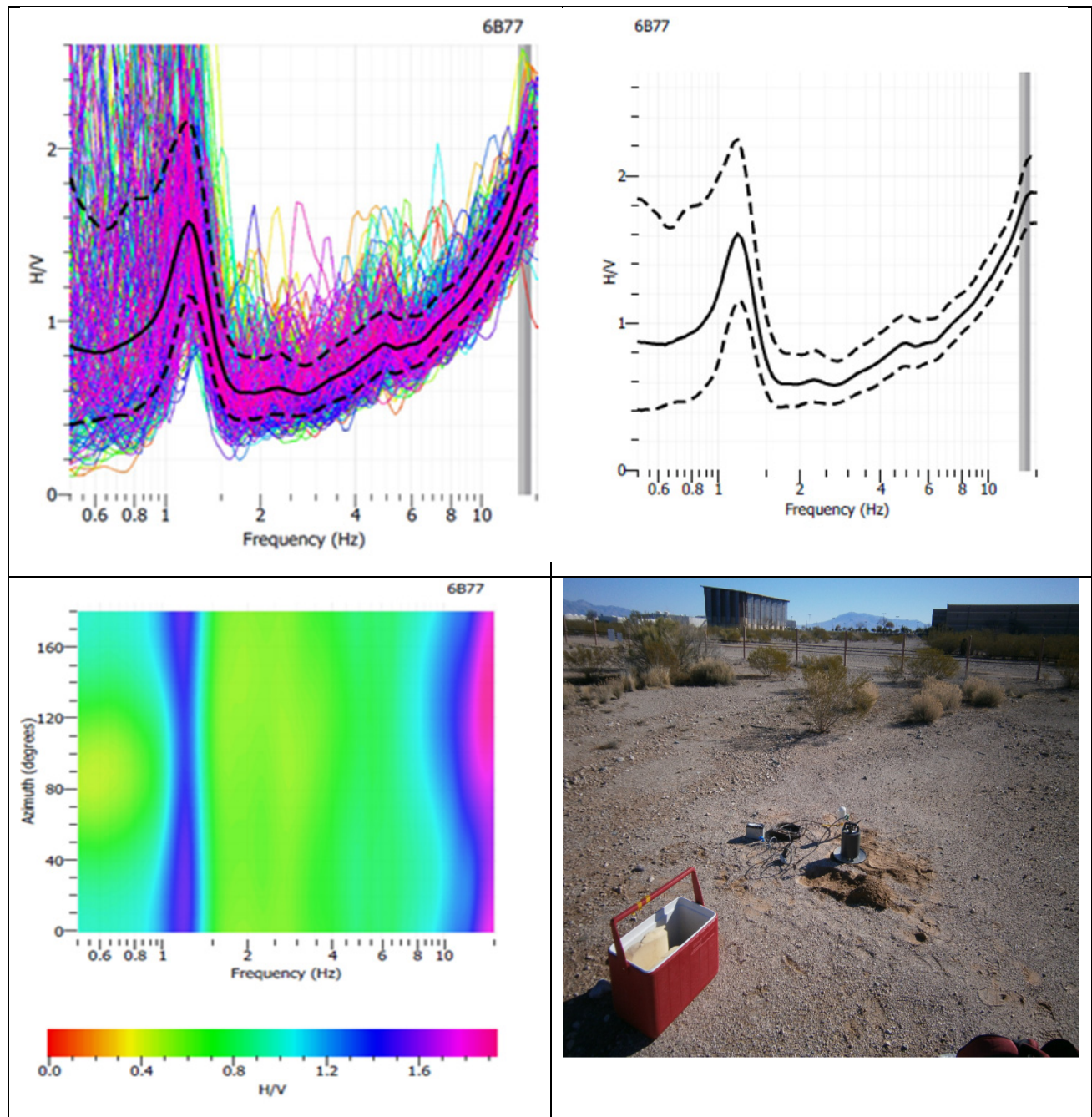


**Figure 6.12:** Seismometer measurement T6B77\_Feb23\_1626 with (a) individual H/V window peaks, (b) mean H/V peak 1 of 1.25 Hz (corresponding depth: 223 m), and mean peak 2 of 13.65 Hz (corresponding depth: 20.4 m) and (c) H/V rotate analysis, indicating a seismic source that seems to arrive in all directions, and (d) a photograph showing the seismometer measurement taken in an open area with no nearby vegetation.

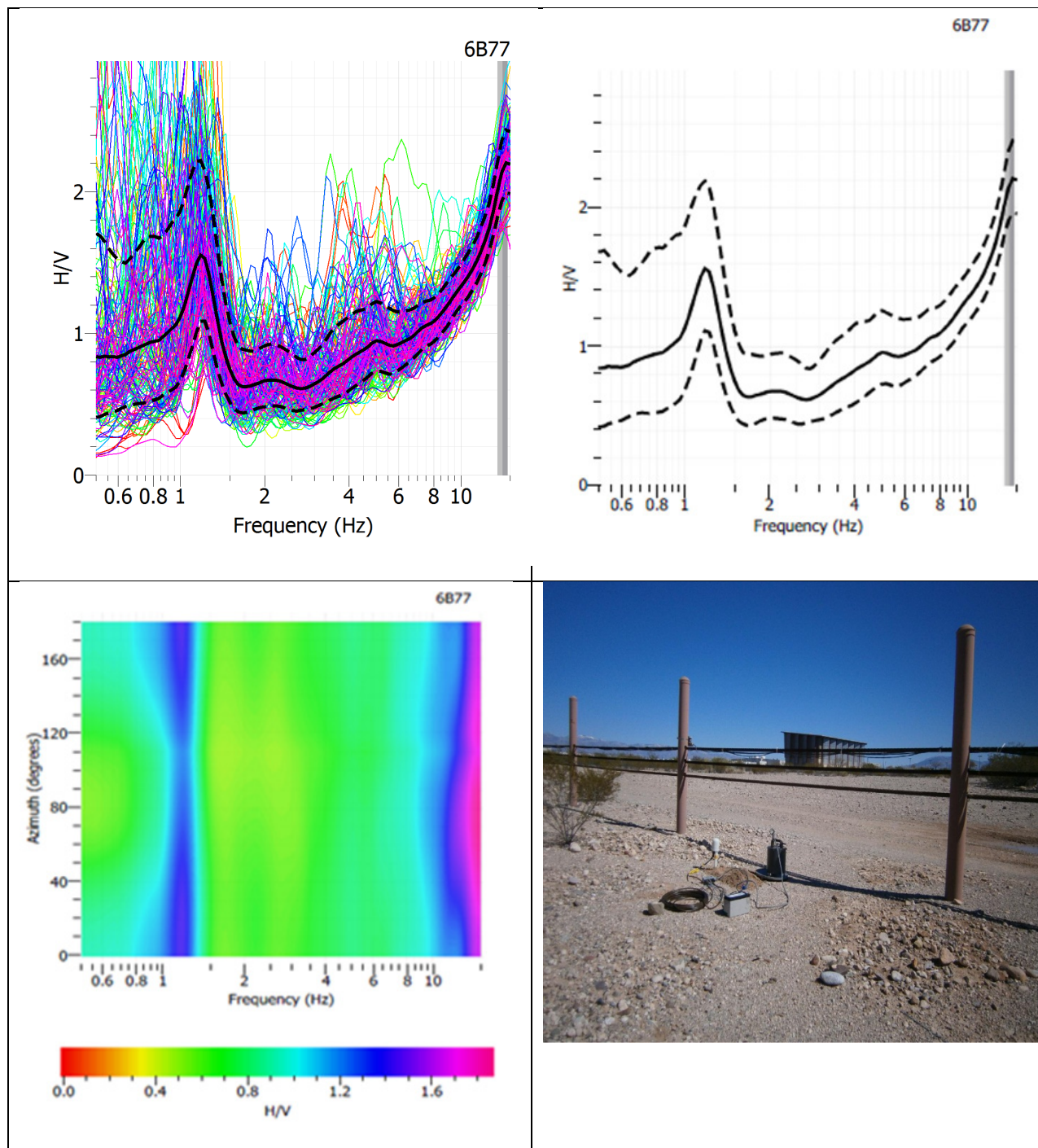


**Figure 6.13:** Seismometer measurement T6B77\_Feb23\_1842 with (a) individual H/V window peaks, (b) mean H/V peak 1 of 1.084 Hz (corresponding depth: 257.1 m), and mean peak 2 of 14.15 Hz (corresponding depth: 19.69m) and (c) H/V rotate analysis, indicating a seismic source that seems to arrive from all directions, and (d) a photograph showing the seismometer measurement taken close to an electrified fence.

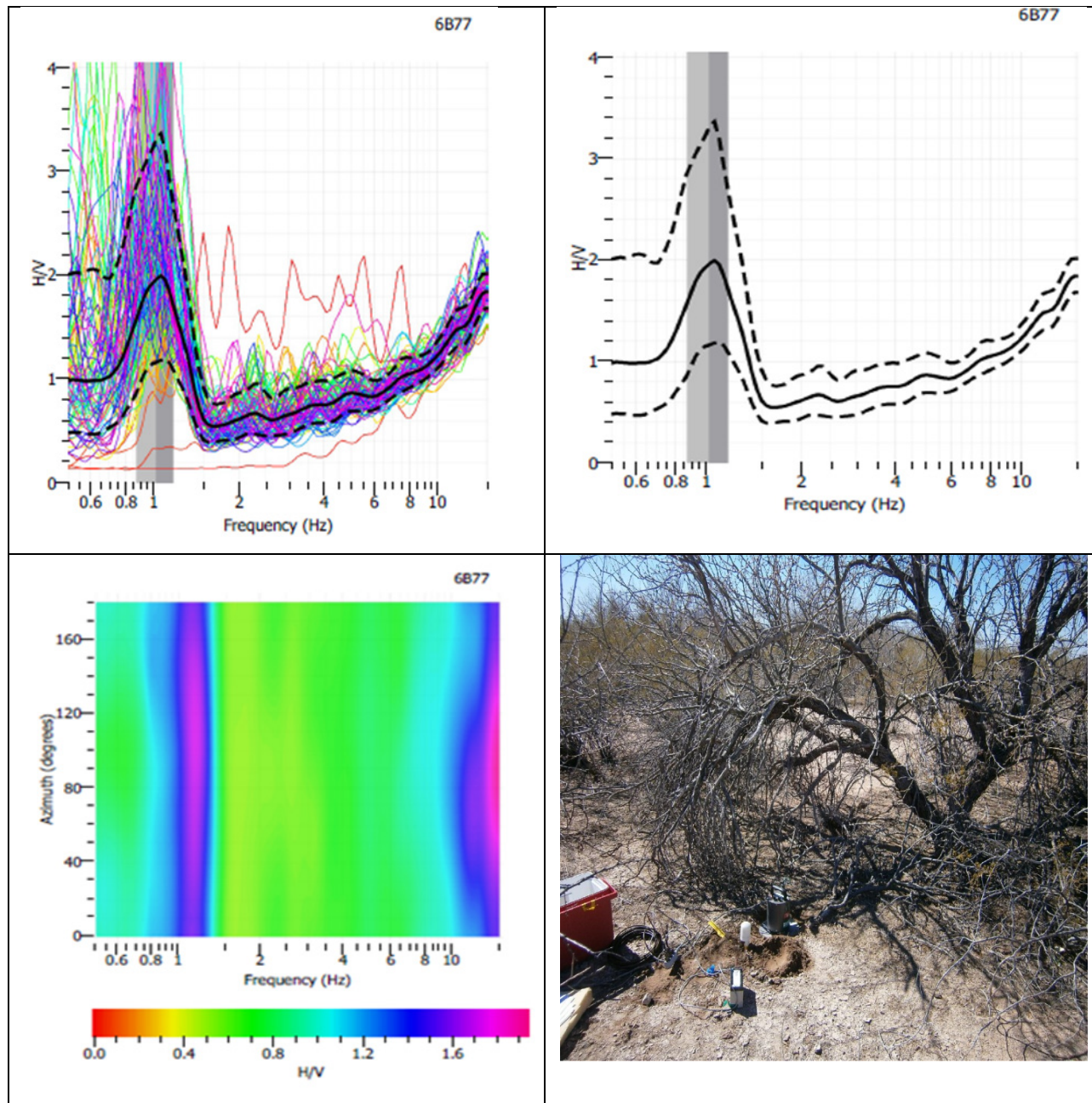


**Figure 6.14:** Seismometer measurement T6B77\_Feb23\_2016 with (a) individual H/V window peaks, (b) mean H/V peak of 1.021 Hz (corresponding depth: 273 m) and (c) H/V rotate analysis, indicating a seismic source that seems to arrive from all directions, and (d) a photograph showing the seismometer measurement taken by a tall tree with roots beneath the seismometer.

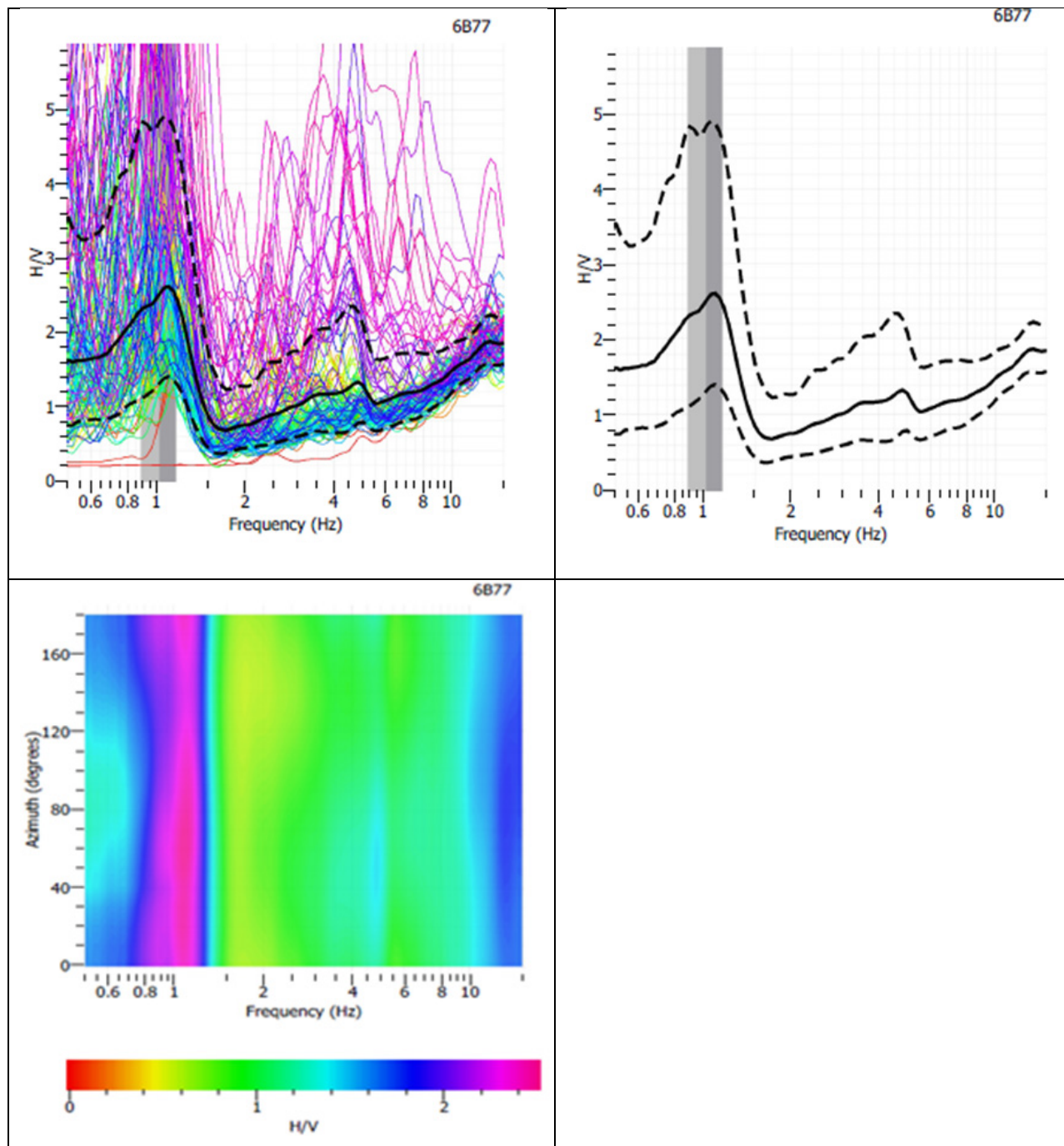


**Figure 6.15:** Seismometer measurement T6BD77\_Feb24\_1510 with (a) individual H/V window peaks, (b) mean H/V peak 1.024 Hz (corresponding depth: 272.1 m) and (c) H/V rotate analysis, indicating a seismic source that seems to arrive from all directions.

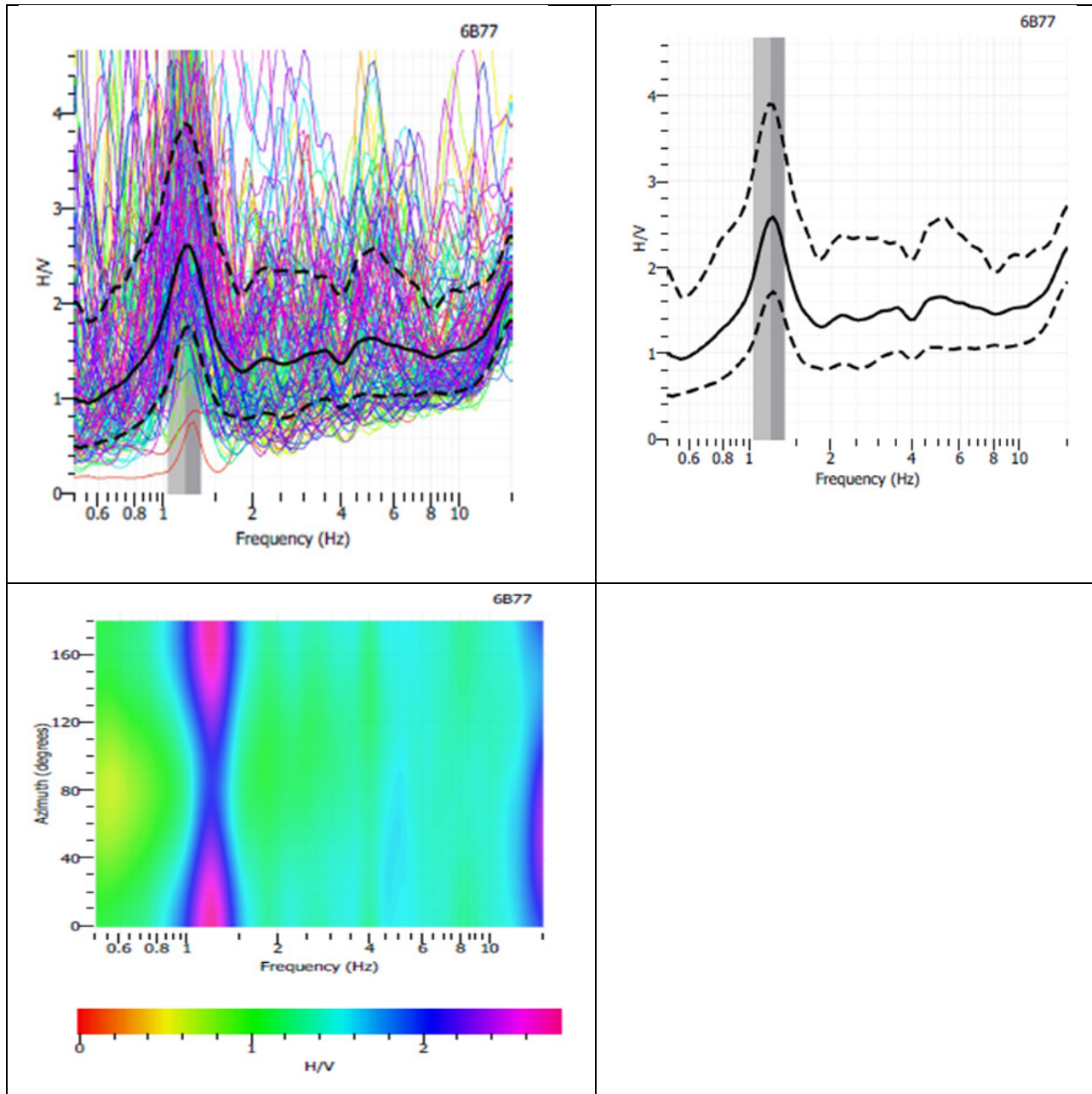


**Figure 6.16:** Seismometer measurement T6B77\_Feb24\_1647 with (a) individual H/V window peaks, (b) mean H/V peak 1.186 Hz (corresponding depth: 235.1 m) and (c) H/V rotate analysis, indicating seismic sources that concentrate from north and south.

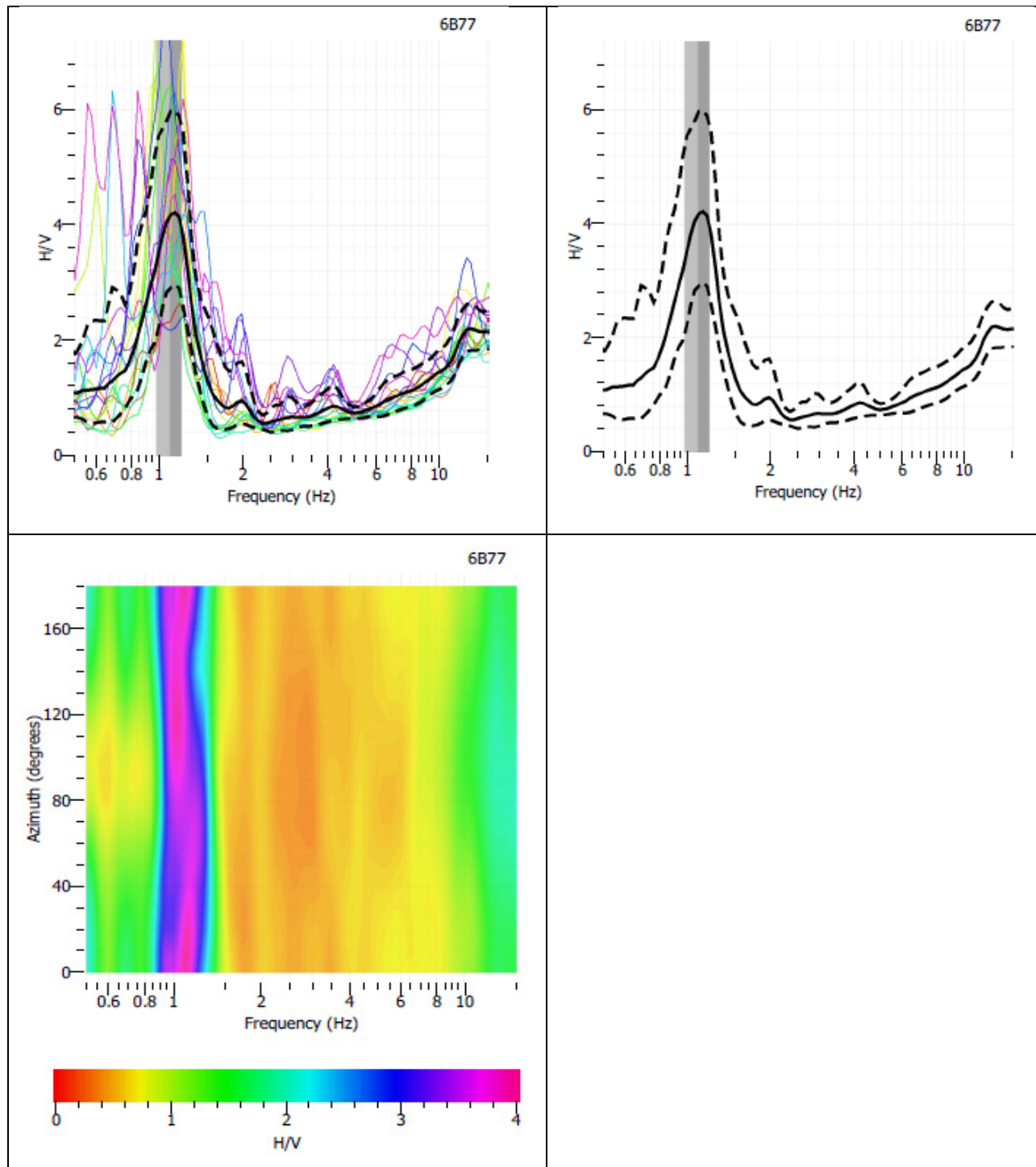


**Figure 6.17:** Seismometer measurement T6B77\_Feb24\_1810 with (a) individual H/V window peaks, (b) mean H/V peak at 1.092Hz (corresponding depth: 235.06m) (c)H/V rotate analysis, indicating source from all direction.

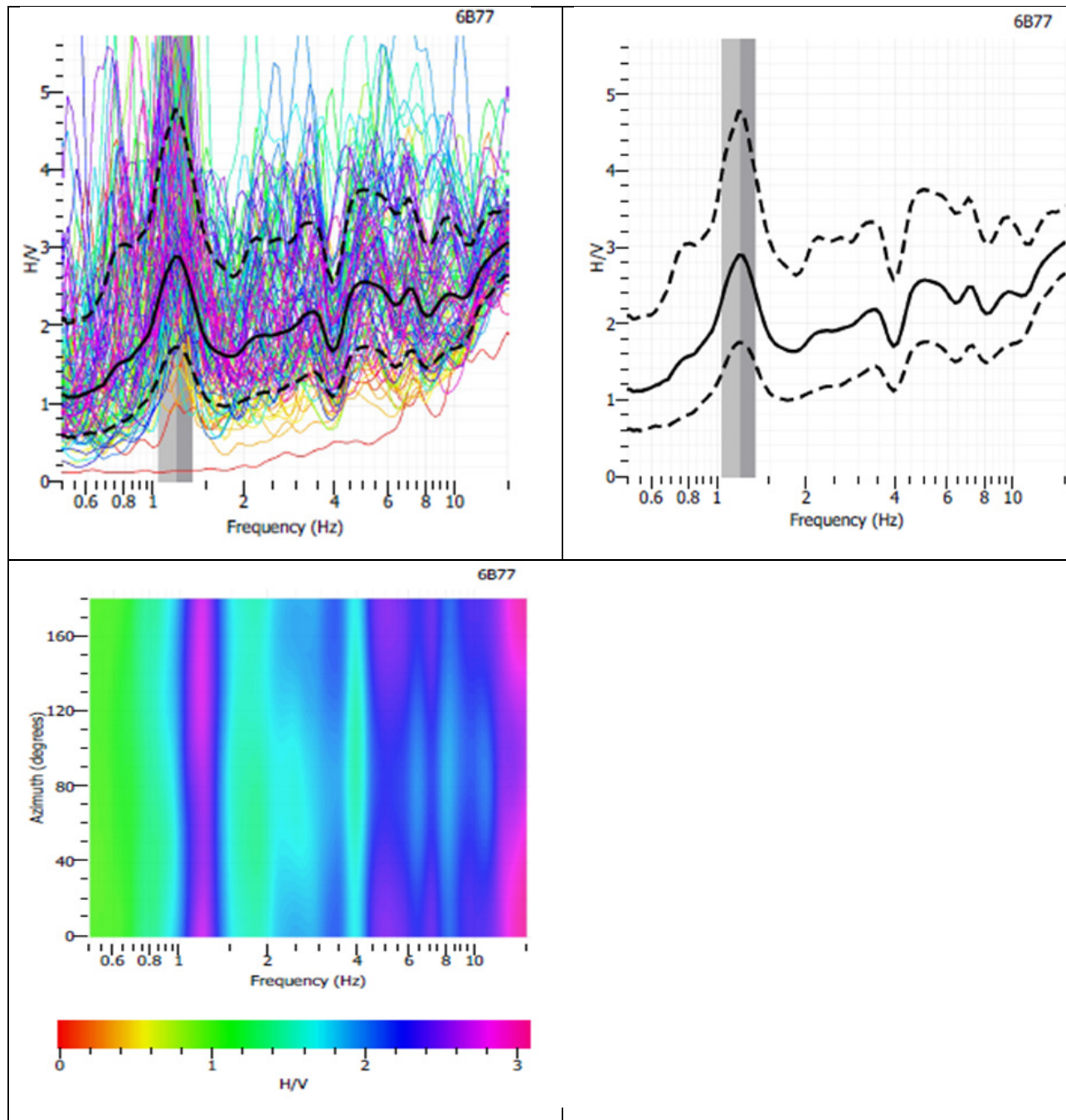


**Figure 6.18:** Seismometer measurement T6B77\_Feb24\_1948 with (a) individual H/V window peaks, (b) mean H/V peak at 1.192 Hz (corresponding depth: 233.8 m) and (c) H/V rotate analysis, indicating seismic sources that arrive from all directions.

### **6.3c. Seismometer A834 H/V and H/V Rotate Analysis**

This section focuses on the H/V and H/V rotate analyses for seismometer A834 presented in Figure 6.19 through Figure 6.21. Seismometer A834\_Feb23\_1603 (Figure 6.19) with a mean H/V peak at 0.864 Hz, with a corresponding depth of 323 m. Its H/V rotate analysis implies seismic sources that arrive from all directions. Seismometer measurement A834\_Feb24\_1520 (Figure 6.20) has a mean H/V peak at 0.729 Hz, with a corresponding depth at 382 m. Its H/V rotate analysis indicates seismic sources that arrive from the north and south. Seismometer measurement A834\_Feb24\_1700 (Figure 6.21) has a mean H/V peak at 0.950 Hz, with a corresponding depth at 293 m. Its H/V rotate analysis indicates that seismic sources that arrive from all directions. In this case only one boundary was detected as well.

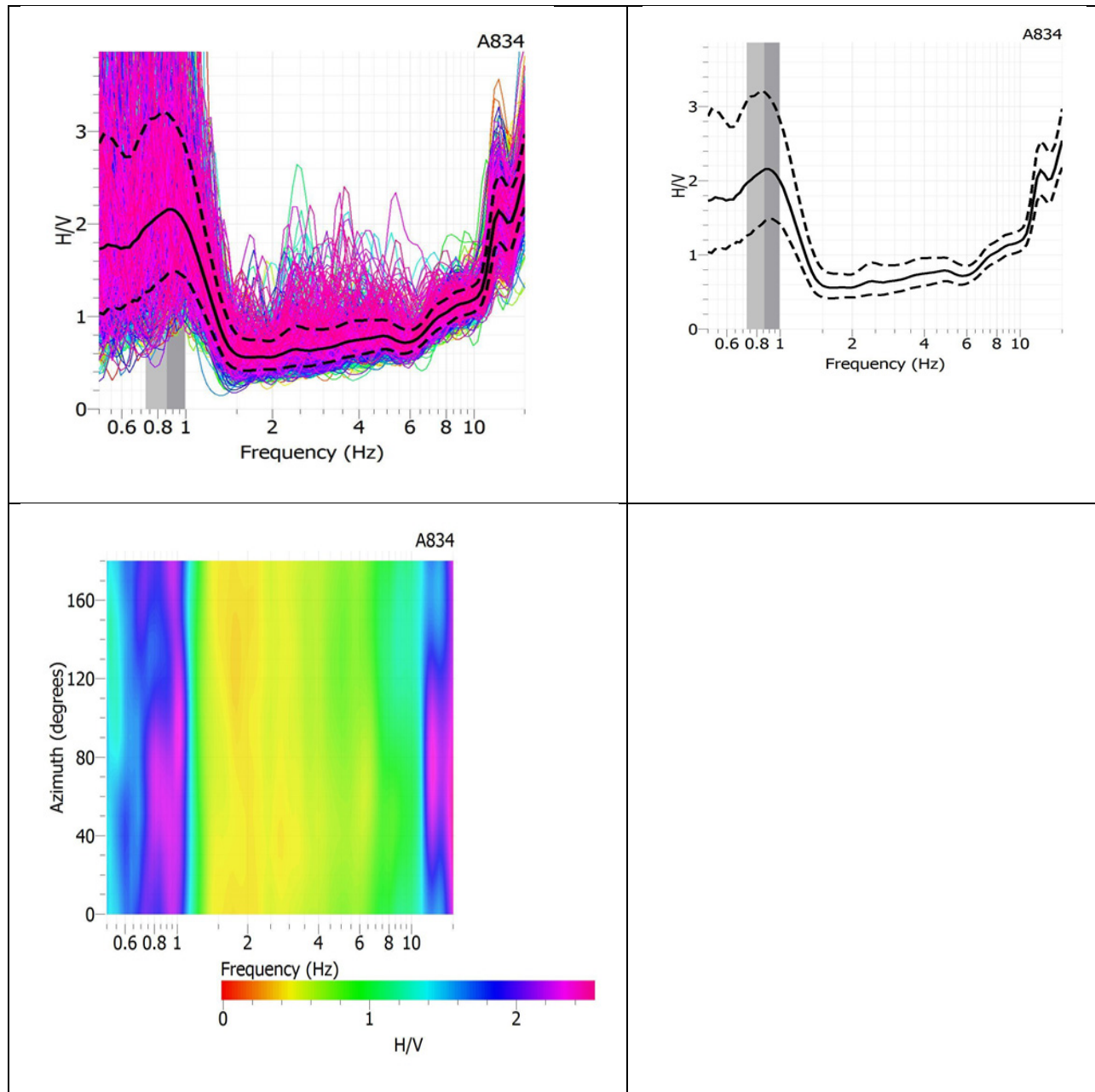


**Figure 6.19:** Seismometer measurement A834\_Feb23\_1603 with (a) individual H/V window peaks, (b) mean H/V peak at 0.864 Hz (corresponding depth: 322.5 m) and (c) H/V rotate analysis, indicating seismic sources that arrive from all directions.

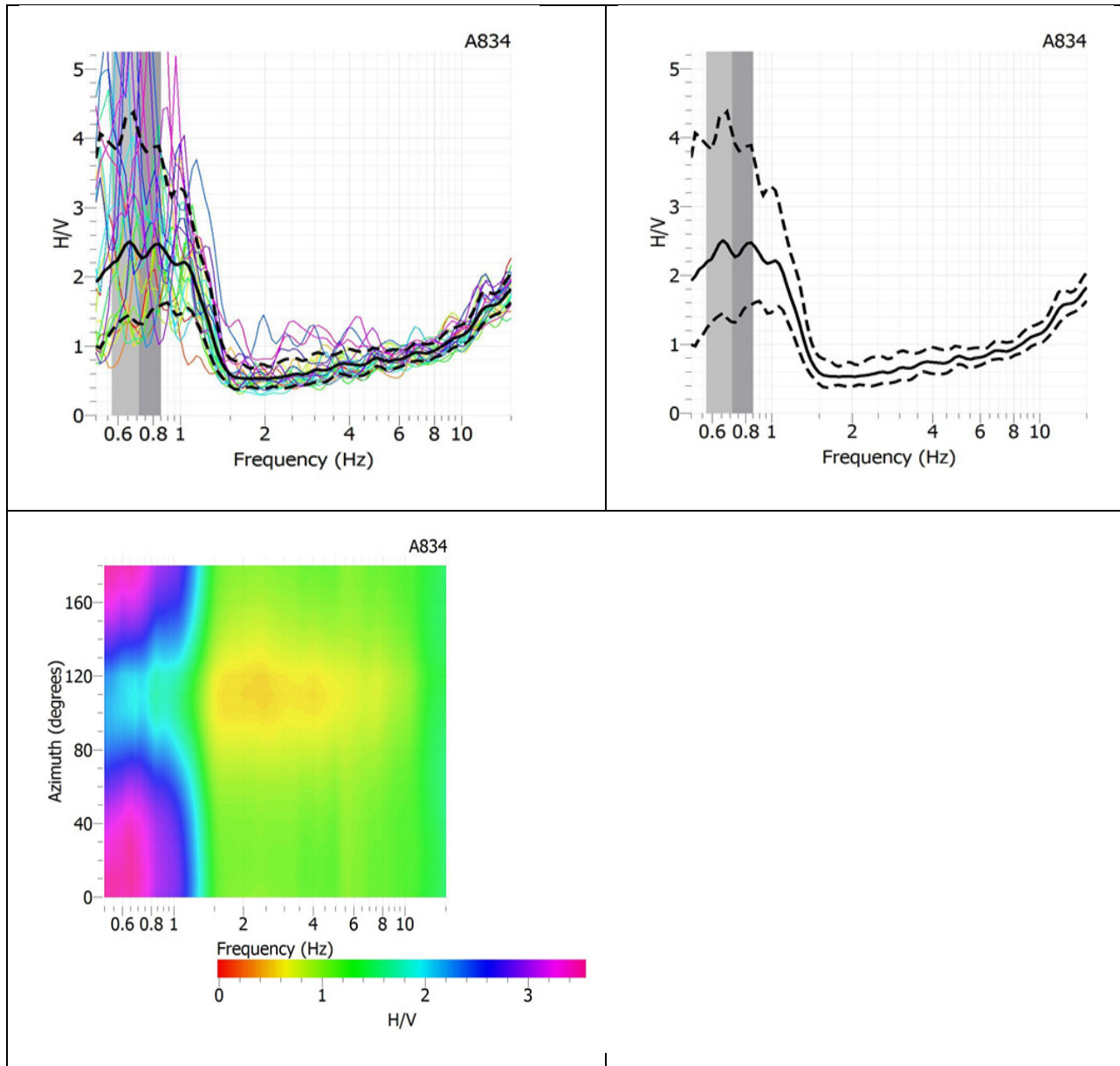


**Figure 6.20:** Seismometer measurement A834\_Feb24\_1525 with (a) individual H/V window peaks, (b) mean H/V peak at 0.729 Hz (corresponding depth: 382.4 m) and (c) H/V rotate analysis, indicating seismic sources that arrive from the north and south.

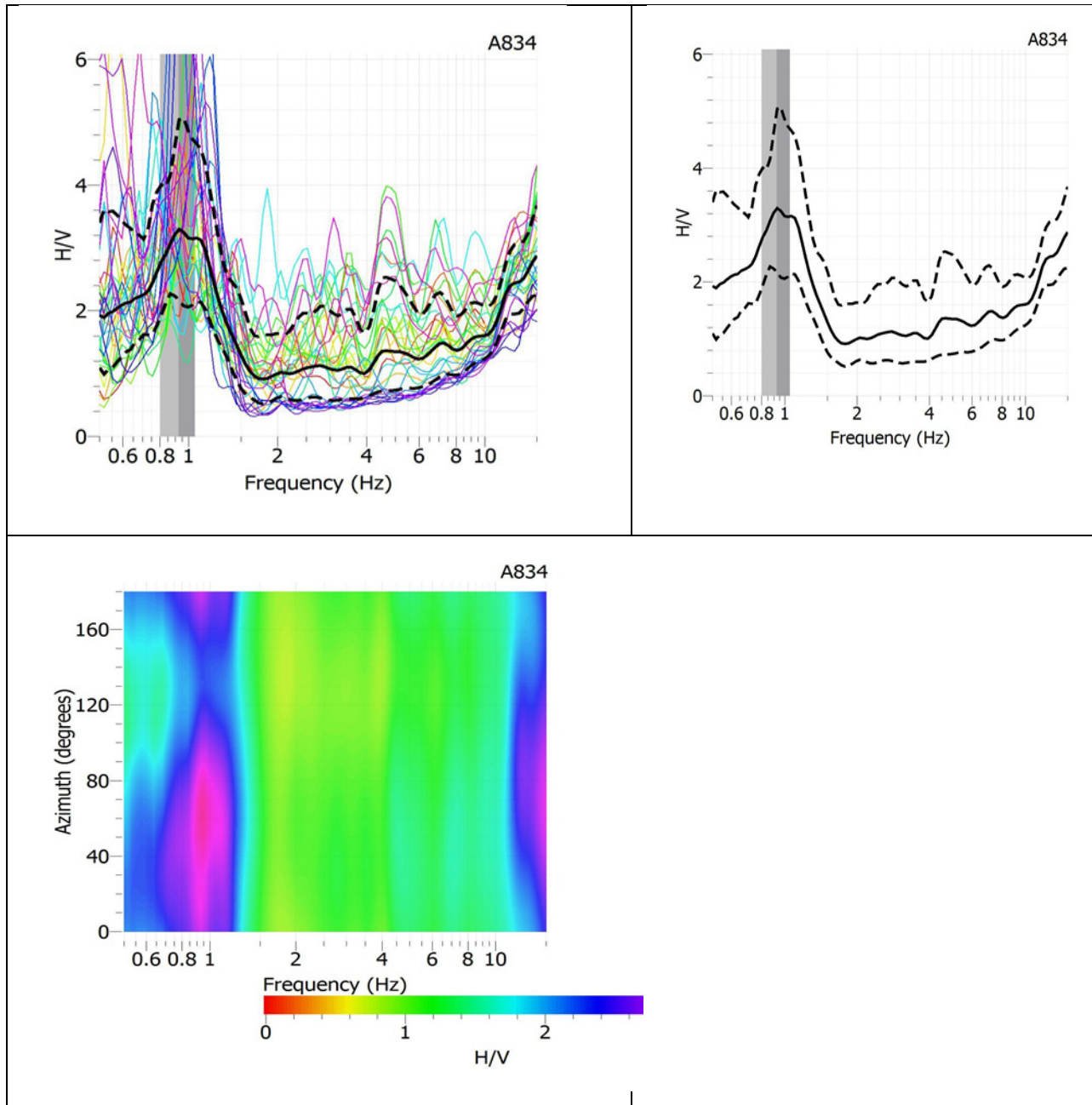


**Figure 6.21:** Seismometer measurement A834\_Feb24\_1700 with (a) individual H/V window peaks, (b) mean H/V peak at 0.950 Hz (corresponding depth: 293.3 m) and (c) H/V rotate analysis, indicating seismic sources that arrive from all directions.

#### 6.4. Data Interpretation

The range of the frequency obtained from the H/V spectral analysis is about 0.70 to 1.25 Hz, and the amplitude ranges from 1.4 to 7.5 (Figures 6.22 and 6.23, respectively). Figures 6.4-6.9 show that the results consist of plateau-like H/V curves more than peak amplitude curves. These plateau-like curves appear at the low-frequency side of the H/V curves. Figure 6.22 show that most of the higher frequencies, 1.08Hz to 1.25 Hz are located at the northern and the lower frequencies, 0.71 Hz to 1.02 Hz are located at the center and southern side. The plateau-like curves may also indicate that the boundary is sloping (SESAME, 2004). The accompanying peak/plateau amplitudes mostly fall in the range of 2.10 to 2.60, which suggests the impedance contrast of this boundary is not incredibly significant. There is no clear correlation between amplitude and plateau or peak frequencies.

The plateau and peak frequencies range corresponds to a depth of about 220 to 400 meters. According to Davidson (1973), this depth range in general correlates with tertiary Tinaja beds. However, the well data that is closest to the study site in F-F' cross section of the Davidson (1973) study does not contain any data for the depth of interest for this study. According to another study, this depth range might correlate with the transition between the upper and lower part of unit A of the Pliocene upper basin fill deposit (Houser & Gettings, 2000). Houser & Gettings (2000) describe the transition as gradational, which implies a low impedance contrast that agrees with low peak or plateau amplitudes of approximately 2. In addition, the calculated depth was derived from a few assumptions, including the Poisson's ratio and the P-wave velocity, which was derived from an area in the Tucson Basin close to, but not on the study site. This offset between the survey location with the Exxon 32-1 Well and the reflection seismic lines locations might explain the mismatch.

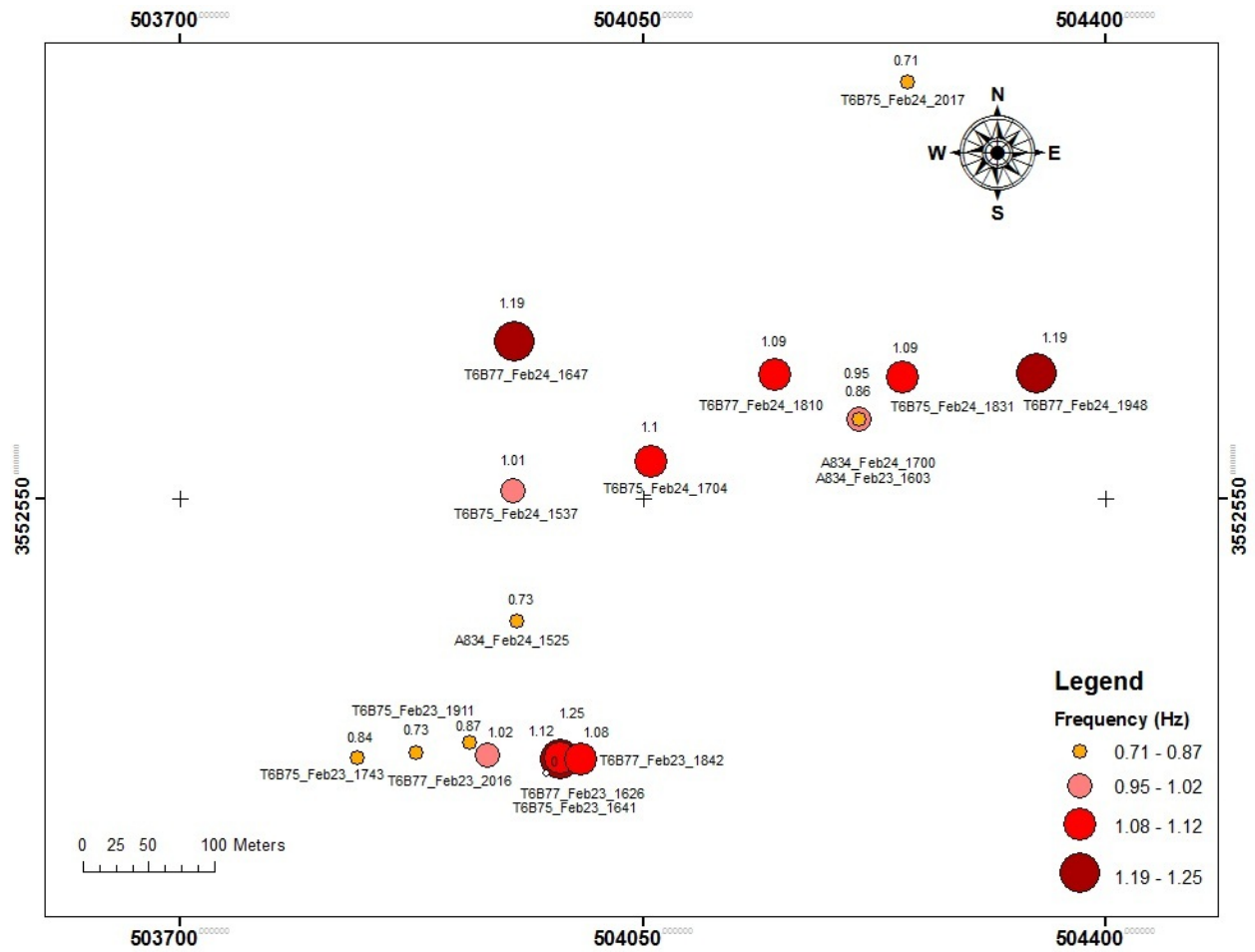


**Figure 6.22:** Frequency ranges in the seismic data with their corresponding seismometers.

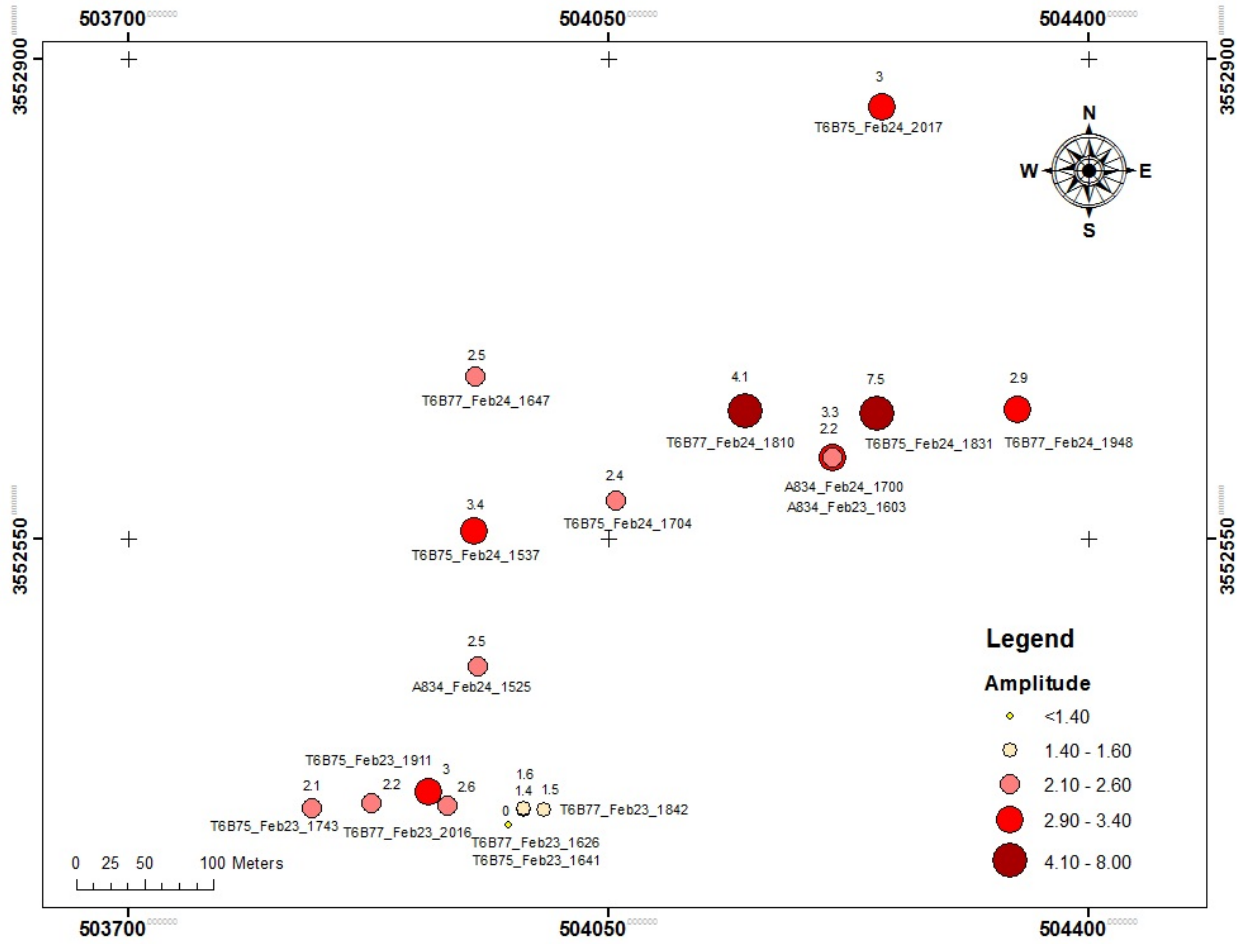
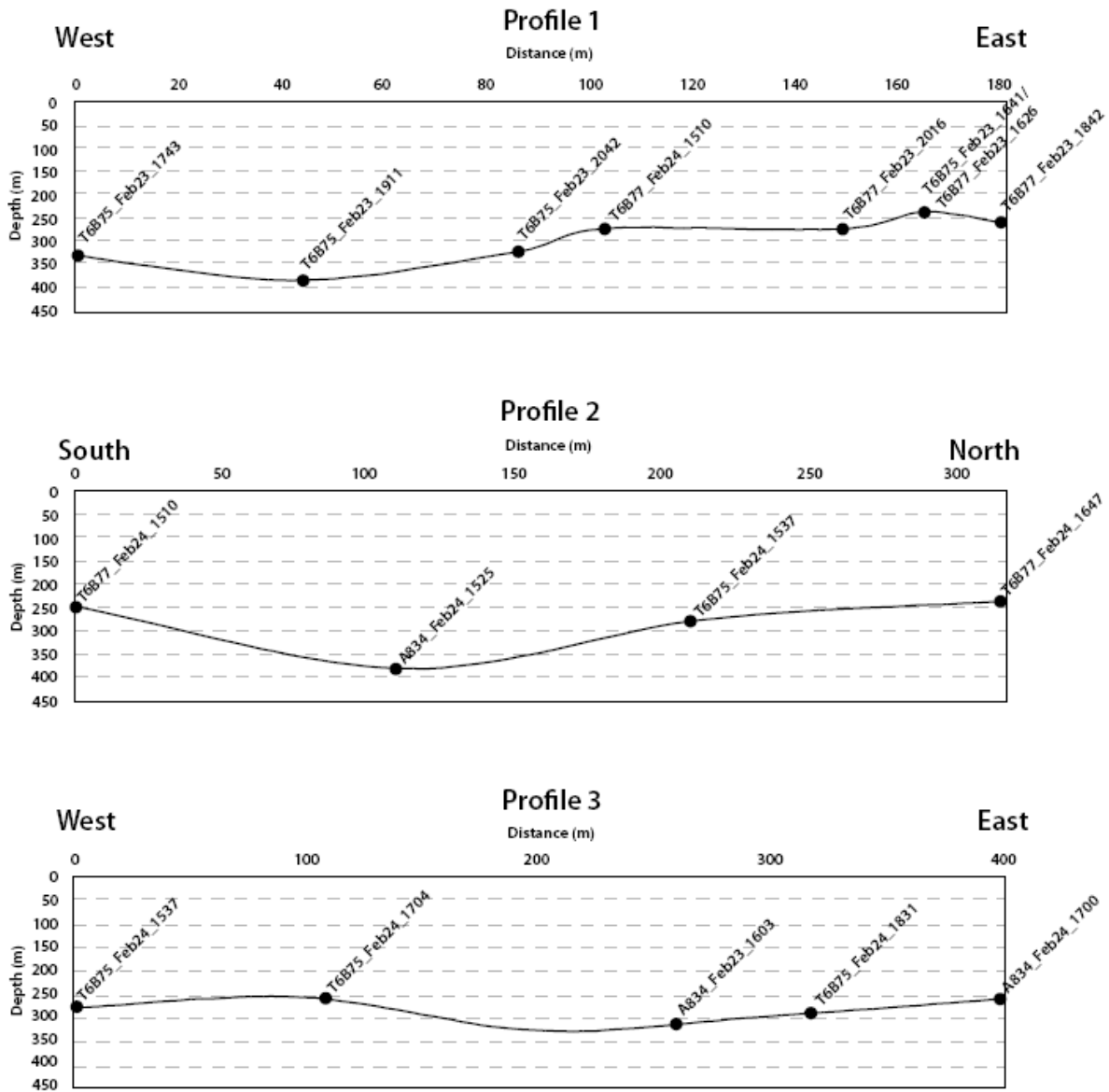


Figure 6.23: Amplitude ranges in the seismic data with their corresponding seismometers.



**Figure 6.24:** Seismic profiles 1-3 with the corresponding seismometers used in the profile generation. Profiles 1 and 2 can be referenced in the aerial map in Figure 6.1, and Profile 3 can be seen in Figure 6.2.

## 6.5. Discussion and Conclusions

One of the reasons why only one boundary is observed is because the H/V technique is most effective in cases where there is a large impedance contrast. If the sampled beds are very similar, the boundaries might not be detected. Thus, even though it can probably be assumed that there are several sedimentary layers in the subsurface of our study site, they are of similar nature and were not detected, with the exception of the boundary between the upper and lower part of unit A of the Pliocene upper basin fill deposit (Houser & Gettings, 2000). Other complications that affected the quality of the data were wind gusts and strong constant winds (especially in the afternoon of February 24), which caused a decrease in the signal-to-noise ratio of some measurements. Furthermore, due to the limited time and number of seismometers in our array, the precision of the data was compromised. Despite these setbacks, a clear boundary ranging from 220 to 400 meters in depth was detected with this technique. Unfortunately, because this boundary was significantly deeper than the observed depths by TEM, this eliminated any overlap between the seismic and TEM data, and we could not make any correlations between the findings of the two techniques.

## 7. TEM Summary and Conclusions

At the Samsonite N. site, there is likely a parallel N-S metal pipeline near the profile, which has a resistivity that is much lower than the earth resistivity and which leads to the low-resistivity response. Because of this, we cannot conclude anything about the presence of porous channels in the section.

The EPA-03 site shows a lower resistivity region at a depth of 35 meters with a resistivity less than 10 Ohm-m. This may indicate higher moisture content, and this may be caused by a porous, water-filled channel passing through that site. It could also indicate a non-porous clay-rich region, which would also be low resistivity.

At Aero Park Blvd. S. site, NS line, there are possible high-moisture porous areas in the region of 30-40 meter depth, at points 10-20 meters and at points 50-100 meters. This raises the possibility of two porous channels passing through this site. This conclusion comes from an agreement of both the results of the EMIGMA and STEMINV programs, except for Figure 5.7, which shows some low resistivity regions at points of 40 meters, 120 meters, and 140 meters. These points do not appear in any of the other models and this may be caused by the Occam inversion method.

At Aero Park Blvd. S. site, EW line, 20 meter loops indicate a possibility of a NS pipeline at a depth of 30-40 meters, around 360 meters, causing low resistivity, which is also indicated by the EM31. Although there is a correlation between the TEM and EM31 on some TEM profiles, the majority of these profiles show no effect from the apparent pipeline. At other places along this profile (0-20 meters, 200-240 meters, and 380-400 meters) there low-resistivity regions at depths of 30-40 meters. This may indicate higher moisture content, and this may be caused by a porous, water-filled channel passing through that site. It could also indicate a non-porous clay-rich region, which would also be low resistivity.

Combining all the information, we see that at Aero Park Blvd South, NS line, has possible crossing channels oriented east west and Aero Park Blvd South, EW line, and EPA-03

has possible crossing channels oriented north south. This results in overall orientation of North West, as expected in this region, which has a flow of water in that orientation.

### 7.1 Comparison of the same site inversion results of EMIGMA and STEMINV

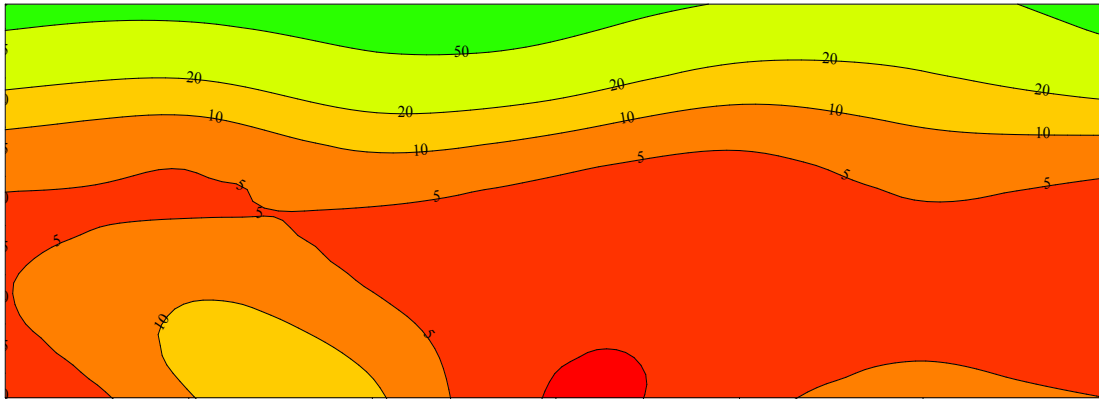


Fig 7.1 EMIGMA inversion results

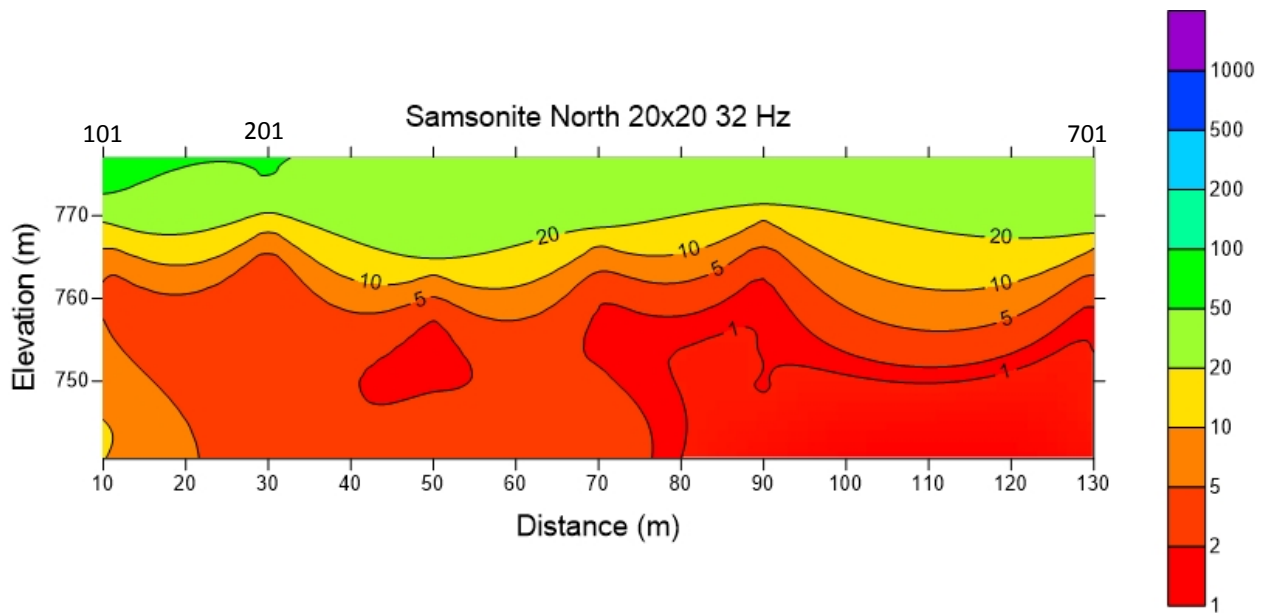


Fig 7.2 STEMINV inversion results

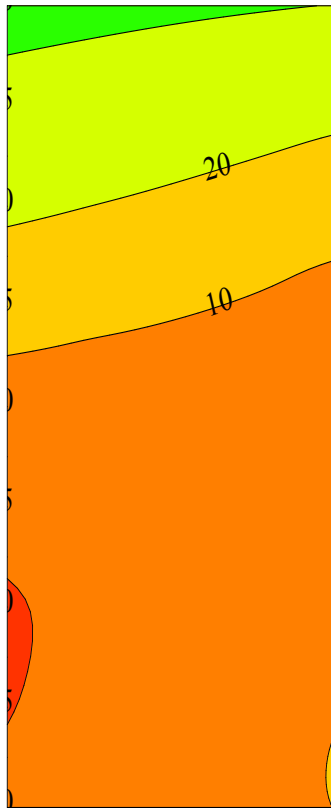


Figure 7.3 EMIGMA inversion results

Samsonite North East line 20x20 32 Hz

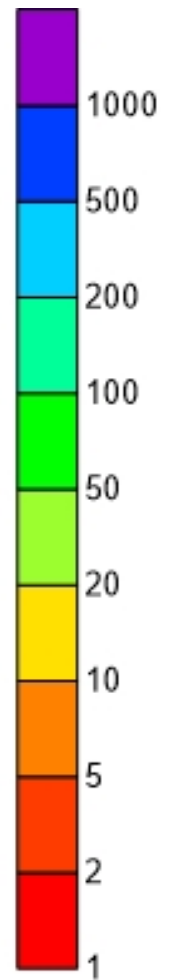
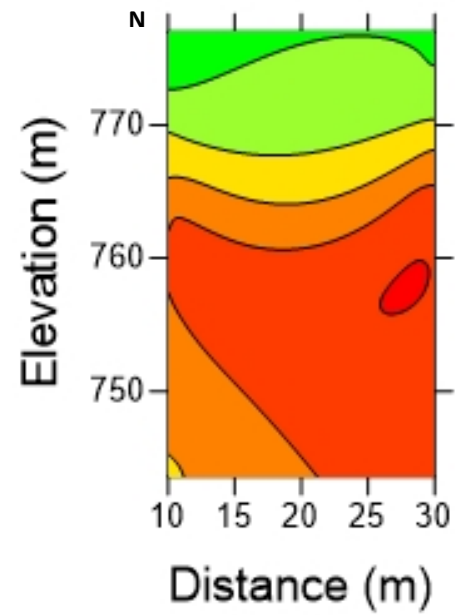


Figure 7.4 STEMINV inversion results

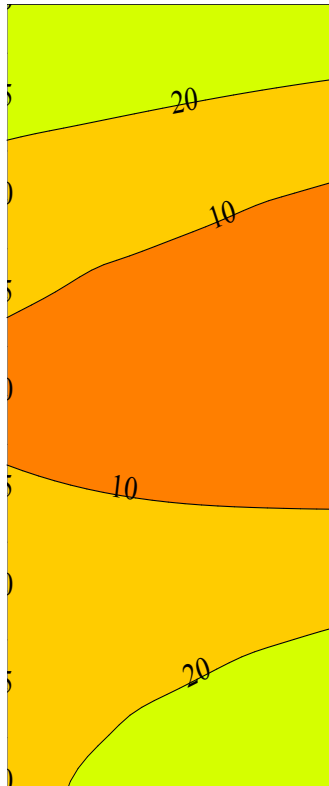


Figure 7.5 EMIGMA inversion results

Samsonite North West line 20x20 32 Hz

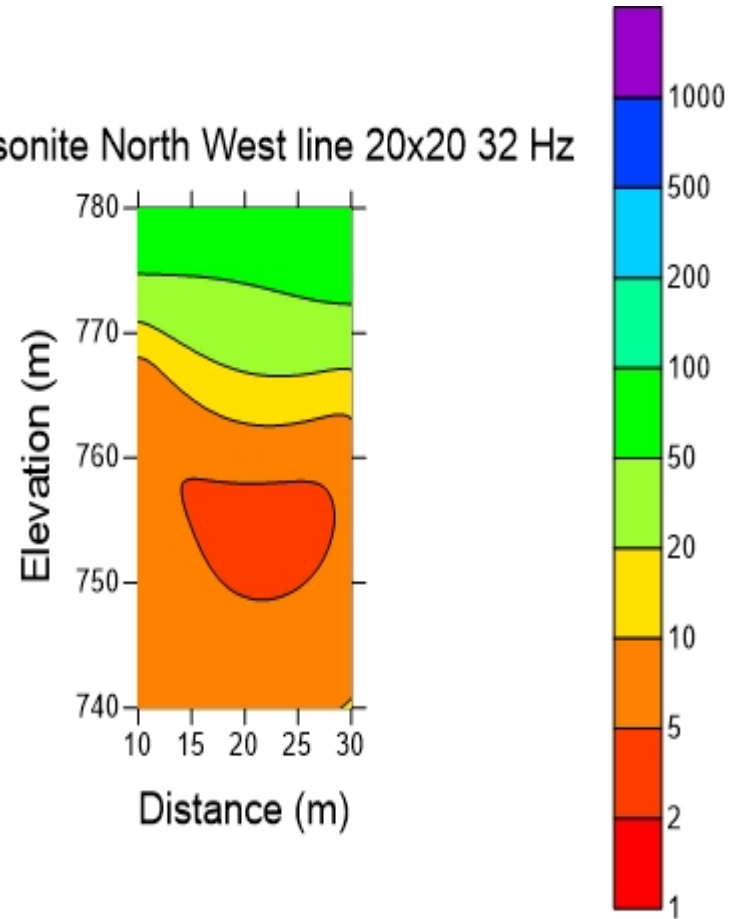


Figure 7.6 STEMINV inversion results

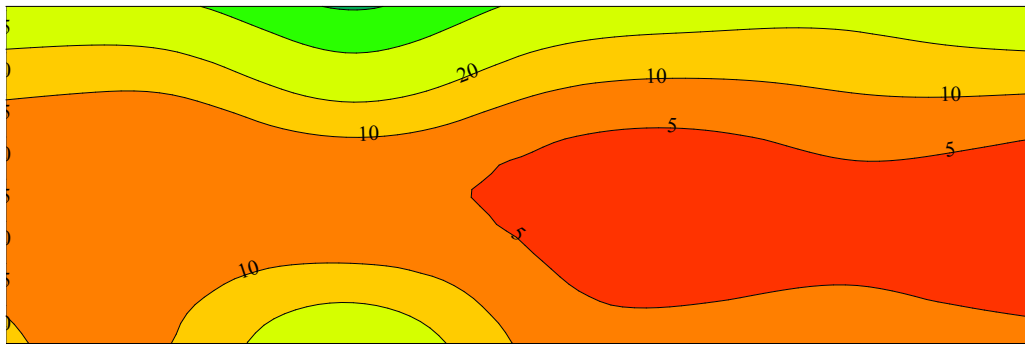


Fig 7.7 EMIGMA inversion results

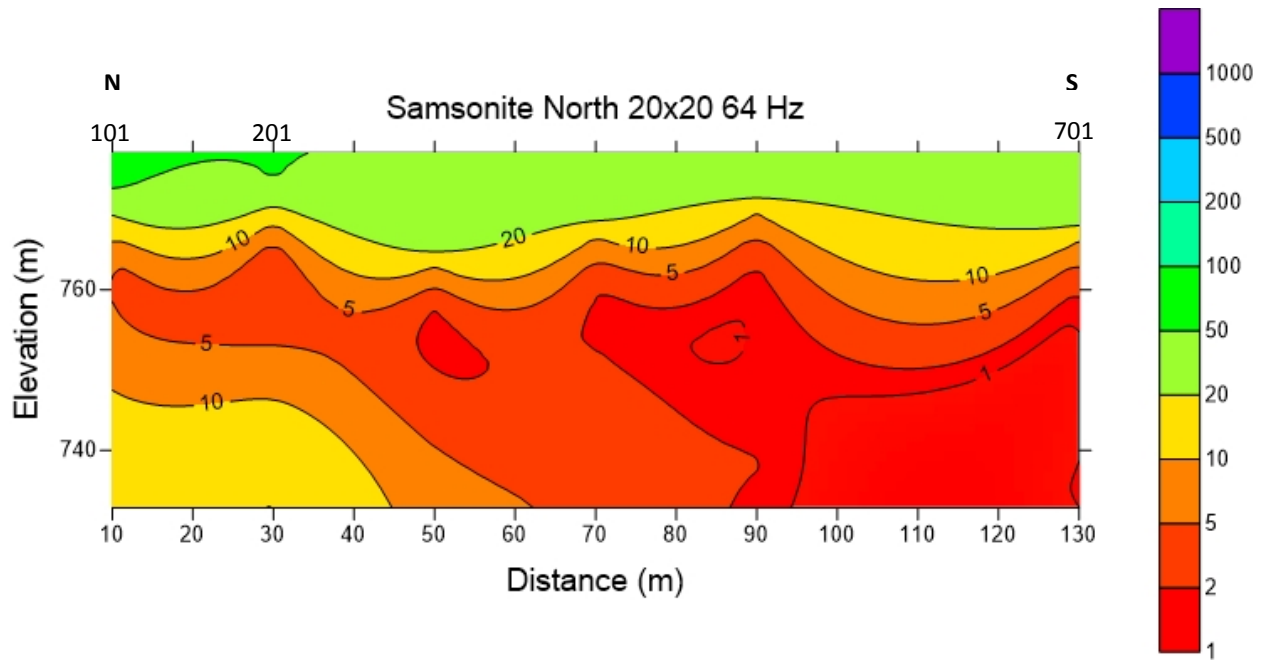


Fig 7.8 STEMINV inversion results

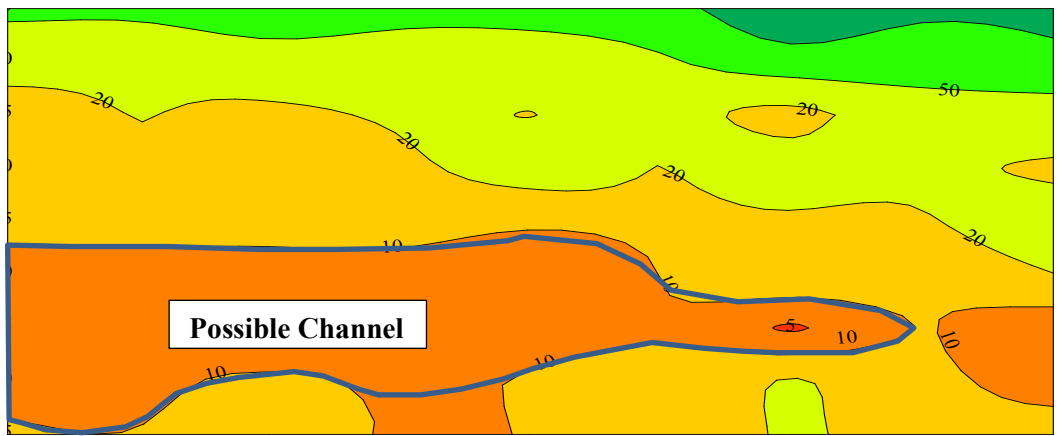


Fig 7.9 EMIGMA inversion results

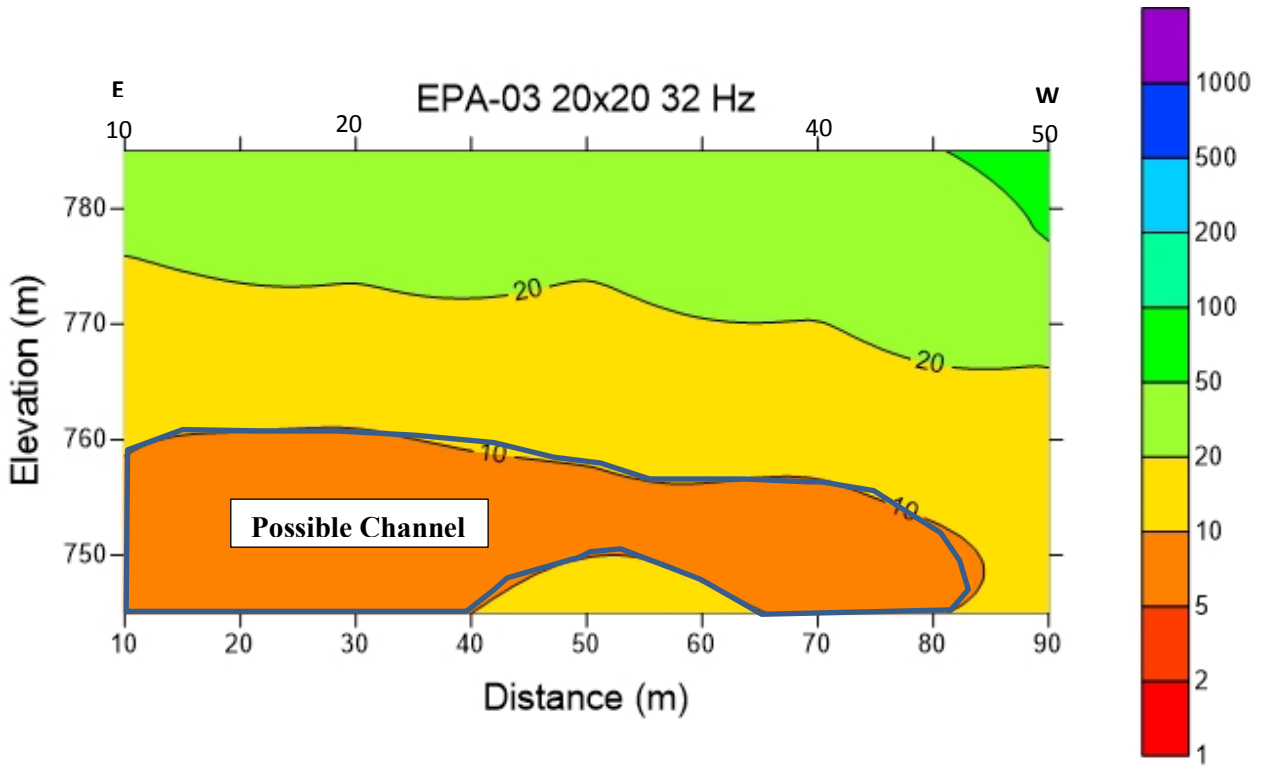


Fig 7.10 STEMINV inversion results

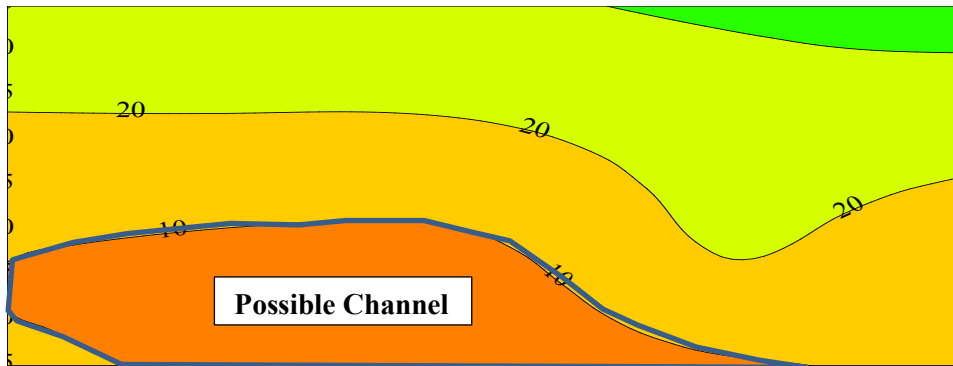


Fig 7.11 EMIGMA inversion results

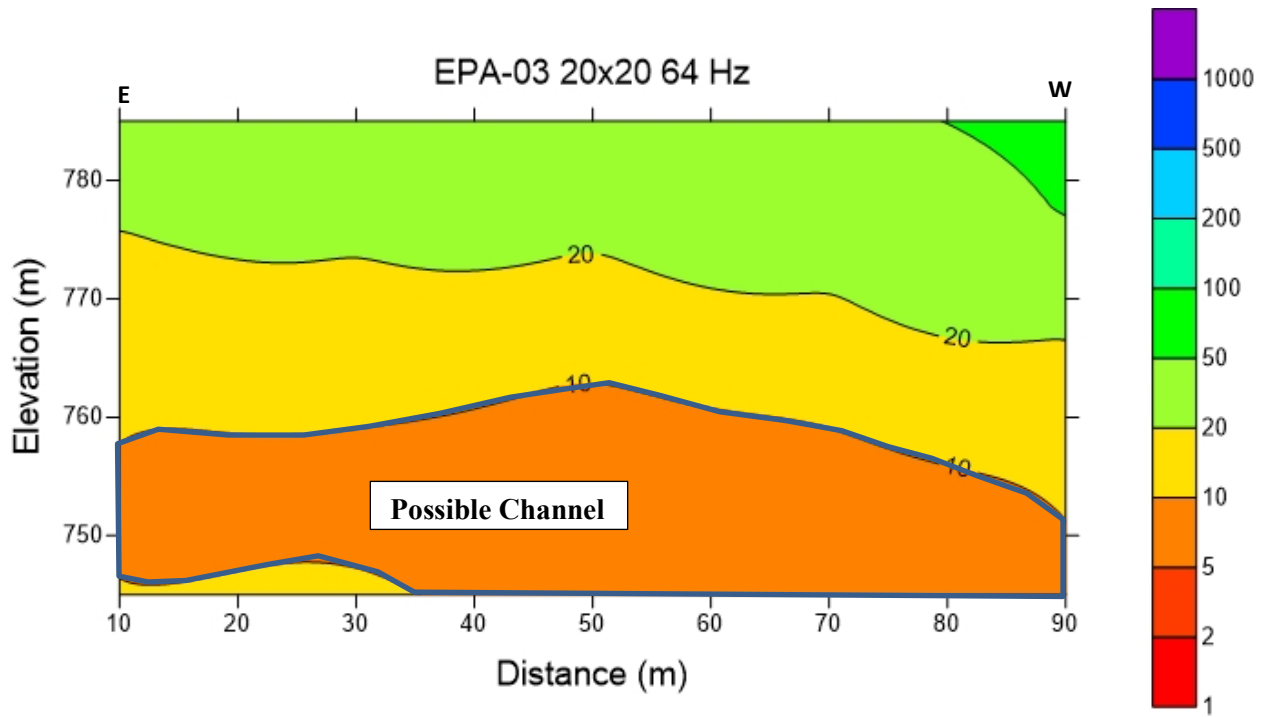


Fig 7.12 STEMINVE inversion results

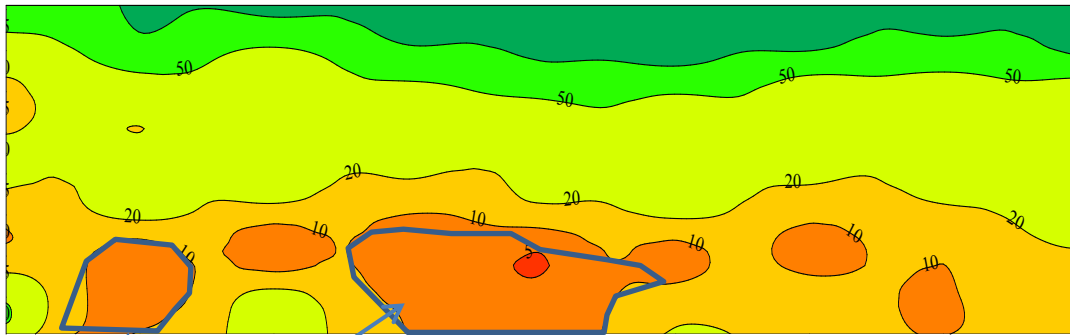


Fig 7.13 EMIGMA inversion results

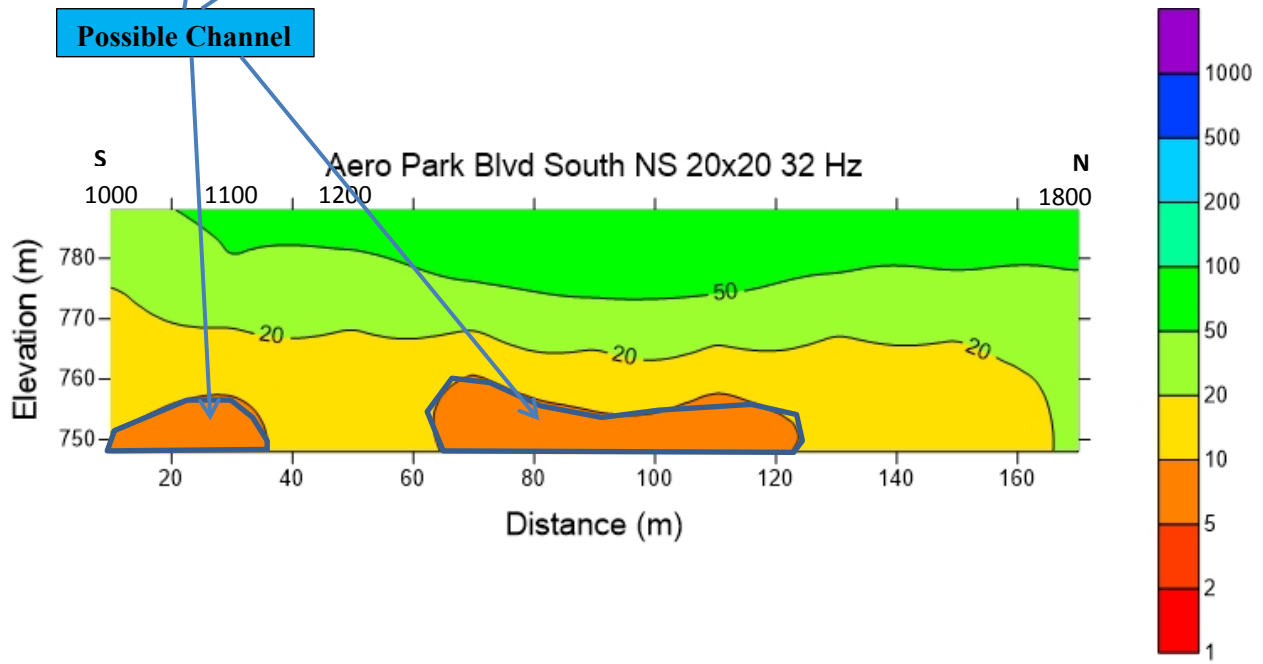


Fig 7.14 STEMINV inversion results

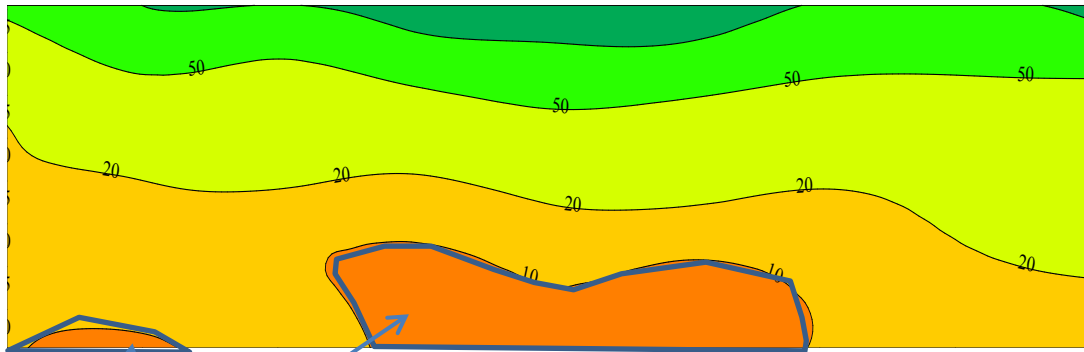


Fig 7.15 EMIGMA inversion results

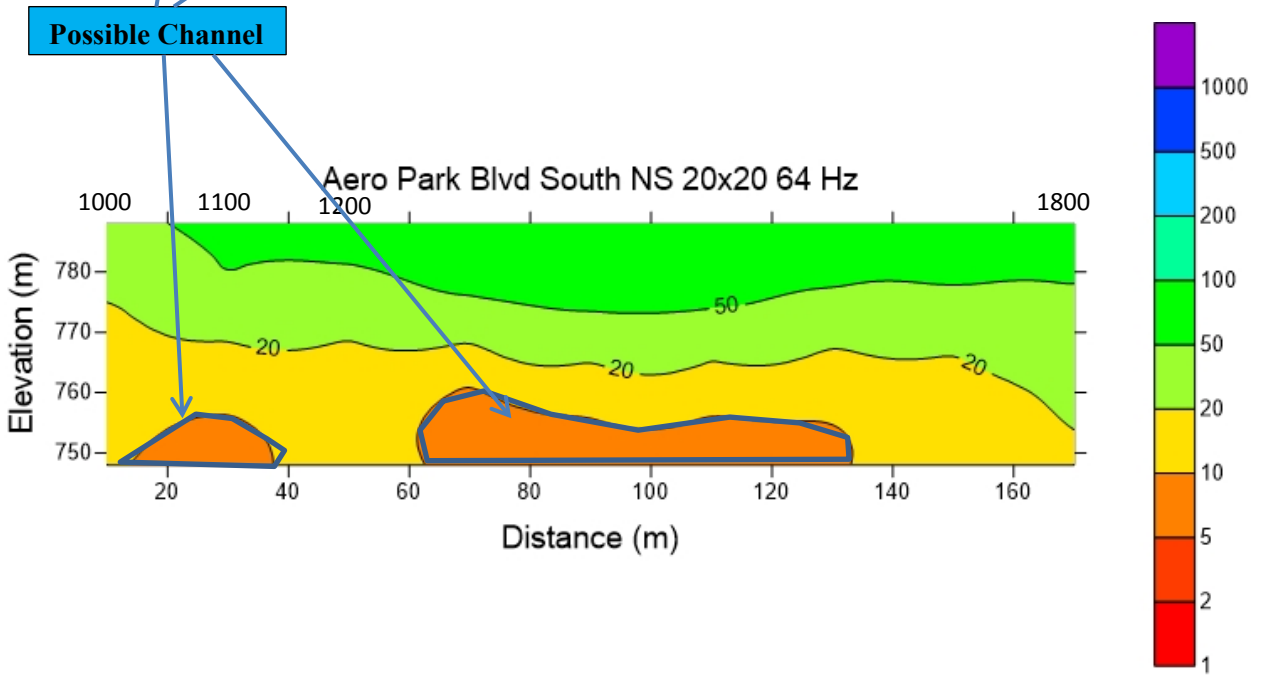


Fig 7.16 STEMINV inversion results

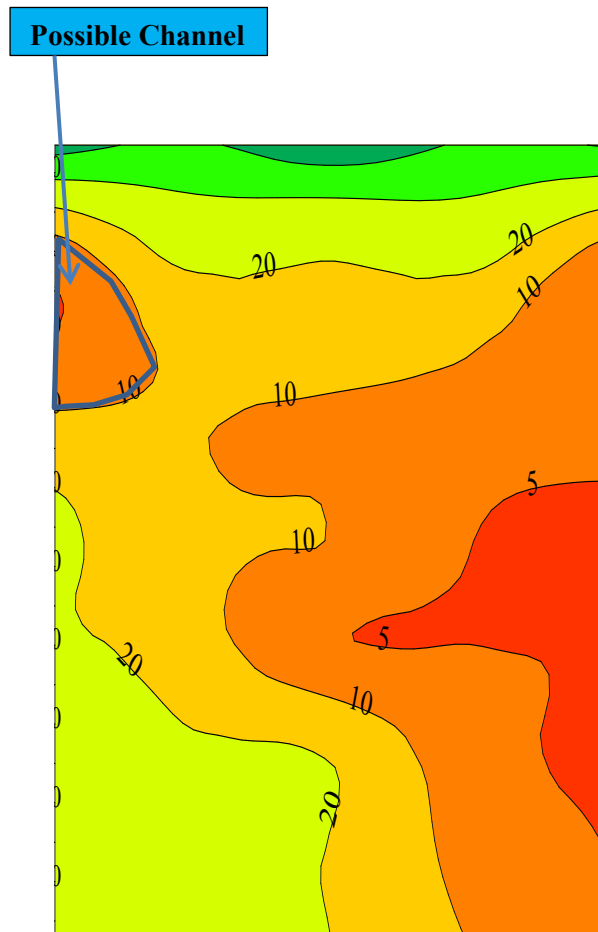


Figure 7.17 EMIGMA inversion results

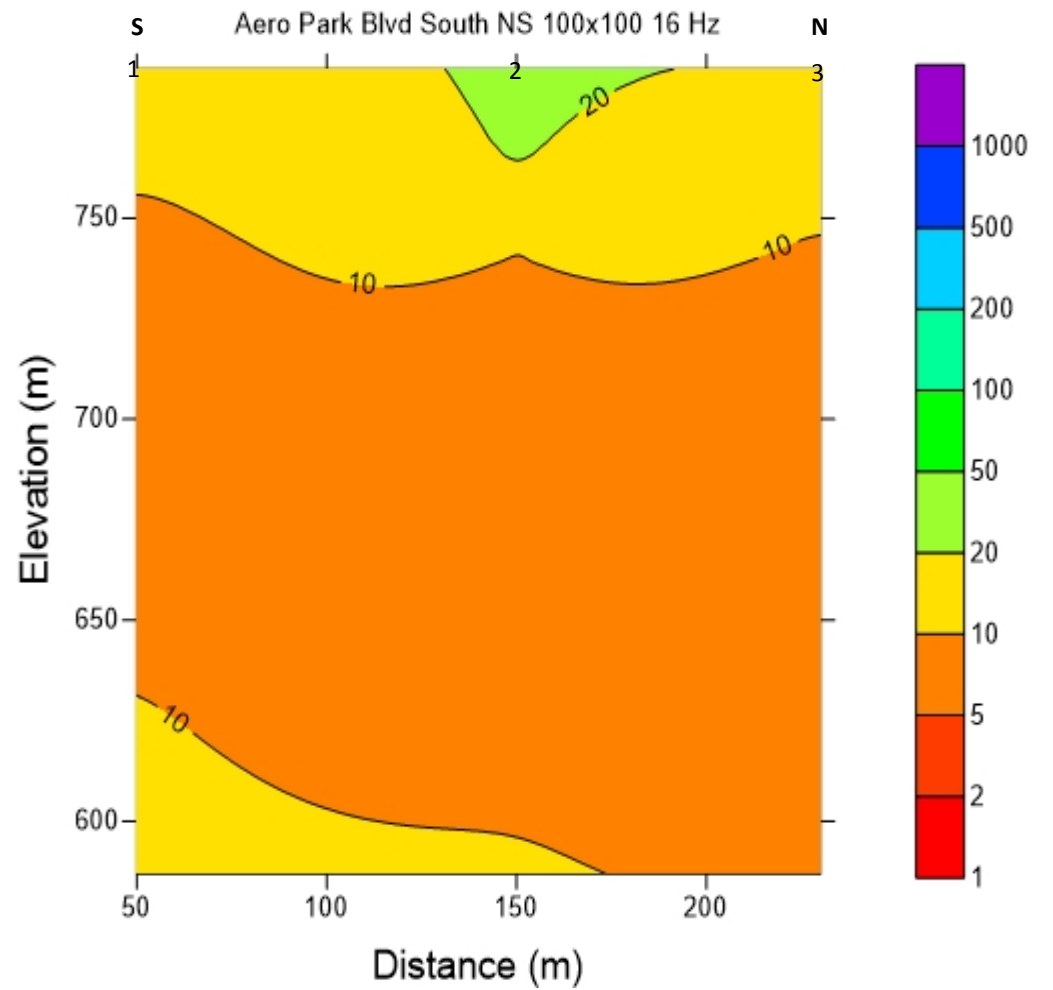


Figure 7.18 STEMINV inversion results



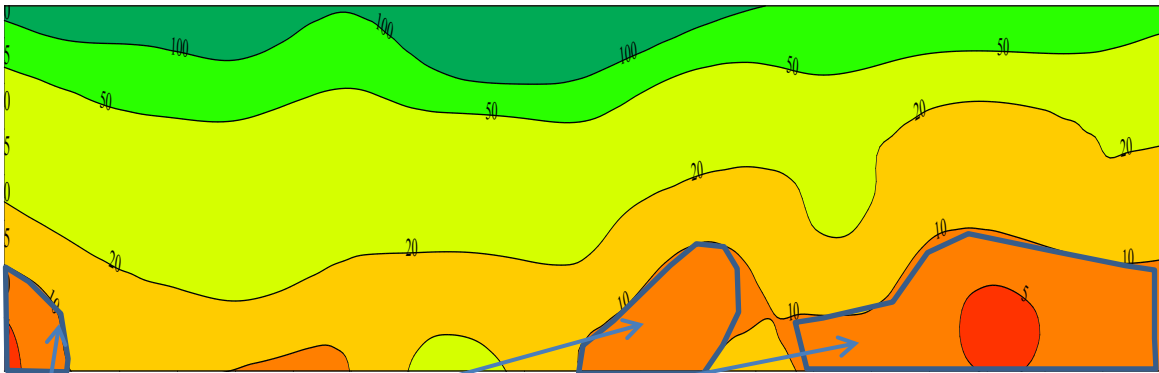


Fig 7.21 EMIGMA inversion results

Possible Channels

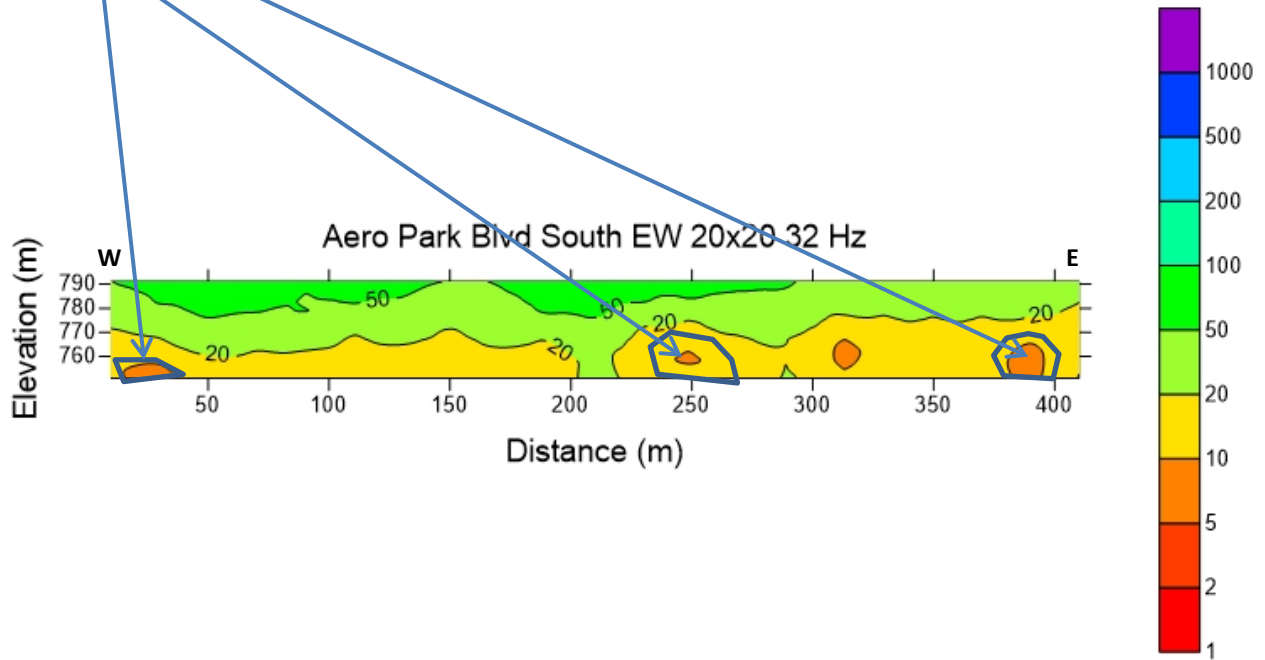


Fig 7.22 STEMINV inversion result

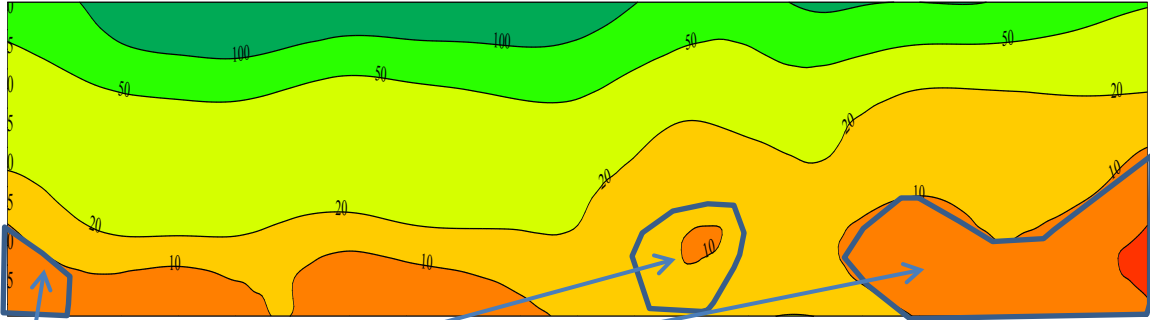


Fig 7.23 EMIGMA inversion results

Possible Channels

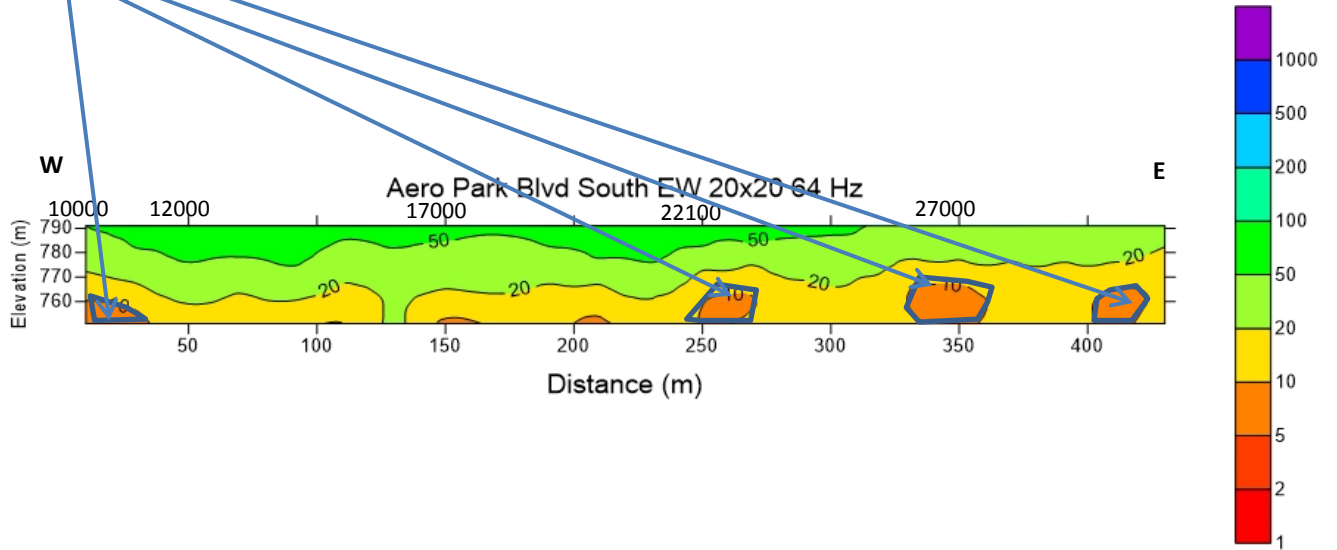


Fig 7.24 STEMINVE inversion results

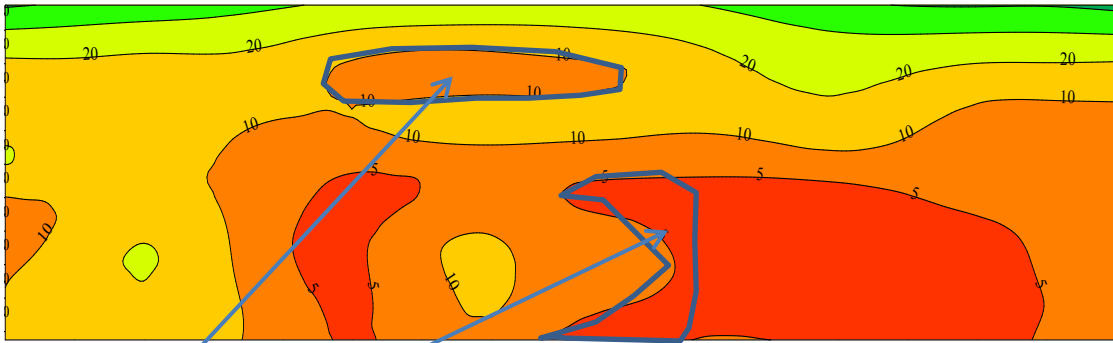


Fig 7.25 EMIGMA inversion results

Possible Channels

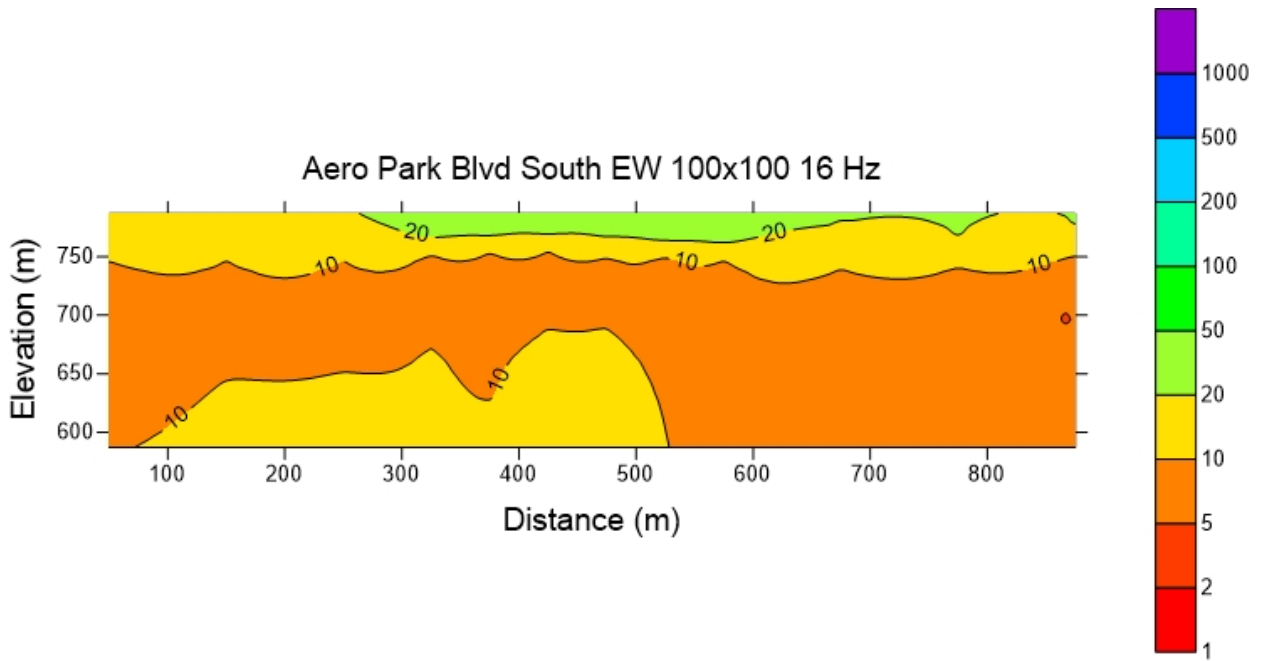


Fig 7.26 STEMINV inversion results

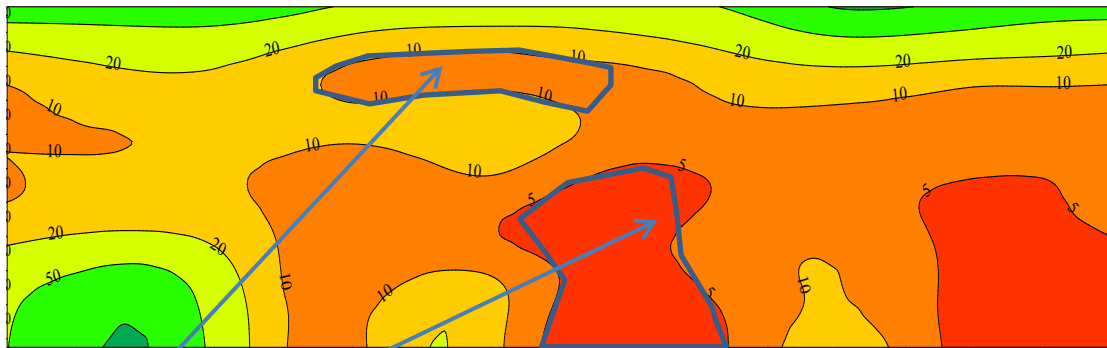


Fig 7.27 EMIGMA inversion results

Possible Channels

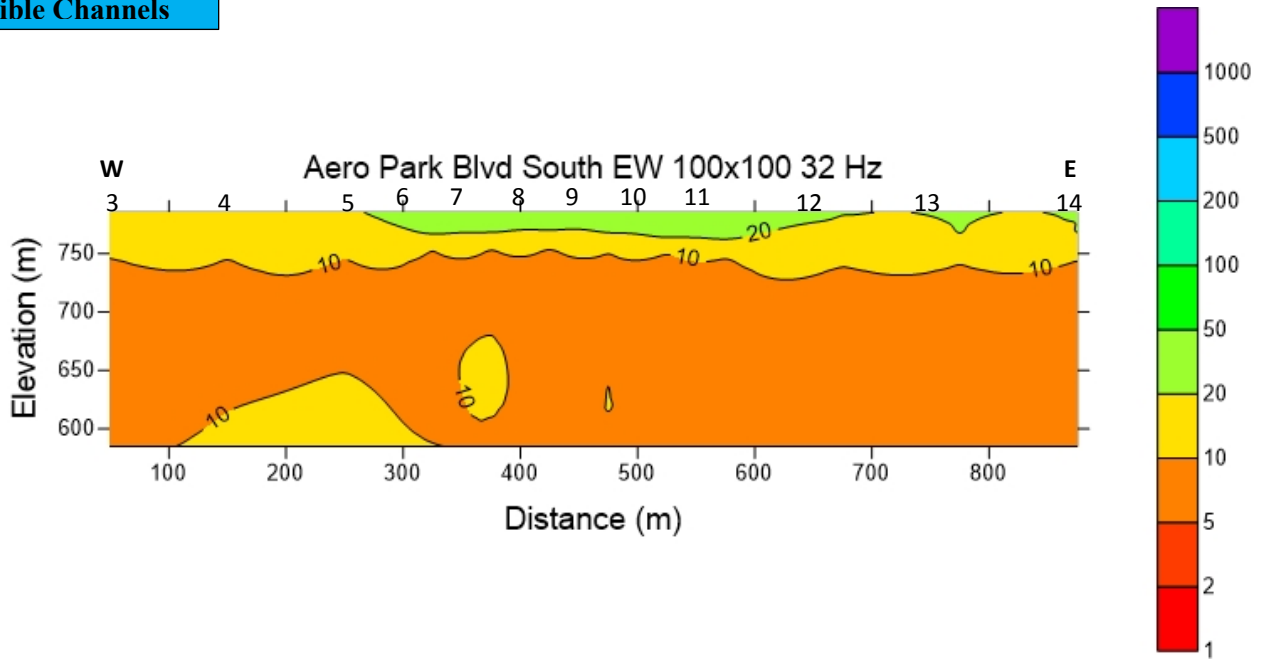


Fig 7.28 STEMINVE inversion results

## 7.2 Comparison of 20m loop and 100m loop at the same site

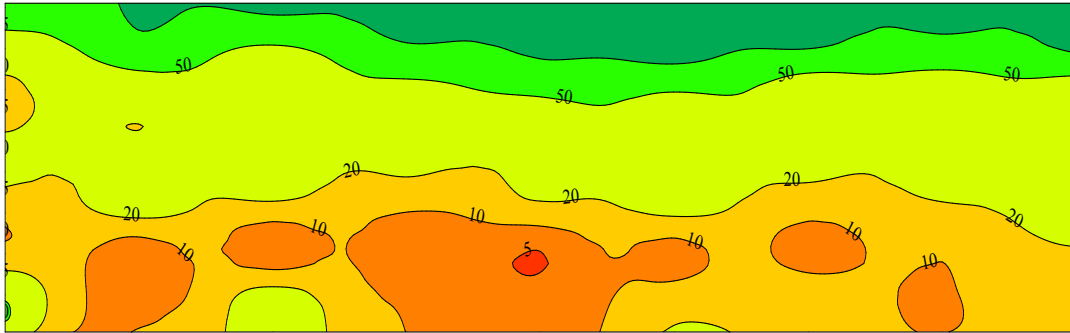


Fig 7.29 EMIGMA inversion results

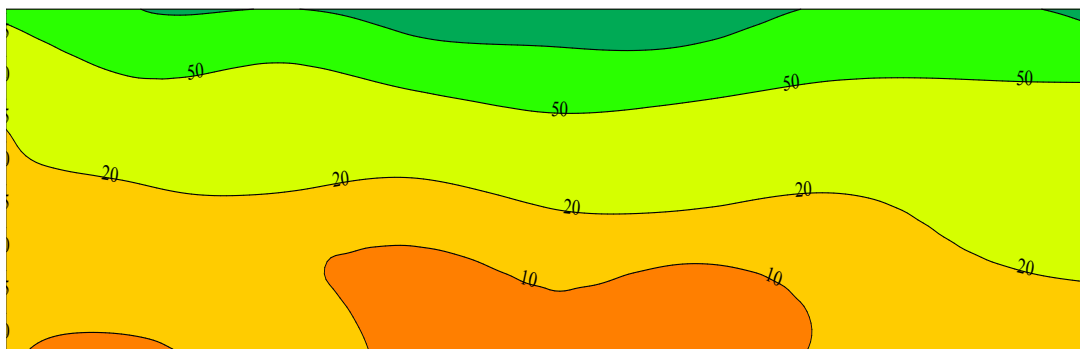


Fig 7.30 EMIGMA inversion results

Comparison region with 20m loop

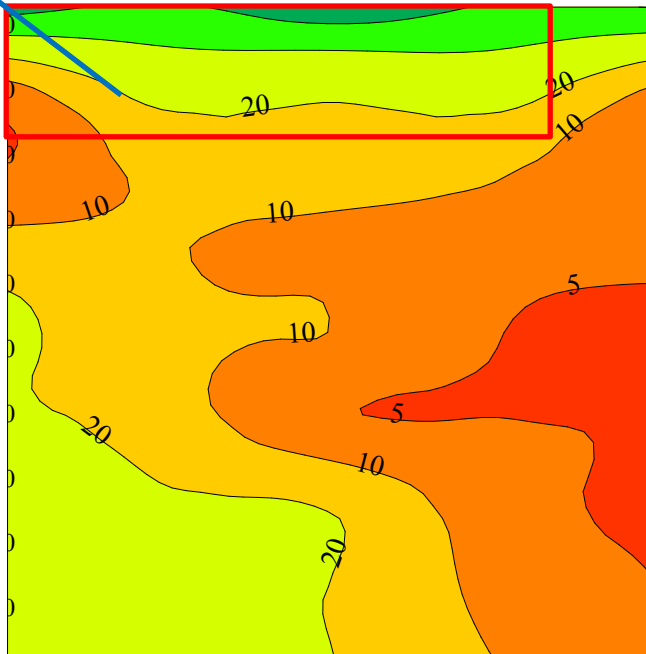


Fig 7.31 EMIGMA inversion results

Comparison region with 20m loop

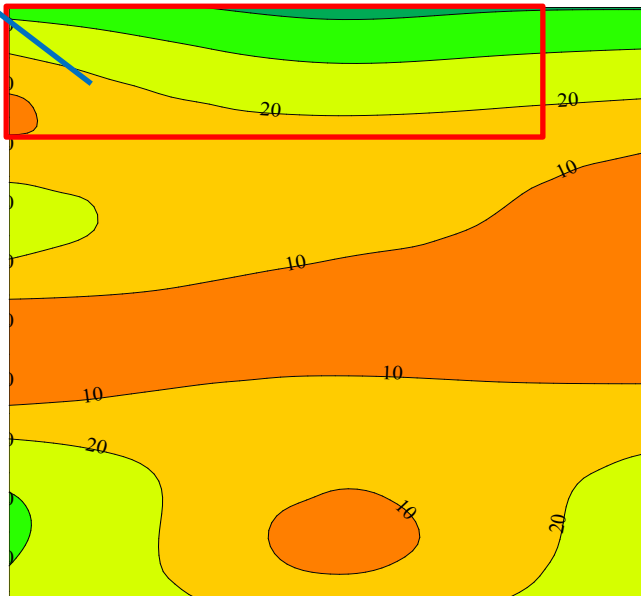


Fig 7.32 EMIGMA inversion results

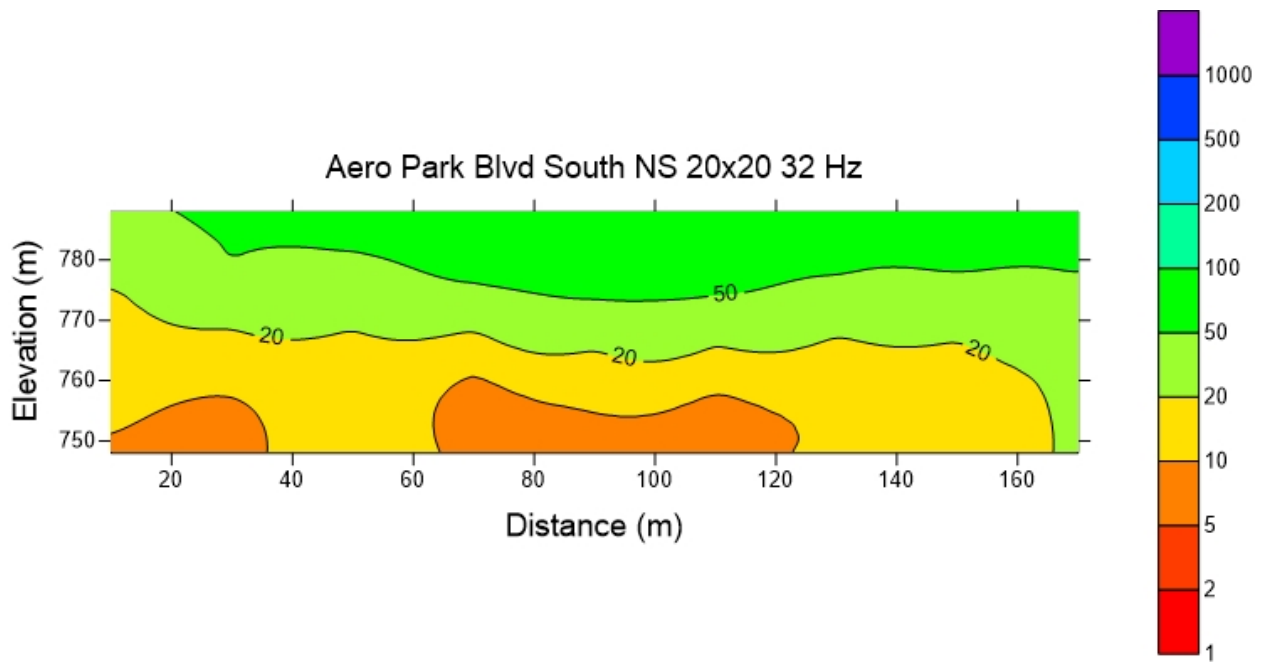


Fig 7.33 STEMINV inversion results

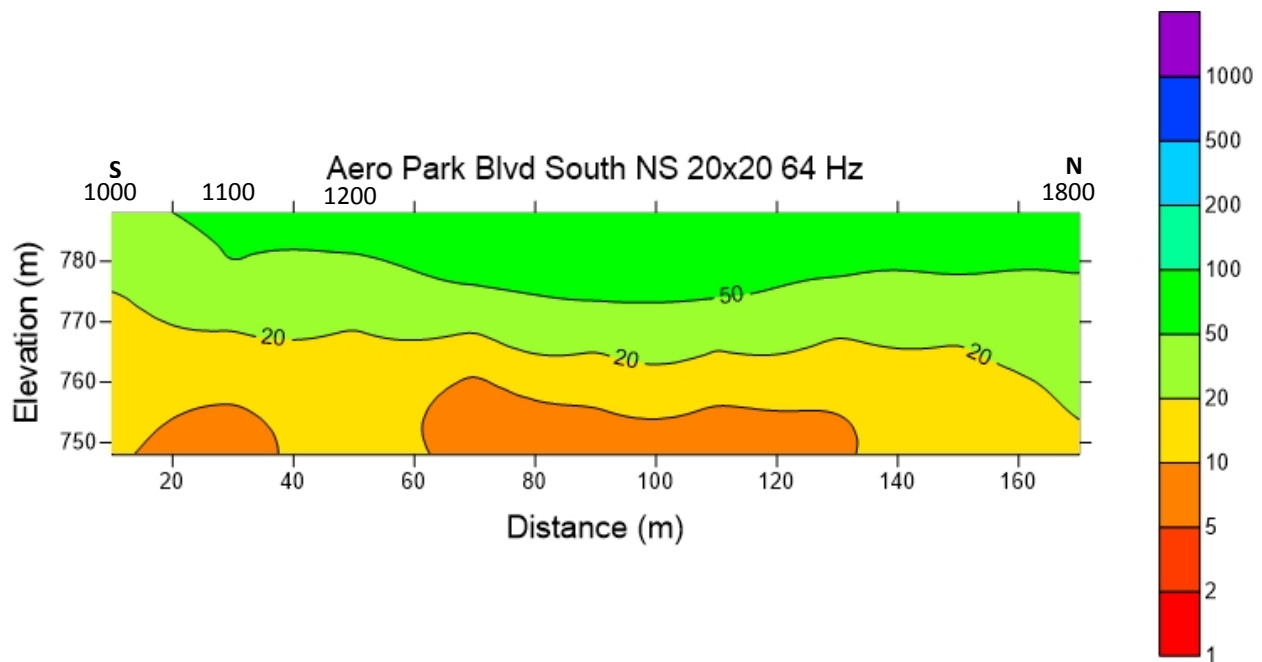


Fig 7.34 STEMINV inversion results

Comparison region with 20m loop

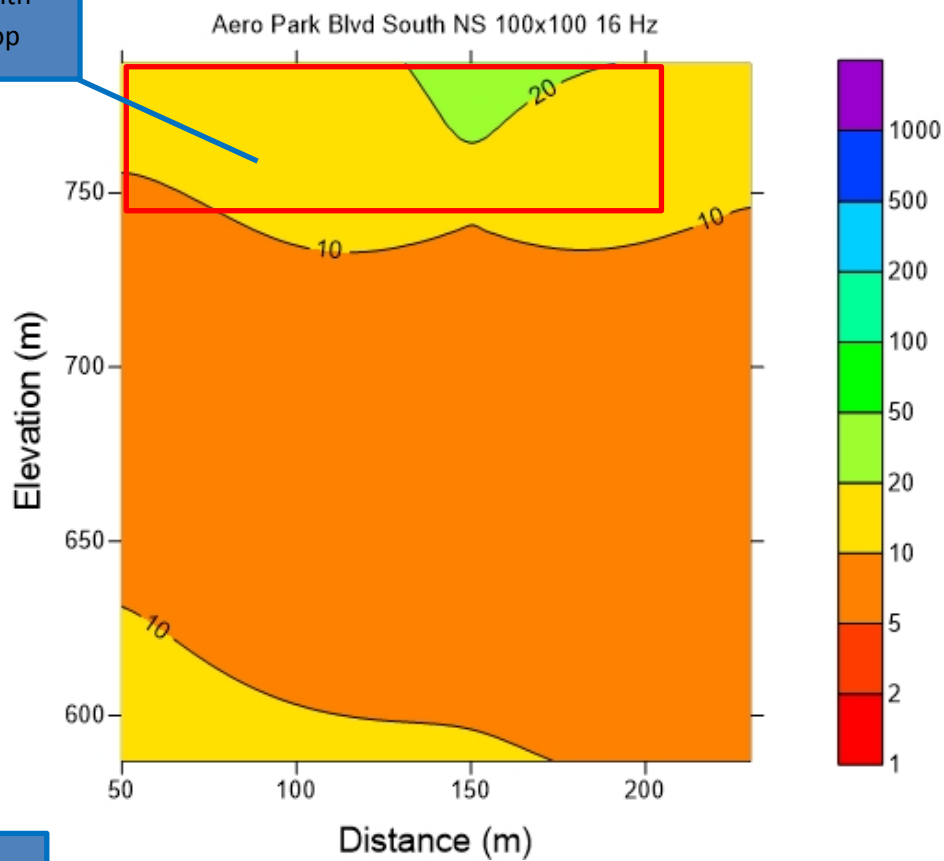


Fig 7.35 STEMINV inversion results

Comparison region with 20m loop

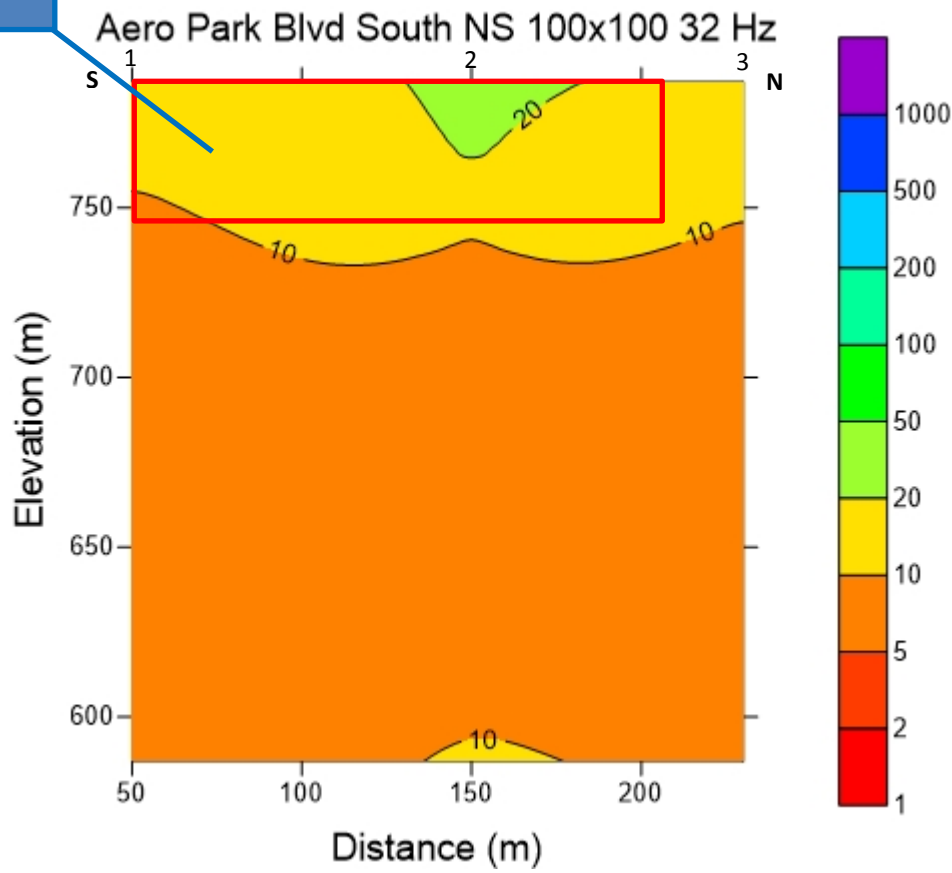


Fig 7.36 STEMINV inversion results



Comparison region with 20m loop

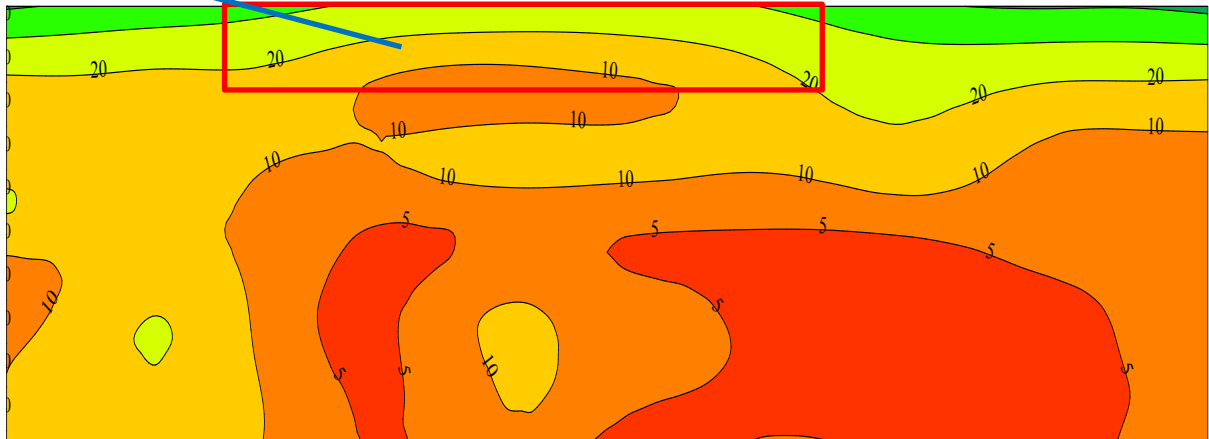


Fig 7.39 EMIGMA inversion results

Comparison region with 20m loop

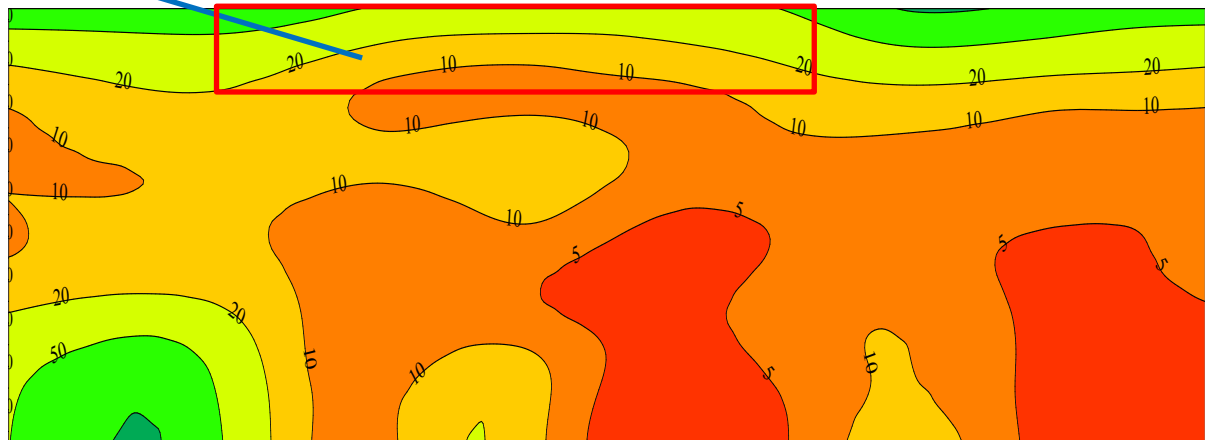


Fig 7.40 EMIGMA inversion results

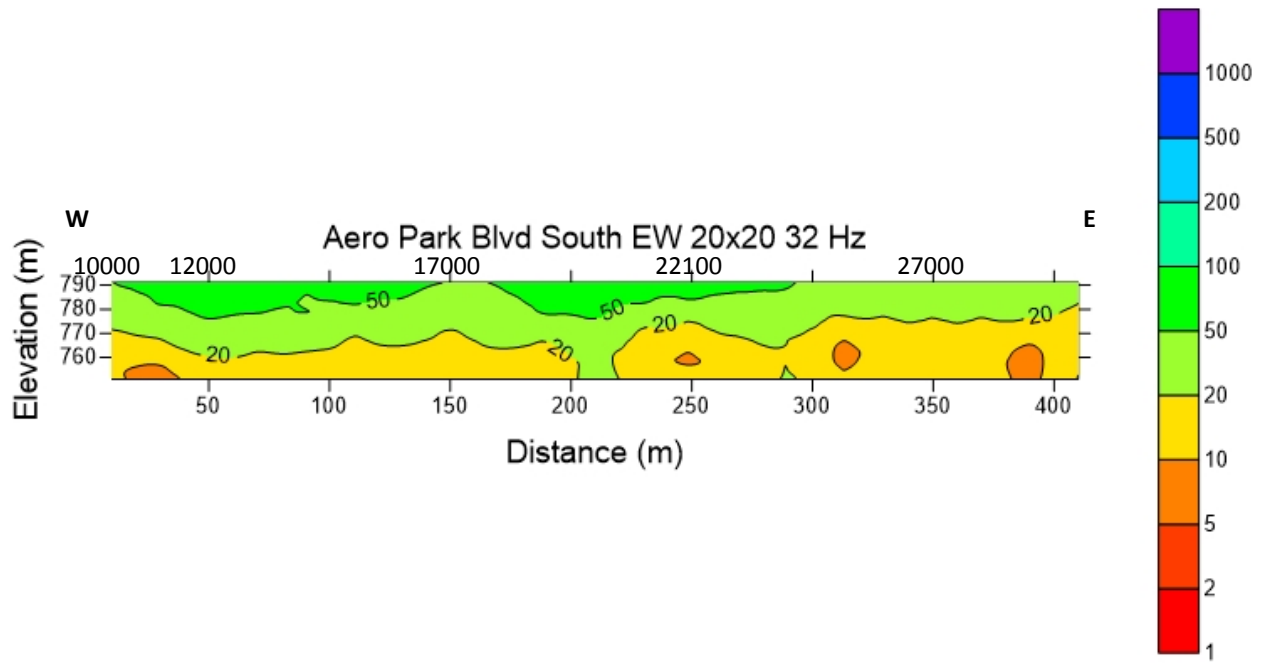


Fig 7.41 STEMINV inversion results

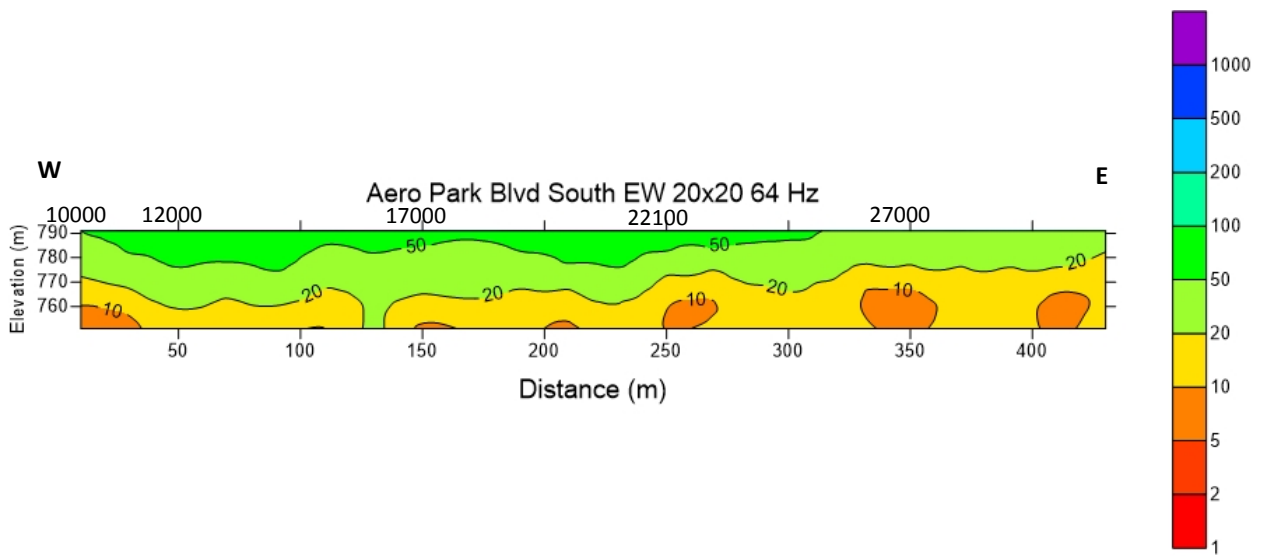


Fig 7.42 STEMINV inversion results

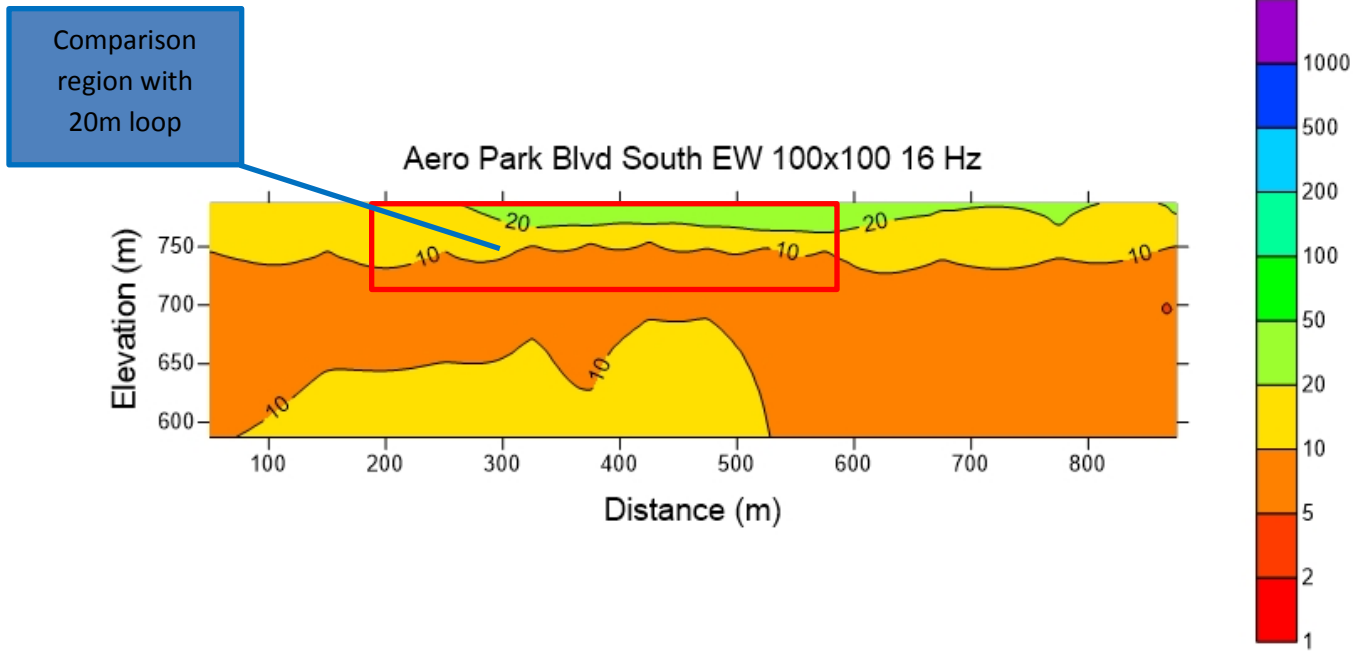


Fig 7.43 STEMINV inversion results

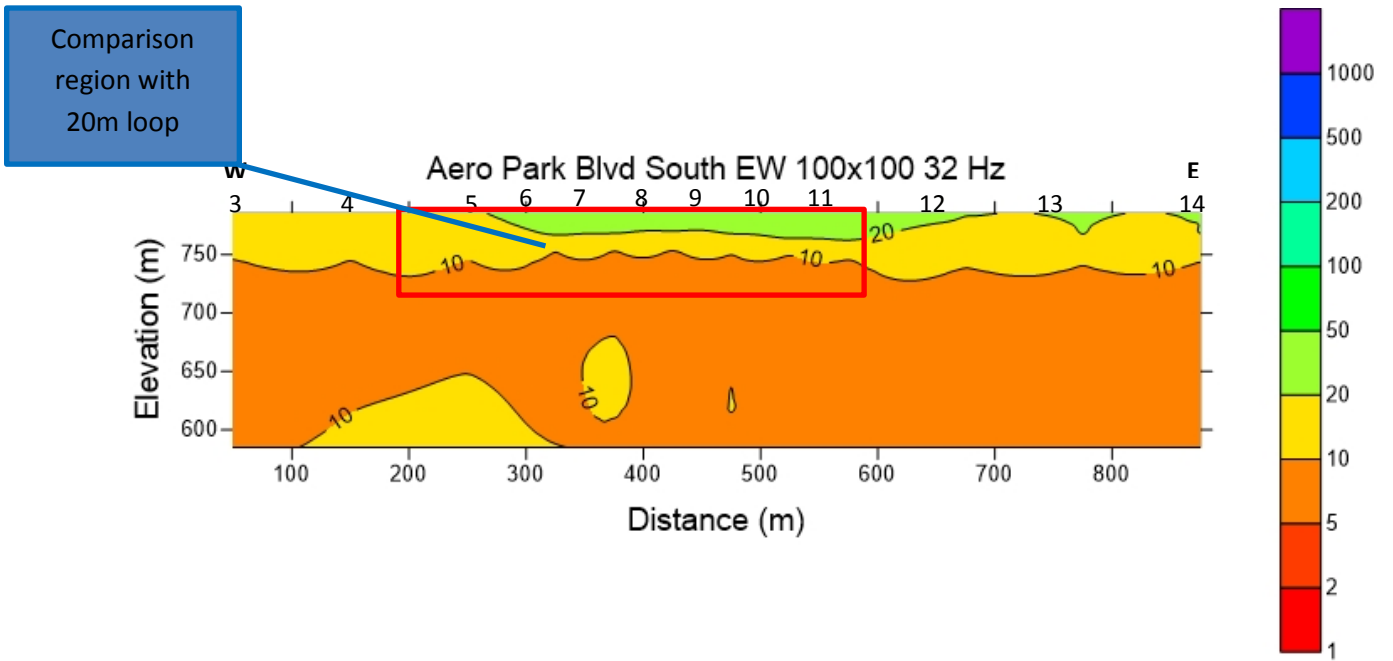


Fig 7.44 STEMINV inversion results

## References

- Bachrach, R., Dvorkin, J., Nur, A. (2002). Seismic velocities and Poisson's ratio of shallow unconsolidated sands, *Geophysics*, **65**, 559-564.
- Conestoga-Rovers and Associates, 2012. Tucson International Airport Superfund site [PowerPoint slides]. Oct 18 2012.
- Davidson, 1973. Geohydrology and water resources of the Tucson, Arizona. USGS paper 1939-E, 90p.
- G. Di Giulio, C. Cornou, M. Ohrnberger, M. Wathelet, and A. Rovellii (2006). Deriving Wavefield Characteristics and Shear-Velocity Profiles from Two-Dimensional Small-Aperture Arrays Analysis of Ambient Vibrations in a Small-Size Alluvial Basin, Colfiorito, Italy. *Bulletin of the Seismological Society of America*, **96**, 1915--1933.
- Houser, B. and M.E. Gettings (2000), Stratigraphy and tectonic history of the Tucson basin, Arizona, based on re-examination of cuttings and geophysical logs of the Exxon State (32)-1 well. *U.S. Geological Survey, Open File Report 00-139*, 1-39.
- EPA, 2013. "EPA Superfund site - region 9 : Tucson International Airport." Accessed April 23, 2013. <http://www.epa.gov/region9/superfund/>
- Loy, K. (1990) Subsurface structure of the Southern and Central Tucson Basin, Pima County, Arizona, M.Sc., 81 p.
- SESAME (2004). Guidelines for the implementation of the H/V spectral ratio technique on ambient vibrations: Measurements, processing and interpretation. SESAME European Research Project.
- Wathelet, M., D. Jongmans, M. Ohrnberger, and S. Bonnefoy-Claudet (2008). Array

performances for ambient vibrations on a shallow structure and consequences over Vs inversion. Journal of Seismology, 12, 1-19.

Zonge, 2009. Introduction to TEM. (<http://www.zonge.com>)

Zonge, 2012. GDP-32". Geophysical receiver. Multi-function receiver. (<http://www.zonge.com>)

Zonge, 2013a. NT-20 TEM Transmitter. Multi-function, battery powered. (<http://www.zonge.com>)

Appendix A. GPS COORDINATES OF TRANSIENT ELECTROMAGNETIC SOUNDINGS (TEM), EM31 AND PASSIVE SEISMIC SURVEYS

Table A.1. GPS coordinates of the center of 20x20 m loops at the Samsonite North and Aero Park Blvd South North line.

Point Name	Description	UTM		Easting	Northing	Elevation_m
		Zone				
1. Samsonite North						
Ap100	2/9/2013 9:30	12		503758	3554806	780
Ap200	2/9/2013 10:11	12		503755	3554787	778
Ap201	2/9/2013 11:04	12		503768	3554783	777
Ap301	2/9/2013 11:24	12		503767	3554761	770
Ap401	2/9/2013 12:06	12		503769	3554744	774
Ap501	2/9/2013 12:33	12		503767	3554724	777
Ap601	2/9/2013 12:37	12		503769	3554703	782
Ap701	2/9/2013 12:51	12		503768	3554682	774
2. Aero Park Blvd South: South - North line						
1000	2/9/2013 13:57	12		503923	3552368	786
1100	2/9/2013 14:06	12		503925	3552387	783
1200	2/9/2013 15:01	12		503925	3552407	788
1300	2/9/2013 15:13	12		503926	3552429	784
1400	2/9/2013 15:18	12		503930	3552446	782
1500	2/9/2013 15:39	12		503930	3552465	783
1600	2/9/2013 15:56	12		503934	3552488	783
1700	2/9/2013 16:08	12		503930	3552506	784
1800	2/9/2013 16:19	12		503935	3552527	783

Table A.2. GPS coordinates of the center of 20x20 m loops at the Aero Park Blvd East West line and EPA-03.

Point Name	Description	UTM		Easting	Northing	Elevation(m)
		Zone				
3. Aero Park Blvd South: East - West line						
10000	2/10/2013 8:15	12		504065	3552630	788
11000	2/10/2013 8:35	12		504085	3552630	786
12000	2/10/2013 8:47	12		504103	3552631	782
13000	2/10/2013 8:57	12		504122	3552627	784
14000	2/10/2013 9:08	12		504141	3552630	780
15000	2/10/2013 9:21	12		504162	3552629	782
16000	2/10/2013 9:49	12		504178	3552627	787
17000	2/10/2013 10:01	12		504199	3552628	782
18000	2/10/2013 10:24	12		504216	3552629	781
19100	2/10/2013 10:51	12		504235	3552606	782
20100	2/10/2013 11:10	12		504254	3552604	782
21100	2/10/2013 11:21	12		504273	3552597	780
22100	2/10/2013 11:27	12		504289	3552592	786
23100	2/10/2013 11:40	12		504307	3552587	788
24100	2/10/2013 13:11	12		504328	3552592	782
25100	2/10/2013 13:16	12		504347	3552585	791
26000	2/10/2013 13:36	12		504365	3552607	786
27000	2/10/2013 13:48	12		504382	3552604	787
28000	2/10/2013 13:56	12		504400	3552600	787
29000	2/10/2013 14:08	12		504421	3552599	788
30000	2/10/2013 14:20	12		504439	3552598	786
31000	2/10/2013 14:30	12		504464	3552600	791
4. EPA-03						
Aj10	2/10/2013 15:15	12		504226	3552826	783
Aj20	2/10/2013 15:20	12		504206	3552830	783
Aj30	2/10/2013 15:26	12		504184	3552830	785
Aj40	2/10/2013 15:35	12		504163	3552831	782
Aj50	2/10/2013 15:50	12		504145	3552834	780

Table A.3. GPS coordinates of the center of 50x50 m loops at the Aero Park Blvd East West line.

Point Name	Date and time	UTM			Elevation (m)
		Zone	Easting	Northing	
3. Aero Park Blvd South: East - West line					
AE3_7	2/24/2013 9:20	12	504245	3552595	784
AE3_8	2/24/2013 9:51	12	504295	3552596	785
AE3_9	2/24/2013 10:07	12	504343	3552595	783
AE3 10L	2/24/2013 10:31	12	504385	3552644	783
AE3 11L	2/24/2013 10:52	12	504434	3552645	782

Table A.4. GPS coordinates of the centers and corners of 100x100 m loops at the Aero Park Blvd South North line.

Point Name	Date and time	UTM			Elevation (m)
		Zone	Easting	Northing	
AE3 2.3	2/23/2013 10:25	12	503922	3552428	777
AE3_20	2/23/2013 8:41	12	503873	3552380	786
AE3_11	2/23/2013 9:46	12	503975	3552478	785
AE3_10	2/23/2013 9:32	12	503976	3552381	781
AE3_21	2/23/2013 8:47	12	503873	3552480	785
AE3 1.1	2/23/2013 9:56	12	503924	3552529	781
AE3 2	2/23/2013 10:18	12	503924	3552530	779
AE3 3.2	2/23/2013 14:09	12	504023	3552613	788
AE3 3.3	2/23/2013 13:30	12	503927	3552518	787
AE3 22	2/23/2013 9:59	12	503872	3552579	781
AE3 13	2/23/2013 11:28	12	503974	3552565	778
AE3 2.1	2/23/2013 10:46	12	503926	3552629	777
AE3 3	2/23/2013 13:25	12	503926	3552617	781
AE3 25	2/23/2013 13:49	12	503979	3552664	785
AE3 24	2/23/2013 14:17	12	503878	3552661	781

Table A.5. GPS coordinates of the centers and corners of 100x100 m loops at the Aero Park Blvd East West line and EPA-03.

Point Name	Date and time	UTM		Easting	Northing	Elevation (m)
		Zone				
3. Aero Park Blvd South: East - West line						
AE3_12	2/23/2013 9:54	12		503975	3552577	782
AE3_14	2/23/2013 14:52	12		504071	3552570	788
AE3_25	2/23/2013 12:57	12		503976	3552667	780
AE3_26	2/23/2013 14:01	12		504074	3552661	788
AE3_5	2/23/2013 4:28	12		504127	3552607	782
AE3_15	2/23/2013 3:46	12		504173	3552568	782
AE3_6.4	2/24/2013 9:15	12		504147	3552593	781
AE3_27.5	2/24/2013 7:54	12		504173	3552618	790
AE3_27	2/23/2013 14:56	12		504174	3552657	783
AE3_35	2/24/2013 10:25	12		504498	3552663	780
AE3_19.5	2/24/2013 10:30	12		504598	3552563	780
AE3_19.4	2/24/2013 10:19	12		504498	3552563	778
AE3_36	2/24/2013 10:33	12		504596	3552663	781
AE3_13L	2/24/2013 11:55	12		504649	3552612	779
AE3_36	2/24/2013 10:33	12		504596	3552663	781
AE3_37	2/24/2013 11:00	12		504695	3552664	780
AE3_14L	2/24/2013 12:34	12		504744	3552615	787
AE3_19.8	2/24/2013 12:14	12		504796	3552565	787
AE3_37	2/24/2013 11:00	12		504695	3552664	780
AE3_39	2/24/2013 12:20	12		504794	3552665	784
4. EPA-03						
BA1	2/24/2013 14:26	12		504191	3552814	787
BA11	2/24/2013 14:23	12		504239	3552765	786
BA1.2	2/24/2013 14:50	12		504289	3552814	789

Table A.6. GPS coordinates along the EM31 transects.

Distance along transect (m)	Easting	Northing	Notes
2. Aero Park Blvd South: south - north line			
0	503932.90	3552358.27	only one transect
50	503932.90	3552408.27	
100	503932.90	3552458.27	
150	503932.90	3552508.27	
200	503932.90	3552558.27	
250	503932.90	3552608.27	
3. Aero Park Blvd South: east - west line			
0	503999.94	3552643.01	first transect
50	504049.94	3552643.01	
50	504055.00	3552620.00	second transect
100	504105.00	3552620.00	
150	504155.00	3552620.00	
200	504205.00	3552620.00	
250	504255.00	3552620.00	
300	504305.00	3552620.00	
350	504355.00	3552620.00	
400	504405.00	3552620.00	
450	504455.00	3552620.00	
4. EPA-03			
0	504239.80	3552826.84	east-west
50	504189.80	3552826.84	
100	504139.80	3552826.84	
0	504189.49	3552761.39	south-north
50	504201.51	3552810.37	
100	504213.53	3552859.34	

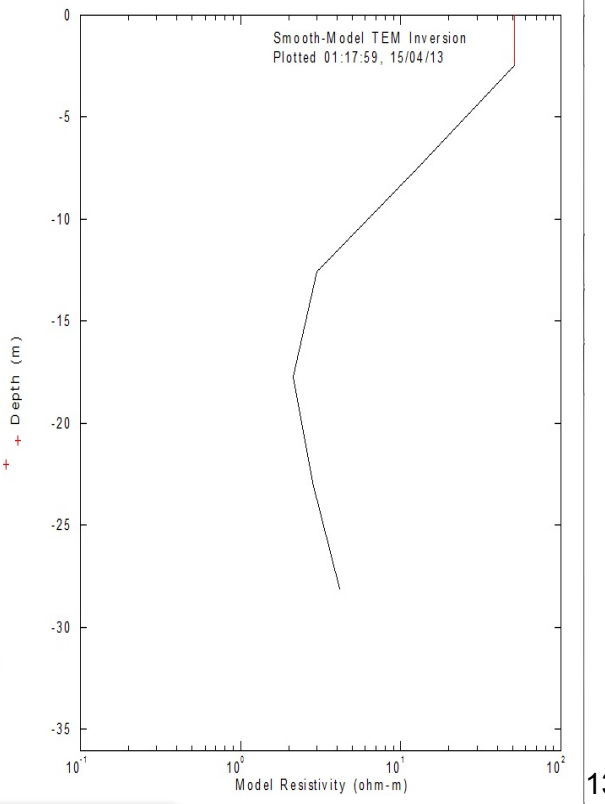
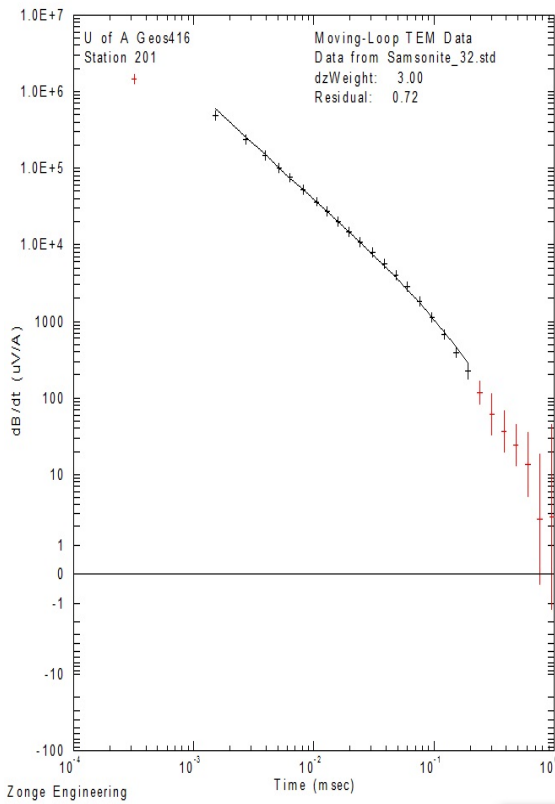
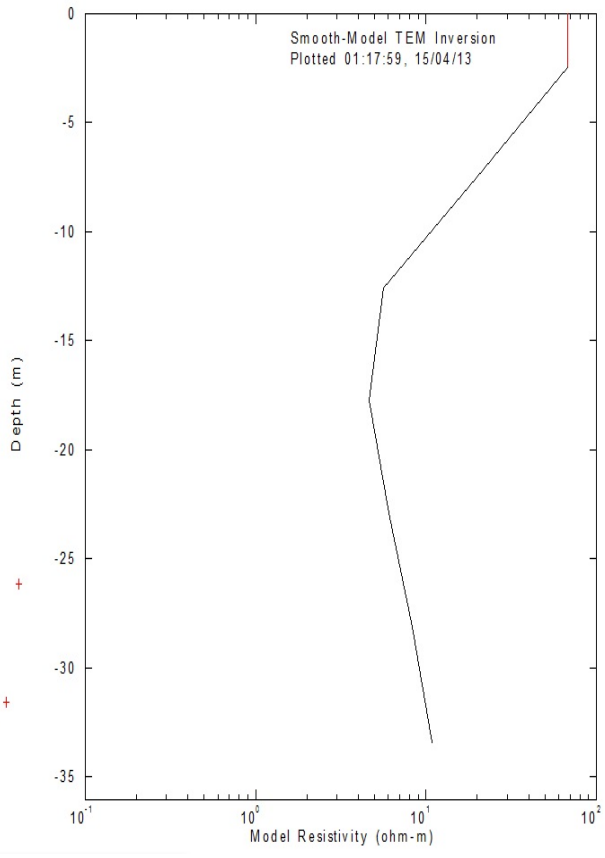
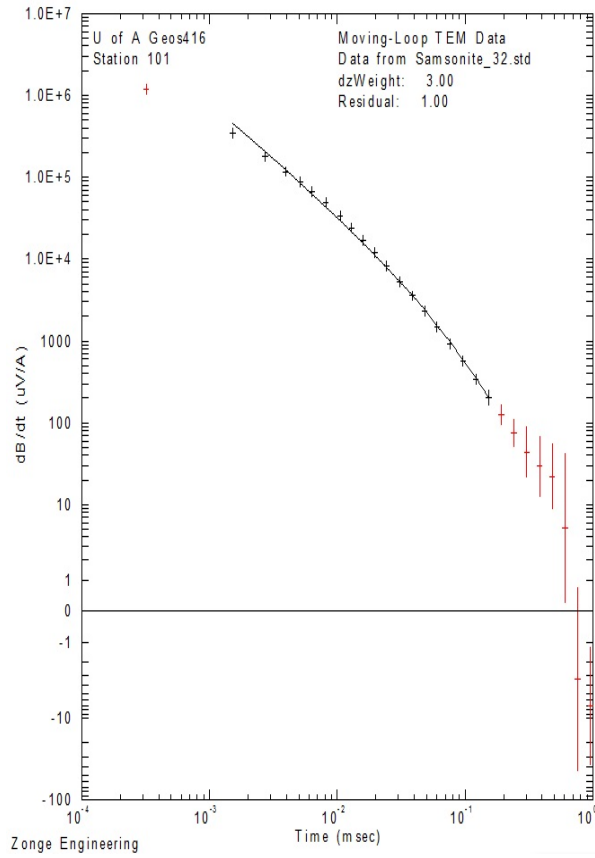
Table A.6. GPS coordinates from passive seismic stations.

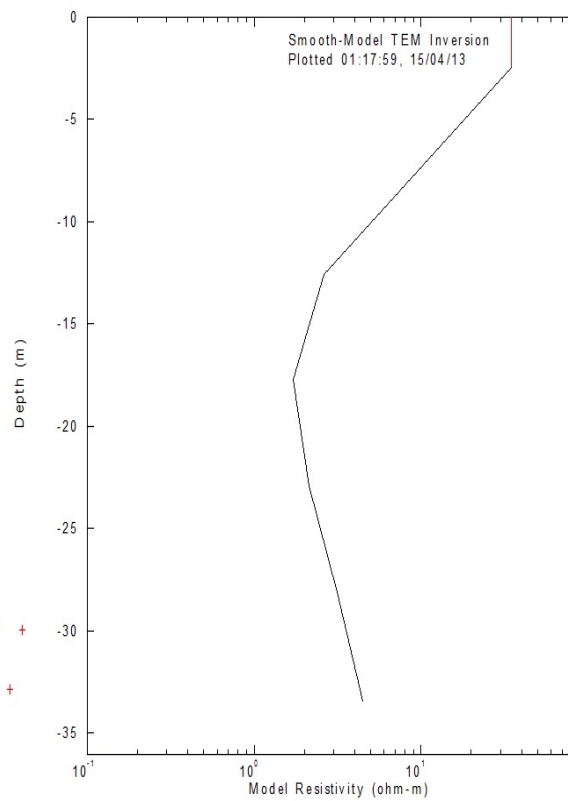
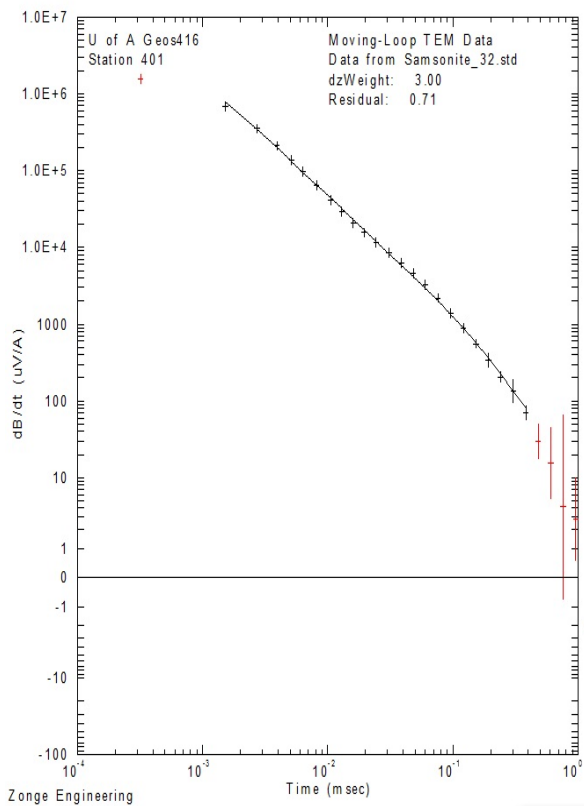
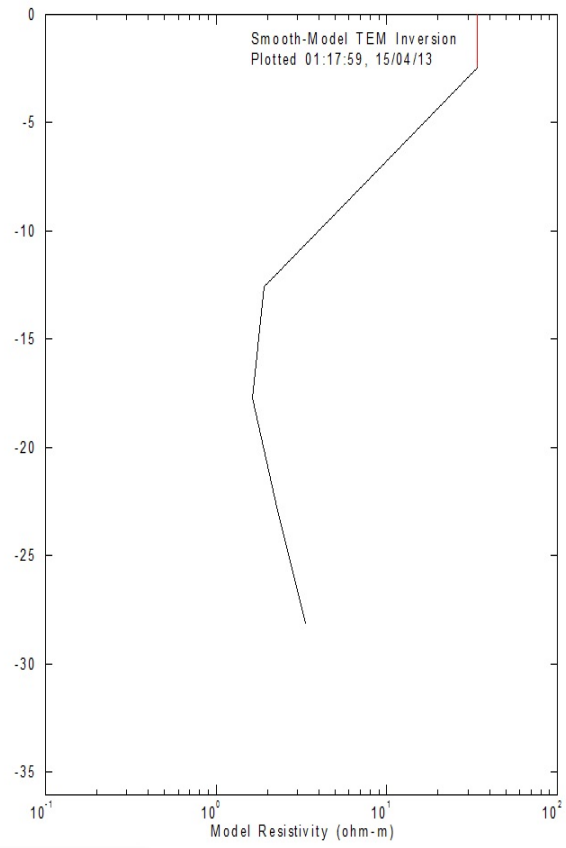
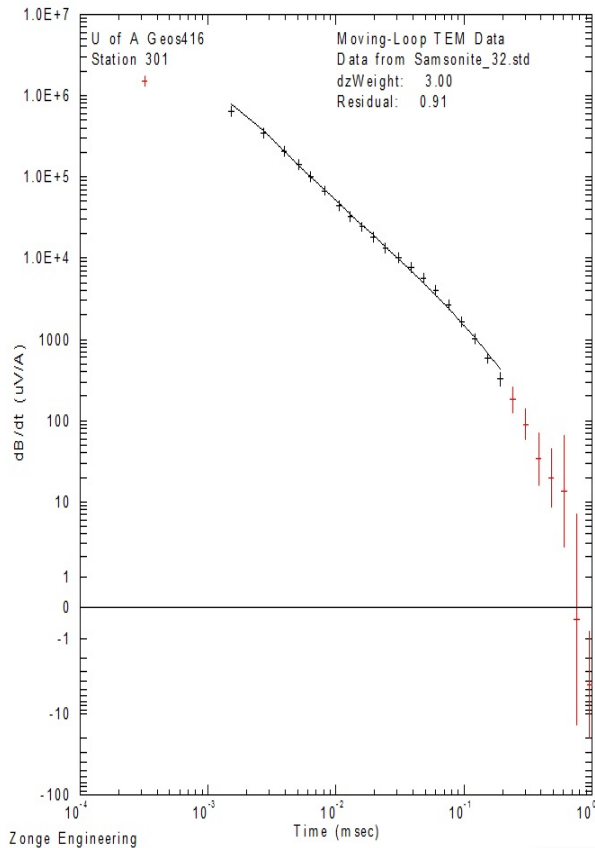
Date	Seismometer	Time (Arizona time)	Northing	Easting
2/23/2013	A834			
	T6B77	9:24 AM	3552353	503988
	T6B75	10:43 AM	3552354	503834
	T6B75	10:23 AM	3552361	503855
	T6B77	11:41 AM	3552353	504003
	T6B75	12:11 PM	3552358	503878
	T6B77	1:16 PM	3552342	503977
	T6B75	1:42 PM	3552366	503919
	T6B77	2:25 PM	3552375	50398
2/24/2013	T6B77	8:09 AM	3552356	503933
	A834	8:26 AM	3552457	503955
	T6B75	8:37 AM	3552556	503952
	A834	9:38 AM		
	T6B77	9:46 AM	3552669	503953
	T6B75	10:04 AM	3552578	504056
	T6B77	11:08 AM	3552644	504150
	T6B75	11:31 AM	3552642	504246
	T6B77	12:49 PM	3552645	504348
T6B75	1:17 PM	3552865	504250	

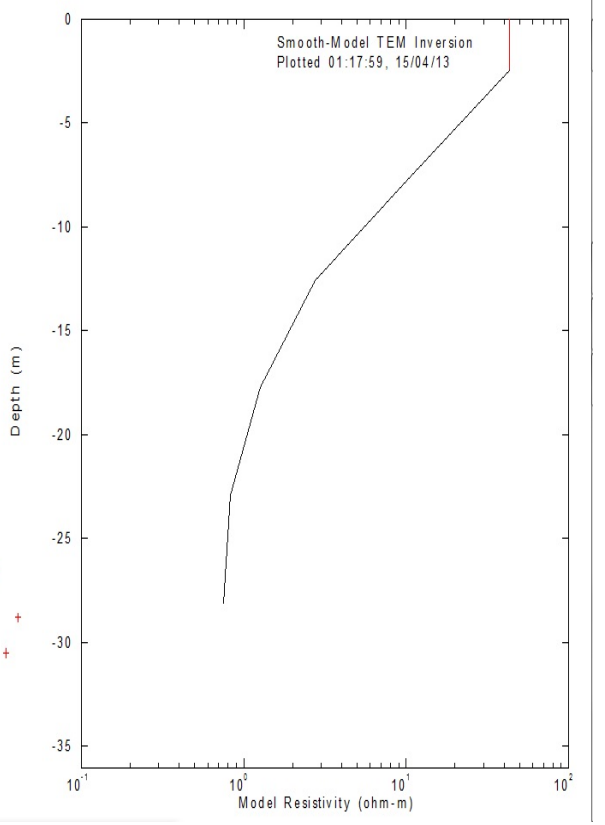
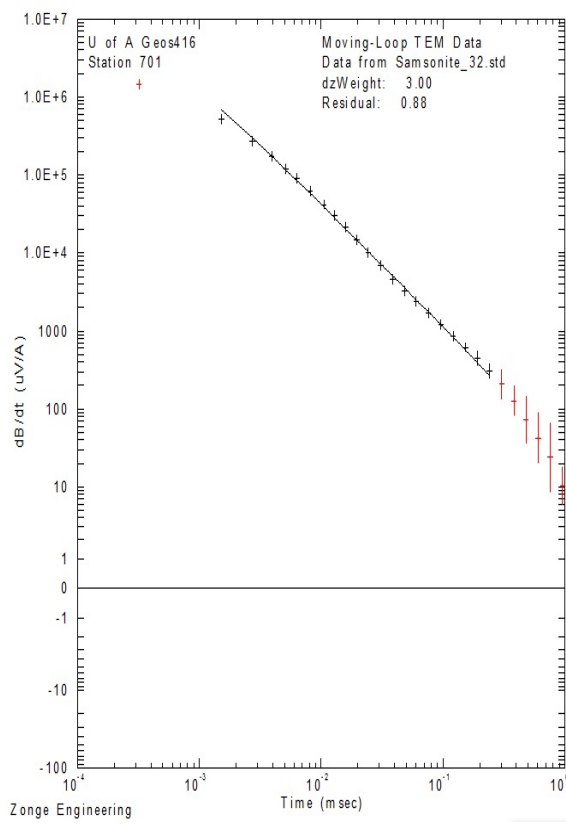
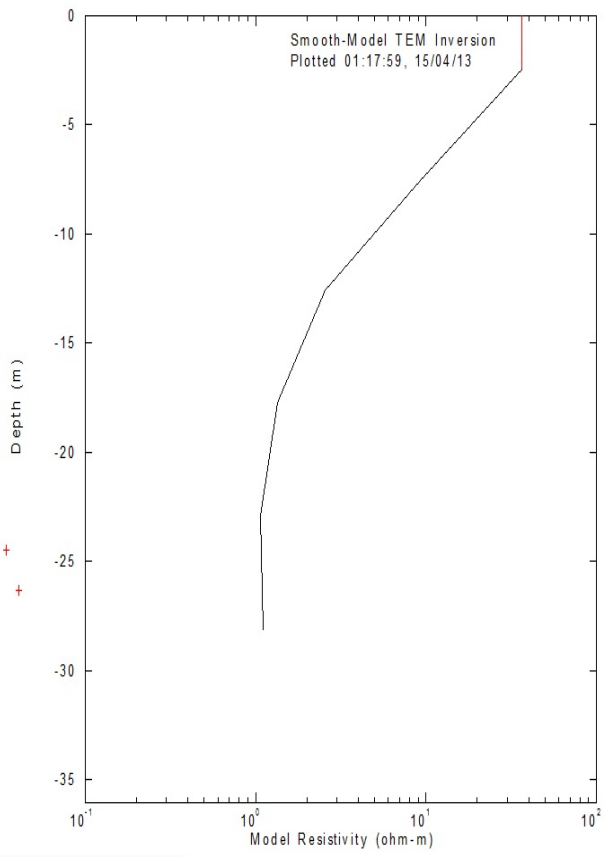
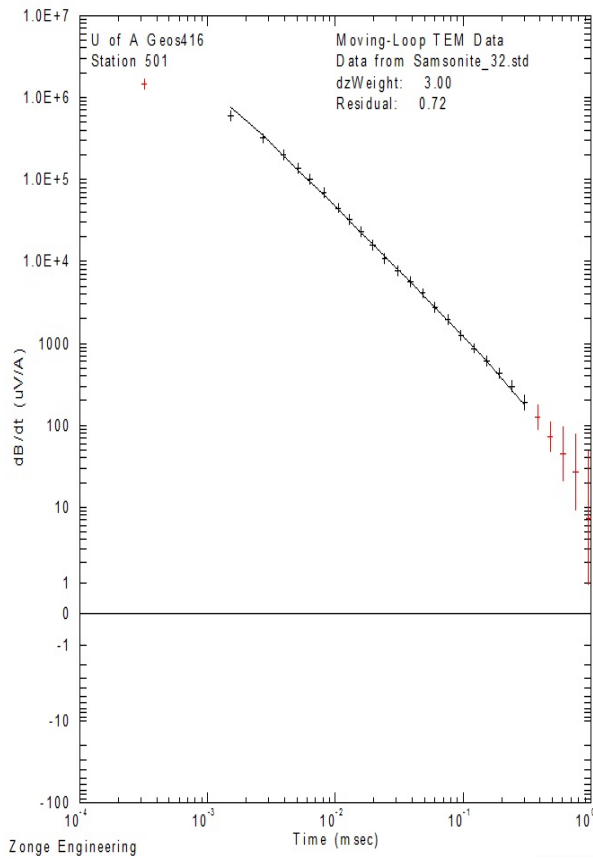
## Appendix B

In this appendix we show the smooth-model TEM inversion for all the loops in each area.

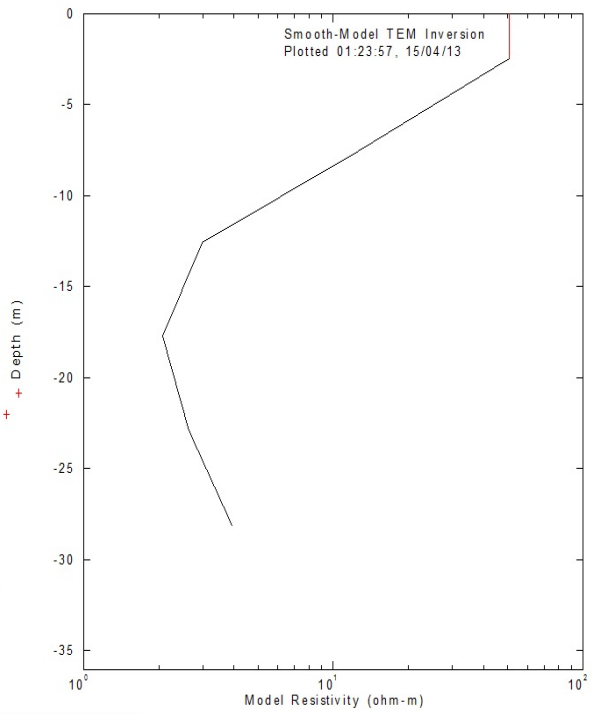
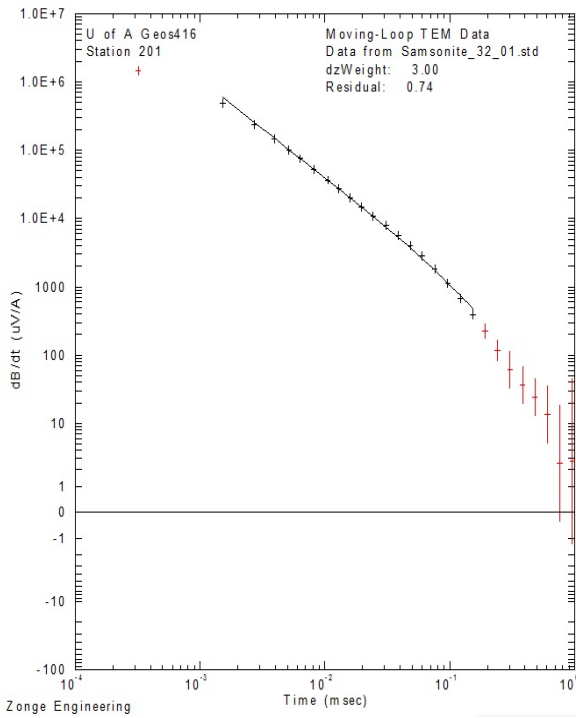
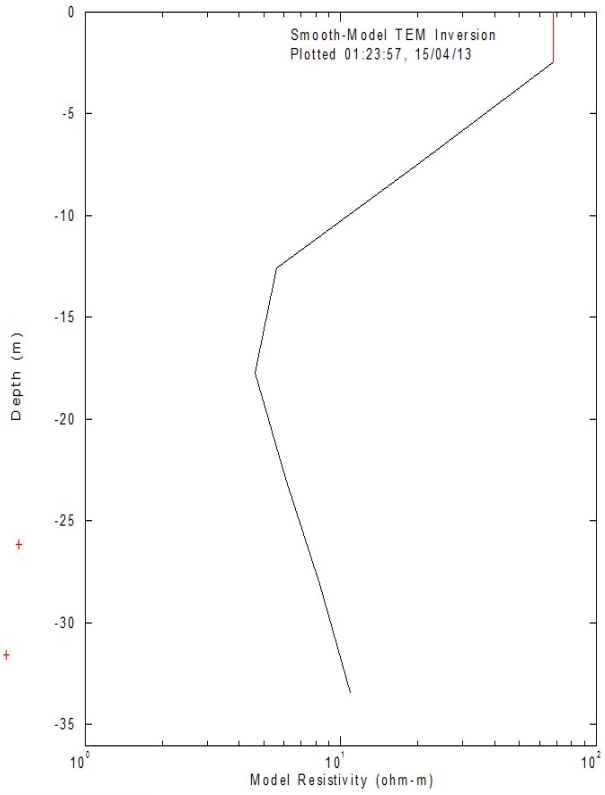
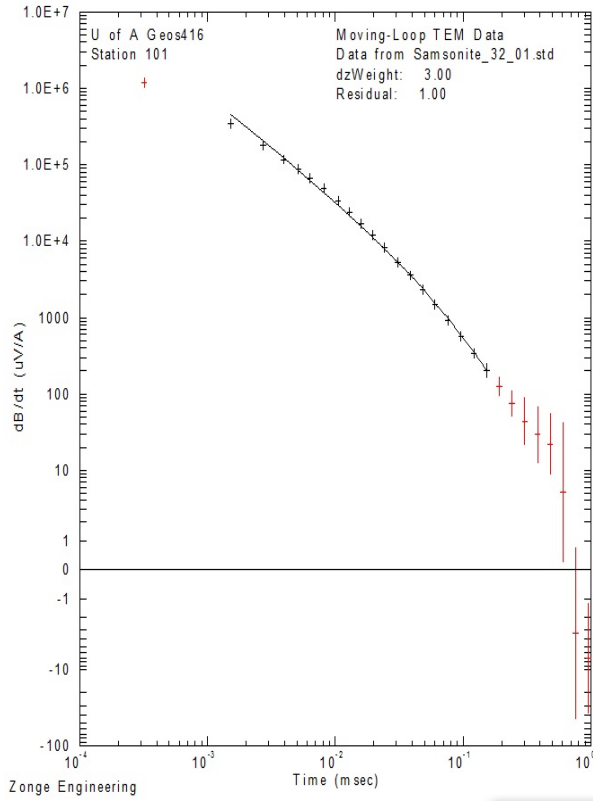
20x20 loops at the Samsonite South site with 32Hz



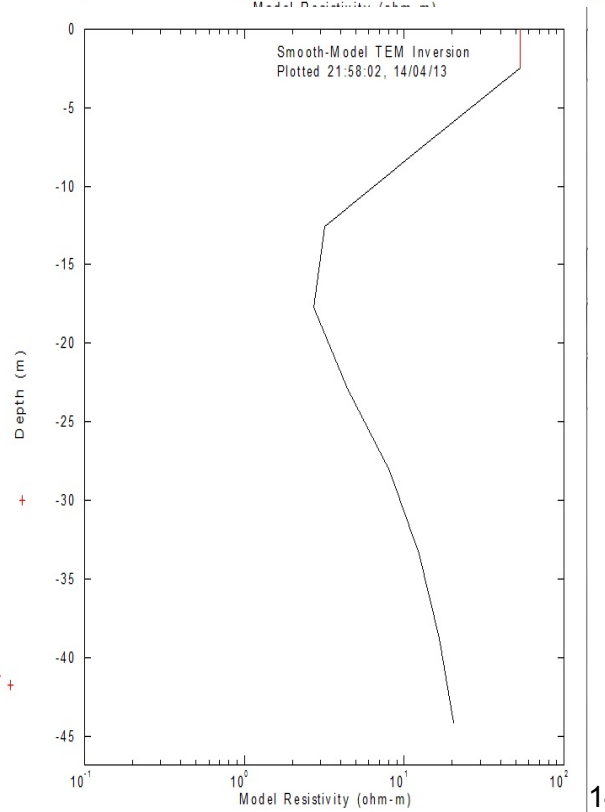
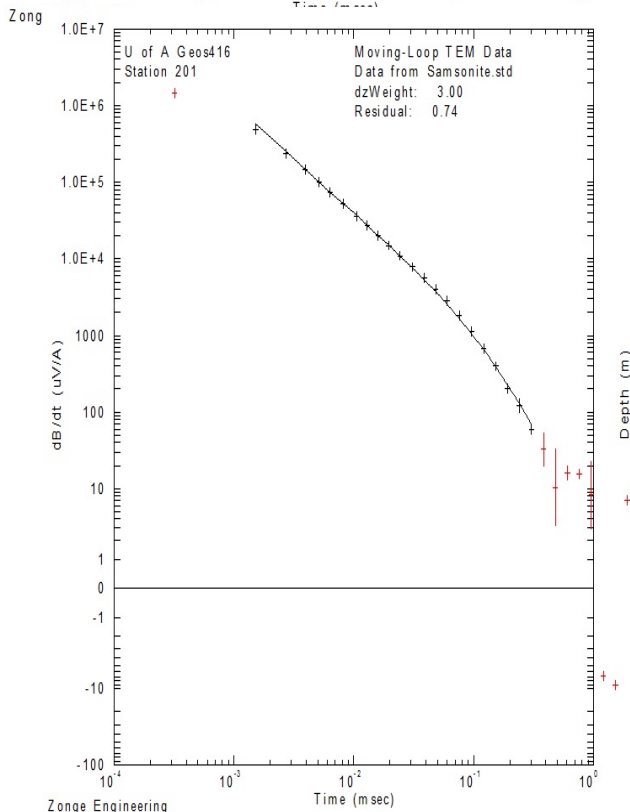
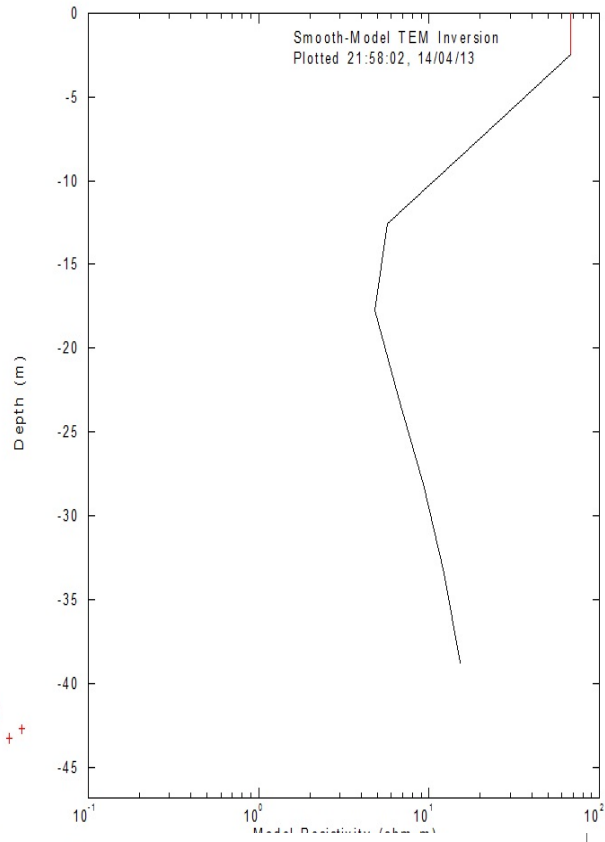
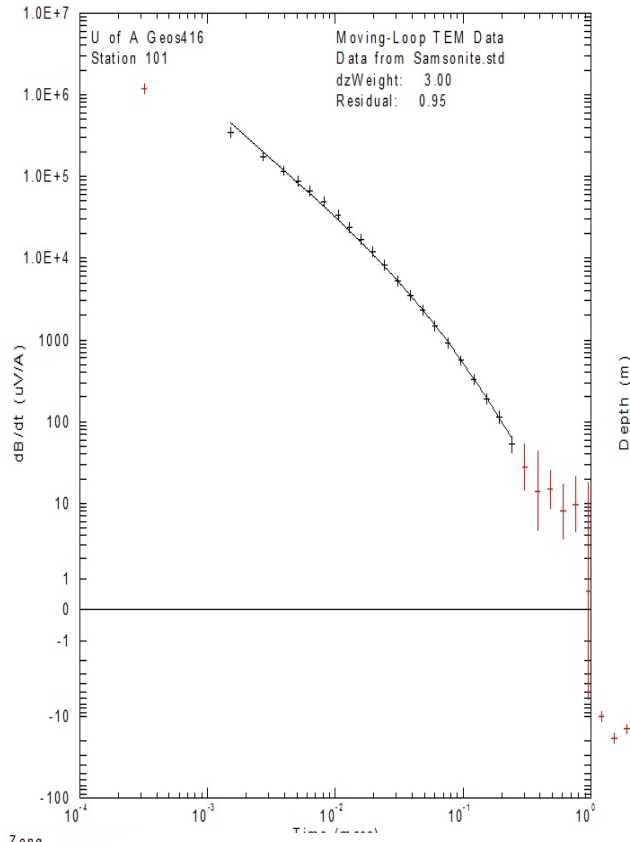


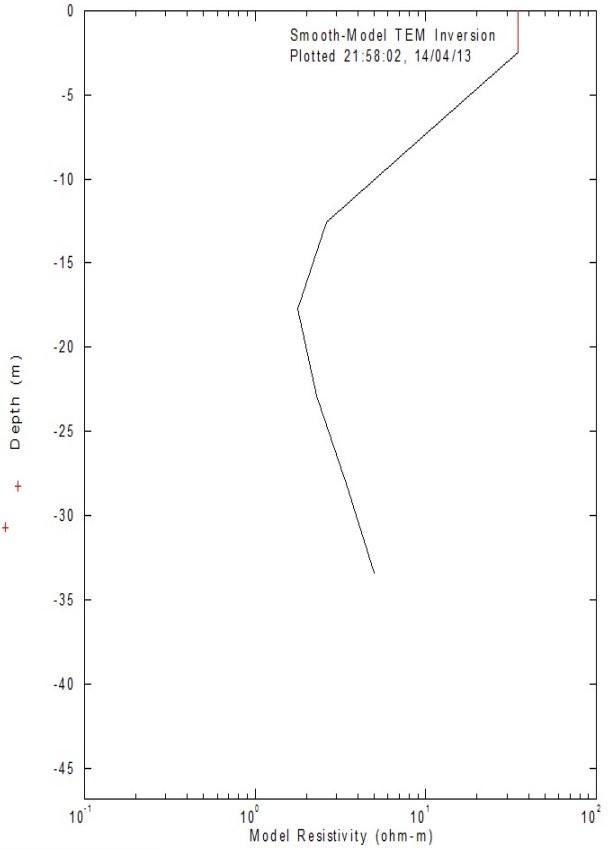
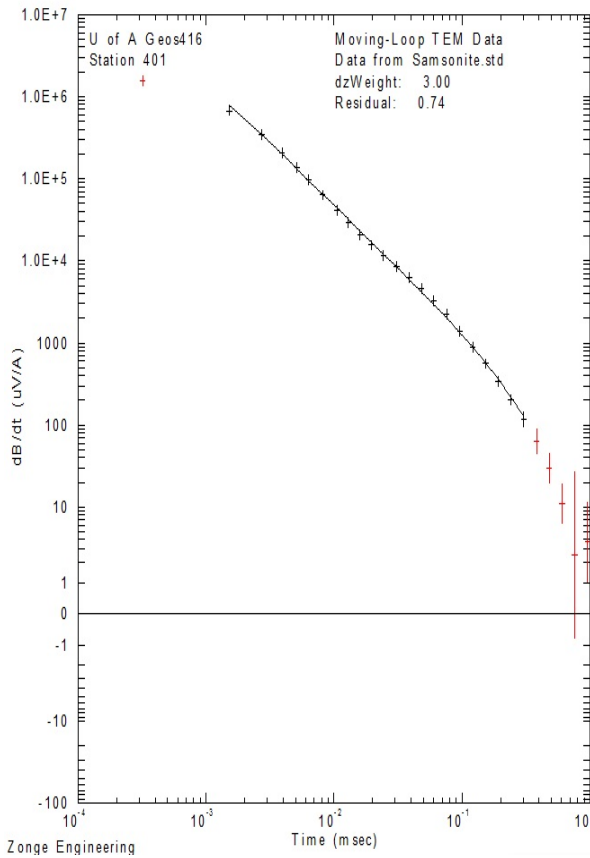
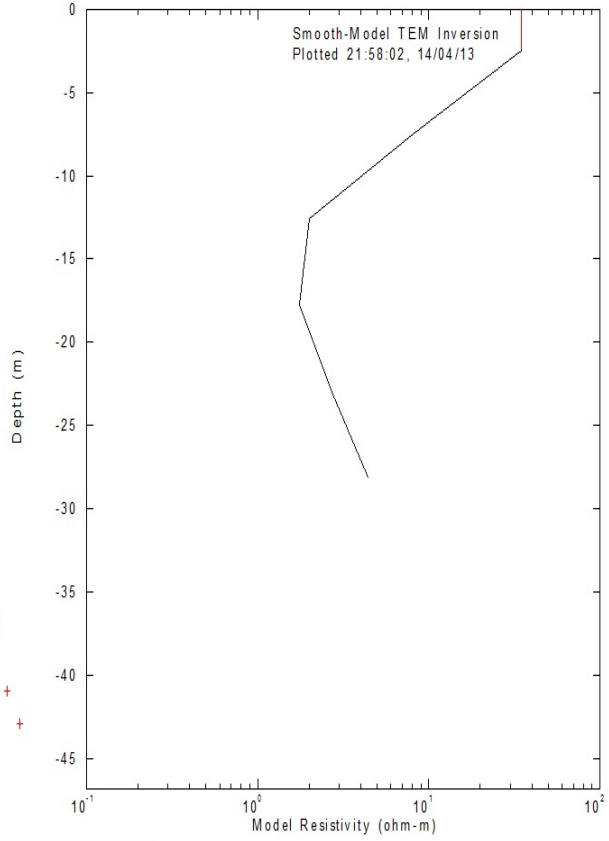
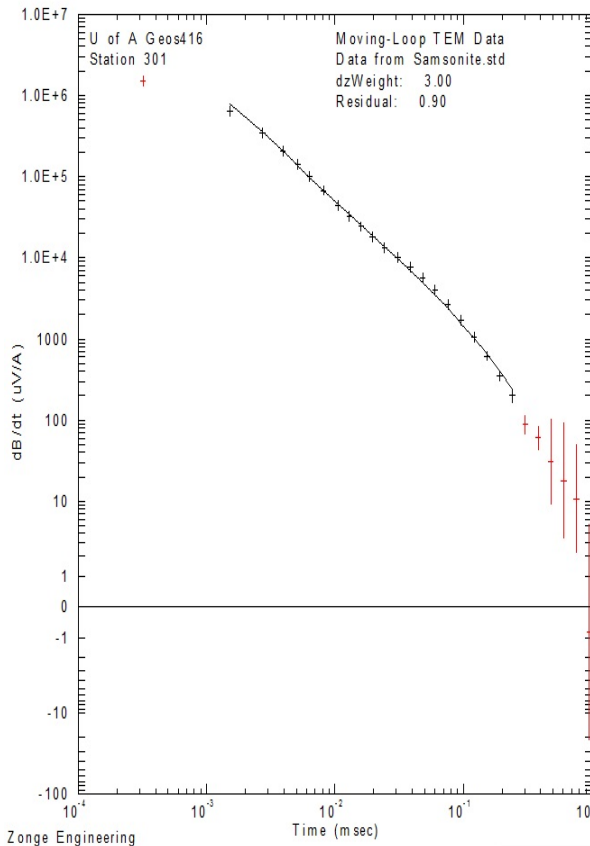


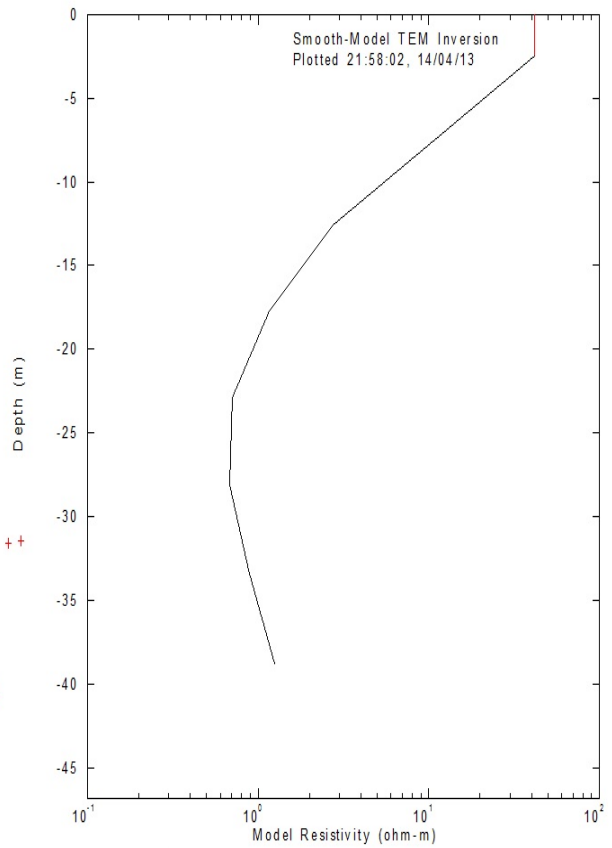
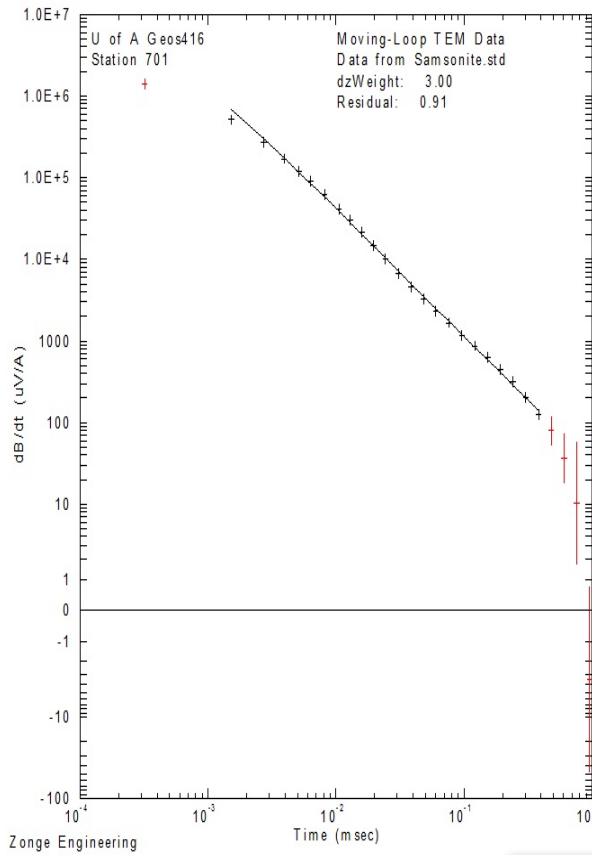
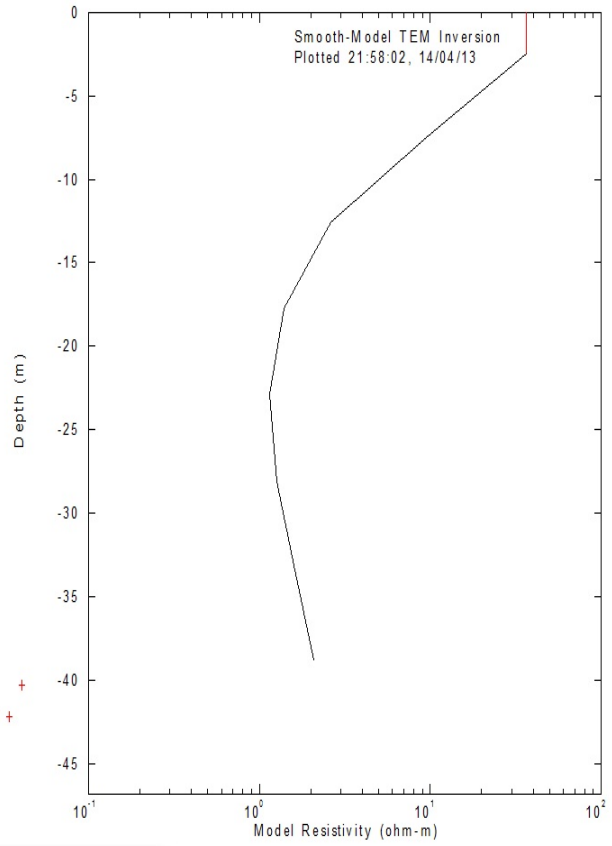
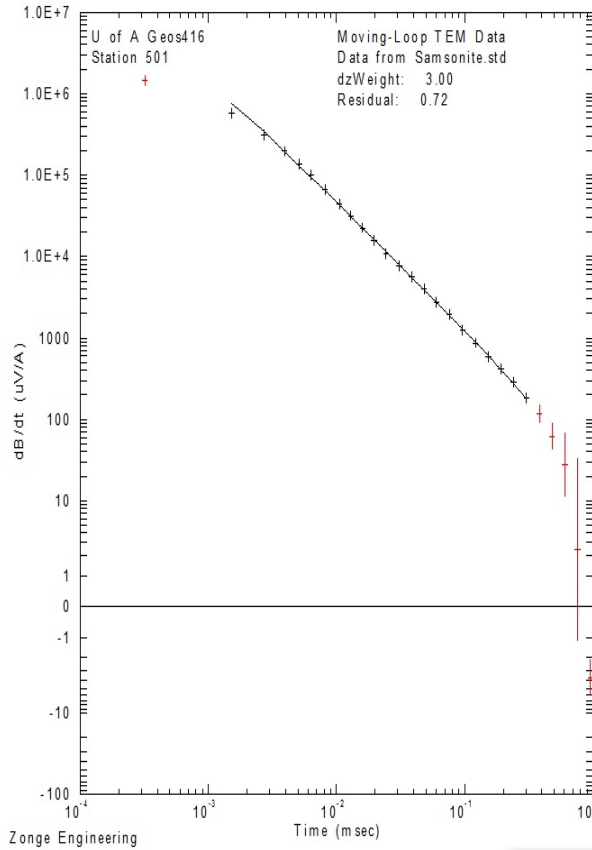
# The Adjacent two loops



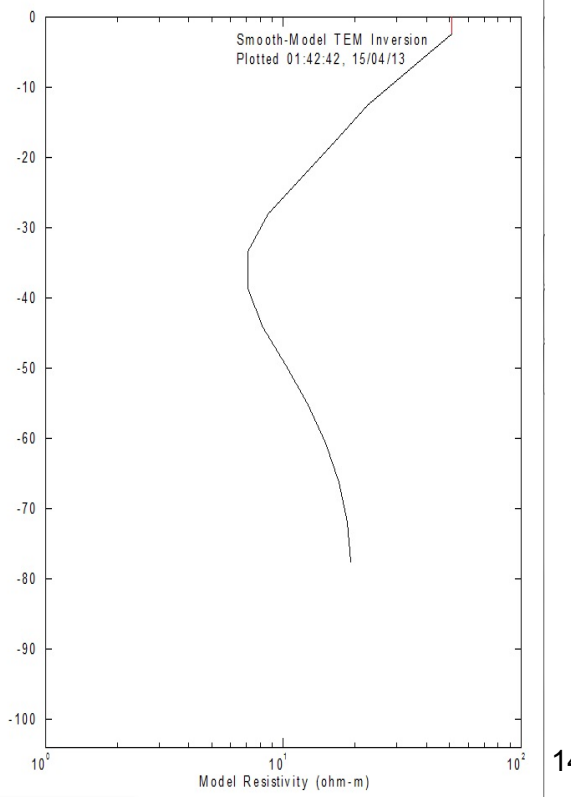
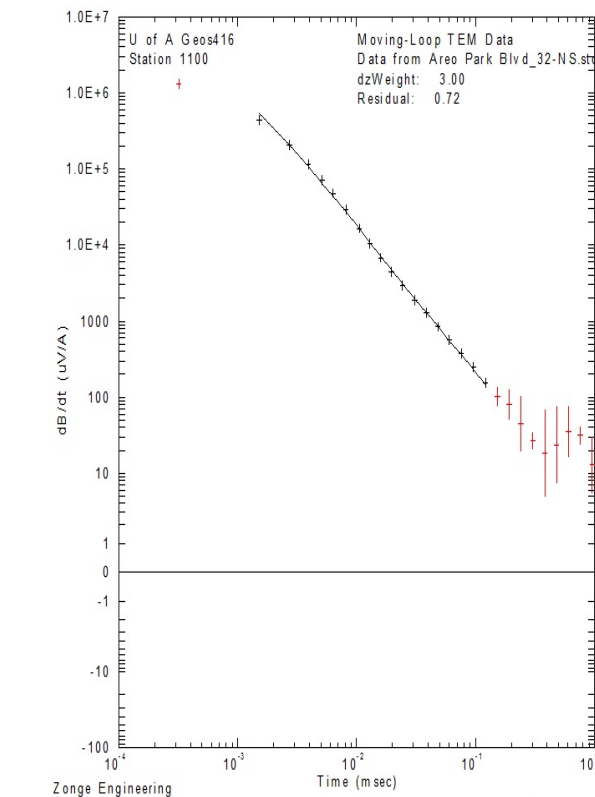
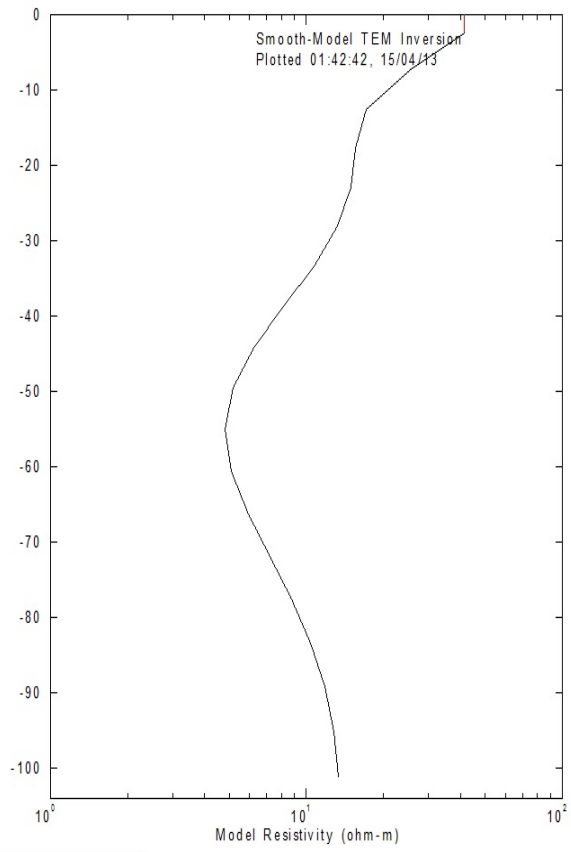
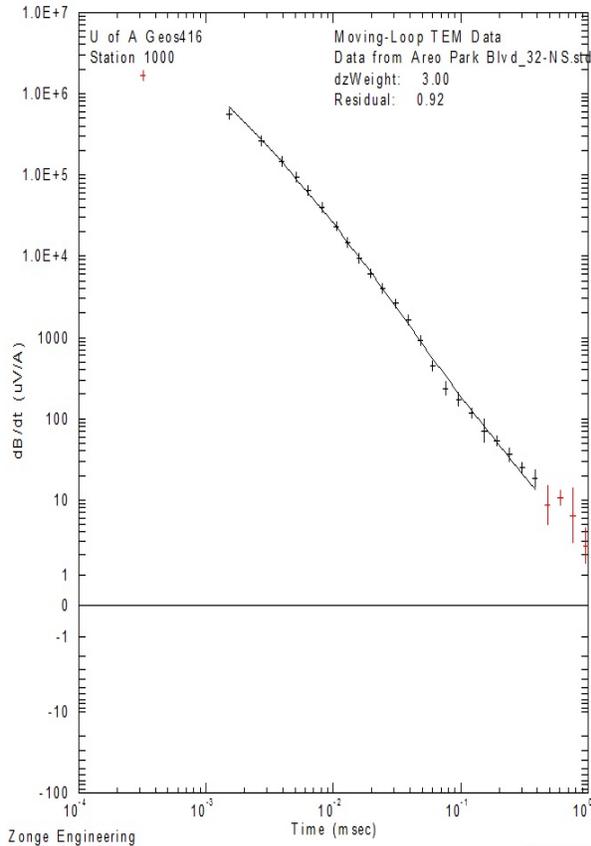
20x20 loops at the Samsonite South site with 64Hz

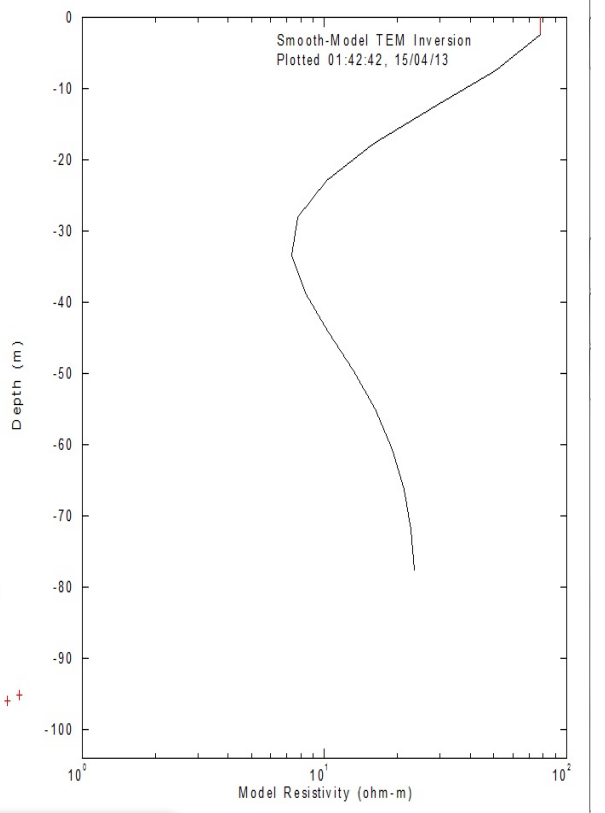
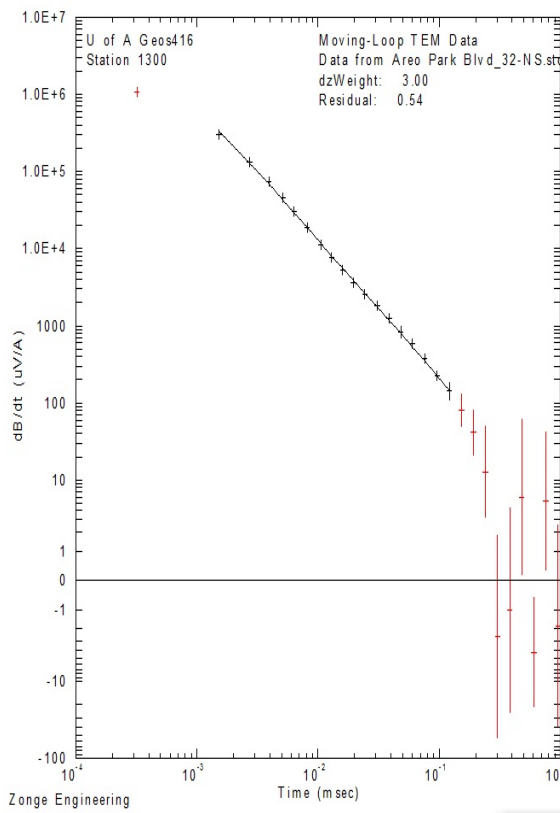
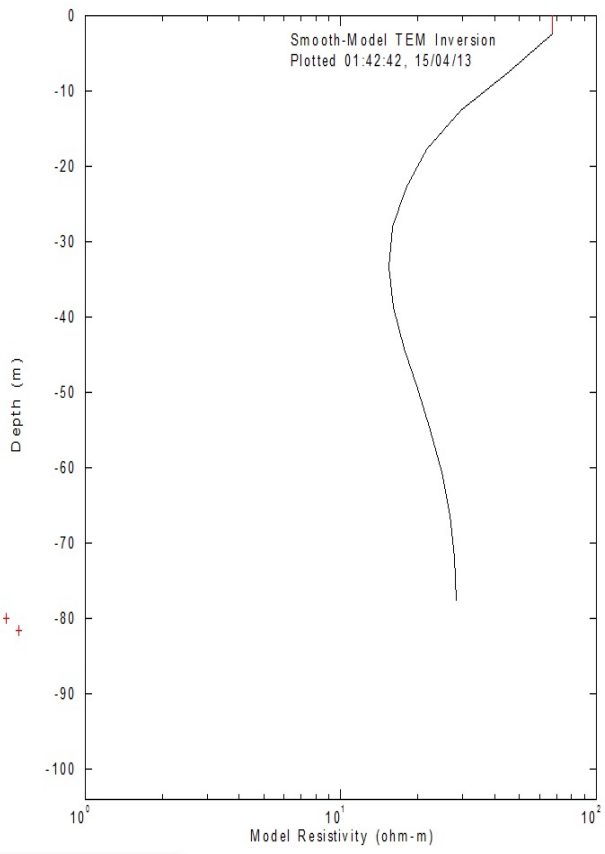
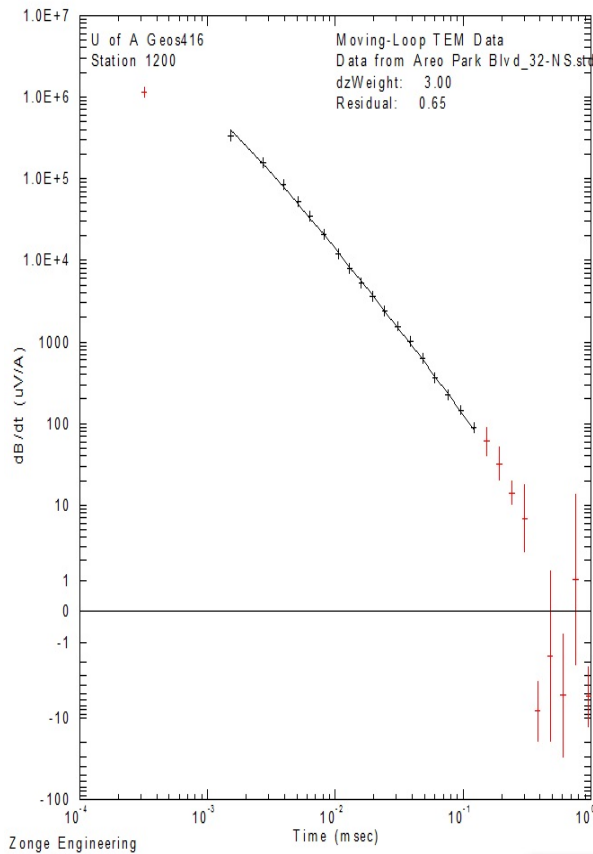


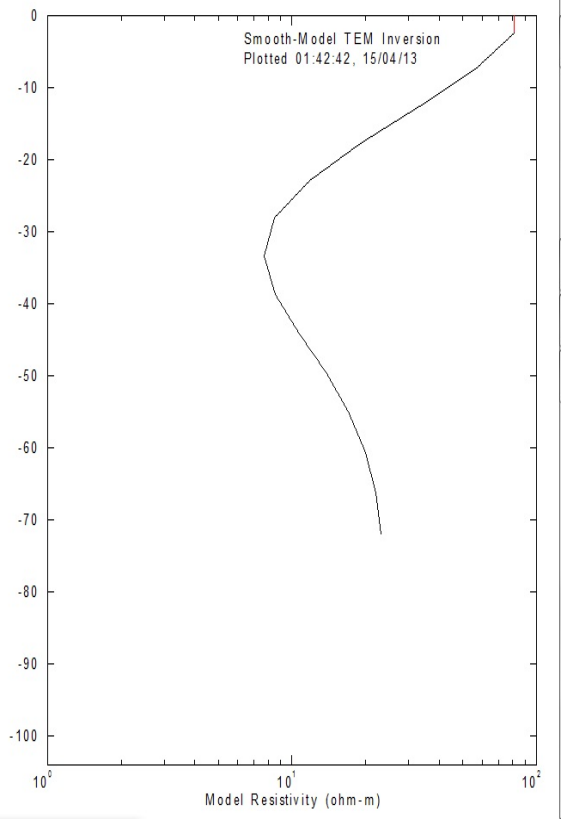
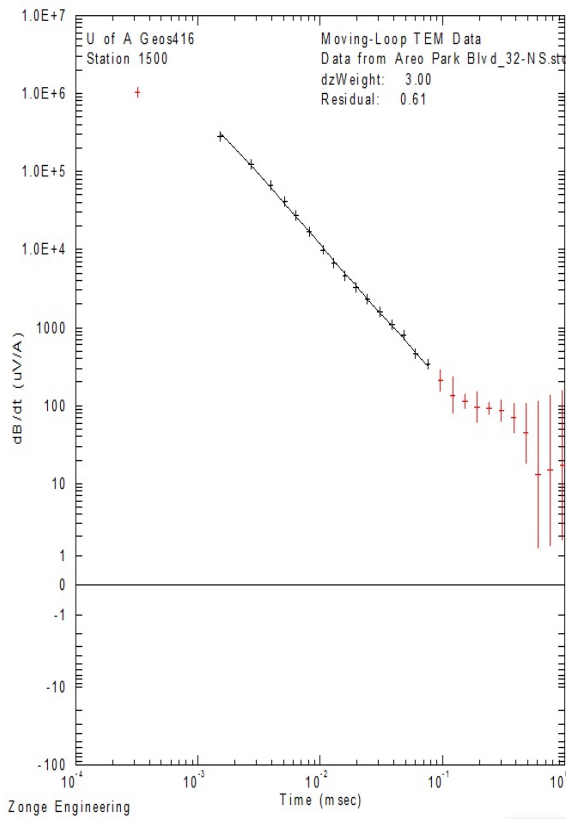
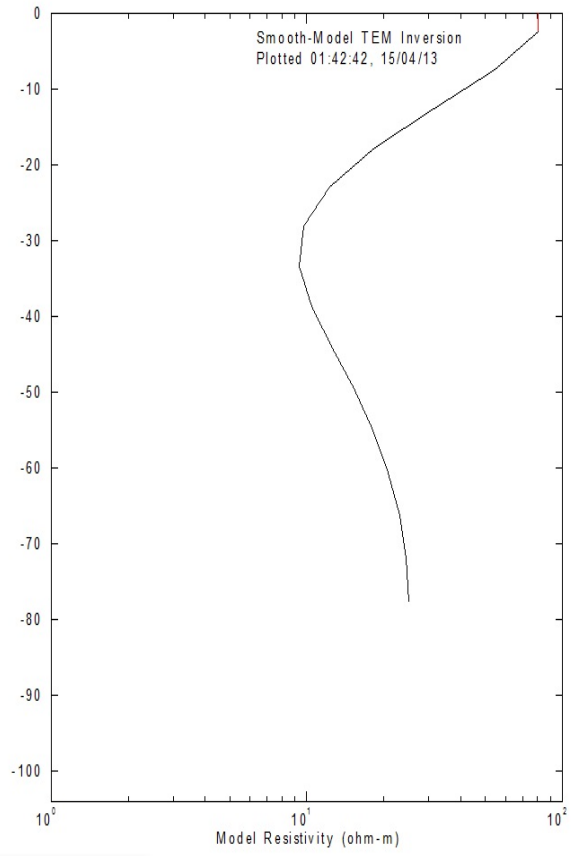
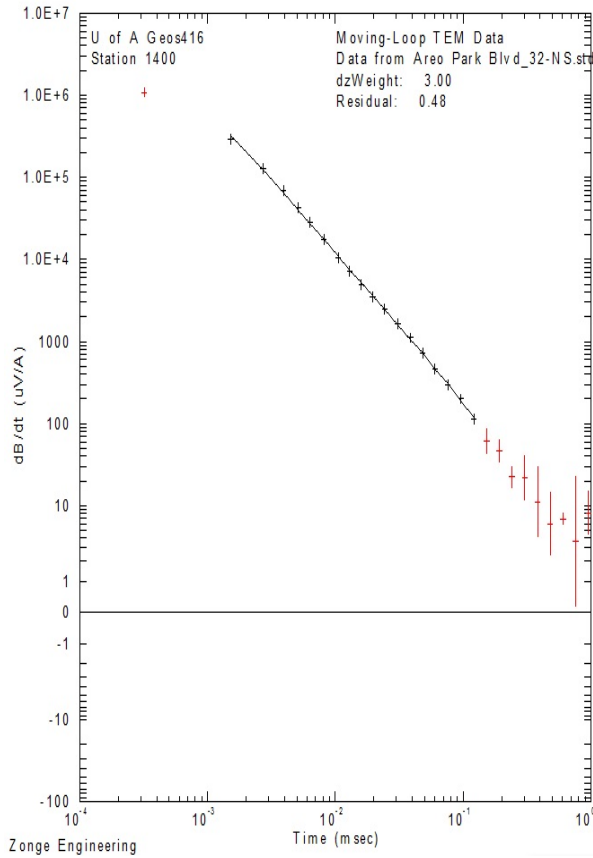


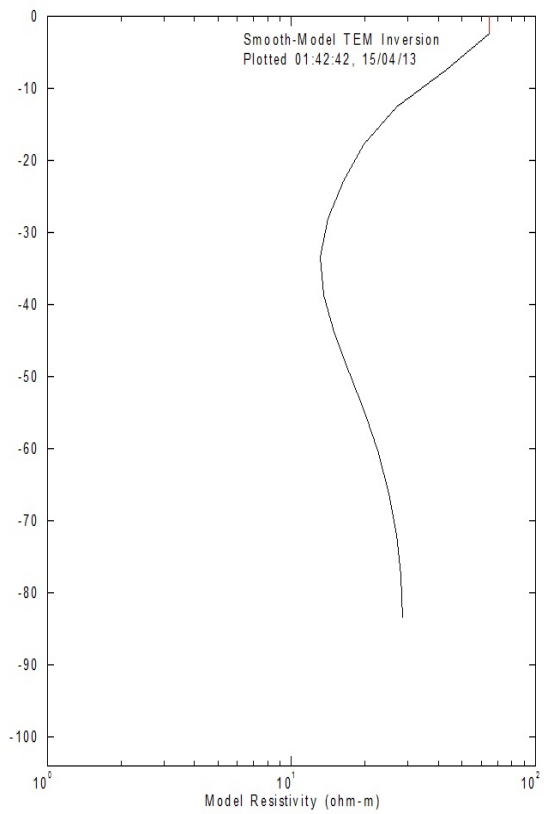
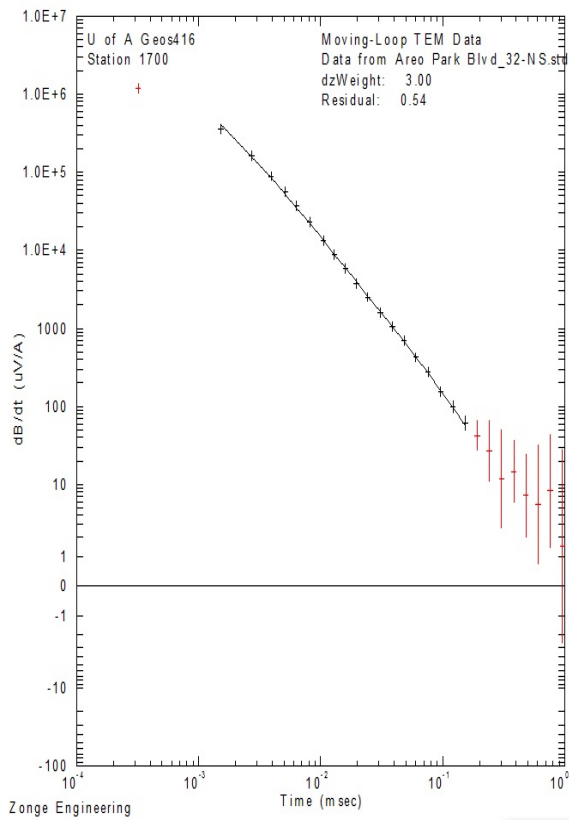
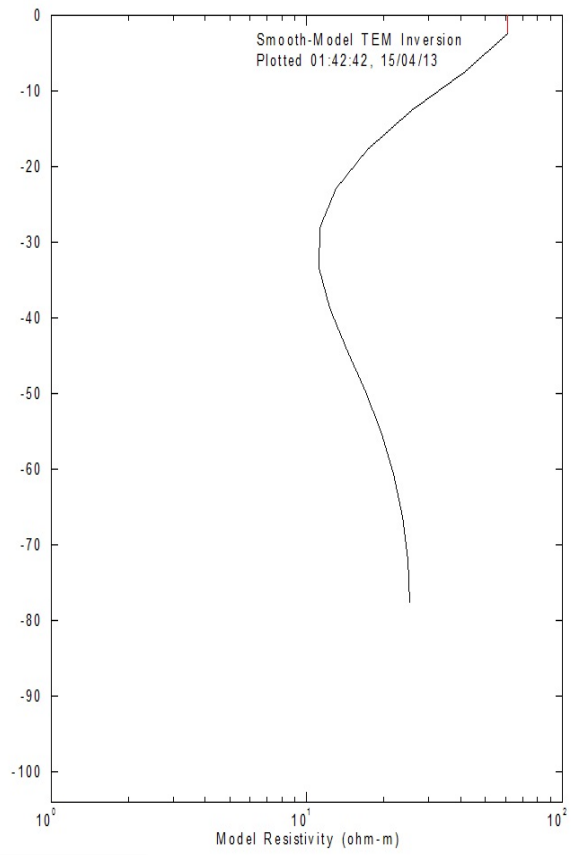
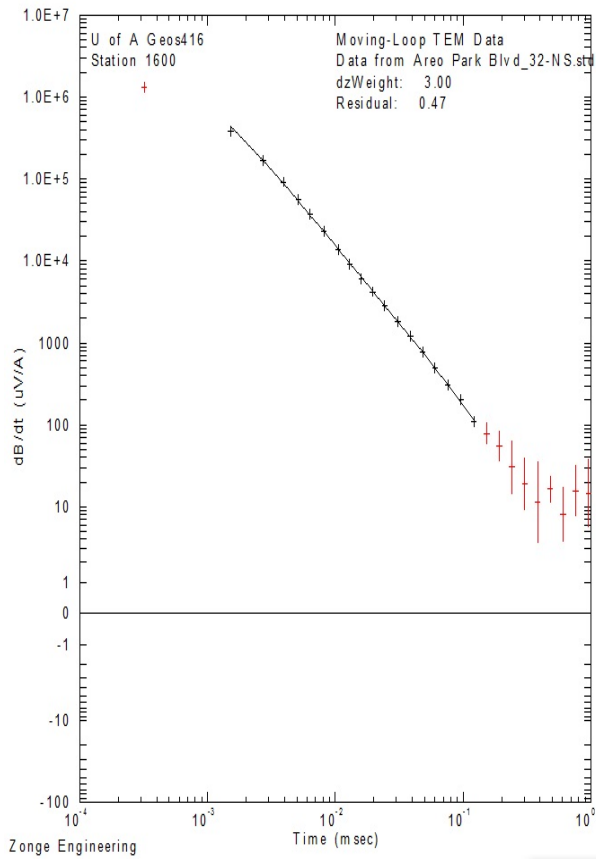


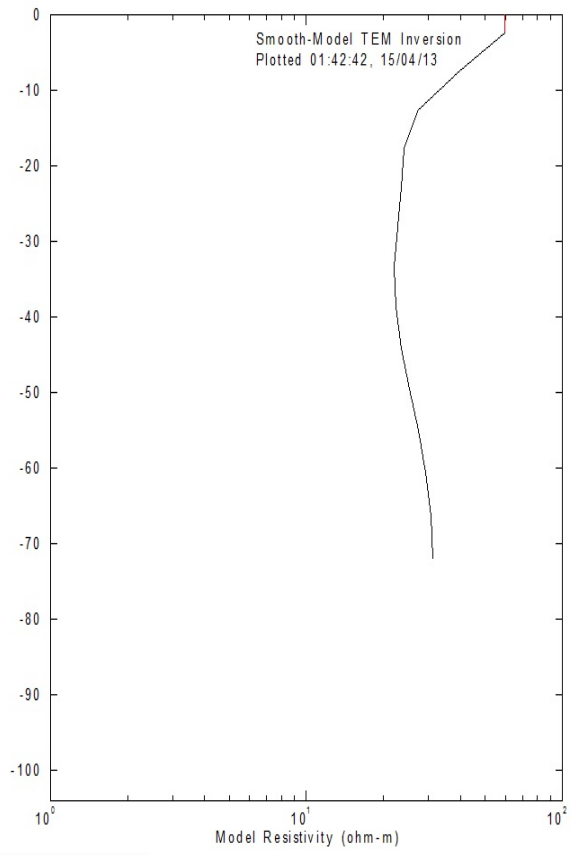
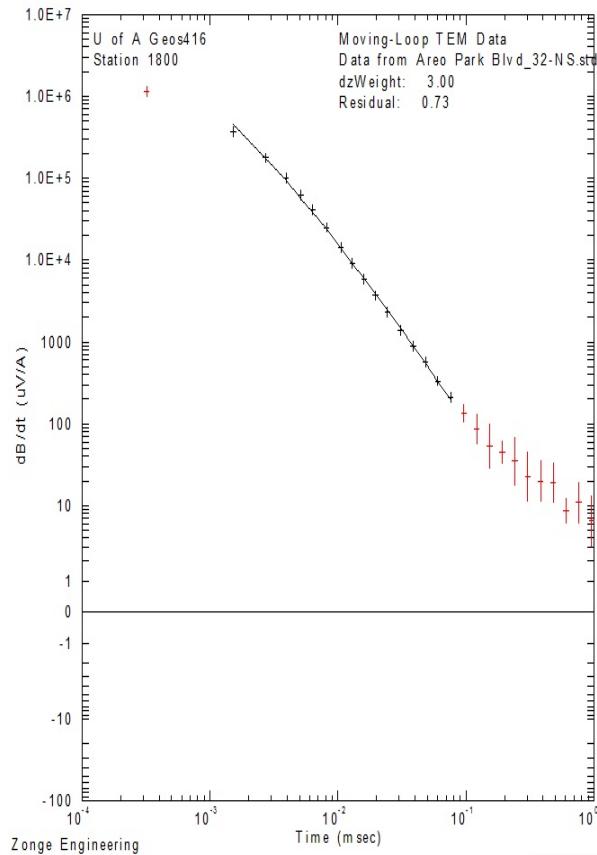
20x20 loops at the Aero Park Blvd South site with 32Hz from south to North



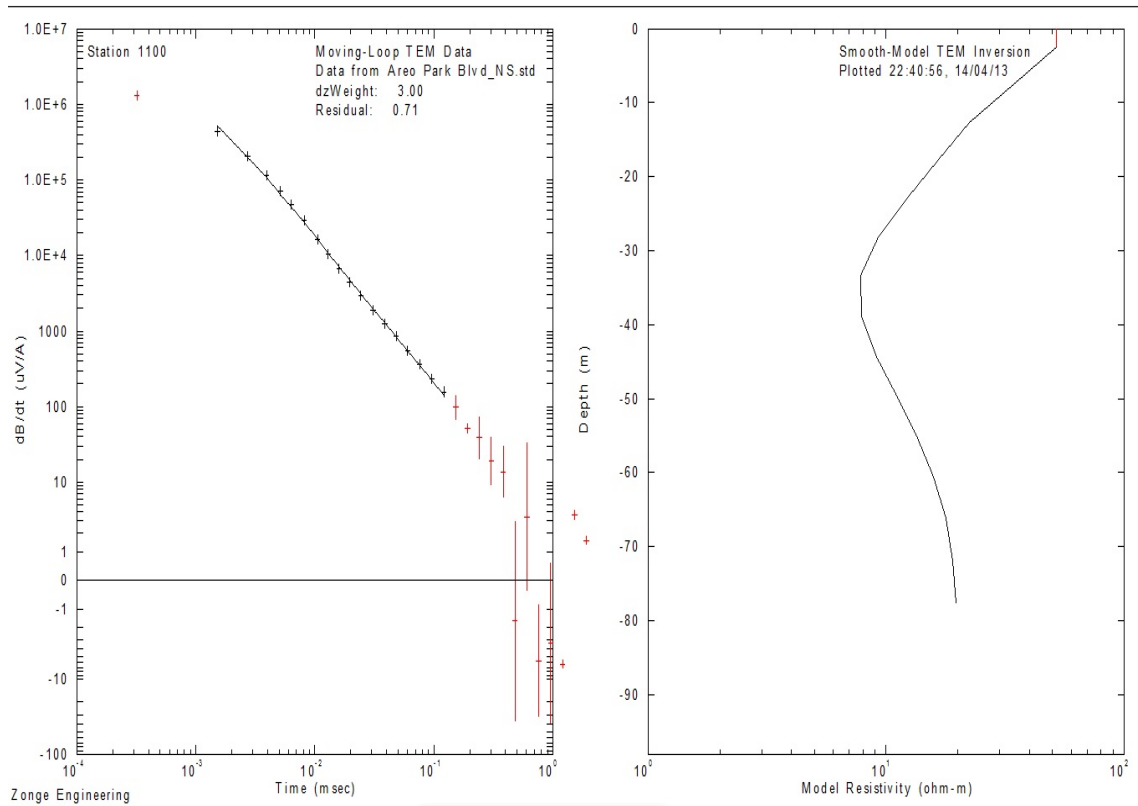
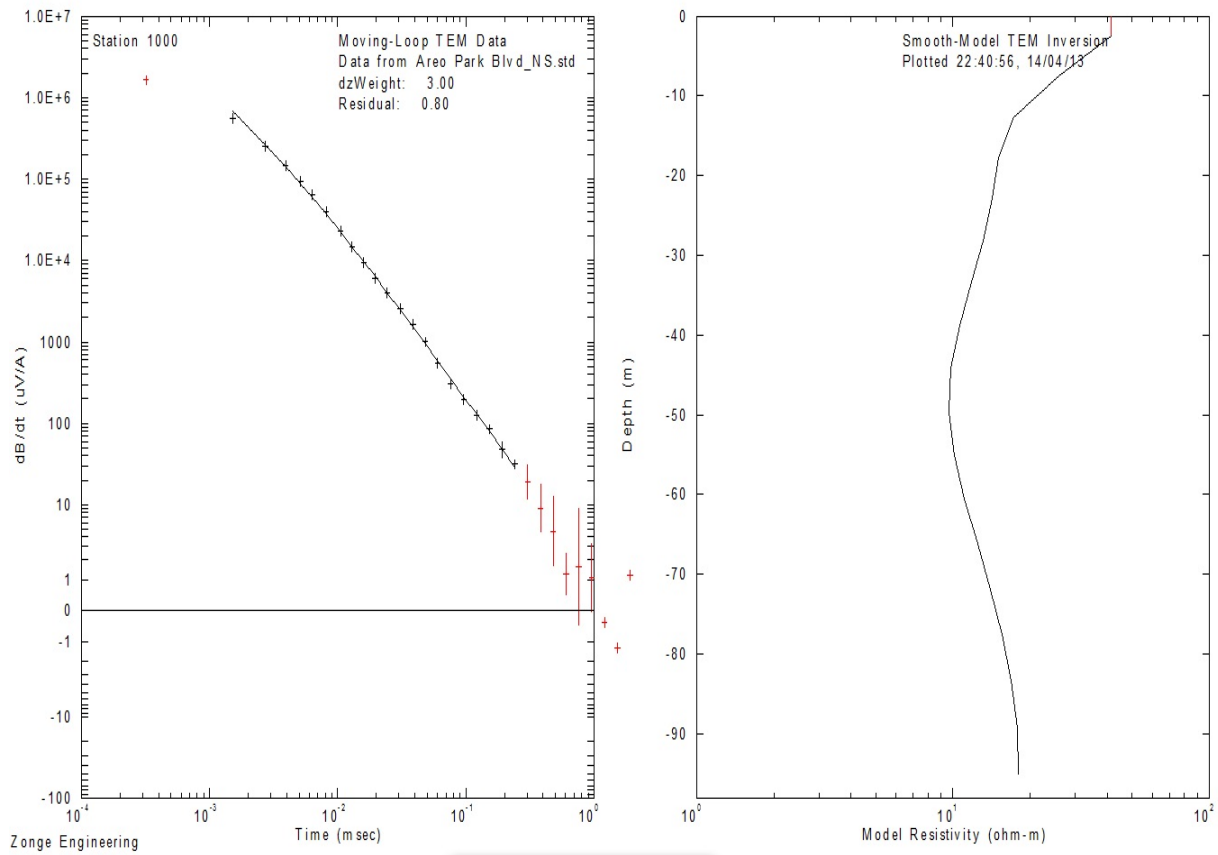


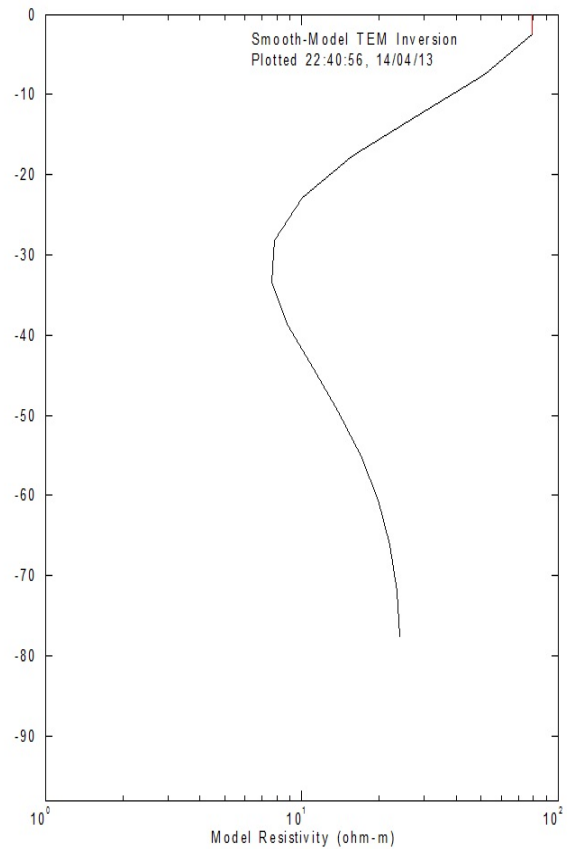
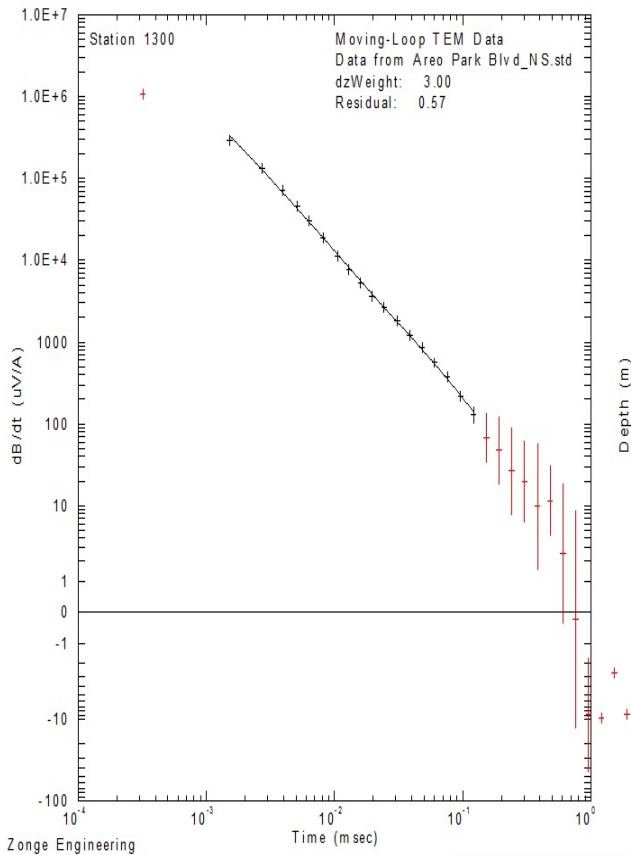
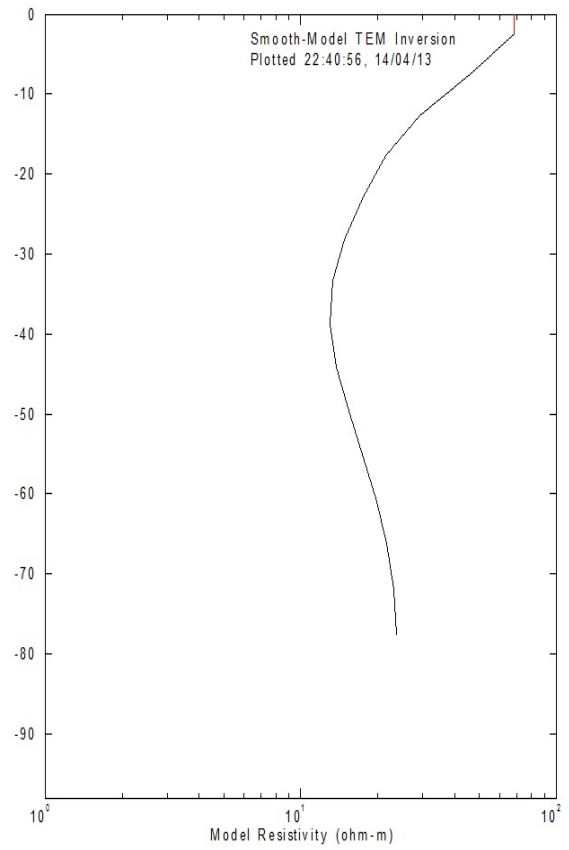
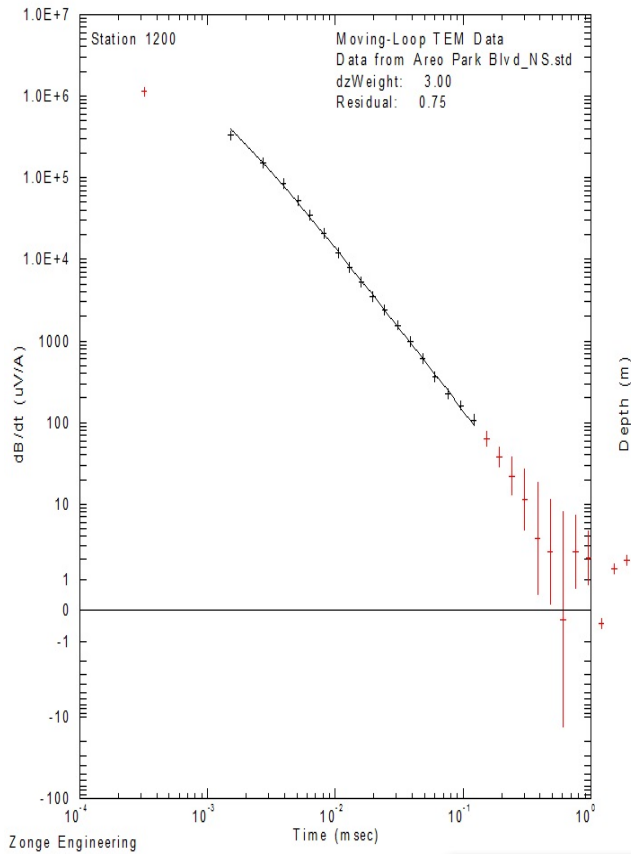


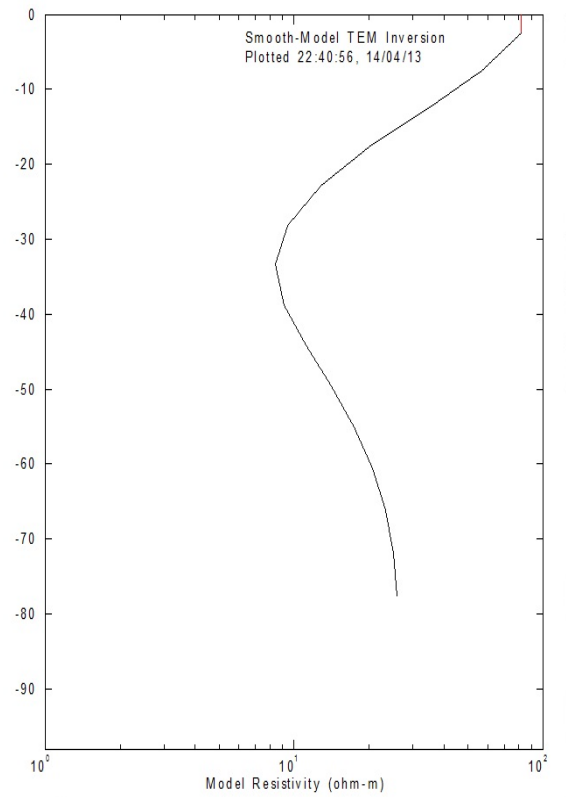
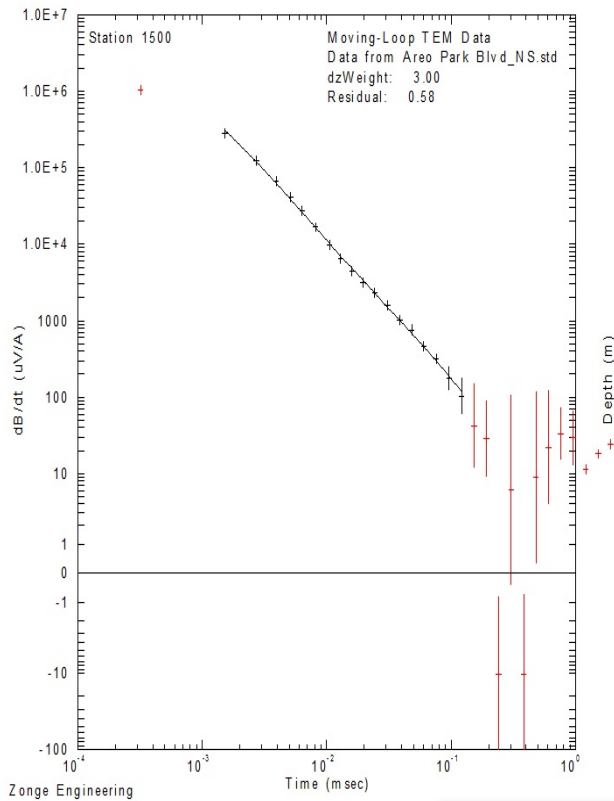
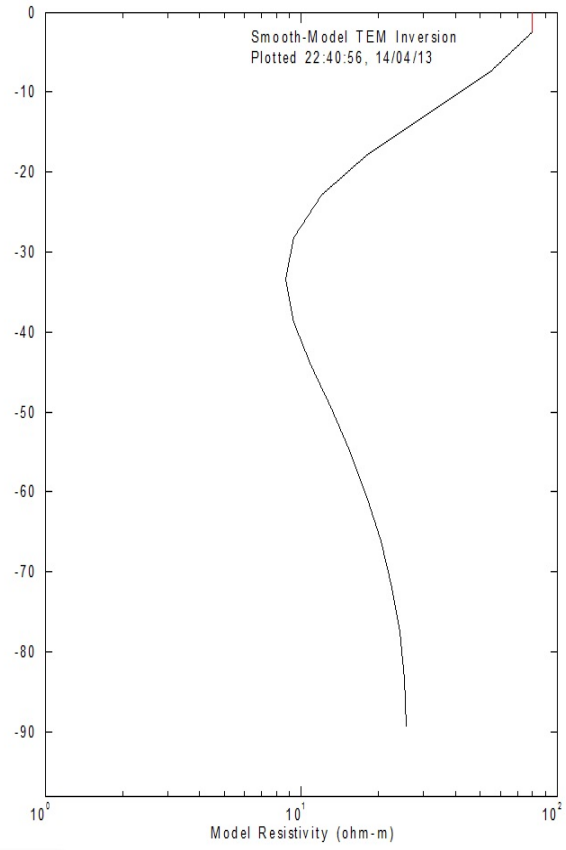
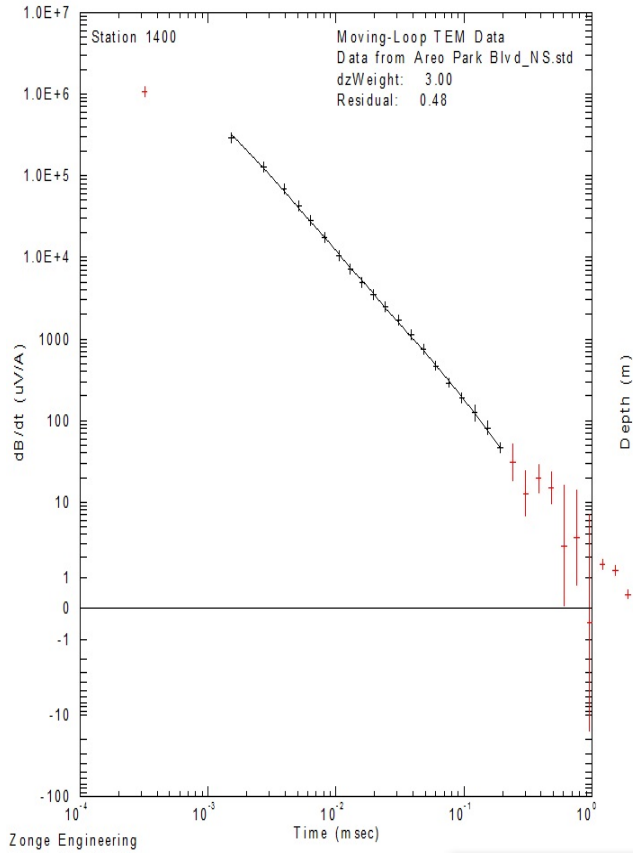


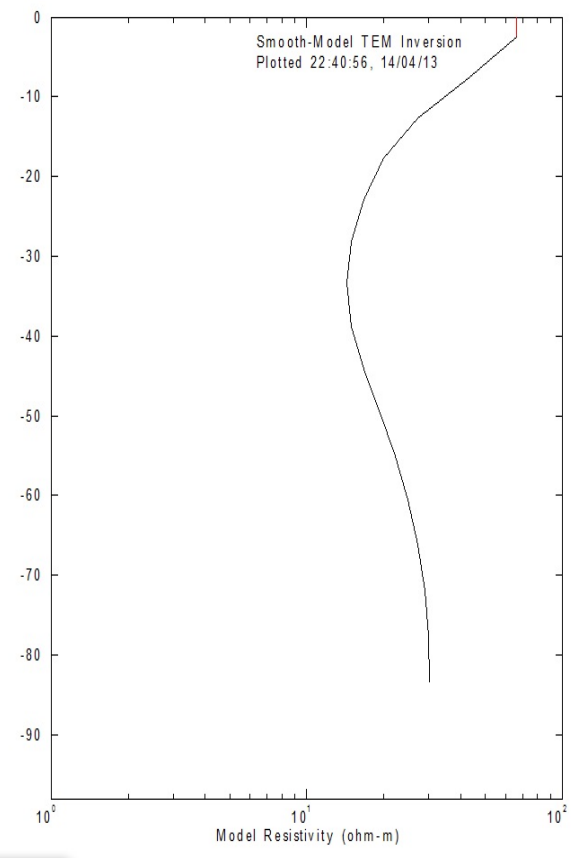
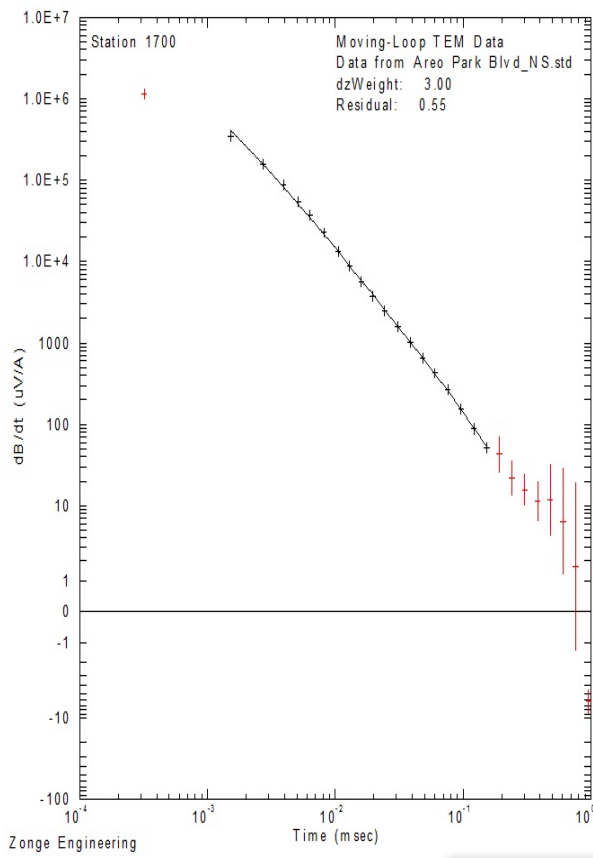
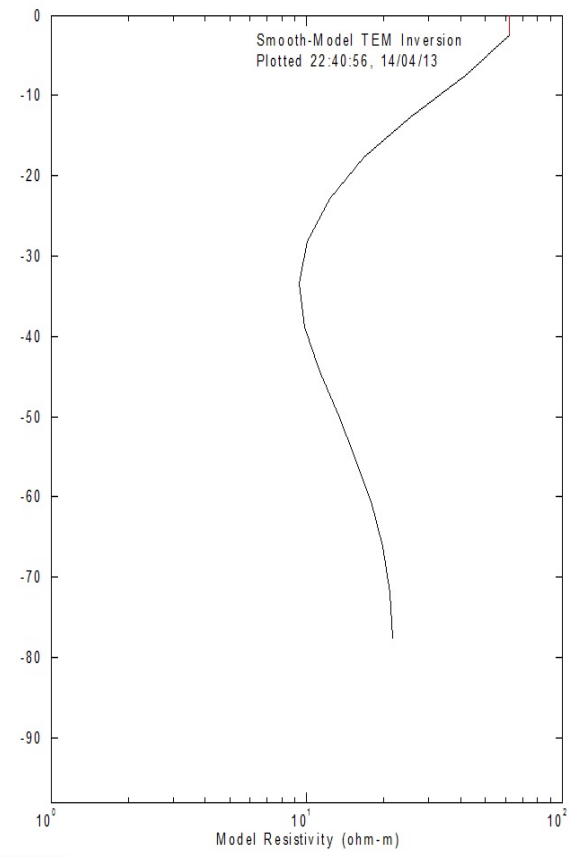
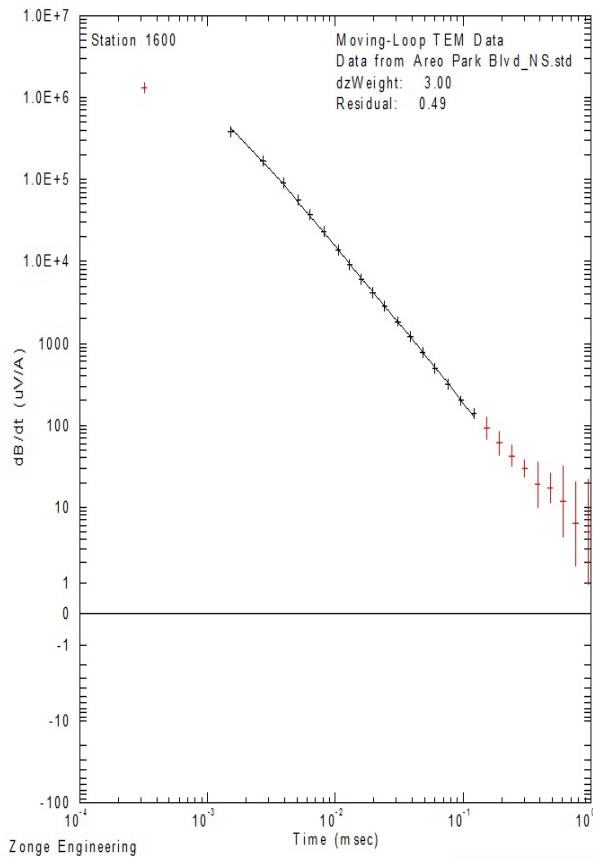


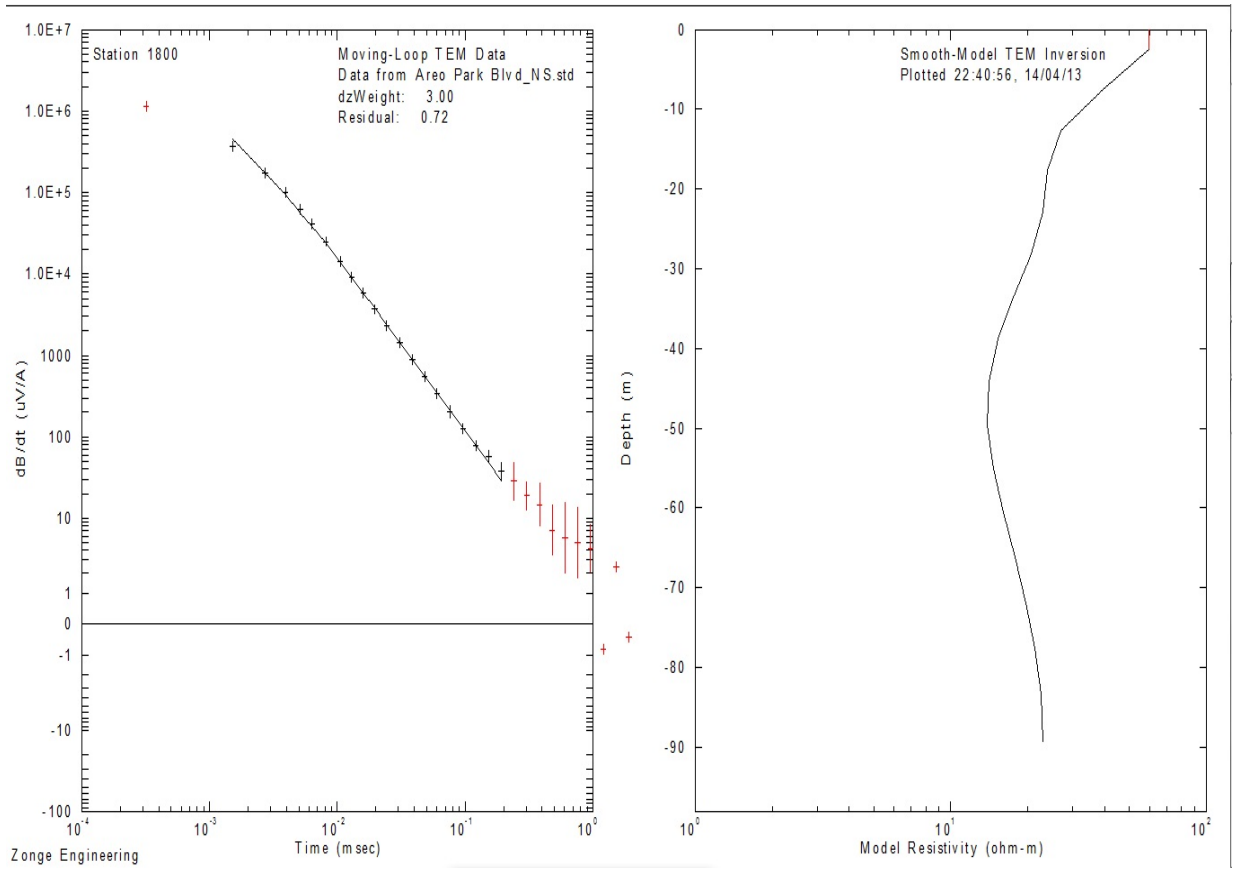
20x20 loops at the Aero Park Blvd South site with 64Hz from south to North



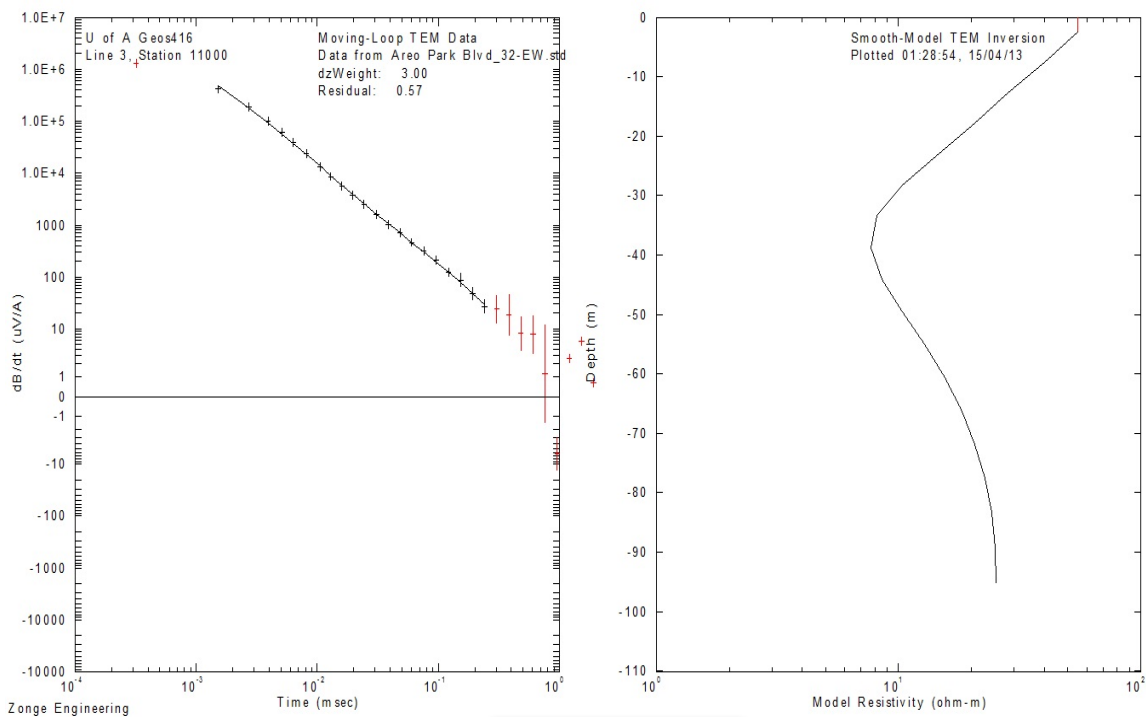
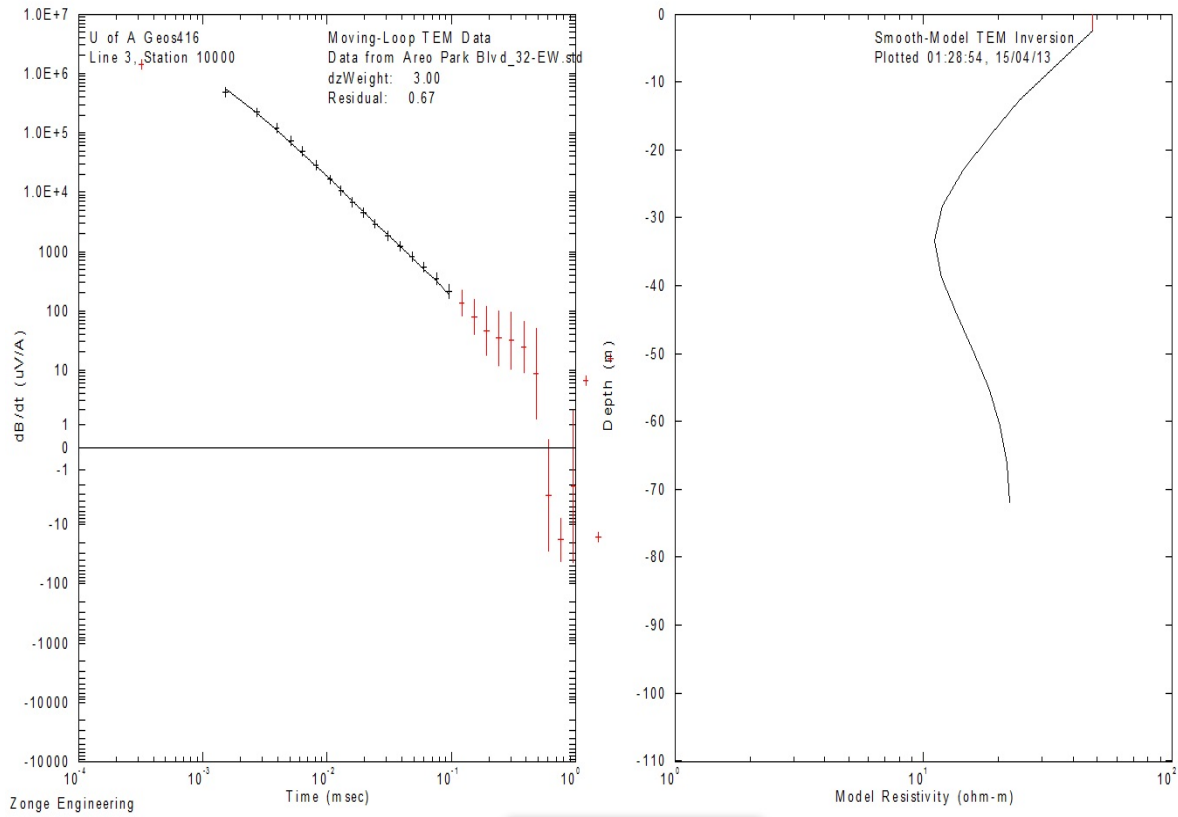


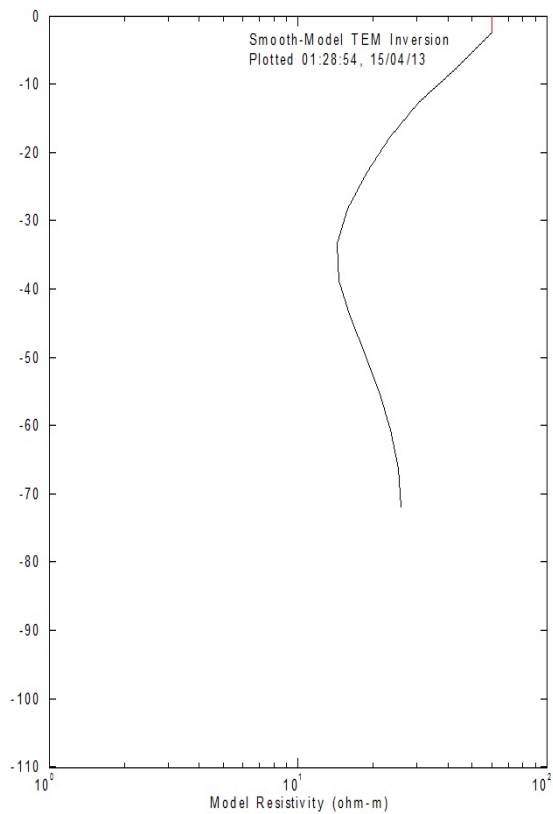
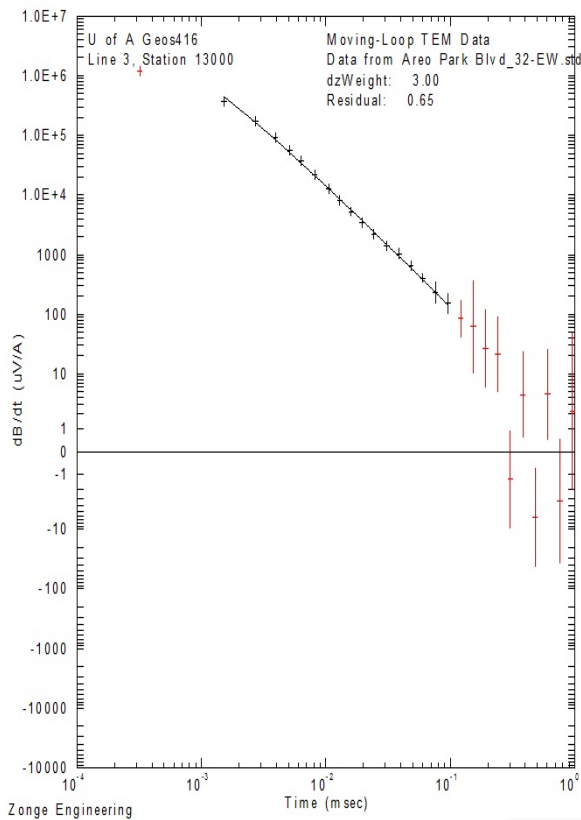
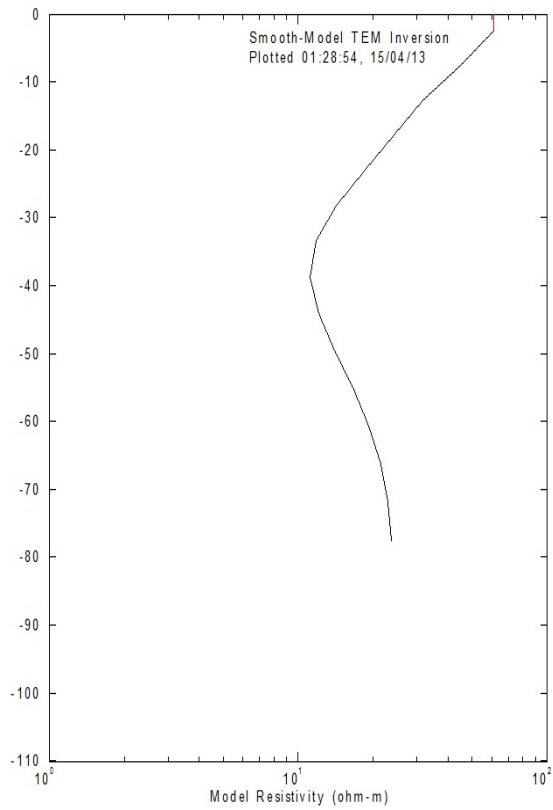
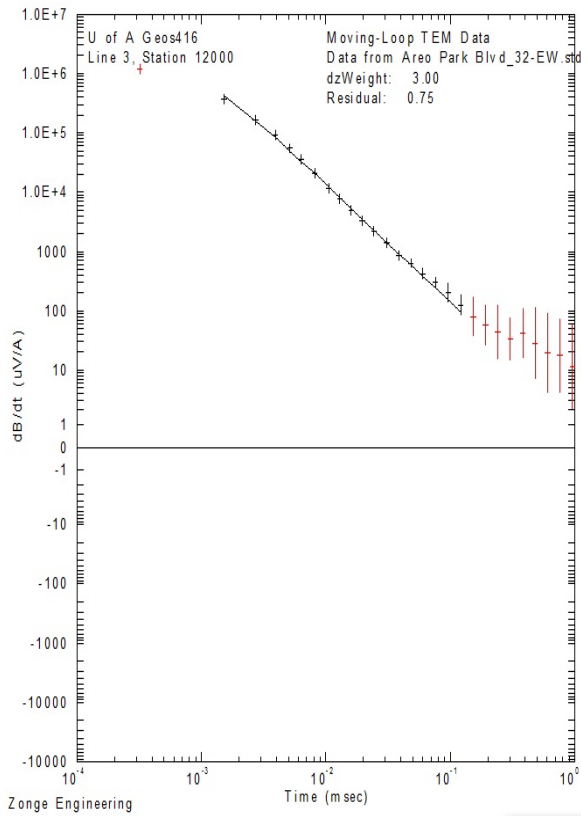


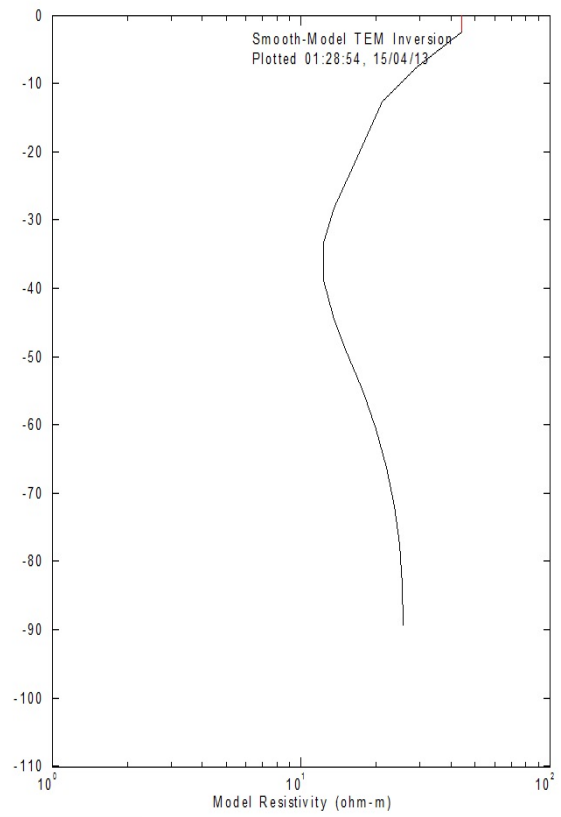
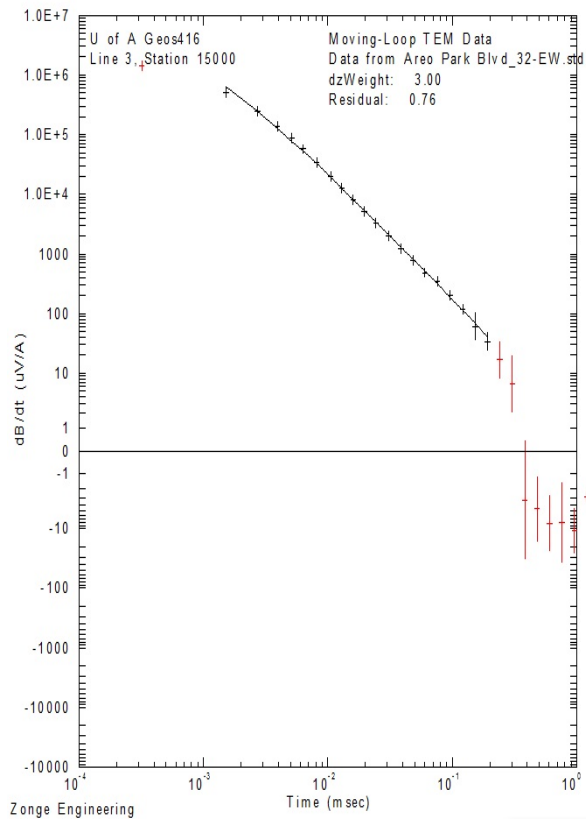
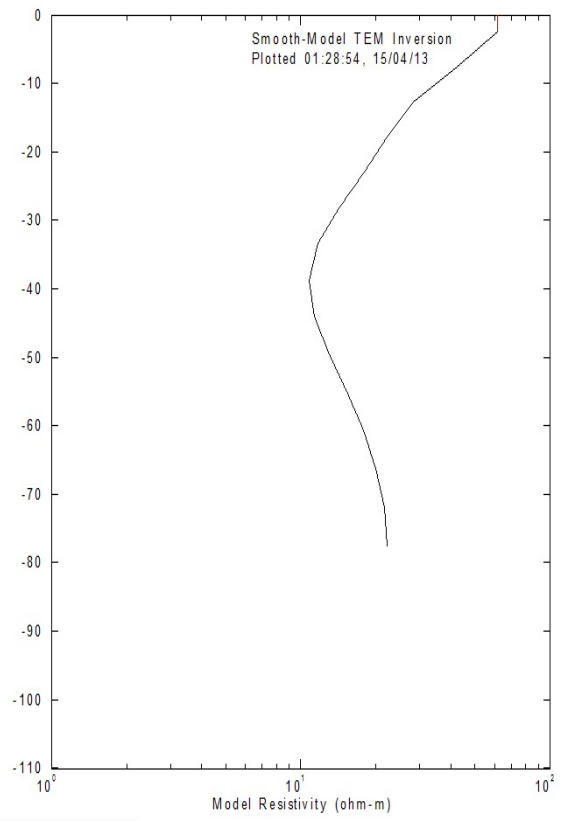
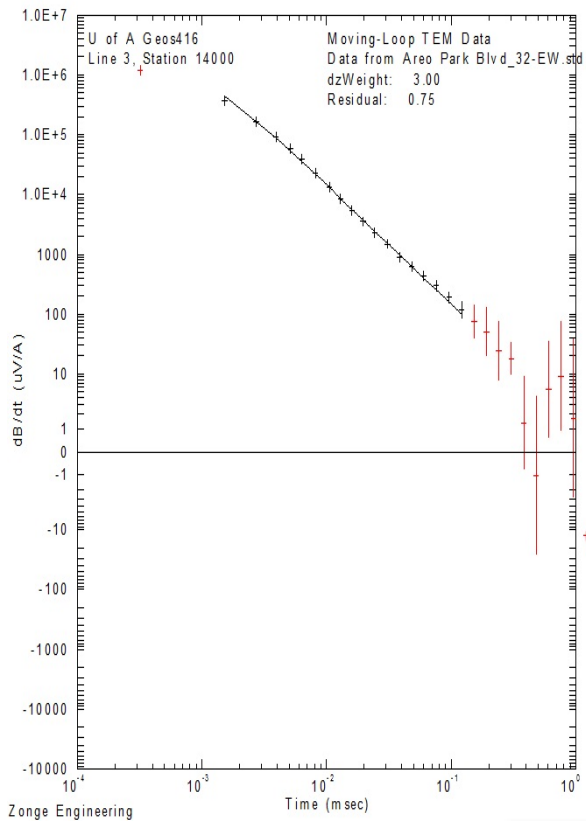


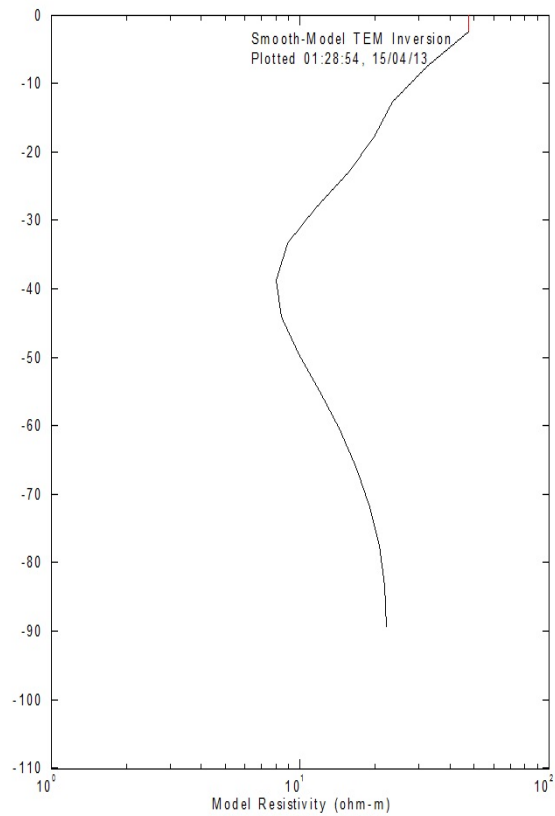
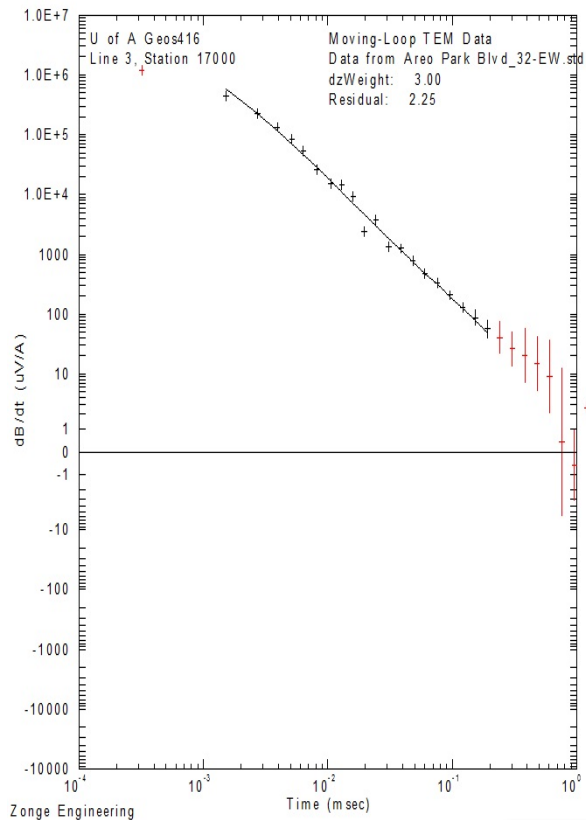
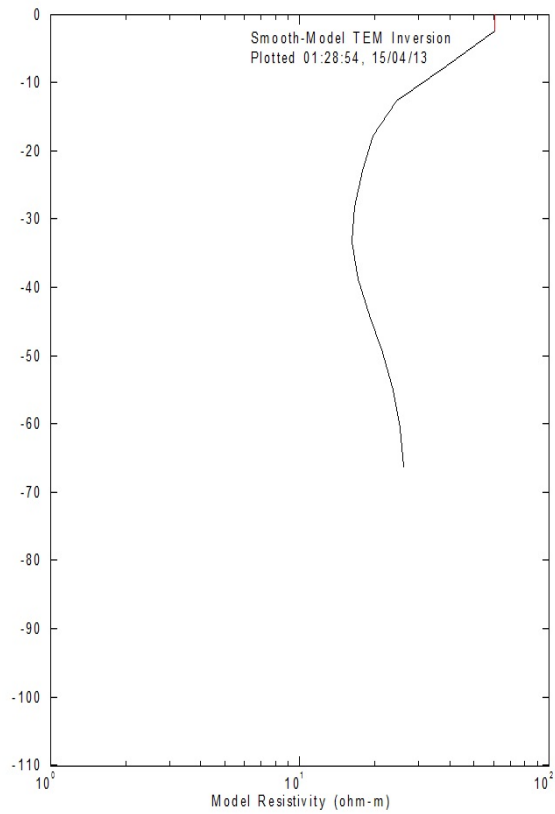
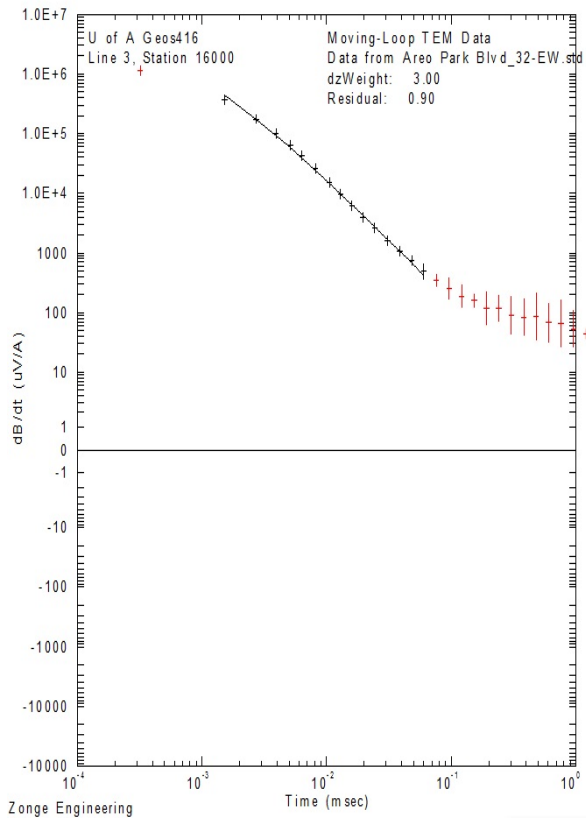


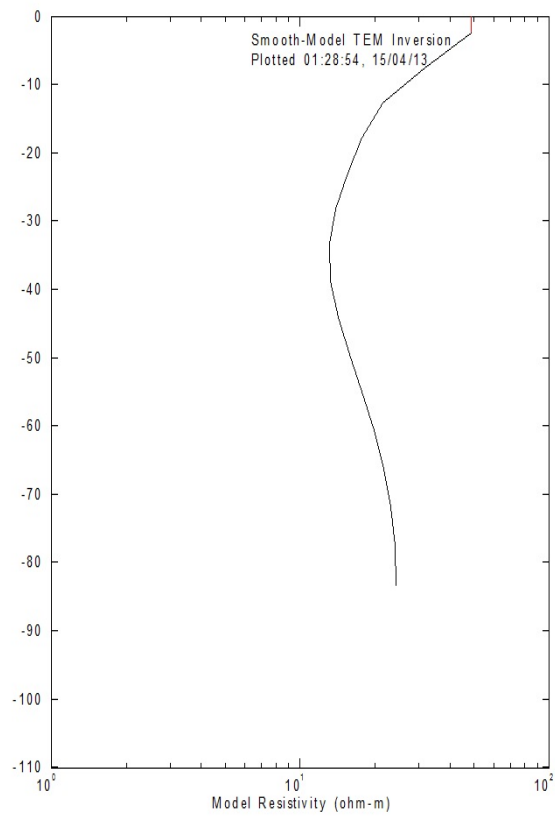
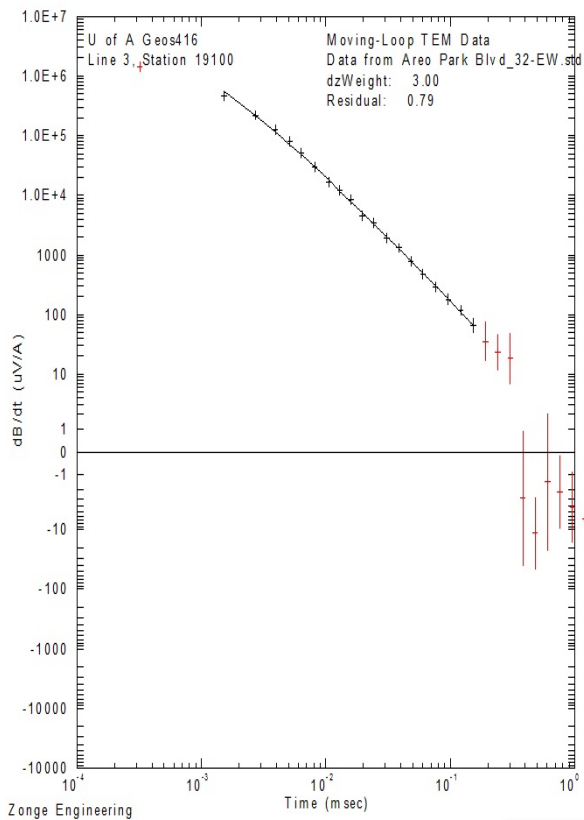
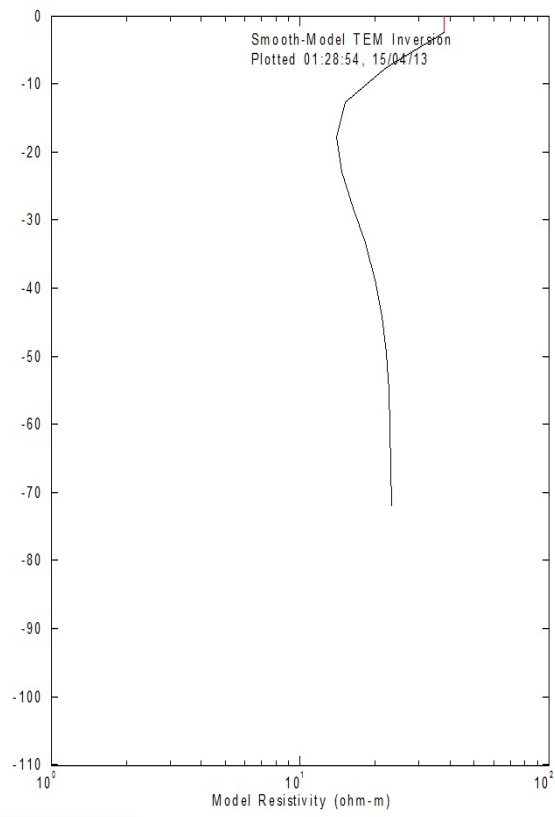
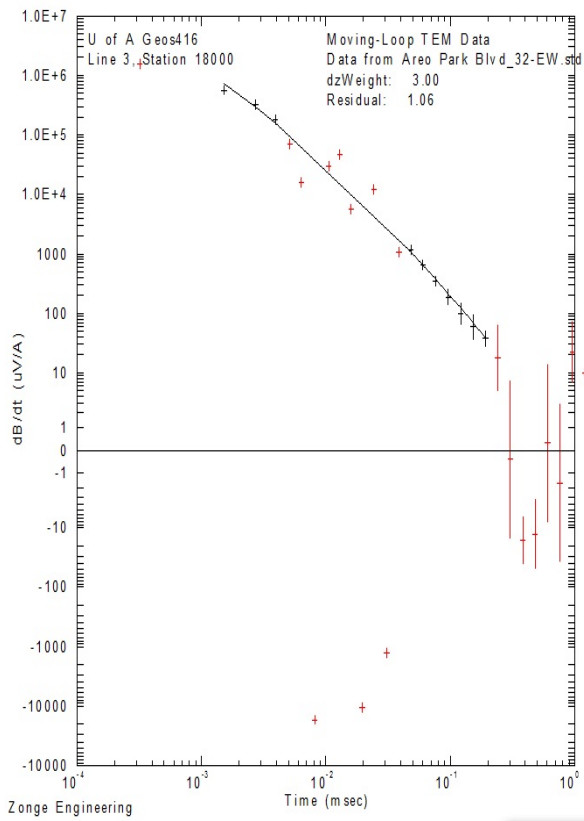
20x20 loops at the Aero Park Blvd South site with 32Hz from West to East

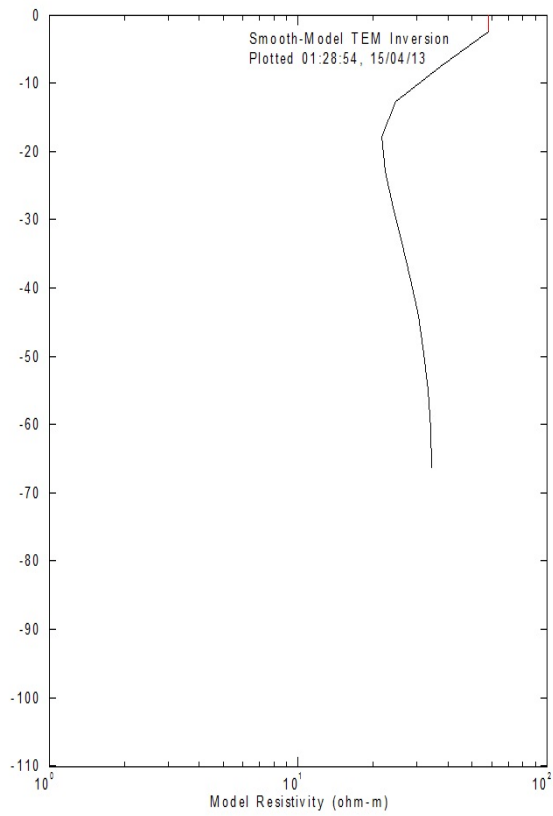
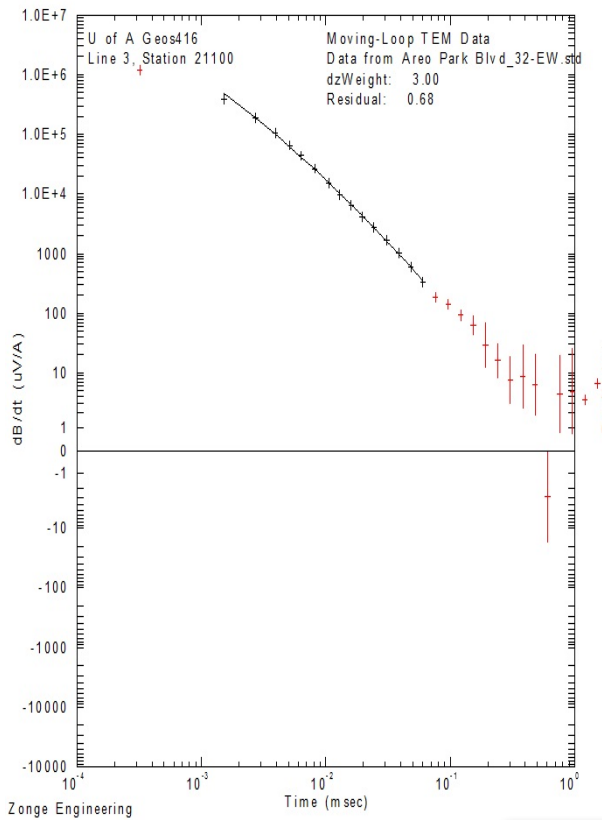
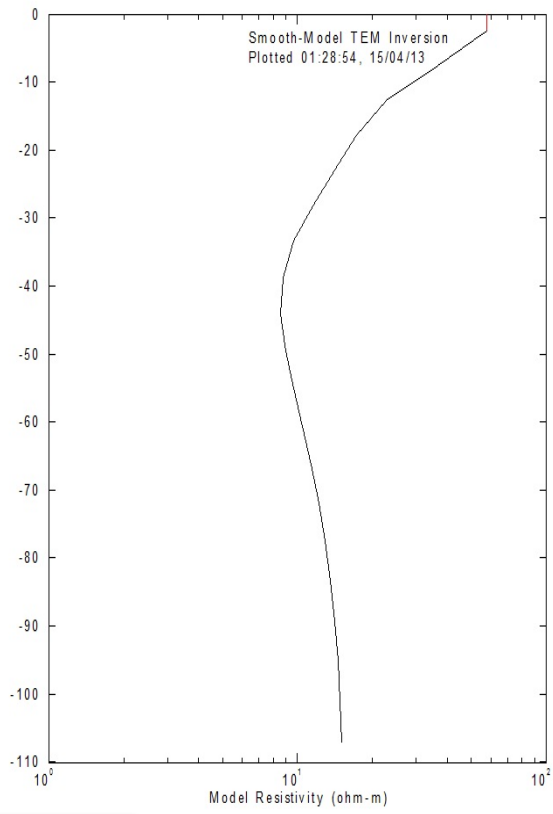
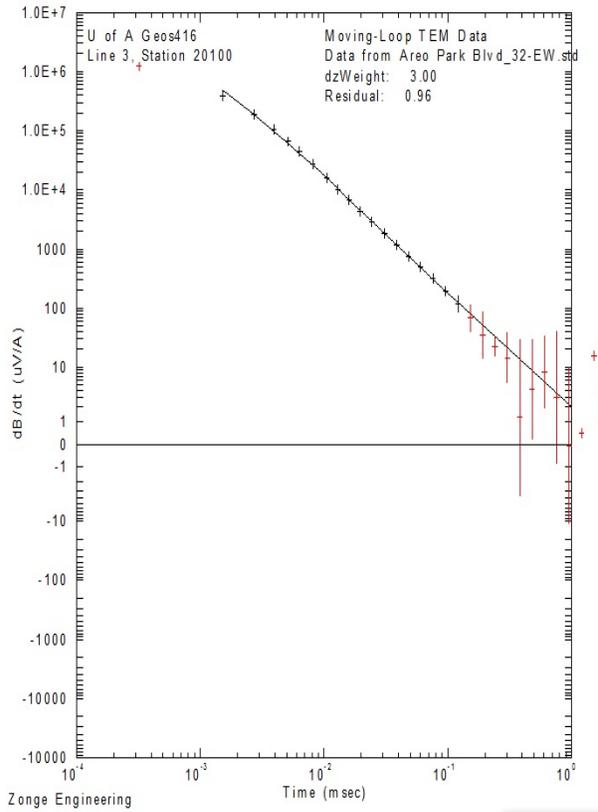


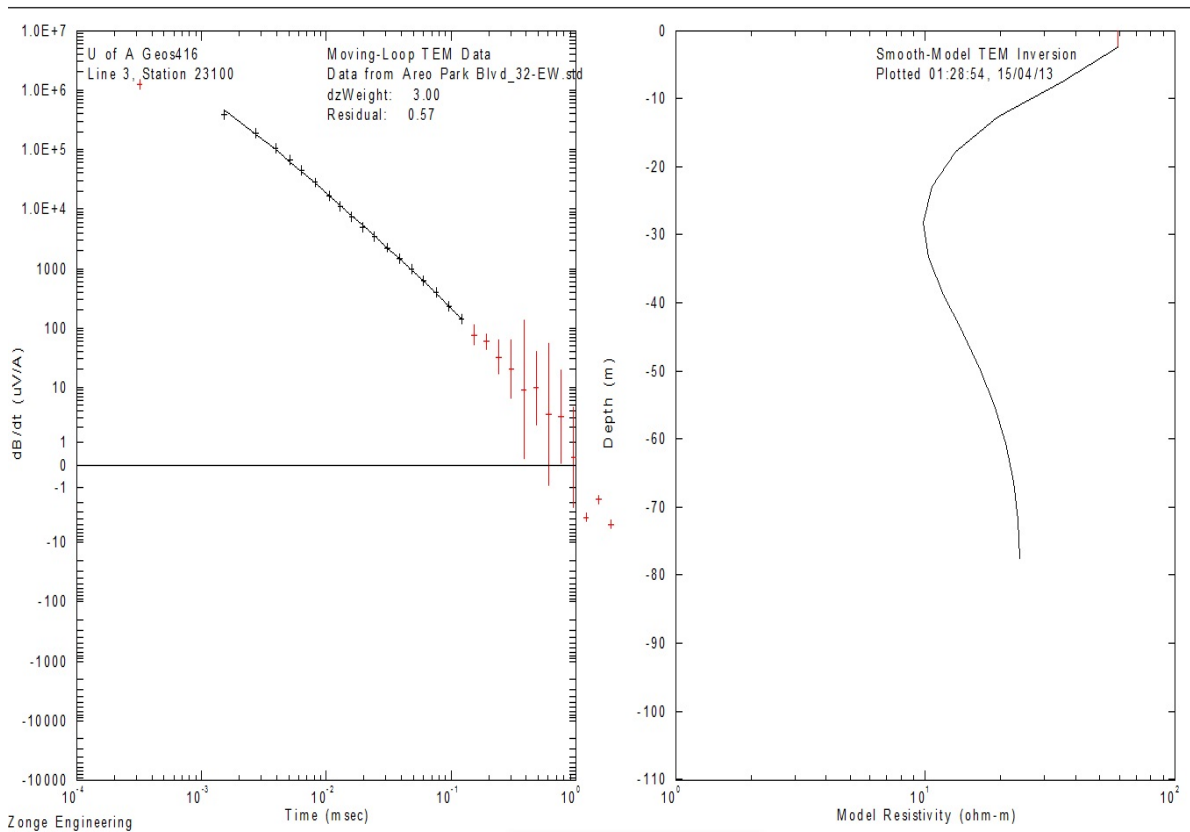
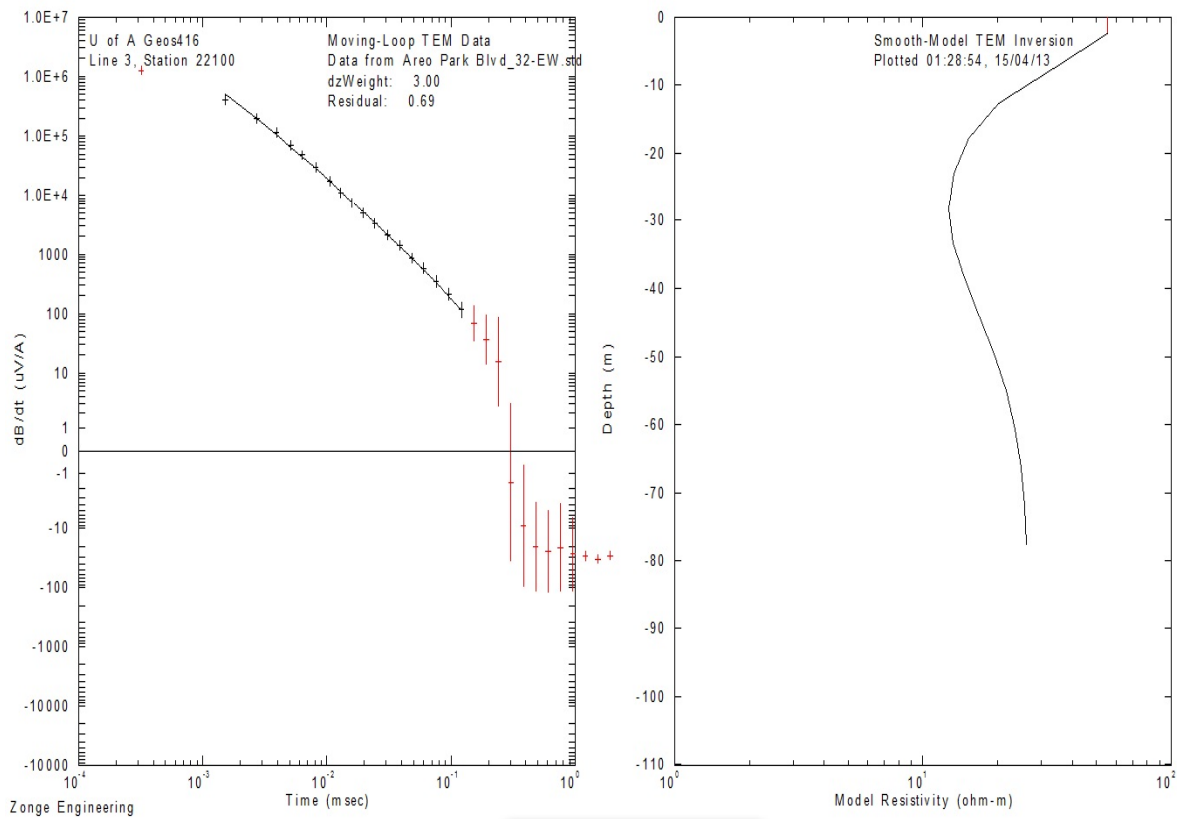


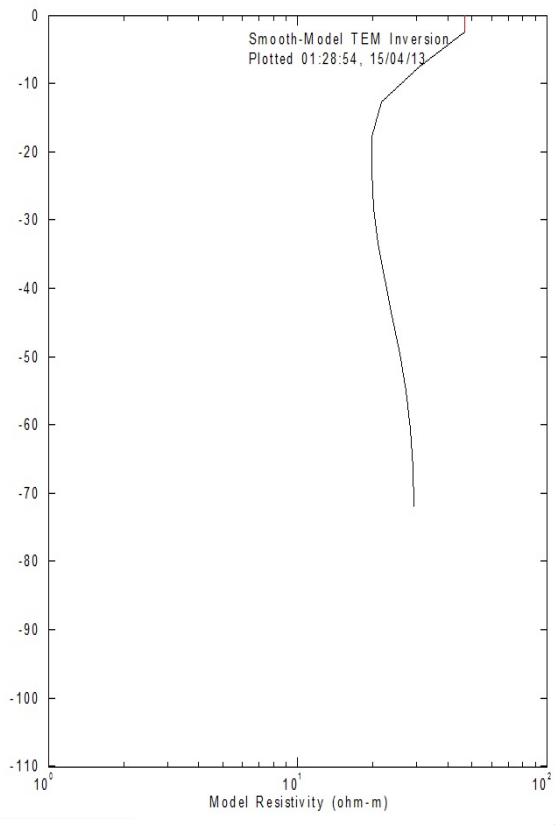
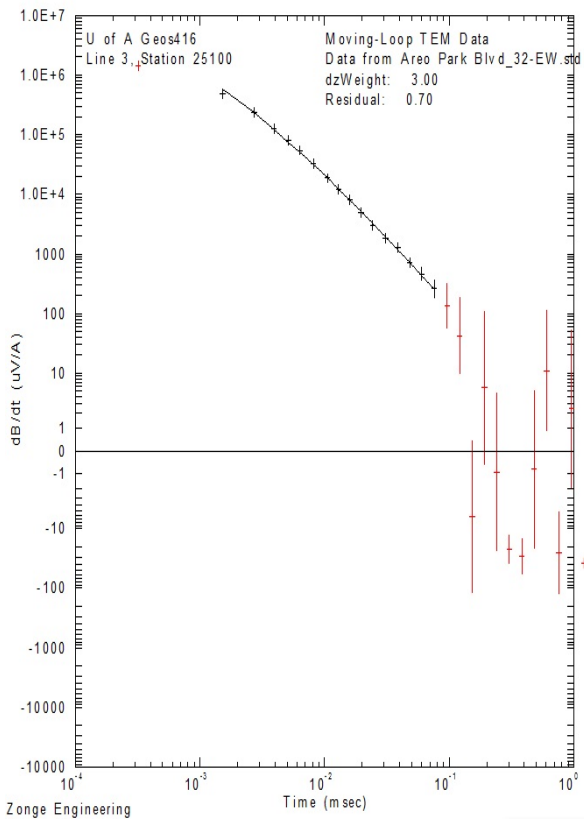
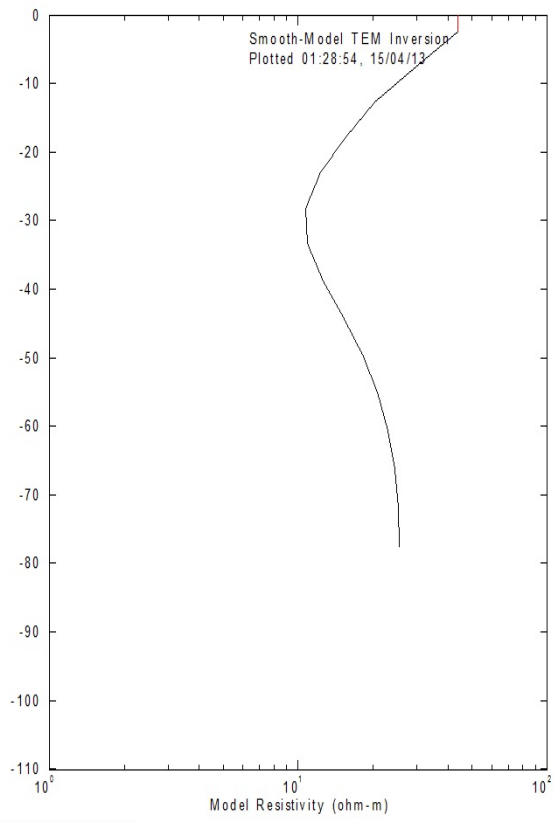
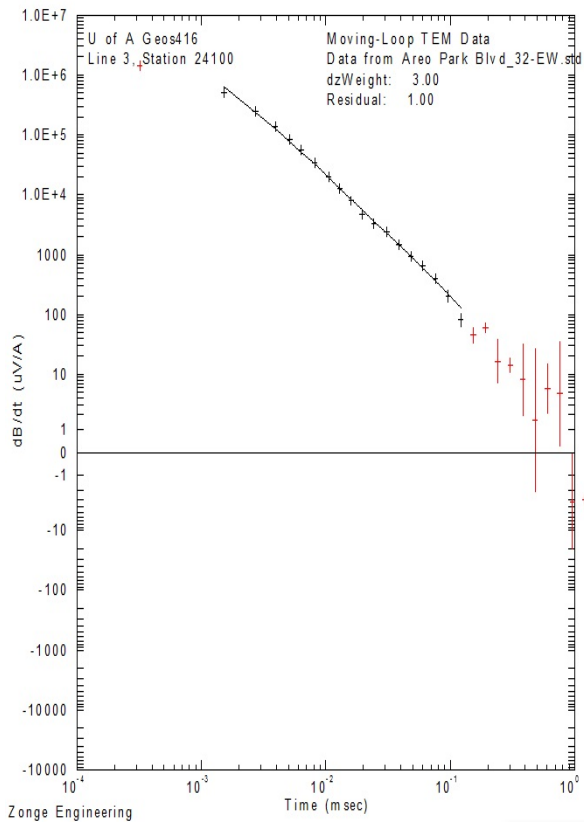


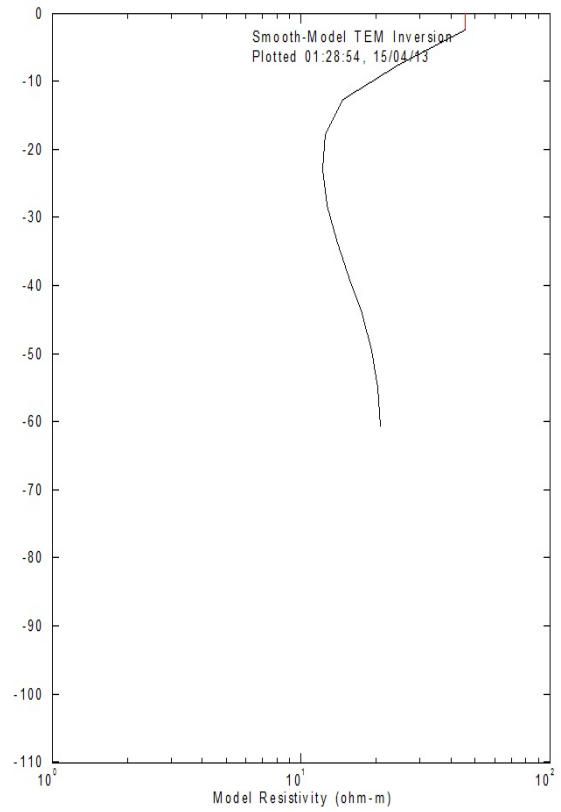
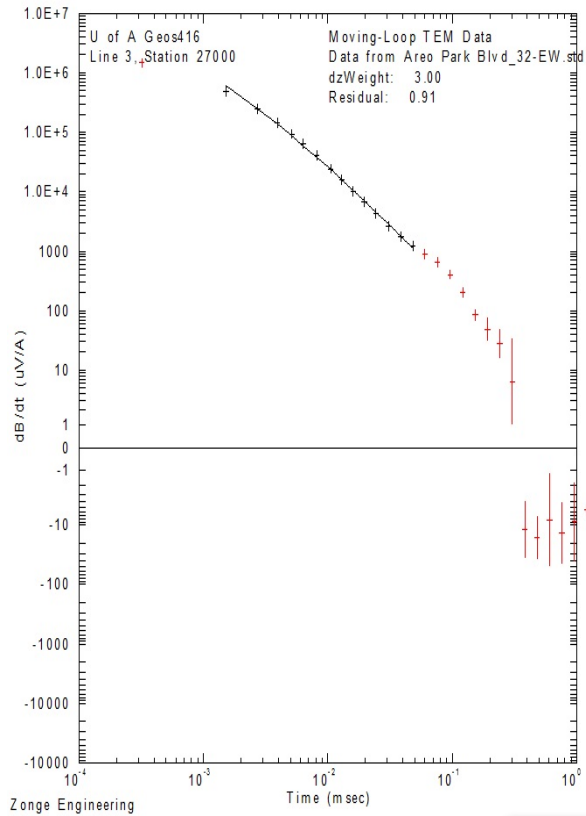
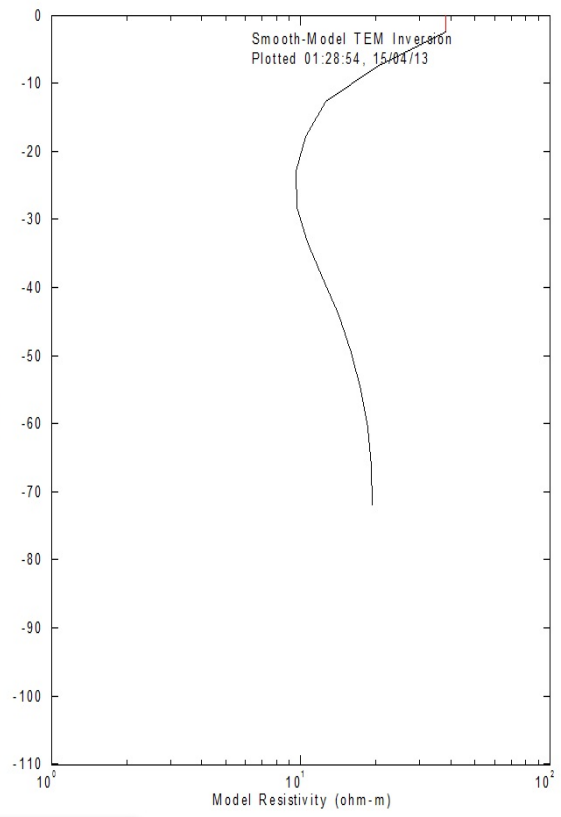
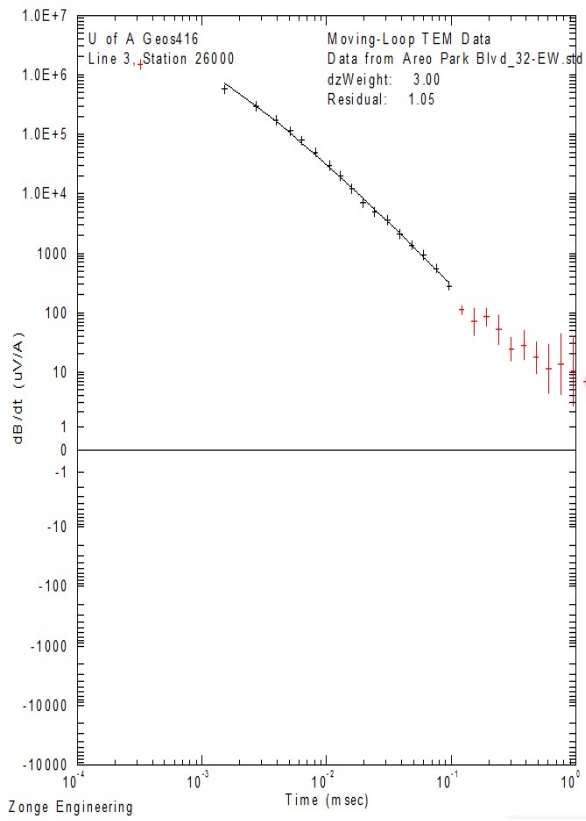


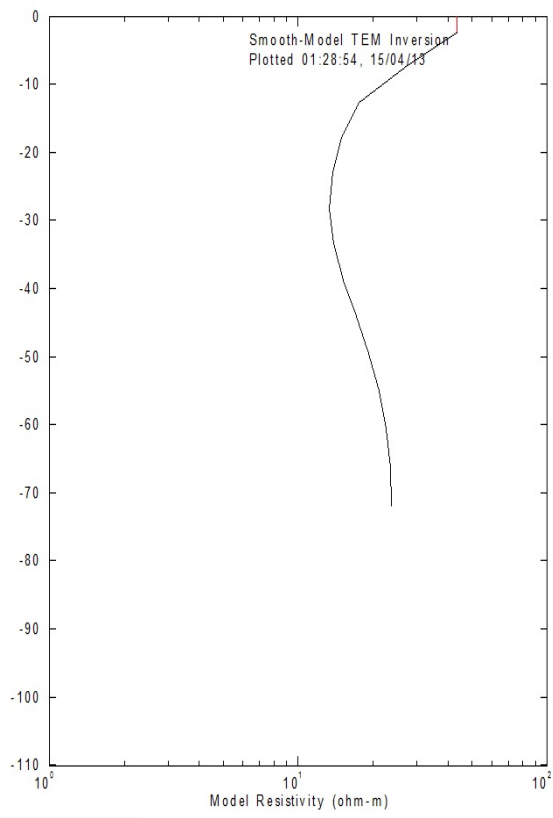
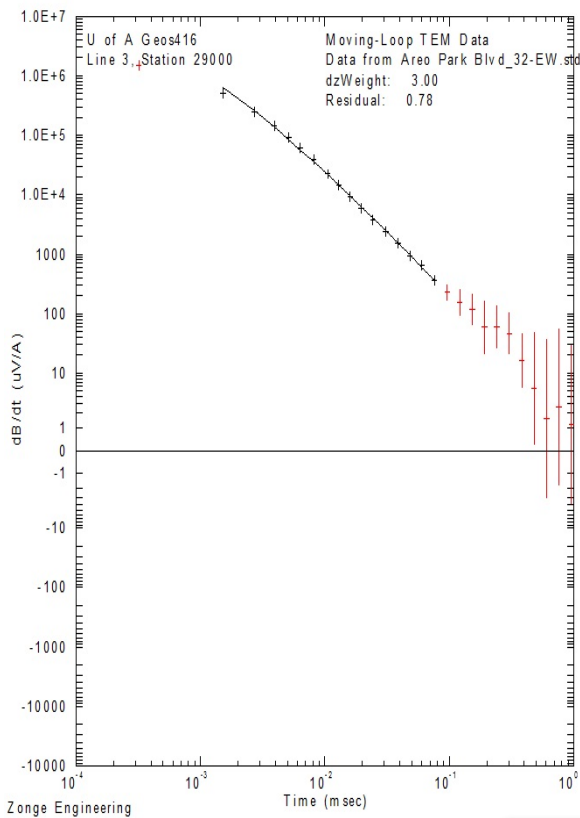
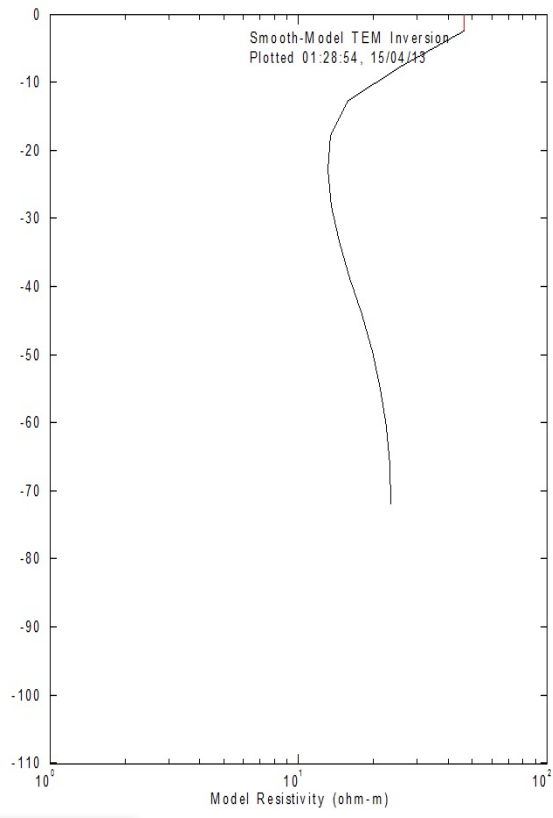
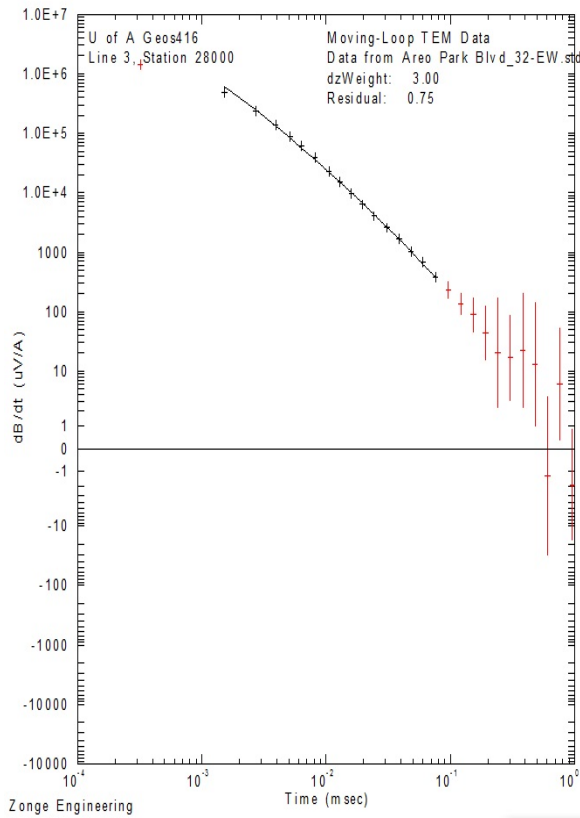


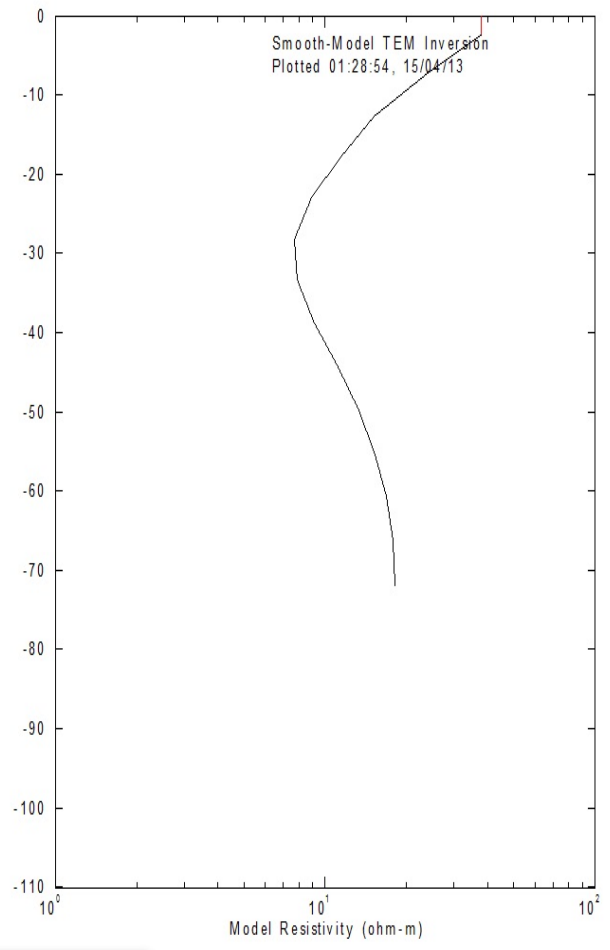
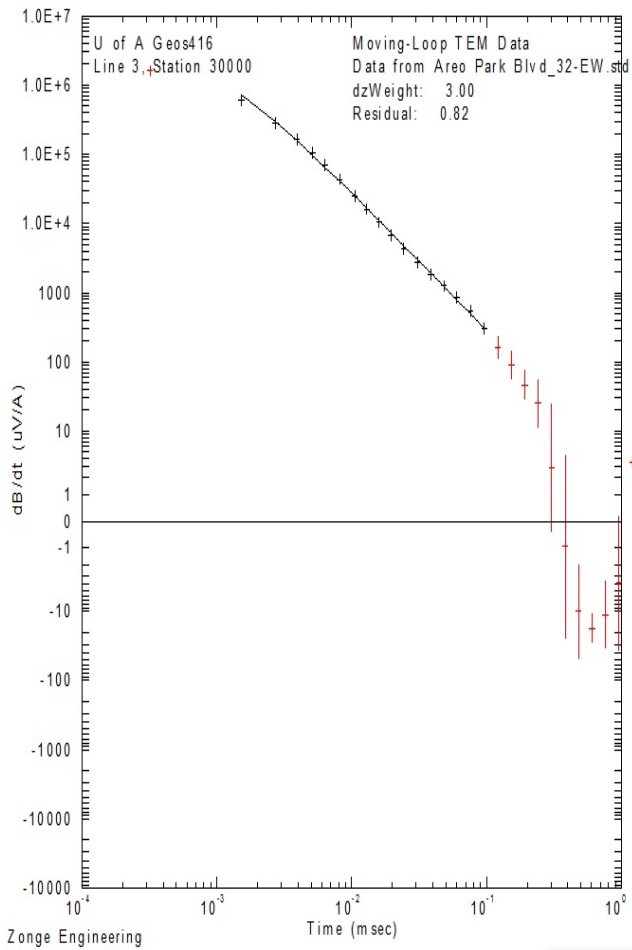




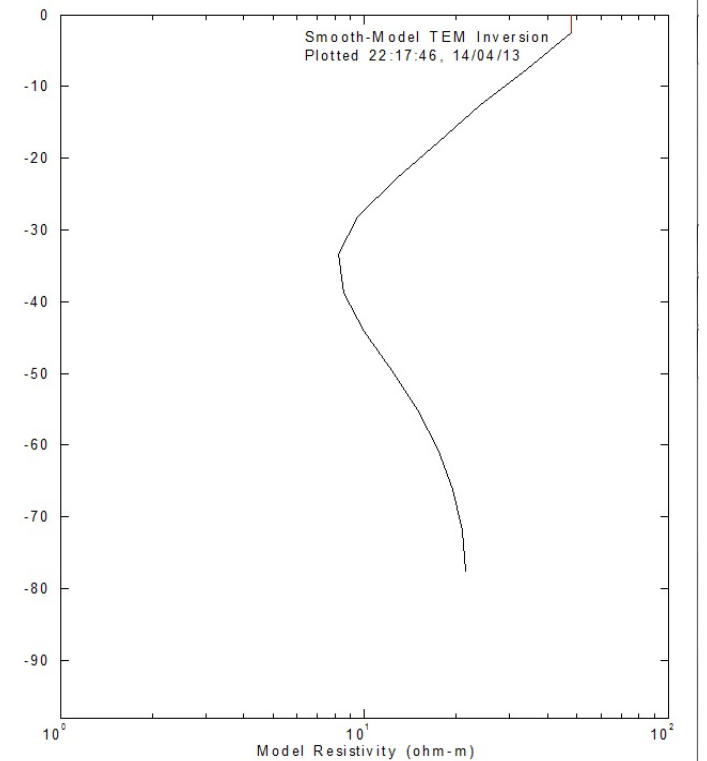
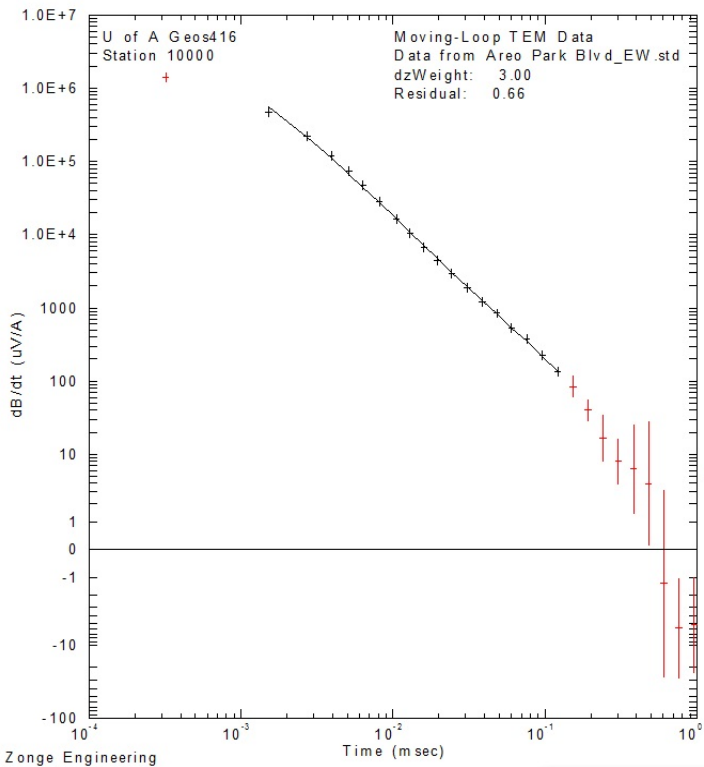
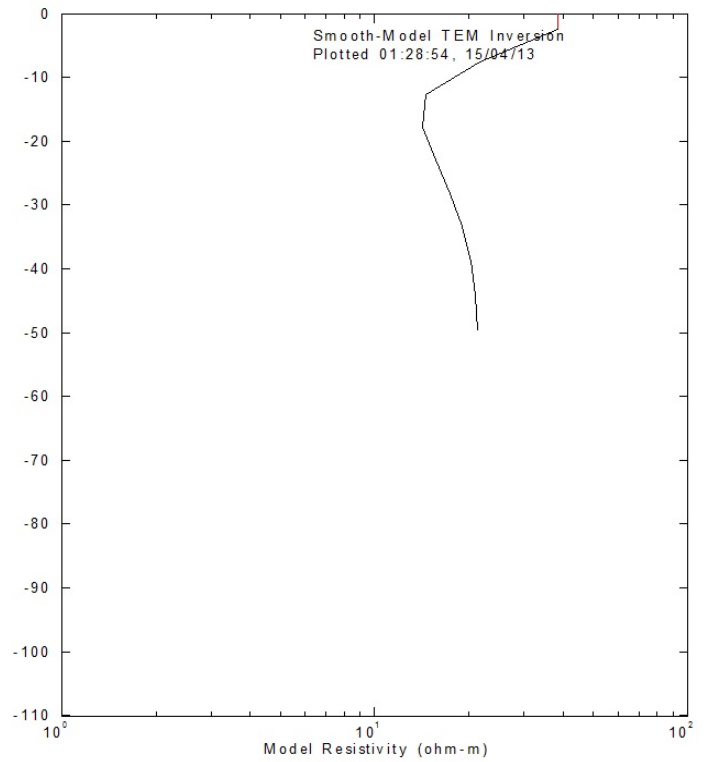
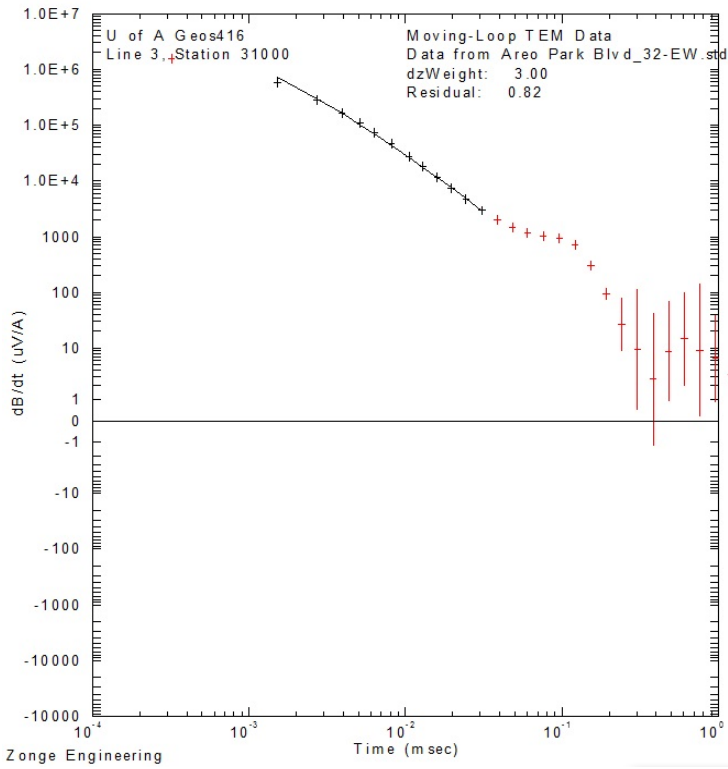


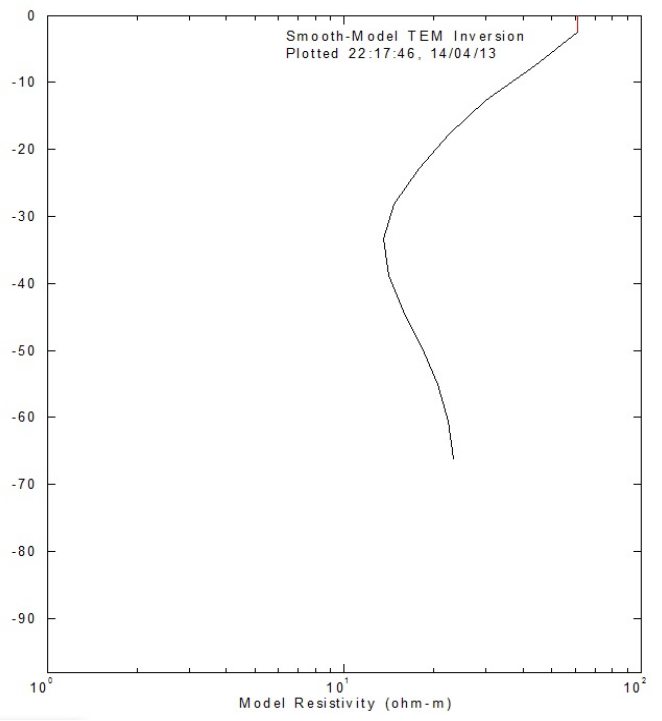
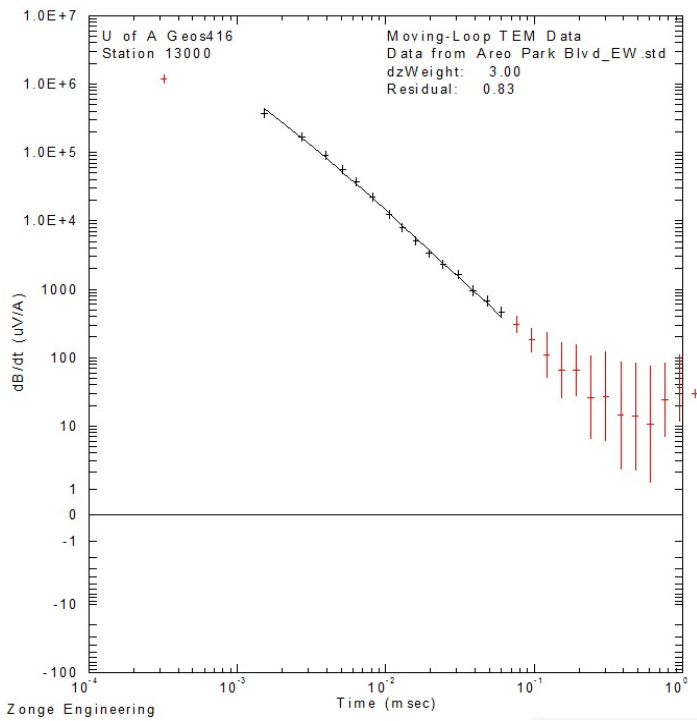
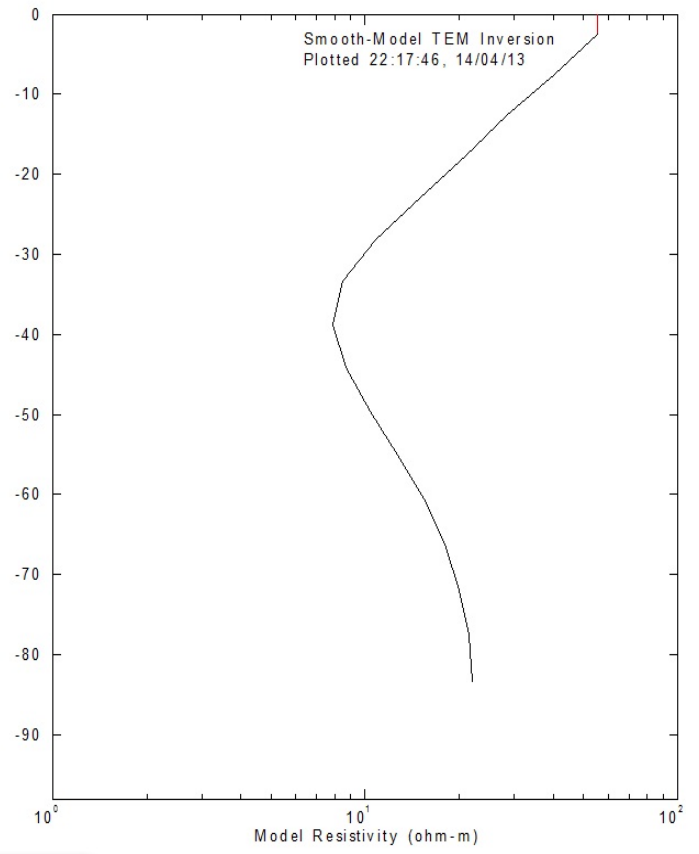
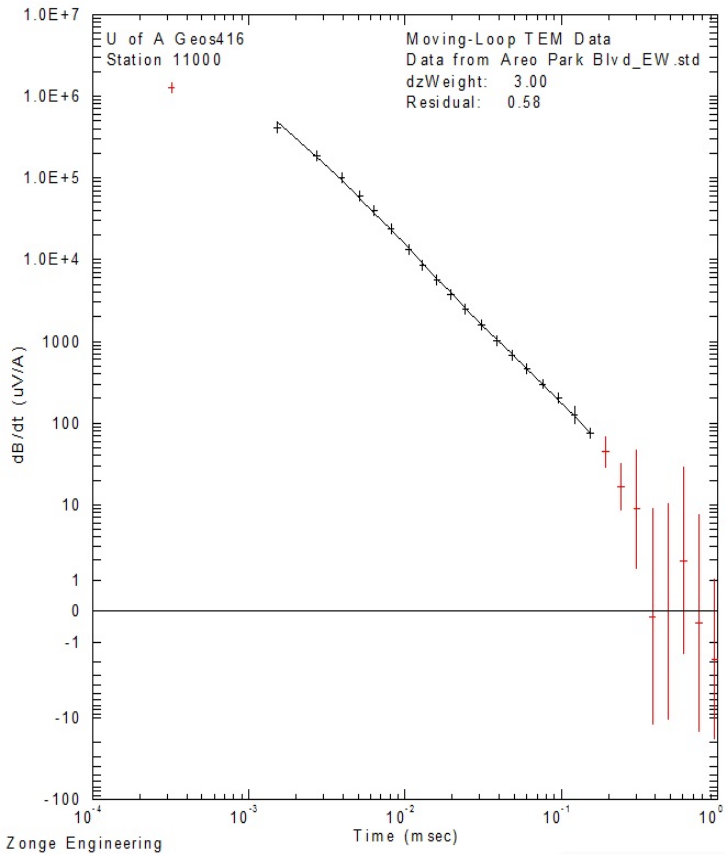


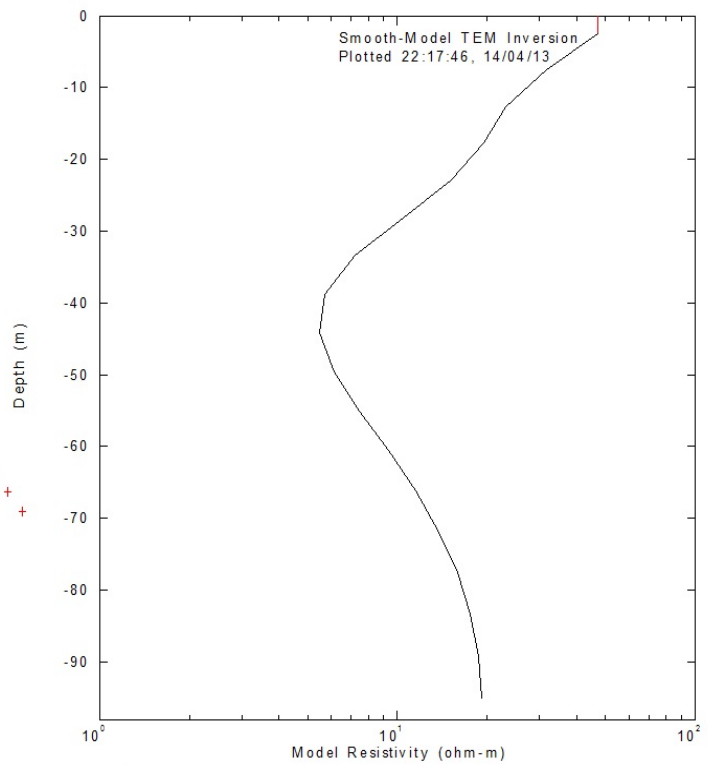
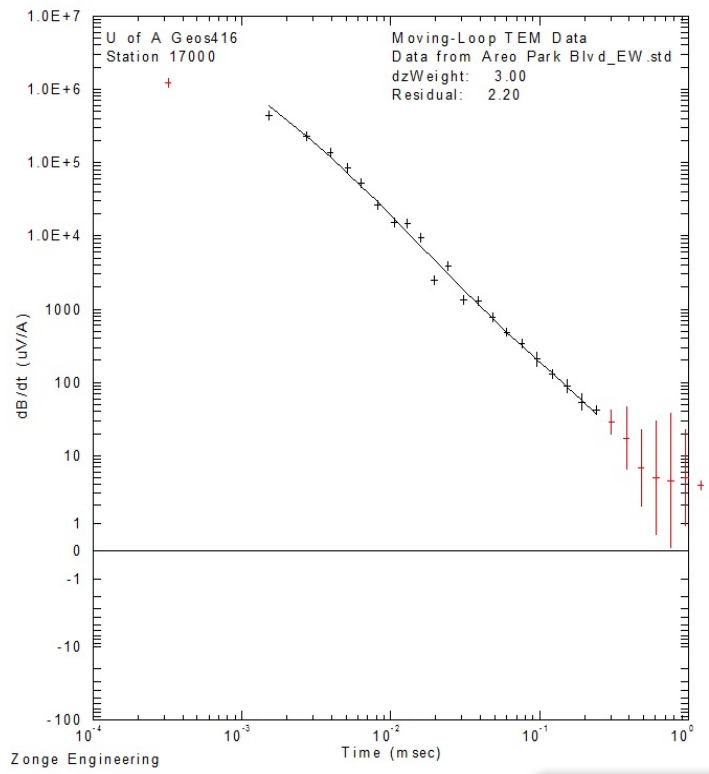
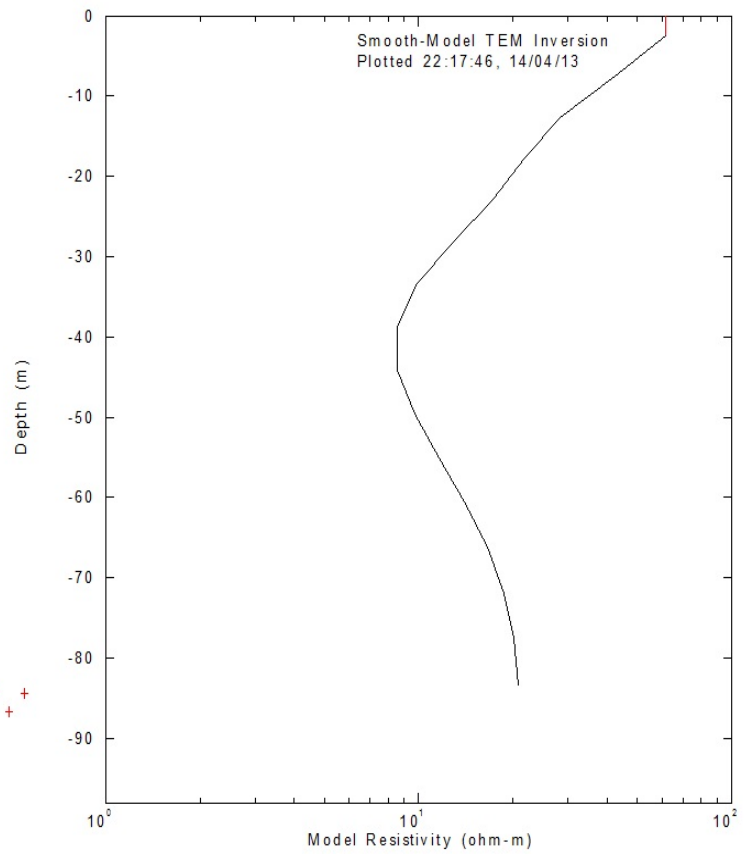
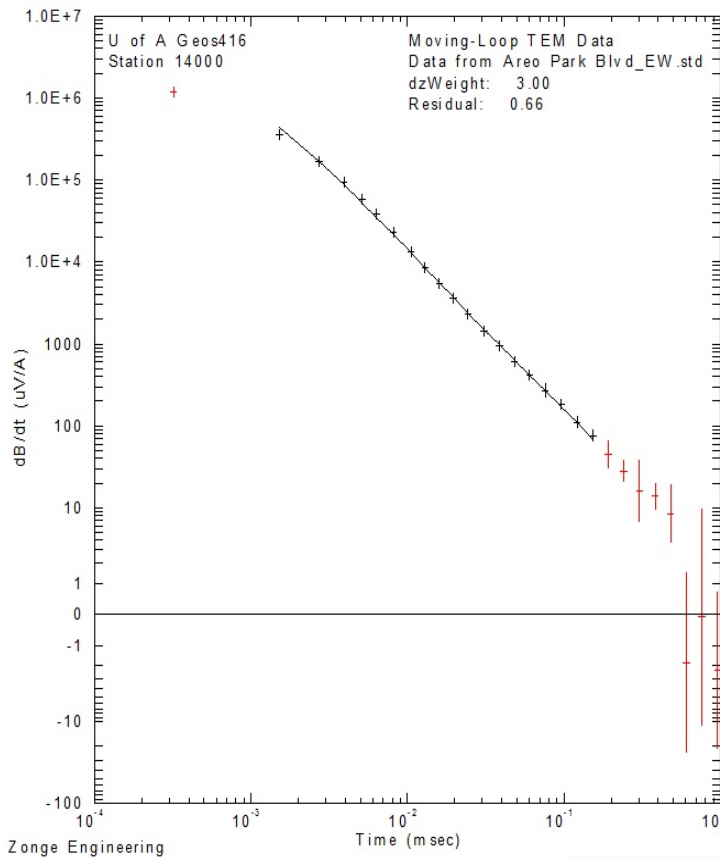


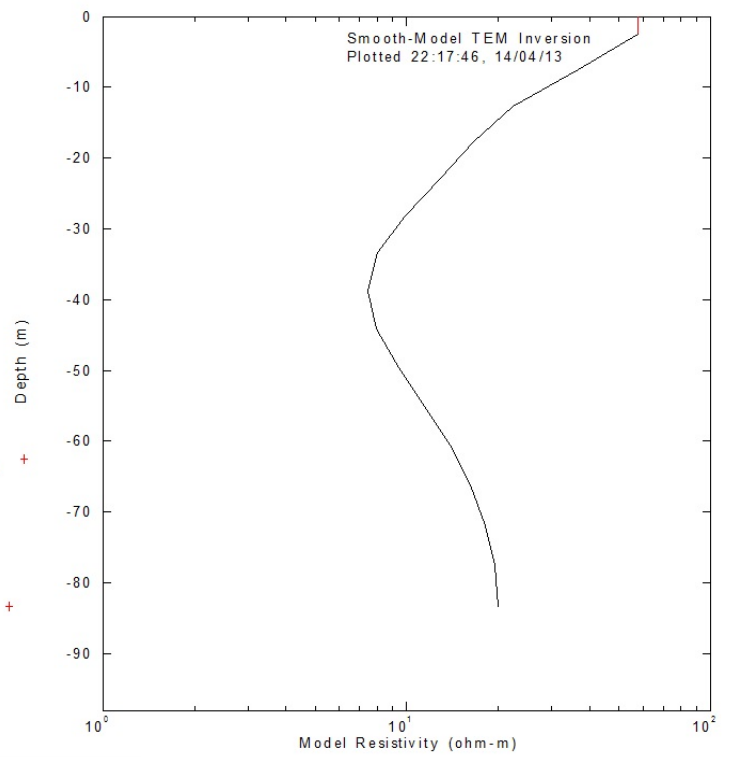
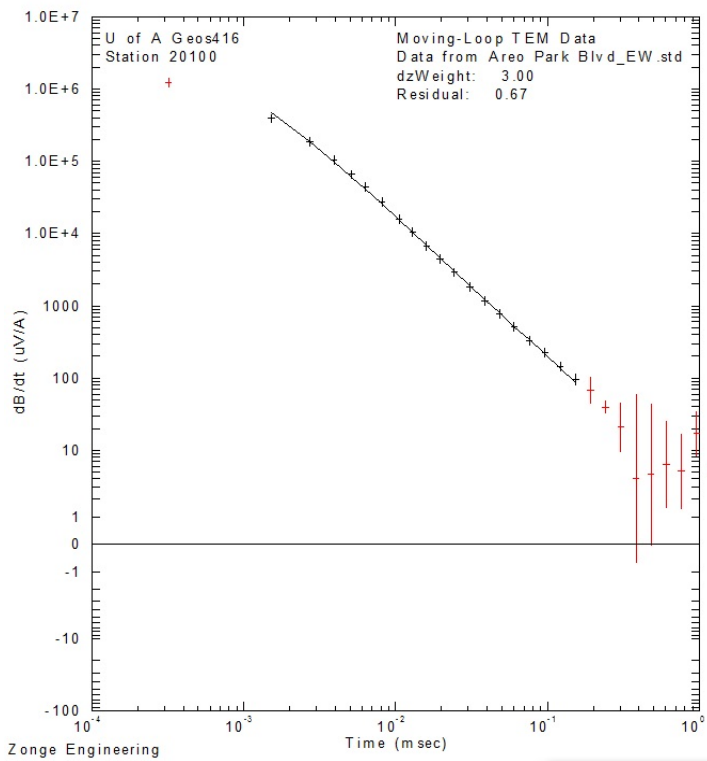
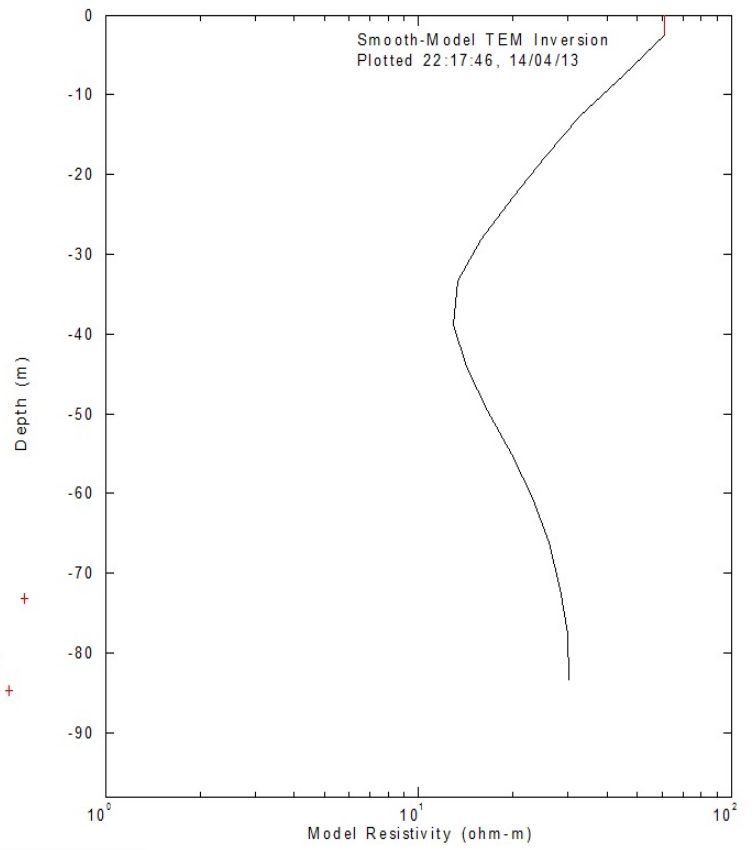
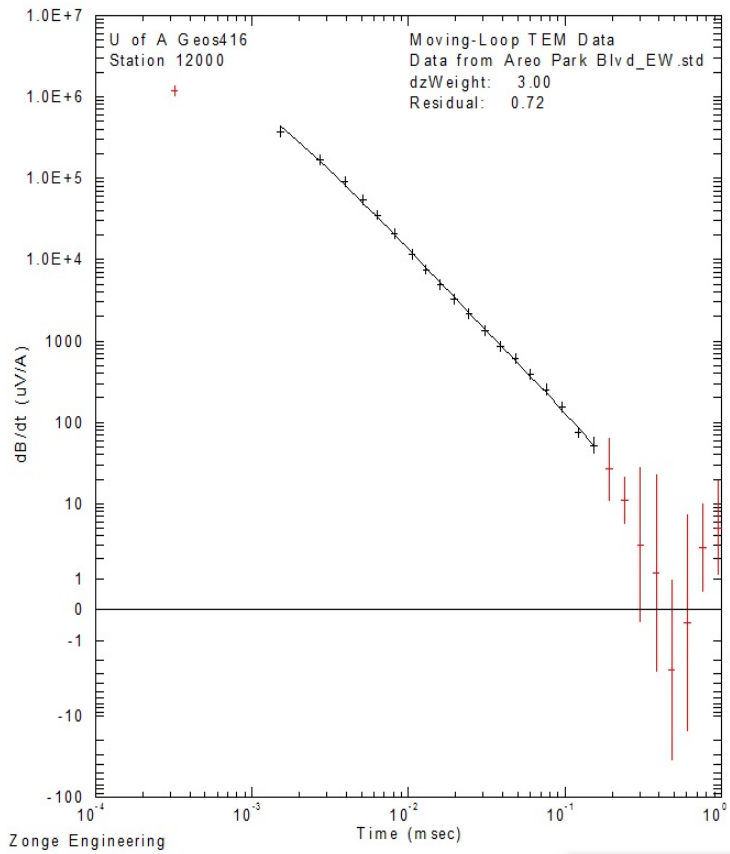


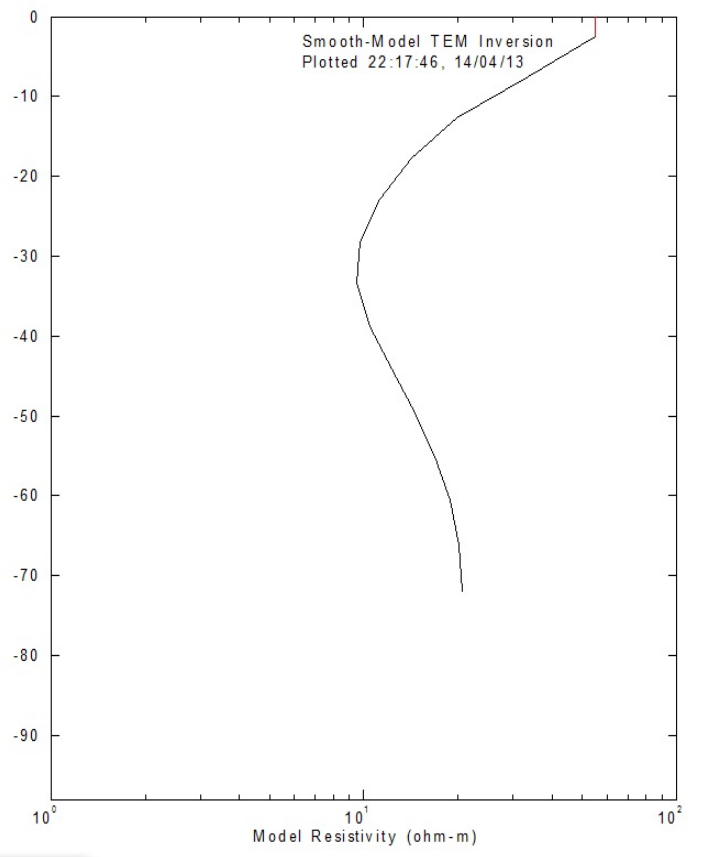
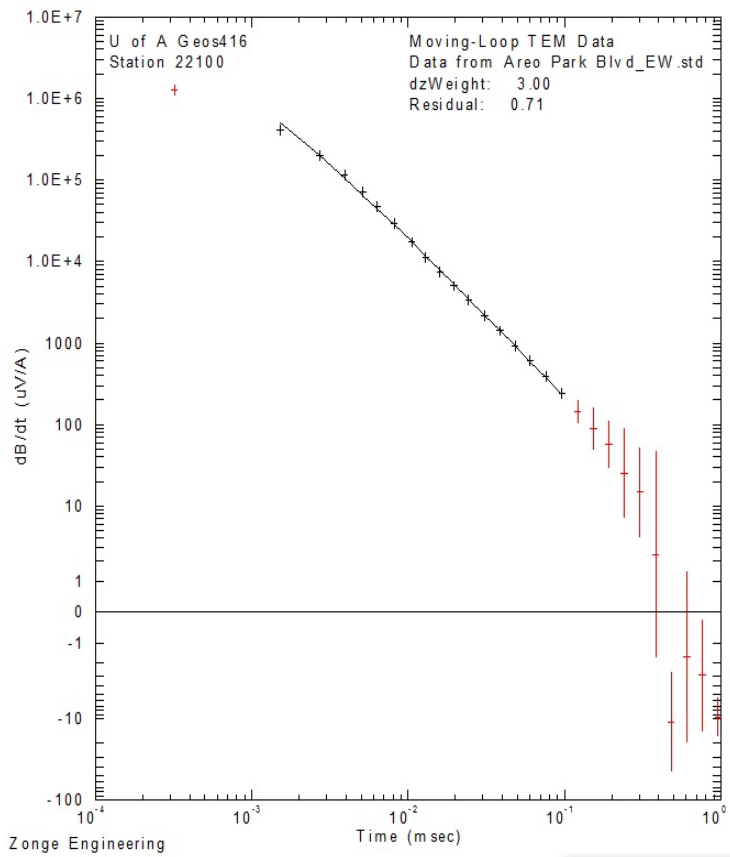
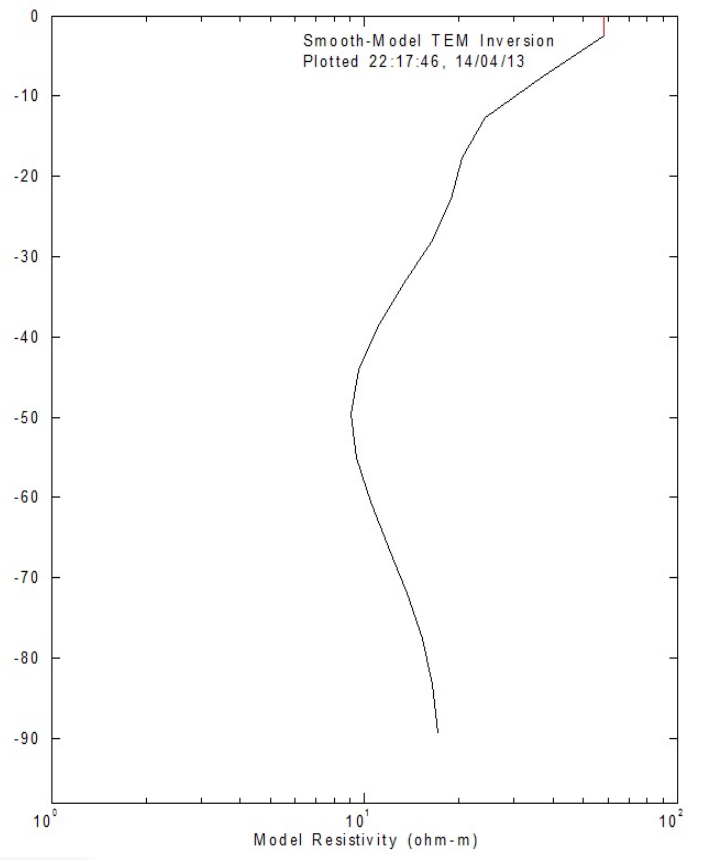
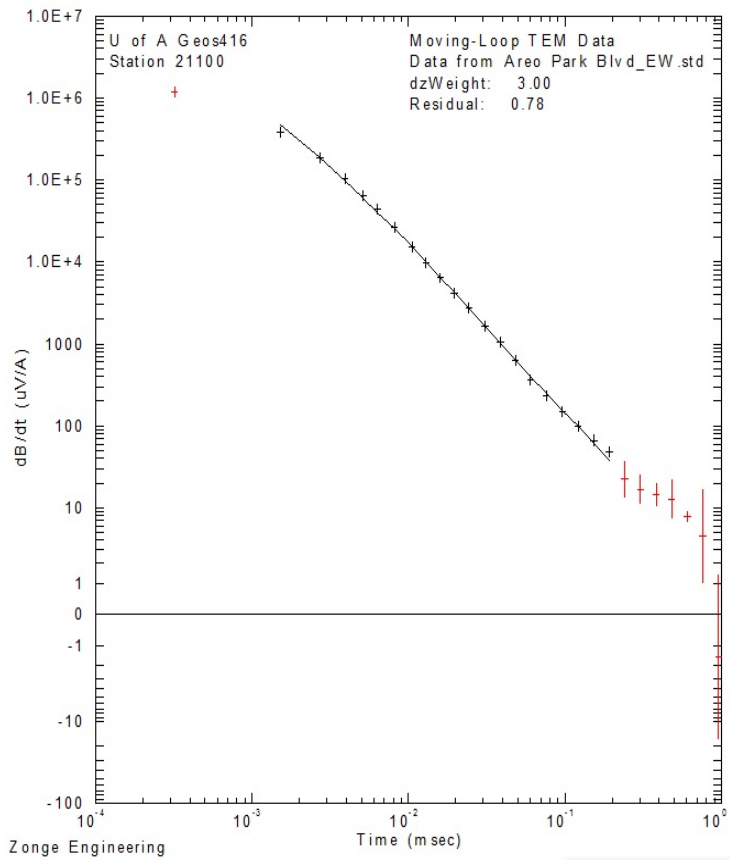
20x20 loops at the Aero Park Blvd South site with 64Hz from south to North

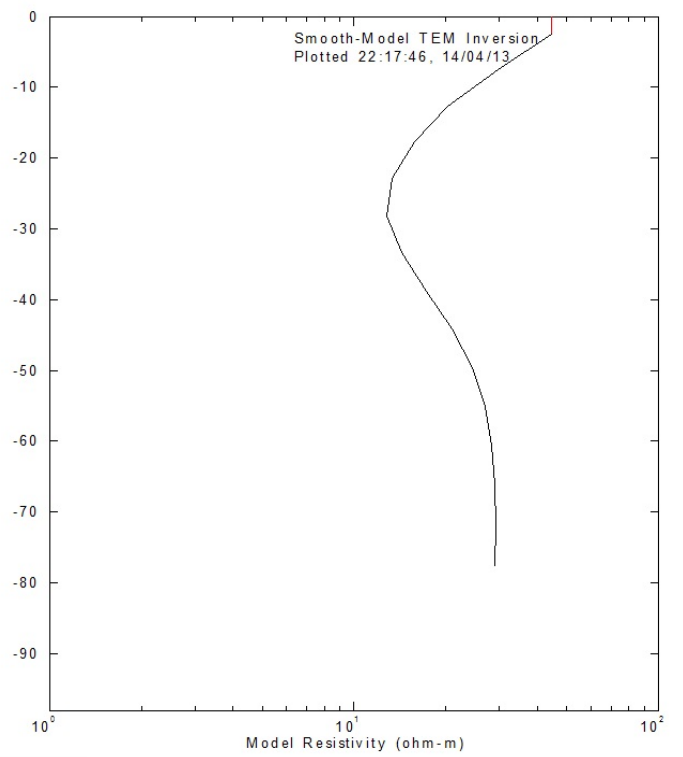
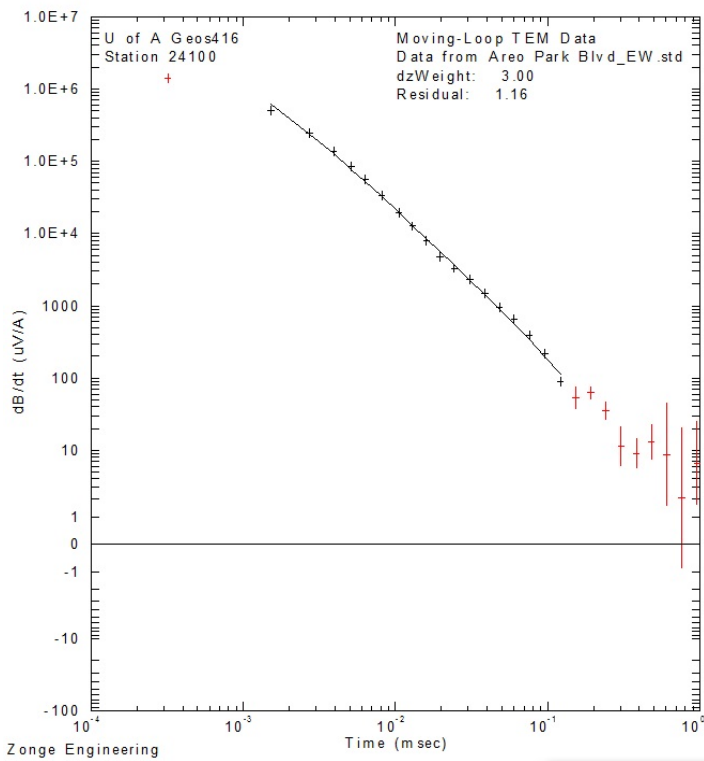
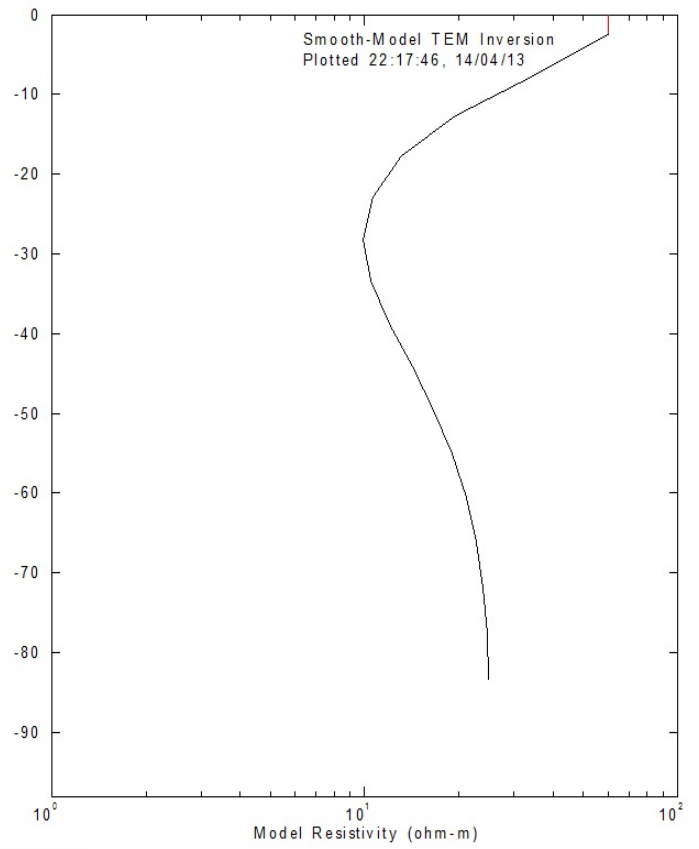
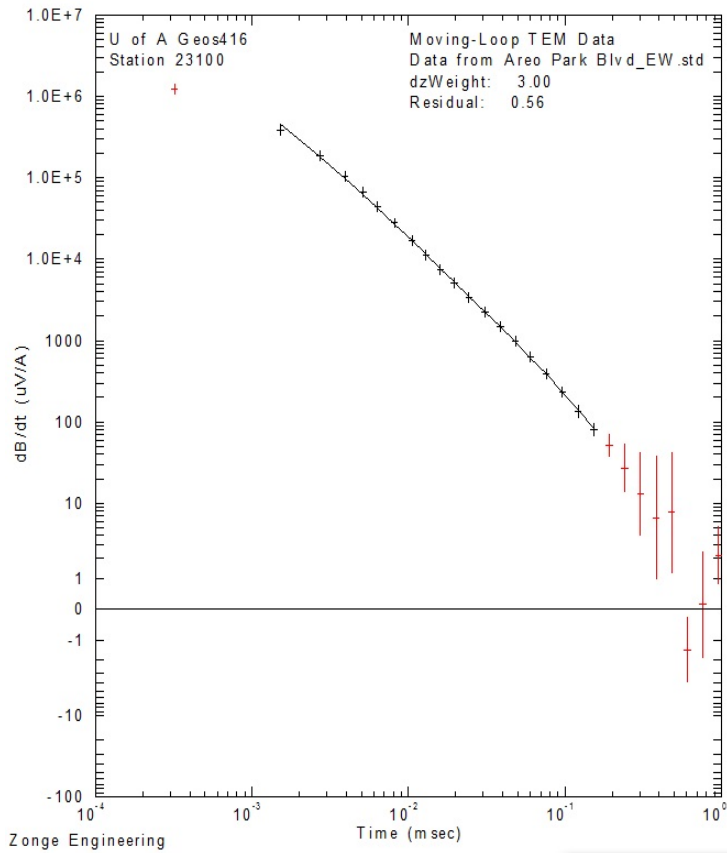


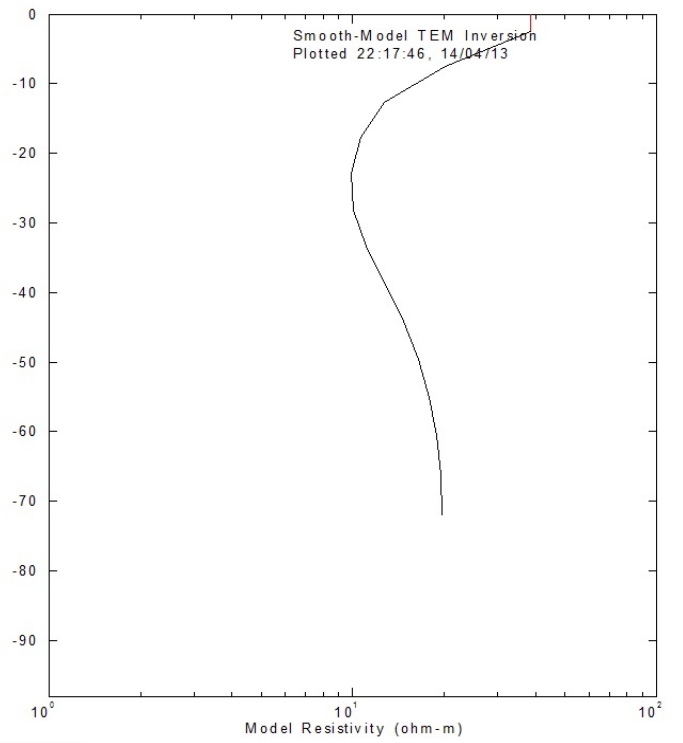
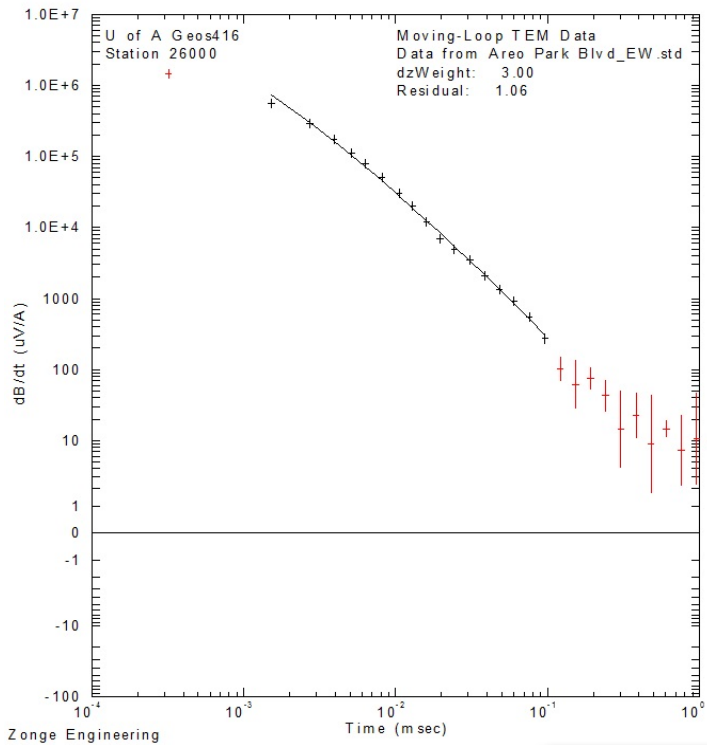
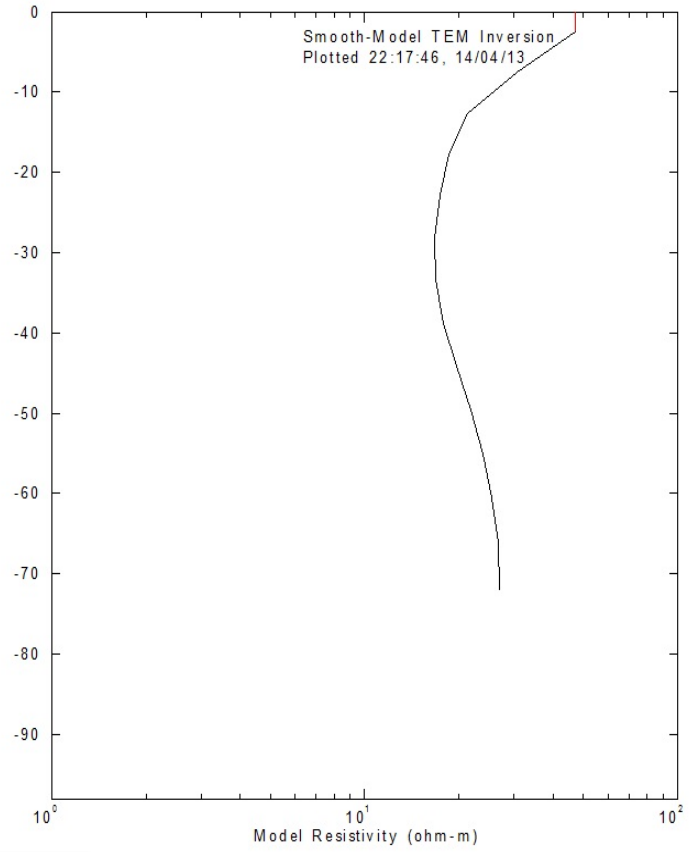
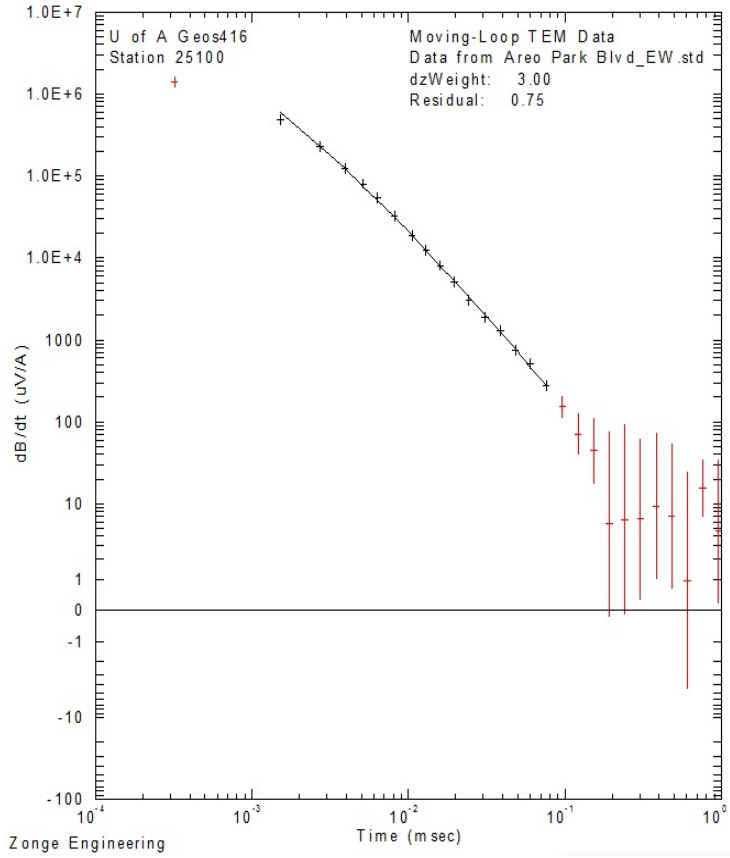


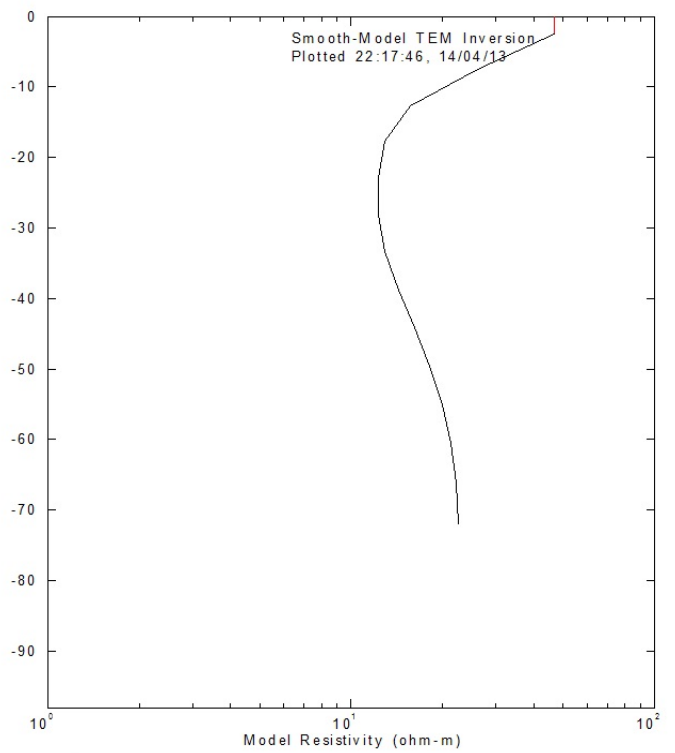
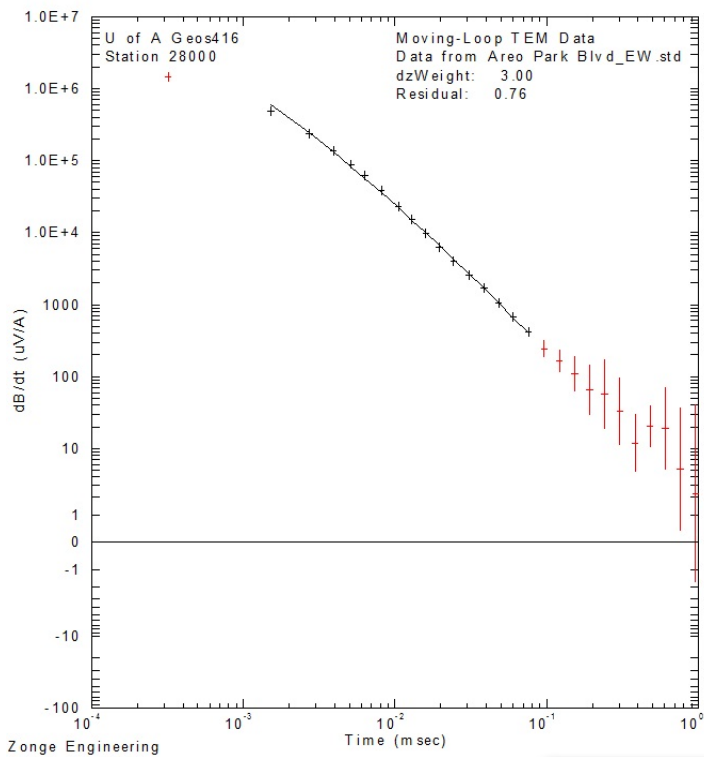
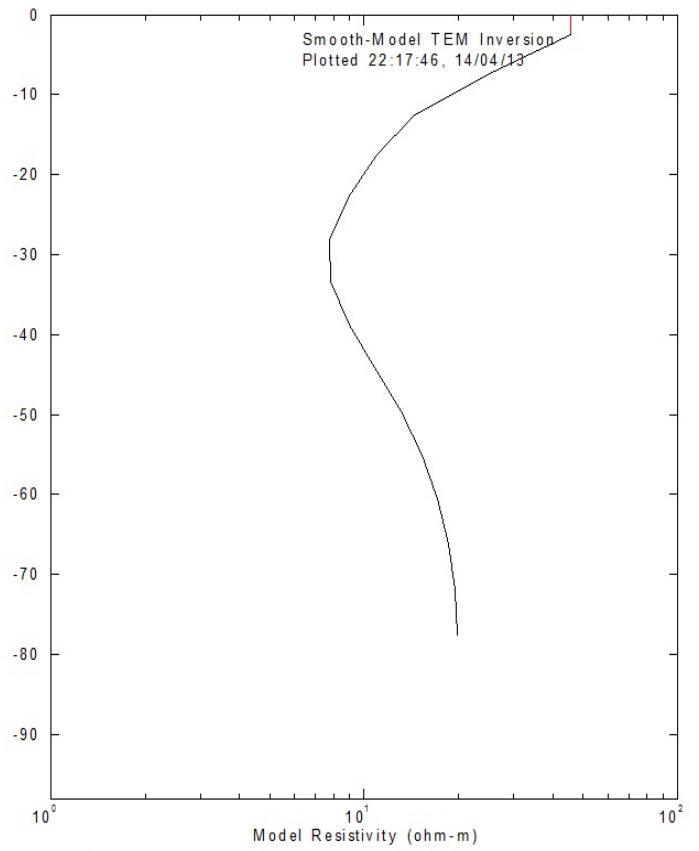
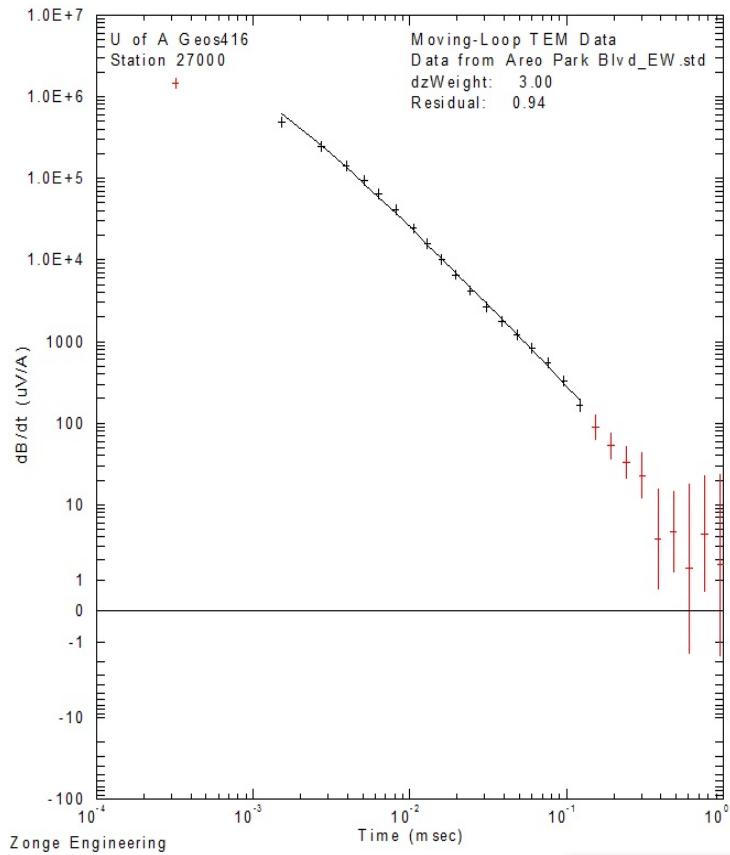


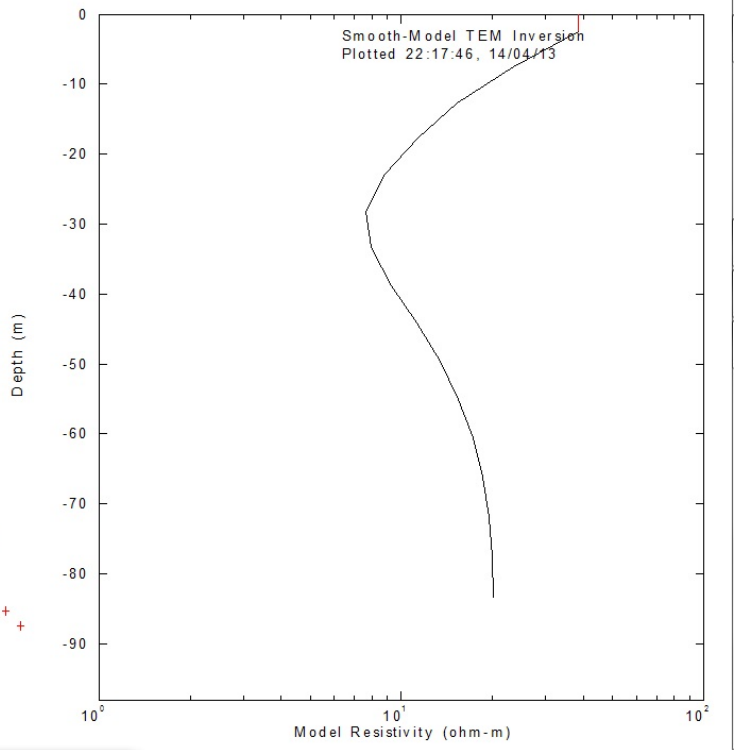
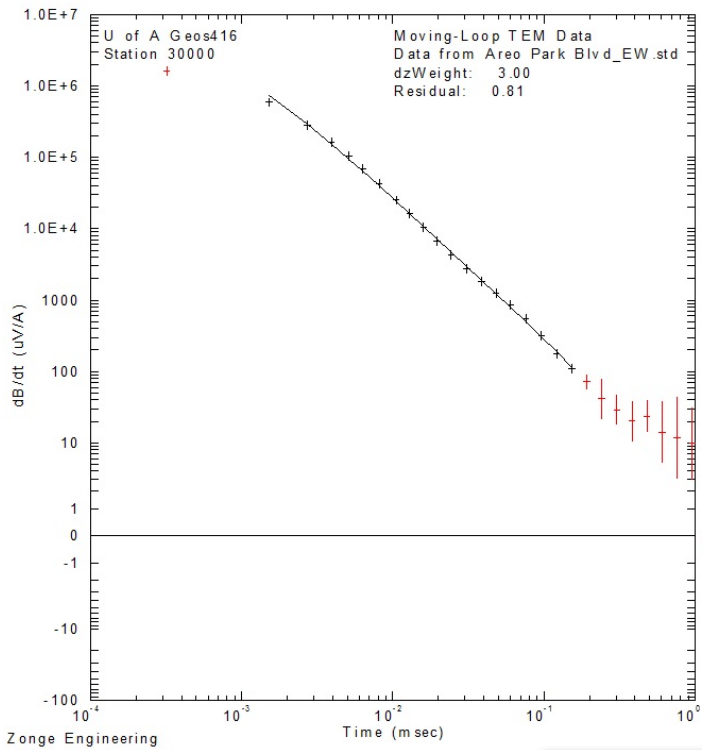
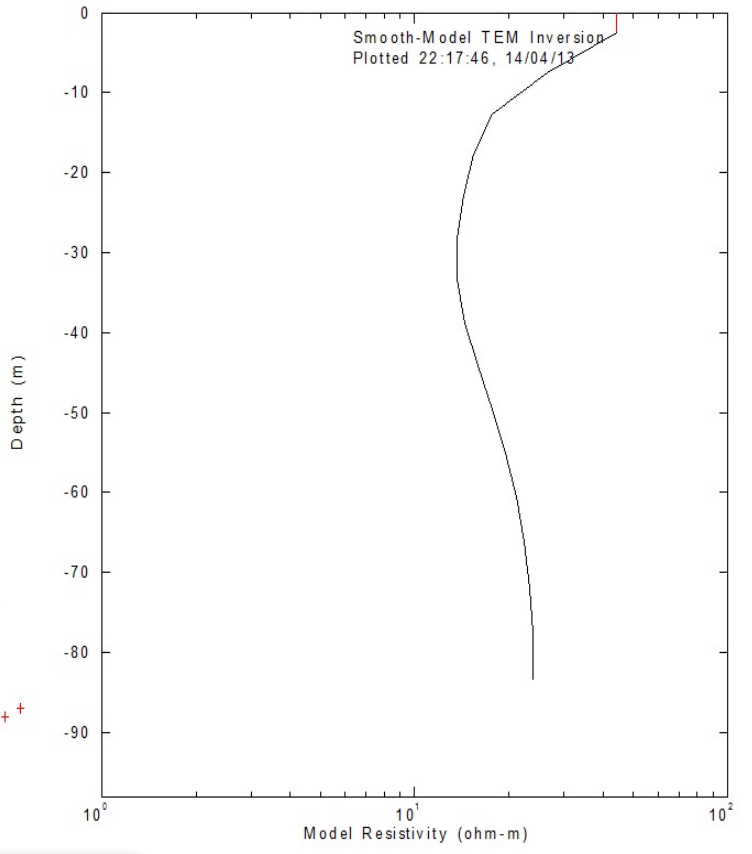
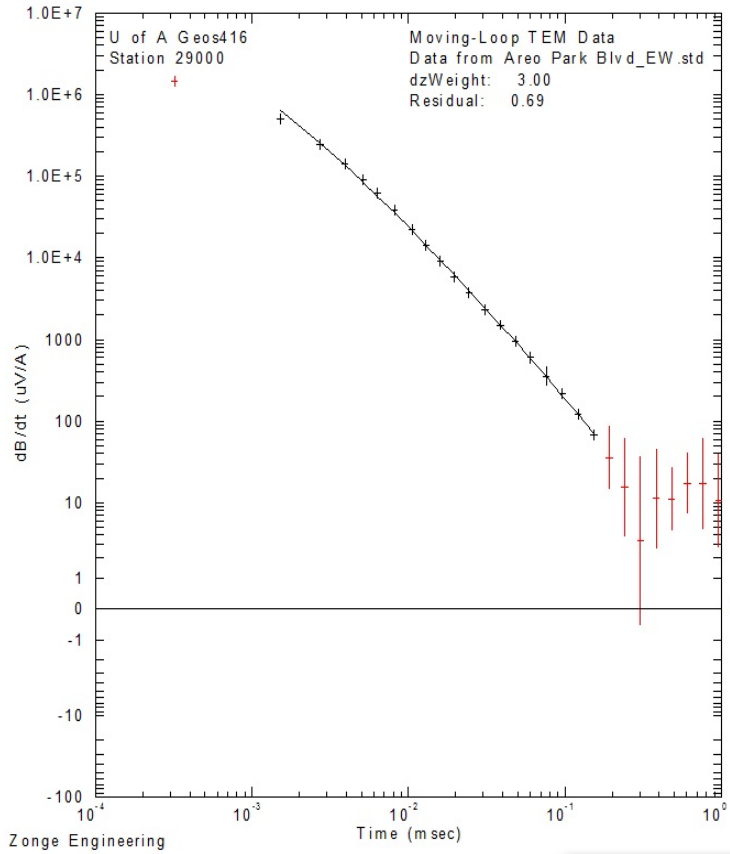


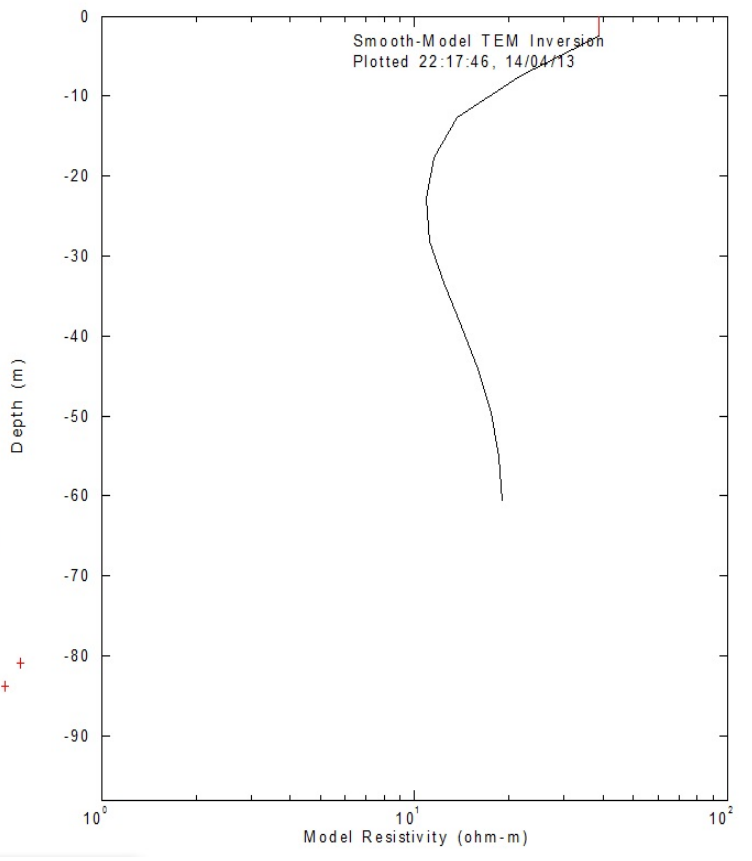
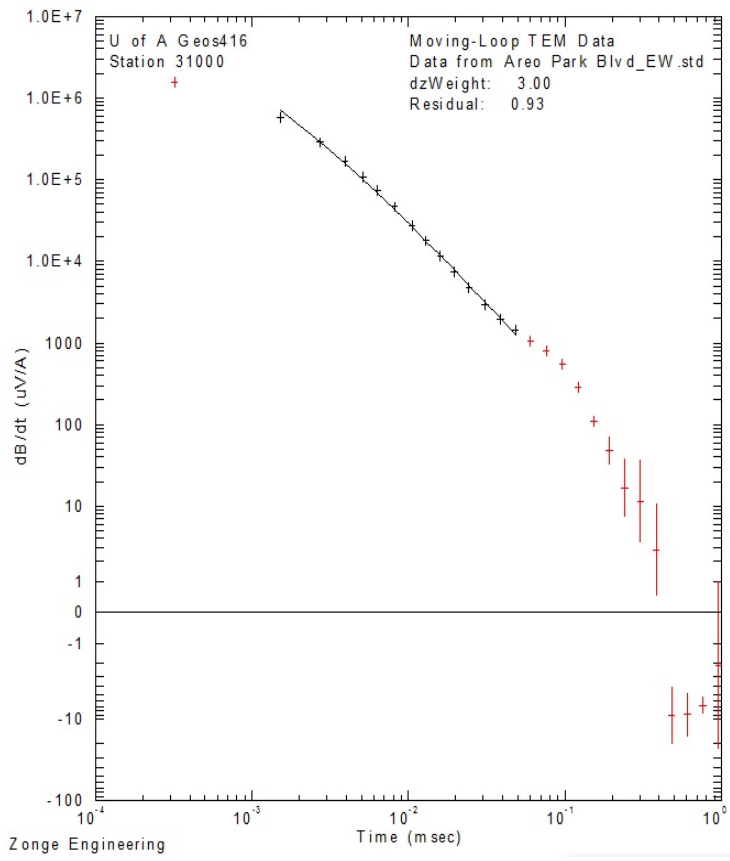




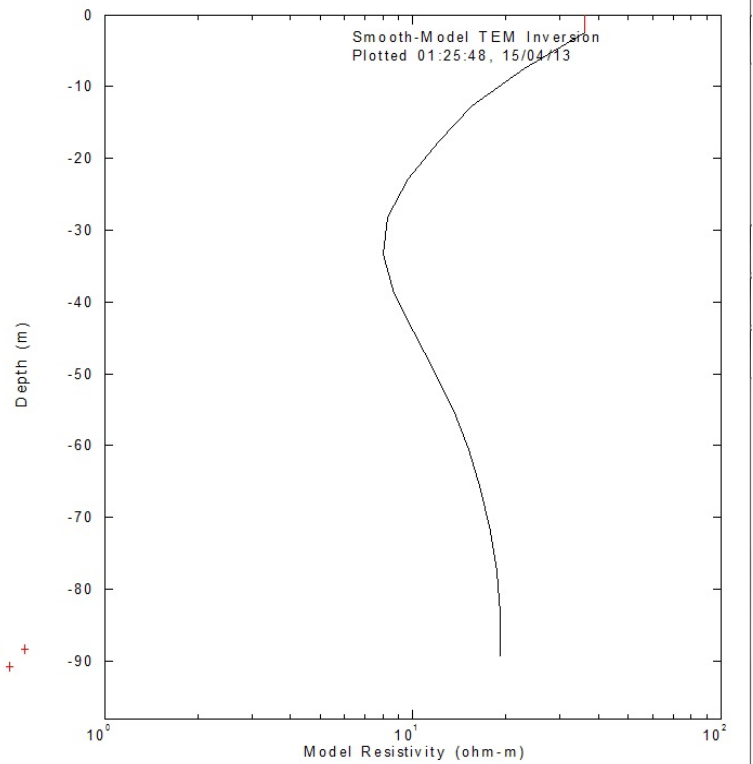
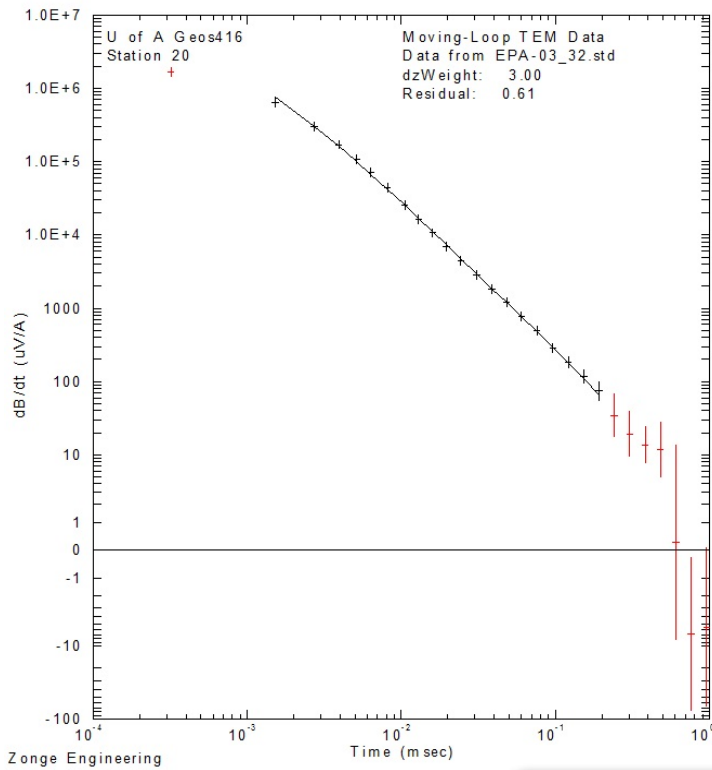
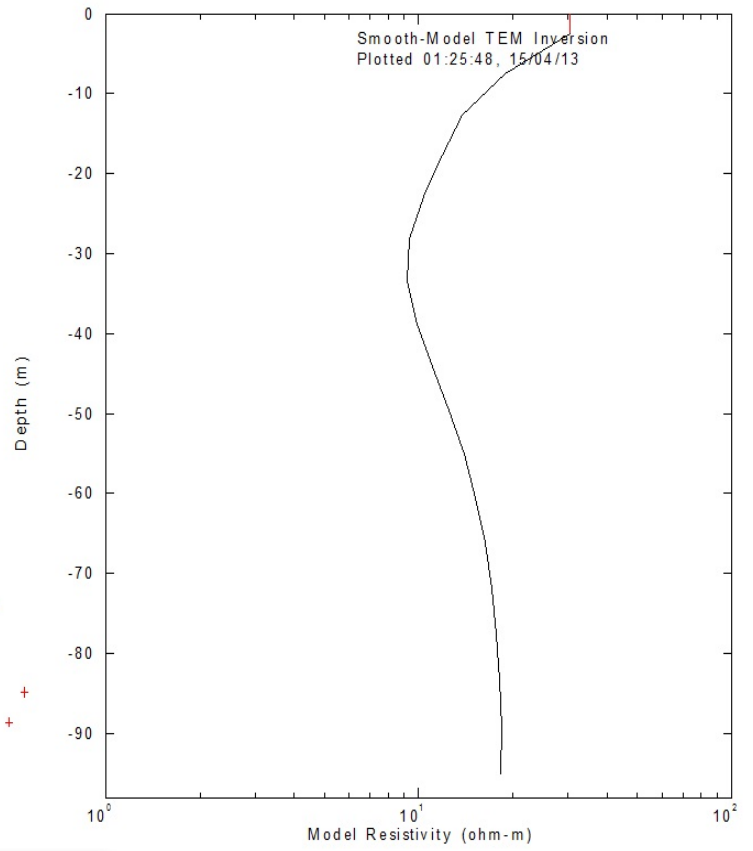
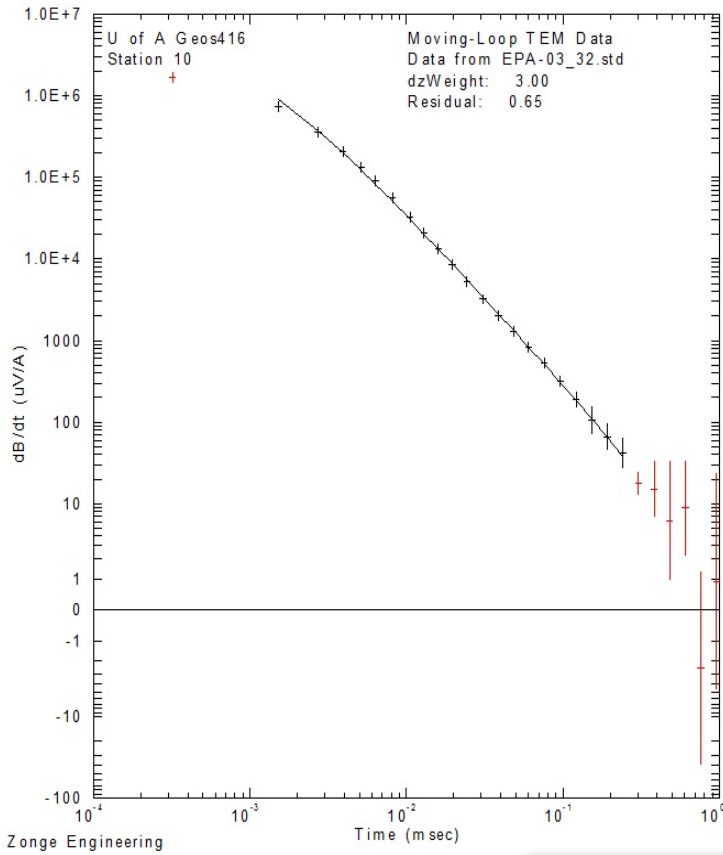


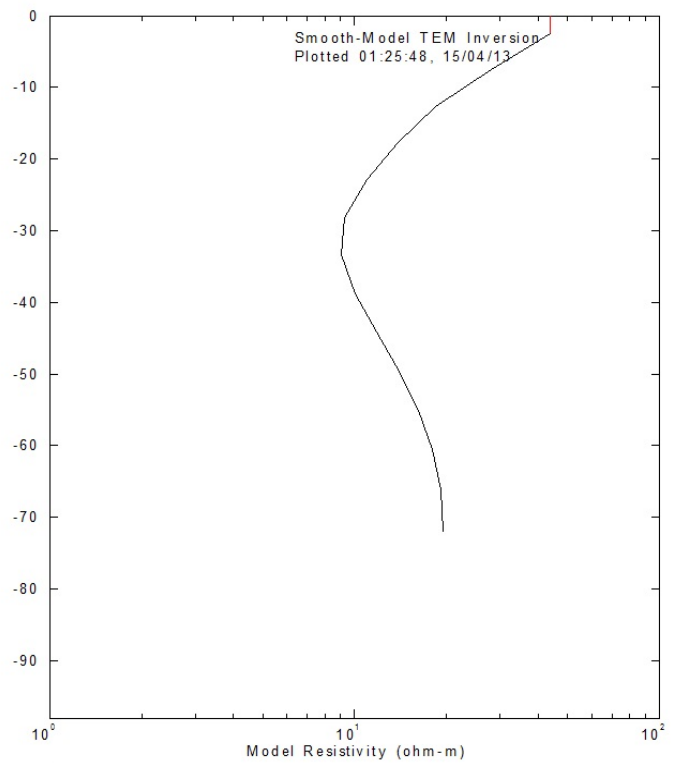
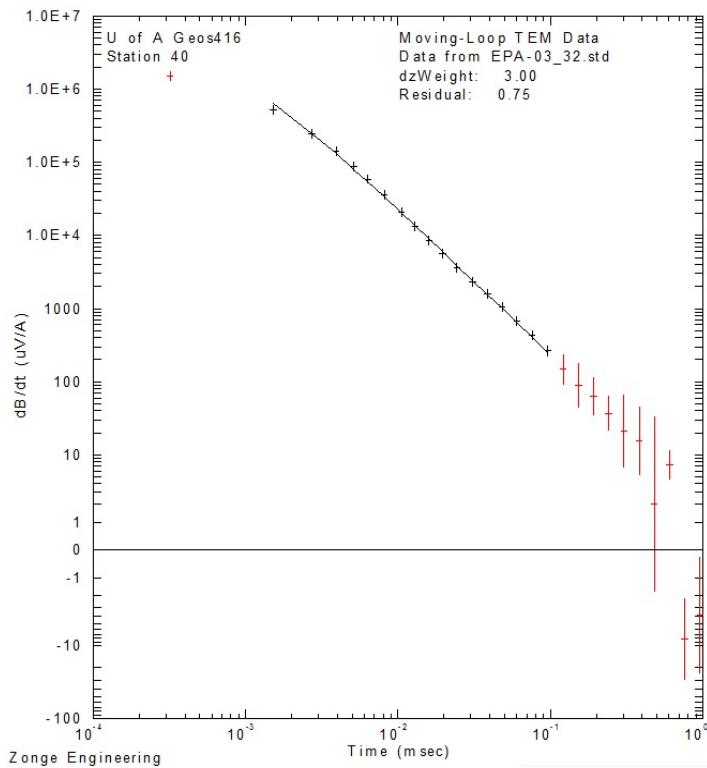
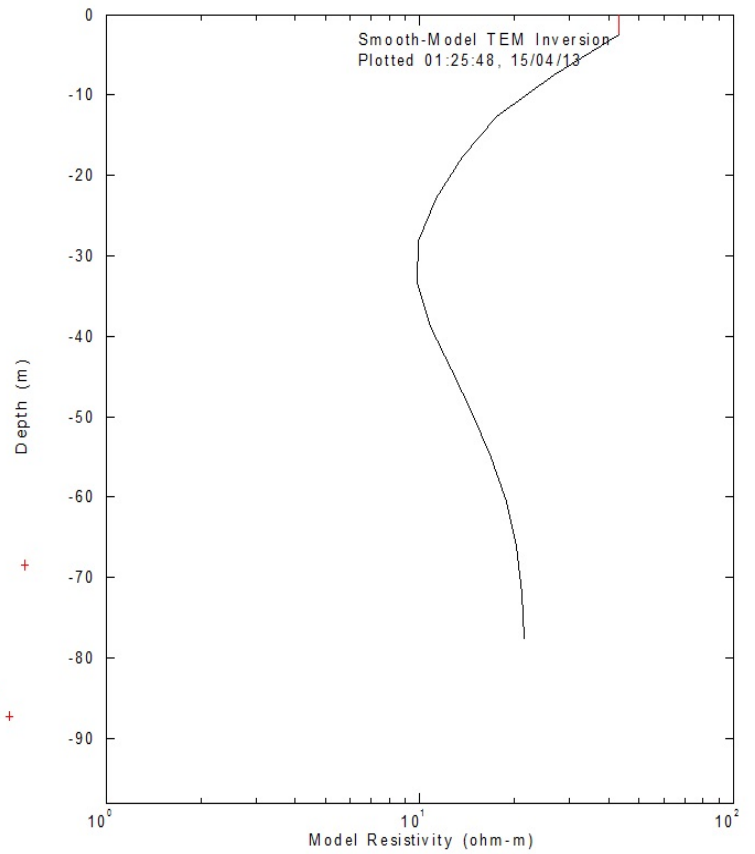
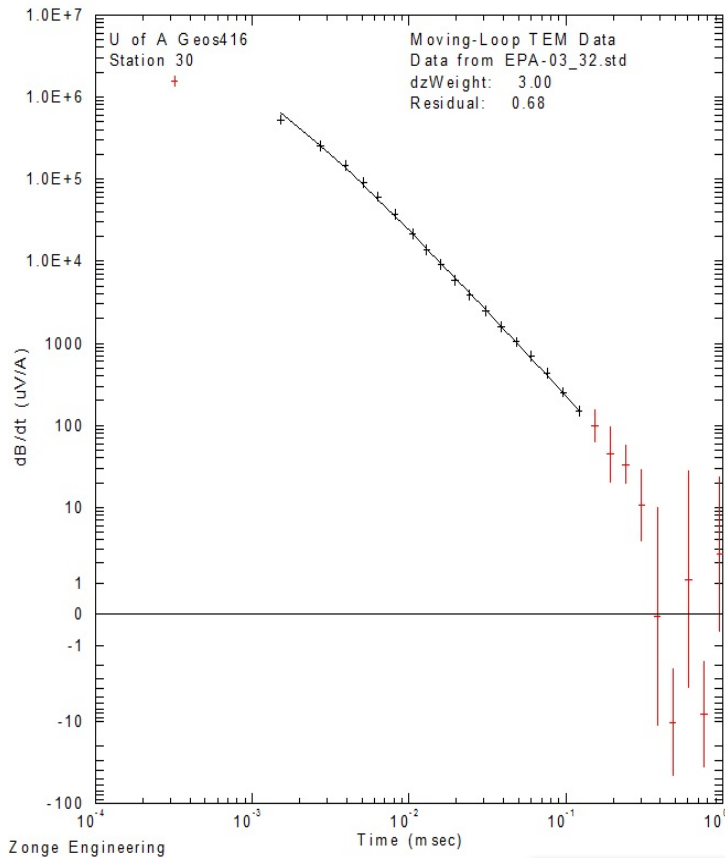


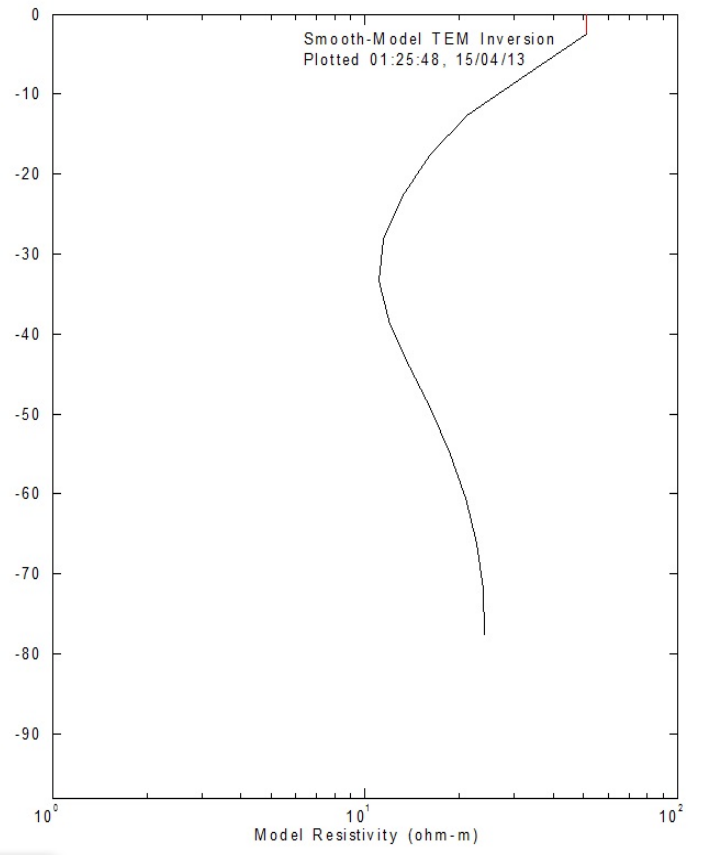
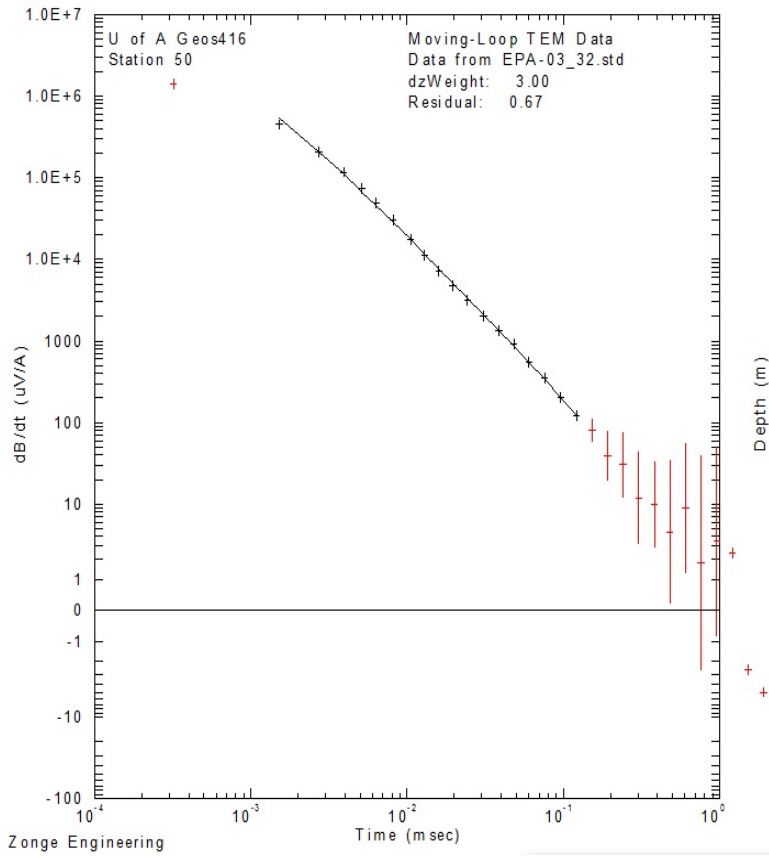




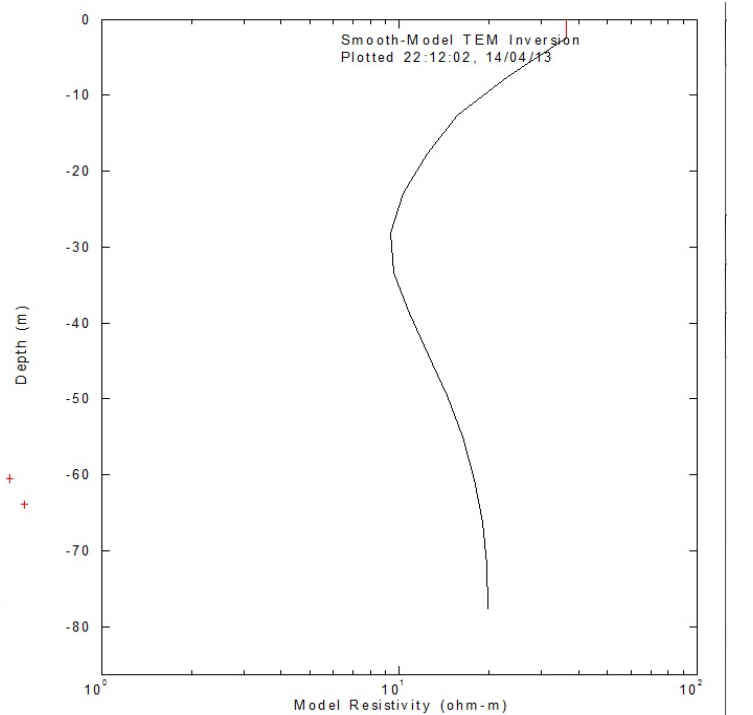
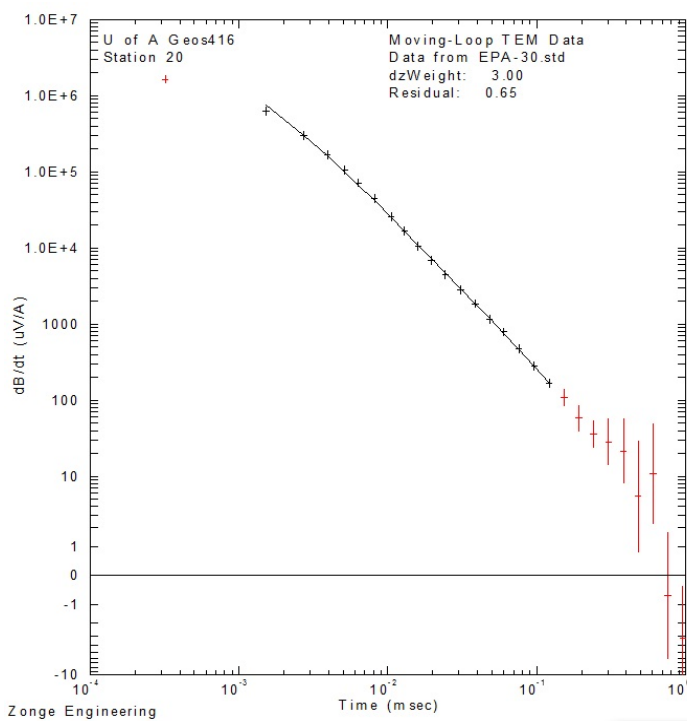
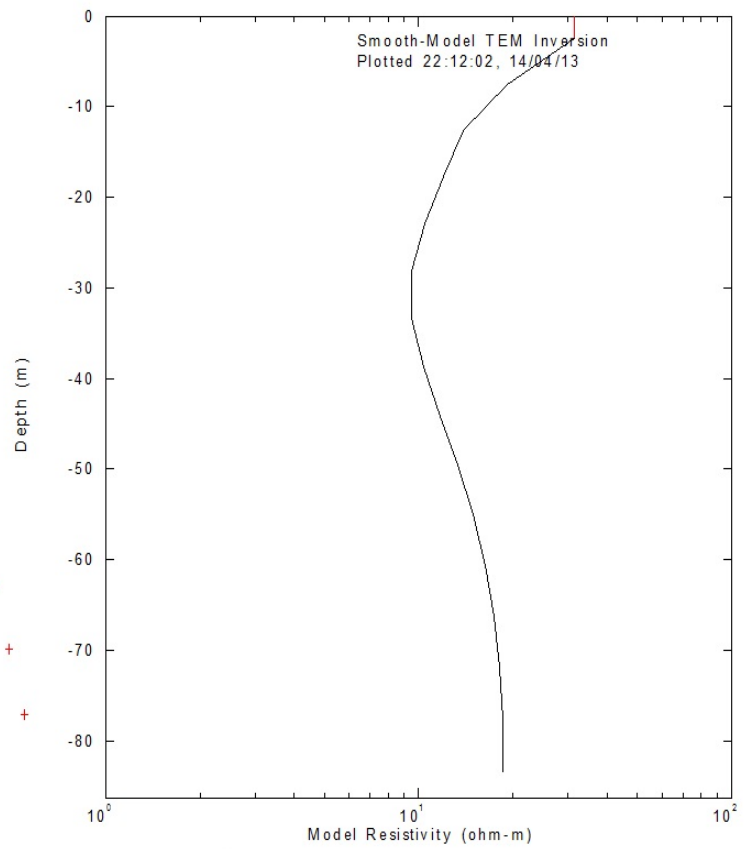
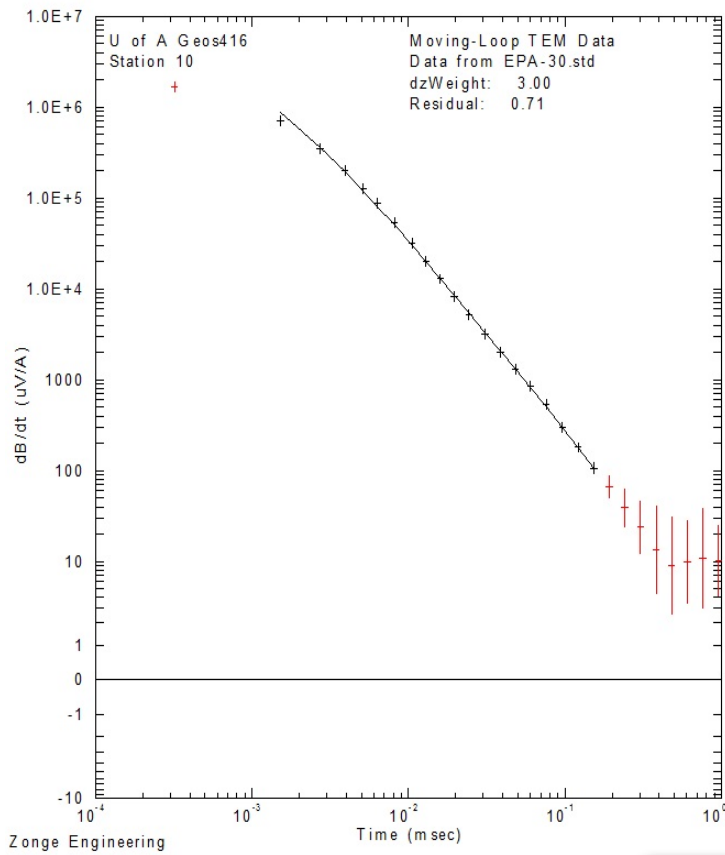
20x20 loops at EPA-03 site with 32Hz from East to West

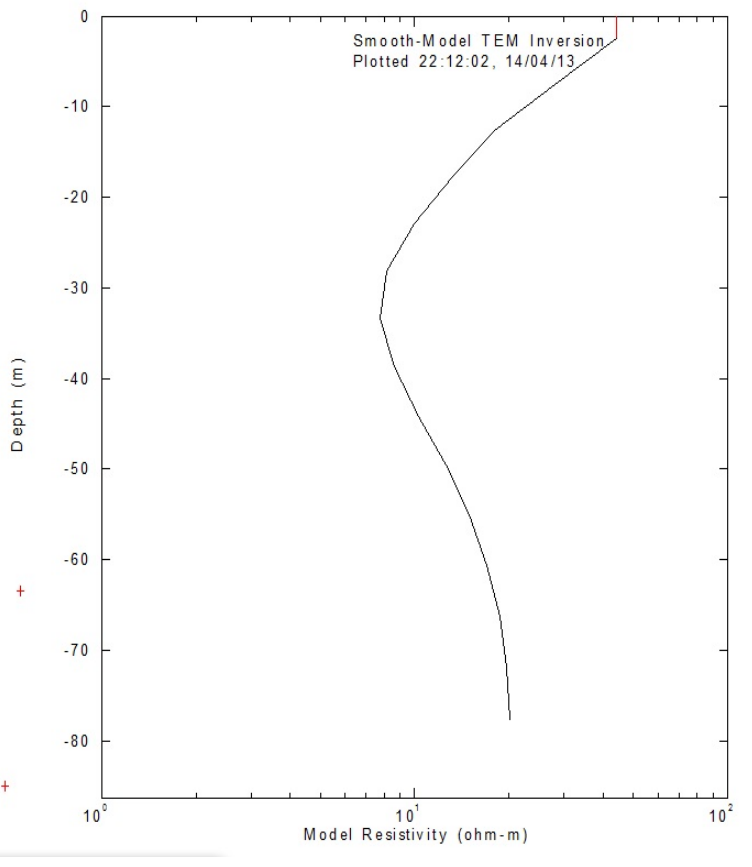
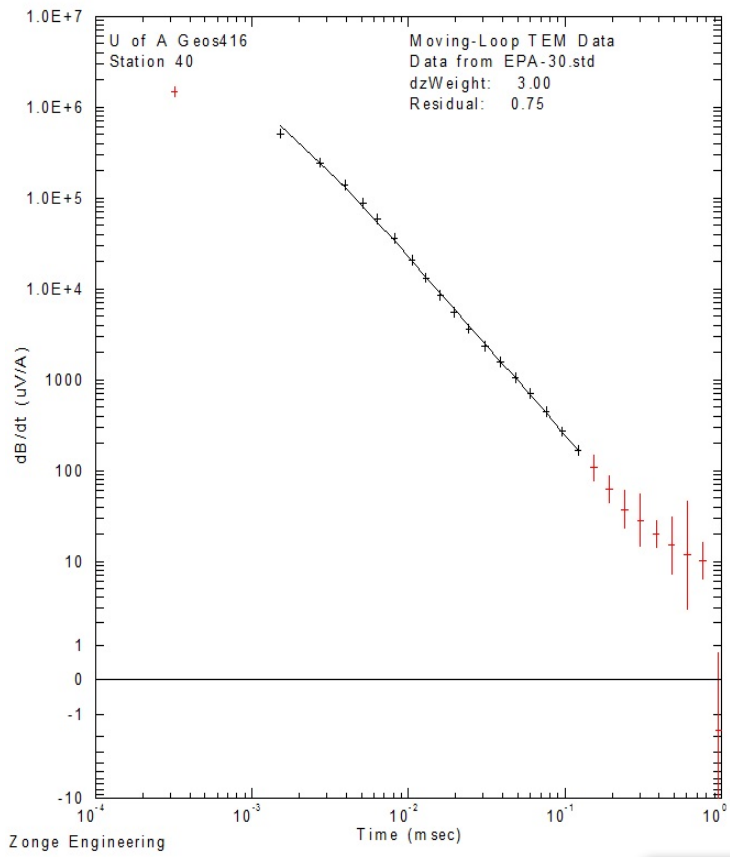
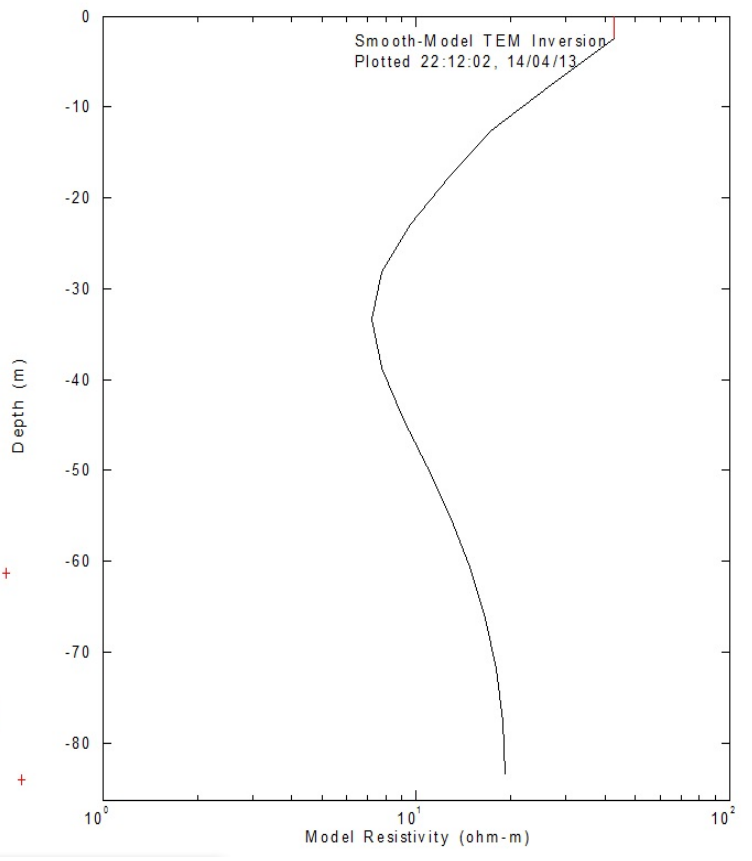
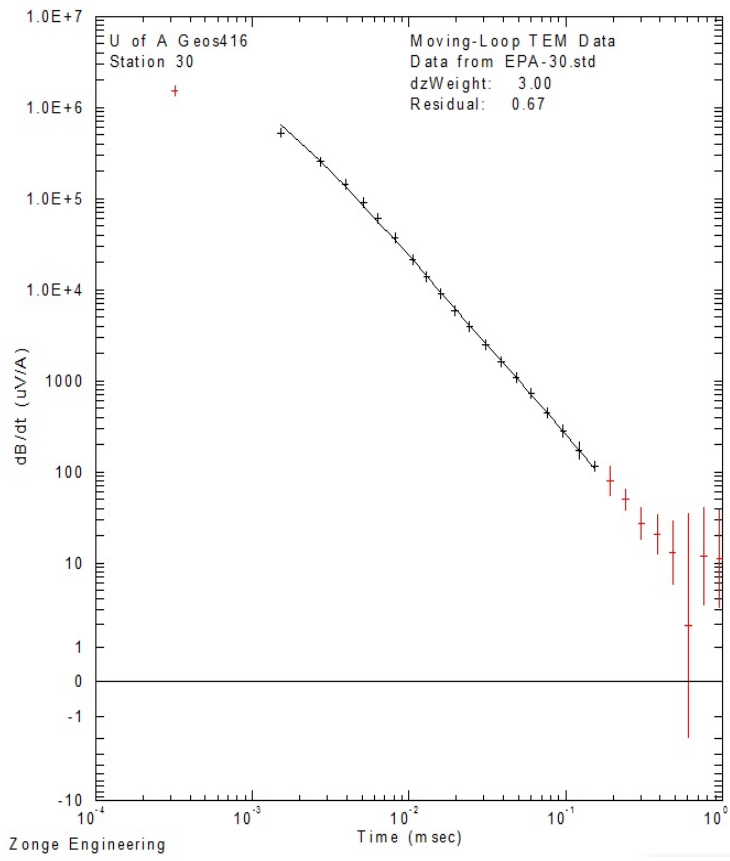


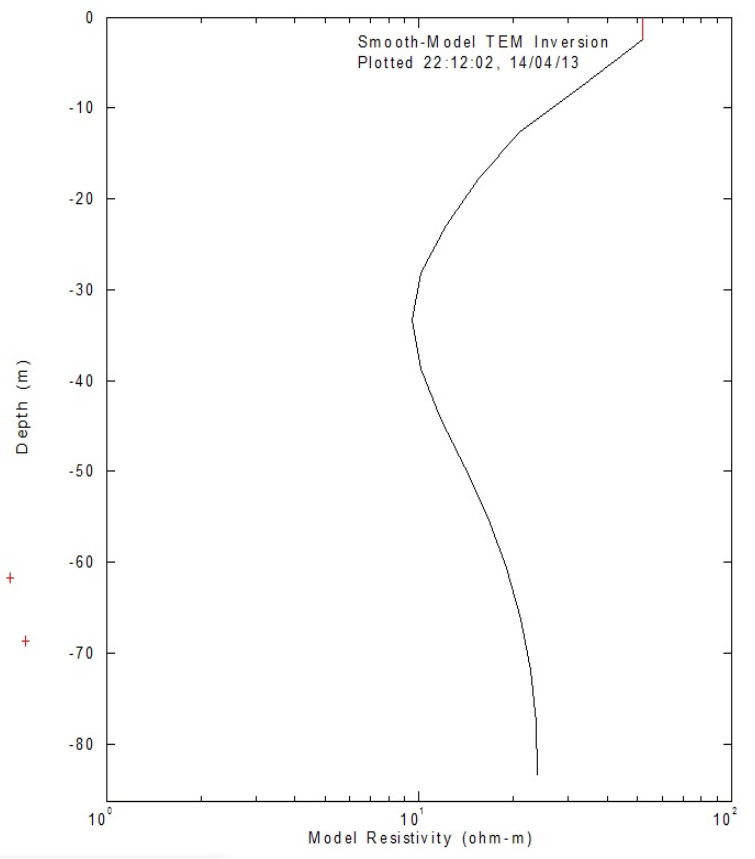
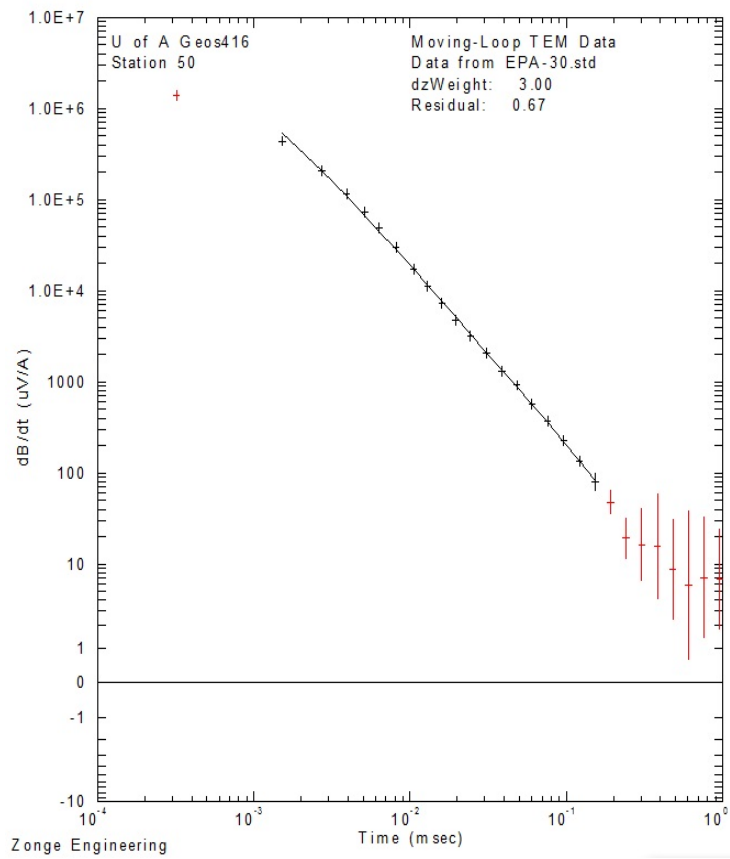




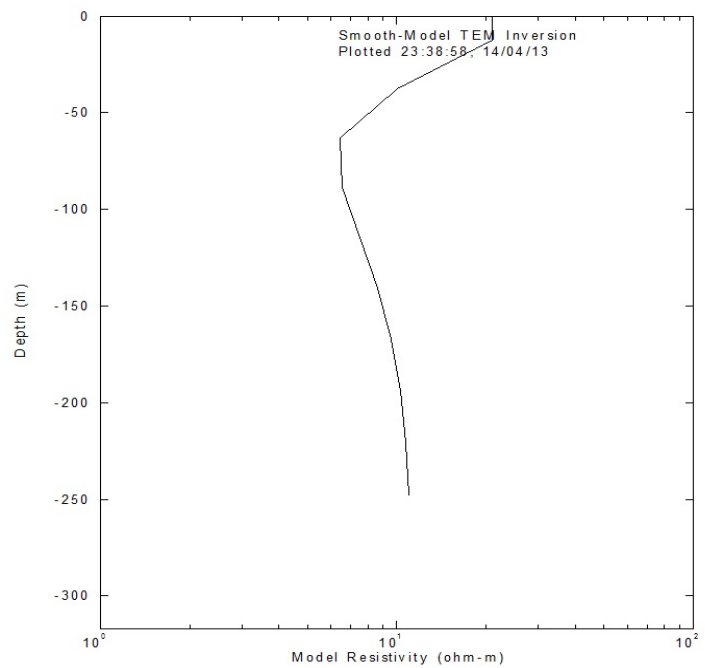
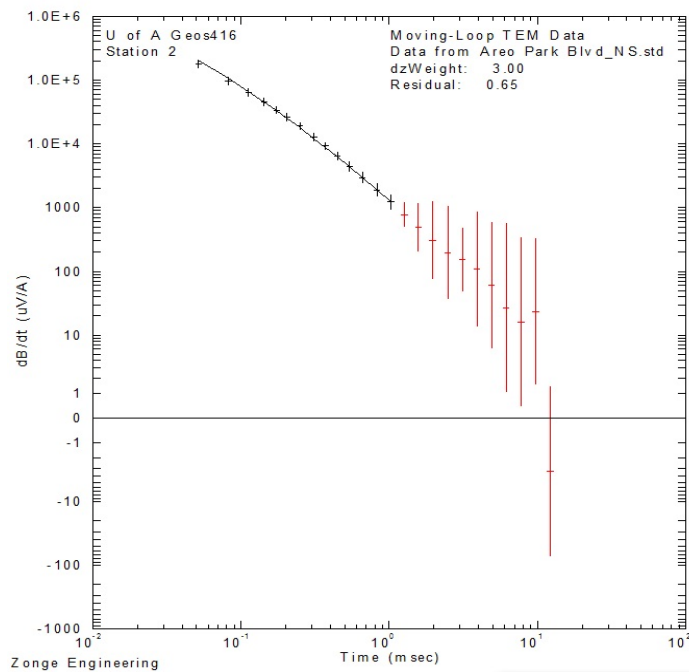
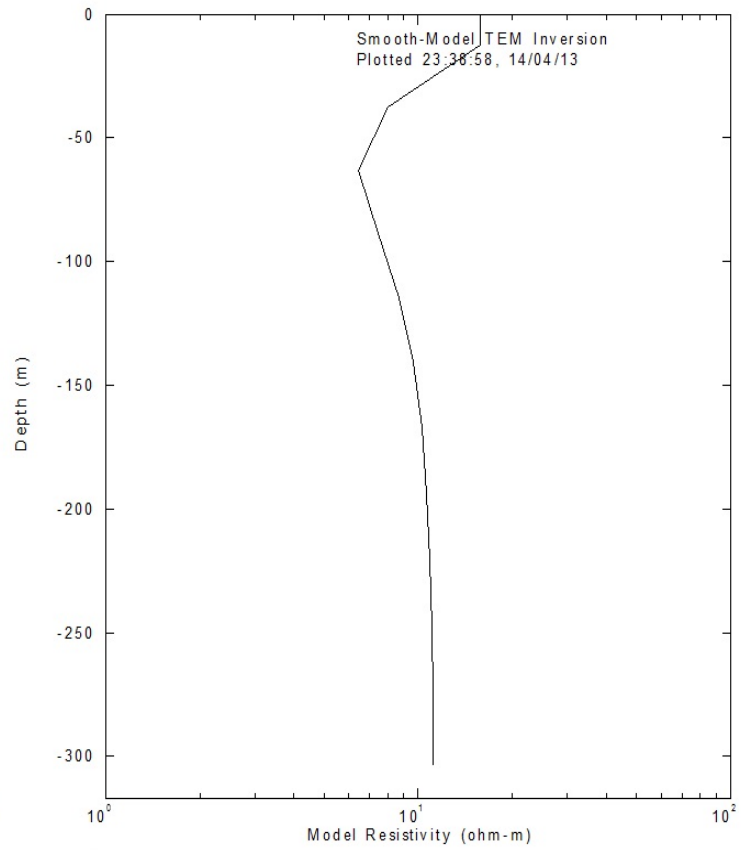
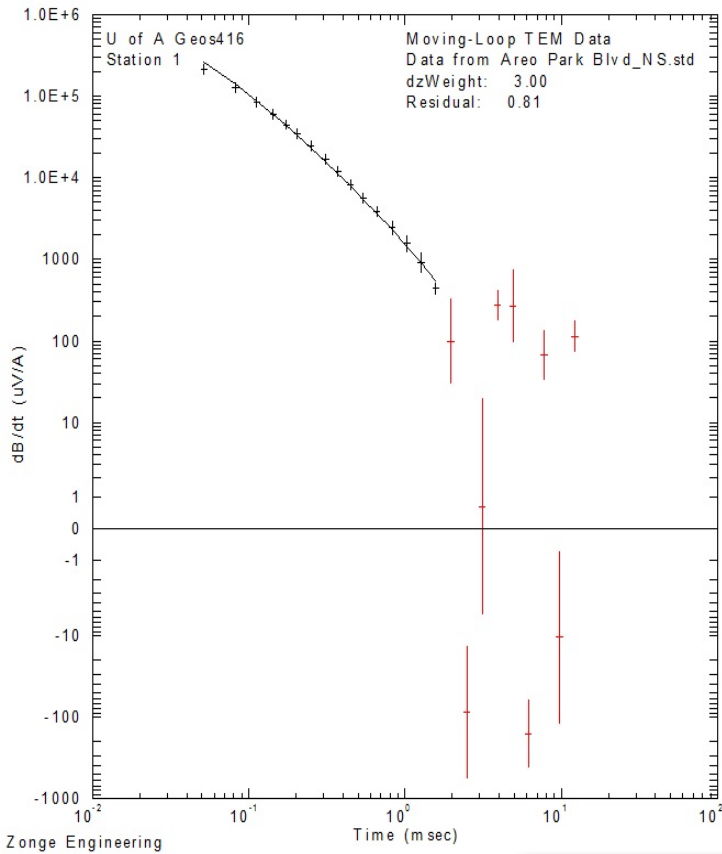
20x20 loops at EPA-03 site with 64Hz from East to West

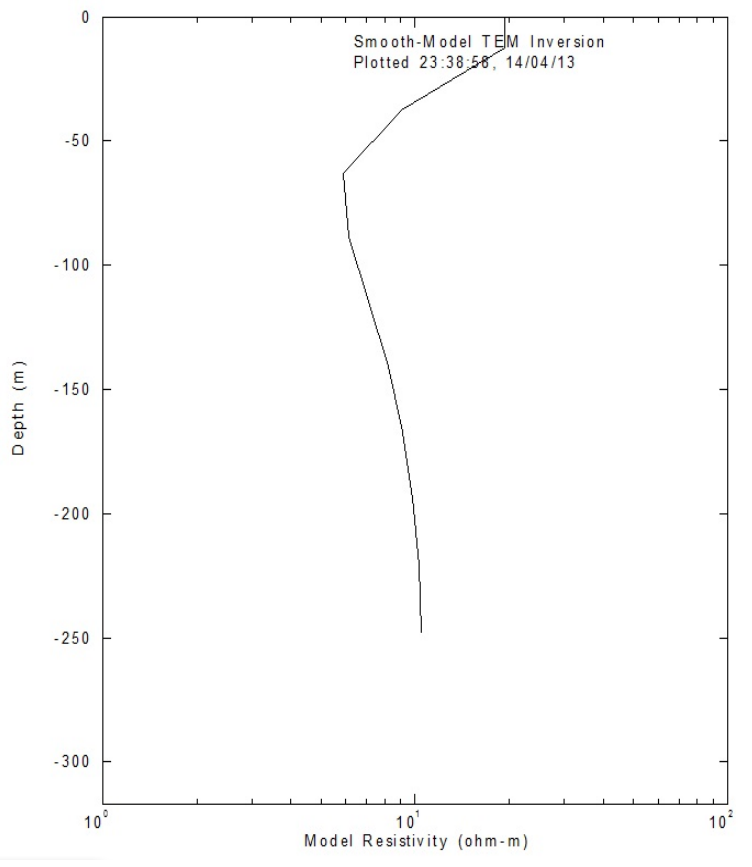
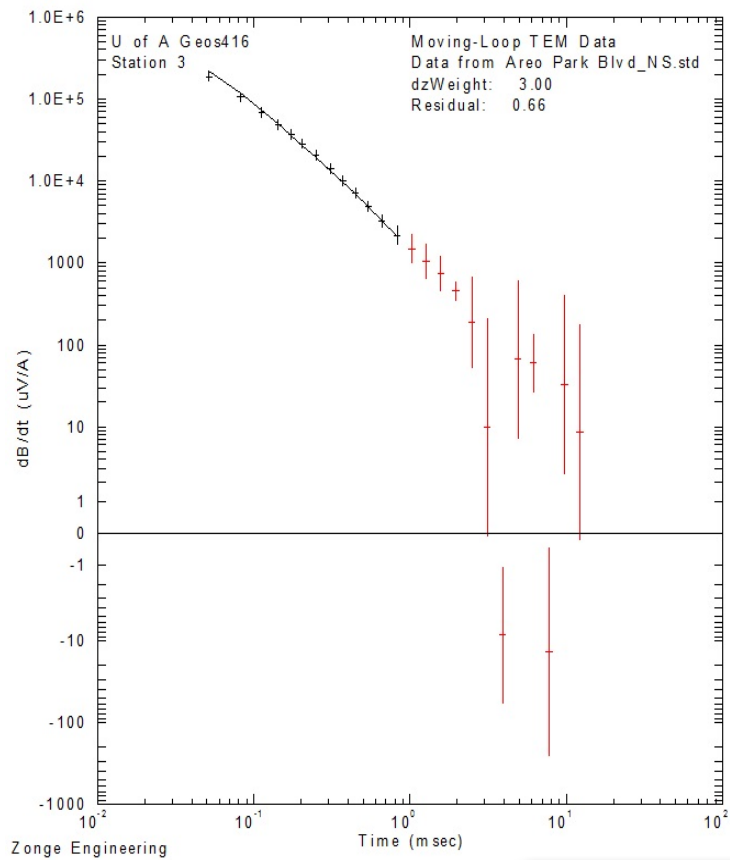




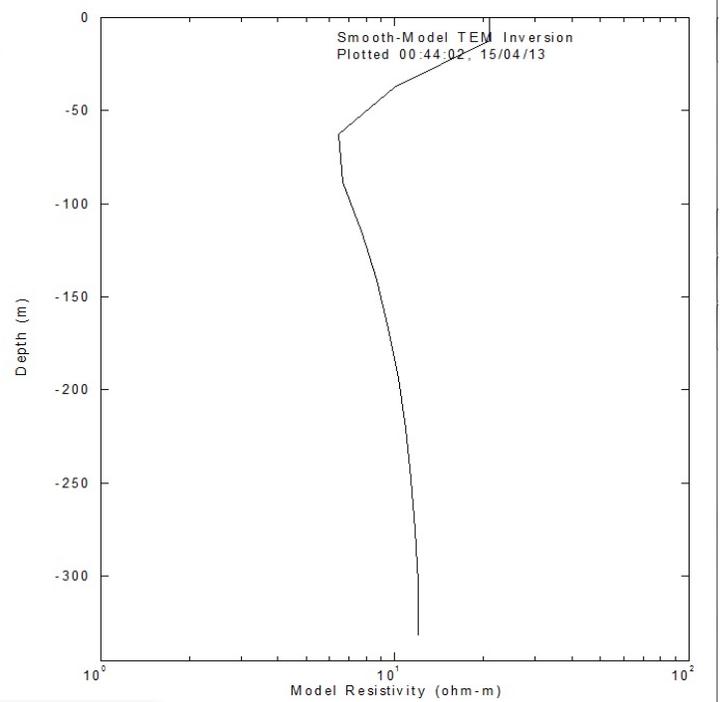
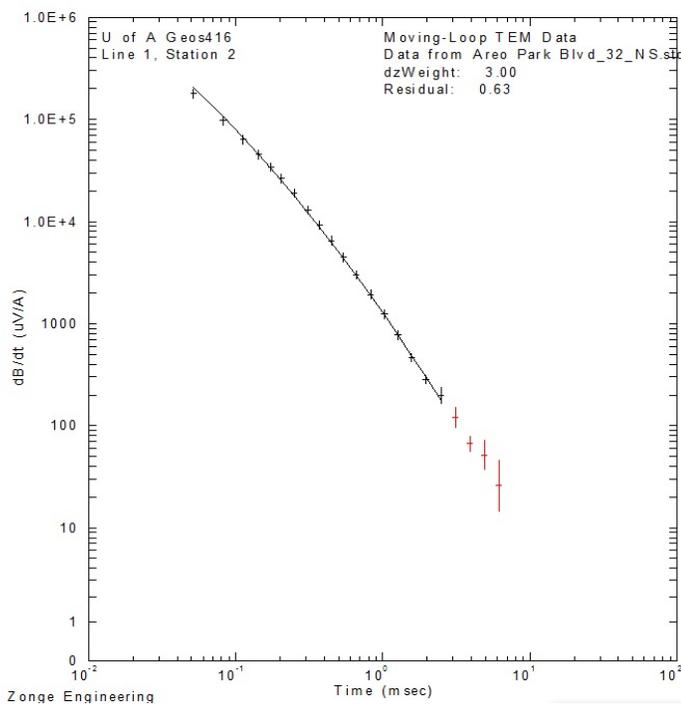
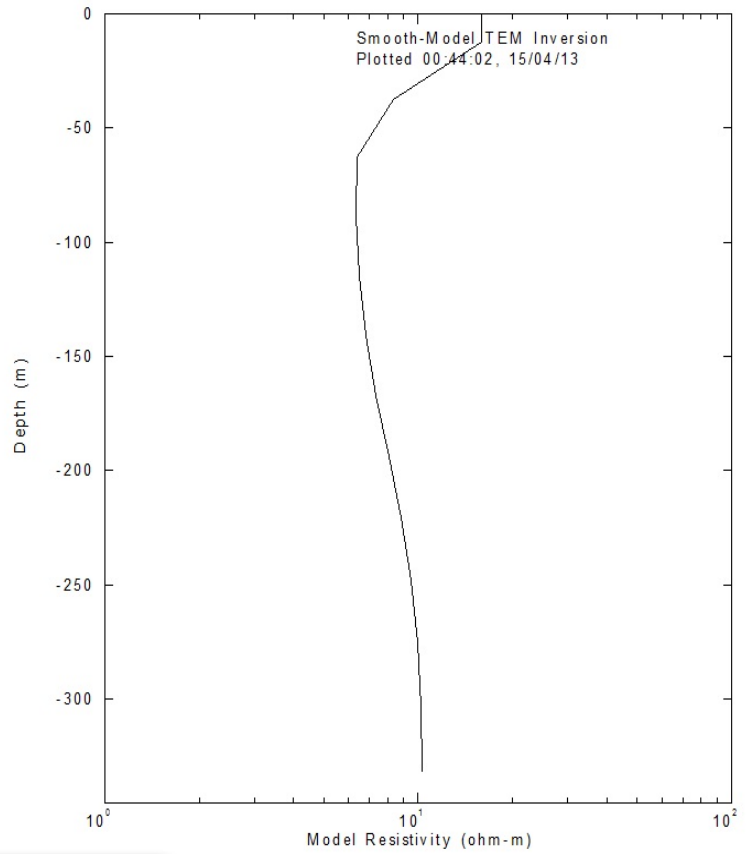
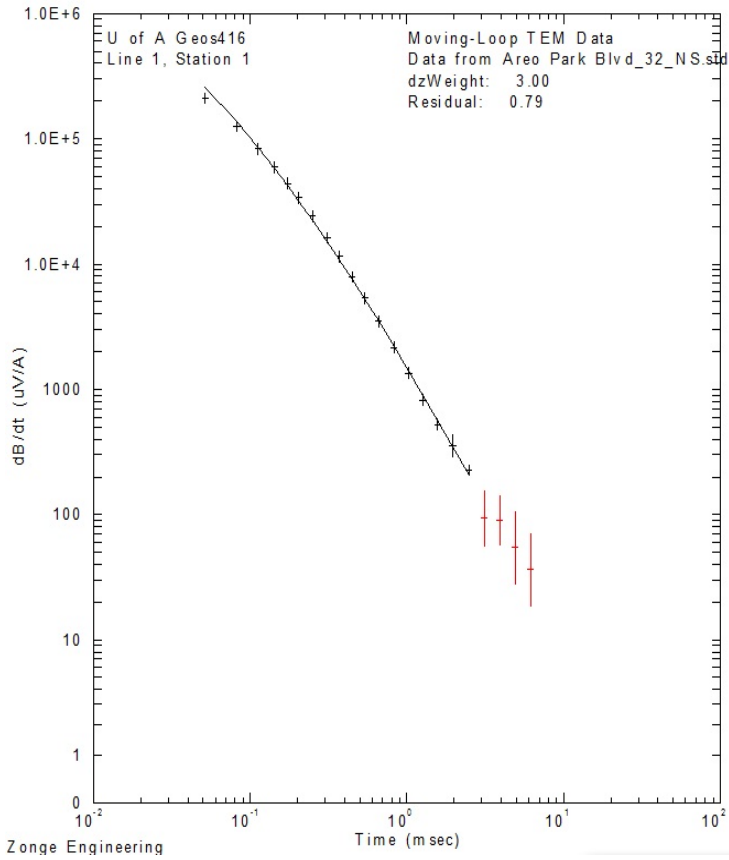


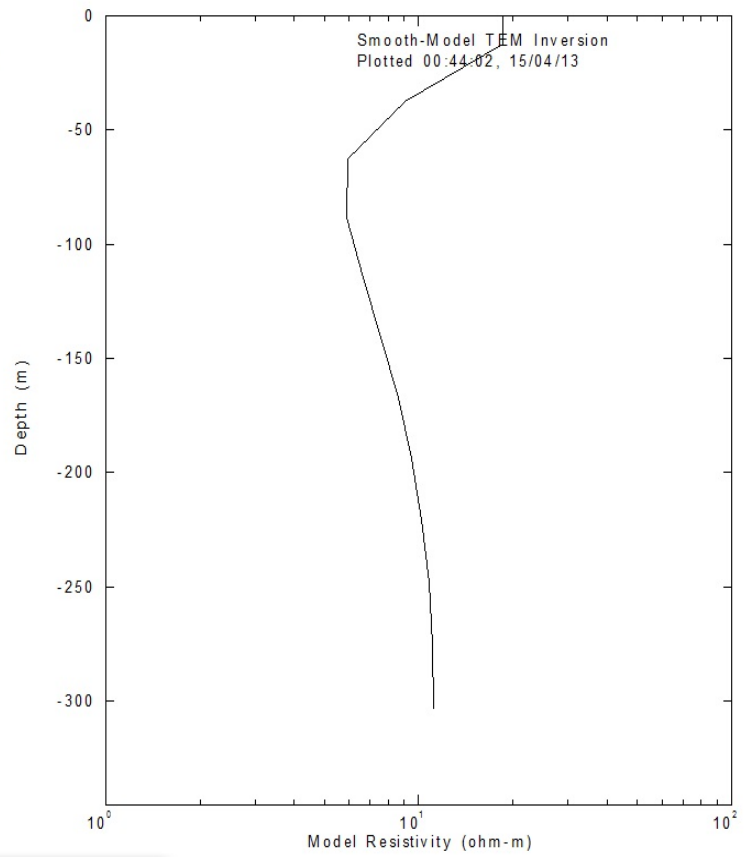
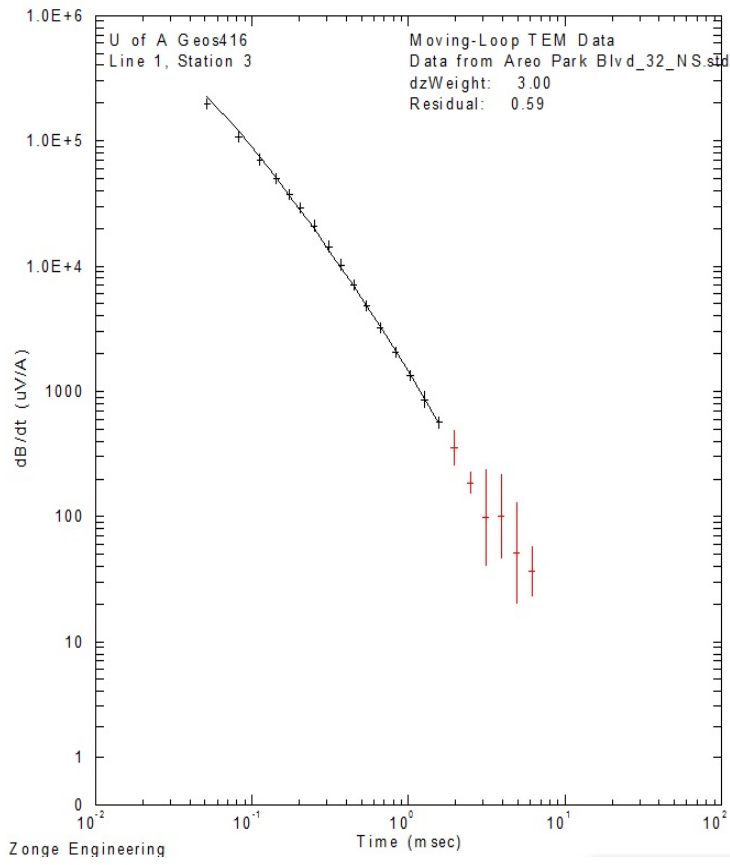
100x100 loops at the Aero Park Blvd South site with 16Hz from south to North



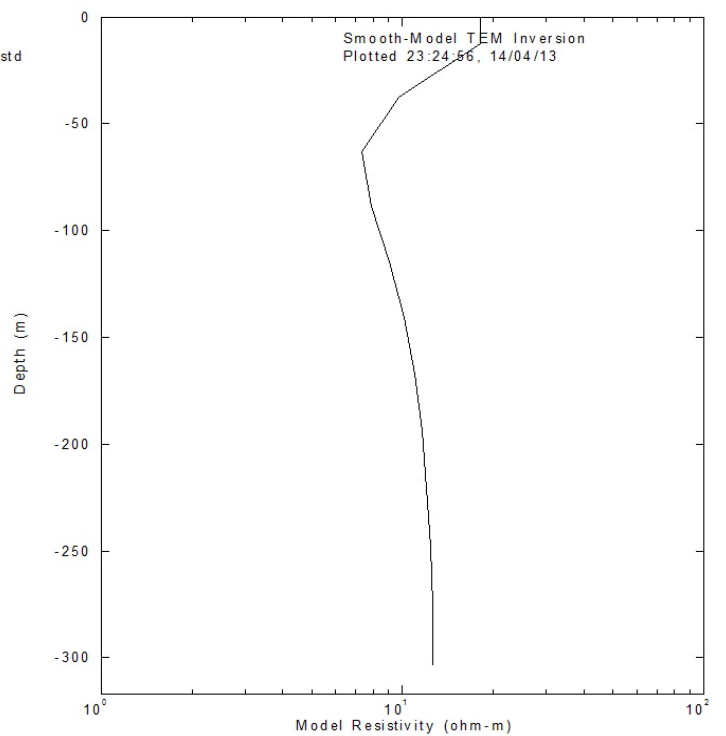
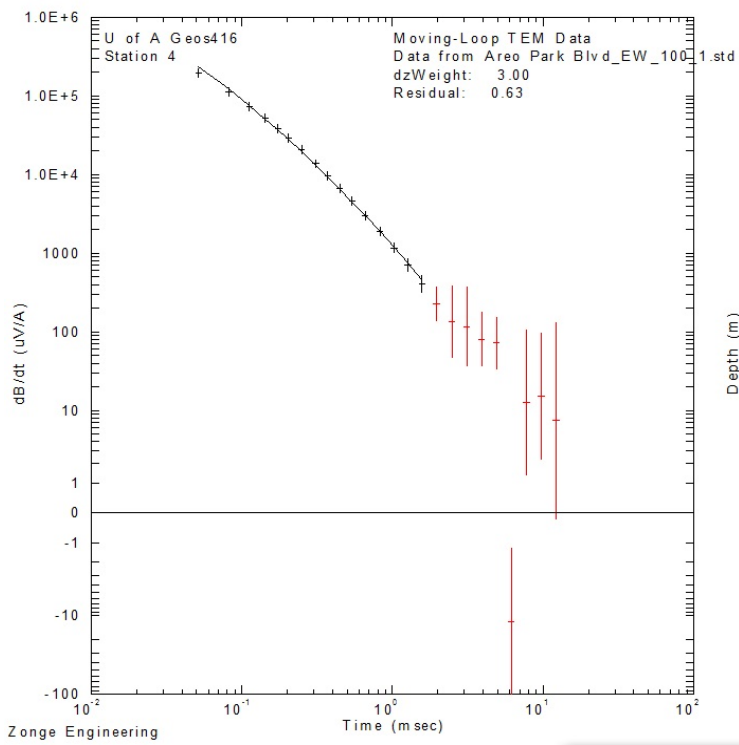
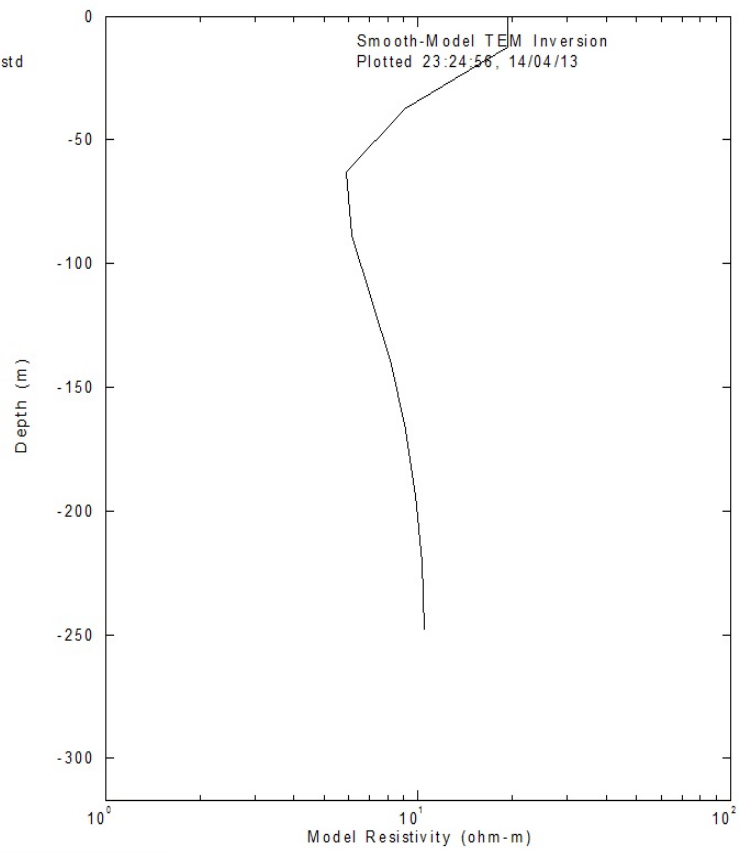
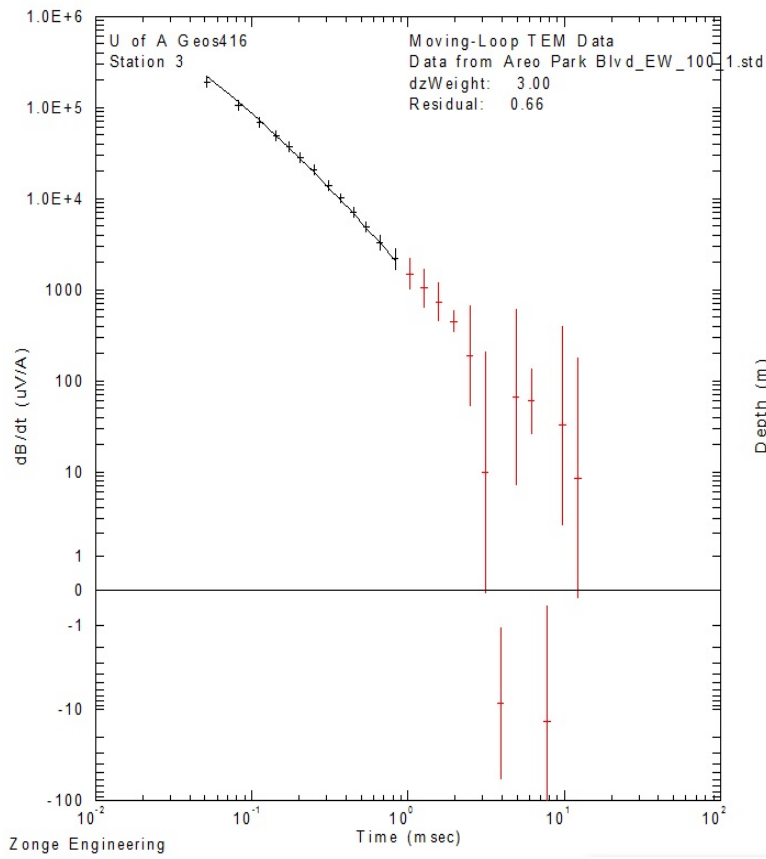


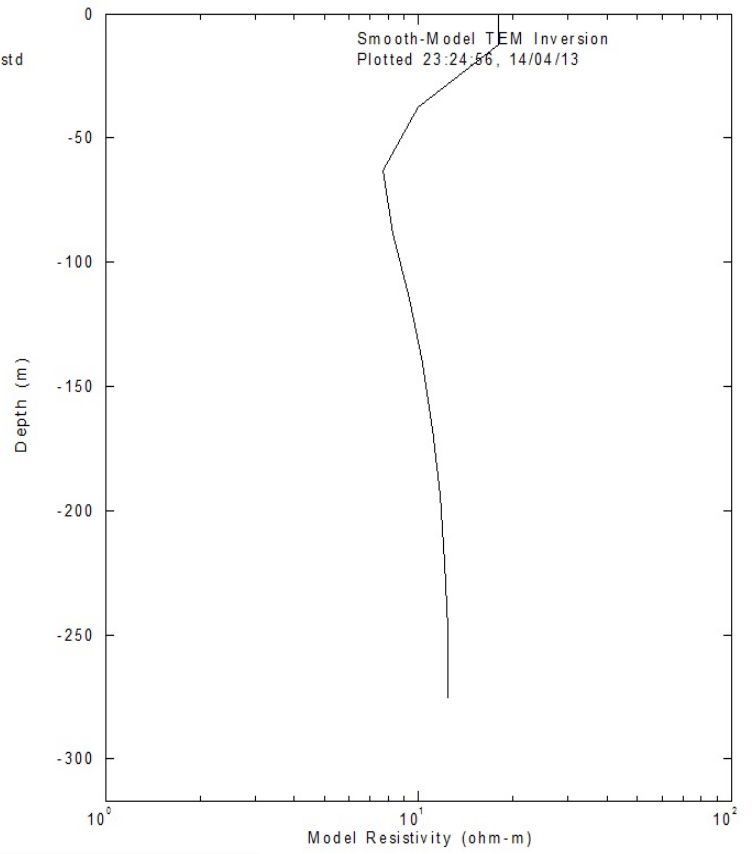
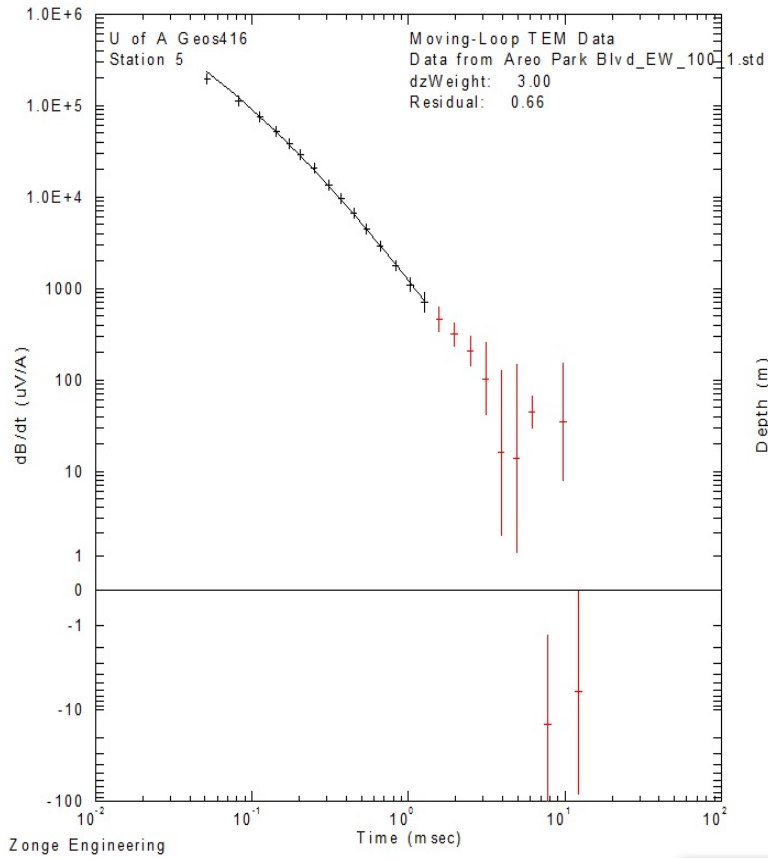
100x100 loops at the Aero Park Blvd South site with 32Hz from south to North



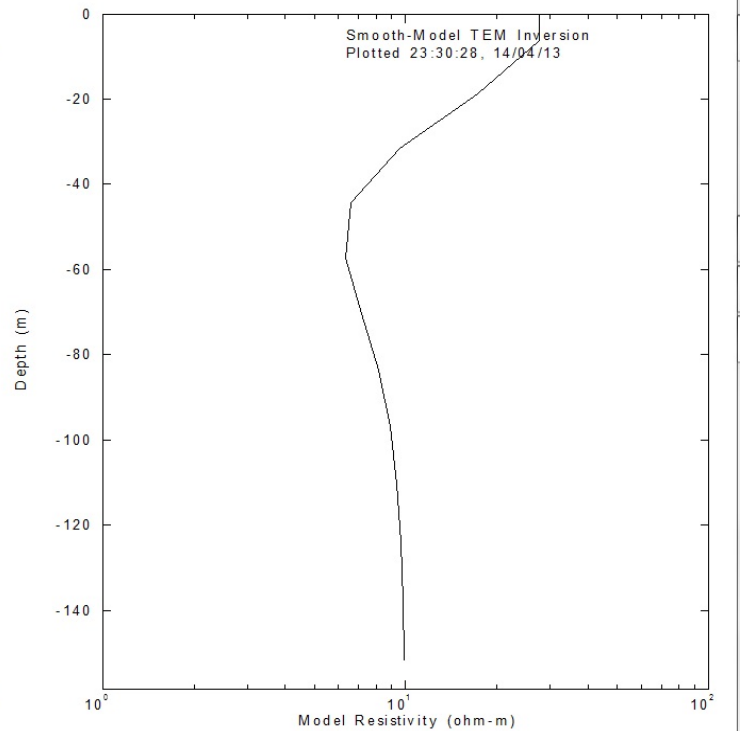
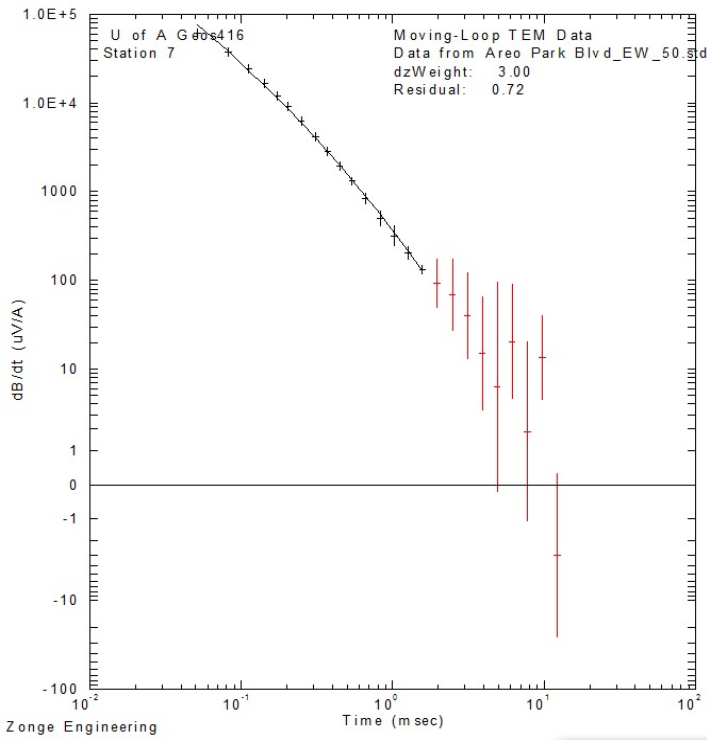
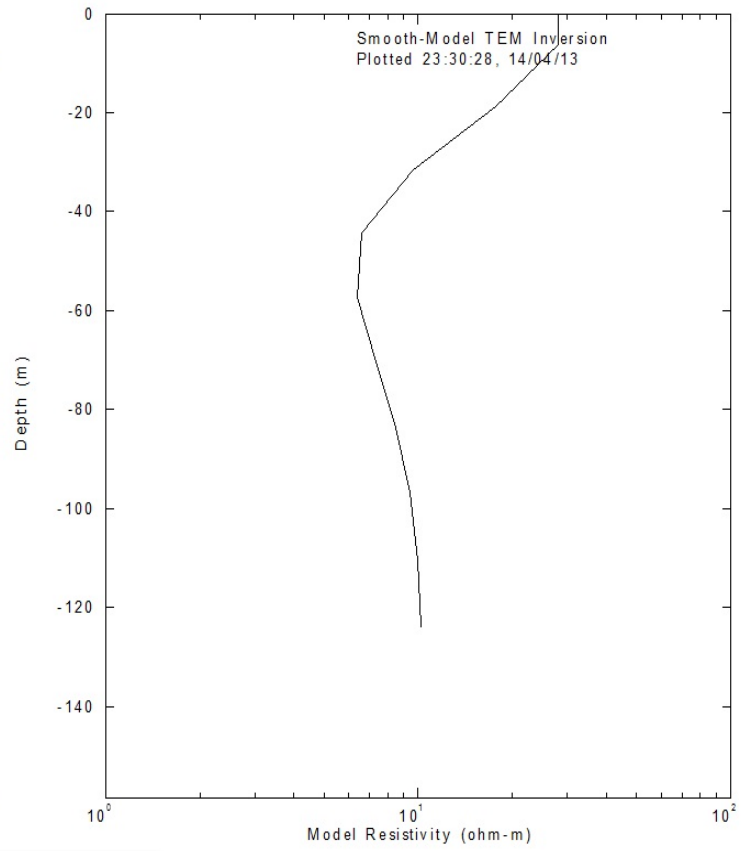
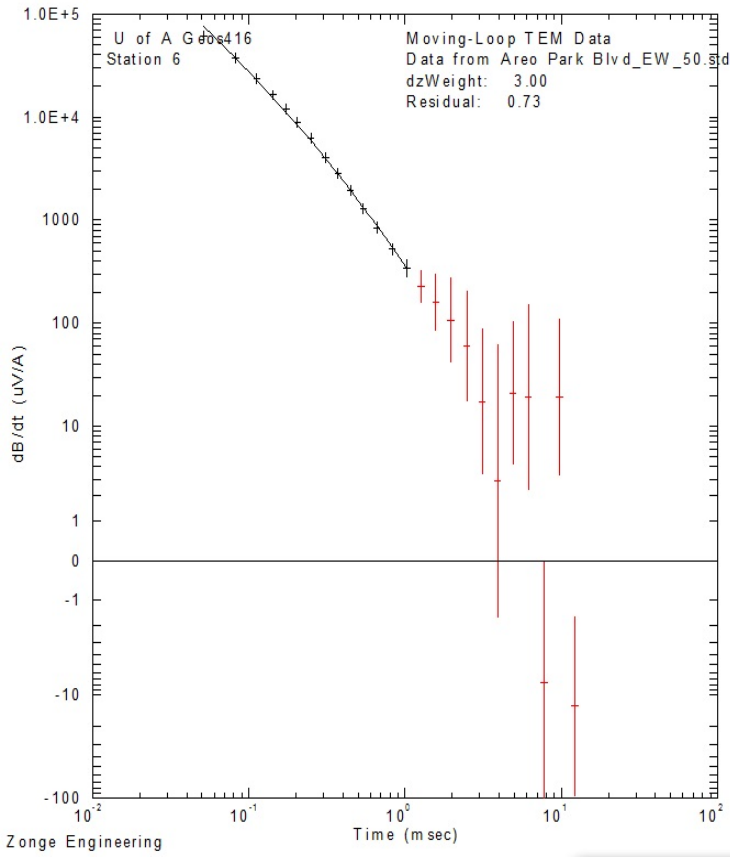


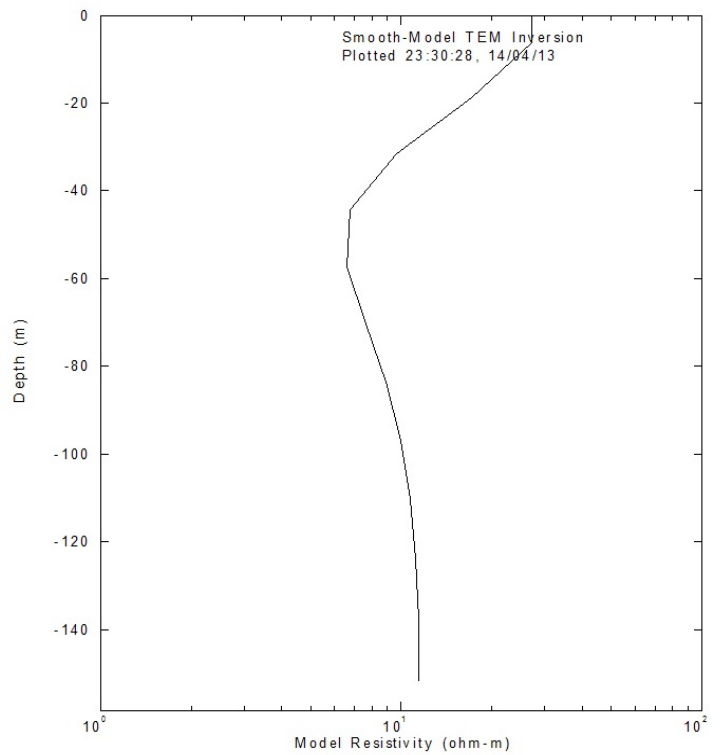
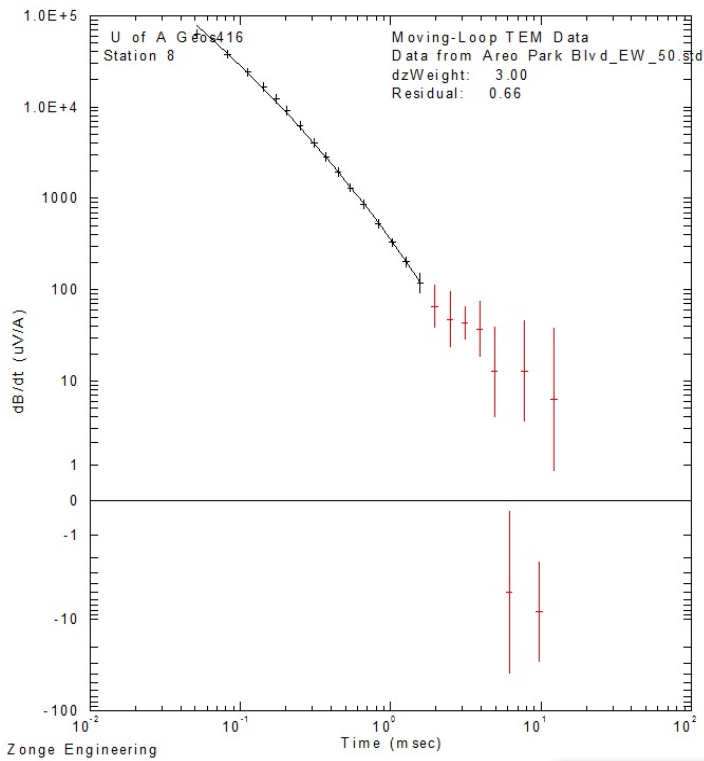
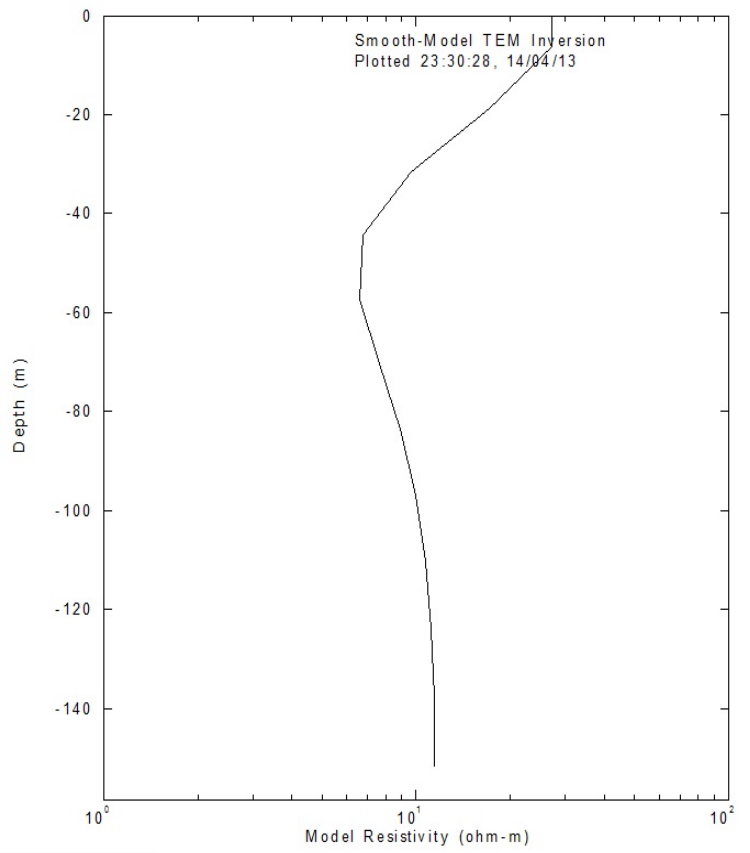
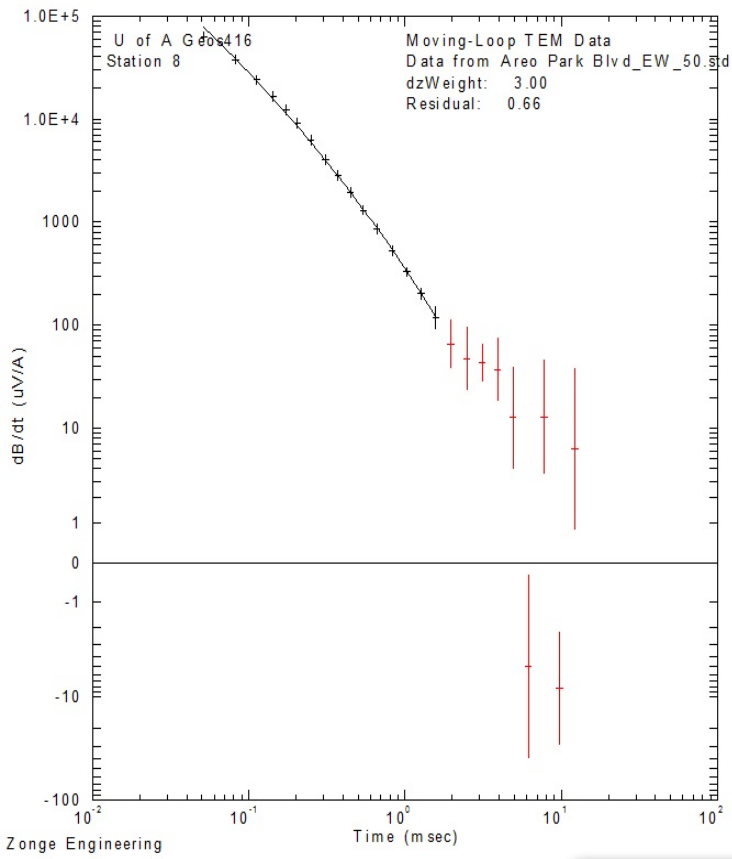
100x100 loops at the Aero Park Blvd South site with 16Hz from West to East

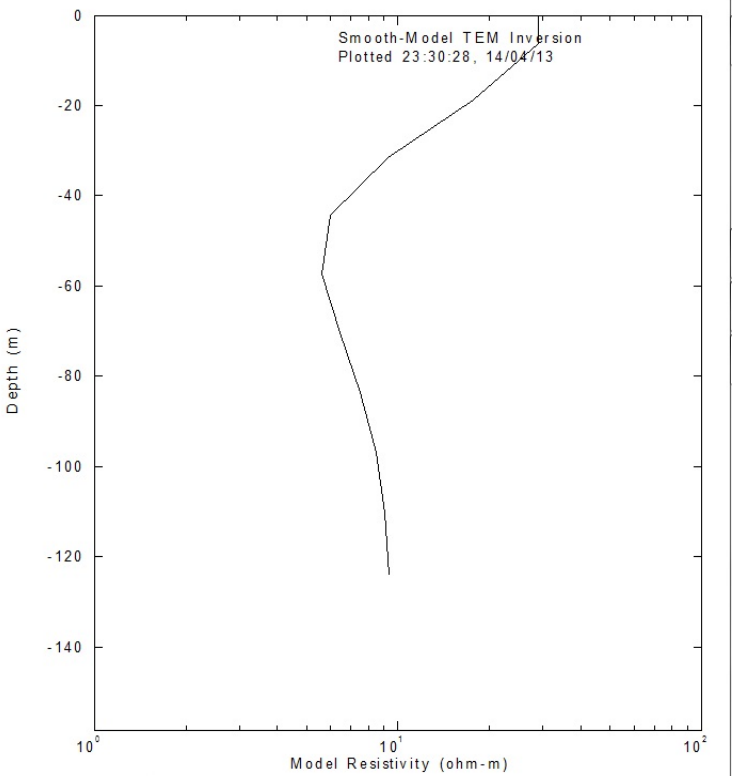
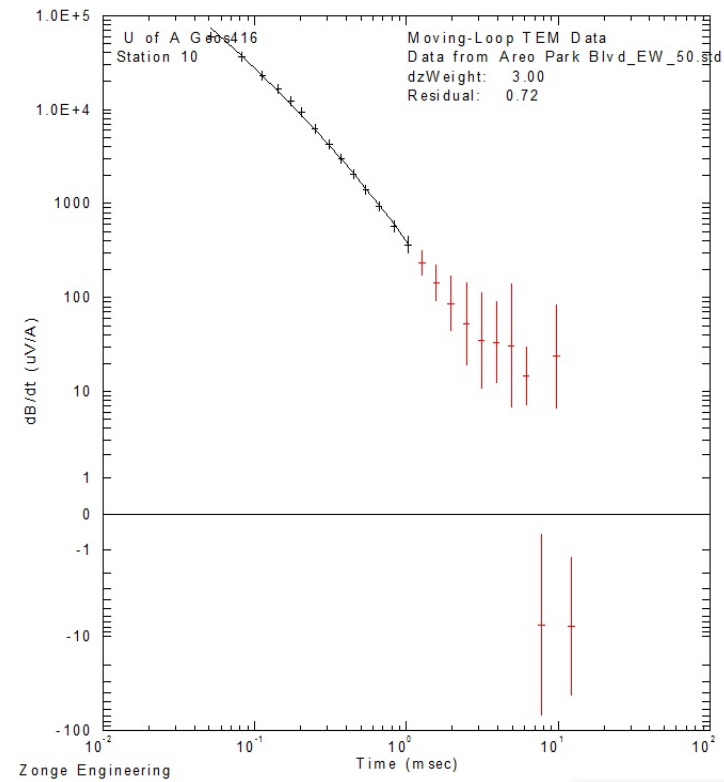
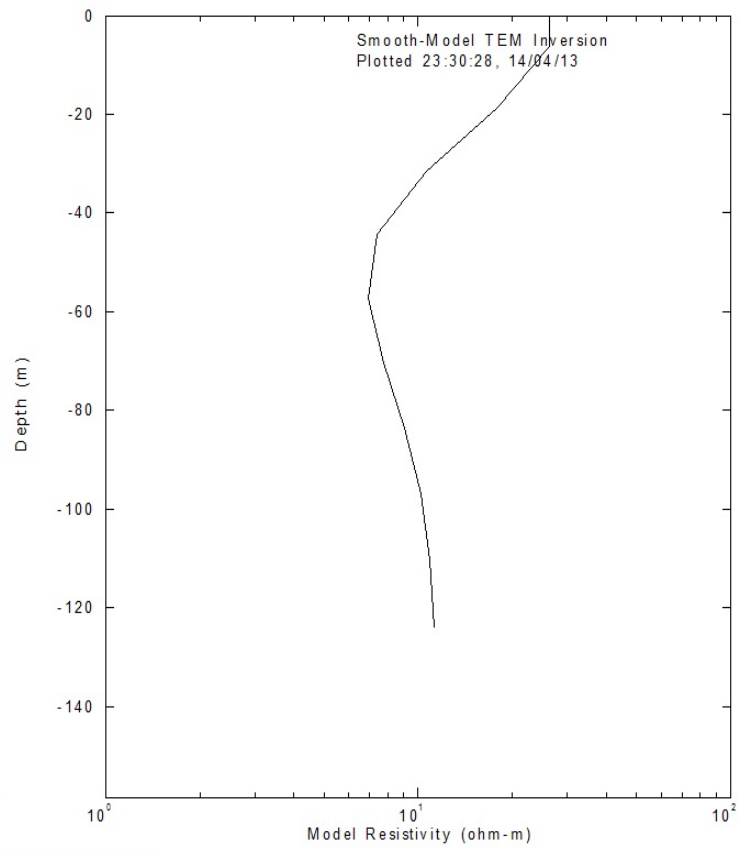
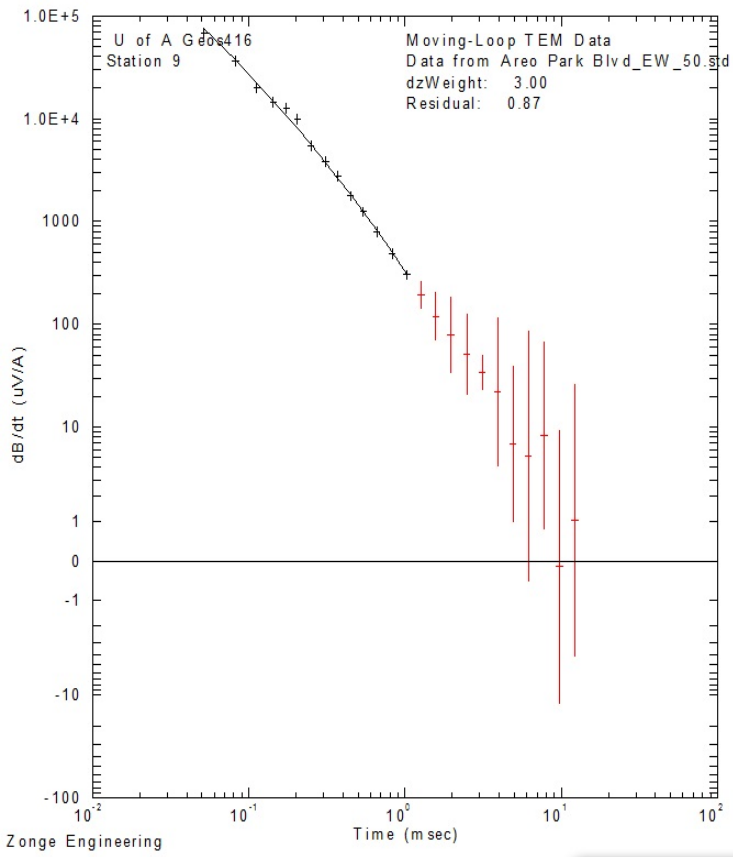


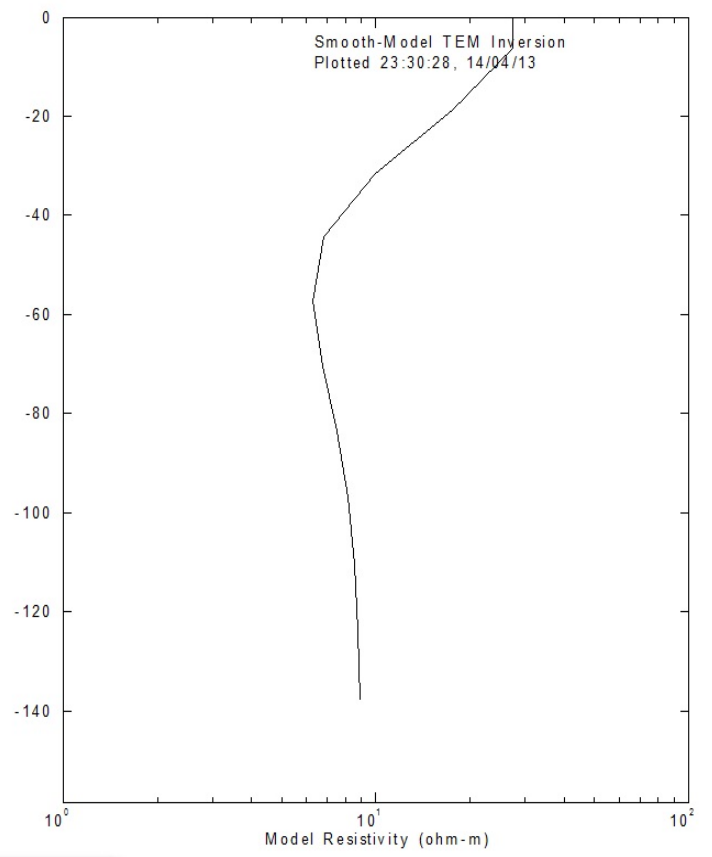
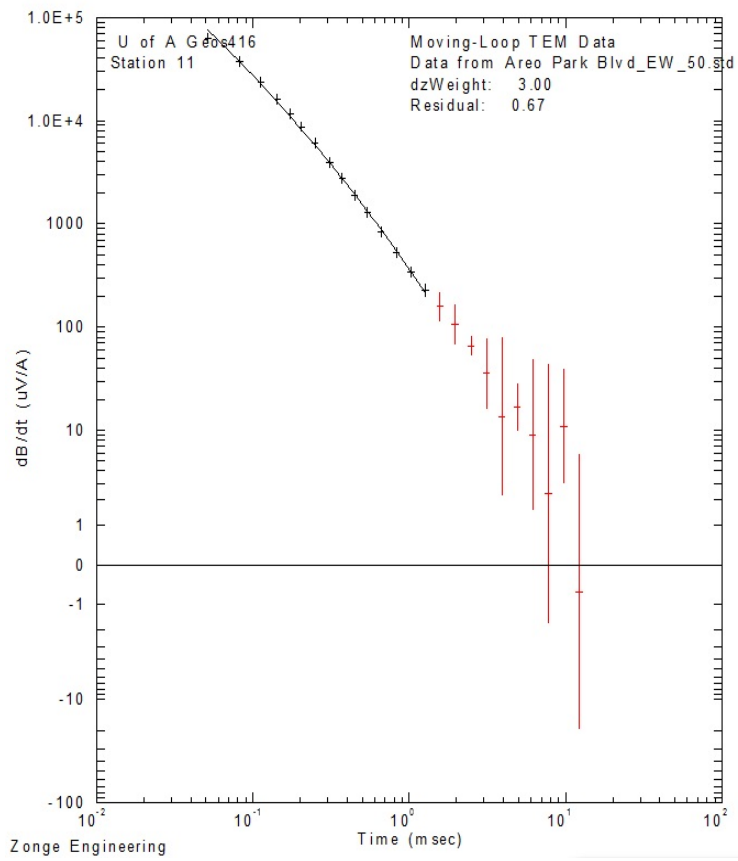


50x50 loops at the Aero Park Blvd South site with 16Hz from West to East

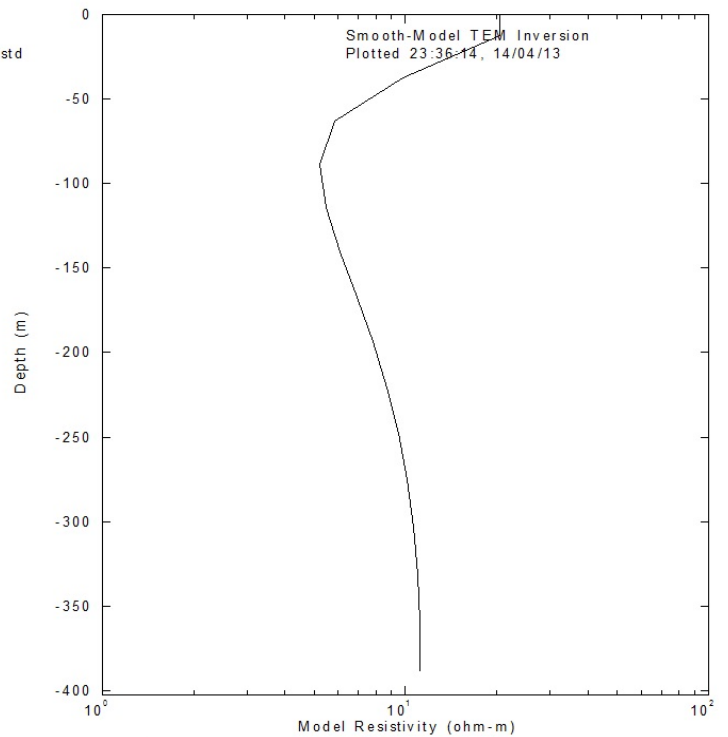
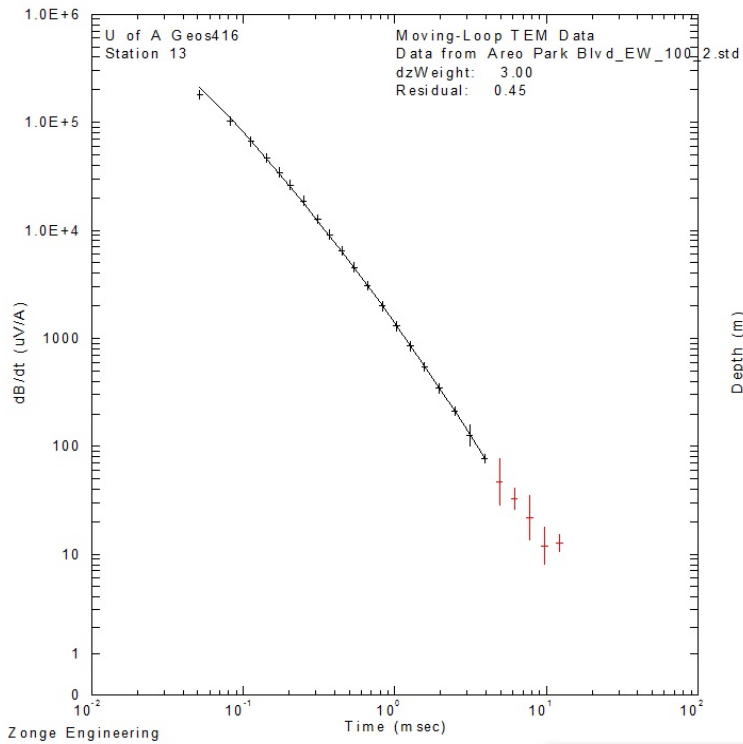
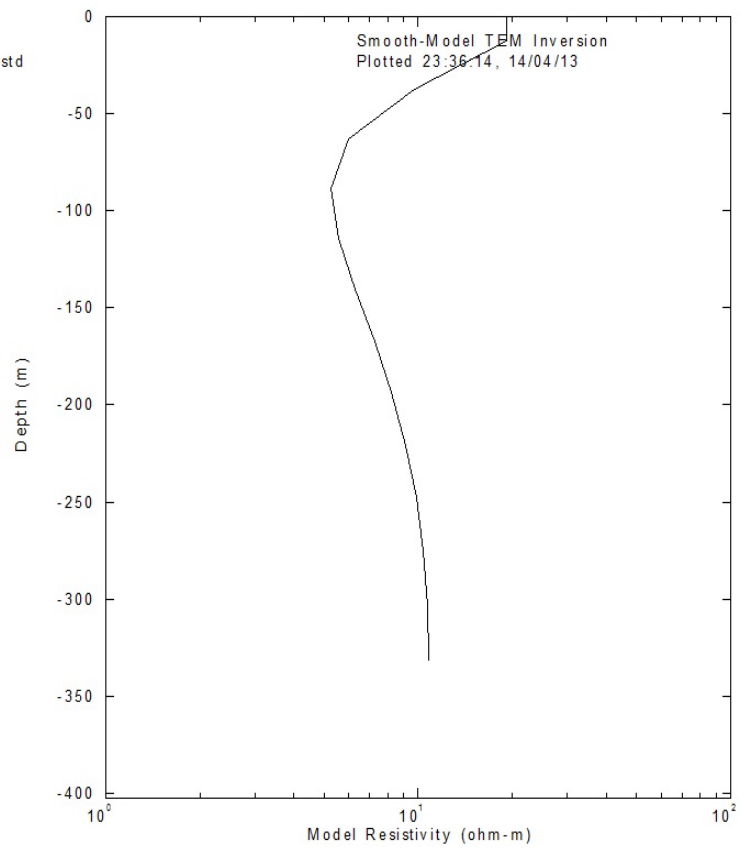
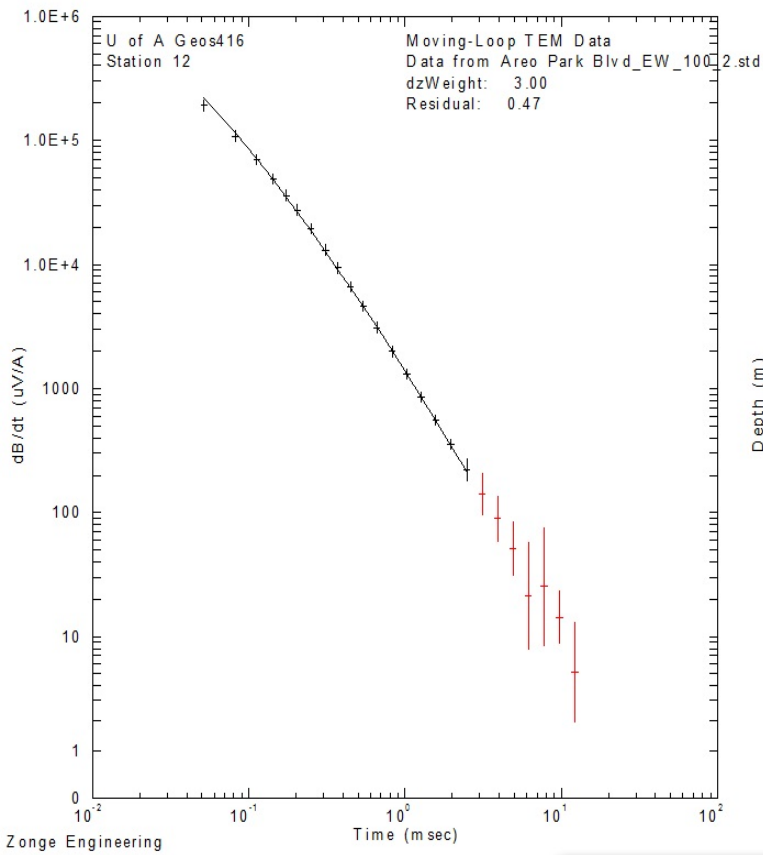


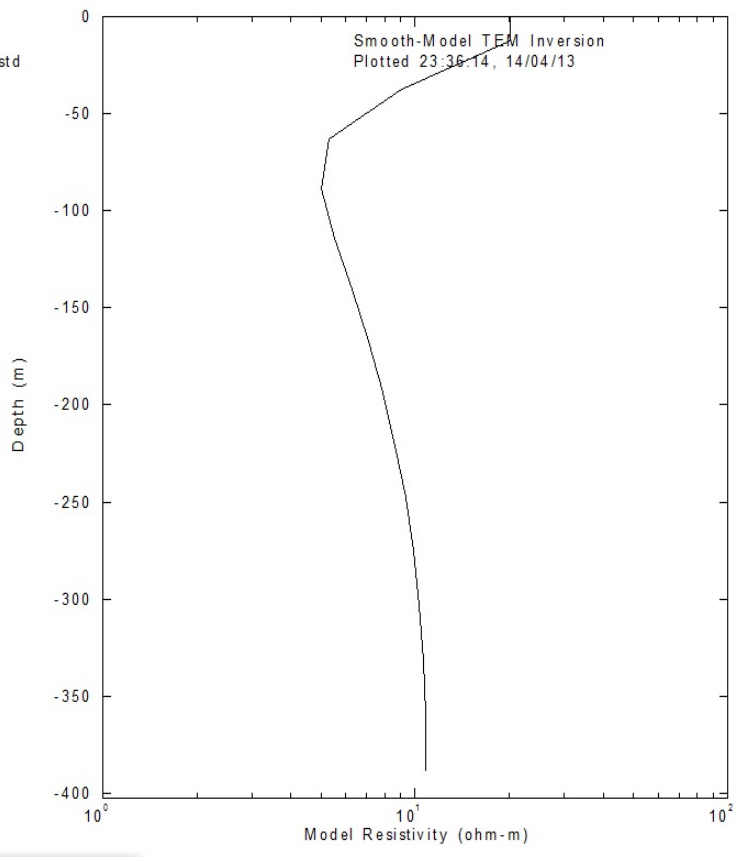
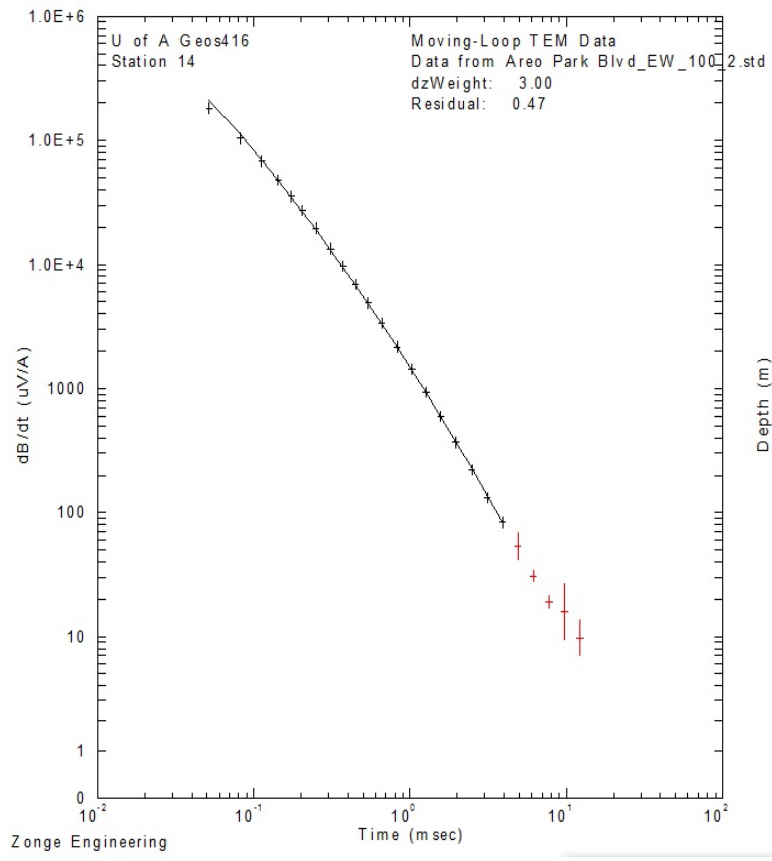




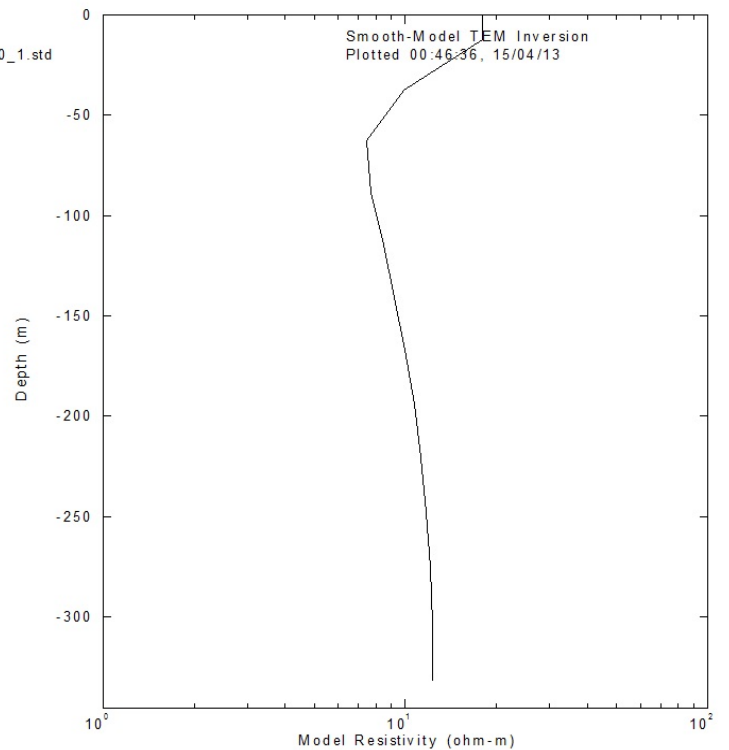
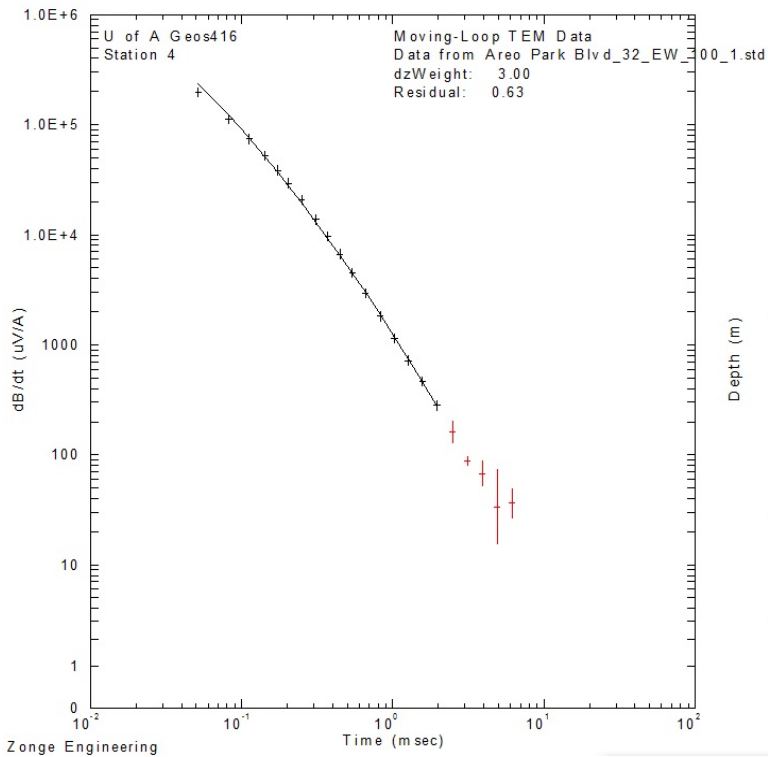
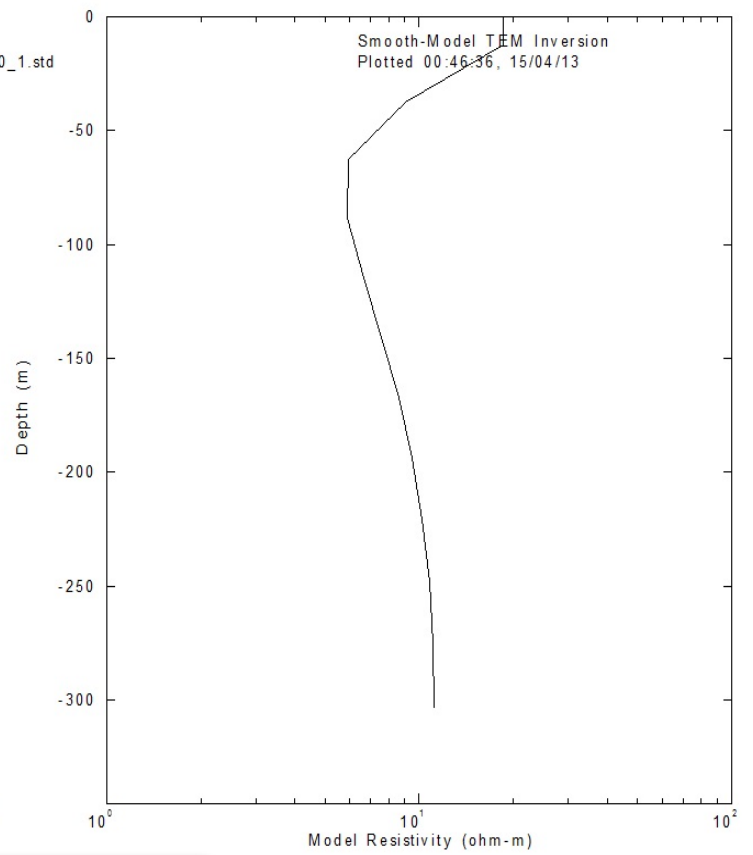
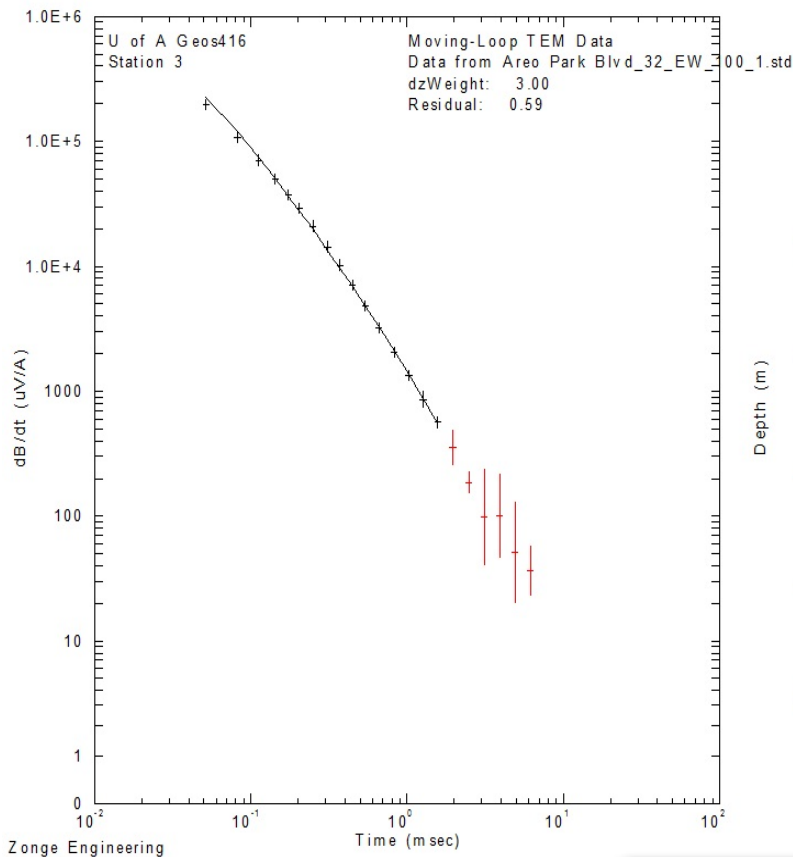


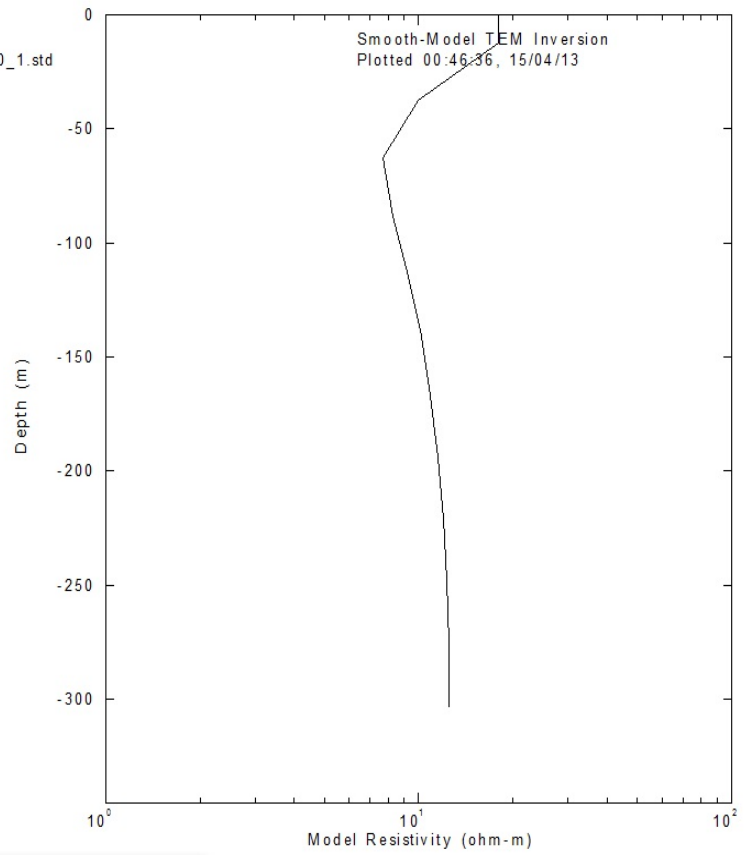
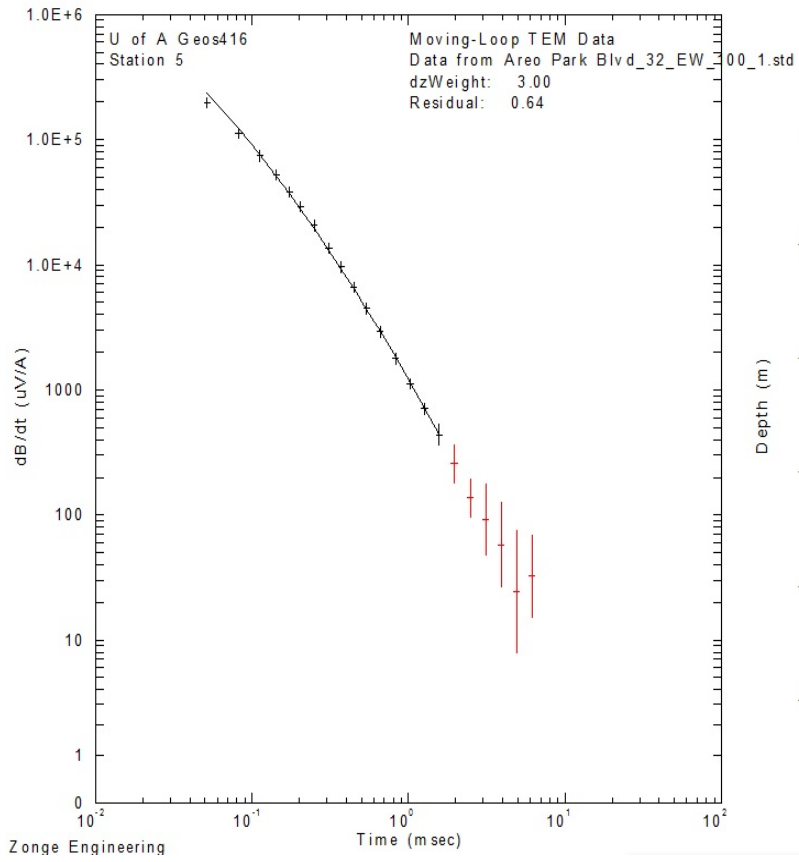
100x100 loops at the Aero Park Blvd South site with 16Hz from West to East after the 50x50 loops



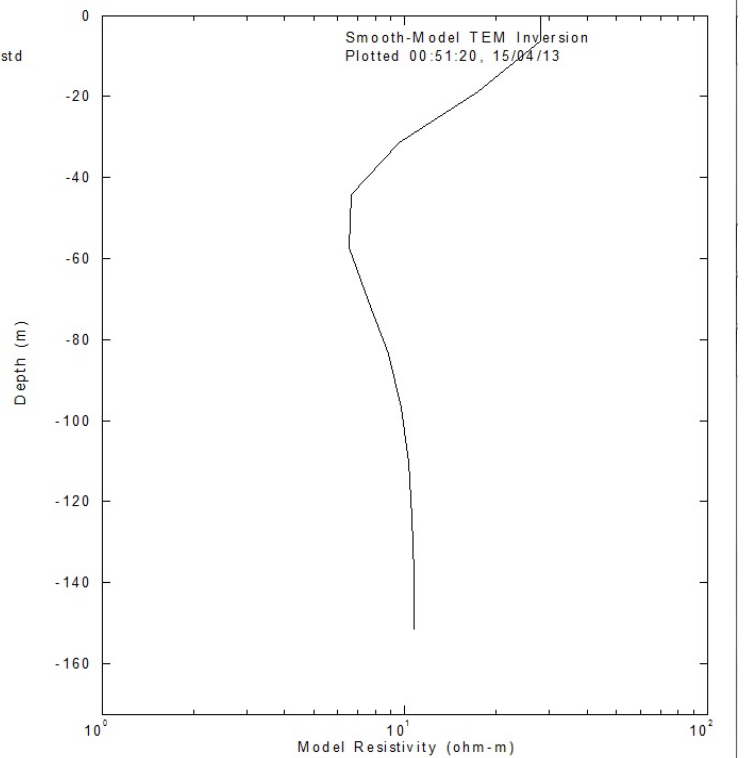
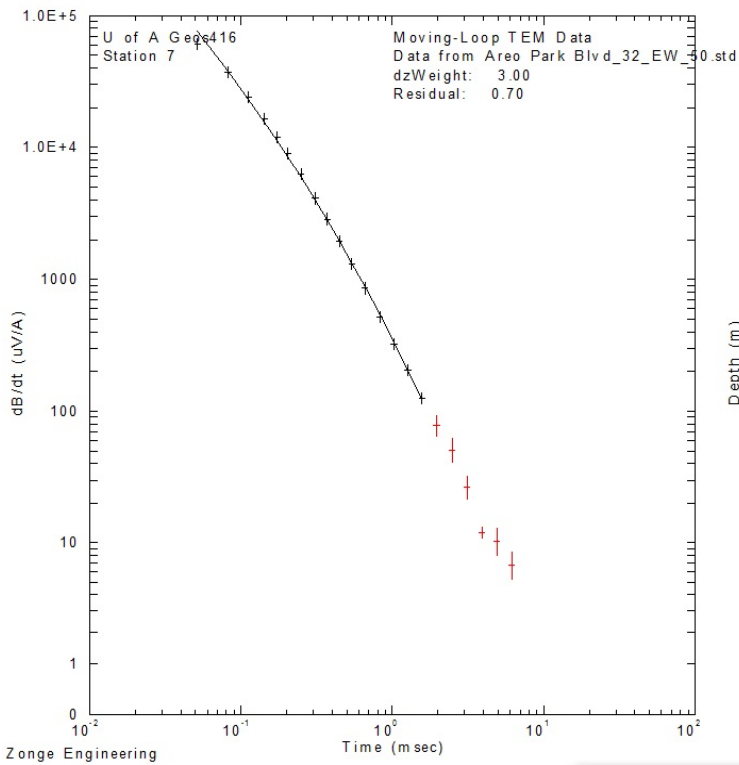
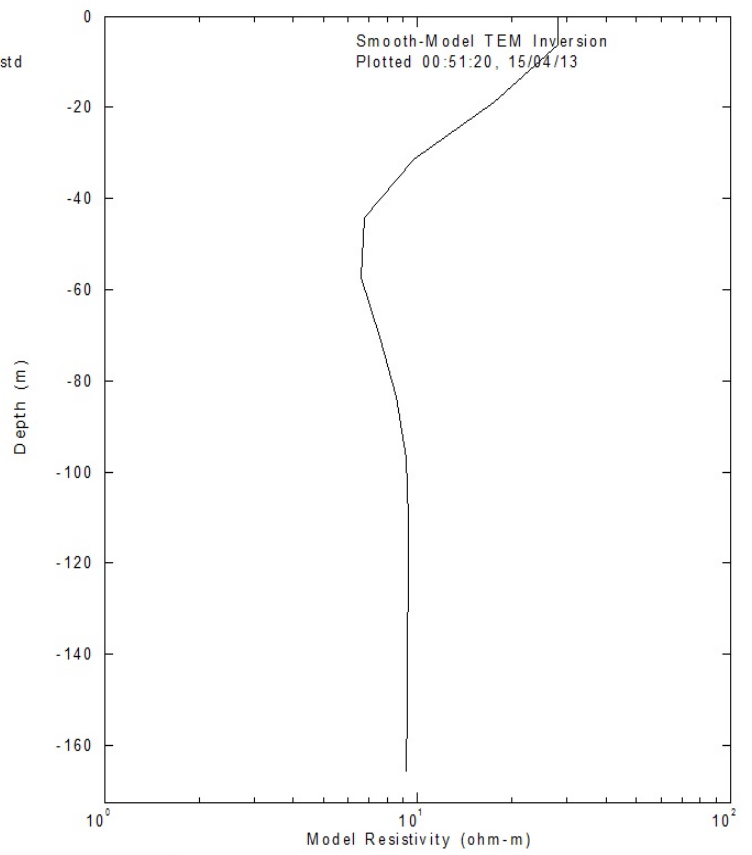
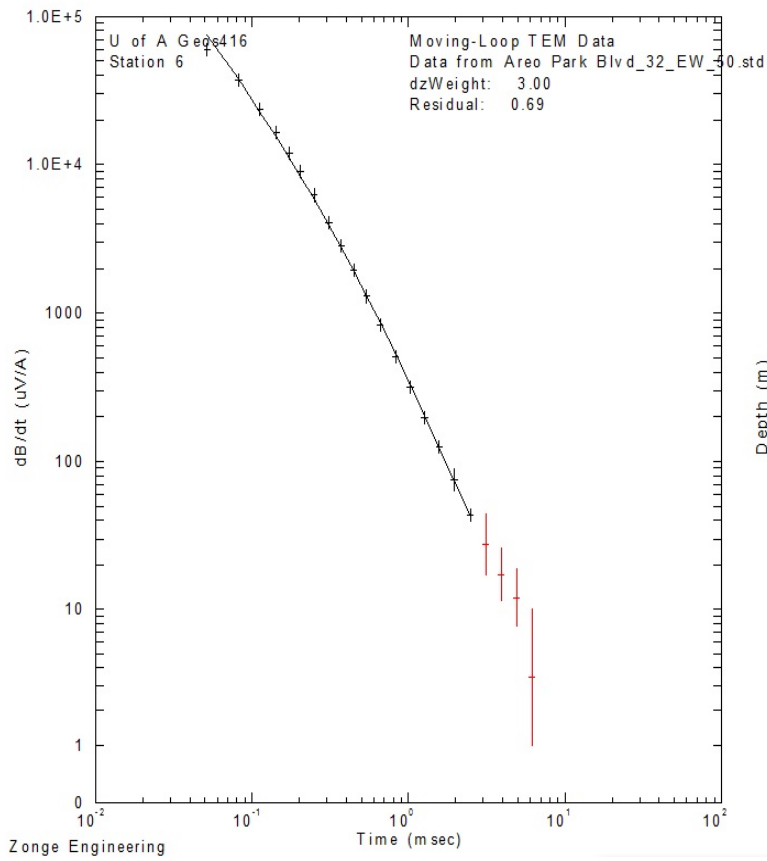


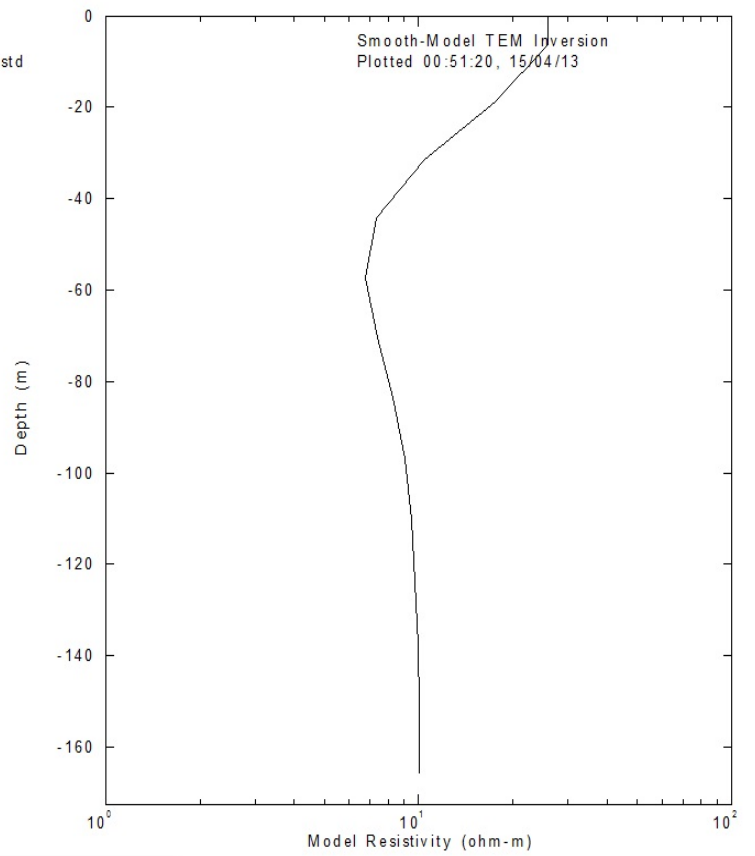
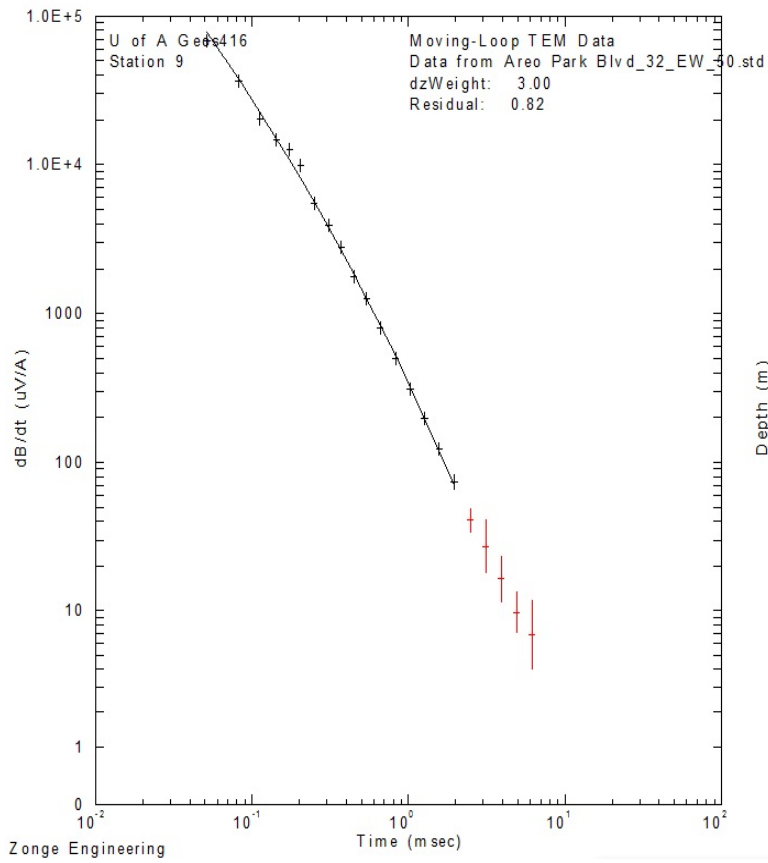
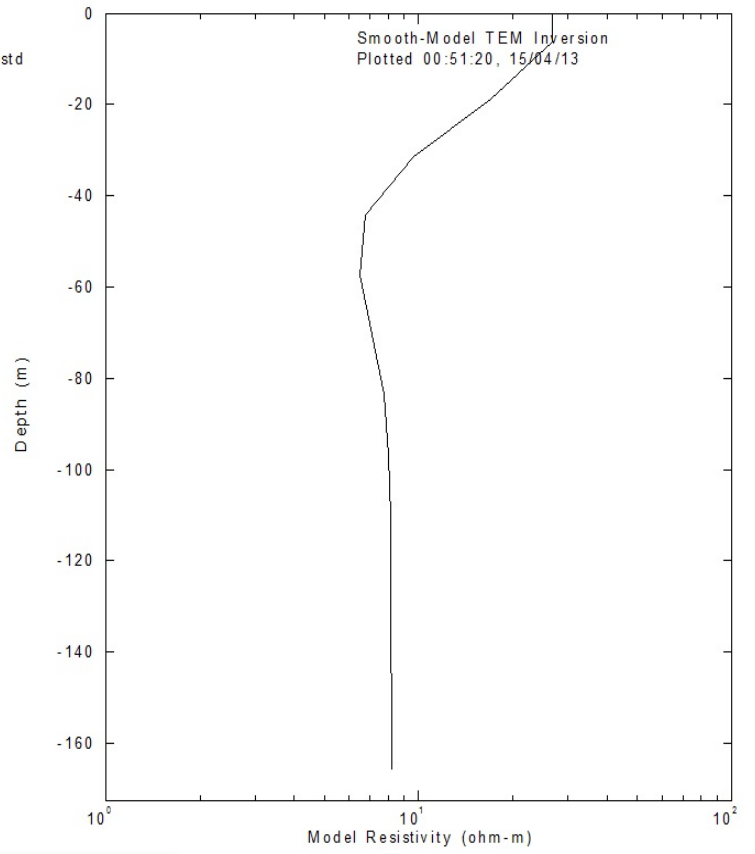
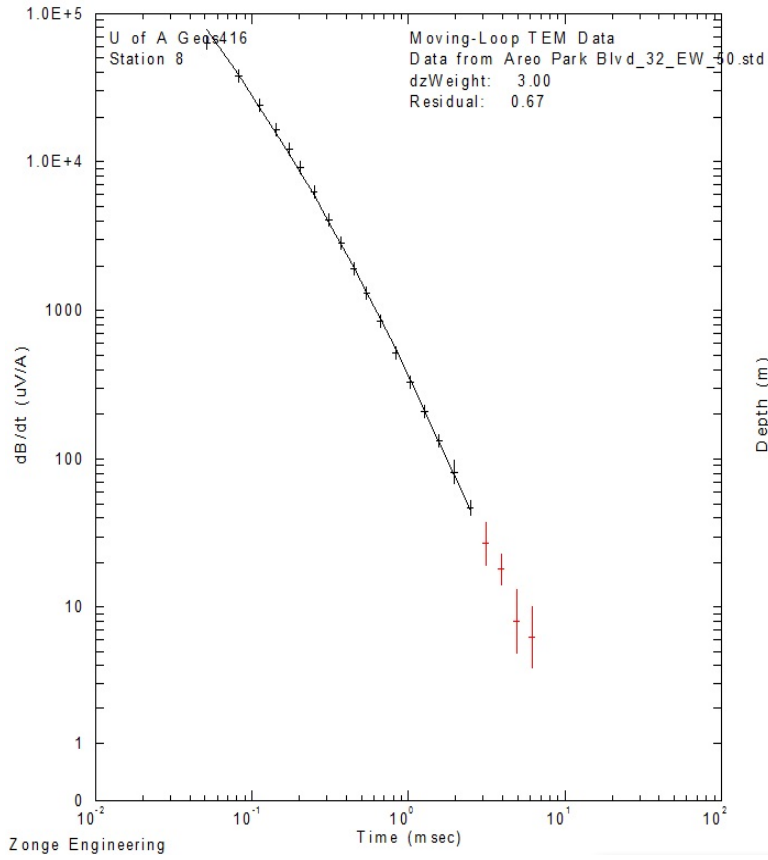
100x100 loops at the Aero Park Blvd South site with 32Hz from West to East

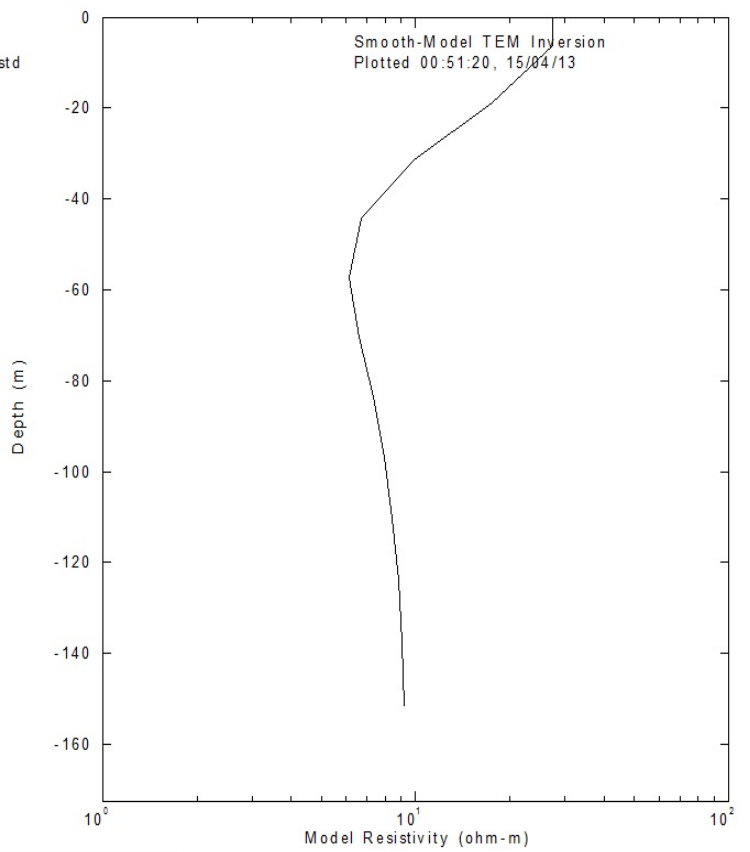
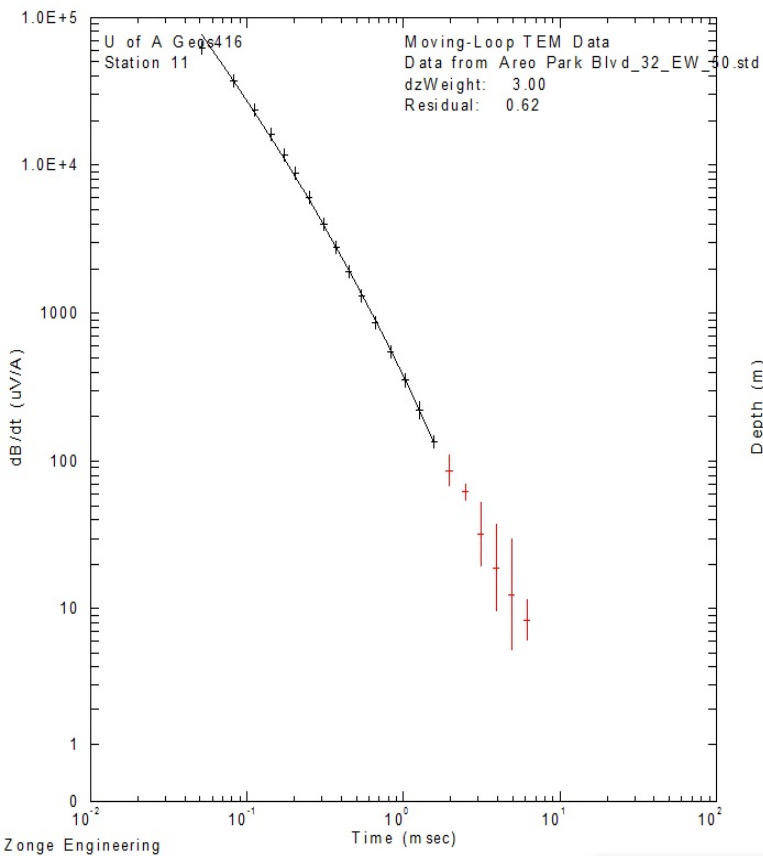
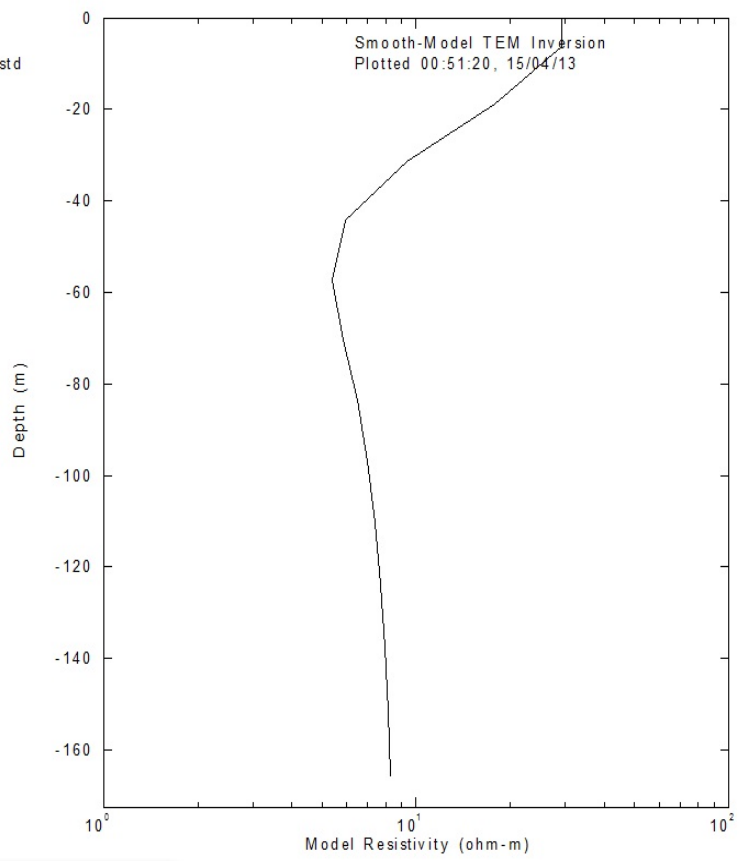
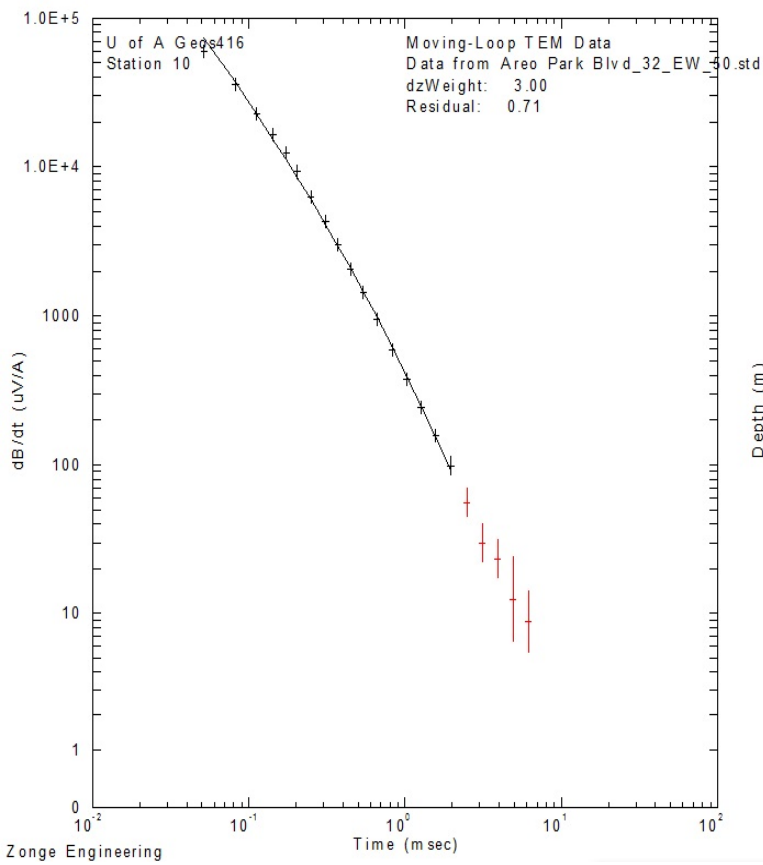




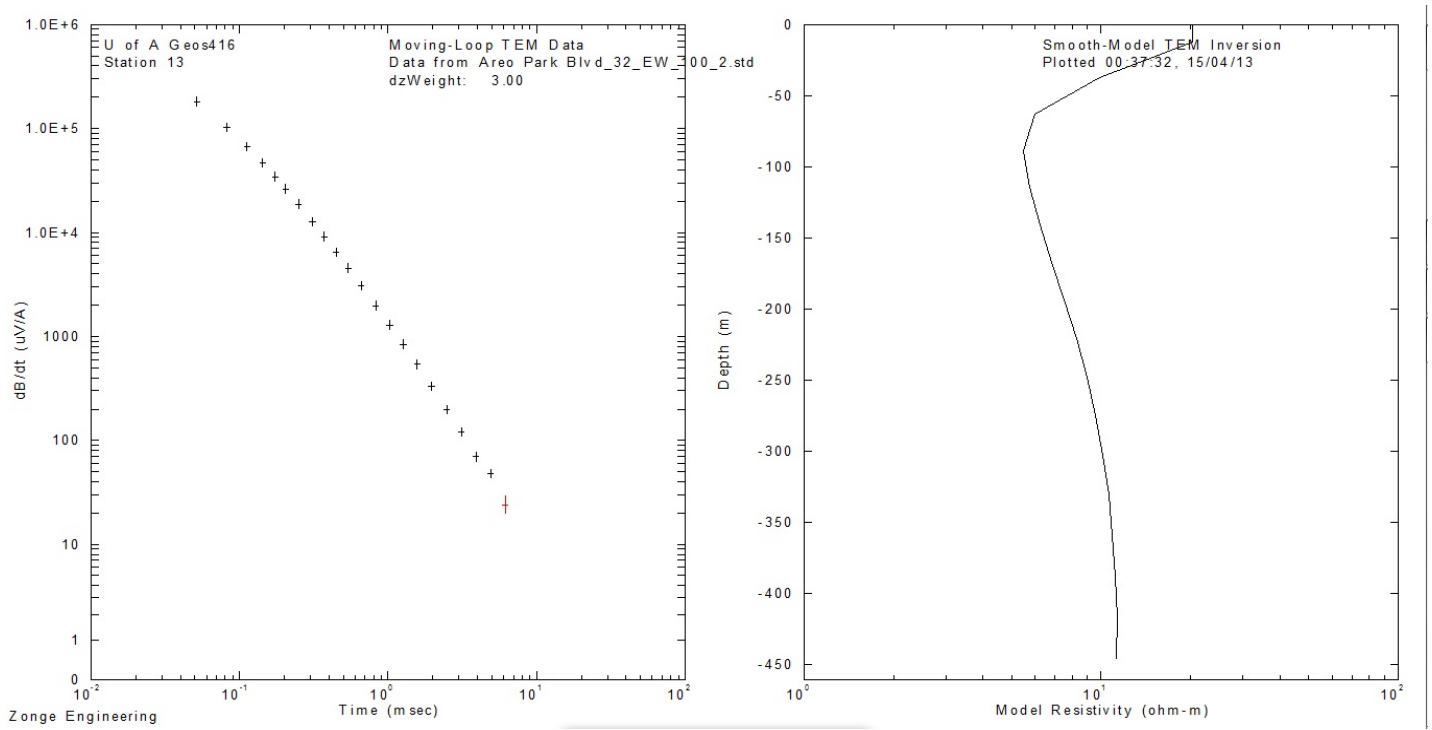
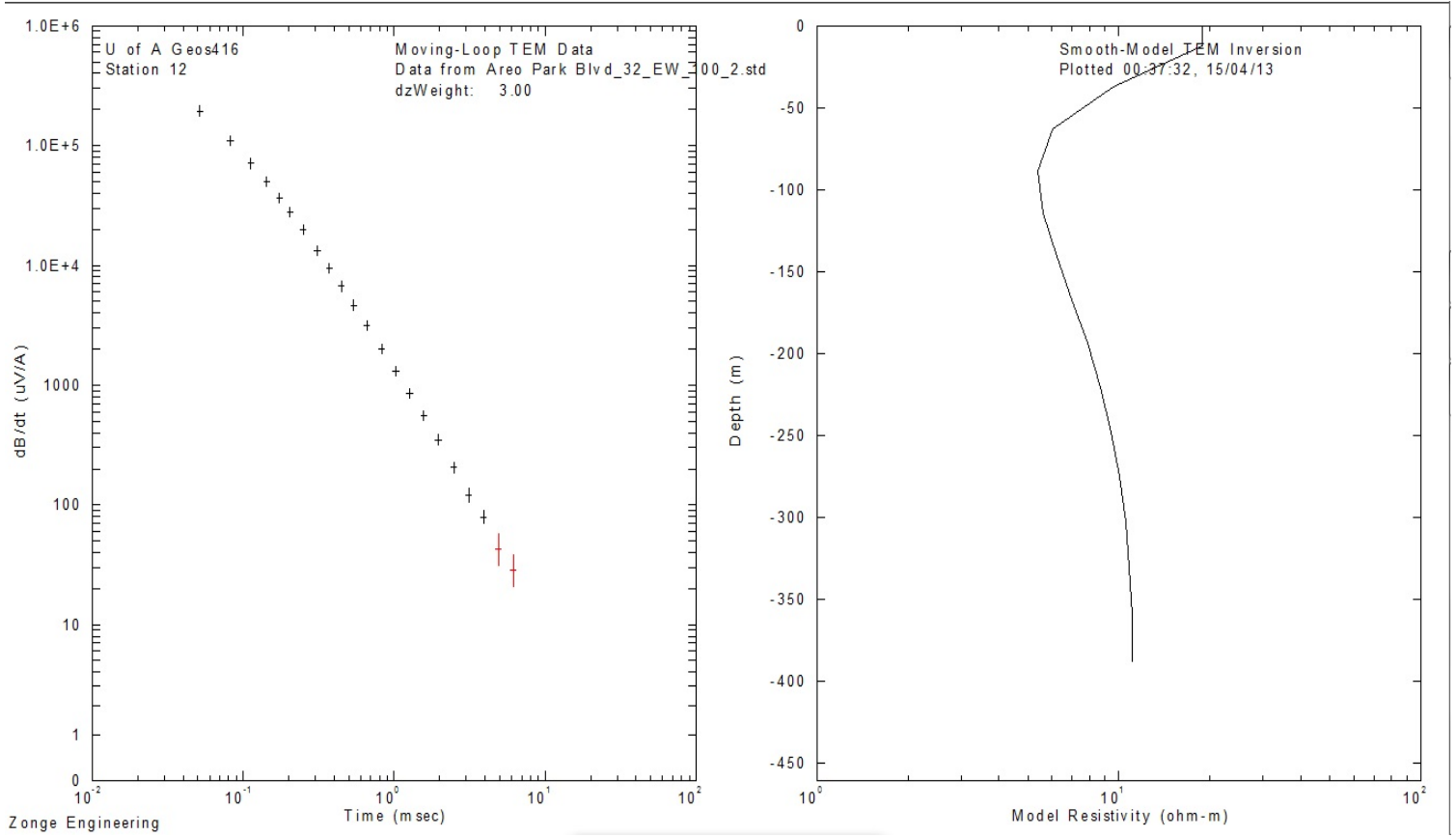
50x50 loops at the Aero Park Blvd South site with 32Hz from West to East

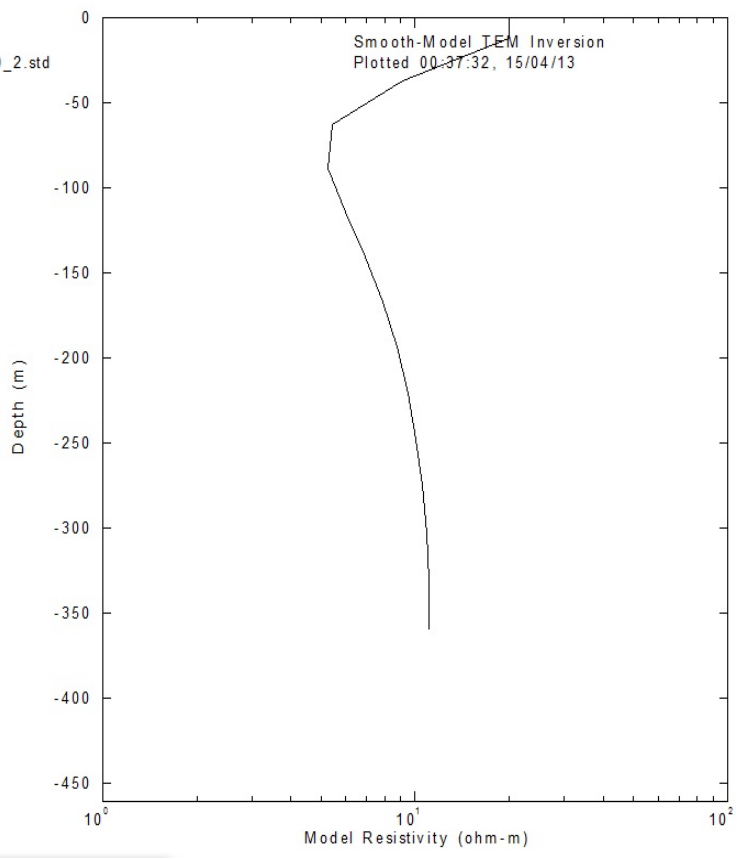
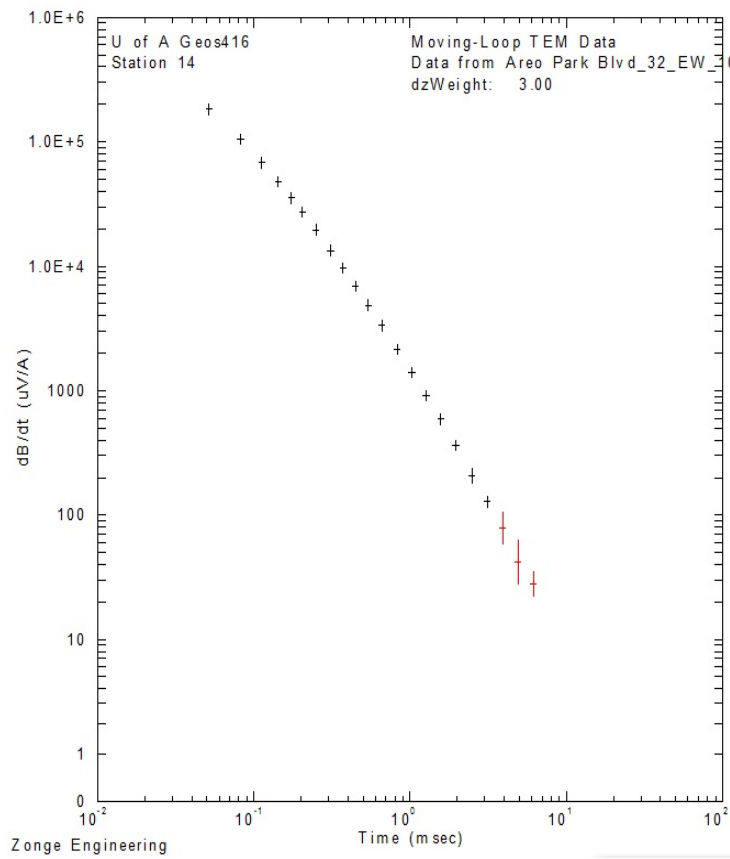




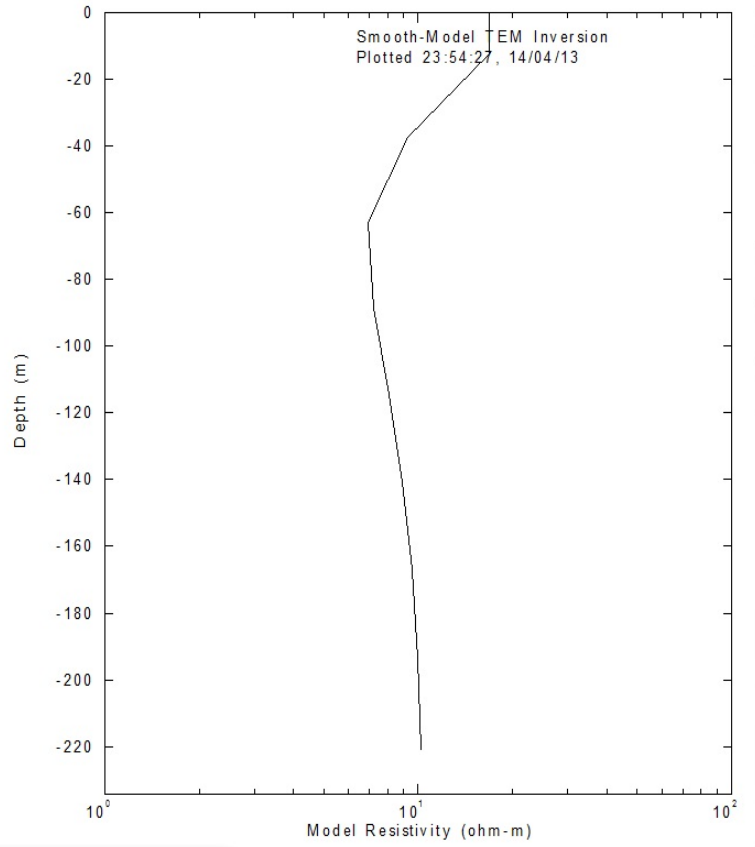
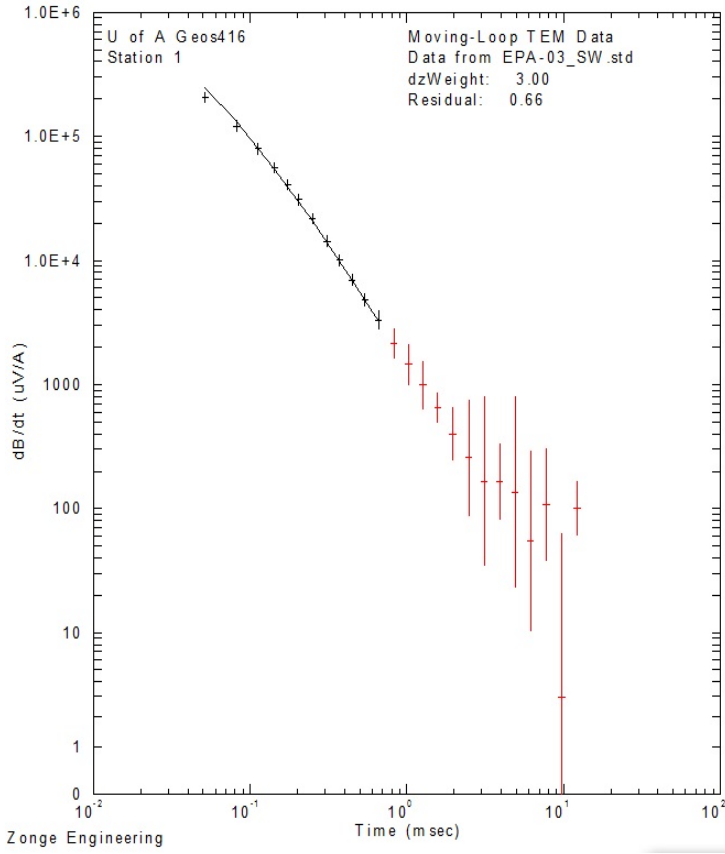


100x100 loops at the Aero Park Blvd South site with 32Hz from West to East after the 50x50 loops

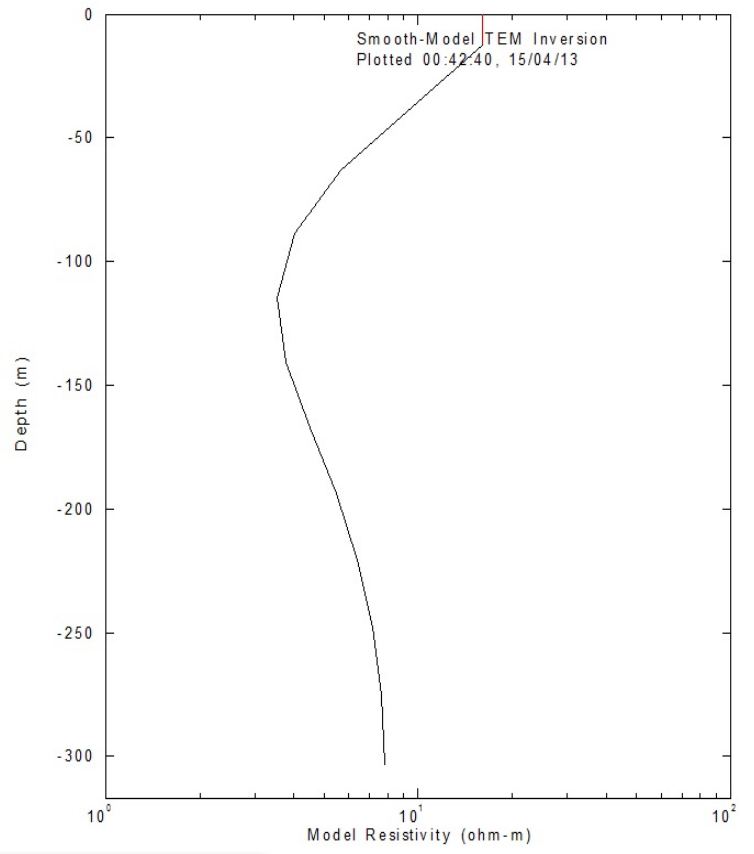
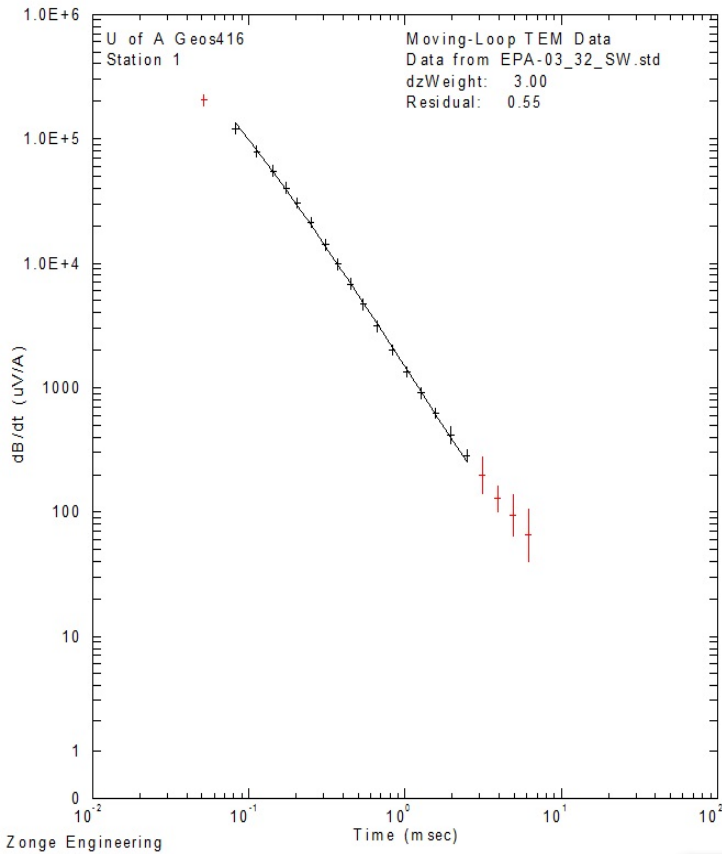




100x100 loop at the EPA-03 site with 16Hz from East to West



100x100 loops at EPA-03 site with 32Hz from East to West

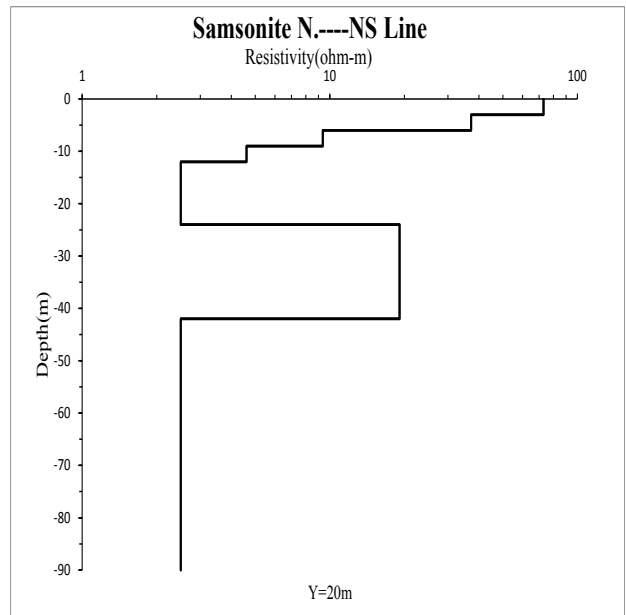
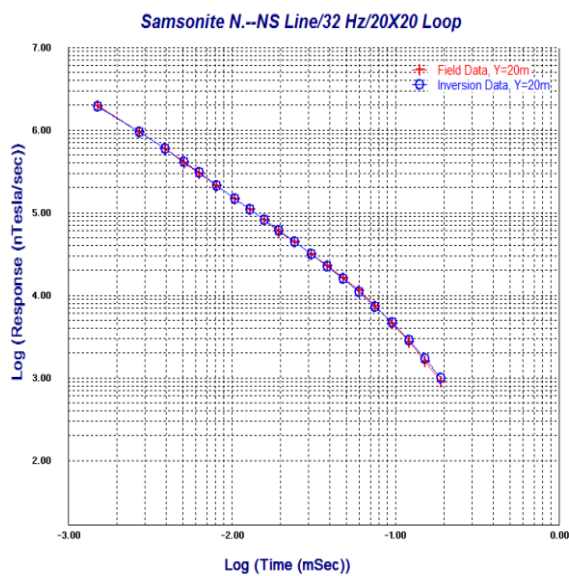
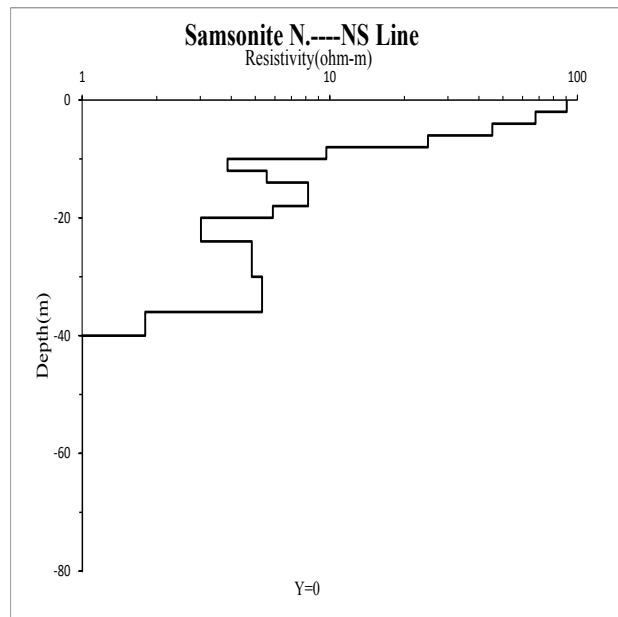
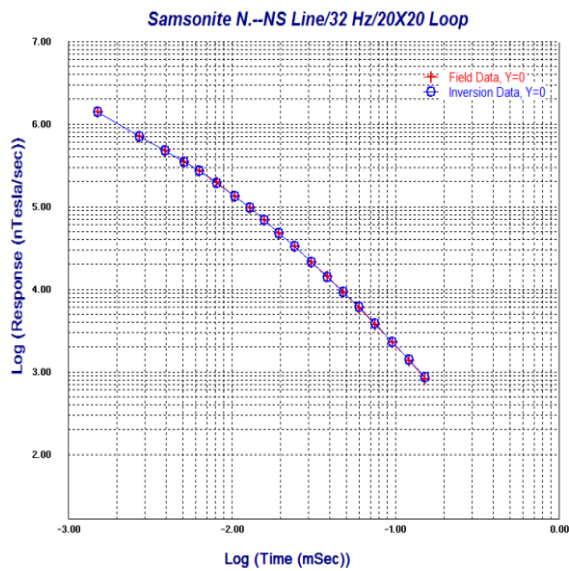


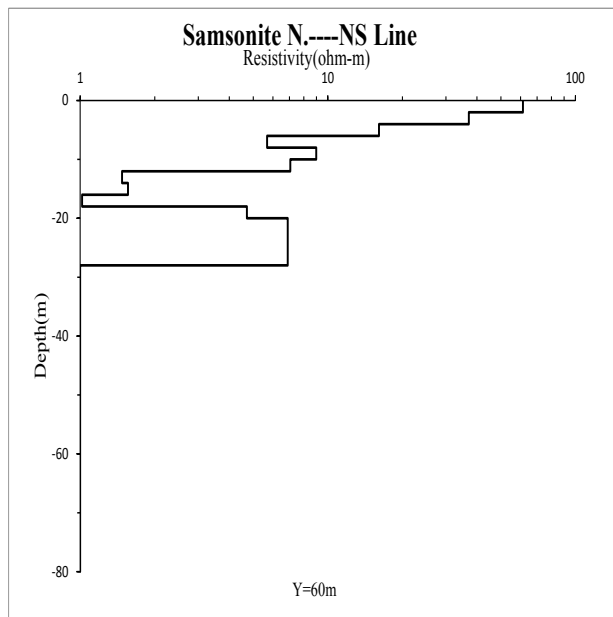
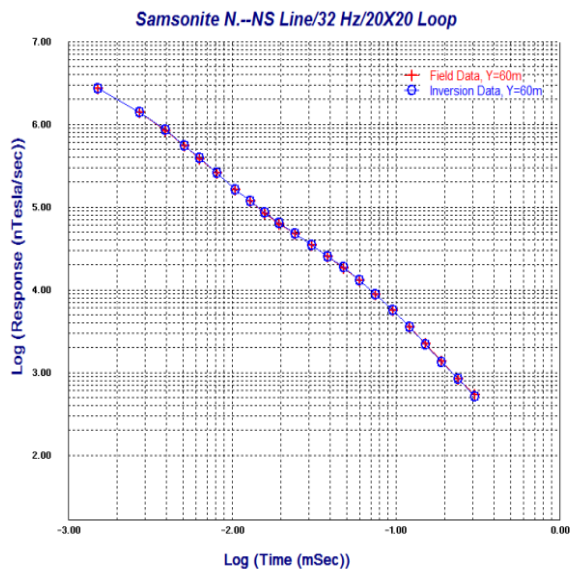
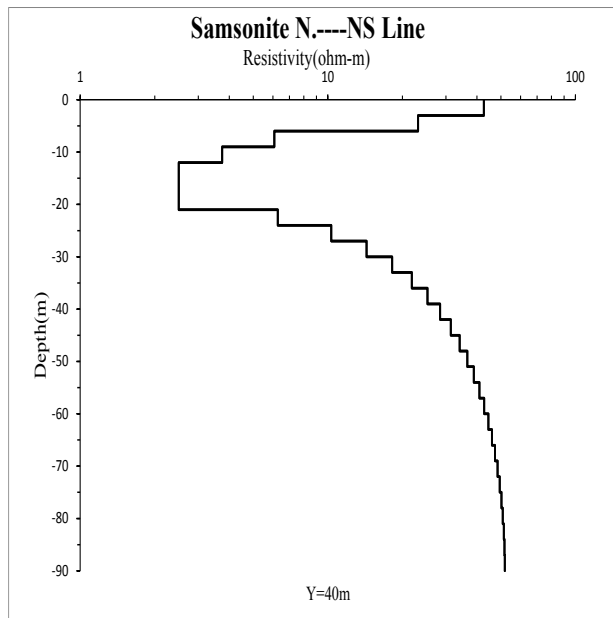
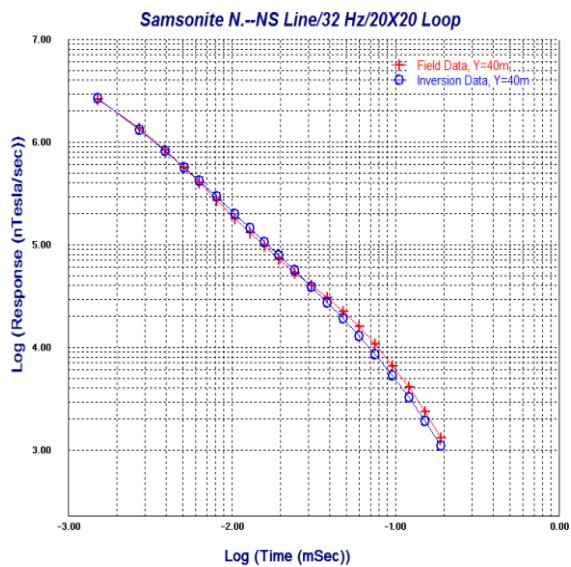
# Appendix C

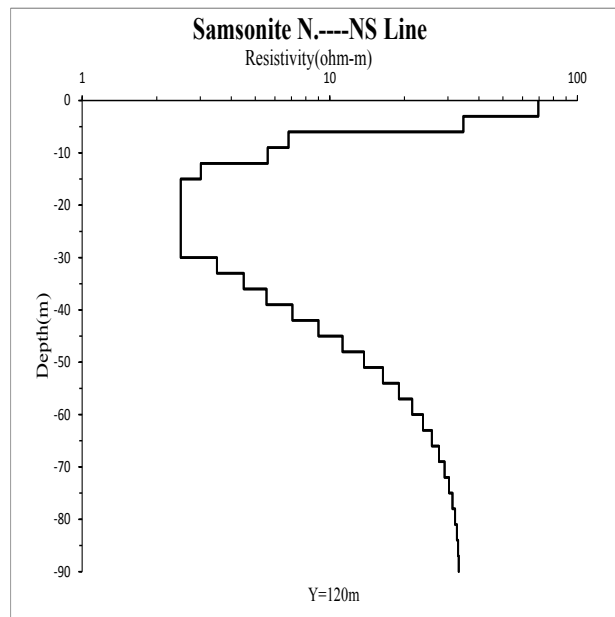
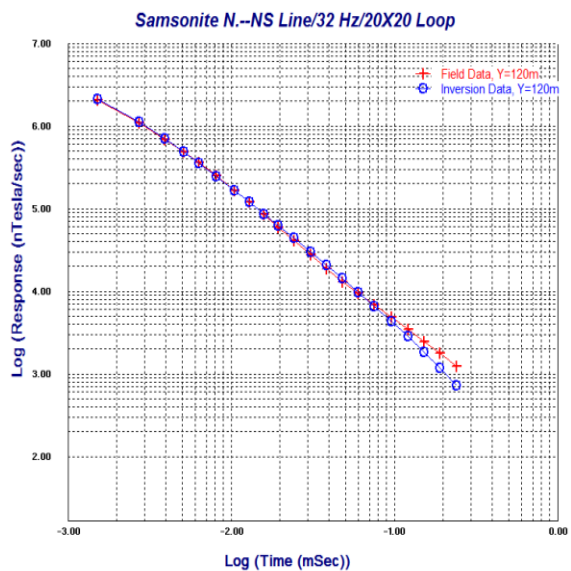
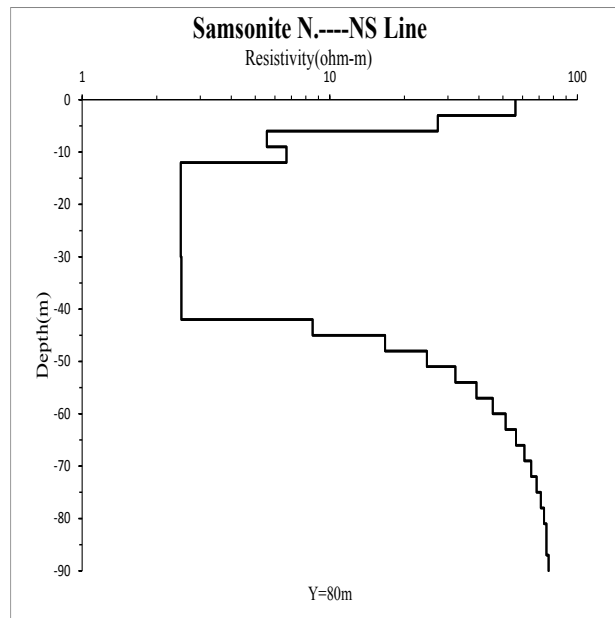
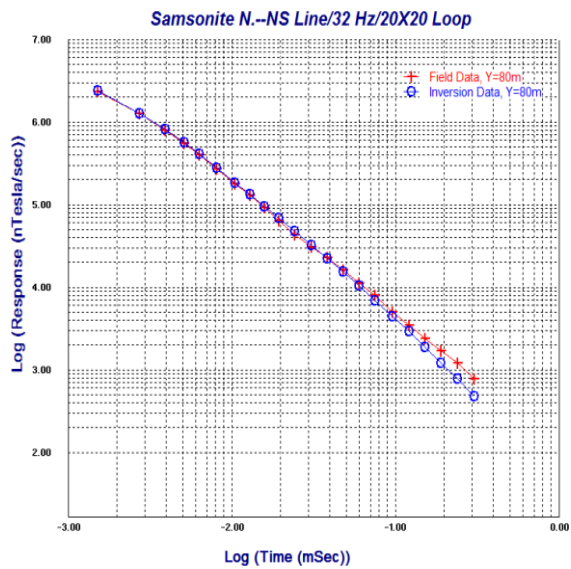
These plots show EMIGMA inversion results and measured data, and their corresponding inversion layer models.

## 1. 32HZ, 20×20m Loop

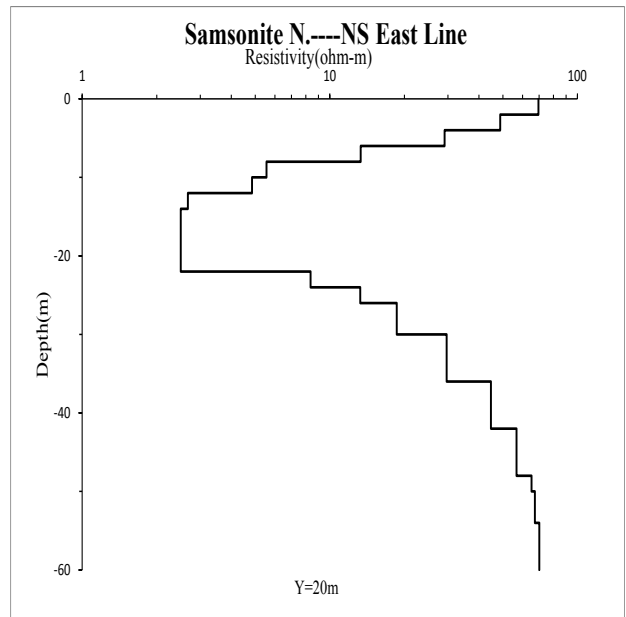
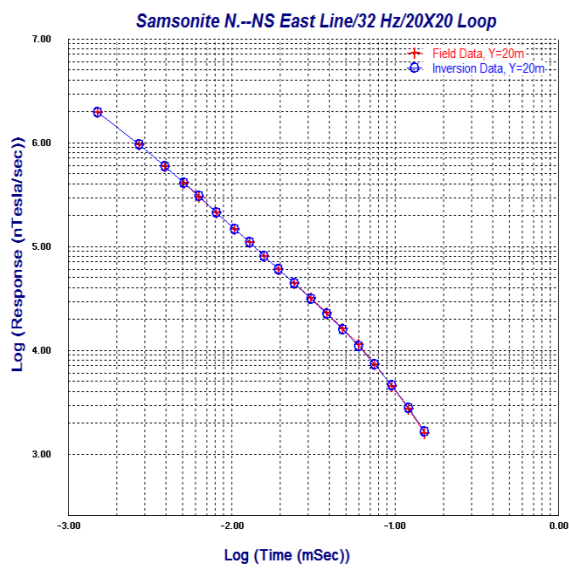
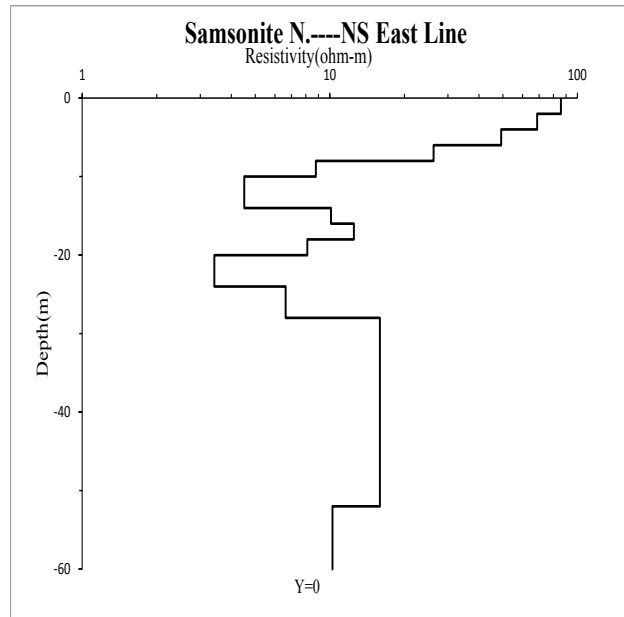
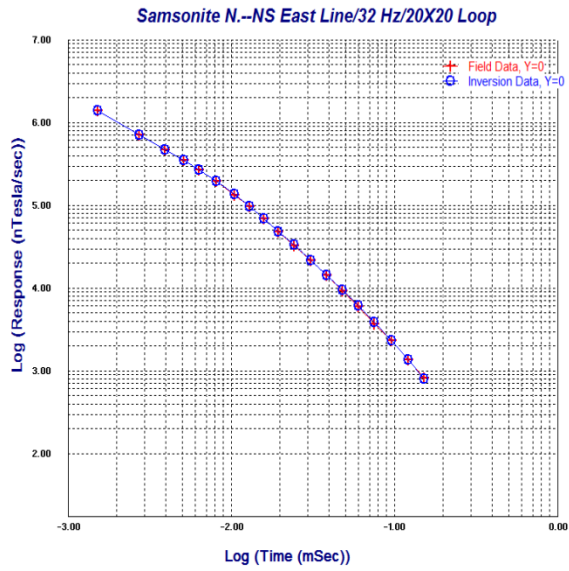
① Samsonite N. NS



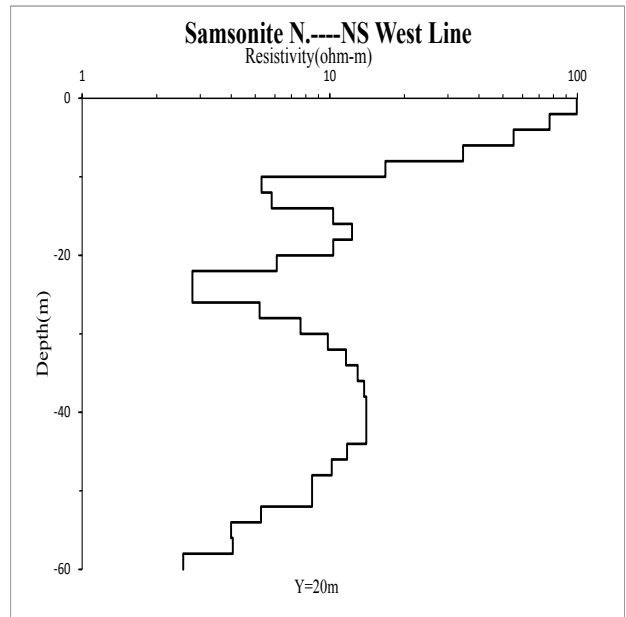
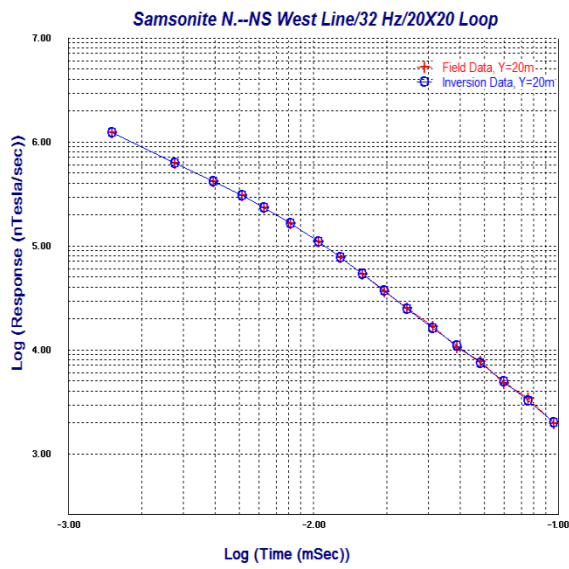
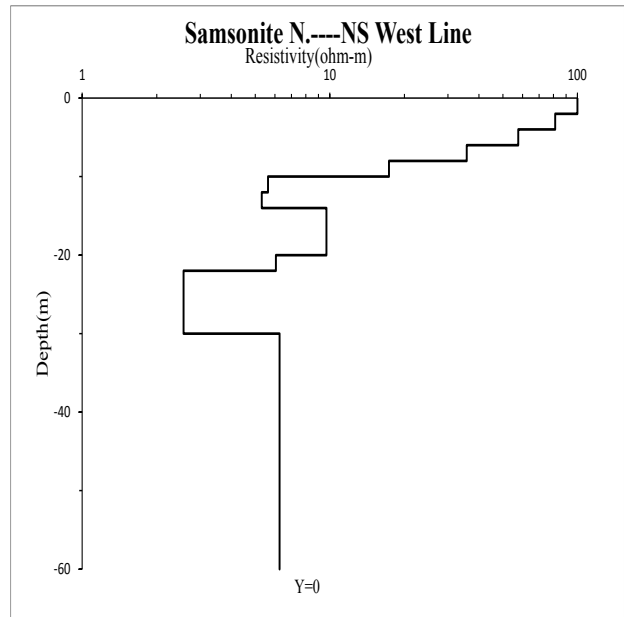
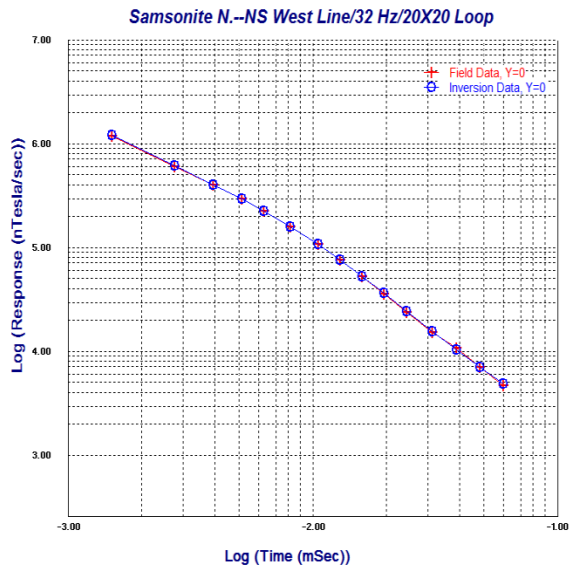




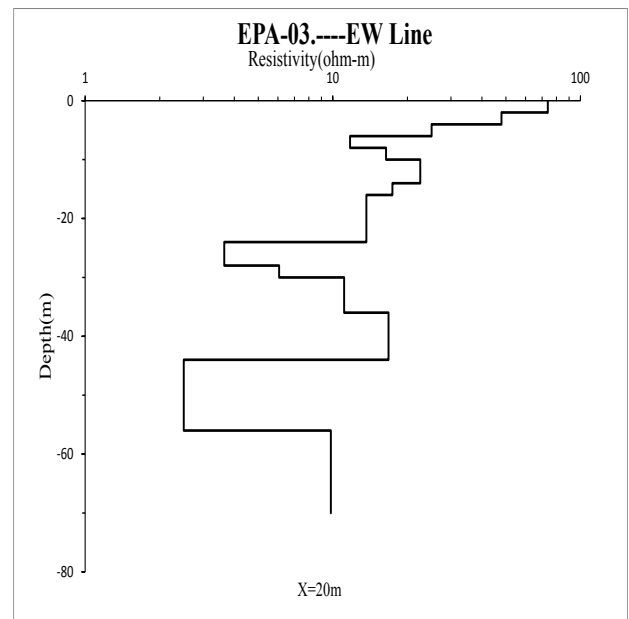
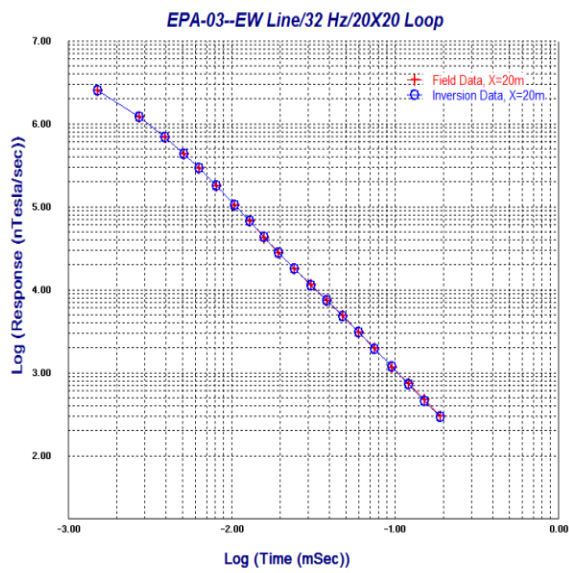
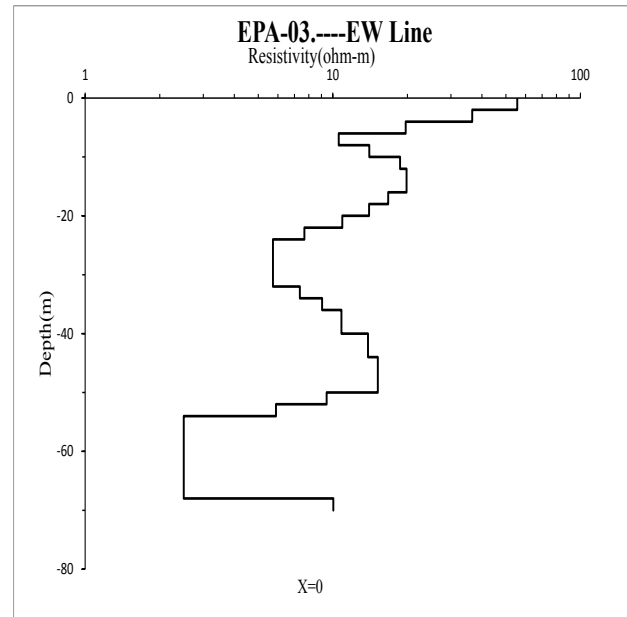
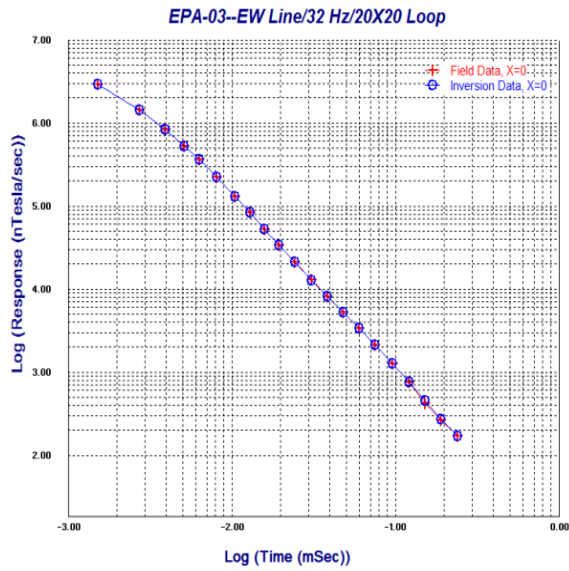
② Samsonite N. NS East Line

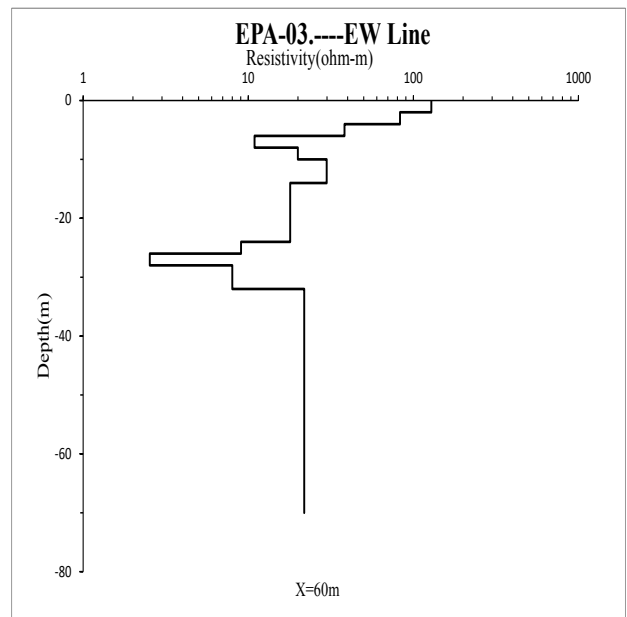
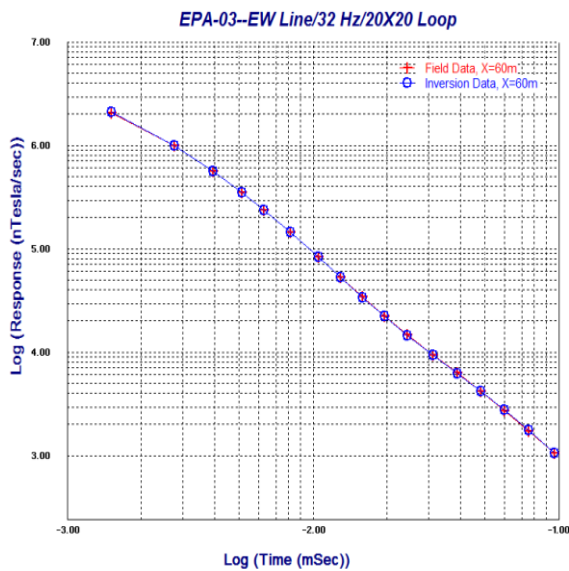
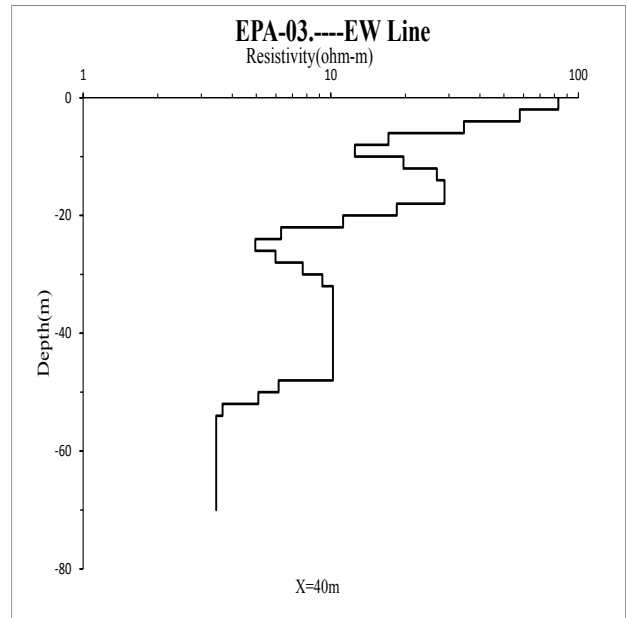
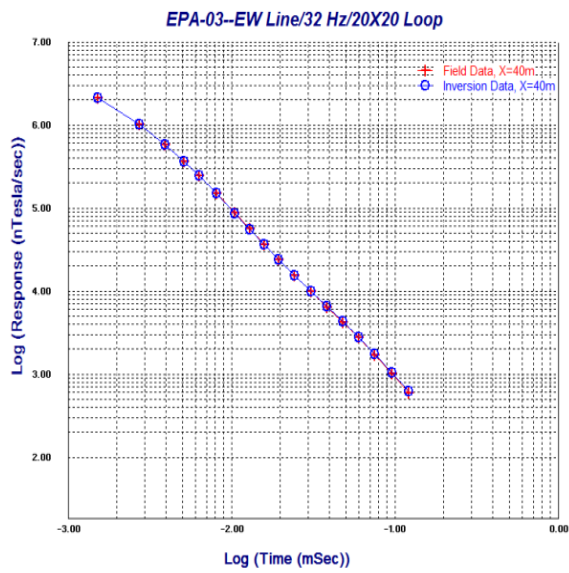


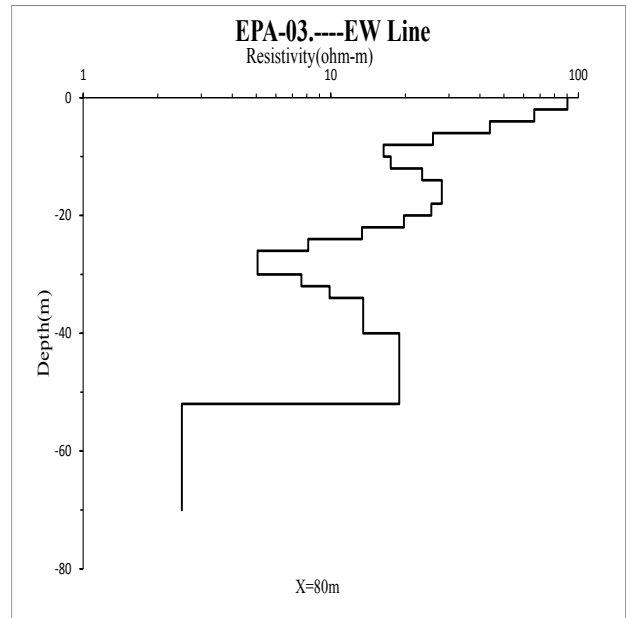
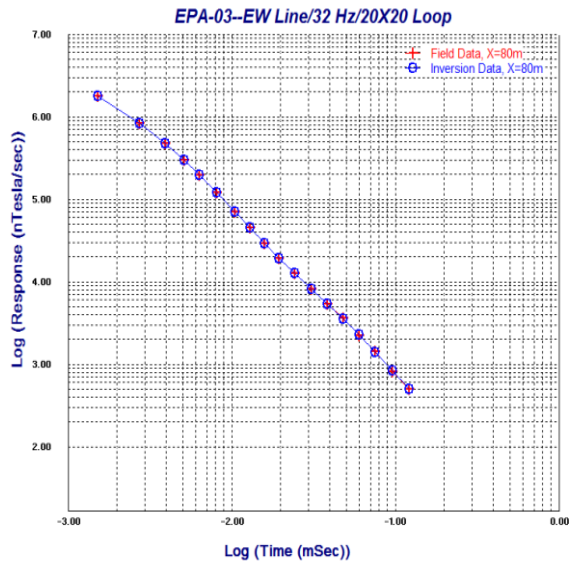
③ Samsonite N. NS West Line



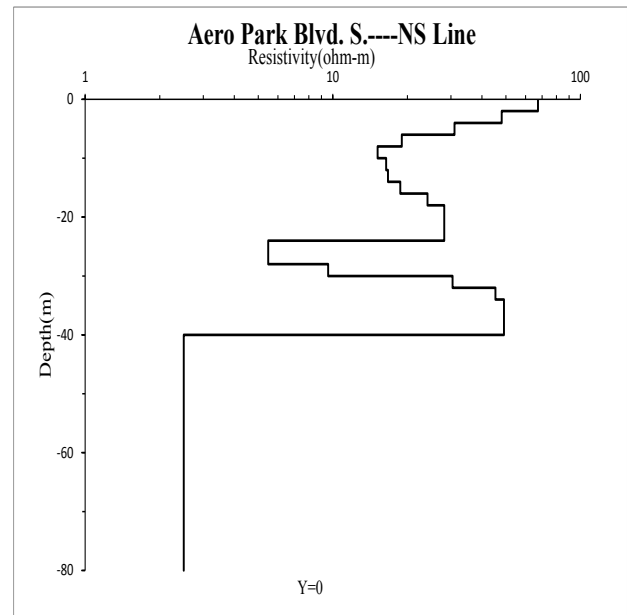
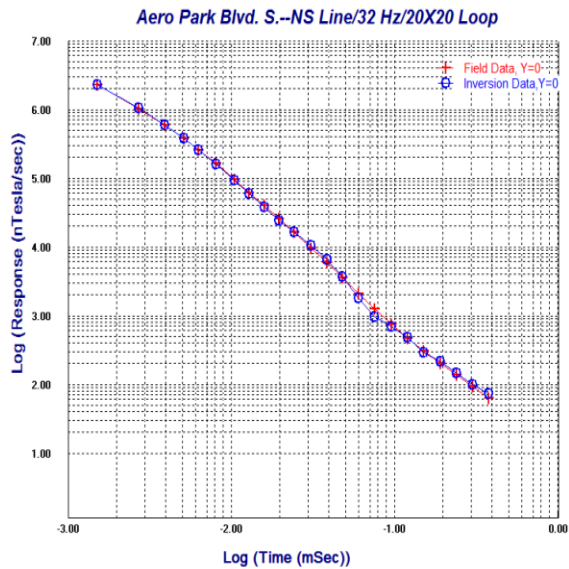
④EPA-03. EW

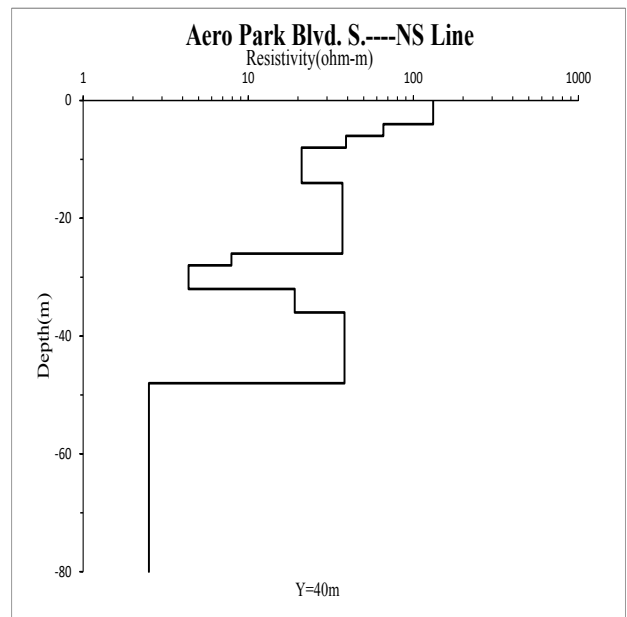
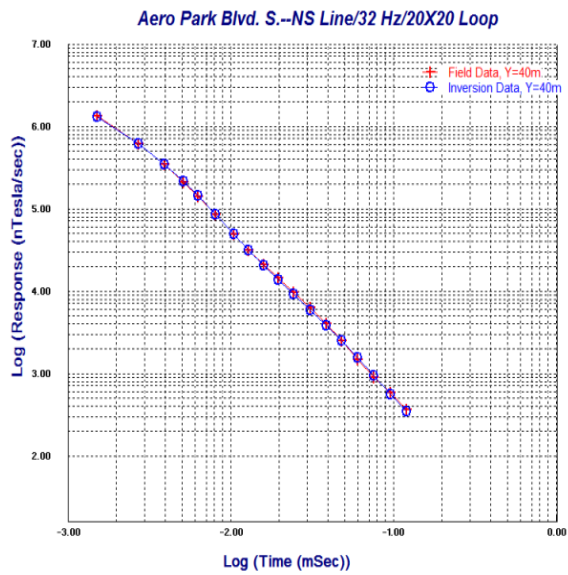
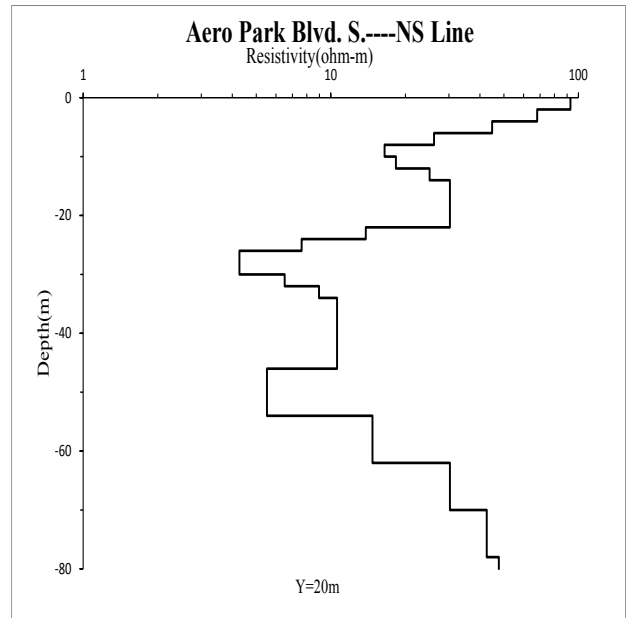
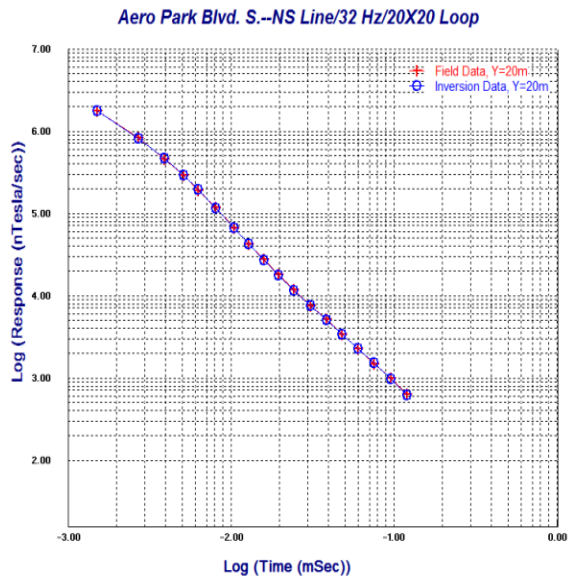


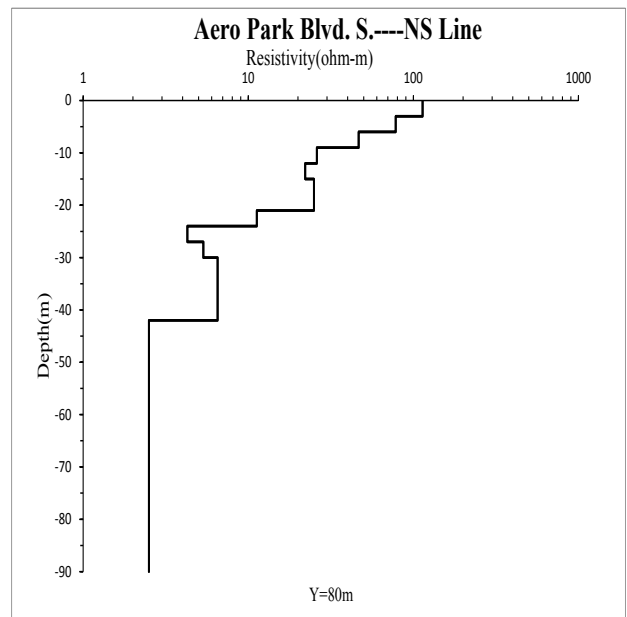
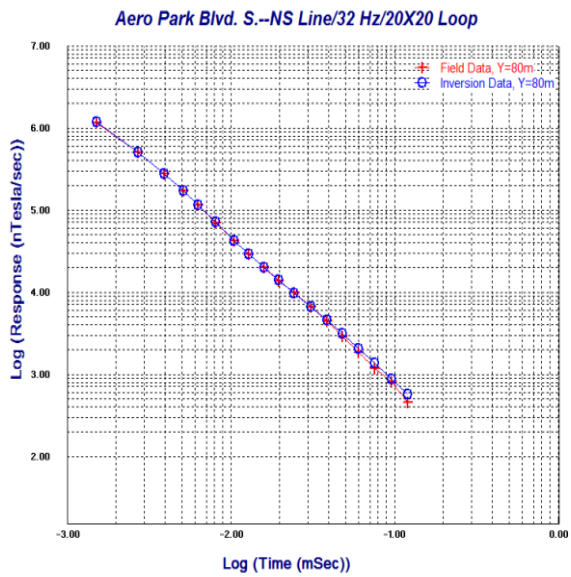
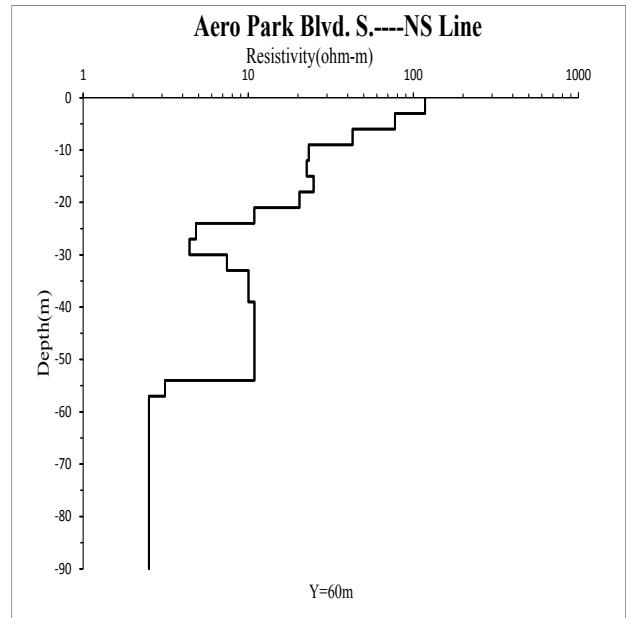
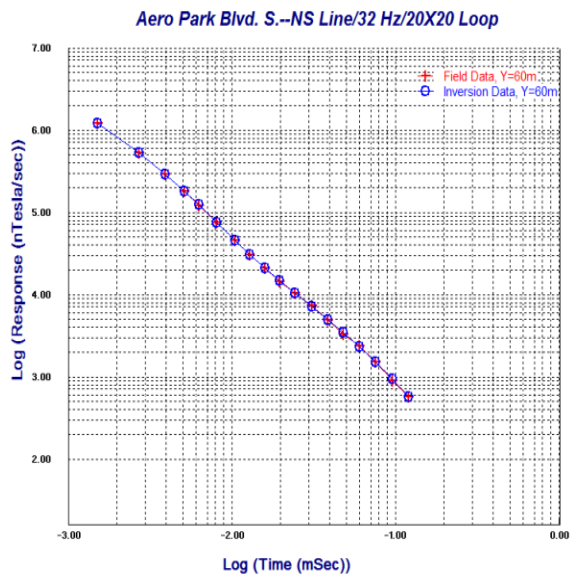


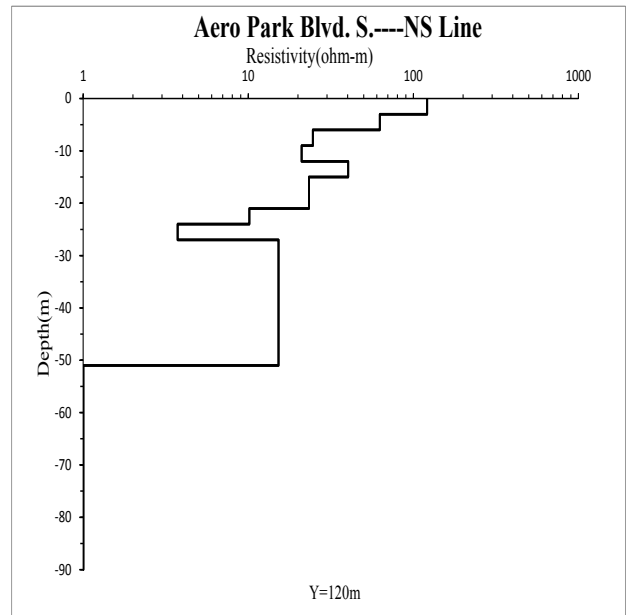
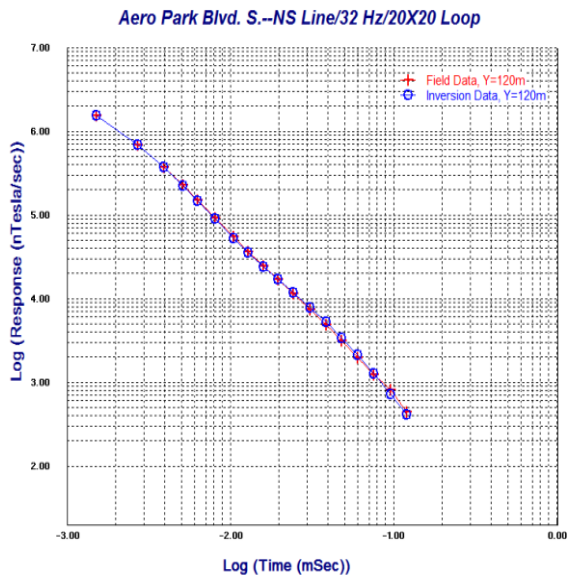
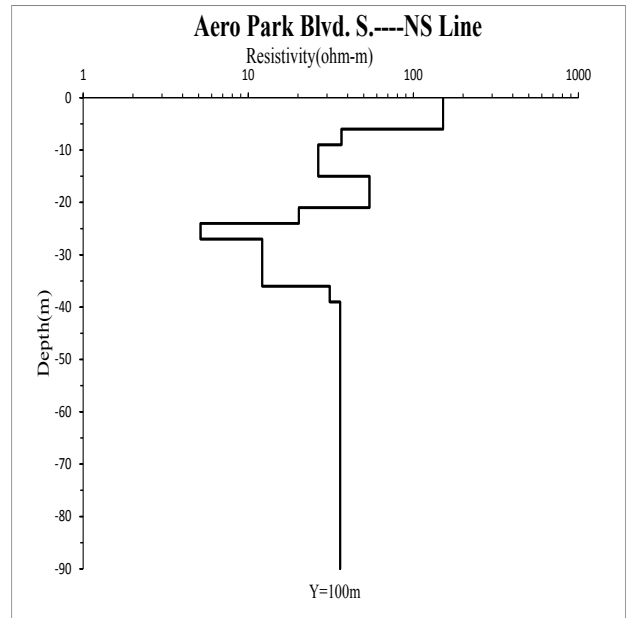
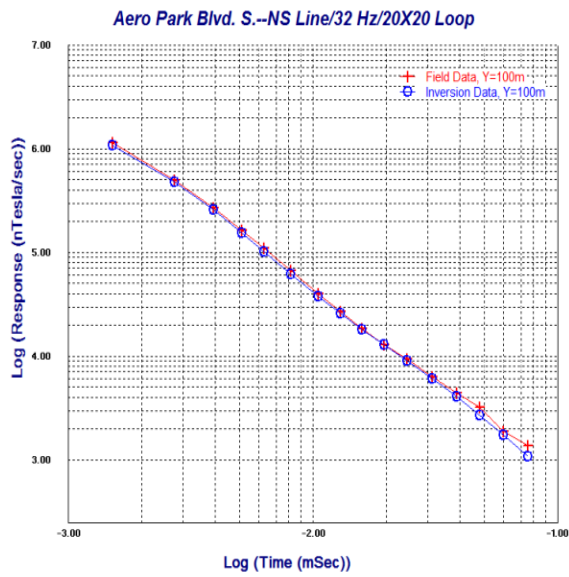


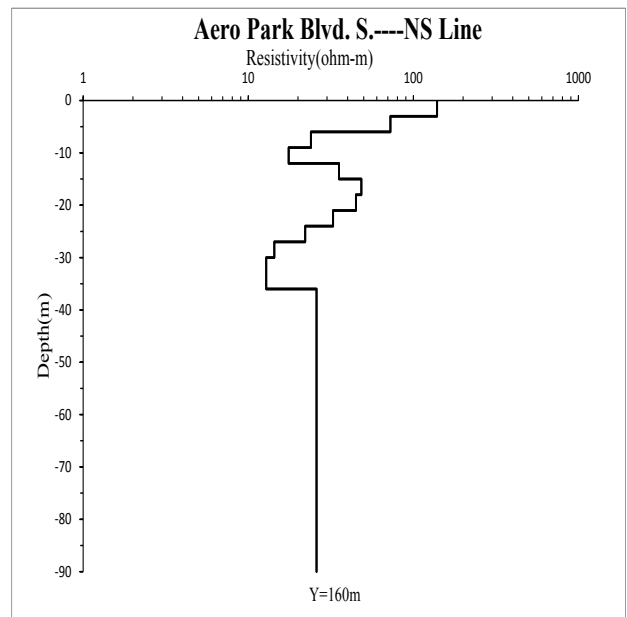
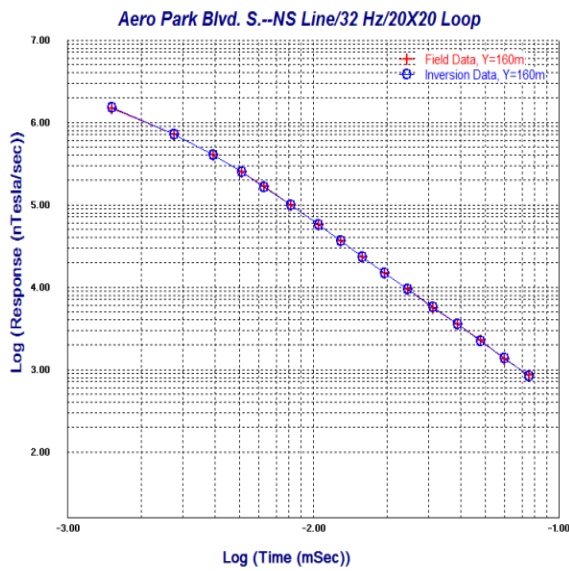
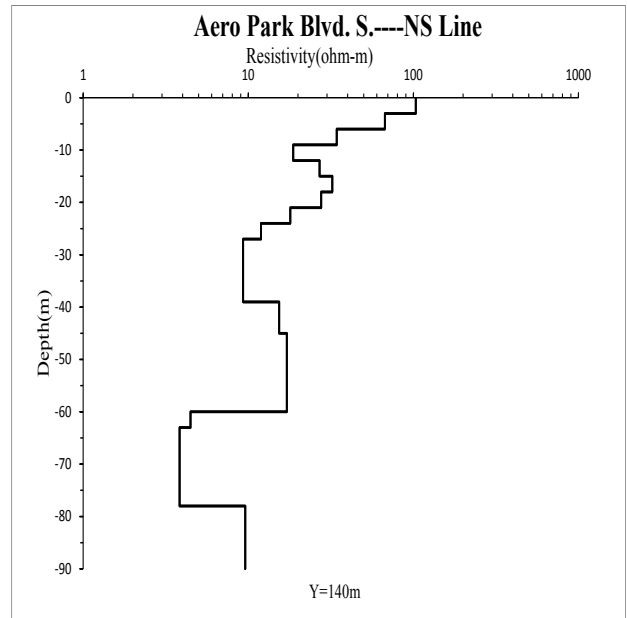
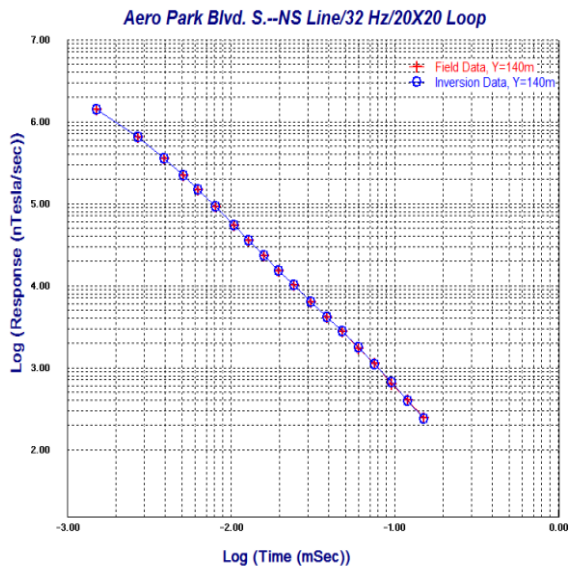
⑤Aero Park Blvd. S.NS



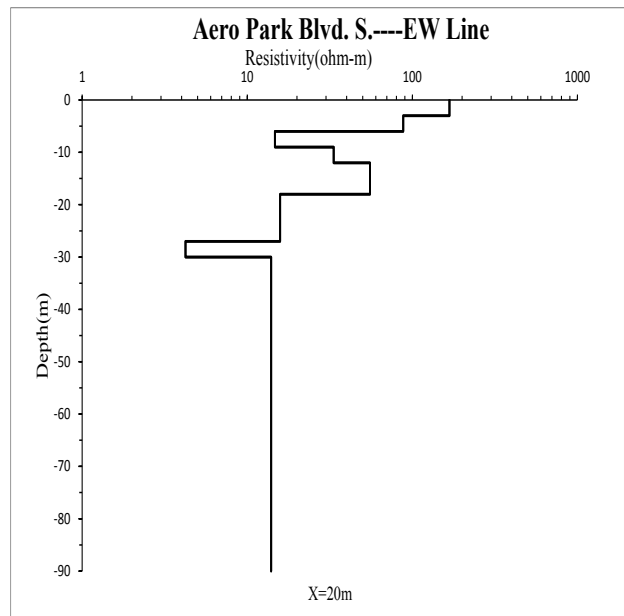
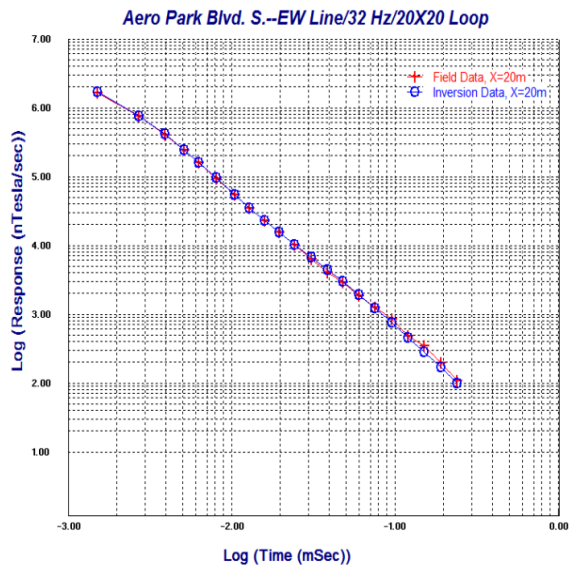
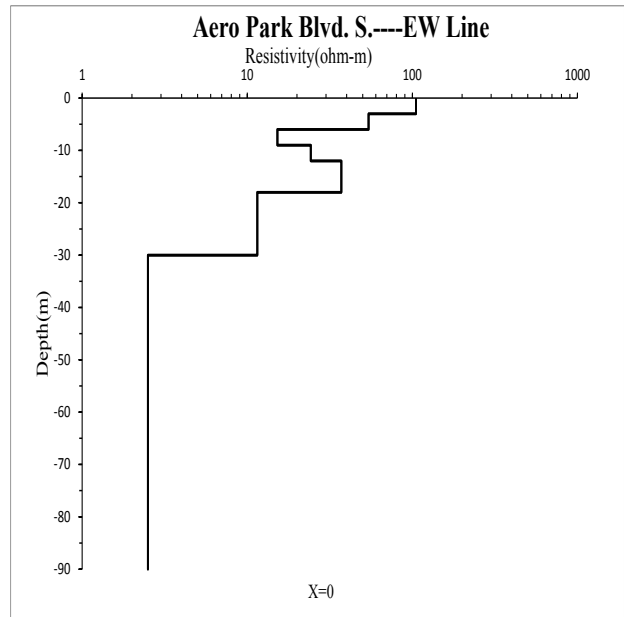
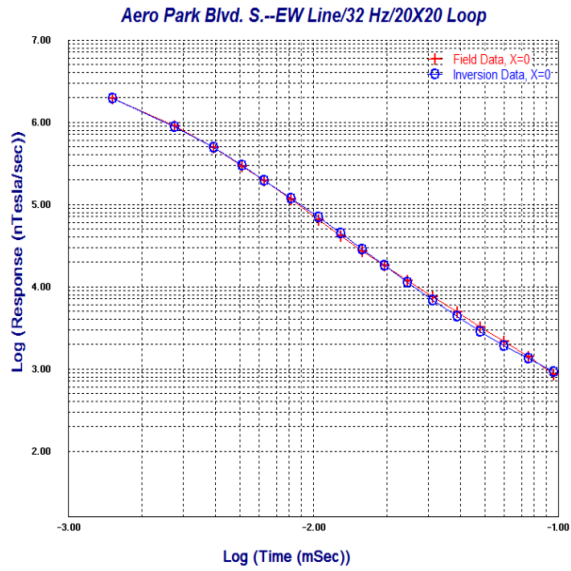


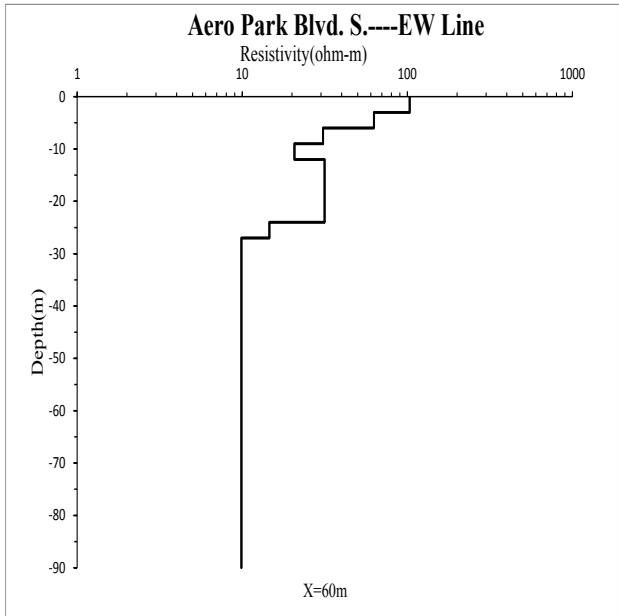
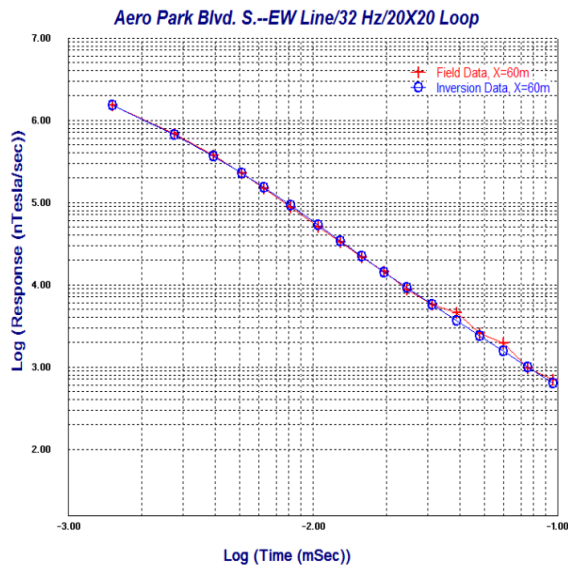
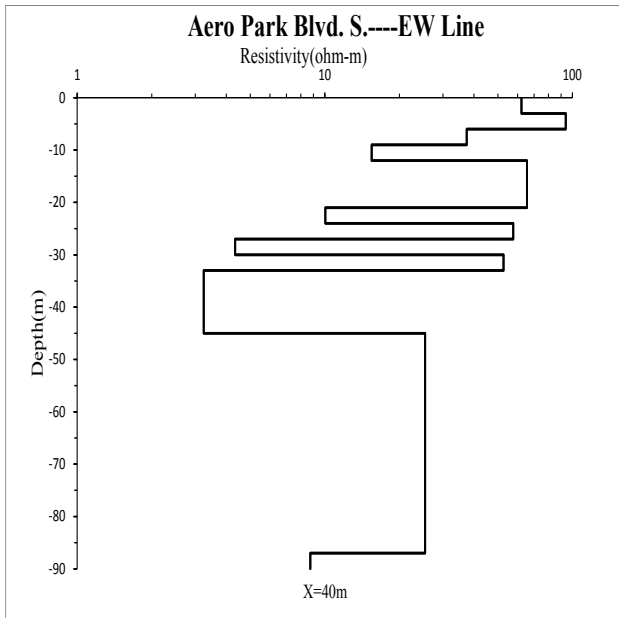
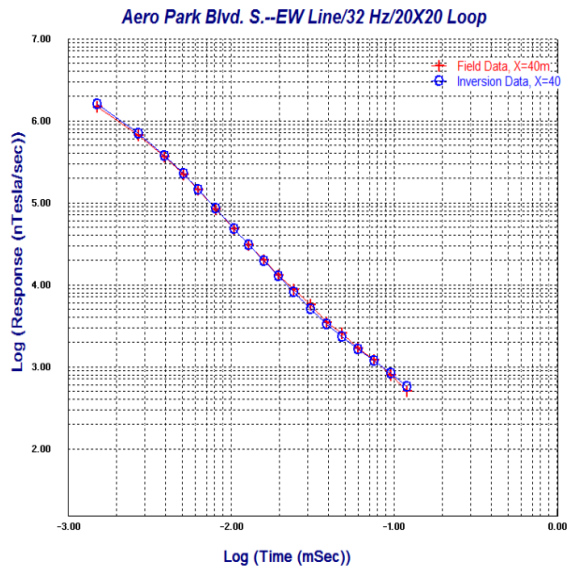


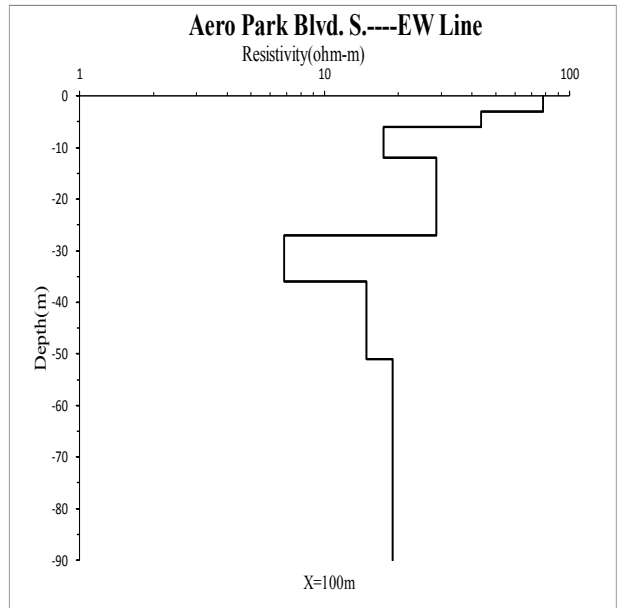
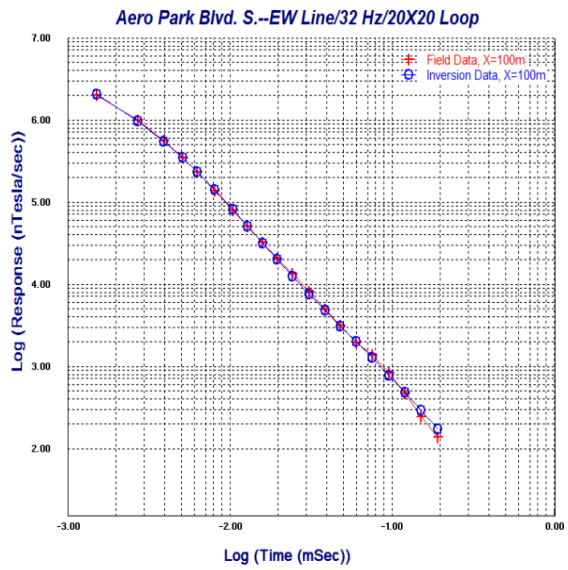
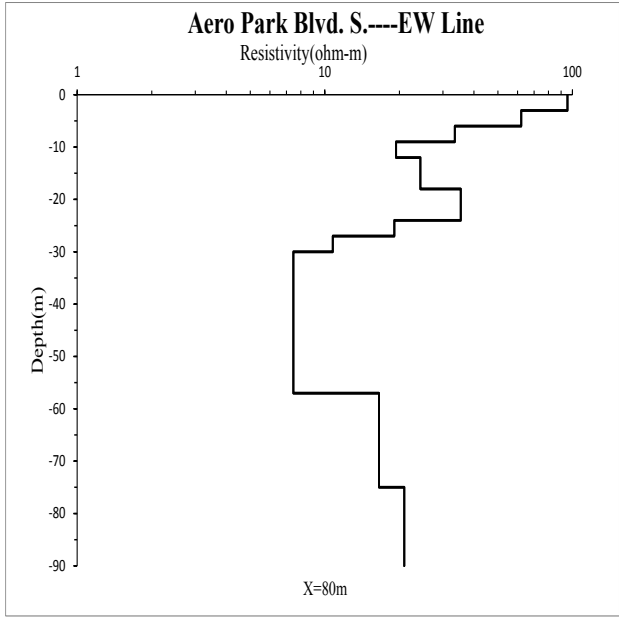
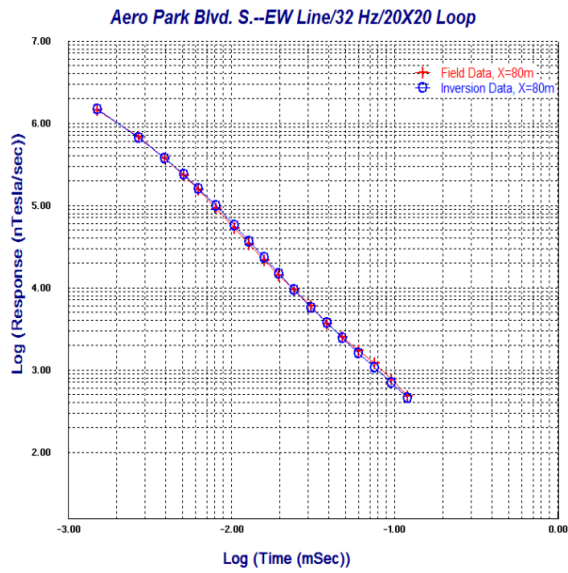


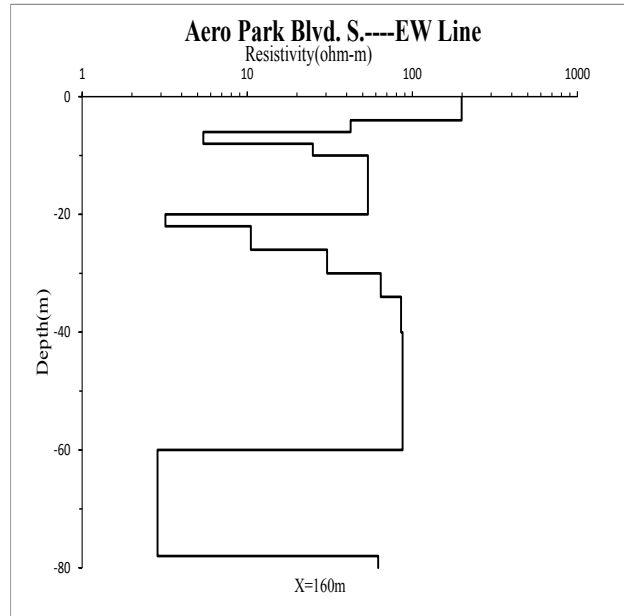
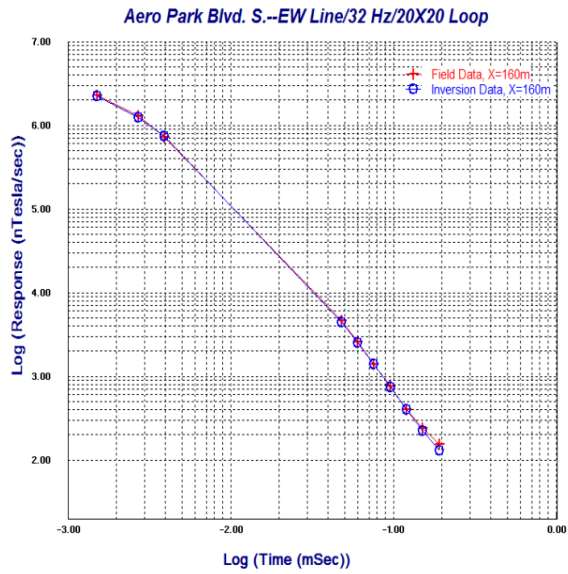
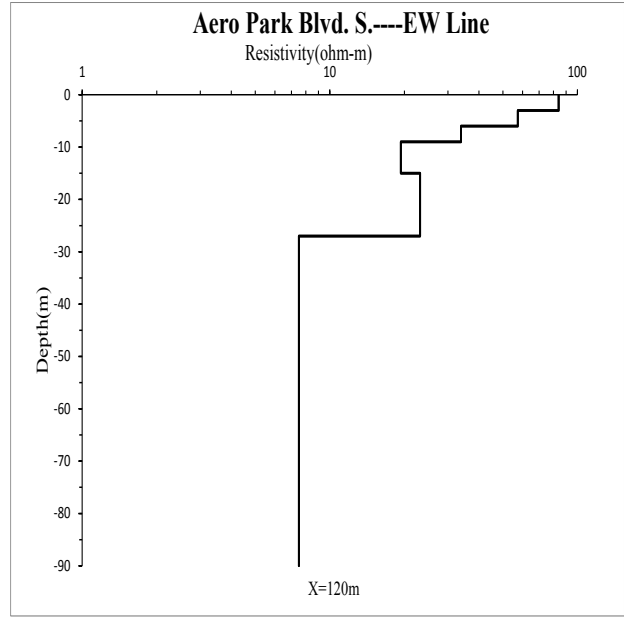
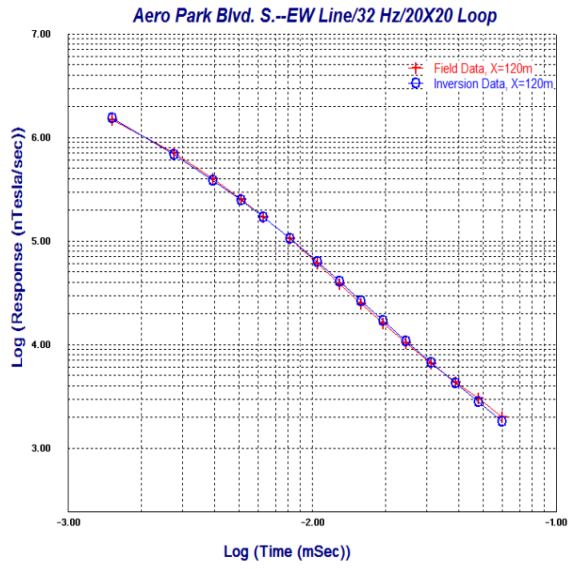


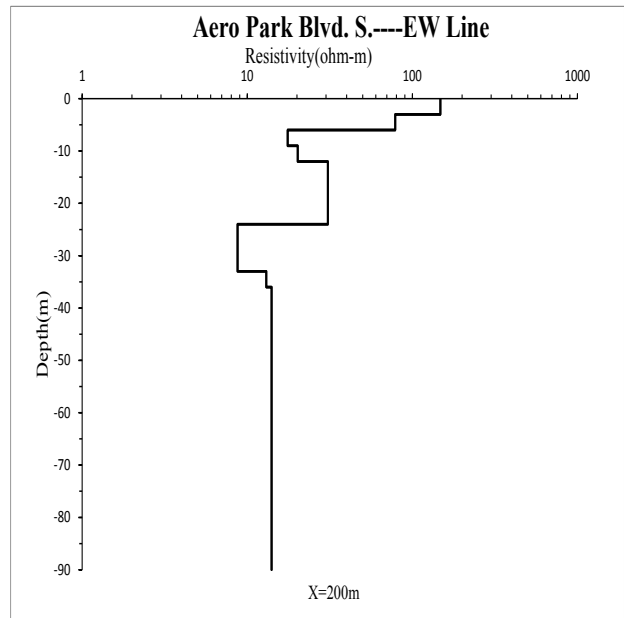
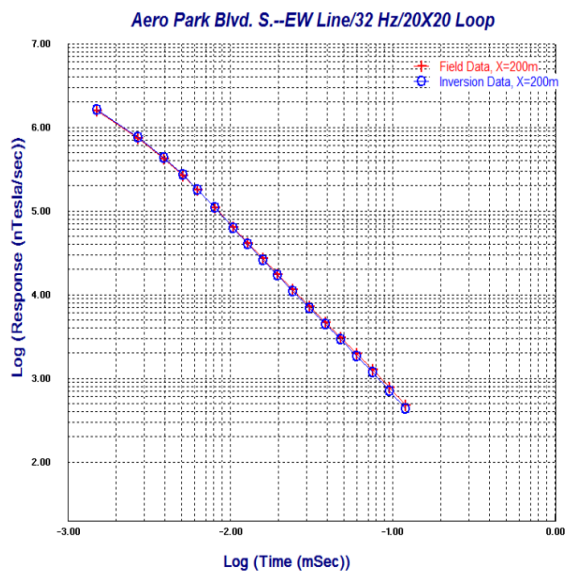
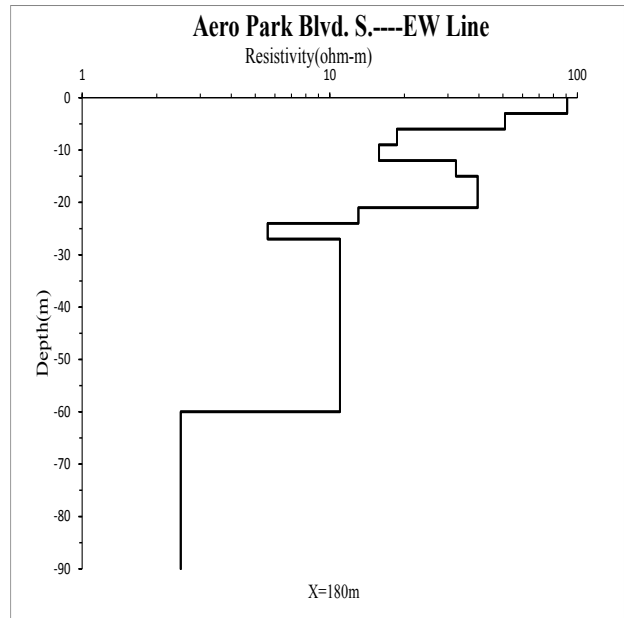
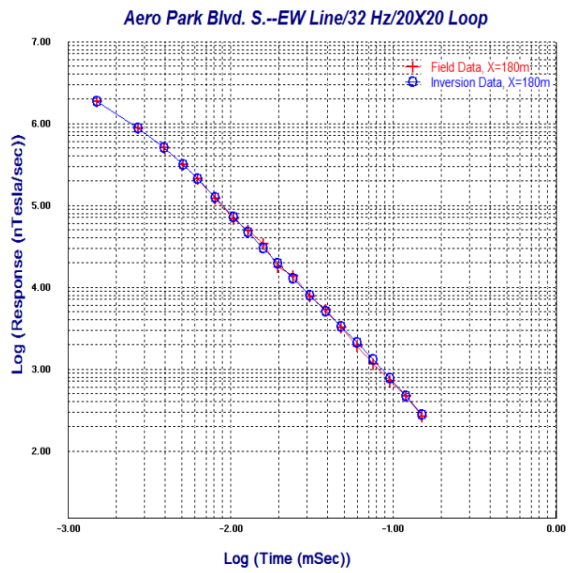
⑥Aero Park Blvd. S. EW

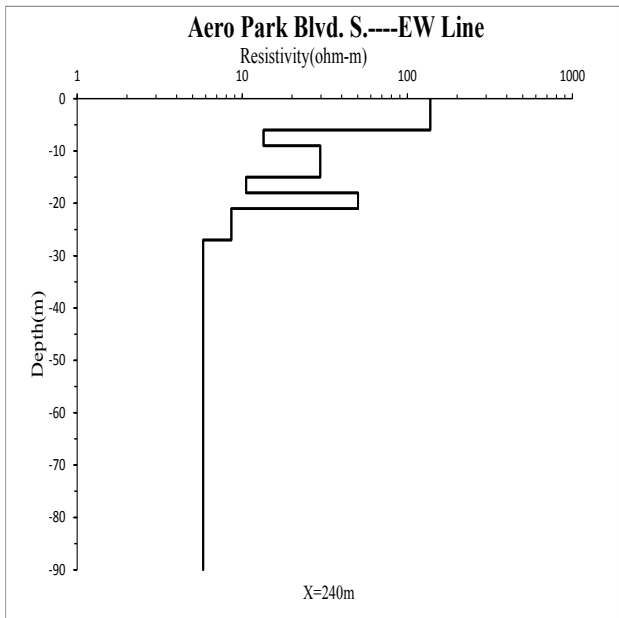
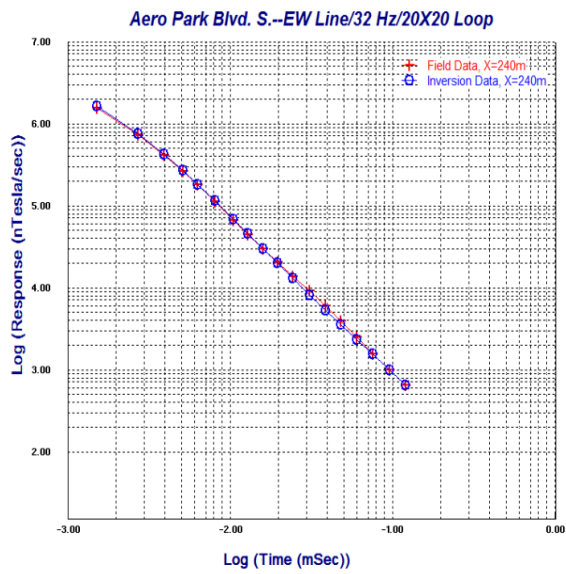
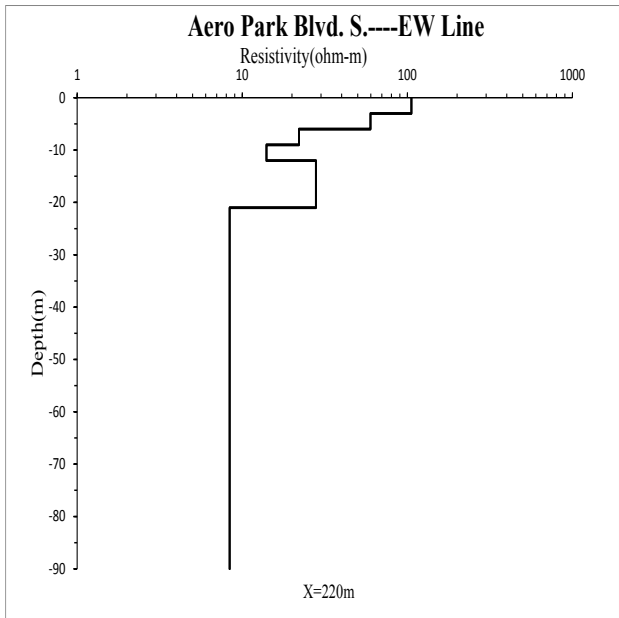
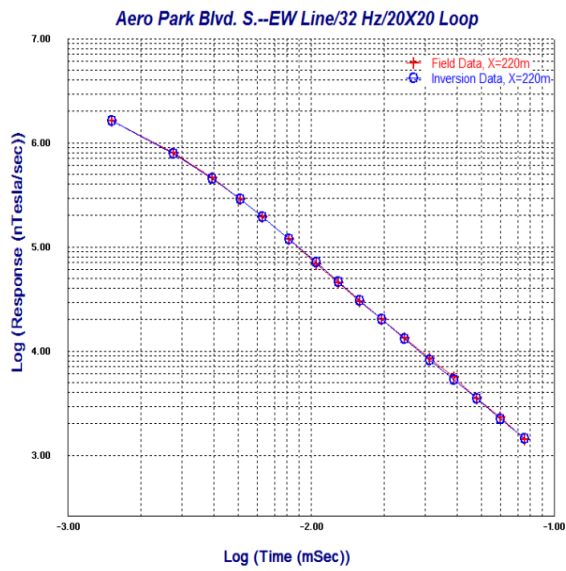


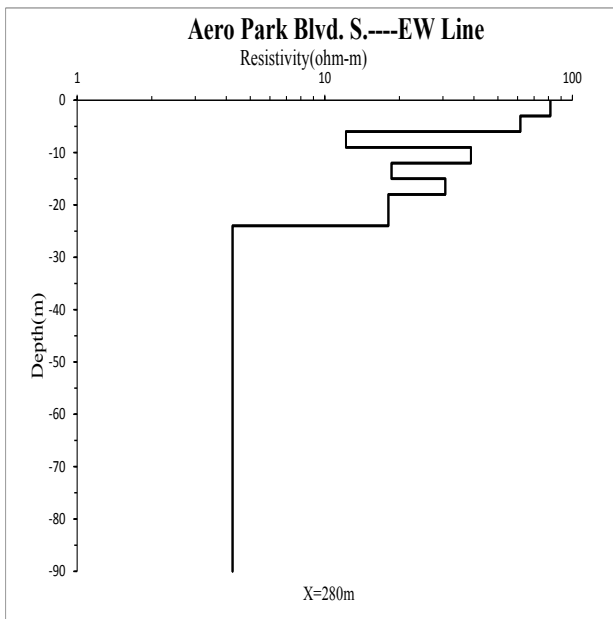
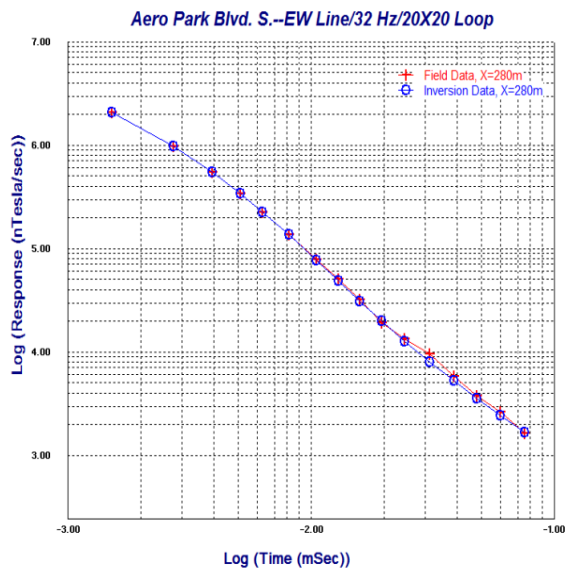
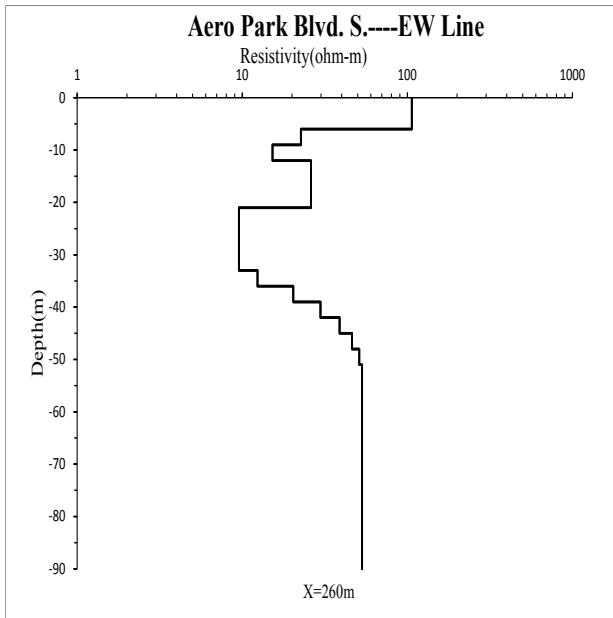
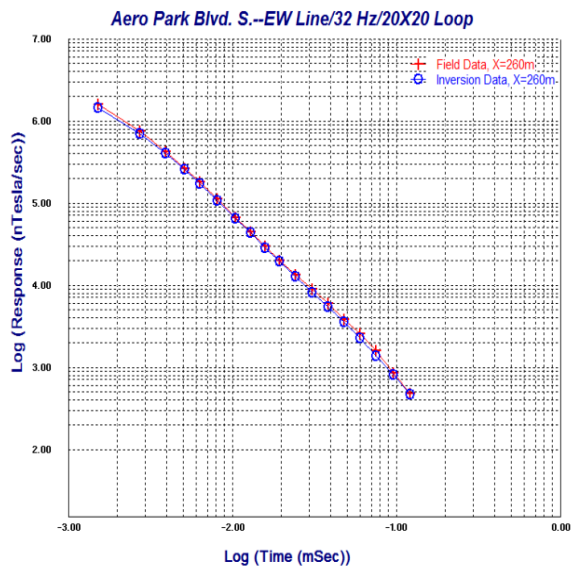


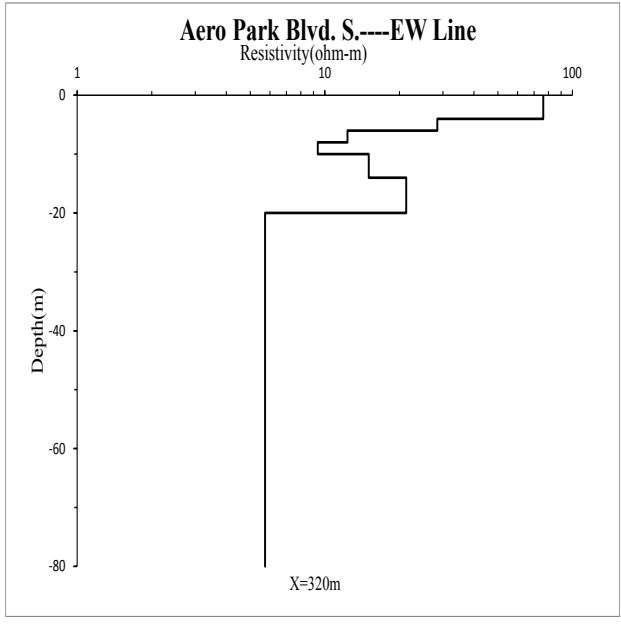
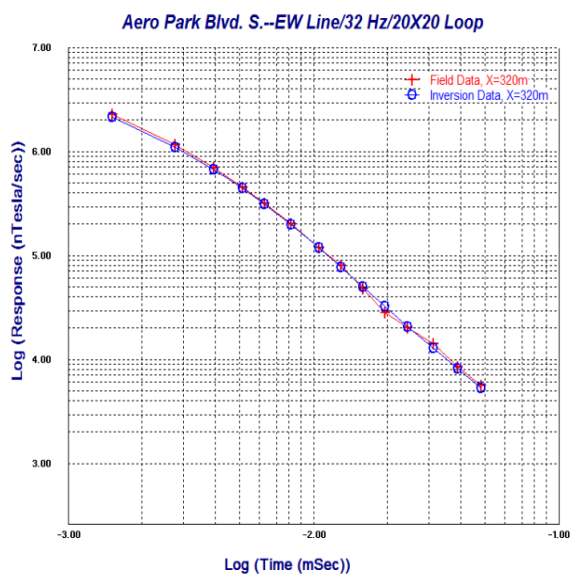
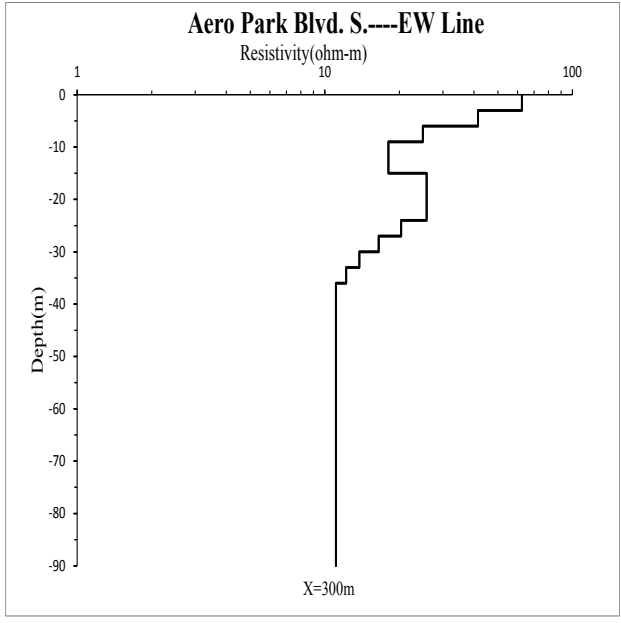
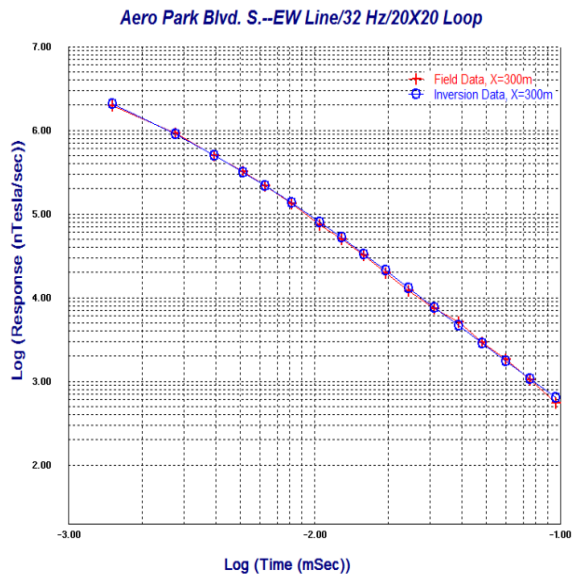


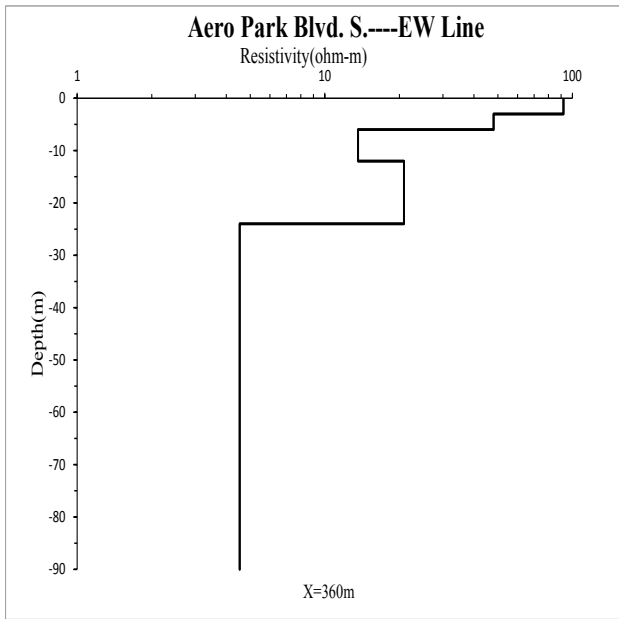
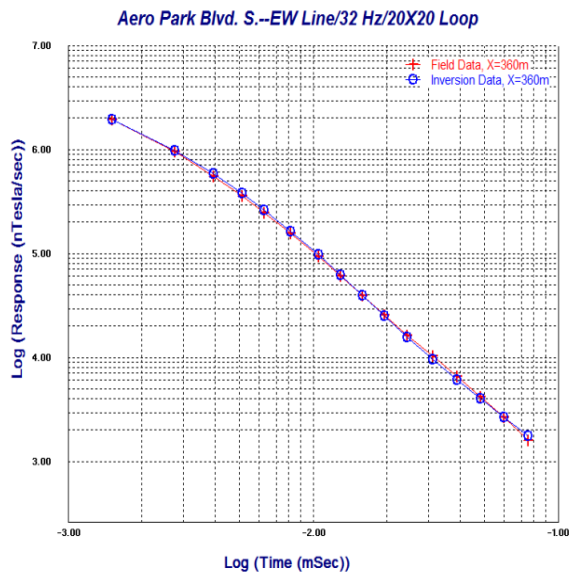
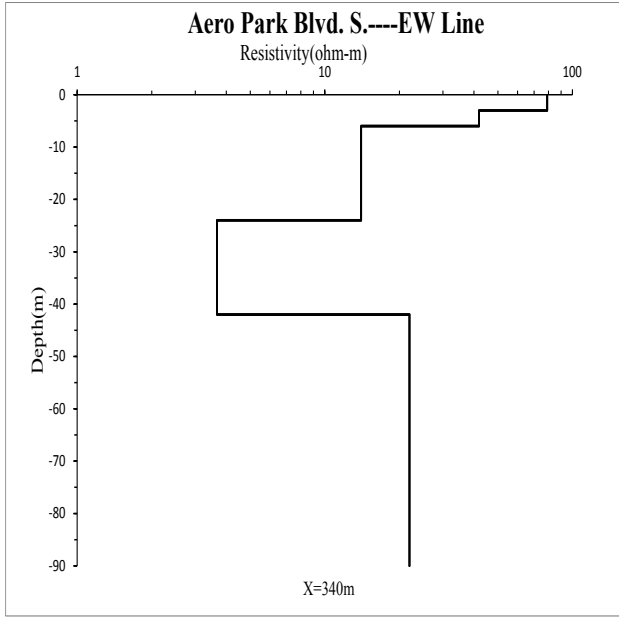
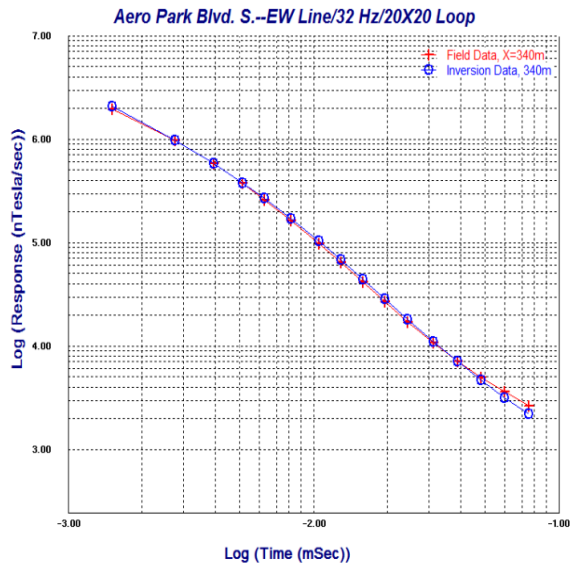


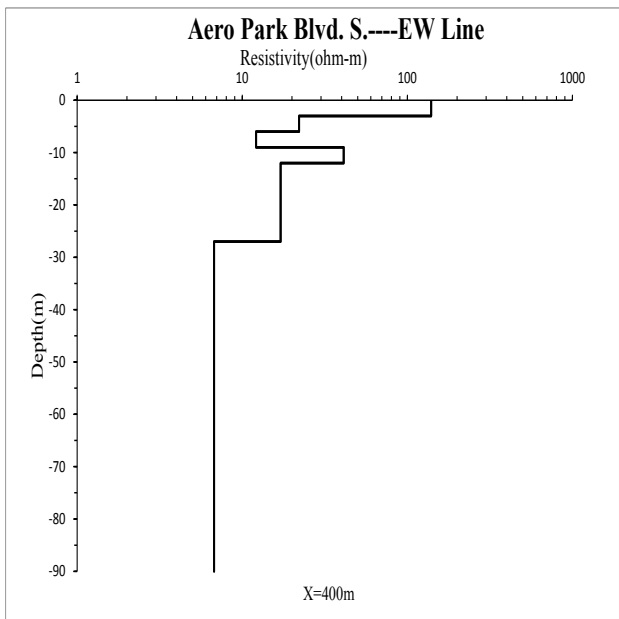
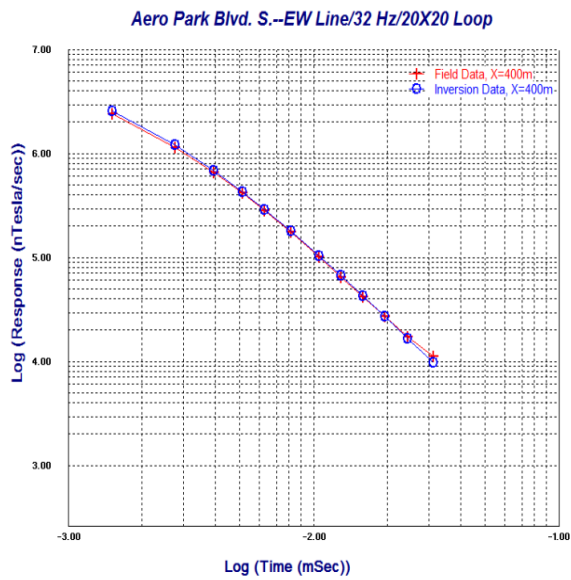
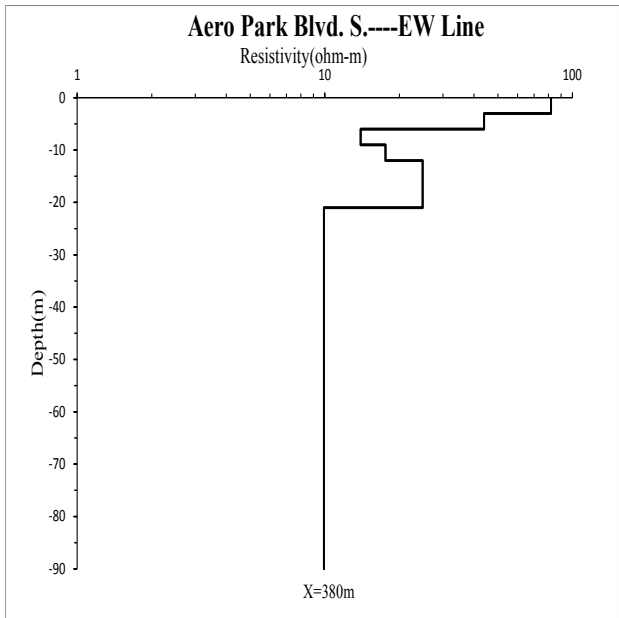
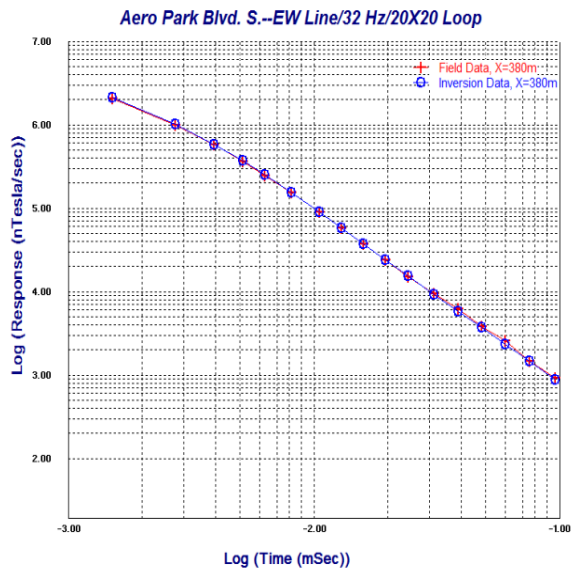






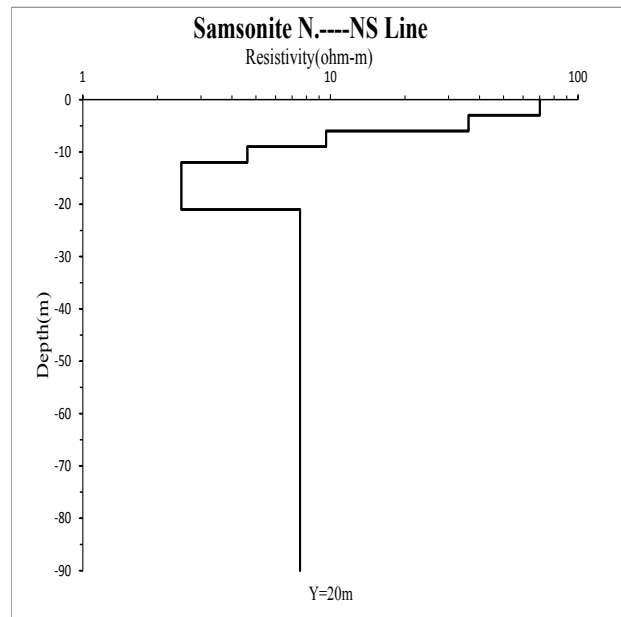
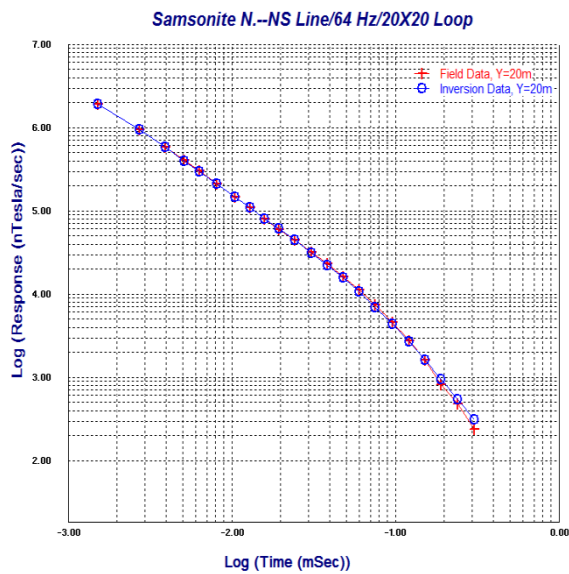
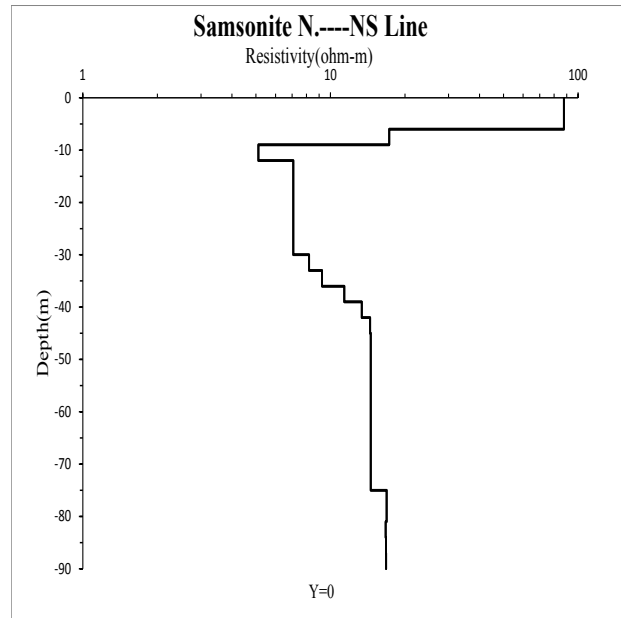
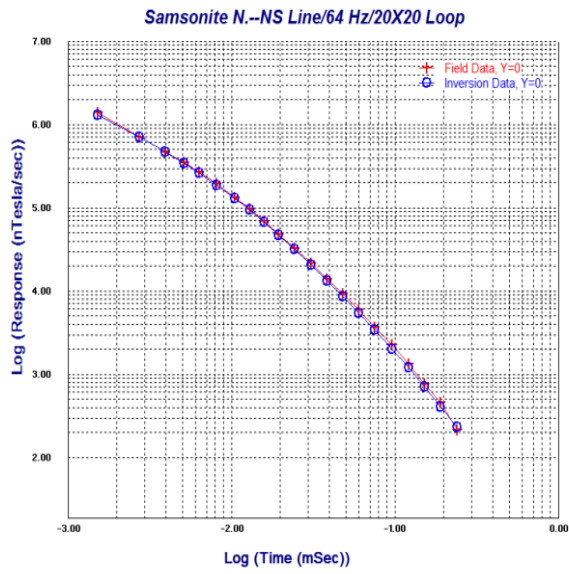


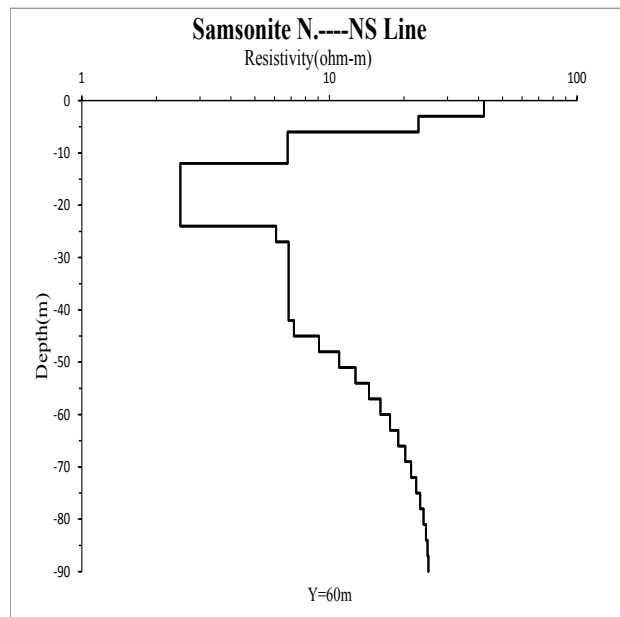
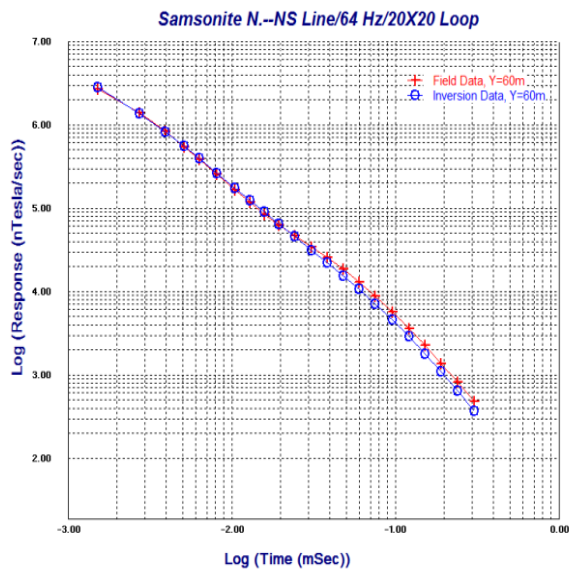
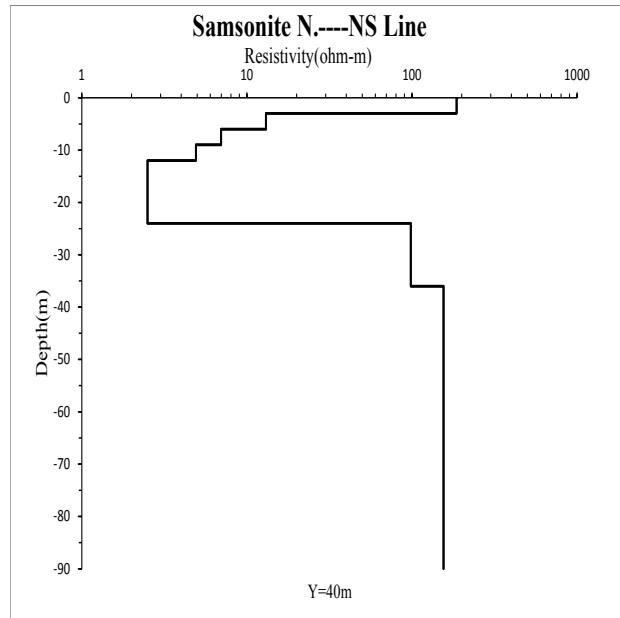
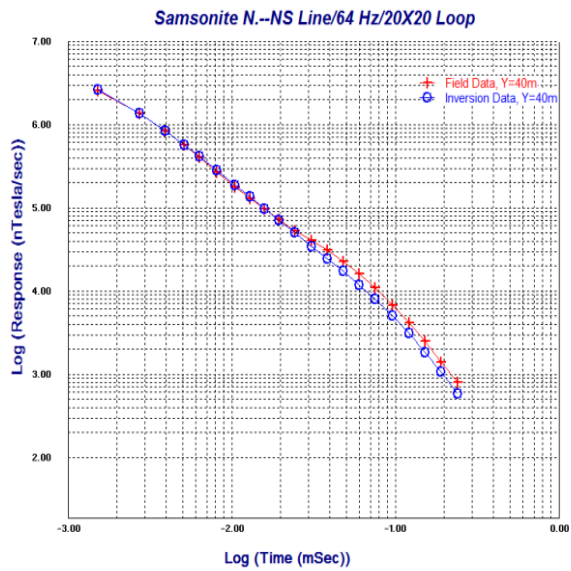


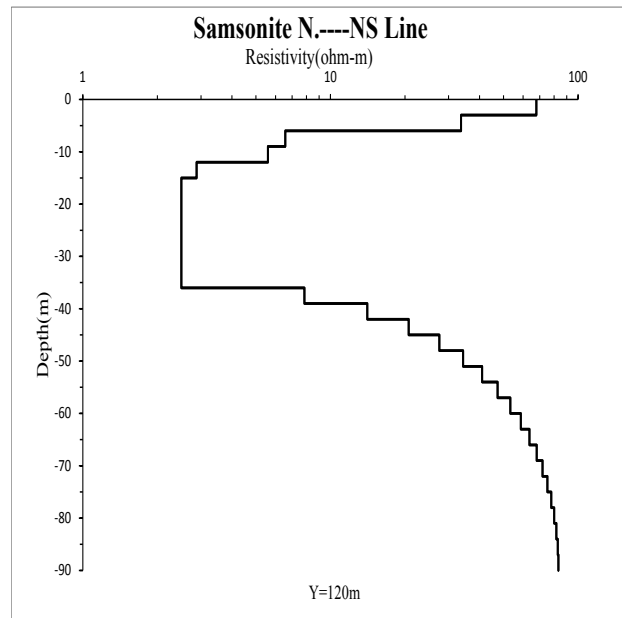
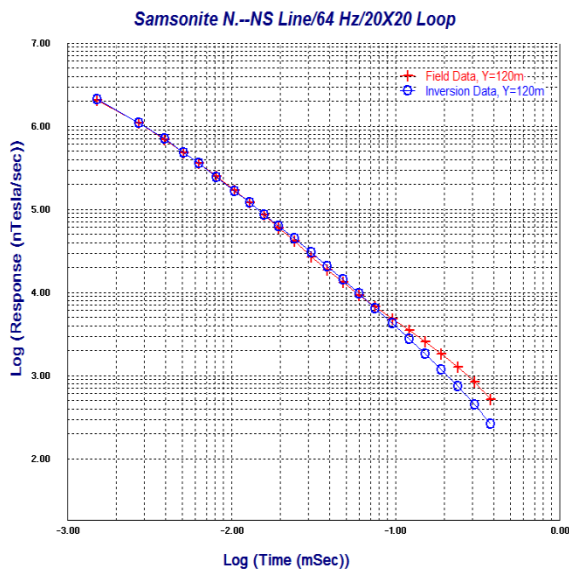
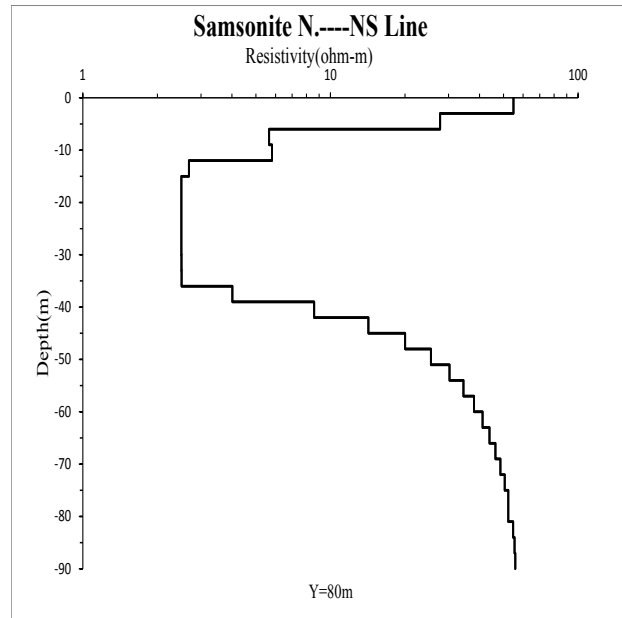
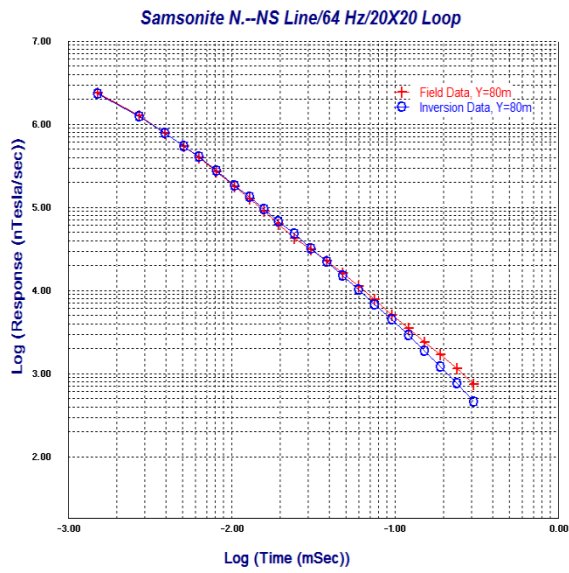


## 2. 64HZ, 20×20m Loop

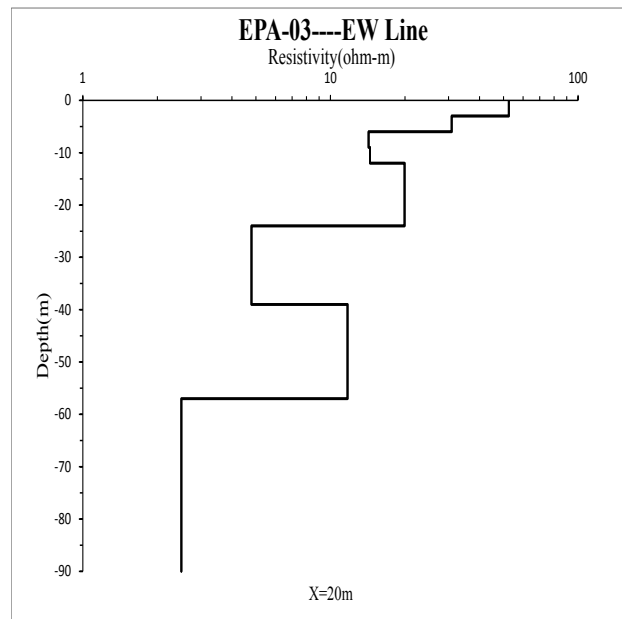
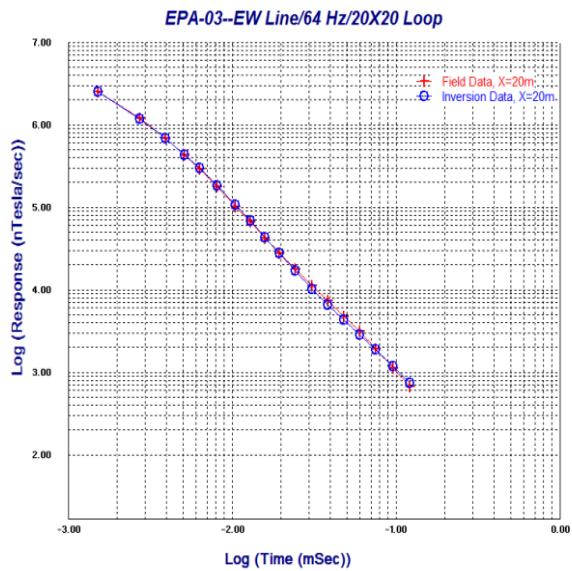
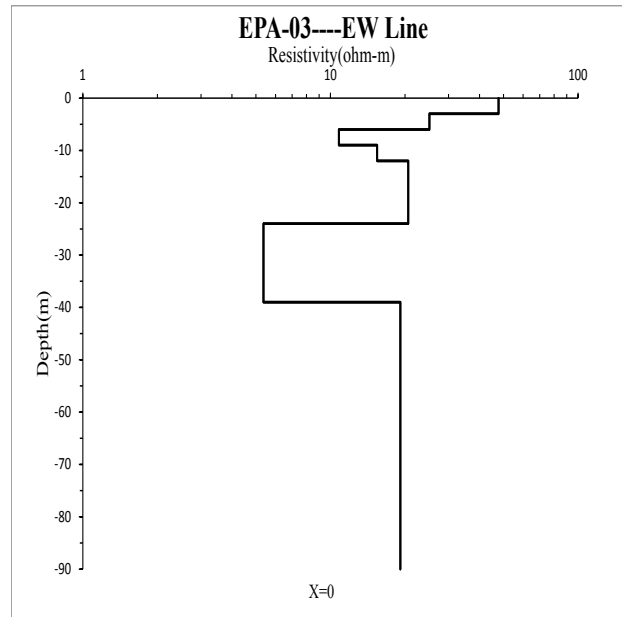
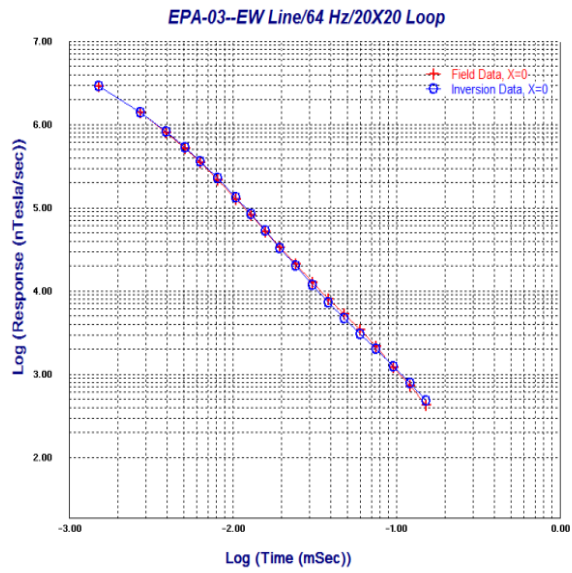
① Samsonite N. NS

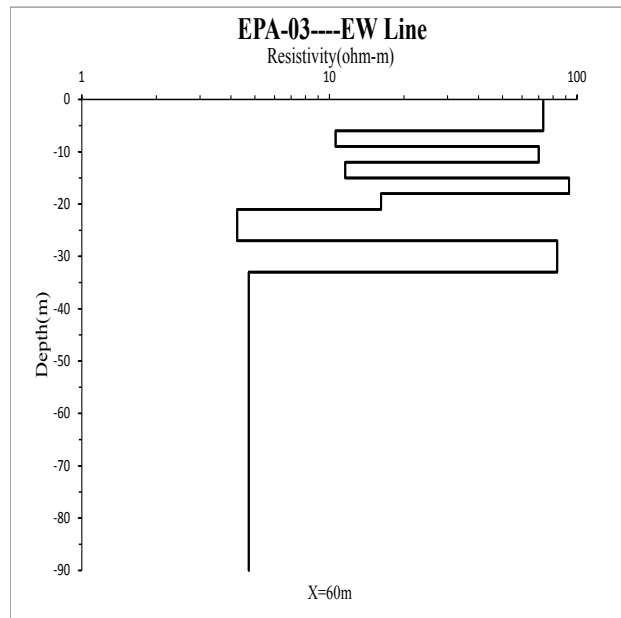
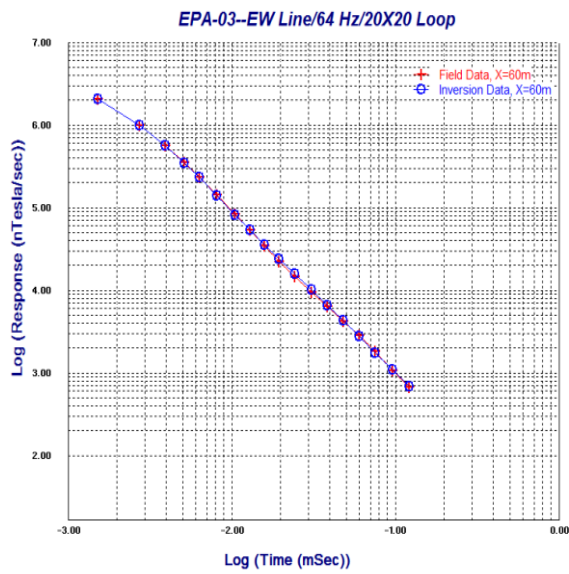
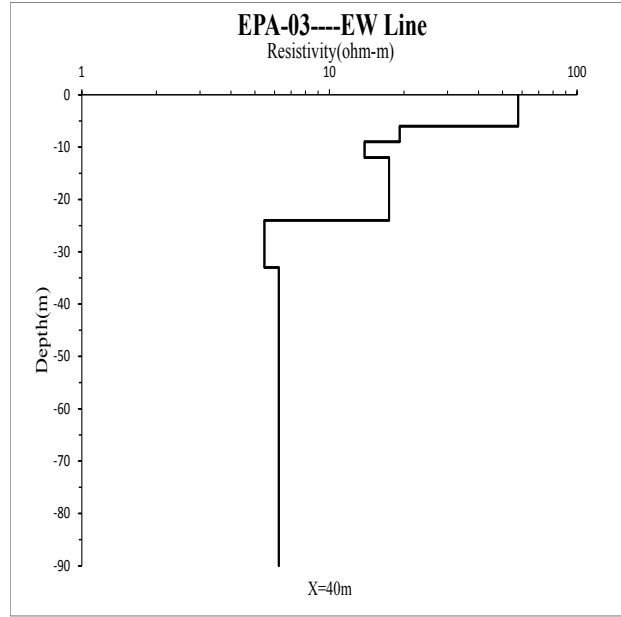
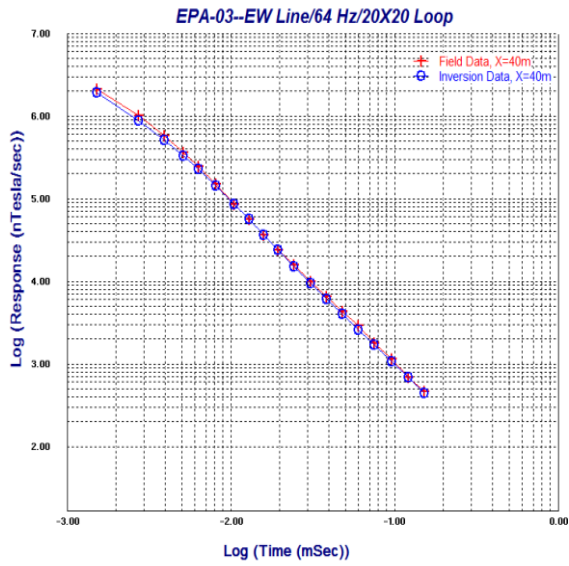


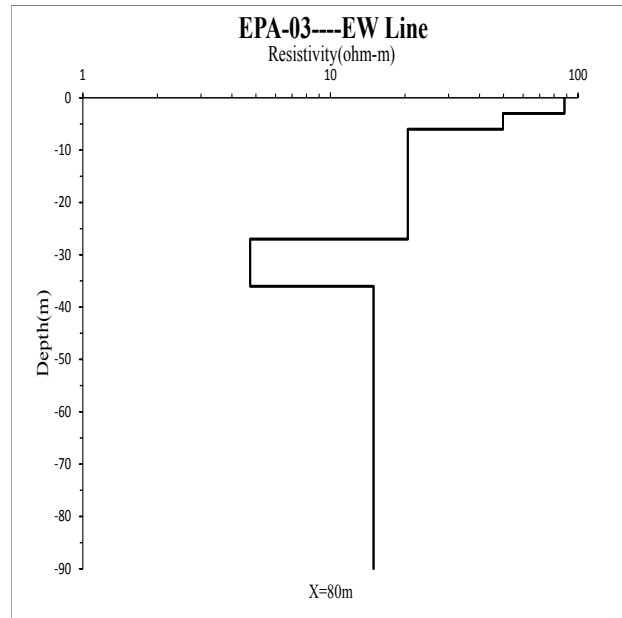
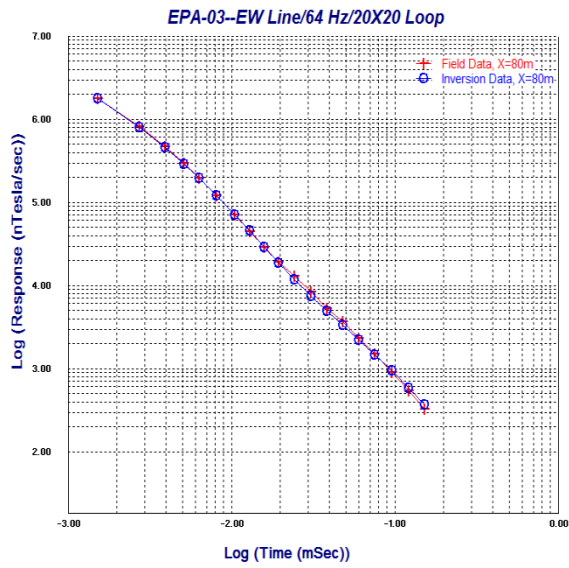




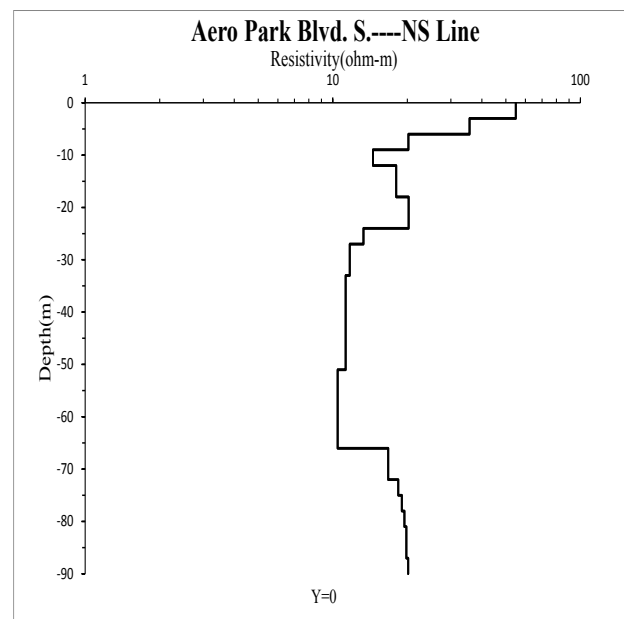
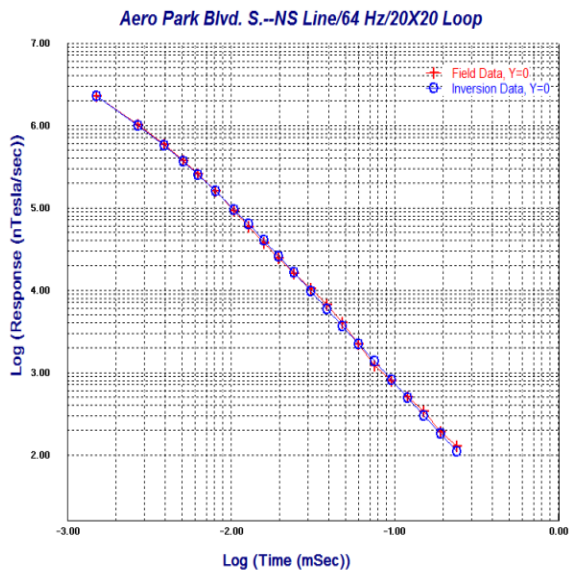
②EPA-03. EW

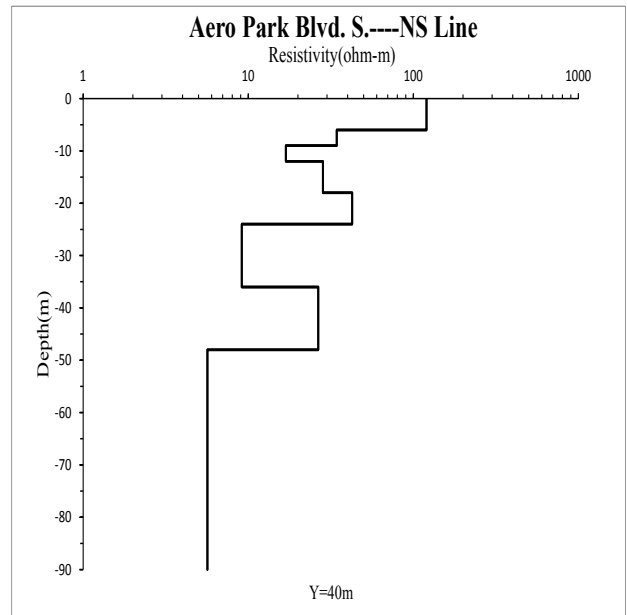
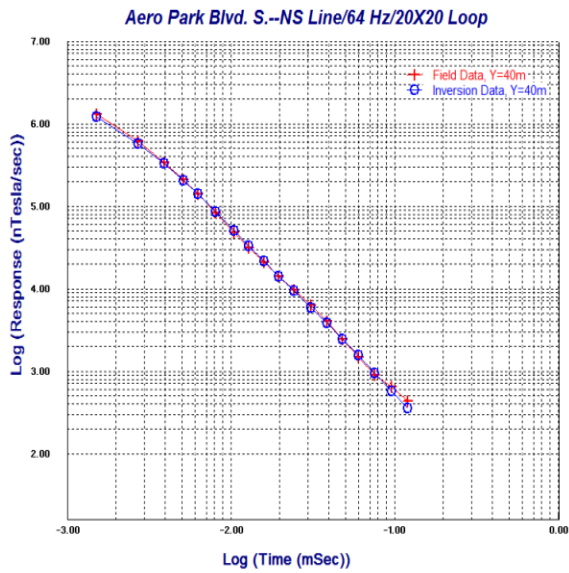
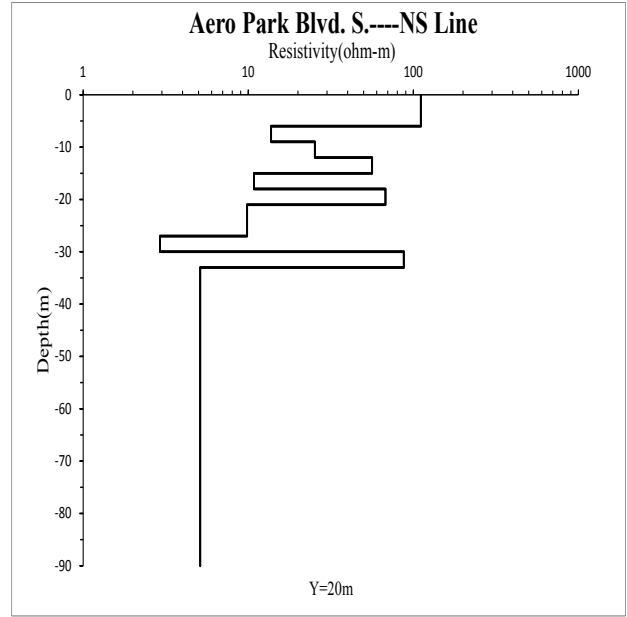
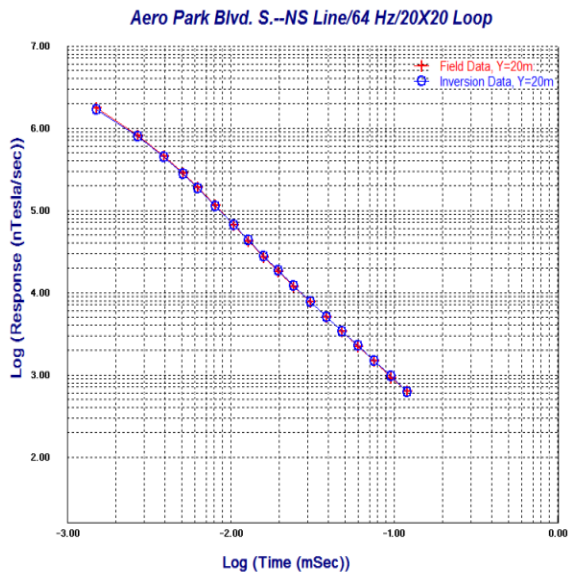


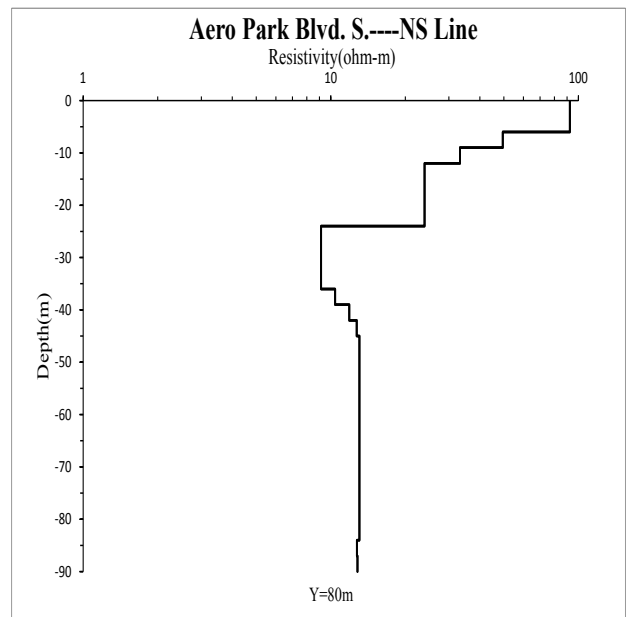
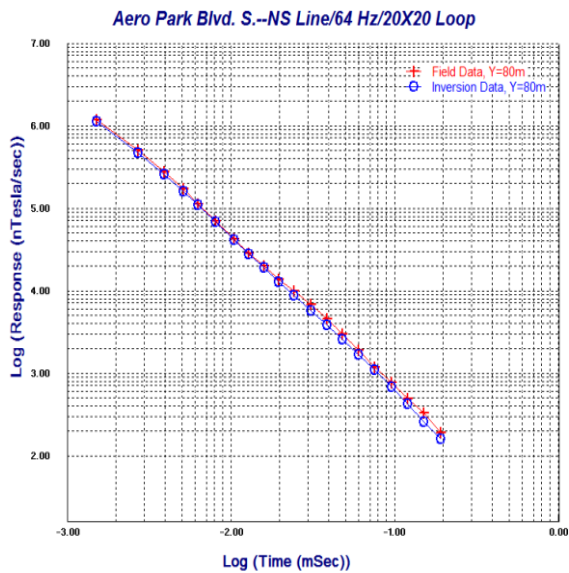
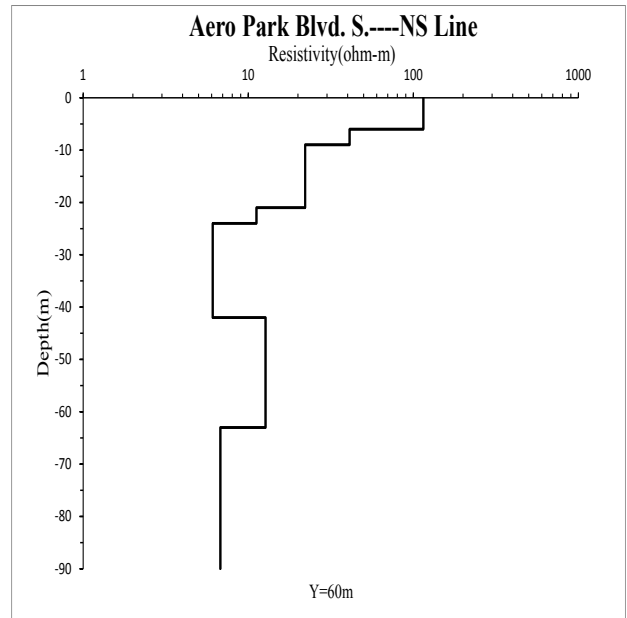
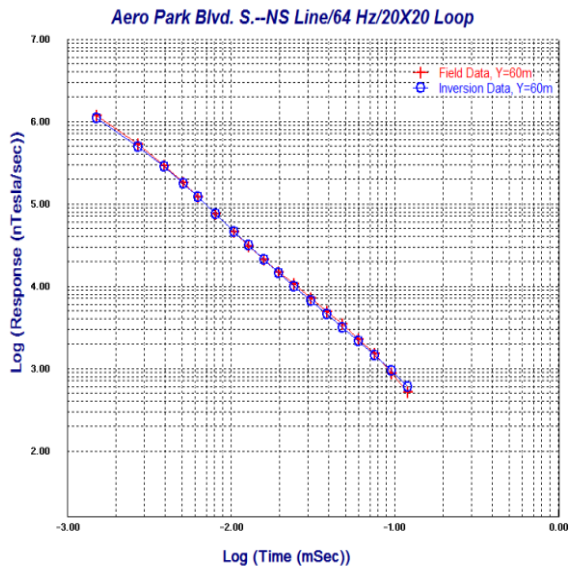


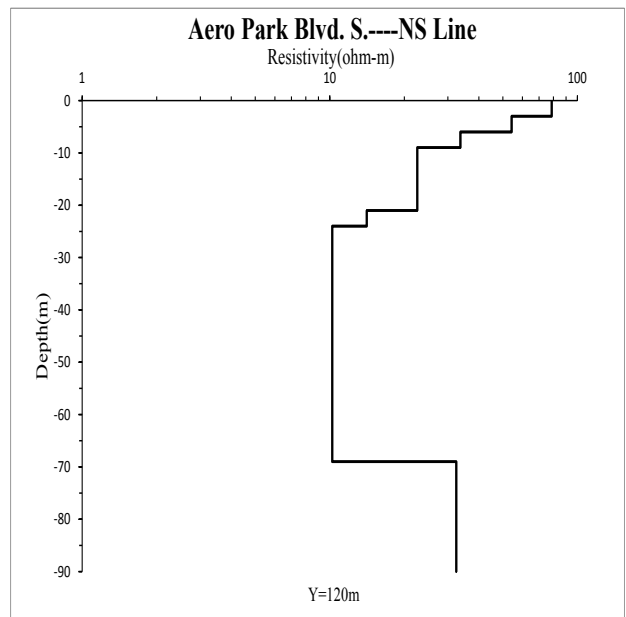
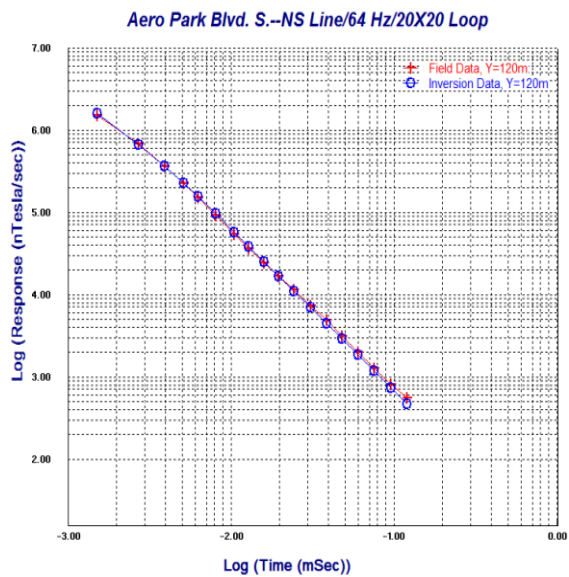
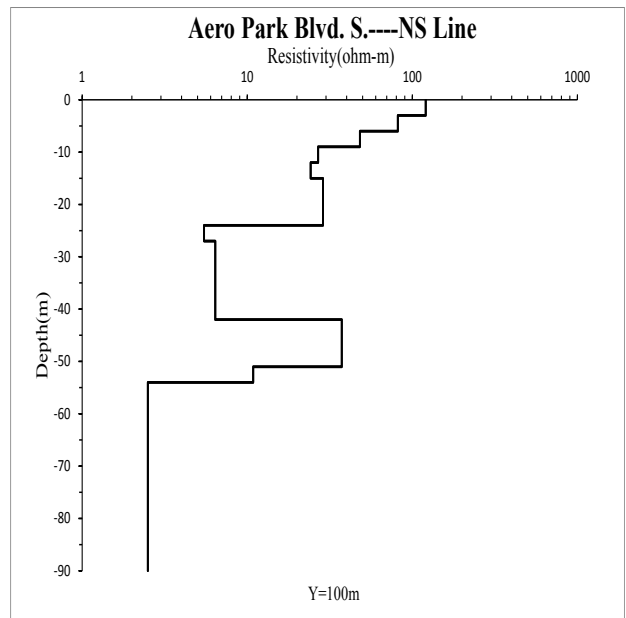
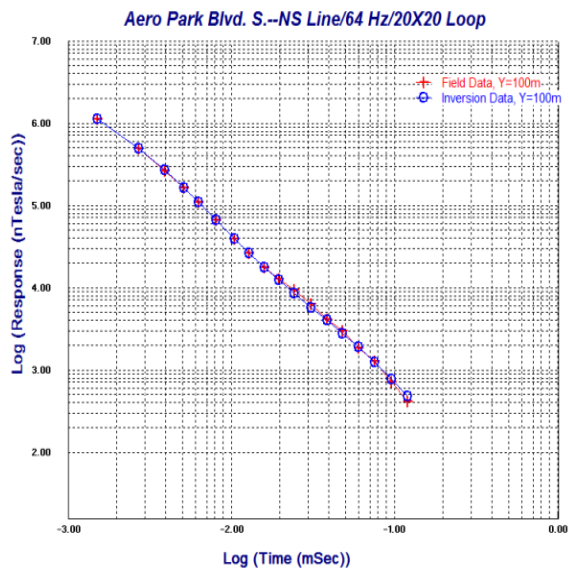


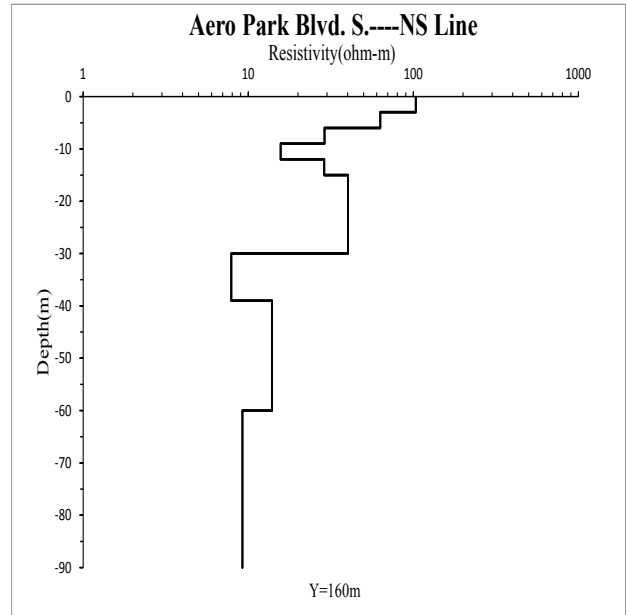
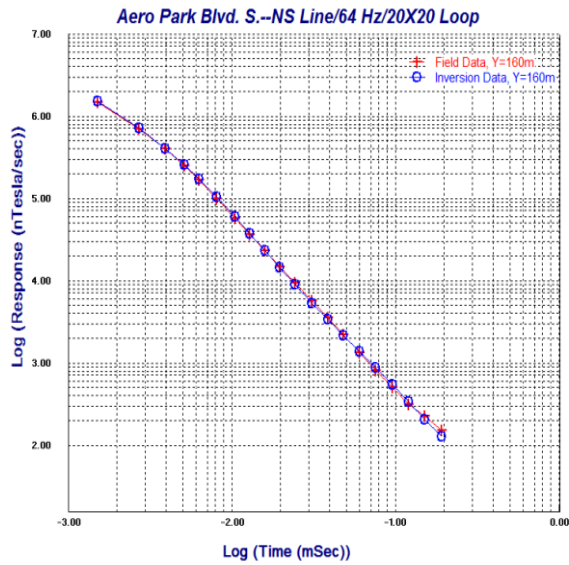
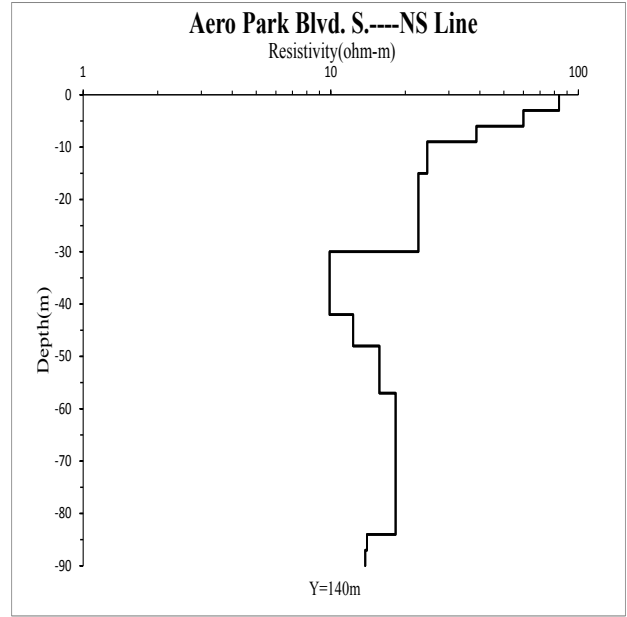
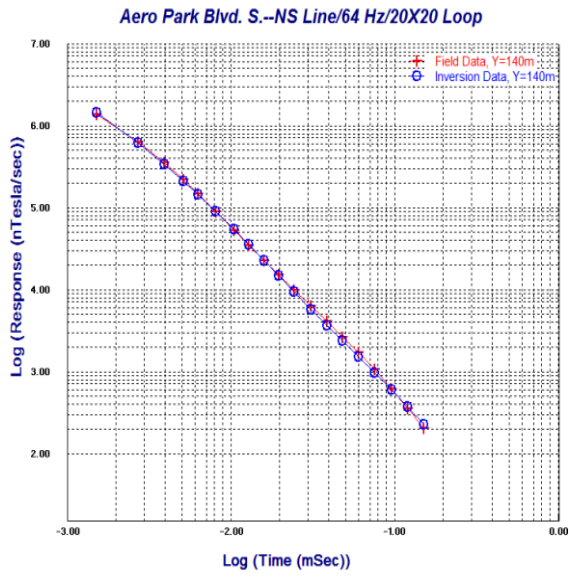
③Aero Park Blvd. S.NS



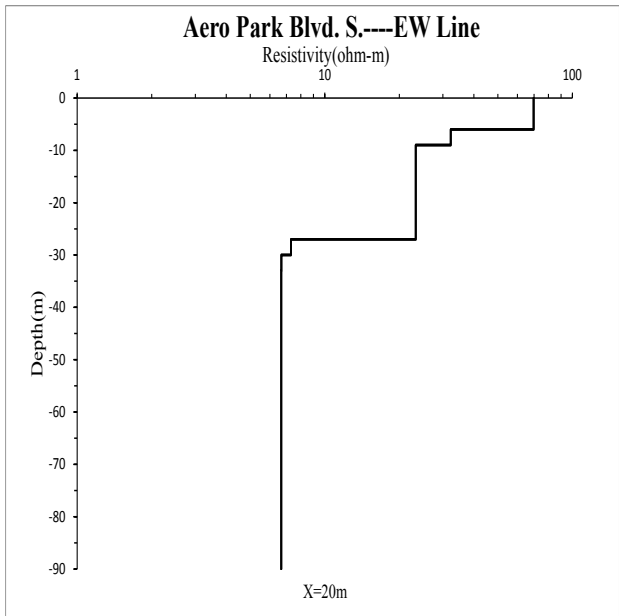
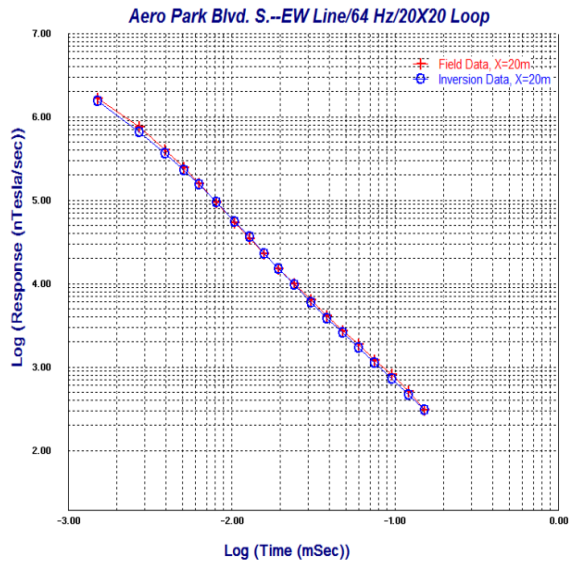
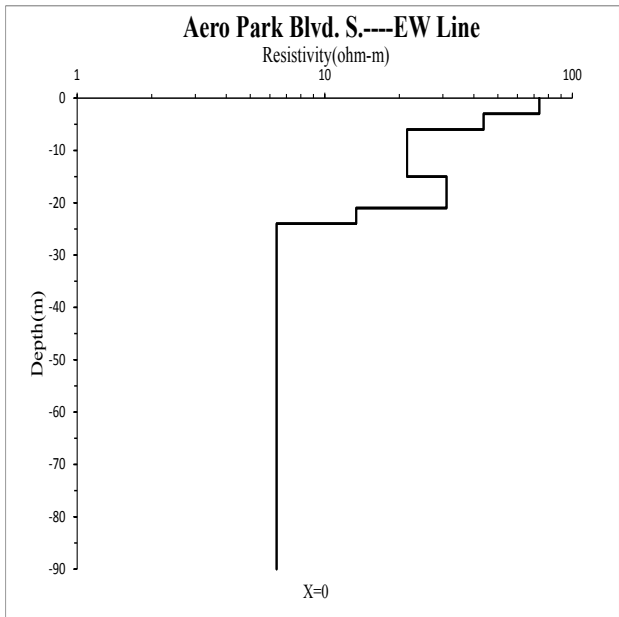
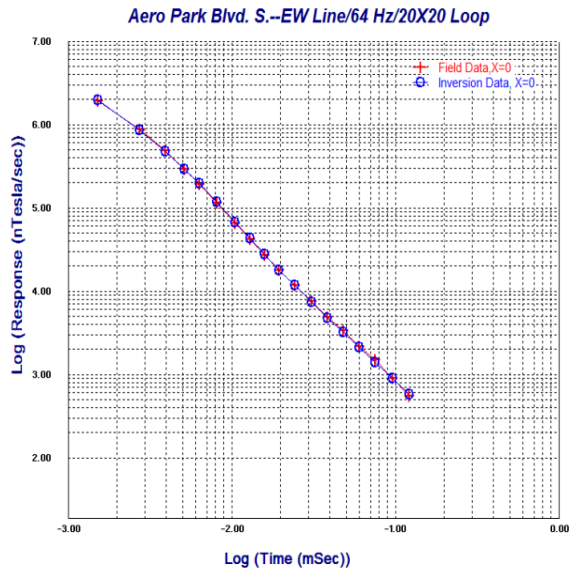


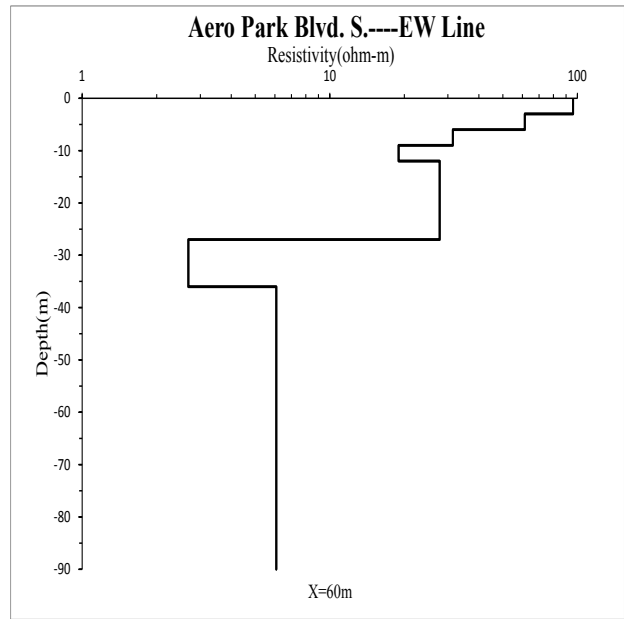
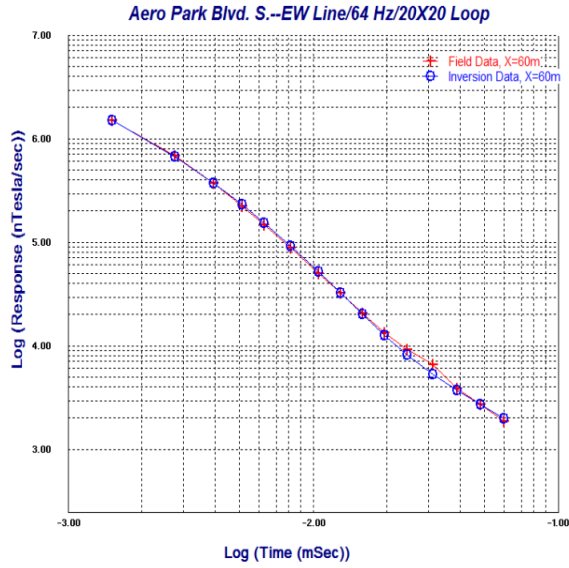
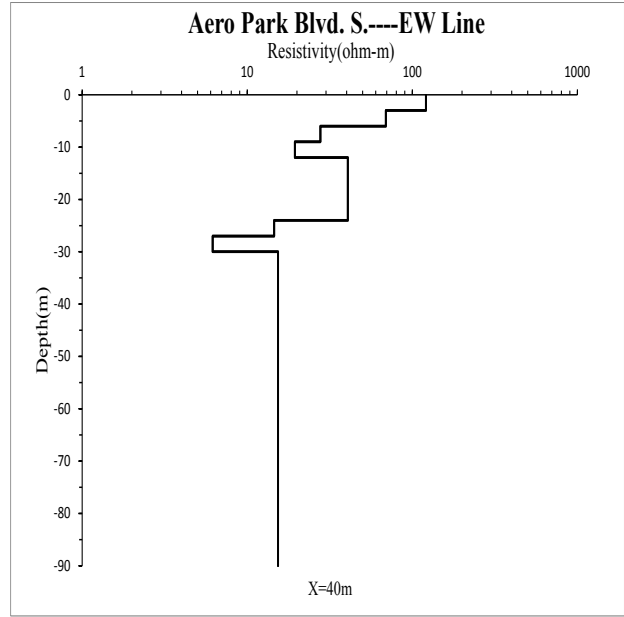
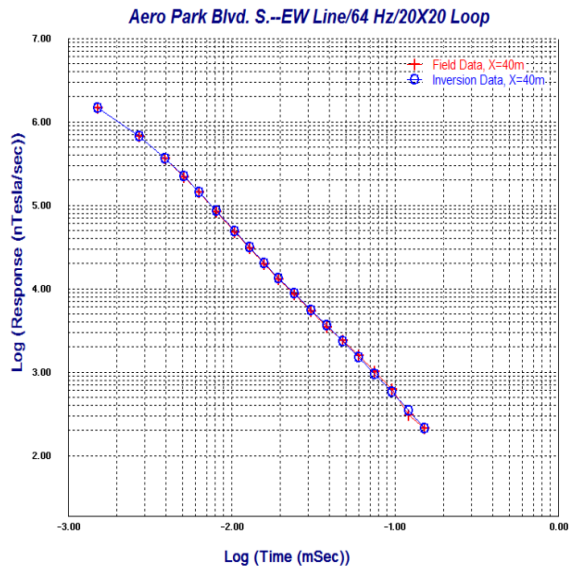


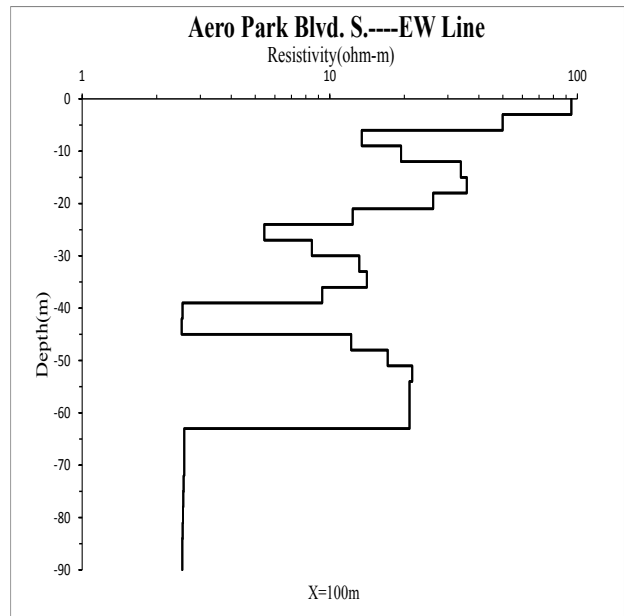
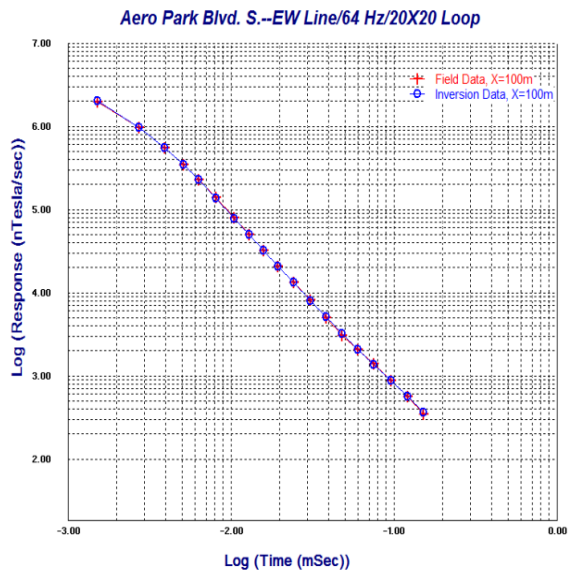
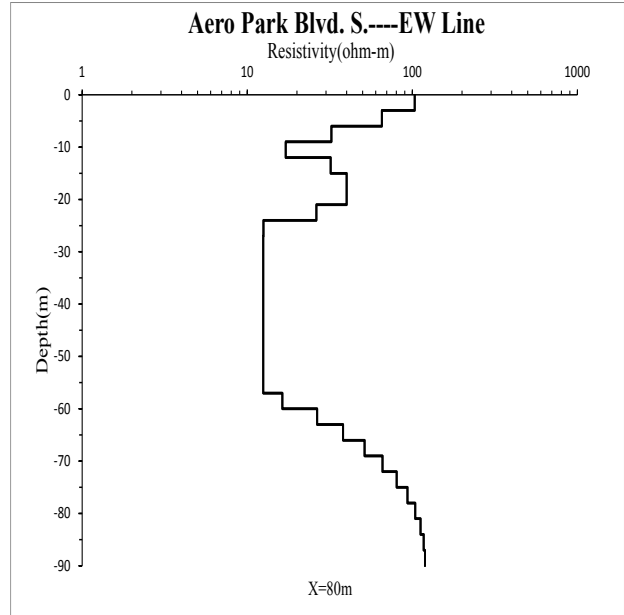
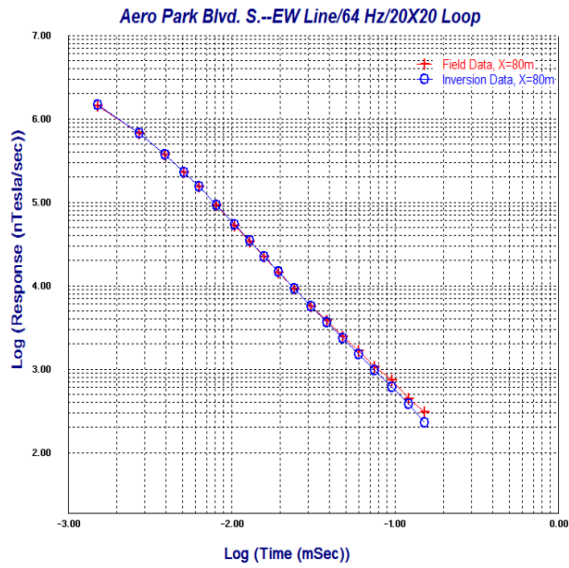


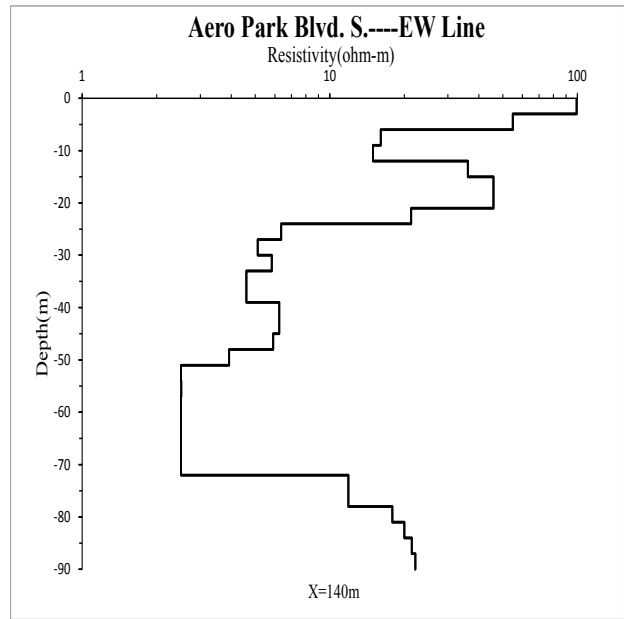
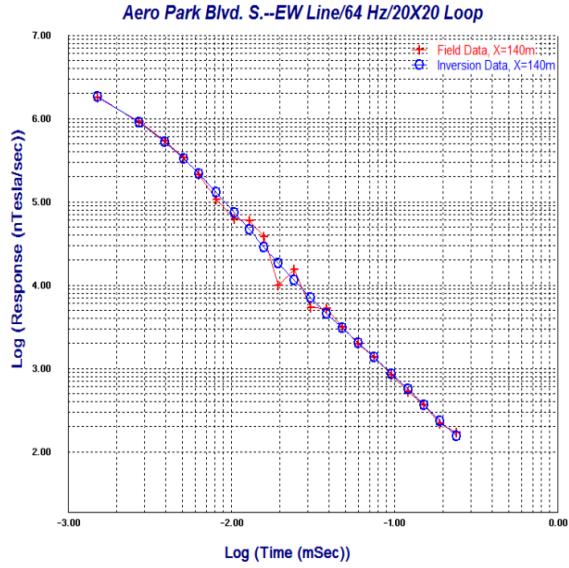
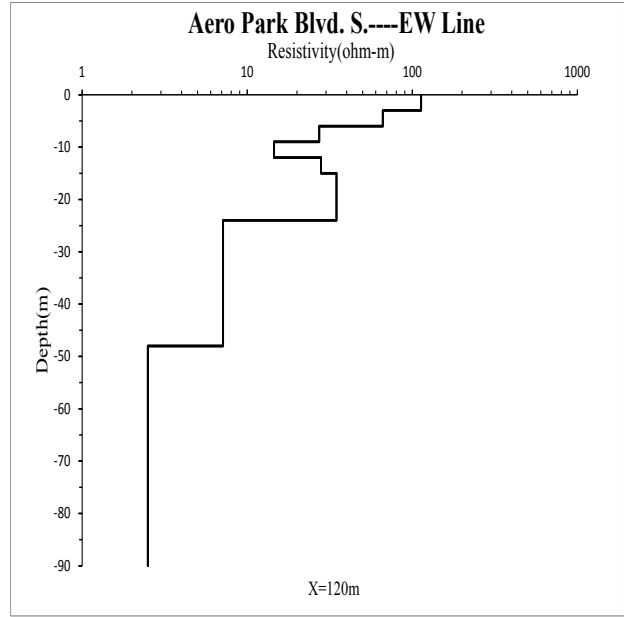
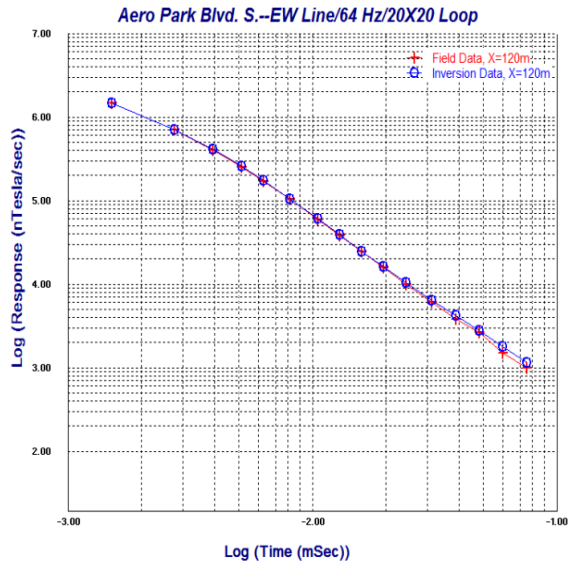


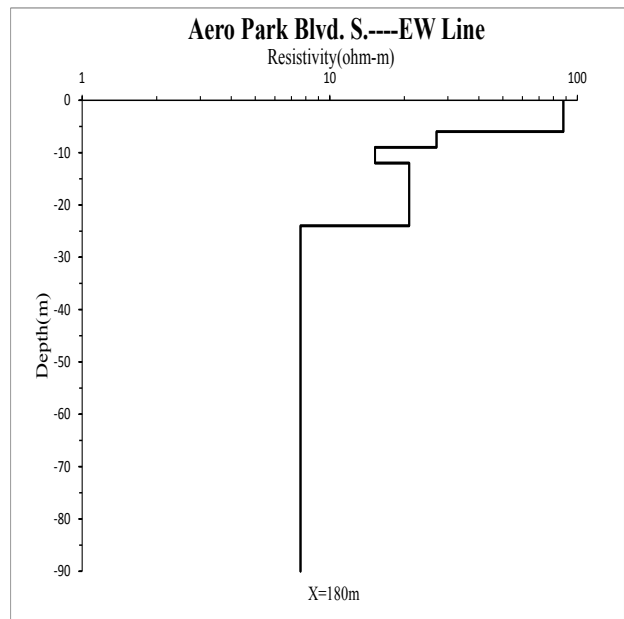
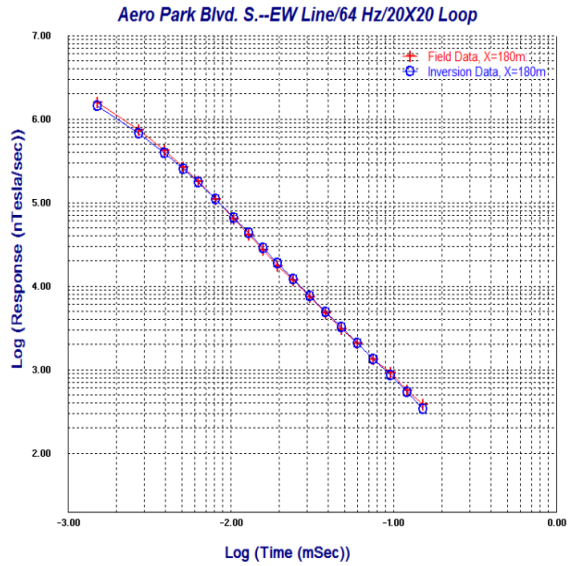
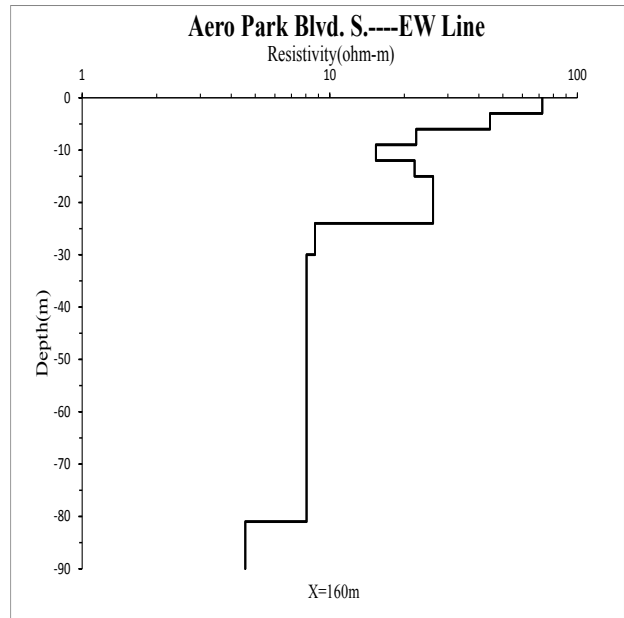
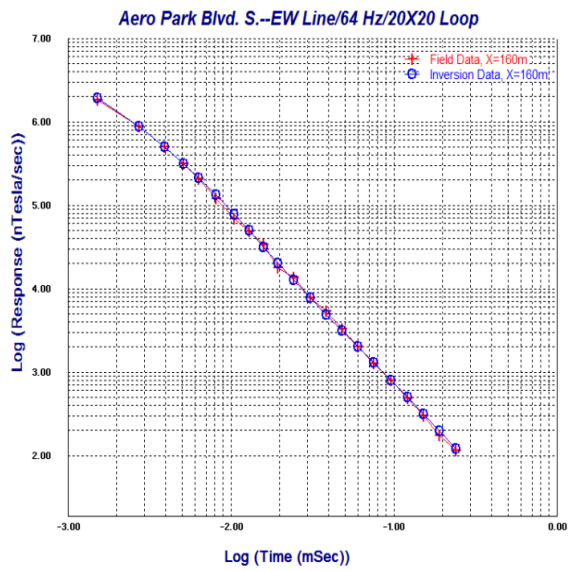
④Aero Park Blvd. S. EW

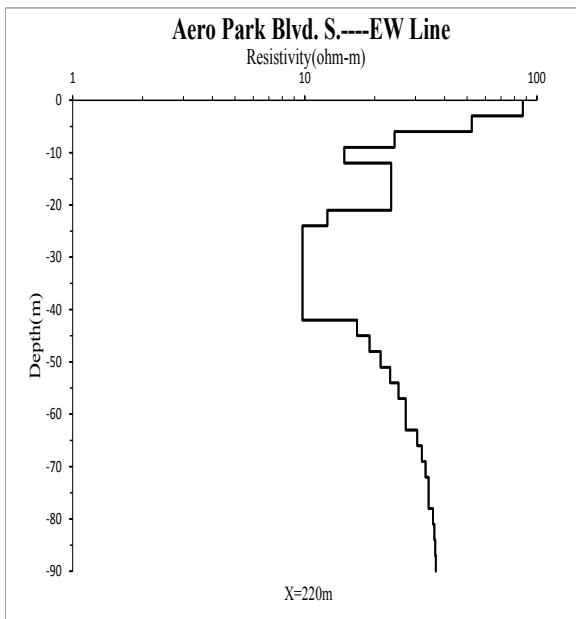
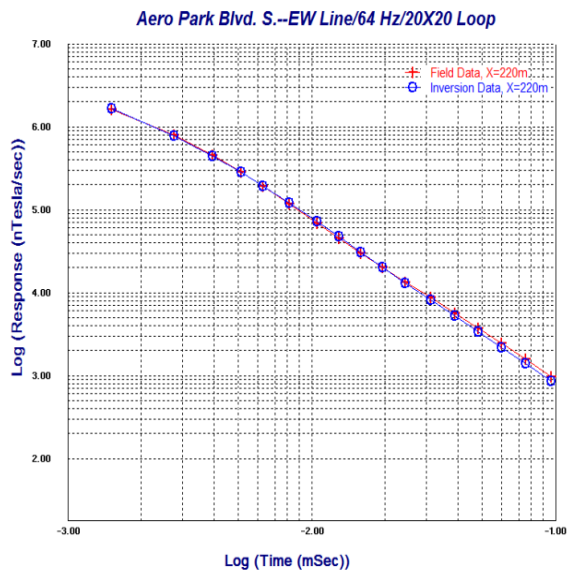
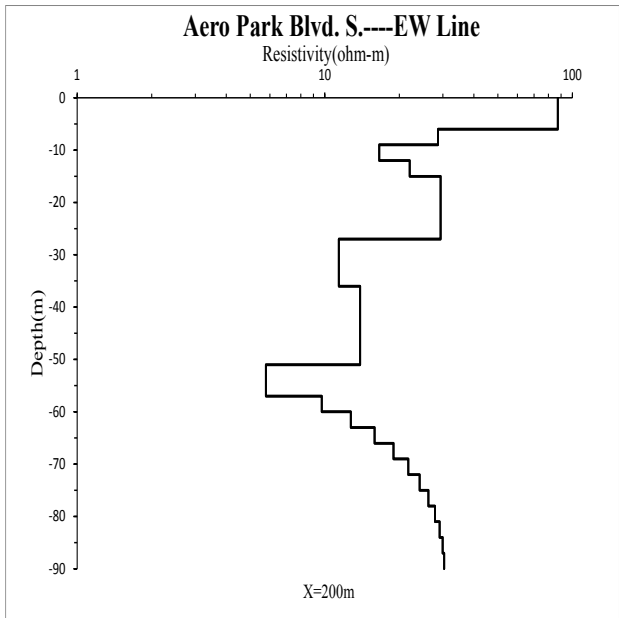
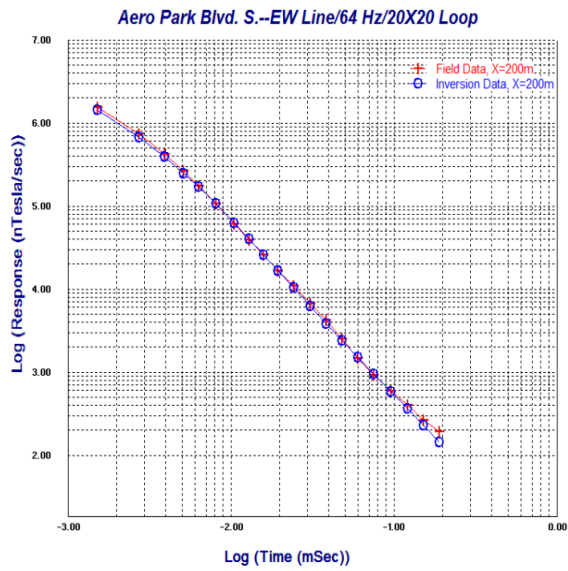


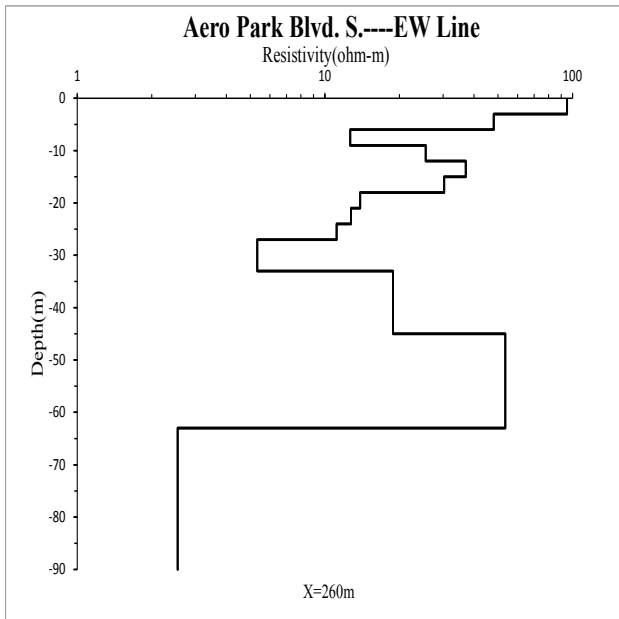
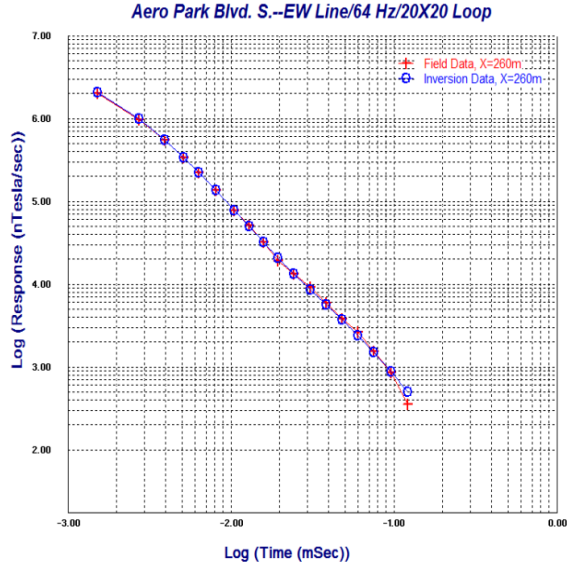
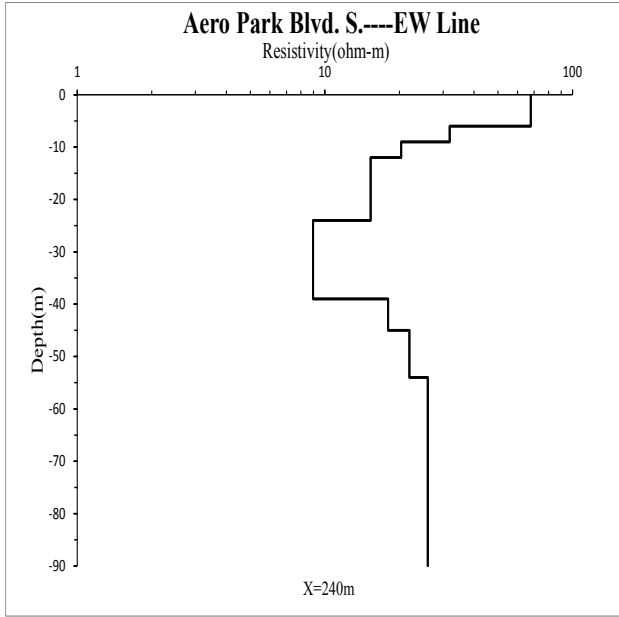
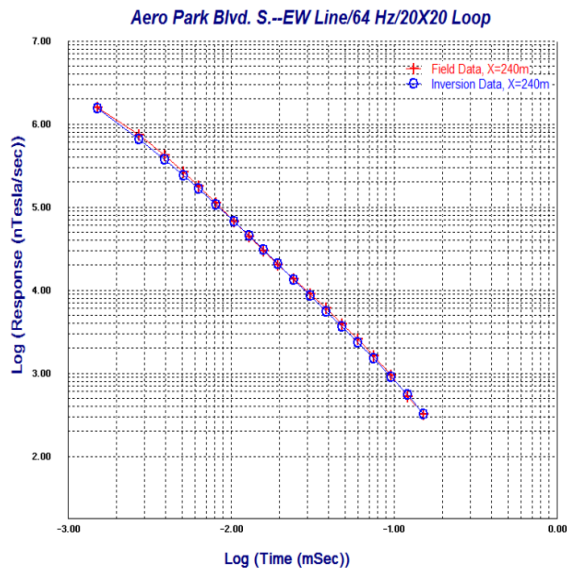


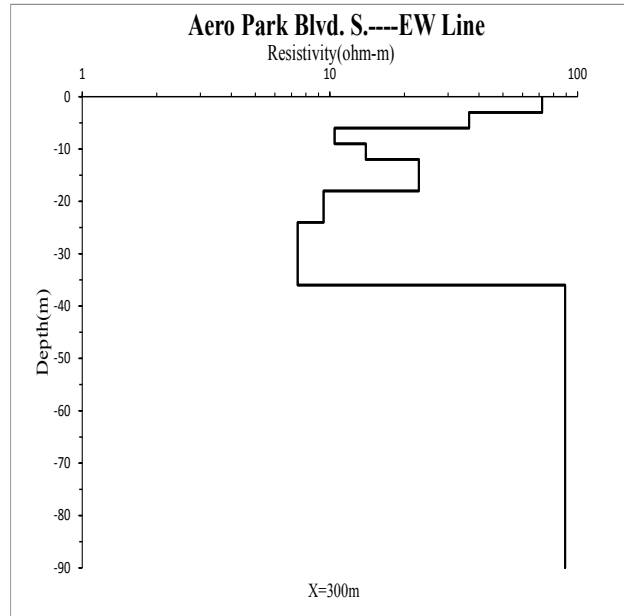
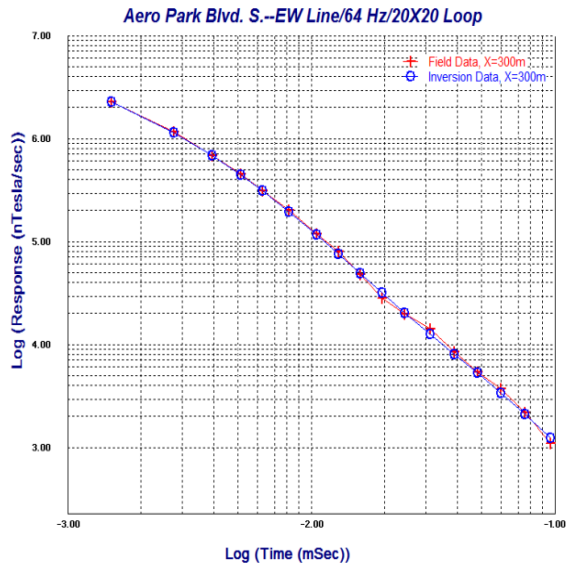
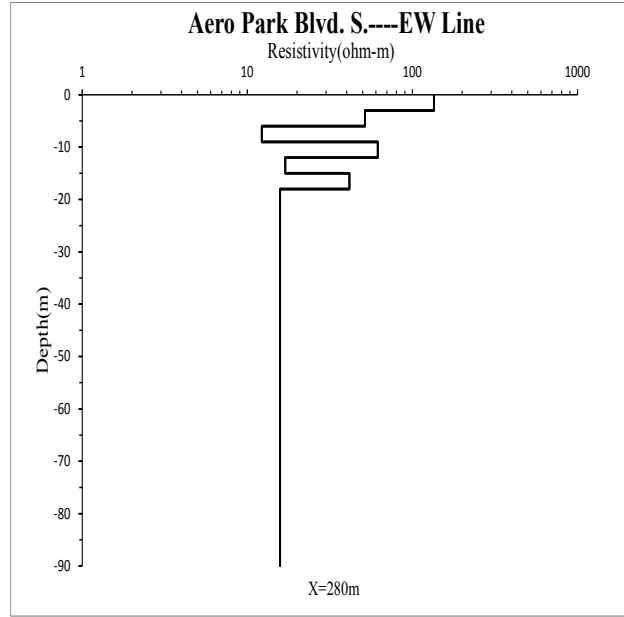
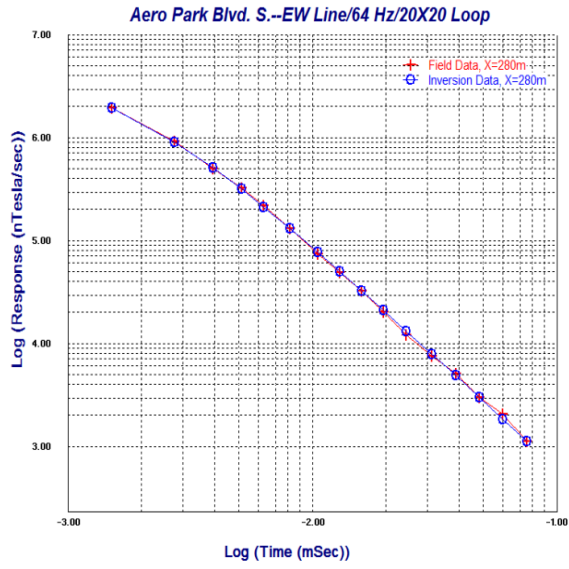


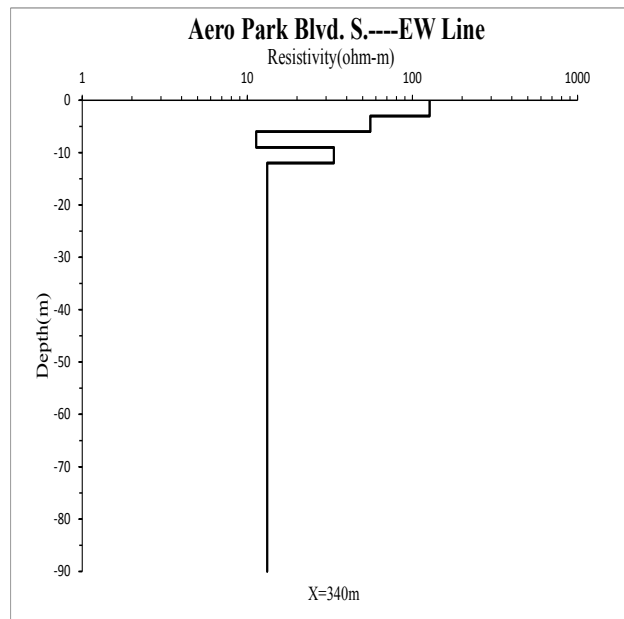
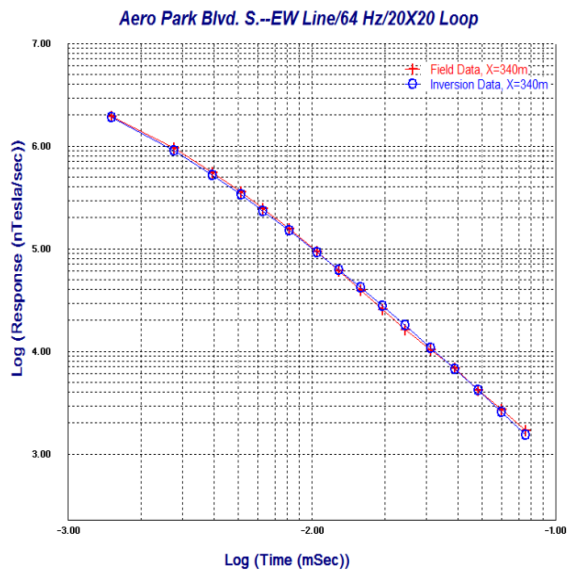
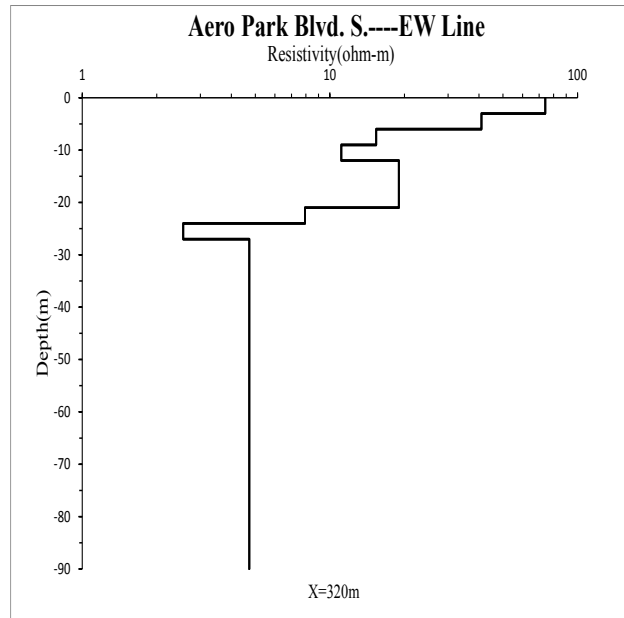
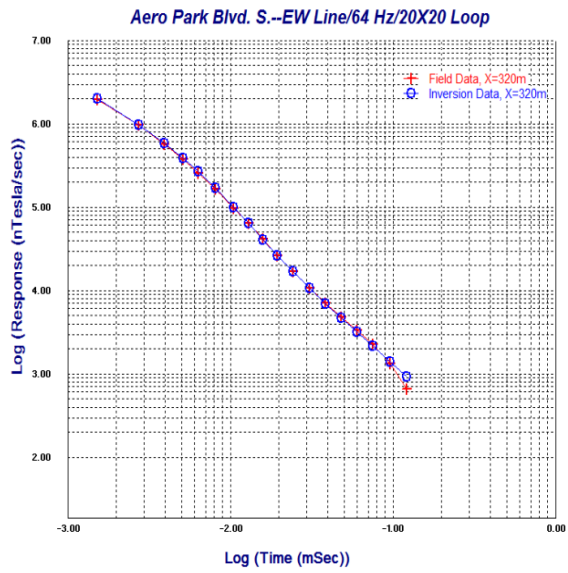


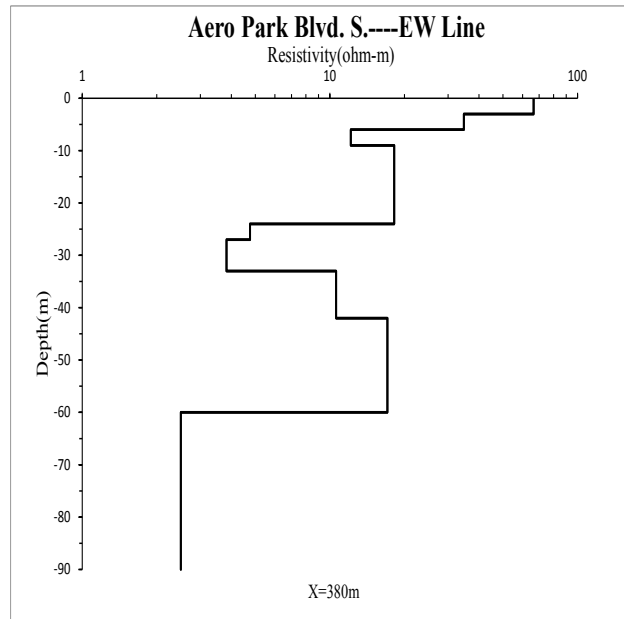
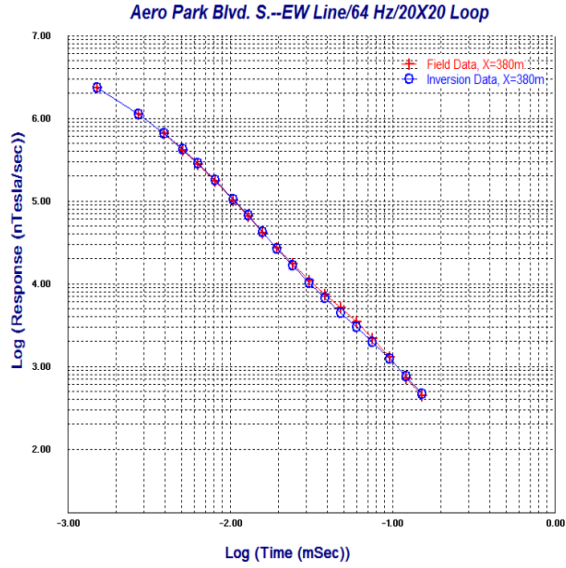
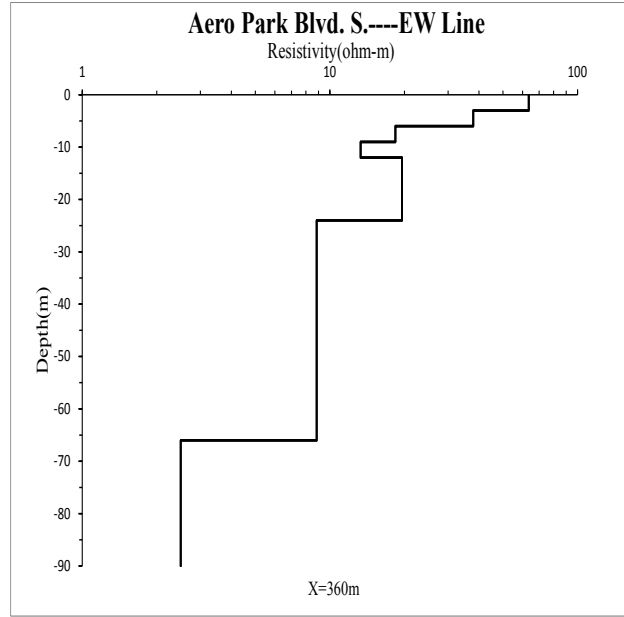
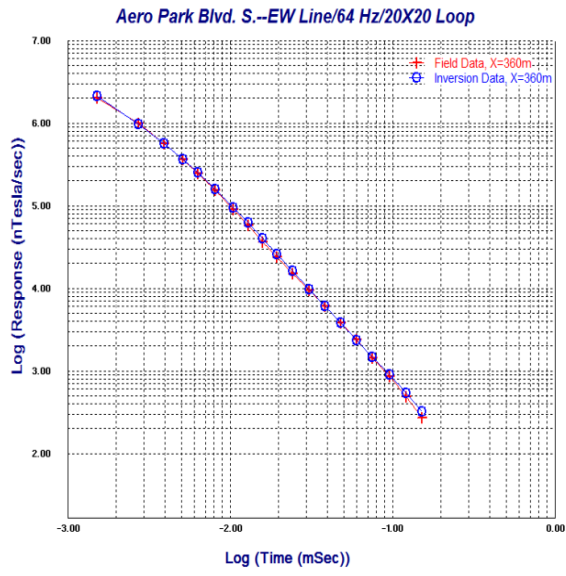


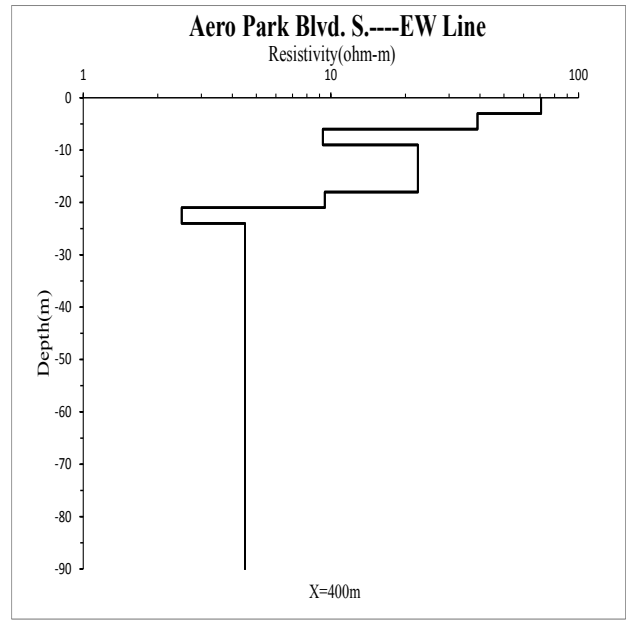
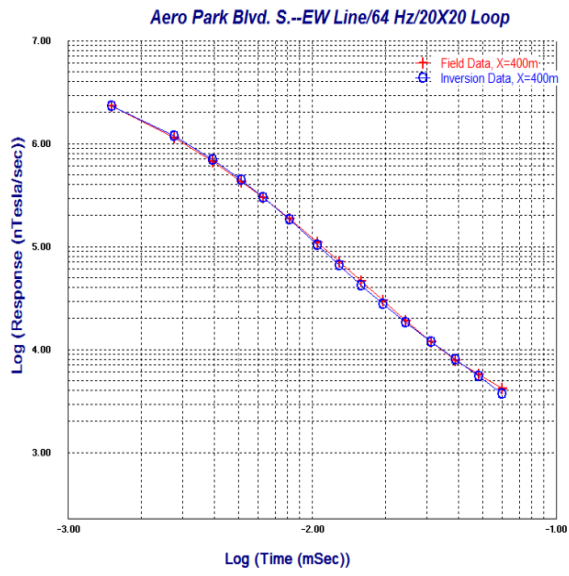






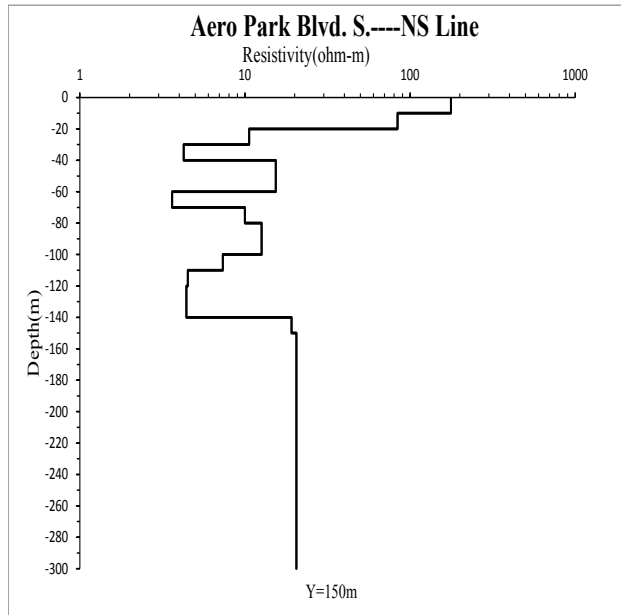
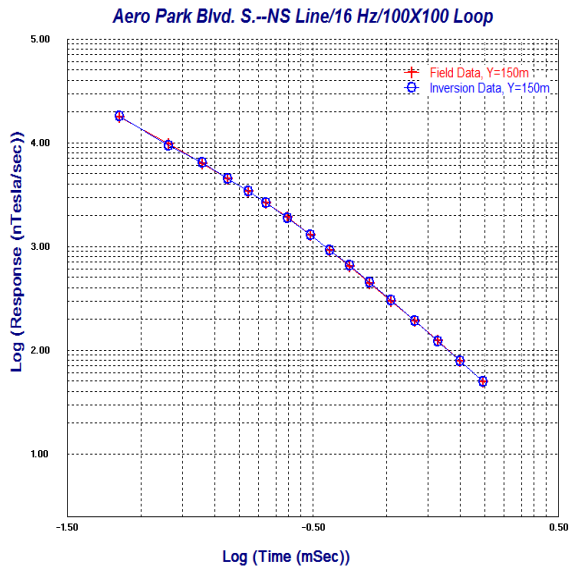
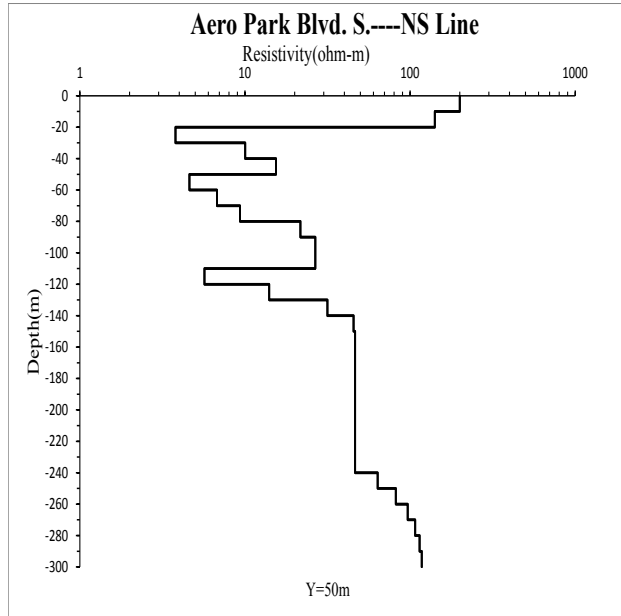
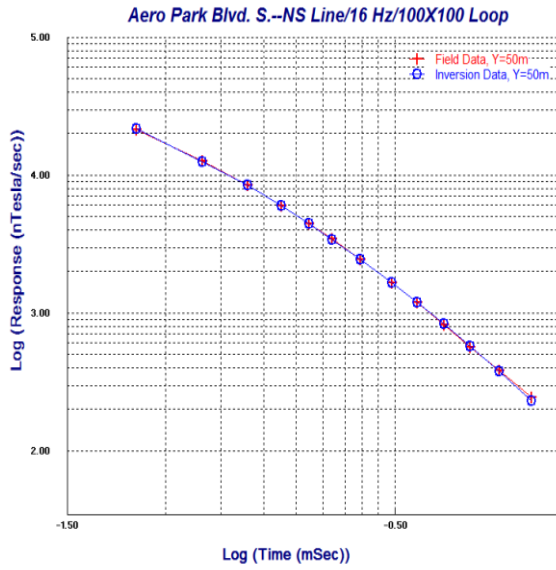


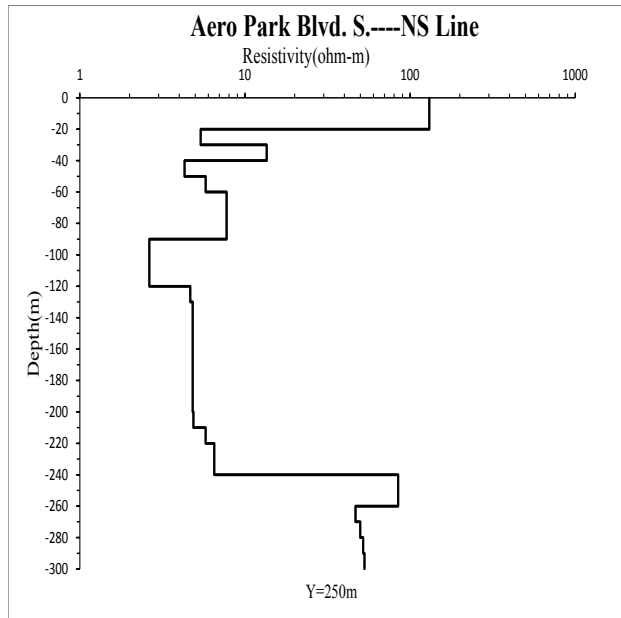
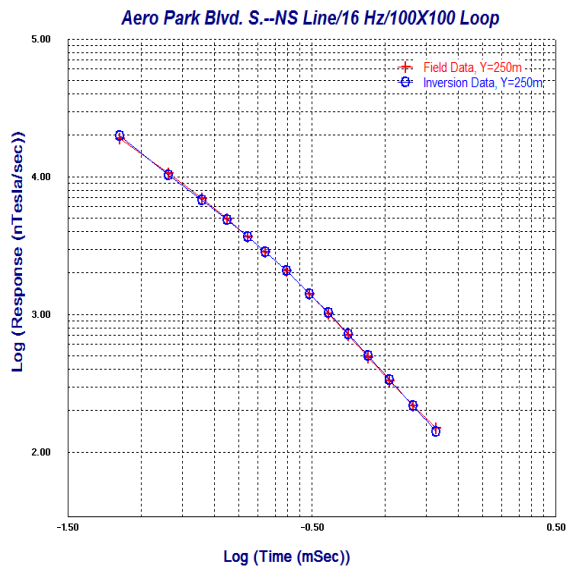




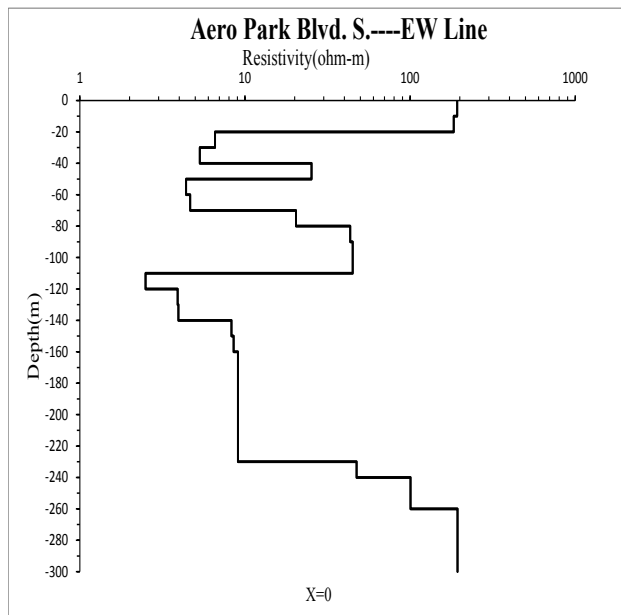
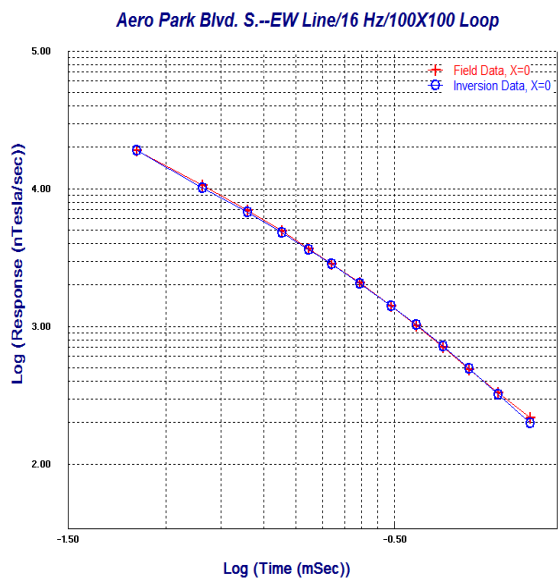
### 3. 16HZ, 100×100m Loop and 50×50m Loop

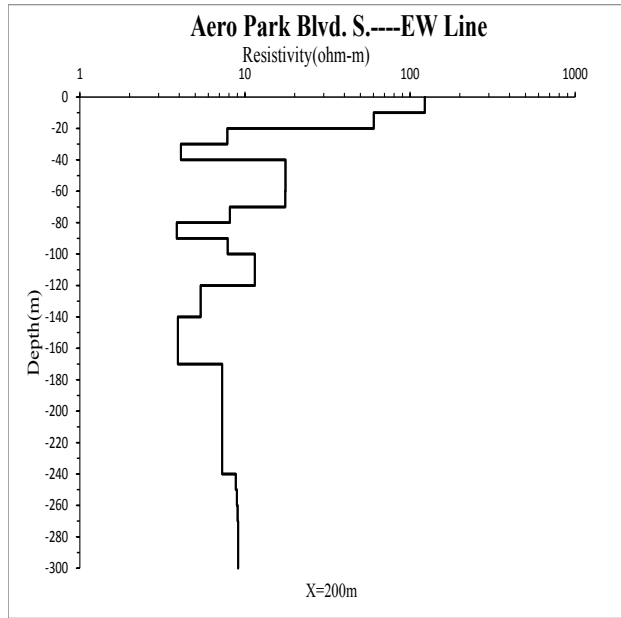
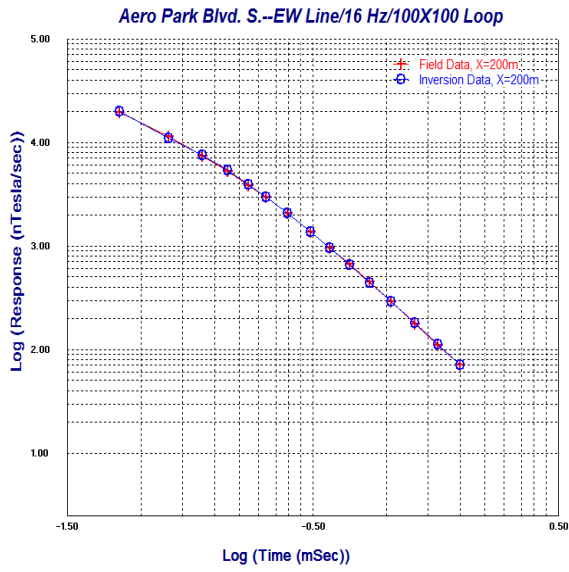
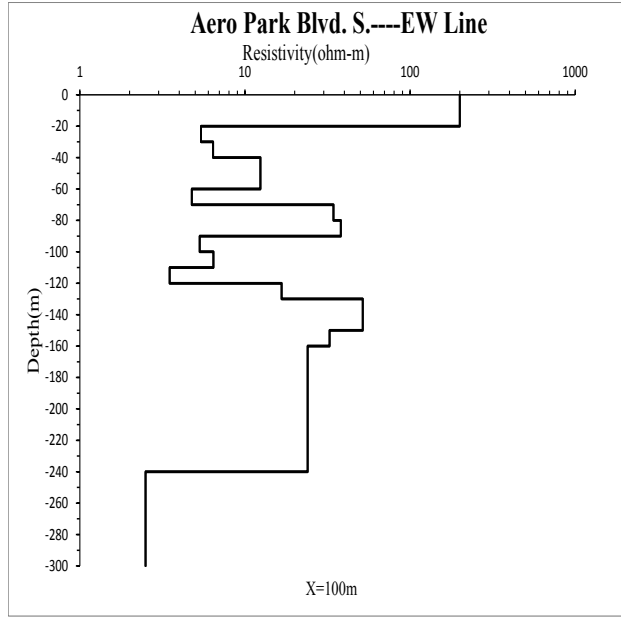
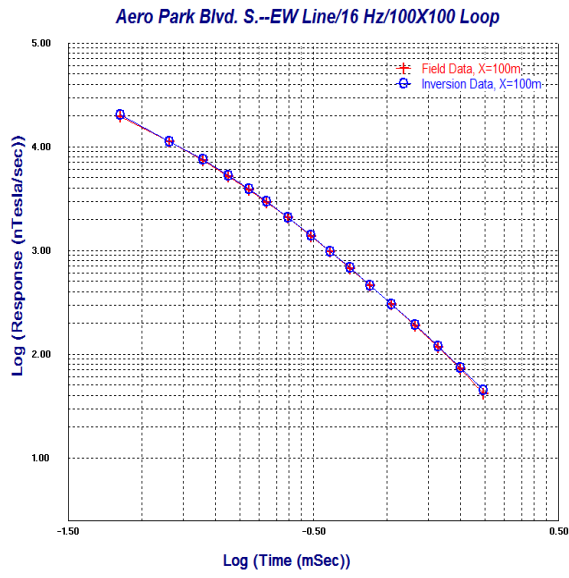
①Aero Park Blvd. S.NS

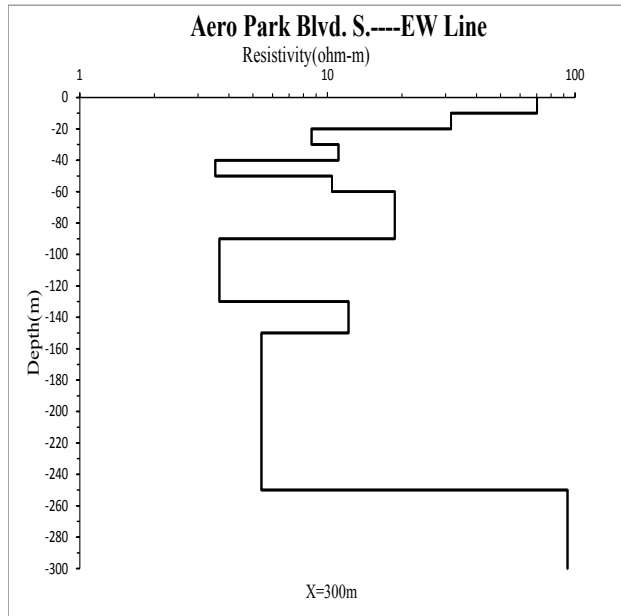
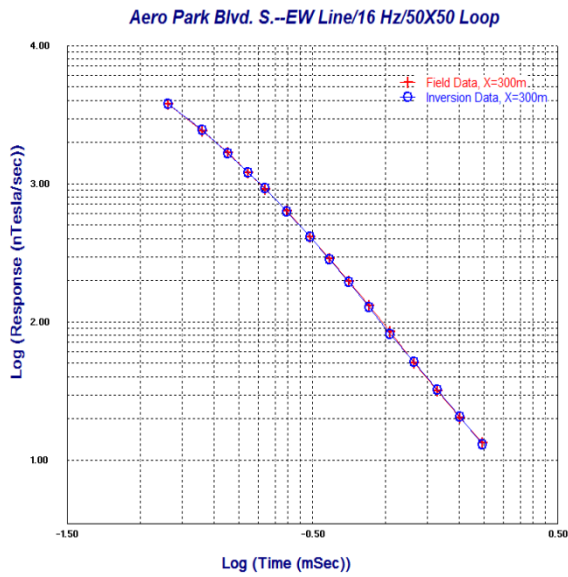
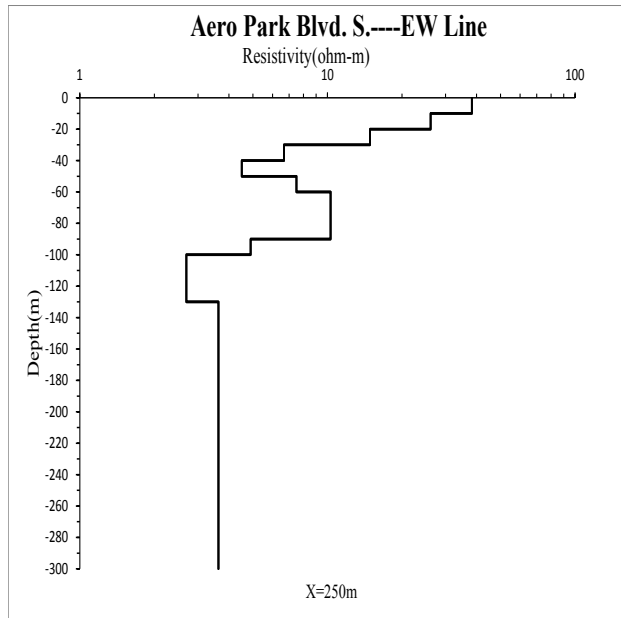
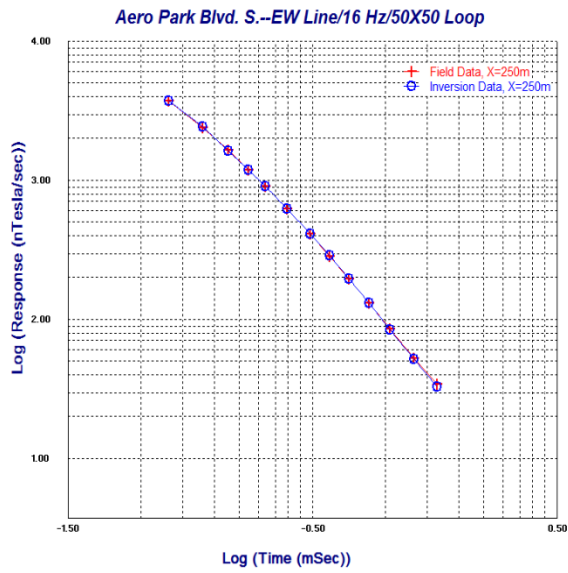


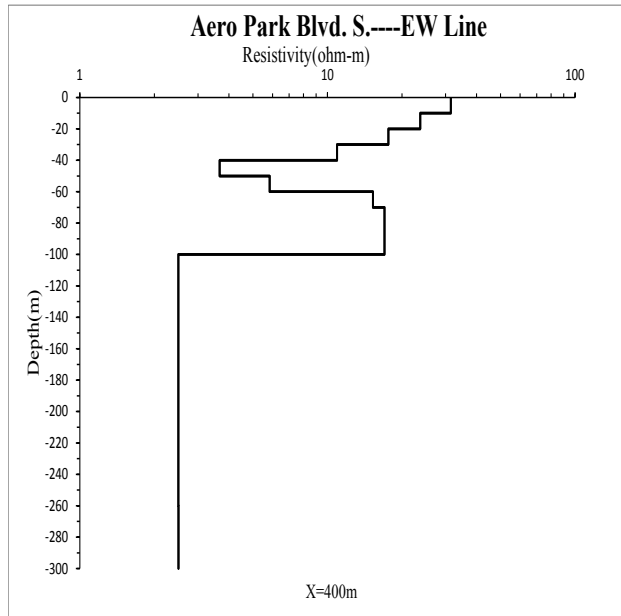
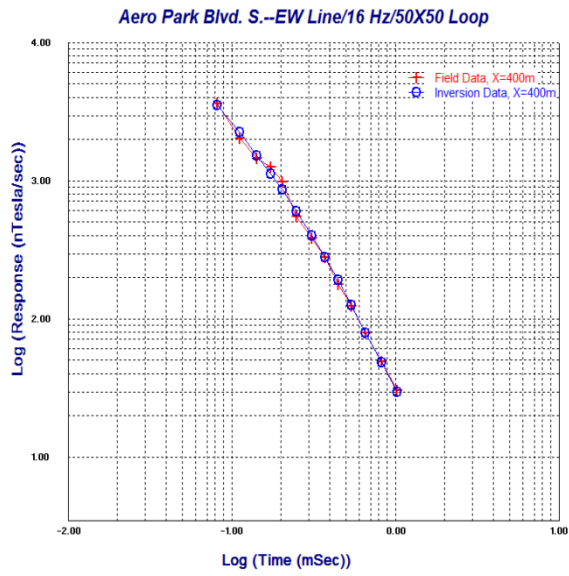
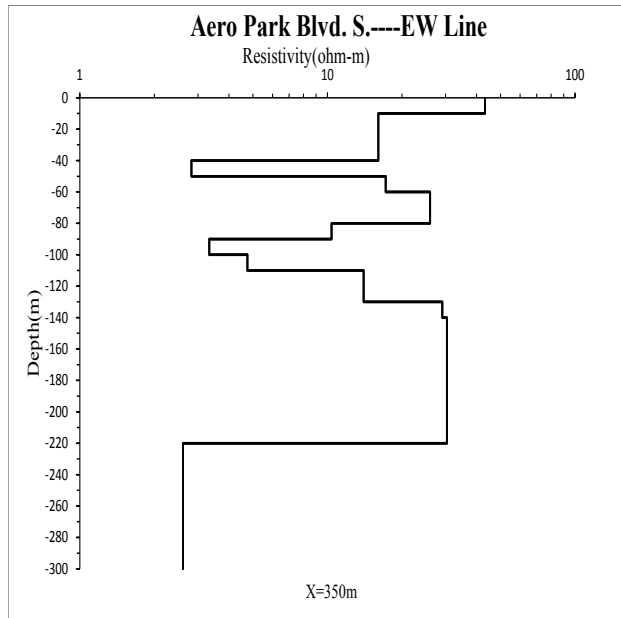
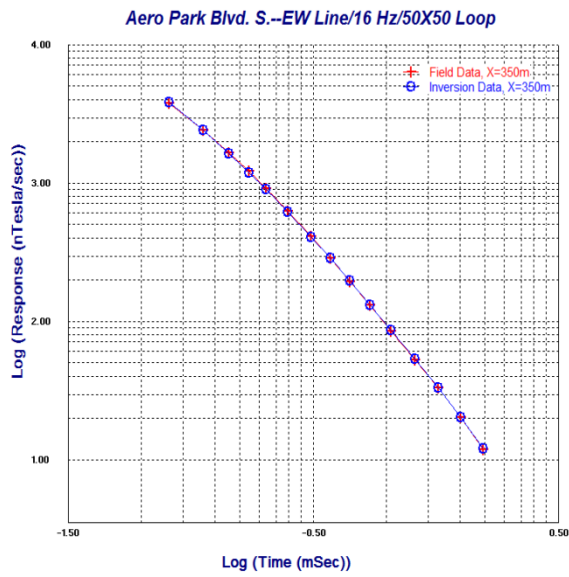


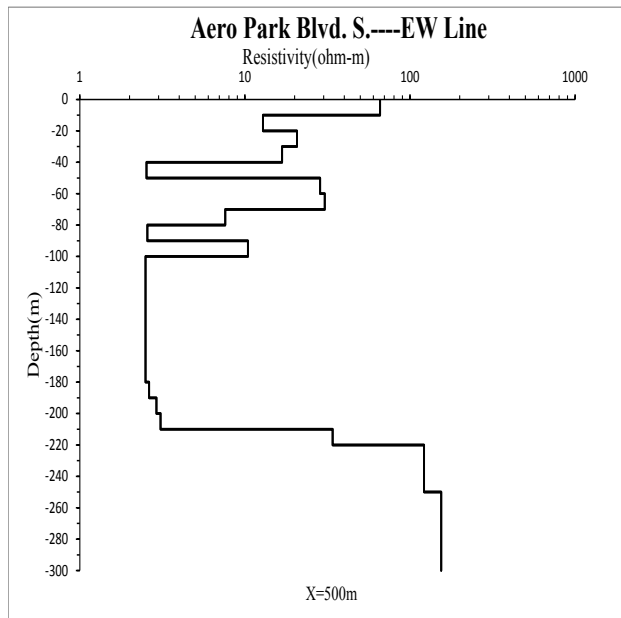
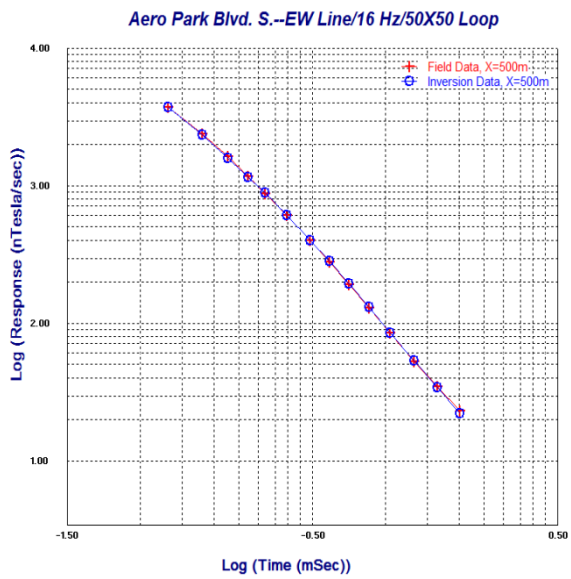
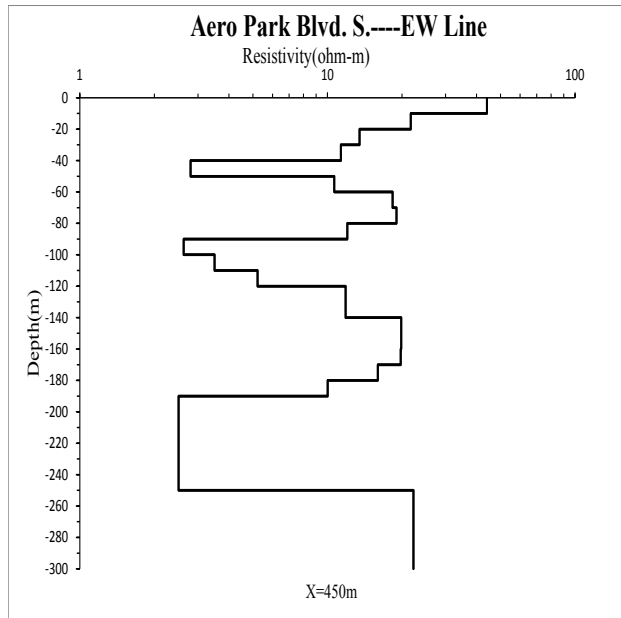
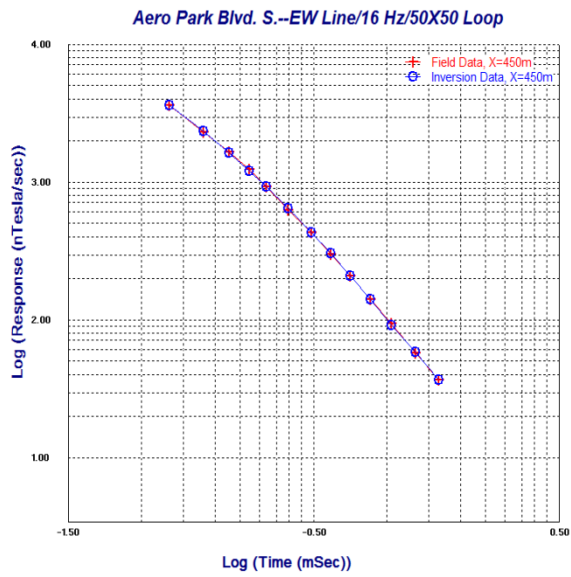
② Aero Park Blvd. S. EW

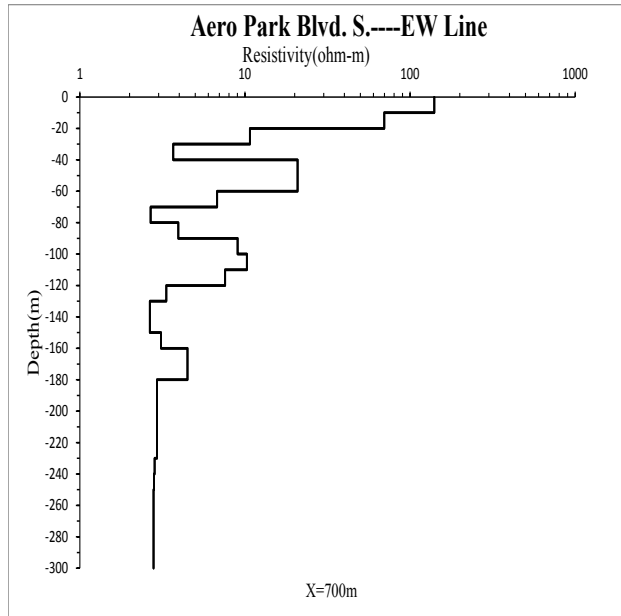
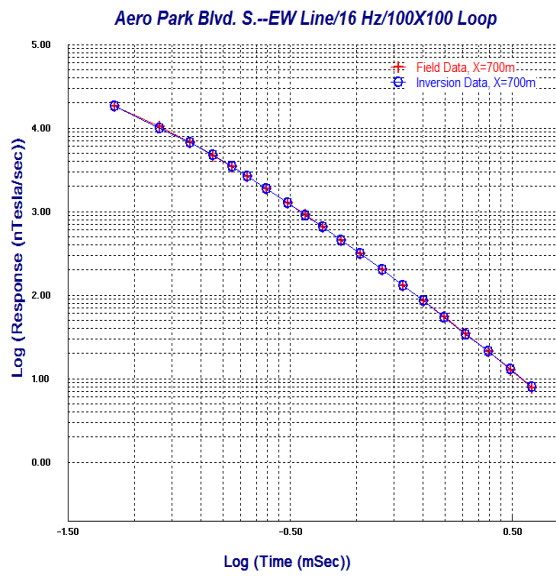
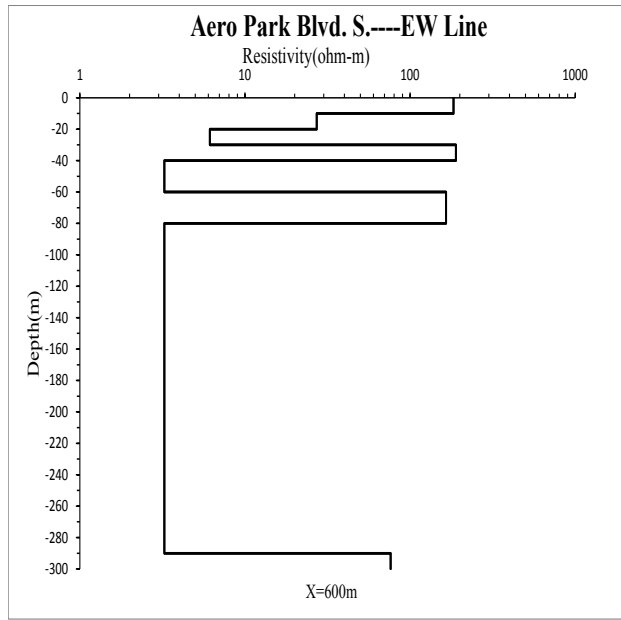
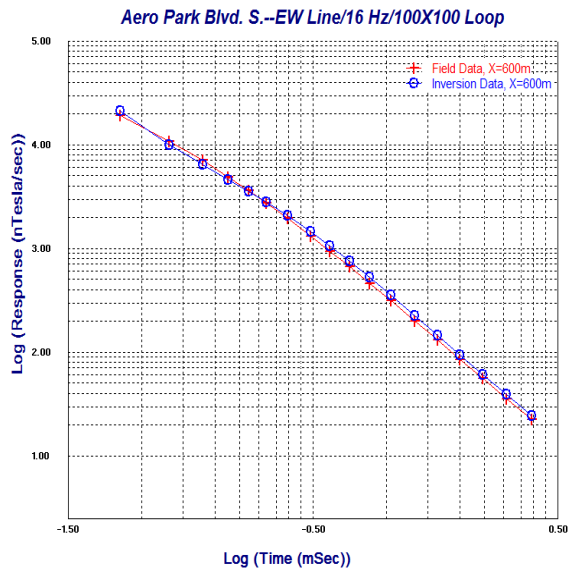


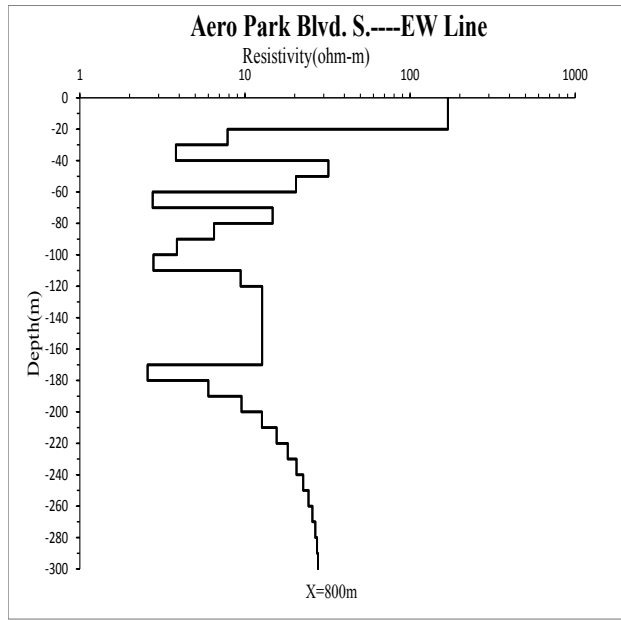
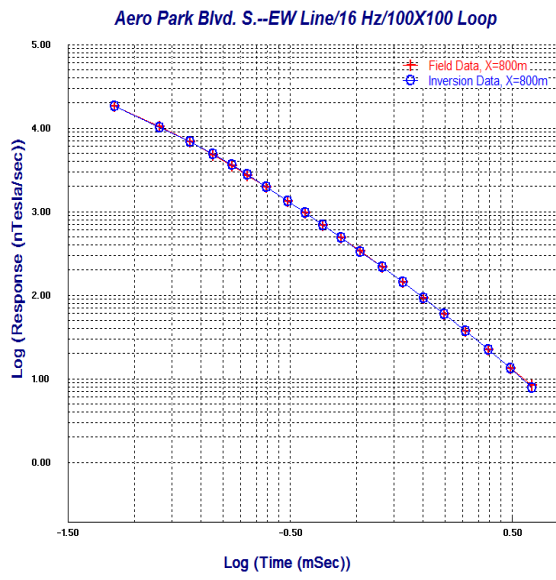






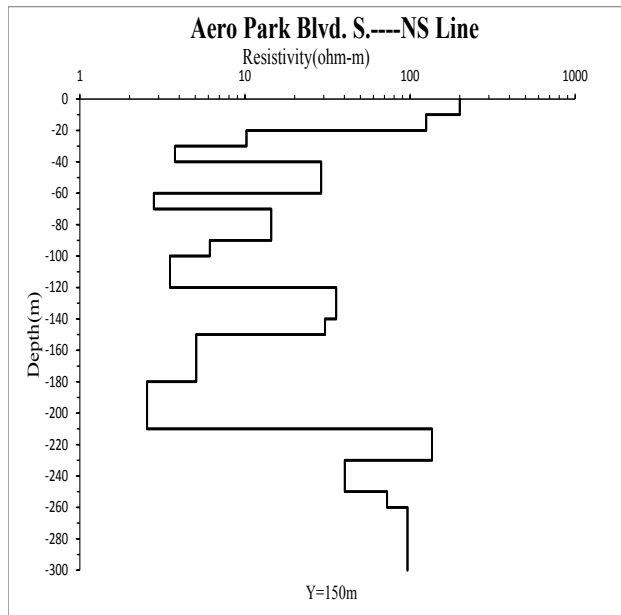
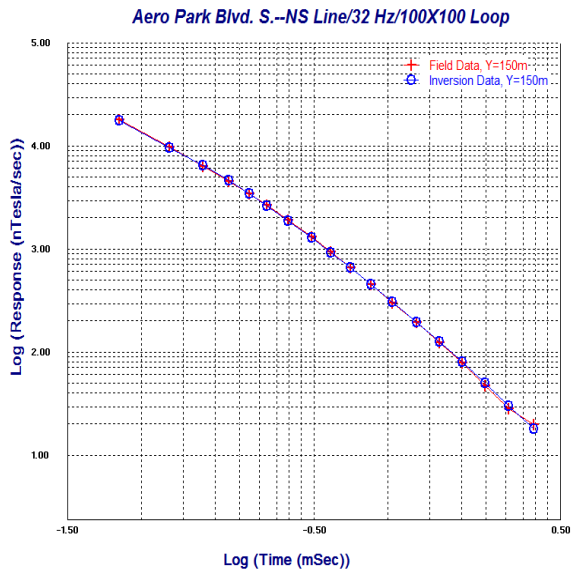
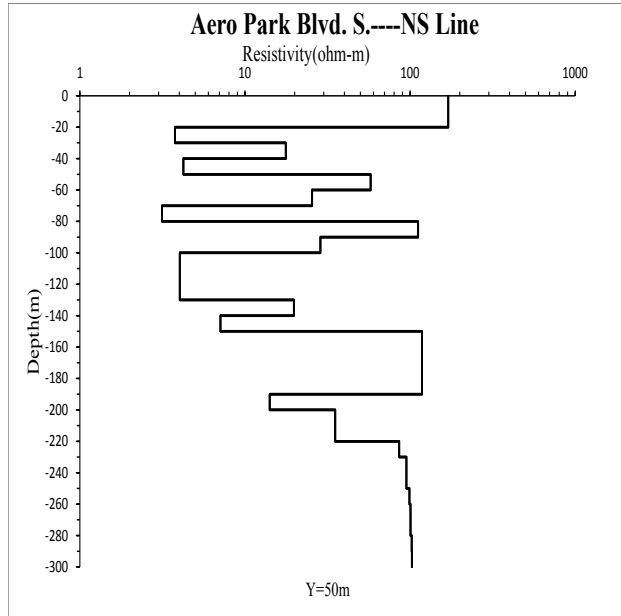
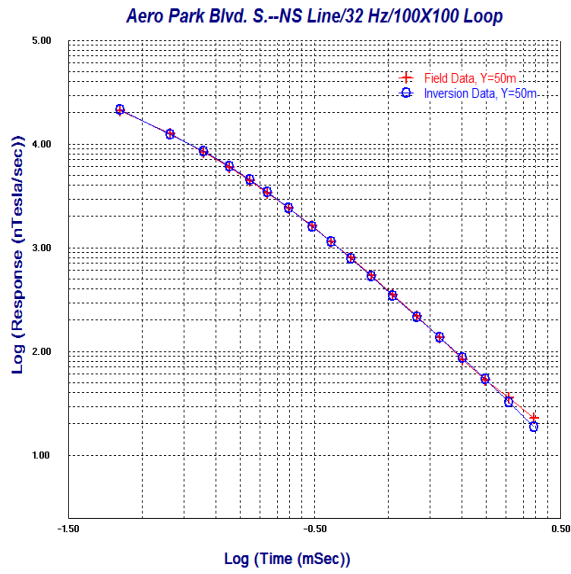


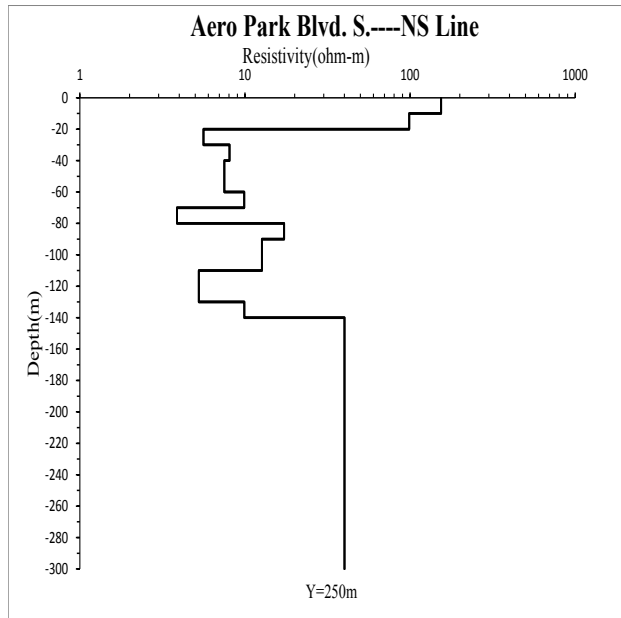
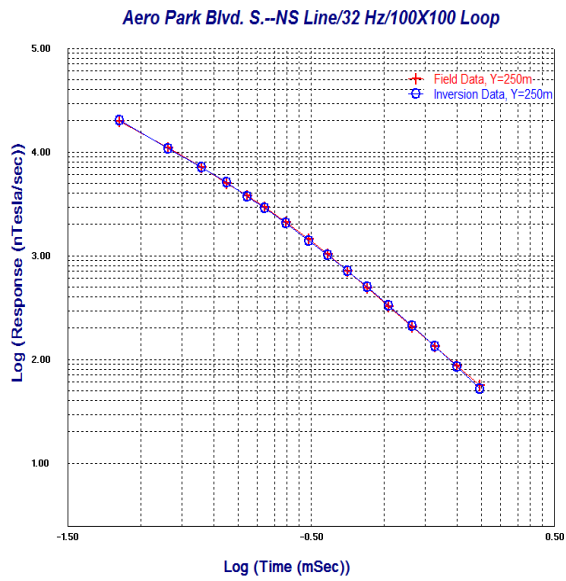




#### 4. 32HZ, 100×100m Loop and 50×50m Loop

①Aero Park Blvd. S.NS





④Aero Park Blvd. S. EW

